



UNIVERSIDADE D  
**COIMBRA**

Renan Câmara Pereira

**QUANTUM CHROMODYNAMICS PHASE  
DIAGRAM UNDER EXTREME CONDITIONS**

**Tese no âmbito do Doutoramento em Física, ramo de Física Nuclear e das Partículas orientada pelo Professor Doutor Pedro Fernando Simões Costa e pela Professora Doutora Maria Constança M. P. da Providência S. e Costa e apresentada ao Departamento de Física da Faculdade de Ciências e Tecnologia da Universidade de Coimbra.**

Dezembro de 2020



UNIVERSITY OF COIMBRA

DOCTORAL THESIS

---

**Quantum Chromodynamics Phase  
Diagram Under Extreme Conditions**

---

*Author:*  
Renan Câmara Pereira

*Supervisors:*  
Prof. Dr. Pedro Costa  
Prof. Dr. Constança Providência

*A thesis submitted in fulfillment of the requirements  
for the degree of Doctor of Philosophy*

*in the*

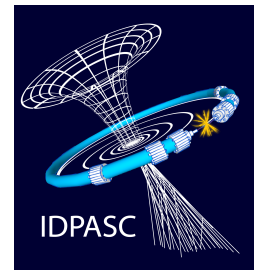
Centre for Physics of the University of Coimbra  
Department of Physics of the University of Coimbra

May 3, 2021



The work presented in this thesis was funded by FCT (Fundação para a Ciência e a Tecnologia, I.P, Portugal) under the FCT-IDPASC PhD program (International Doctorate Network in Particle Physics, Astrophysics and Cosmology), through the grant PD/BD/128234/2016.

**FCT** Fundação  
para a Ciência  
e a Tecnologia





*“People think dreams aren’t real just because they aren’t made of matter, of particles. Dreams are real. But they are made of viewpoints, of images, of memories and puns and lost hopes.”*

- Neil Gaiman, *The Sandman*

*“We live on an island surrounded by a sea of ignorance. As our island of knowledge grows, so does the shore of our ignorance.”*

- John Archibald Wheeler, *Scientific American* (1992), Vol. 267

*“Are you really sure that a floor can’t also be a ceiling?”*

*“My work is a game, a very serious game.”*

- Maurits Cornelis Escher



## *Preface*

The present work is the result of research carried out under the supervision of Professor Doctor Pedro Costa and Professor Doctor Constança Providência, at the Centre for Physics of the University of Coimbra. The original contributions that resulted from this research work are partially contained in this thesis and gave origin to several scientific publications:

1. *Phase Diagram, Scalar-Pseudoscalar Meson Behavior and Restoration of Symmetries in (2+1) Polyakov-Nambu-Jona-Lasinio Model*  
 Pedro Costa and Renan Câmara Pereira  
 Symmetry 11 (2019) 4, 507-538  
 DOI: 10.3390/sym11040507  
 arXiv:1904.05805;
2. *One-meson-loop NJL model: Effect of collective and noncollective excitations on the quark condensate at finite temperature*  
Renan Câmara Pereira and Pedro Costa  
 Phys. Rev. D 101, 054025 (2020)  
 DOI: 10.1103/PhysRevD.101.054025  
 arXiv:2003.08430;
3. *Probing the interior of Neutron Stars and the QCD phase diagram with SKA*  
 Constança Providência, Pedro Costa, Márcio Ferreira, Helena Pais, and  
Renan Câmara Pereira  
 Contribution to the Portuguese whitebook of the SKA-Square Kilometre Array “Portuguese SKA White Book”, UA Editora – Universidade de Aveiro, 2020, pgs. 69-74  
 arXiv:2005.01140;
4. *Neutron stars with large quark cores*  
 Márcio Ferreira, Renan Câmara Pereira and Constança Providência  
 Phys. Rev. D 101, 123030 (2020)  
 DOI: 10.1103/PhysRevD.101.123030  
 arXiv:2005.10543;
5. *Functional renormalization group study of the critical region of the quark-meson model with vector interactions*  
Renan Câmara Pereira, Rainer Stiele and Pedro Costa  
 Eur. Phys. J. C 80, 712 (2020)  
 DOI: 10.1140/epjc/s10052-020-8296-9  
 arXiv:2003.12829;

6. *The strange critical endpoint and isentropic trajectories in an Extended PNJL Model with Eight Quark Interactions*  
Renan Câmara Pereira, João Moreira and Pedro Costa  
Eur. Phys. J. A 56, 214 (2020)  
DOI: 10.1140/epja/s10050-020-00223-8  
arXiv:2006.02385;
7. *Role of the conserved charges in the chiral symmetry restoration phase transition*  
Pedro Costa, Renan Câmara Pereira and Constança Providência  
Phys. Rev. D 102, 054010 (2020)  
DOI: 10.1103/PhysRevD.102.054010  
arXiv:2009.01781;
8. *Quark matter in light neutron stars*  
Márcio Ferreira, Renan Câmara Pereira and Constança Providência  
Phys. Rev. D 102, 083030 (2020)  
DOI: 10.1103/PhysRevD.102.083030  
arXiv:2008.12563;
9. *Aspects of isentropic trajectories in chiral effective models*  
Rainer Stiele, Wanda Maria Alberico, Andrea Beraudo, Renan Câmara Pereira, Pedro Costa, Hubert Hansen and Mario Motta  
J. Phys. Conf. Ser. 1667 1, 012043 (2020)  
DOI: 10.1088/1742-6596/1667/1/012043  
arXiv:1909.03216;

# *Abstract*

In this work, different aspects of the phase diagram of strongly interacting matter are explored using effective models of Quantum Chromodynamics (QCD) under various approximations. We use the Nambu–Jona-Lasinio (NJL) model, in its two and three flavour versions, including different types of quark interactions. We also consider the two flavour Quark-Meson (QM) model with vector interactions, which can be interpreted as a bosonized version of the NJL model.

Considering the usual mean field approximation, an extended three flavour NJL model, which includes the Polyakov loop, with eight-quark scalar and pseudoscalar interactions is used to study the QCD phase diagram. We also analyse the properties of isentropic trajectories along the different regions of the diagram, including the crossing of the first-order phase transitions. We find that, within this model, it is possible to have two different critical endpoints with the respective first-order lines, related to the light and strange sectors of QCD.

We apply the zero temperature three flavour NJL model, in  $\beta$ -equilibrium to study the stability of neutron stars in accordance with the latest astrophysical constraints from NICER, LIGO/Virgo and the pulsars with approximately two solar masses, PSR J1614-2230 and PSR J0348+0432. The model includes four-quark and eight-quark vector-isoscalar interactions. We find quark matter in the core of moderately low mass neutron stars. The existence of quark matter inside these neutron stars imprints the tidal deformability when compared to the expected results for purely hadronic neutron stars. It follows that, low values of tidal deformability for low/intermediate mass stars, might be a possible observational signature for the existence of quark matter in the core of neutron stars.

In a second part, we perform beyond mean field studies including the so-called one-meson-loop approximation to the NJL model and the Functional Renormalization Group (FRG) method applied to the QM model.

In the case of the one-meson-loop NJL, quantum fluctuations are introduced in a symmetry conserving way, by including collective and non-collective modes in the gap equation of the model which originate from poles and branch cuts in the complex plane, respectively. The inclusion of these modes leads to a non-standard quark condensate as a function of temperature. However, it is possible to distinguish two regions, one with a large quark condensate and the other with a small quark condensate. These regions are separated by the melting temperature of the collective modes, the so-called Mott temperature.

The application of the FRG to the two flavour QM model is known to lead to an unphysical region of negative entropy density, near the first-order phase transition of the model. We explore the connection between this unphysical region and the chiral critical region, especially the first-order and spinodal lines, using different vector interactions. We find scenarios where the phase diagram presents a first-order phase transition, without negative entropy, for a high enough vector interaction.



## *Resumo*

Neste trabalho exploram-se diferentes aspetos do diagrama de fases de matéria que interage fortemente, usando modelos efetivos da Cromodinâmica Quântica (QCD) sob várias aproximações. Para isso, recorre-se a modelos efetivos da QCD, nomeadamente ao modelo de Nambu–Jona-Lasinio (NJL), nas suas variantes de dois e três sabores, incluindo diferentes tipos de interações entre quarks, e também ao modelo Quark-Mesão (QM) com interações vetoriais, na versão de dois sabores, que pode ser interpretado como uma versão bosonizada do modelo de NJL.

Numa primeira fase, considera-se a aproximação de campo médio para uma versão generalizada do modelo NJL, com três sabores, incluindo o *loop* de Polyakov e com interações de oito quarks escalares e pseudoescalares, para estudar o diagrama de fases da QCD. Também são analisadas as propriedades de trajetórias isentrópicas ao longo de diferentes regiões do diagrama de fases, incluindo as linhas que cruzam a região onde existe uma transição de fase de primeira ordem. Conclui-se que, neste modelo, é possível encontrar dois pontos críticos diferentes, assim como as respetivas linhas de transição primeira ordem, associados aos sectores leve e estranho da QCD.

Numa aplicação à descrição de objetos compactos, usamos uma versão de três sabores do modelo NJL no limite de temperatura zero, em equilíbrio- $\beta$  para estudar a estabilidade de estrelas de neutrões que estão de acordo com as restrições astrofísicas impostas pelas observações de NICER, LIGO/Virgo e dos pulsares PSR J1614-2230 e PSR J0348+0432 com cerca de duas massas solares. O modelo também inclui interações vectoriais-isoscalares de quatro e oito quarks. Neste contexto, verificou-se que pode existir matéria de quarks no interior de estrelas de neutrões moderadamente leves. A existência de matéria de quarks no interior dessas estrelas de neutrões afeta a deformabilidade de maré, quando comparado ao resultado esperado de estrelas compostas apenas por matéria hadrónica. Conclui-se que valores baixos de deformabilidade de maré para estrelas com massas baixas/moderadas, pode ser usado como uma possível assinatura observacional da existência de matéria de quarks no núcleo de estrelas de neutrões.

Numa segunda fase, realizaram-se estudos para além da aproximação de campo médio usando a aproximação de um-*loop*-mesónico no modelo de NJL e o Grupo de Renormalização Funcional (FRG) aplicado ao modelo de QM.

No estudo envolvendo o modelo NJL com um-*loop*-mesónico, as flutuações quânticas são introduzidas de modo a não quebrar as simetrias do modelo, incluindo os modos coletivos e não coletivos na equação do gap com origem, respetivamente, nos polos e linhas de corte no plano complexo. A introdução destes modos leva a um comportamento não convencional do condensado de quarks em função da temperatura. Contudo, ainda é possível distinguir duas regiões, uma em que o condensado de quarks tem um valor elevado e outra onde ele é muito suprimido. Estas regiões são separadas pela temperatura em que os modos coletivos “derretem”, a chamada temperatura de Mott.

É sabido que a aplicação do FRG ao modelo QM de dois sabores leva ao aparecimento de uma região não-física de densidade de entropia negativa na vizinhança da linha de transição de primeira ordem do modelo. Ao investigar a ligação dessa região não-física e a região quirál crítica na presença de interações vetoriais diferentes, com ênfase na linha de primeira ordem e respectivas linhas *spinodais*, encontraram-se cenários, para interações vetoriais suficientemente intensas, em que o diagrama de fases apresenta uma transição de primeira ordem sem entropia negativa.

## *Agradecimentos*

Em primeiro lugar, gostaria de agradecer aos meus orientadores, Prof. Dr. Pedro Costa e Prof<sup>a</sup>. Dra. Constança Providência. Para além de serem excelentes cientistas, professores e orientadores, são pessoas excepcionais. Sem a vossa ajuda, apoio e orientação este trabalho não existiria.

Desejo agradecer os meus colegas e colaboradores, Dr. João Moreira, Dr. Márcio Ferreira e Dr. Rainer Stiele. Trabalhar convosco foi extremamente enriquecedor, tanto a nível intelectual como pessoal. Igualmente, gostaria de agradecer o meu colega Marcos Gouveia, pela ajuda disponibilizada com a interface *OpenMP*.

Gostaria de agradecer ao Prof. Dr. Hubert Hansen e ao Prof. Dr. Guy Chanfray, por comentários que disponibilizaram a cerca de alguns tópicos abordados neste trabalho. Quero também mencionar, e agradecer, correspondência por email que tive com Konstantin Otto, a respeito do Grupo de Renormalização Funcional.

Quero deixar o meu agradecimento ao *Institute of Nuclear physics of Lyon* (IPNL) e ao *Istituto Nazionale di Fisica Nucleare* (INFN) - *Sezione di Torino*, pelo financiamento parcial que recebi durante a minha estadia em cada uma dessas instituições, no âmbito de missões científicas de curto prazo (STSM).

Não posso deixar de agradecer à Ação COST CA16214 (“PHAROS: *The multi-messenger physics and astrophysics of neutron stars*”) pelo financiamento parcial de uma STSM no INFN - *Sezione di Torino*, e pela bolsa de conferência (ITC Conference Grants) que me permitiu participar no workshop “*Multi-Messenger Astrophysics in the Gravitational Wave Era*” realizado no *Yukawa Institute for Theoretical Physics* em Quioto, Japão. Igualmente, agradeço financiamento parcial da Ação COST CA15213 (“THOR: *Theory of hot matter and relativistic heavy-ion collisions*”) para uma STSM realizada no IPNL.

Agradeço também ao Laboratório de Computação Avançada da Universidade de Coimbra por terem providenciado tempo de cálculo no *cluster Navigator*.

Este trabalho foi financiado através de fundos nacionais providenciados pela FCT (Fundação para a Ciência e a Tecnologia, I.P, Portugal), sob o programa de doutoramento IDPASC (*International Doctorate Network in Particle Physics, Astrophysics and Cosmology*), através da bolsa de doutoramento PD/BD/128234/2016. Os projetos UID/FIS/04564/2019, UID/04564/-2020 e PTDC/FIS-NUC/29912/2017 com financiamento do POCI (“Programa Operacional Competitividade e Internacionalização” - COMPETE 2020) na sua componente FEDER, também contribuíram financeiramente para este trabalho, apoiando deslocações ao estrangeiro para participação em conferências e missões científicas.

Aos meus pais e irmã, não consigo sequer expressar a minha gratidão e apreço. Estou eternamente grato pela nossa história. Os vários sacrifícios que fizeram por mim, e o vosso amor incondicional, fizeram de mim aquilo que sou hoje.

Aos meus amigos, muitos para serem nomeados, obrigado pelo apoio, encorajamento e partilha.

Por mais estranho que pareça, agradeço também ao gato Blu, que foi o meu assistente em inúmeras noitadas de trabalho.

Por último, quero agradecer à Maria. Acompanhaste-me em mais uma aventura, estando sempre lá quando precisei de ti. Estou pronto para a próxima aventura, ao teu lado. *“It’s dangerous to go alone! Take this.” – The Legend of Zelda.*

# List of Abbreviations

<b>CEP</b>	<b>Critical Endpoint</b>
<b>EoS</b>	<b>Equation of State</b>
<b>FRG</b>	<b>Functional Renormalization Group</b>
<b>GW</b>	<b>Gravitational Wave</b>
<b>HIC</b>	<b>Heavy Ion Collision</b>
<b>IR</b>	<b>Infrared</b>
<b>MF</b>	<b>Mean Field</b>
<b>NJL</b>	<b>Nambu–Jona-Lasinio</b>
<b>NS</b>	<b>Neutron Star</b>
<b>PNJL</b>	<b>Polyakov–Nambu–Jona-Lasinio</b>
<b>QCD</b>	<b>Quantum Chromodynamics</b>
<b>QGP</b>	<b>Quark-Gluon Plasma</b>
<b>QM</b>	<b>Quark-Meson</b>
<b>RHIC</b>	<b>Relativistic Heavy Ion Collision</b>
<b>UV</b>	<b>Ultraviolet</b>



# Contents

<b>Preface</b>	<b>vii</b>
<b>Abstract</b>	<b>ix</b>
<b>Resumo</b>	<b>xi</b>
<b>Agradecimentos</b>	<b>xiii</b>
<b>PART I - The phase diagram of strongly interacting matter</b>	<b>1</b>
<b>1 Introduction</b>	<b>3</b>
1.1 Discussion Layout . . . . .	5
<b>2 Quantum Chromodynamics</b>	<b>7</b>
2.1 Quantum Chromodynamics with light quarks . . . . .	10
<b>3 QCD phase diagram</b>	<b>13</b>
3.1 What is known theoretically . . . . .	16
3.1.1 Theoretical tools . . . . .	16
3.1.2 External magnetic field . . . . .	18
3.1.3 What can affect the transitions? . . . . .	18
3.2 What is known from Heavy Ion Collisions . . . . .	19
3.3 What is known from Astrophysics . . . . .	20
<b>4 Modelling the QCD phase diagram</b>	<b>23</b>
4.1 The Nambu–Jona-Lasinio model . . . . .	27
4.1.1 Coupling to the Polyakov loop . . . . .	30
4.1.2 Regularization Procedure . . . . .	31
4.2 The Functional Renormalization Group . . . . .	32
4.2.1 Applying the FRG to NJL-type models . . . . .	36
<b>PART II - Studies in the mean field approximation</b>	<b>41</b>
<b>5 The strange CEP and isentropic trajectories in the PNJL model</b>	<b>43</b>
5.1 Introduction . . . . .	43
5.2 Model and formalism . . . . .	44
5.2.1 Thermodynamics . . . . .	47

5.2.2	Meson masses . . . . .	50
5.3	Results . . . . .	54
5.3.1	Parameter fitting . . . . .	54
5.3.2	The NJL phase diagram . . . . .	60
5.3.3	The PNJL phase diagram: the strange critical endpoint and isentropic trajectories . . . . .	62
5.4	Conclusions and outlook . . . . .	69
<b>6</b>	<b>Quark matter in light neutron stars</b>	<b>71</b>
6.1	Introduction . . . . .	71
6.2	Model and Formalism . . . . .	74
6.3	Results . . . . .	78
6.4	Conclusions and outlook . . . . .	87
	<b>PART III - Studies beyond the mean field approximation</b>	<b>89</b>
<b>7</b>	<b>One-meson-loop NJL model: collective and non-collective excitations</b>	<b>91</b>
7.1	Introduction . . . . .	91
7.2	Model and Formalism . . . . .	92
7.2.1	The one-meson-loop gap equation at finite temperature . . . . .	98
7.3	Results . . . . .	104
7.3.1	Vacuum . . . . .	104
7.3.2	Finite temperature . . . . .	105
7.4	Conclusions and outlook . . . . .	110
7.4.1	The one-meson-loop Polyakov–Nambu–Jona-Lasinio . . . . .	112
<b>8</b>	<b>FRG study of the critical region of the QM model with vector interactions</b>	<b>115</b>
8.1	Introduction . . . . .	115
8.2	Model and Formalism . . . . .	116
8.2.1	The FRG method . . . . .	119
8.2.2	The flow equations . . . . .	121
The effective potential flow equation . . . . .	121	
Flow equations for the MF vector fields . . . . .	124	
The entropy flow equation . . . . .	127	
The quark density flow equation . . . . .	129	
Solving the flow equations . . . . .	131	
8.3	Results . . . . .	132
8.4	Conclusions and outlook . . . . .	140
	<b>PART IV - Conclusion</b>	<b>145</b>
<b>9</b>	<b>Conclusion</b>	<b>147</b>
	<b>PART V - Appendix</b>	<b>151</b>

<b>A</b>	<b>Units, conventions and the Matsubara summation</b>	<b>153</b>
A.1	Conventions . . . . .	153
A.2	The Heaviside step function and the Dirac delta function . . . . .	154
A.3	Sokhotski–Plemelj formula . . . . .	155
A.4	Dirac matrices . . . . .	155
A.5	Matsubara summation . . . . .	156
A.5.1	Thermodynamic relations . . . . .	157
<b>B</b>	<b><math>SU(N)</math> and <math>U(N)</math> matrices</b>	<b>159</b>
B.1	$SU(N)$ matrices . . . . .	159
B.2	$U(N)$ matrices . . . . .	160
<b>C</b>	<b>Expansion of the product between <math>N</math> operators</b>	<b>163</b>
C.1	Linear expansion of the product between $N$ operators . . . . .	163
C.1.1	The general formula . . . . .	163
C.2	Quadratic expansion of the product between $N$ operators . . . . .	165
C.2.1	The general formula . . . . .	165
<b>D</b>	<b>Grand canonical potential for fermions in the mean field approximation</b>	<b>169</b>
<b>E</b>	<b><math>f_0(S)</math> loop function</b>	<b>173</b>
<b>F</b>	<b><math>f_1(S, q)</math> loop function</b>	<b>175</b>
F.1	The Real and Imaginary parts of $F(S, \mathbf{q}, \omega)$ . . . . .	178
F.2	Change of variables . . . . .	179
F.3	The pair creation/annihilation contribution, $F_p(S, \mathbf{q}, \omega)$ . . . . .	183
F.4	The scattering contribution, $F_s(S, \mathbf{q}, \omega)$ . . . . .	186
F.5	Calculation of $\partial_{S^2} F(S, \mathbf{q}, \omega)$ . . . . .	187
F.5.1	Calculation of $\partial_{S^2} 16\pi^2 q \operatorname{Re} [F_p(S, \mathbf{q}, \omega)]$ . . . . .	188
F.5.2	Calculation of $\partial_{S^2} 16\pi^2 q \operatorname{Im} [F_p(S, \mathbf{q}, \omega)]$ . . . . .	190
F.5.3	Calculation of $\partial_{S^2} 16\pi^2 q \operatorname{Re} [F_s(S, \mathbf{q}, \omega)]$ . . . . .	191
F.5.4	Calculation of $\partial_{S^2} 16\pi^2 q \operatorname{Im} [F_s(S, \mathbf{q}, \omega)]$ . . . . .	192
F.6	Calculation of $\partial_\omega \operatorname{Re} [F(S, \mathbf{q}, \omega)]$ . . . . .	192
F.6.1	Calculation of $\partial_\omega 16\pi^2 q \operatorname{Re} [F_p(S, \mathbf{q}, \omega)]$ . . . . .	192
F.6.2	Calculation of $\partial_\omega 16\pi^2 q \operatorname{Re} [F_s(S, \mathbf{q}, \omega)]$ . . . . .	195
F.7	Noncommutative limits of the $f_1(S, q \rightarrow 0)$ loop function . . . . .	197
<b>G</b>	<b><math>f_2(S, q)</math> loop function</b>	<b>199</b>
<b>H</b>	<b>Non-existence of the <math>\sigma</math>-meson collective excitation at finite temperature</b>	<b>201</b>
H.1	The zero temperature case, $T = 0$ . . . . .	201
H.2	The finite temperature case, $T > 0$ . . . . .	203
<b>I</b>	<b>Integral contributions to the one-meson-loop gap equation</b>	<b>207</b>
I.1	The $I_M(S)$ contribution . . . . .	207

I.2	The $I_{1M}(S)$ contribution . . . . .	210
I.3	The $I_{2M}(S)$ contribution . . . . .	211
<b>J</b>	<b>Useful identities and important results</b>	<b>217</b>
J.1	Useful identities . . . . .	217
J.2	Leibniz integral rule . . . . .	217
J.3	$\eta$ -Sum Identity . . . . .	218
<b>K</b>	<b>FRG applied to the QM model: numerical details</b>	<b>221</b>
<b>L</b>	<b>FRG applied to the QM model: derivatives of the vector field</b>	<b>225</b>
L.1	Derivative of the vector fields with respect to temperature . . . . .	225
L.2	Derivative of the vector fields with respect to chemical potential . . . . .	227
	<b>Bibliography</b>	<b>231</b>

# PART I

The phase diagram of strongly interacting matter



## Chapter 1

# Introduction

In the current state of modern physics, there are four known fundamental forces: the gravitational force, the electromagnetic force and the weak and strong nuclear forces. If we put aside the mysteries imposed by dark matter and dark energy, all physical phenomena in nature, can be described by elementary matter particles, interacting via these fundamental forces. There are a total of twelve flavours of fundamental matter particles, six quarks (up, down, strange, charm, bottom, top) and six leptons (electron, muon, tau, electron neutrino, muon neutrino, tau neutrino). It is from the existence of these particles and their interactions via the fundamental forces that the complexity of the Universe emerges: from atoms and molecules, from planets and galaxies, to life itself.

From this set of four fundamental interactions, gravity, was the first to receive a mathematical model by Isaac Newton, which was later improved by Albert Einstein, with the theory of general relativity, a geometrical theory. The other three interactions, electromagnetism and the weak and strong nuclear forces are described by quantum field theories in what is called the Standard Model of particle physics. Quantum field theory occupies a central role in the description of the laws of nature. It has the ability of describing the creation and annihilation of particles and an incredible predictive power when compared to empirical results, making it an essential tool in modern physics.

The Standard Model of particle physics is built by gauge theories which are described by Lagrangian densities that are invariant under local transformations of specific symmetry groups. These symmetry requirements imply the existence of gauge fields. These fields are identified as gauge bosons and are the mediators of the fundamental forces. Hence, to each fundamental interaction, corresponds a set of gauge bosons. For the electroweak interaction, for example, the gauge bosons are the massless photon and the massive W and Z, while the massless gluons carry the strong nuclear force. Another very important part in the Standard Model is the Higgs particle which, after the inclusion of the Yukawa interaction, gives mass to the fermions and explains the massive nature of the W and Z gauge bosons and the massless nature of the photon through the electroweak symmetry breaking. Only very recently, in 2012, the Higgs boson, the quanta of the Higgs field, was discovered in the Large Hadron Collider (LHC) at CERN<sup>1</sup> by the

---

<sup>1</sup>Organisation Européenne pour la Recherche Nucléaire.

CMS<sup>2</sup> and ATLAS<sup>3</sup> collaborations.

It is possible to unify the electromagnetic interaction and the weak nuclear force under the same field theory, the electroweak interaction. The unification with the strong force would lead to what is called a Grand Unified Theory, a single interaction which, at very high energies, would contain the electroweak and strong interactions. Gravity, on the other hand, currently does not have a quantum field description, making the unification with the other three forces even more challenging. The ultimate unification of the four known forces would lead to the so-called Theory of Everything. Investigation to find both a Grand Unified Theory and a Theory of Everything are currently under development by the theoretical physicists community.

The lack of a quantum theory of gravity is not the only flaw on the Standard Model of particle physics. Currently, the biggest mysteries unanswered by the model are: the nature of dark matter or dark energy, the mass of neutrinos and the matter-antimatter asymmetry in the early Universe.

This work is focused on the strong interacting sector of the Standard Model, described by Quantum Chromodynamics (QCD). This theory was developed in the last half of the twenty century with the proliferation of high energy deep elastic scatterings experiments and features unprecedented properties like scaling, asymptotic freedom and confinement. In this theory, all hadrons are composed of quarks, more fundamental particles which carry colour charge, a new quantum number. The observed hadrons however, are colourless. This implies that some mechanism must exist in QCD that confines coloured particles into colourless bound states. Another ground breaking property of this theory is asymptotic freedom. Calculating the running coupling of QCD leads to a weak coupling regime at high momentum transfers (or small distances) that grows at low momentum transfer (or large distances). As a consequence, QCD has a strong coupling at low energies, making imperative the use of non-perturbative techniques in order to understand its low energy dynamics.

The interplay of all the properties of quantum chromodynamics leads to a very rich phase structure for strongly interacting matter, often referred as the QCD phase diagram [1, 2]. Different phases of a physical system can be displayed in a phase diagram spanned by different external parameters like temperature, density, magnetic field, etc. The Quark-Gluon plasma (QGP), which existed milliseconds after the Big Bang [3], matter inside neutron stars (NS), which prevents the gravitational collapse of the dying star into a black hole, and the confined quarks inside hadrons, that constitute the nucleons, are some examples of different phases of the same underlying structure, strongly interacting matter. The study of the QCD phase diagram, the different transitions and the search for the conjectured QCD critical endpoint (CEP), have led to remarkable theoretical and experimental developments in recent years [1, 4].

The goal of the present thesis is to explore different aspects of the phase diagram of QCD using effective models under different approximations. Understanding matter under such extreme conditions is one of the most challenging and interesting topics in modern physics due to its

---

<sup>2</sup>Compact Muon Solenoid experiment.

<sup>3</sup>A Toroidal LHC ApparatuS experiment.

relevance for studies involving compact objects like neutron stars, magnetars [5, 6], measurements in heavy ion collisions (HIC) at very high energies [7, 8] or the first phases of the Universe [9, 10].

## 1.1 Discussion Layout

The present thesis is organized in five different parts each containing several chapters:

- Part I - The phase diagram of strongly interacting matter;
- Part II - Studies in the mean field approximation;
- Part III - Studies beyond the mean field approximation;
- Part IV - Conclusion;
- Part V - Appendix.

After analysing Part I, the reader can choose to read any other chapter in Parts II and III in any particular order. The chapters that constitute these parts are self-contained, except for auxiliary calculations presented in Part V, the Appendix.

The current chapter is contained in Part I, where all the necessary theoretical tools in order to understand the remaining work are discussed. This includes an introduction to the theory of strong interactions and the phase diagram of strongly interacting matter; an introduction to modelling low energy QCD using effective models in the so-called mean field (MF) approximation and tools to go beyond such approximation like the background field expansion and the Functional Renormalization Group technique (FRG). We also discuss the Nambu–Jona-Lasinio (NJL) quark model and the very closely related Quark-Meson (QM) model as effective models of QCD.

In Part II we discuss two different mean field studies. In the first study, presented in Chapter 5, we use an extended Polyakov–Nambu–Jona-Lasinio (PNJL) model in the MF approximation to study the possible existence of several critical endpoints in the phase diagram of strongly interacting matter. Besides, we also study the isentropic trajectories crossing both (light and strange) chiral phase transitions and around the CEP in both the crossover and first-order transition regions. The second study of Part II, presented in Chapter 6, is related to neutron stars. We use an extended Nambu–Jona-Lasinio model, with higher-order repulsive interactions, in the mean field approximation, in order to describe the quark phase of a hybrid neutron star. The effect of such higher-order repulsive interaction is studied and the stability of hybrid star configurations is explored. The properties of the resulting hybrid neutron stars are analysed against the latest constraints coming from astrophysical observations.

In Part III, we turn our attention to studies beyond the usual MF approximation and perform two different studies. In the first, presented in Chapter 7, we explore the effect of including quantum fluctuations in the two flavour Nambu–Jona-Lasinio model at finite temperature. This is accomplished, in a symmetry preserving way, by including collective and non-collective modes in the one-meson-loop gap equation which originate from poles and branch cuts in the complex plane, respectively. In such methodology a new parameter has to be introduced, the boson

cutoff. This new parameter is used to study the influence of going beyond the usual mean field approximation in the quark condensate at finite temperature. In Chapter 8, we examine the critical region of the two flavour Quark-Meson model with vector interactions using the Functional Renormalization Group, a non-perturbative method that takes into account quantum and thermal fluctuations. Special attention is given to the low temperature and high density region of the phase diagram, which is very important to construct the equation of state (EoS) for compact stars. This model under this approximation is known to predict an unphysical region of negative entropy density near the first-order chiral phase transition. We study the connection between this unphysical region and the chiral critical region, especially the first-order line and spinodal lines, using different vector interactions.

Finally, in Part IV, some general conclusions are drawn.

In the Appendix A, we define the units and conventions we are using in this work.

## Chapter 2

# Quantum Chromodynamics

Quantum Chromodynamics is currently viewed as the theory that describes the strong interaction. Historically, it was originally proposed by Harald Fritzsch, Heinrich Leutwyler and Murray Gell-Mann in 1972 with colour being promoted to a local gauge symmetry, in a similar spirit to the electromagnetic and weak interactions [11]. This additional quantum number is essential for the quark model to correctly reproduce the quantum numbers of hadrons, in particular the spin statistics<sup>1</sup>. However, QCD only started to be accepted amongst the community, when David Gross, Frank Wilczek and, independently, David Politzer [14, 15], demonstrated that such theory was compatible with the contemporary experimental observations, in particular, with the results coming from SLAC<sup>2</sup> [11]. However, the history is not that linear: in 1973, Gross and Wilczek were actually trying to prove that quantum field theory was not the correct framework to describe the strong interaction. They would do this by following a “plan”, as entitled by David Gross [16], that was rooted on two concepts: scaling and asymptotic freedom. Scaling<sup>3</sup> is a phenomenon first discovered by James Bjorken in 1968 which in essence states that hadrons, when probed at very high energies (as in the case of deep inelastic scattering experiments), behave as ensembles of point-like components. The first point of the “plan” was to show that scaling was needed to explain the results found in the SLAC experiments and that a quantum field theory only displays scaling if its running coupling constant vanishes at high momentum transfers, a property that was coined as asymptotic freedom<sup>4</sup>. Finally, they would show that there were no asymptotically free field theories. In this process however, they ended up discovering that the non-Abelian theory of Yang and Mills was asymptotically free, allowing for the construction of a Lagrangian that respected the symmetries of the strong interaction and at the same time, was able to explain the experiments performed at SLAC [17–19]. Experimentally, a single quark was never observed

---

<sup>1</sup>The introduction of the colour charge is essential to describe the  $\Delta^{++}$  baryon by a total antisymmetric wave function with the quark model, while respecting the Pauli exclusion principle [12]. This is also true for other baryon states. Another experimental evidence for the existence of colour comes from the cross section of electron-positron annihilation into hadrons [13].

<sup>2</sup>Stanford Linear Accelerator Center.

<sup>3</sup>Generally, in a scattering experiment, the spatial resolution can be improved by increasing the absolute energy of the collisions. However, certain properties are said to scale if they do not depend on the absolute energy but only on dimensionless quantities (scattering angles, ratios of energies...). Hence, scaling occurs for point-like structures once increasing energy does not entail improved resolution.

<sup>4</sup>Actually, Gerard 't Hooft showed one year early, in an unpublished work, that non-Abelian field theory was asymptotically free for certain numbers of fermions and scalar fields [11, 13].

in nature which is interpreted as the colour confinement hypothesis: only colour singlet states can exist in nature as free particles.

QCD is based on the gauge group  $SU(3)_c$ , the special unitary group in three dimensions, whose elements are the set of unitary  $3 \times 3$  matrices with determinant one [12]. The QCD Lagrangian is:

$$\mathcal{L} = \bar{\psi}_i [i\gamma^\mu (D_\mu)_{ij} - m_{ij}] \psi_j - \frac{1}{4} \mathcal{F}_{\mu\nu}^a \mathcal{F}^{a\mu\nu}, \quad (2.1)$$

where  $\psi_i$  is a quark field with colour index  $i = \{1, 2, 3\}$ , indicating that they are in the fundamental representation of  $SU(3)_c$ , and  $N_f$ -components in flavour space, with  $N_f$  the number of quark flavours.  $\mathcal{F}_{\mu\nu}^a$  is the gluon field strength tensor for a gluon with colour index  $a$ , and it is given by:

$$\mathcal{F}_{\mu\nu}^a = \partial_\mu \mathcal{A}_\nu^a - \partial_\nu \mathcal{A}_\mu^a + g_s f_{abc} \mathcal{A}_\mu^b \mathcal{A}_\nu^c, \quad (2.2)$$

with  $\mathcal{A}_\mu^a$  the gluon field with colour index  $a = \{1, 2, \dots, 8\}$ ,  $g_s$  the strong coupling and  $f_{abc}$  the totally antisymmetric structure constants of  $SU(3)_c$  (see Appendix B). The quark field is coupled to the gluon field through the covariant derivative,  $D_\mu$ , which is explicit given by:

$$(D_\mu)_{ij} = \delta_{ij} \partial_\mu - \frac{ig_s}{2} (\lambda_a)_{ij} \mathcal{A}_\mu^a. \quad (2.3)$$

Here,  $\lambda_a$  are the eight hermitian and traceless Gell-Mann matrices of  $SU(3)_c$  (see Appendix B). Finally,  $m_{ij}$  is a colour-independent phenomenological mass matrix in flavour space, that can be written in diagonal form through flavour-mixing transformations, so that:

$$\bar{\psi}_i m_{ij} \psi_j = \bar{\psi} \hat{m}_f \psi. \quad (2.4)$$

The matrix  $\hat{m}_f$  is diagonal and can be estimated through current algebra relations, after all, they are not asymptotic observables of QCD because of the confinement properties of the theory. These are called the current quark masses, generated by the Higgs mechanism, see Table 2.1. From the order of magnitude of the masses of the different quark flavours, one can clearly distinguish the so-called light sector of QCD, constructed from the three lightest flavours of quarks. In the present thesis, we will focus on this sector due to its importance to the dynamics of chiral symmetry breaking and deconfinement.

QCD is invariant under local transformations of the  $SU(3)_c$  symmetry group by construction: it is this exact symmetry that defines the theory. Another very important symmetry of QCD (and the whole Standard Model) is its invariance under CPT transformations i.e., charge conjugation (C), parity (P) and time reversal transformations (T). However, considering only gauge invariance, the QCD Lagrangian could also incorporate the so-called  $\theta$ -term, which implies an explicit CP violation. Contemporary experimental information indicates that this term, if it is non-zero, is very small [22]. The fact that this term is extremely small when it does not have any theoretical reason for being so, is termed in the literature as the strong CP problem.

The remaining symmetries of QCD are easily identified if the quark field is decomposed in its

Quark name	Symbol	Mass [20]
up	$u$	$2.3_{-0.5}^{+0.7}$ MeV
down	$d$	$4.8_{-0.3}^{+0.5}$ MeV
strange	$s$	$95 \pm 5$ MeV
charm	$c$	$1.275 \pm 0.025$ GeV
bottom	$b$	$4.18 \pm 0.03$ GeV
top	$t$	$173.21 \pm 0.51$ GeV

TABLE 2.1: The  $u$ ,  $d$  and  $s$  quark masses are estimates from a mass-independent subtraction scheme such as  $\overline{\text{MS}}$  at a scale  $\mu \approx 2$  GeV. The  $c$  and  $b$  quark masses are the “running” masses in the  $\overline{\text{MS}}$  scheme. The  $t$  mass is taken from direct measurements (direct reconstruction of the decays of the top quark into final states using Monte Carlo simulations for example [21]).

right and left components,  $\psi_{R/L}$ . This can be performed using the right and left projection operators<sup>5</sup>,  $P_{R/L} = (1 \pm \gamma_5)/2$ , which act in the quark field as:

$$\psi_R = P_R \psi = \frac{1 + \gamma_5}{2} \psi, \quad (2.5)$$

$$\psi_L = P_L \psi = \frac{1 - \gamma_5}{2} \psi. \quad (2.6)$$

QCD, for the massless quarks, is invariant under independent global rotations of the left-handed and the right-handed components of the quark field,  $\psi_{R/L}$ . This symmetry of QCD is called chiral symmetry and it means that the Lagrangian is invariant under a global transformation  $U$ , that belongs to the group following symmetry group:

$$U(N_f)_R \times U(N_f)_L = SU(N_f)_V \times SU(N_f)_A \times U(1)_V \times U(1)_A. \quad (2.7)$$

We summarize the continuous symmetries of QCD and respective conserved quantities in Table 2.2. The symmetry transformation defined above is not exact for massive quarks because the quark mass term in Eq. (2.4), mixes right- and left-handed fields, explicitly breaking the chiral symmetry of the theory:

$$\bar{\psi} \hat{m}_f \psi = \bar{\psi}_R \hat{m}_f \psi_L + \bar{\psi}_L \hat{m}_f \psi_R. \quad (2.8)$$

The existence of different quark masses will give rise to the physical pseudoscalar meson spectra i.e., will give mass to the Goldstone bosons (the meson octet for  $N_f = 3$  [23]).

In the chiral limit, when the quarks current mass goes to zero, QCD has only one parameter, the coupling  $g_s$  defined at a certain energy scale. This means that all the complexity arising from confinement, chiral symmetry breaking, hadron masses, decay rates, the QCD phase diagram and properties of nuclei and their interactions, are microscopically defined by a known theory with only one free parameter. However, it does not matter how incredible this fact is, if one is

<sup>5</sup>These operators have the following properties:  $P_R + P_L = \mathbb{1}$ ,  $P_{R/L} P_{L/R} = 0$  and  $(P_{R/L})^n = P_{R/L}$  for  $n \geq 1$ .

Symmetry	Transformation	Current
$SU(N_f)_V$	$\psi \rightarrow e^{-i\tau_a \Theta_a/2} \psi$	$j_a^\mu = \bar{\psi} \gamma^\mu \frac{\tau_a}{2} \psi$
$SU(N_f)_A$	$\psi \rightarrow e^{-i\tau_a \Theta_a \gamma_5/2} \psi$	$j_a^\mu = \bar{\psi} \gamma^\mu \gamma_5 \frac{\tau_a}{2} \psi$
$U(1)_V$	$\psi \rightarrow e^{-i\alpha} \psi$	$j^\mu = \bar{\psi} \gamma^\mu \psi$
$U(1)_A$	$\psi \rightarrow e^{-i\alpha \gamma_5} \psi$	$j^\mu = \bar{\psi} \gamma^\mu \gamma_5 \psi$
$SU(3)_c$	$\psi \rightarrow e^{-i\lambda_a \Theta_a/2} \psi$	$j_a^\mu = \bar{\psi} \gamma^\mu \frac{\lambda_a}{2} \psi$

TABLE 2.2: QCD continuous symmetries and respective conserved currents. Here,  $\tau_a$  are  $N_f^2 - 1$  operators that form the  $SU(N_f)$  algebra and  $\lambda_a$  are the Gell-Mann matrices of  $SU(3)_c$  (see Appendix B).

not able to solve the theory. Indeed, due to the magnitude of the coupling at typical conditions, QCD is non-perturbative, rendering the perturbative Feynman diagram technique inappropriate. For theories with a small coupling, one sums up the most relevant Feynman diagrams until the desired accuracy is reached. When perturbation theory fails, the procedure is not trivial: one may use lattice QCD simulations in a supercomputer or a plethora of non-perturbative techniques, each having their own advantages and disadvantages. Even results like the colour confinement hypothesis, decades after the discovery of QCD are still mysterious. “From large-scale computer simulations, we know that the result is true, but we do not really have a human understanding of why” – Edward Witten [24].

Finding a way to solve QCD or at least gather a greater understanding of all its fundamental phenomena which, fundamentally, are the reason of the existence of our world as it stands today, is still one of the most difficult, important and challenging tasks in theoretical particle and nuclear physics.

## 2.1 Quantum Chromodynamics with light quarks

Hadron physics runs over the MeV – GeV energy range so, it should be well described by the dynamics of the lightest quarks: the up, down and strange quarks ( $u$ ,  $d$  and  $s$ ). Considering these three flavours of quarks, the quark field can be written as:

$$\psi^T = (\psi_u \quad \psi_d \quad \psi_s), \quad (2.9)$$

and the diagonal mass matrix as  $\hat{m} = \text{diag}(m_u, m_d, m_s)$ . For massless ( $u$ ,  $d$  and  $s$ ) quarks, the Lagrangian density (2.1) is invariant under the transformation

$$\psi \rightarrow \psi' = U\psi, \quad (2.10)$$

where  $U$  is a global transformation that belongs to the group:

$$U(3)_L \times U(3)_R = SU(3)_V \times SU(3)_A \times U(1)_V \times U(1)_A. \quad (2.11)$$

The transformations under  $U(1)_V$  and  $SU(3)_V$  are related to baryon number conservation and isospin/strangeness conservation, respectively. While the first is always conserved in nature, the second is only approximately conserved due to different quark masses (Eightfold Way). This symmetry is almost respected in the two flavour case ( $m_u \approx m_d$ ) but it is more severely broken in the three flavour case due to the value of  $m_s$ .

The invariance under transformations  $SU(3)_A$  and  $U(1)_A$  constitute the chiral (or axial) symmetries. These transformations change the parity of a given physical state and can be realized physically in a Wigner–Weyl<sup>6</sup> way or in the Nambu–Goldstone<sup>7</sup> mode. If the  $SU(3)_A$  symmetry occur in nature in the Wigner–Weyl way, it would imply that each flavour multiplet would have a degenerate copy, with opposite parity. In the case of the  $U(1)_A$  symmetry also realizing in the Wigner–Weyl way, there would exist a degenerate parity partner for each hadron. However, such states are not observed in nature, which means that  $SU(3)_A$  and  $U(1)_A$  should not be directly realized by QCD. The  $SU(3)_A$  symmetry is realized in the previously mentioned Nambu–Goldstone mode, via chiral symmetry breaking, giving origin to the meson octet:  $\pi^0$ ,  $\pi^+$ ,  $\pi^-$ ,  $K^+$ ,  $K^-$ ,  $K^0$ ,  $\bar{K}^0$  and  $\eta$ . Likewise, the breaking of  $U(1)_A$  symmetry should generate another Goldstone boson, a pseudoscalar meson with zero isospin and a mass of the same order as the pion mass [25], being the  $\eta'$  the main candidate. Nevertheless, the experimental value for the mass of the  $\eta'$  is not in accordance with the expectation due to its higher mass, and no boson with such properties is observed experimentally. So, this symmetry must not exist at the quantum level, being broken by the axial anomaly [25]. This problem was solved by Gerard 't Hooft [26, 27], who showed that, at a classical level, the  $U(1)_A$  symmetry should not result in physical manifestations due to instanton induced effects. The violation of this symmetry is essential to lift the mass of the  $\eta'$  meson to about 1 GeV and is also responsible for flavour mixing, which contributes to spoil the supposed degeneracy between the  $\pi^0$  and the  $\eta$  mesons [28].

Another very important result related to chiral symmetry breaking is the partially conserved axial-vector current (PCAC). Considering the  $SU(2)_f$  case, the matrix element of the divergence of the axial vector current<sup>8</sup>,  $A_a^\mu = \bar{\psi}\gamma^\mu\gamma_5\frac{\tau_a}{2}\psi$ , between the vacuum and a pion state with momentum  $q$ ,  $|0\rangle$  and  $|\pi^b(q)\rangle$ , respectively, can be written as (for a derivation see Ref. [29]):

$$\langle 0|\partial_\mu A_a^\mu|\pi^b(q)\rangle = -f_\pi m_\pi^2 \delta_a^b e^{-iq\cdot x}. \quad (2.12)$$

In this expression,  $f_\pi$  is the leptonic decay of the pion (whose experimental value is  $f_\pi = (92.07 \pm 0.85)$  MeV [30]) and  $m_\pi$  is the pion mass. As previously mentioned, chiral symmetry is realized in the Nambu–Goldstone mode and the pion corresponds to the massless Goldstone mode. Since  $f_\pi$  is non-zero, a massless pion mode would imply that this current is perfectly conserved however, as previously discussed, the pion has a finite mass, and this current is only partially conserved.

<sup>6</sup>Wigner–Weyl realization of a symmetry: invariance of the Lagrangian density under a symmetry group should lead to a degeneracy of the energy eigenstates [23].

<sup>7</sup>Nambu–Goldstone realization of a symmetry: non invariance of the vacuum under the symmetry operation. In this case the Goldstone theorem implies the existence of massless spinless particles [23].

<sup>8</sup>The axial-vector current is related with the conservation of the  $SU(N_f)_A$  symmetry, see Table 2.2.

Two (approximate) low-energy theorems can be derived from current algebra results. One of those, is the Gell-Mann–Oakes–Renner (GMOR) relation [31], which (approximately) relates pionic quantities with quark properties and can be written as:

$$f_\pi^2 m_\pi^2 = -m_q \langle \bar{\psi}\psi \rangle, \quad (2.13)$$

where  $m_q$  is the light quark masses and  $\langle \bar{\psi}\psi \rangle$  is the light quark condensate. The other (approximate) low-energy theorem is the Goldberger-Treiman relation, which can be expressed by [29]:

$$g_{\pi NN} f_\pi = g_A m_N. \quad (2.14)$$

In the above,  $g_{\pi NN}$  is the pion–nucleon coupling,  $g_A$  is the nucleon axial charge, which determines the neutron decay rate and  $m_N$  is the nucleon mass. In later chapters we will apply this relation to a theory of quarks interacting with mesons, the Quark-Meson model. In such case, we can set  $g_A = 1$  and  $g_{\pi NN} = h$ , to get [32, 33]:

$$h f_\pi = m_q. \quad (2.15)$$

Here,  $h$  is the Yukawa coupling between the quark and the meson fields in the Quark-Meson model.

## Chapter 3

# QCD phase diagram

The QCD phase diagram is a very challenging and interesting topic in modern physics and was first conjectured in the seventies by N. Cabibbo and G. Parisi [34], see Fig. 3.1.

At high enough energies QCD is asymptotically free meaning that quarks and gluons interact very weakly, behaving almost like free particles. This weakly interacting phase of matter is called the Quark-Gluon plasma. At low energies however, quarks and gluons are confined inside hadrons. The existence of these two phases of QCD matter, at different energies, suggests that there must be a transition between the low energy and the high energy regimes of QCD, the so-called deconfinement transition. The very first version of the QCD phase diagram only displayed these two phases, the confined and deconfined phases. Since then, several other phases have been theoretically proposed, but they still lack experimental evidence to support their existence, in spite all the tremendous effort that has been done, see [35, 36].

Chiral symmetry breaking explains the observed spectra of hadrons and the constituent quark mass. Since the mechanism of chiral symmetry breaking must be rooted in the strong interaction between quarks and gluons, chiral symmetry is expected to get restored as energy increases. If the interaction is very weak, chiral symmetry should be partially or totally restored. Thus, another transition is expected to also occur, a chiral transition, between the low energy region of QCD where chiral symmetry is broken and another, at high energies, where chiral symmetry is restored.

One can attribute order parameters<sup>1</sup> to these transitions, which will correspond to changes of the system's overall symmetries. A phase transition can be classified as follows [37, 38]:

- First-order phase transition: in the so-called Ehrenfest classification, this type of transition is characterized by a discontinuity of the first derivative of the free energy with respect to some thermodynamic variable. From the modern perspective, in this type of phase transition, the system absorbs or releases energy in the form of latent heat, displaying a mixed-phase, where portions of the system have completed the transition while others have not;

---

<sup>1</sup>An order parameter is a quantity which is able to distinguish two different phases of a particular system by its behaviour along the transition. Some examples are the magnetization in a ferromagnetic system, or, the density in a liquid/gas transition.

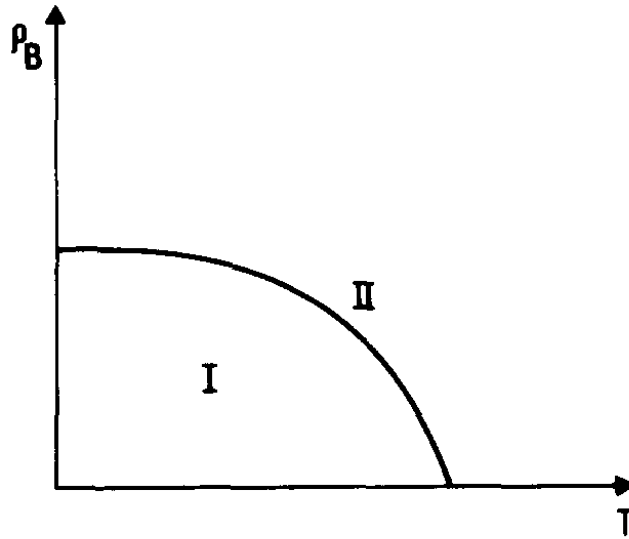


FIGURE 3.1: Schematic phase diagram of hadronic matter. Quarks are confined in phase I and deconfined in phase II (phase diagram from [34]).

- Second-order phase transition: in the Ehrenfest classification, this type of transition is characterized by a discontinuity on the second derivative of the free energy with respect to some thermodynamic variable, while the first derivative remains continuous. In these transitions, correlation length diverges and the entire system is in the same critical phase. In such scenario, physical quantities have power law behaviours near the transition point, which can be described by critical exponents.
- Crossover: in this type of transition the system changes its properties, continuously. Such change is not associated with any discontinuity in the free energy, or its derivatives. Hence, the transition happens over a region instead of a specific point and it becomes necessary to specify how the transition point is defined.

The Polyakov loop acts as an exact order parameter for the confined and deconfined phases of matter in pure Yang–Mills theory [39]. In the imaginary time formalism, bosons and fermions have to respect periodic and antiperiodic boundary conditions. Pure Yang–Mills theory have boundary conditions that are symmetric under the discrete group  $Z(3)$ , the center group of  $SU(3)_c$ . Fermions on the other hand do not have boundary conditions that respect this symmetry, implying that fermions explicitly break the discrete  $Z(3)$  symmetry of the boundary conditions. One can define the Polyakov loop as [39, 40]:

$$\Phi = \frac{1}{N_c} \text{tr}_c \mathcal{P} \exp \left[ i \int_0^\beta d\tau A_4(\tau, \mathbf{x}) \right]. \quad (3.1)$$

Here,  $\mathcal{P}$  is the path ordering operator and  $A_4 = ig_s \mathcal{A}_\mu^a \frac{\lambda_a}{2} \delta_0^\mu$ . This quantity transforms like the quarks under a  $Z(3)$  symmetry: if the Polyakov loop is zero, the  $Z(3)$  symmetry is preserved while, if it is non-zero, the  $Z(3)$  symmetry is broken. If one calculates the free energy of a system of quarks in a static gluonic background field, one can see that, if the vacuum expectation of the

Polyakov loop is zero, the free energy of the quark is infinite while, if it is bigger than zero, the free energy is finite [39, 41]. Thus, the Polyakov loop can be viewed as an order parameter for the confined and deconfined phases of matter:

$$\begin{aligned}\langle\Phi\rangle\sim 0 &\rightarrow \text{confined phase;} \\ \langle\Phi\rangle > 0 &\rightarrow \text{deconfined phase.}\end{aligned}$$

The chiral condensate acts as an order parameter for chiral symmetry. Finite current quark masses explicitly break chiral symmetry, giving a very small mass to the supposed massless Goldstone bosons (the meson octet for  $SU(3)_f$  [23]). The chiral condensate transforms like a mass term under axial symmetries and is related to the pion mass through the GMOR relation, see Eq. (2.13) and Chapter 2.1.

If the quark condensate is non-zero, chiral symmetry is broken while, if it is (approximately) zero, chiral symmetry is (partially) restored:

$$\begin{aligned}|\langle\bar{\psi}\psi\rangle| > 0 &\rightarrow \text{chiral symmetry is broken;} \\ |\langle\bar{\psi}\psi\rangle| \sim 0 &\rightarrow \text{chiral symmetry is restored.}\end{aligned}$$

Both of these transitions are displayed in the QCD phase diagram in Fig. 3.2. In the early Universe, about 1 millisecond after the Big Bang, where the difference between matter and anti-matter was really small, such phase transitions must have occurred. Is there some connection between these transitions? Does one transition imply the other? Do they coincide at some finite value of chemical potential? What is their nature? Is there a first-order phase transition which changes to a crossover? If so, where is the critical endpoint (CEP) located? What are good experimental signatures for the first-order phase transition or the CEP? These are some of the open questions in the field.

It is also expected that, at large baryonic densities, colour superconducting phases can occur [42]. In such region of the diagram, weak coupling techniques can be applied to QCD, and several methods used in condensed matter physics can be utilized [43]. In analogy with electrons forming Cooper pairs in metals at low temperatures, due to an attractive interaction between electron pairs<sup>2</sup>, quarks can also form colour superconducting pairs in quark matter. Since quarks have the additional colour degree of freedom, the pairing mechanism can give rise to different superconducting phases. One particular example of a colour superconducting phase is the so-called colour flavour locking phase (CFL), where all three colours and all three flavours form Cooper pairs (ignoring the three heaviest quarks flavours) [43–46]. Variations of this phase are also possible, where one specific quark flavour does not form a cooper pair with the remaining phases. For example, the uSC and dSC phases in which there is no pairing between the strange quark and the down and up quarks, respectively. The intricate behaviour of all these phases

<sup>2</sup>The attractive interaction between electron pairs in metals originates from the displacement of ions in the lattice.

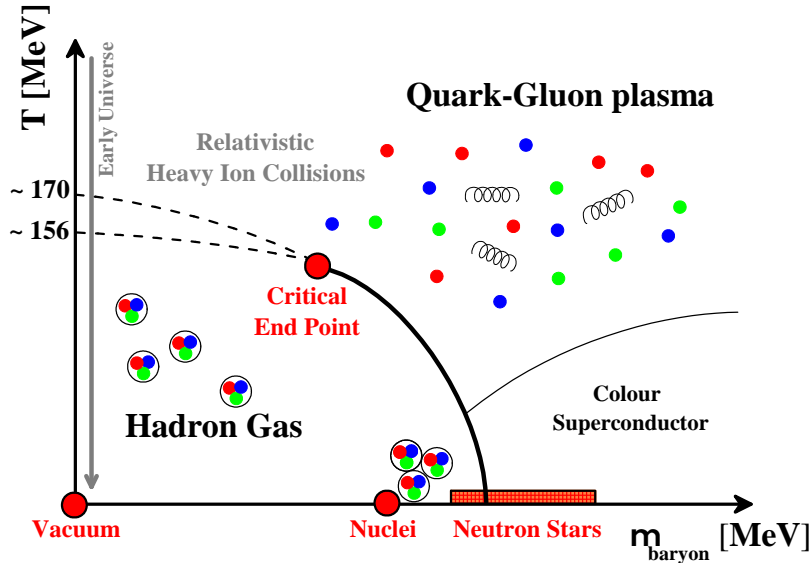


FIGURE 3.2: A conjectured QCD phase diagram. At zero baryon chemical potential lattice QCD predicts a smooth crossover transition around 156-170 MeV. Neutron star matter is described in the region of low temperature and large baryon chemical potentials while, superconducting phases are expected at even higher chemical potentials. At high temperatures, the QGP phase dominates the phase diagram. It has been conjectured that the crossover transition at zero chemical potential, predicted by lattice QCD calculations, transforms into a first-order phase transition, implying the existence of a CEP.

culminates in an extremely rich phase diagram. For more details about superconducting phases see [43].

### 3.1 What is known theoretically

To theoretically study the QCD phase diagram, the options are limited, due to the non-perturbative nature of the theory at low energies. Some options are lattice gauge theory applied to QCD (lattice QCD), Dyson–Schwinger equations and effective field models.

#### 3.1.1 Theoretical tools

Lattice QCD is a discrete realization of QCD with the advantage of being derived from first principles. In this method, the goal is to compute the functional integral numerically, using the Monte Carlo method. The integrand includes the exponential of the Euclidean action,  $\exp(-\mathcal{S}_E)$ , where the Euclidean action  $\mathcal{S}_E$ , is positive definite. Supposedly, to perform the integration, one has to take into account the infinite field configurations that can contribute to the generating functional. However, due to the negative phase in the exponential, there is a suppression of several field configurations and just a small number of field configurations will contribute to the calculation. The method used to make this distinction among the configurations is known as importance sampling [47].

Another caveat of this method is the large amount of computation power needed and the use of two distinct extrapolations, one which takes from the discrete grid to the continuum, and the

thermodynamic limit, both of which carry systematic uncertainties.

At finite density, when including a finite baryonic chemical potential  $\mu_B$ , the Euclidean action becomes complex. A complex exponential corresponds to an oscillatory function, rendering the importance sampling needed in Monte Carlo simulations ineffective: this is known as the “infamous” sign problem [48]. In these conditions, how are the important configurations chosen to calculate the integral? Currently, there have been several attempts to solve or circumvent this problem like: reweighting, Taylor expansions, complex Langevin dynamics [48, 49] and considering an imaginary chemical potential and then making an analytical continuation to the real quantity [47]. However, these methods are still under development and their convergence to the correct result is not assured, mainly in the high density and low temperature region of the phase diagram.

Despite the technical difficulties that arise when using a first principles method, the only solid theoretical evidence regarding the phase diagram, comes from lattice QCD results at zero baryonic chemical potential. It has been shown the existence of an analytic crossover, from a low-temperature region characterized by chiral symmetry breaking, to a high-temperature (partially) chirally restored region. From lattice QCD, the pseudocritical temperature for the chiral crossover is found to be  $T_c = (156.5 \pm 1.5)$  MeV [50–53]. It has also been found by these types of calculations a different pseudocritical temperature related to the Polyakov loop and the strange quark number susceptibility<sup>3</sup> of  $T_c = (170^{+4}_-3)$  MeV and  $T_c = (169 \pm 3)$  MeV, respectively [50]. These critical temperatures can be associated with the breaking of the  $Z(3)$  symmetry and the deconfinement transition [55].

Dyson–Schwinger equations is a method based on the QCD effective action [29, 56]. This method generates an infinite tower of integro-differential equations for the Green’s functions of the theory that need to be truncated at some order. The main difficulty lies in the fact that the  $n$ -order equation will depend on the equation of order  $n + 1$  and even on the  $n + 2$  order. Hence, dealing with the hierarchy of equations (diagrams) to make a proper truncation is not a simple task and several techniques have been invented and applied throughout the years [57]. Recently some studies using this method have been applied to study the region of small chemical potentials of the phase diagram and search for the conjectured CEP [57–60].

Effective models are widely used method to study a complicated theory. A model for QCD must be built, a la Landau, in such a way to incorporate the most important features of QCD, at a certain energy scale. The main advantage of this method is that it works in the entire phase diagram and it can be rooted in experimental data or lattice QCD calculations. The big caveat of using effective models lies in the existence of free parameters in the theory that need fixing to some experimental data, lattice calculation or sometimes be left free [61]. Since effective models are not fundamental theories, one should take caution and not use them outside their range of applicability.

---

<sup>3</sup>The strange quark number susceptibility can be used as an order parameter for the deconfinement transition. Not only its behaviour with increasing temperature (at zero chemical potential) is empirically similar to that of the Polyakov loop [54, 55], one can also show that, due to the large strange quark mass, it is proportional to the Polyakov loop [55].

Interestingly, some model calculations, namely in an extended version of the NJL model with multi-quark interactions and explicit chiral symmetry breaking interactions<sup>4</sup> [62, 63], show that it is possible for the strange sector to also have a first-order phase transition, meaning that a second CEP for this sector can also exist in the phase diagram [64]. In Chapter 5 of the present work we also find a strange CEP, but for an NJL model without these extra explicit chiral symmetry breaking interactions.

### 3.1.2 External magnetic field

The effect of an external magnetic field has been studied both by lattice QCD and effective models. At finite magnetic field, lattice QCD does not present the sign problem [65]. Considering the phase diagram spanned by temperature and magnetic field, lattice QCD predicts a change of nature for the chiral transition as the magnetic field is increased. Hence, the crossover turns into a first-order phase transition, implying the existence of a CEP for finite temperature and magnetic field [50, 66]. In the literature most of the models predict magnetic catalysis: the external magnetic field has a strong tendency to enhance (“catalyse”) the quark condensates. This has consequences on the chiral symmetry breaking mechanism: the quark condensate assumes higher values as the magnetic field increases and the transition into a chiral symmetric phase takes place at larger temperatures. However, this behaviour is contrary to lattice QCD results that foresee a decreasing temperature for the phase transition for an increasing magnetic field, the so-called inverse magnetic catalysis [67–69]. Some effective models are able to reproduce this feature and observe that increasing the magnetic field drives the CEP at finite temperature and density to lower densities and temperatures until the zero density axis [70, 71]. Besides affecting the location of the CEP [72], the influence of external magnetic fields can lead to the appearance of several CEPs, including in the strange sector in some effective models [73].

### 3.1.3 What can affect the transitions?

The phase diagram and respective transitions, can be affected by several physical factors: the presence of an external magnetic field, isospin and strangeness content of the medium. Consequently, it is very important to develop various theoretical tools that are able to make predictions within these different scenarios.

When using effective models for example, unconstrained degrees of freedom, like the strength of vector interactions, can drastically alter the predictions of the model [74–76]. When calculating the phase diagram, the inclusion of quantum fluctuations, change the thermodynamics of effective models at finite temperature and density. When correctly accounted for, quantum fluctuations smooths the phase transition and changes the location of the CEP [77, 78]. Not only this position is model dependent but it can depend on the method one uses to solve the given model [79–81]. Hence, quantum fluctuations play a major role in the phase diagram and they must be included if one wishes to make better qualitative predictions. Consequently, the location of the CEP predicted by effective models is extremely sensitive [82]. Indeed, if one identifies every possible

<sup>4</sup>The authors considered only explicit chiral symmetry breaking interactions that were relevant in an  $1/N_c$  expansion.

effective model prediction for the chiral CEP in a diagram, or the space parameter of a model [83], a great region of the phase diagram would be filled. Thus, experimental knowledge of the location of the possible CEP would highly constrain QCD effective models and their physical predictions.

## 3.2 What is known from Heavy Ion Collisions

From the experimental point of view, the study of the QCD phase diagram is one of the major goals of heavy ion collision (HIC) experiments. Current experiments like J-PARC<sup>5</sup>, RHIC<sup>6</sup> and SPS<sup>7</sup> performed by the STAR and NA61/SHINE collaborations, respectively, are not only trying to map the chiral and deconfinement phase boundaries of QCD, but are also studying the properties of the QGP. As a matter of fact, the second and last experiments validated the existence of the QGP [3]. Characterizing these phase transitions and looking for the possible existence of CEPs, predicted by many model calculations, is another goal of these experiments. The CEP is a second order phase transition point. In this type of phase transitions, correlation length diverges implying criticality [43]. If discovered, the CEP would be one of the first discovery of in-medium QCD properties. Upcoming experiments like NICA<sup>8</sup> and FAIR<sup>9</sup> will continue this experimental effort. In this experiments, heavy ions travel at very high energies in opposite directions creating powerful magnetic fields [65], even if lasting for a short period of time [84]. The magnetic field created in such experiments are dependent on the collision energy and effective distance between incoming particles (impact parameter).

It is quite possible that the detection of the first-order phase-coexistence region is easier to achieve than that of the CEP. Indeed, it is conjectured that when the expanding matter created in a HIC passes through a putative first-order phase transition line, the system will probably spend enough time in this region to develop measurable signals [85].

Some experimental observables in HIC include particle yields and spectra and event by event fluctuations. In recent years, fluctuations of conserved charges (like the baryonic number, electric charge or strangeness) and their higher order cumulants (derivatives of the logarithm of the generating functional, for more information see [86]) have been intensively studied by lattice QCD calculations as possible observable signatures of the phase transition and even the existence of the CEP. Actually, certain ratios between different order cumulants, are able to distinguish if a given region is described by hadronic or quarks degrees of freedom. Such conclusion can be reached by calculating these ratios using the Hadron Resonance Gas model and the quark model, and then comparing to lattice QCD results, giving information about the deconfinement transition [86]. The second order cumulant of the baryonic number (proportional to the susceptibility of the baryonic number) diverges at the CEP and so it behaves like direct evidence for the existence of the CEP [80]. Fluctuation enhancement due to spinodal instabilities are a generic trait in

<sup>5</sup>Japan proton accelerator research complex.

<sup>6</sup>Relativistic Heavy Ion Collision at the Brookhaven National Laboratory.

<sup>7</sup>Super Proton Synchrotron at CERN.

<sup>8</sup>Nuclotron-based Ion Collider fAcility at the Joint Institute for Nuclear physics.

<sup>9</sup>Facility for Antiproton and Ion Research at GSI.

systems undergoing a first-order phase transition, as such, despite the short lifetime and finite size of these systems, it has been conjectured, as a possible telltale sign of this scenario, the appearance of enhanced fluctuations in the strangeness sector. These can result, for instance, in enhanced kaon-to-pion fluctuations (see [85] for a review).

Experimentally, after the collision, the fireball undergoes hadronization and only hadrons are observed in the final state. Thus, there is not yet a simple one-to-one comparison between experimental data and theoretical calculations and further efforts have to be made in this direction if one wishes to pin down the location of the conjectured CEP [86, 87]. The correlated electron-positron pairs (dileptons) from decays of vector mesons, (specially the  $\rho$  meson due to its low invariant mass) are good candidates to study in-medium modifications since they escape the interaction region unaffected by subsequent strong interactions [88]. Also, due to its low viscosity, the QGP is considered an ideal fluid whose expansion after the collision is expected to be isentropic. Combining this with the conservation of baryon number, it makes the trajectories of constant entropy per baryon number ( $s/\rho_B$ ) in the phase diagram a valuable place to gather information from the system [75].

### 3.3 What is known from Astrophysics

From a completely different perspective, the low temperature and high density region of the phase diagram is not only interesting for nuclear and particle physics studies, but also extremely important for astrophysical applications, namely to study the evolution and properties of neutron stars (NS) [89, 90].

Since its discovery in 1967 [91], NS have been the focus of many experimental and theoretical studies in astrophysics, nuclear and particle physics, due to its extreme properties not attainable in terrestrial laboratories. These objects originate from the gravitational collapse of stars, being one of the three main endpoints of stellar evolution. The evolution of a star is played out by the balance between the four fundamental forces: the collapsing attraction from the star's own gravity and the repulsive radiation pressure coming from nuclear processes. Inside a star, lighter elements are fused into heavier ones that are accumulated in the core of the star. In a very simplistic analysis, when fusions processes stop inside the star, the only pressure fighting the gravitational collapse comes from quantum degeneracy pressure (owing to the Pauli exclusion principle). After the core-collapse supernova, and depending on the progenitor's mass, the remnant will be either a black hole or a neutron star. Typically a neutron star has a mass of about  $1.4M_\odot$  (solar masses) and a radius of 10 – 15 km [92]. The maximum threshold for which a dying star collapses into a black hole, called the NS maximum mass, is still unknown.

As previously discussed, in the location of the QCD phase diagram, occupied by NS (low temperature, high density), our theoretical knowledge coming from first principles fails. Thus, the nuclear matter equation of state (EoS) derived from QCD in the relevant regimes for NS, which encodes these objects composition, is currently unknown. This implies that the core composition of these objects is an open question. As a matter of fact the EoS is only known for low densities i.e., for the outer crust of the star. As a result of the extreme densities reached in

the core of these objects, exotic matter including hyperons, Bose–Einstein condensates or quark matter, may exist [93]. In the latter scenario, baryons begin to overlap and baryonic matter might undergo a deconfinement phase transition to quark matter [94].

In recent years multi-messenger astrophysics has been providing a deeper insight on some properties of these objects by combining information from astrophysical observations and, more recently, gravitational wave (GW) information coming from the binary NS merger GW170817, provided by the LIGO<sup>10</sup>/Virgo collaborations [95, 96]. Another source of observational data is coming from the NICER<sup>11</sup> experiment by NASA. NICER was able to estimate the mass and radius of the millisecond-pulsar PSR J0030+0451 and also infer some thermal properties of hot regions present in the star [97].

The two solar mass pulsars PSR J1614-2230 ( $M = 1.908 \pm 0.016 M_{\odot}$ ) and PSR J0348+0432 ( $M = 2.01 \pm 0.04 M_{\odot}$ ) [98] allied to the gravitational wave signal coming from the NS binary merger GW170817 event, define substantial constraints on the EoS, both on the maximum mass and the tidal deformability of the star. The GW detection was supplemented by the follow up of the electromagnetic counterpart, the gamma-ray burst GRB170817A [99], and the electromagnetic transient AT2017gfo [100], that set extra constraints on the lower limit of the tidal deformability [101–105]. The denser region of the EoS is severely unconstrained, being very difficult to build models with exotic degrees of freedom inside the stars. More precisely, soft EoS at high densities were ruled out by the discovery of the above-mentioned massive pulsars while EoS that are too stiff and have large radii are incompatible with the tidal deformability coming from GW observations [106]. One way to balance both these features might be with an EoS describing a first-order phase transition, which would be soft enough at low densities, satisfying the constraints from GW physics and stiff enough after the transition to attain stars with a sufficiently high mass [106].

The major difficulty on inferring the presence of exotic matter inside neutrons stars, lays on detecting observational signatures that clearly separate a NS described by a purely nucleonic EoS from an EoS with exotic degrees of freedom. In the case of hadron and quark matter, even though there is a clear physical distinction between the two, in practice, it is very difficult to distinguish the effects of each type of matter using observables as the star mass, radius and tidal deformability. As discussed in [106–108], the presence of a first-order phase transition between hadronic matter and quark matter can lead to observational signatures that could be exploited in more NS binary mergers or observations, favouring the hypothesis of quark matter in the NS core.

In order to study matter under such extreme conditions and the possibility of the existence of NSs with a quark core, theoretical models must take into consideration that the low density EoS, near the saturation, is dominated by hadron degrees of freedom while, at high densities, quarks are the relevant degree of freedom. Hence, to study the possibility of NSs with a quark core, hybrid models should be employed to build the hybrid star EoS.

<sup>10</sup>Laser Interferometer Gravitational-wave Observatory.

<sup>11</sup>Neutron Star Interior Composition Explorer.

Finally, very strong magnetic fields exist inside certain types of NS, magnetars [109]. These may be several orders of magnitude larger than the magnetic fields in ordinary NSs. On the surface, the magnetic field may be as strong as  $10^{14} - 10^{15}$  Gauss and it could be as strong as  $10^{16} - 10^{18}$  Gauss in the interior of the star [110]. The influence of external magnetic fields in quark stars and hybrid stars has been also studied [111], with the results indicating that strong magnetic fields do not favour the possibility of hybrid stars with a core containing deconfined quark matter.

## Chapter 4

# Modelling the QCD phase diagram

Owing to asymptotic freedom, at high momentum transfers, QCD is a perturbative theory. However, at low momentum transfers, perturbation theory is not applicable. As stated in the previous section, one way to study low energy QCD lies in the use of effective models.

The goal of effective theories is to isolate the relevant physics of some phenomena by creating mathematically tractable models. For field theories, the most powerful tool in the construction of effective models are the symmetries of the physical system (and their possible breaking). When building an effective field theory, symmetry arguments may be not sufficient to describe a given phenomena. In this case, the effective interaction should be guided by phenomenology.

The importance of effective theories within the history of physics is undeniable. Theories like Quantum Electrodynamics, the Fermi theory of Weak interactions and even the Standard Model itself are effective field theories that break down at some mass scale. Hence, the use of effective theories, i.e., theories that work within a certain energy scale, is completely justified.

Usually, when dealing with field theories, one starts with the respective Lagrangian density,  $\mathcal{L}$ , from which one can calculate the generating functional,  $\mathcal{Z}$ . The generating functional for a scalar field,  $\phi$ , in a  $D$ -dimensional Euclidean spacetime, can be written as:

$$\mathcal{Z}[J] \propto \int \mathcal{D}\phi \exp \left\{ -\mathcal{S}_E[\phi] + \int d^D x J(x)\phi(x) \right\}. \quad (4.1)$$

Here,  $J(x)$ , is known as the external source current and,  $\mathcal{S}_E$ , is the Euclidean action, which can be obtained from the Wick rotated Lagrangian<sup>1</sup> as:  $\mathcal{S}_E = -\int d^D x \mathcal{L}_E$ . It can be shown that calculating the  $n$ -functional derivatives of the generating functional,  $\mathcal{Z}[J]$ , with respect to the source  $J$  (located at the points  $x_1, \dots, x_n$ ), with an appropriate normalization at  $J = 0$ , gives origin to the  $n$ -point correlation functions of the theory, also known as the Greens functions of the theory [56]. In different terms, using the generating functional, one can obtain all the Feynman diagrams of a given theory, both the connected and disconnected ones [56].

---

<sup>1</sup>Starting from a theory in Minkowski spacetime, one can work in Euclidean spacetime after the so-called Wick rotation,  $t \rightarrow -i\tau$ , see Appendix A.

Having the generating functional as a starting point, one can also define the energy functional,  $\mathcal{W}$ , which stores only the connected diagrams [56]. It is defined as:

$$\mathcal{W}[J] = \ln \mathcal{Z}[J]. \quad (4.2)$$

Another way to store physical information about the field theory is the effective action,  $\Gamma$ . To obtain this functional, one must calculate the expectation value of the fields in the presence of an external source  $J$ , known as the classical field<sup>2</sup>  $\langle \phi \rangle_J = \varphi$ . This quantity is defined as:

$$\langle \phi \rangle_J = \frac{\delta \mathcal{W}[J]}{\delta J(x)} = \varphi(x). \quad (4.3)$$

We highlight that the classical field, is a functional of the source,  $\varphi = \varphi[J]$ . It is possible to show, by symmetry arguments, that in the limit of vanishing external source,  $J(x) \rightarrow 0$ , in order for the theory to have an unique and Poincaré invariant vacuum, the classical field,  $\varphi$ , must be a constant,  $\varphi = \text{cte}$  [29, 56]. Finally, using the classical field, and its relation to the energy functional (see Eq. (4.3)), it is possible to construct the previously mentioned effective action,  $\Gamma[\varphi]$ . It is defined through the following Legendre transformation:

$$\Gamma[\varphi] = -\mathcal{W}[J_\varphi] + \int d^D x J_\varphi(x) \varphi(x). \quad (4.4)$$

In the above, the source,  $J_\varphi = J[\varphi]$ , is the source written as a functional of the classical field,  $\varphi$ , by inverting the relation given in Eq. (4.3). It can also be shown<sup>3</sup> that the effective action must obey the following equation [29, 56]:

$$\frac{\delta \Gamma[\varphi]}{\delta \varphi(x)} = J(x). \quad (4.5)$$

This result implies that, in the  $J \rightarrow 0$  limit, the effective action must be an extremum with respect to the classical field. As discussed earlier, in the same limit (of  $J = 0$ ) the classical field must be a constant, independent of spacetime variables. So, the classical field configuration which extremizes the effective action, for  $J = 0$ , is a constant (this equation might have different solutions which depend on spacetime, the so-called soliton solutions [29]).

<sup>2</sup>The name of this quantity stems from the classical limit. One can derive a quantum analogue of the Euler-Lagrange equations for quantum field theory. Taking the  $\hbar \rightarrow 0$  limit, one can arrive at the classical Euler-Lagrange equations written in terms of  $\varphi$  [56].

<sup>3</sup>Consider the functional derivative of Eq. (4.4) with respect to the classical field,  $\varphi$ . We can write:

$$\begin{aligned} \frac{\delta \Gamma[\varphi]}{\delta \varphi(y)} &= -\frac{\delta \mathcal{W}[J_\varphi]}{\delta \varphi(y)} + \int d^D x \frac{\delta J_\varphi(x)}{\delta \varphi(y)} \varphi(x) + \int d^D x J_\varphi(x) \frac{\delta \varphi(x)}{\delta \varphi(y)} \\ &= -\int d^D x \frac{\delta \mathcal{W}[J]}{\delta J(x)} \Big|_{J=J_\varphi} \frac{\delta J_\varphi(x)}{\delta \varphi(y)} + \int d^D x \frac{\delta J_\varphi(x)}{\delta \varphi(y)} \varphi(x) + J_\varphi(y) \\ &= -\int d^D x \varphi(x) \frac{\delta J_\varphi(x)}{\delta \varphi(y)} + \int d^D x \frac{\delta J_\varphi(x)}{\delta \varphi(y)} \varphi(x) + J_\varphi(y) = J_\varphi(y). \end{aligned}$$

Here, we used the definition of classical field given in Eq. (4.3) and the definition of the Dirac delta for functional calculus in  $D$ -dimensions:  $\frac{\delta \varphi(x)}{\delta \varphi(y)} = \delta^D(x - y)$ .

The effective action functional also generates all the one-particle irreducible (1PI) diagrams of a theory i.e., diagrams that cannot be made simpler by cutting an internal line. Calculating exactly the effective action means to completely solve a field theory [56].

From the definition of the effective action in Eq. (4.4), one can derive a *master* equation for the effective action [56]. Consider the definition of the effective action given in Eq. (4.4), exponentiate both sides of the equation and use Eqs. (4.1), (4.2) and (4.5), to write:

$$e^{-\Gamma[\varphi]} = \int \mathcal{D}\phi \exp \left\{ -\mathcal{S}_E[\phi] + \int d^D x \frac{\delta\Gamma[\varphi]}{\delta\varphi(x)} (\phi(x) - \varphi(x)) \right\}. \quad (4.6)$$

Making a change of variables in the integration as  $\phi \rightarrow \phi + \varphi$ , we can finally arrive at the final result:

$$e^{-\Gamma[\varphi]} = \int \mathcal{D}\phi \exp \left\{ -\mathcal{S}_E[\phi + \varphi] + \int d^D x \frac{\delta\Gamma[\varphi]}{\delta\varphi(x)} \phi(x) \right\}. \quad (4.7)$$

From this equation one can conclude that the effective action is governed by a first-order, non-linear integro-differential functional equation. One approach to obtain solutions of this equation lies in the vertex expansion:

$$\Gamma[\varphi] = \sum_{n=0}^{\infty} \frac{1}{n!} \int d^D x_1 \dots d^D x_n \Gamma^{(n)}(x_1, \dots, x_n) \varphi(x_1) \dots \varphi(x_n). \quad (4.8)$$

Where  $\Gamma^{(n)}(x_1, \dots, x_n) = \delta^n \Gamma / \delta\varphi(x_1) \dots \delta\varphi(x_n)$ . The coefficients  $\Gamma^{(n)}(x_1, \dots, x_n)$  correspond to the 1PI  $n$ -point vertex function of the theory. Using this expansion in Eq. (4.7) leads to an infinite tower of coupled integro-differential equations for the coefficients  $\Gamma^{(n)}(x_1, \dots, x_n)$ , the Dyson–Schwinger equations.

Another approach lies in considering small fluctuations around the classical field,  $\varphi$ , and essentially treating it as a background field. Expanding the action  $\mathcal{S}_E[\phi + \varphi]$  around  $\varphi$ , we can write:

$$\mathcal{S}_E[\phi + \varphi] = \mathcal{S}_E[\varphi] + \int d^D x \frac{\delta\mathcal{S}_E[\varphi]}{\delta\varphi(x)} \phi + \int d^D x d^D y \frac{1}{2!} \frac{\delta^2\mathcal{S}_E[\varphi]}{\delta\varphi(x)\delta\varphi(y)} \phi^2 + \dots \quad (4.9)$$

Truncating this expansion in the second order term, substituting it in Eq. (4.7) and considering  $\Gamma[\varphi] = \mathcal{S}_E[\varphi]$  on the right hand side of Eq. (4.7), we can write:

$$e^{-\Gamma[\varphi]} \simeq e^{-\mathcal{S}_E[\varphi]} \int \mathcal{D}\phi \exp \left\{ - \int d^D x d^D y \frac{1}{2} \frac{\delta^2\mathcal{S}_E[\varphi]}{\delta\varphi(x)\delta\varphi(y)} \phi^2 \right\}. \quad (4.10)$$

The path integral has a gaussian form and can be computed explicitly to yield:

$$e^{-\Gamma[\varphi]} \simeq e^{-\mathcal{S}_E[\varphi]} \left( \det \left[ \frac{\delta^2\mathcal{S}_E[\varphi]}{\delta\varphi^2} \right] \right)^{-\frac{1}{2}}. \quad (4.11)$$

In the above, the negative sign is for bosonic fields and the positive sign is for fermionic fields. One can finally write the famous one-loop approximation of the effective action as [112]:

$$\Gamma[\varphi] \simeq \mathcal{S}_E[\varphi] \pm \frac{1}{2} \ln \det \left[ \frac{\delta^2 \mathcal{S}_E[\varphi]}{\delta \varphi^2} \right]. \quad (4.12)$$

Here, the positive sign is for bosonic fields and the negative sign is for fermionic fields. The first term is simply the classical action while, the second term, incorporates the first quantum corrections to the theory (loop effects). For more details about the effective action functional formalism, see [56].

Several studies of the QCD phase diagram using effective models consider only the first term in Eq. (4.12) i.e., in the so-called mean field approximation (or Hartree approximation). In this approximation, the effective action is just the classical action and the only field configuration taken into account is the classical one, all quantum fluctuations are left aside.

If one wishes to do more realistic studies of the QCD phase diagram using effective models, quantum fluctuations are of ultimate importance to get more accurate results. To correctly account for quantum fluctuations in QCD effective models, one can try to calculate the second term in Eq. (4.12). This is usually referred to as an  $1/\varepsilon$  expansion, where  $\varepsilon$  is some parameter considered to be large. Usually, in chiral effective models, this parameter corresponds the inverse Planck constant  $\hbar$  or to the number of colours  $N_c$ .

When dealing with chiral effective models, in particular with the Nambu–Jona-Lasinio model, the parameter of choice is the latter. Truncating Eq. (4.12) in the first term corresponds the one-quark-loop approximation and a  $N_c^1$  calculation. Considering the second term of the same equation<sup>4</sup> yields the meson-loop approximation [113], that corresponds to a  $N_c^0$  correction term with a  $1/N_c$  suppression factor. The inclusion of this term can become very important not only because  $N_c = 3$  in the real world but also in situations where, due to their low mass, pionic effects are important, like the sigma decay into two pions [113].

A great difficulty of using this kind of expansion in effective models, comes from the  $N_c$  counting. If one wishes to maintain important symmetries of low energy hadron physics like the Goldstone boson theorem, the GMOR relation (see Eq. (2.13)) and the Goldberger–Treiman relation (see Eq. (2.14)), the  $N_c$  counting has to be done consistently or there will be violations of these symmetries and the pion, for example, may not be massless in the chiral limit. This means that for a calculation of order  $N_c^0$ , terms of lower power in  $N_c$  have to be thrown away. This is not always a trivial task and there has been an effort in developing the so-called symmetry-conserving approximations [113].

Using these methods in a non-renormalizable model like the Nambu–Jona-Lasinio model carries another disadvantage: the original model has a momentum cutoff, that only limits the quark momentum space and does not constraint the meson momenta. This in turn leads again, to ultraviolet divergences in the bosonic sector and the need of regularization through another

<sup>4</sup>In a small (perturbative) coupling expansion this corresponds to the one-loop approximation.

momentum cutoff. This is another parameter that has to be fixed by some hadron properties in the vacuum [113].

Another method to include quantum fluctuations in effective models is the Functional Renormalization Group (FRG). Usual quantum field theory techniques integrate all quantum fluctuations at once. The FRG is a powerful non-perturbative method that incorporates the Wilsonian ideas of a gradual momentum integration. The FRG can be used to incorporate quantum fluctuations in the equations of state of strong coupled systems in different physical scenarios like finite temperature, finite density and in the presence and absence of an external magnetic field [114–116]. This method will be discussed in more detail in Section 4.2.

## 4.1 The Nambu–Jona-Lasinio model

As motivated in previous sections, to study low energy QCD, one can use chiral effective models. These models should display (approximate) chiral symmetry at the Lagrangian level i.e., invariance under  $SU(N_f)_R \times SU(N_f)_L$  transformations and some breaking mechanism that leads to an asymmetric vacuum and the existence of  $N_f^2 - 1$  Goldstone bosons. The Nambu–Jona-Lasinio is a classical example of a field theory used to study low energy QCD. In this work we will consider this model, within different number of flavours and types of interactions. Additionally, we will study the so-called Quark-Meson model, which can be interpreted as a partial bosonized version of the NJL model (more details will be given in Section 4.2.1).

Introduced by Yoichiro Nambu and Giovanni Jona-Lasinio in 1961, before the assertion of Quantum Chromodynamics as the theory of strong interactions, the Nambu–Jona-Lasinio model had its debut as a model of nucleons [117, 118]. In the original model, the nucleon fields interact locally to generate the mass gap in the Dirac spectrum, in analogy with the Bardeen–Cooper–Schrieffer theory of superconductivity. After the establishment of QCD as the theory of strong interactions, the nucleon field was substituted by a quark field [119, 120]. Since then, this model has been widely used as an effective model of QCD, as a result of sharing all the global symmetries of strong interaction, while providing a mechanism for spontaneous breaking and restoration of chiral symmetry. Several improvements have been made to the model throughout the years like the inclusion of finite quark current quark masses [121–123], extending the model for several quark flavours and adding six-quark and eight-quark interactions to better reproduce the hadron spectra [124–126]. One of the most important extensions of the model was the inclusion of the Polyakov loop by K. Fukushima [40]. This improvement allowed the incorporation in the model of the ability to describe statistical deconfinement with the spontaneous breaking of  $Z(N_c)$  symmetry at finite temperature [127, 128]. This extension of the model will be discussed in more detail in Section 4.1.1. We emphasize the following review works on this model [45, 129–131].

The general Lagrangian density of the NJL model, for  $N_f$  flavours of quarks, can be described by the following Lagrangian density:

$$\mathcal{L} = \bar{\psi}(i\cancel{\partial} - \hat{m})\psi + \mathcal{L}_{\text{int}}. \quad (4.13)$$

Here,  $\psi$  is a  $N_f$ -component vector in flavour space, where each component is a Dirac spinor and  $\hat{m} = \text{diag}(m_1, \dots, m_{N_f})$  is the quark current mass matrix, diagonal in flavour space. The term  $\mathcal{L}_{\text{int}}$ , can include any type of multi-quark interactions, as long as the symmetries of interest are preserved. However, to be an NJL-type of model, it must contain some interaction capable of breaking chiral symmetry in the vacuum. This can be achieved by including, in the Lagrangian density, a four-quark scalar and pseudoscalar interaction which, for  $N_f = 2$  and  $N_f = 3$ , can be respectively written by:

$$\mathcal{L}_4 \propto \left\{ (\bar{\psi}\psi)^2 + (\bar{\psi}i\gamma_5\tau_a\psi)^2 \right\} \quad (N_f = 2, a = 1, 2, 3), \quad (4.14)$$

$$\mathcal{L}_4 \propto \left\{ (\bar{\psi}\lambda_a\psi)^2 + (\bar{\psi}i\gamma_5\lambda_a\psi)^2 \right\} \quad (N_f = 3, a = 0, 1, \dots, 8). \quad (4.15)$$

Where  $\tau_a$  (with  $a = 1, 2, 3$ ) are the three Pauli matrices and  $\lambda_a$  (with  $a = 1, \dots, 8$ ) the eight Gell-Mann matrices. These set of matrices constitute the  $SU(2)$  and  $SU(3)$  algebras, respectively. The matrix  $\lambda_0$  is defined to be proportional to the unit matrix:  $\lambda_0 = \sqrt{2/3}\mathbb{1}$  and its inclusion leads to the  $U(3)$  algebra (for more details about the  $SU(N)$  and  $U(N)$  groups, see the Appendices B.1 and B.2). For high enough coupling, this interaction leads to dynamical chiral symmetry breaking, generating a quark-antiquark condensation (the quark condensate) and, consequently, a large constituent quark mass.

Considering only the previous four-quark interaction, the NJL model has a  $U(1)_A$  symmetry which, as already stated, is not a symmetry of the QCD vacuum and, as suggested by 't Hooft, should not display physical manifestations [26, 27]. To explicitly break this symmetry at the Lagrangian level the so-called Kobayashi–Maskawa–'t Hooft (KMT) determinant interaction,

$$\mathcal{L}_{2N_f} \propto \left\{ \det(\bar{\psi}P_R\psi) + \det(\bar{\psi}P_L\psi) \right\}, \quad (4.16)$$

must be added to a phenomenological model. Here,  $P_{R/L}$ , are the right-handed (R) and left-handed (L) projection operators, defined as:  $P_{R/L} = (1 \pm \gamma_5)/2$ . The determinant in Eq. (4.16), is taken over flavour space and corresponds to a maximally flavour mixing  $2N_f$ -point interaction, involving an incoming and an outgoing quark of each flavour. This term not only imposes the correct symmetries but it also allows model calculation to account for the correct mass splitting between the  $\eta$  and  $\eta'$  mesons in  $SU(3)_f$  [130, 132]. We point out that for two flavours, this term is a four-quark interaction while, for three quark flavours, it represents a six-quark interaction which, in the latter case, is known to destabilize the vacuum of the model making the potential unbounded by below [133]. This can be understood as a necessity to include other interactions at the Lagrangian level.

As pioneered by A. Osipov et al. in [124, 125], it is possible to introduce eight-quark interactions in order to stabilize the ground state of the model. The authors suggested the following

scalar-pseudoscalar eight-quark interactions:

$$\mathcal{L}_8^{(1)} \propto \left\{ (\bar{\psi}_i P_R \psi_j) (\bar{\psi}_j P_L \psi_i) \right\}^2, \quad (4.17)$$

$$\mathcal{L}_8^{(2)} \propto \left\{ (\bar{\psi}_i P_R \psi_j) (\bar{\psi}_j P_L \psi_k) (\bar{\psi}_k P_R \psi_l) (\bar{\psi}_l P_L \psi_i) \right\}. \quad (4.18)$$

These interactions constitute the most general spin-zero and chirally symmetry preserving interactions that can be introduced in the model without derivative terms. More details about these interactions will be given in Chapter 5.

The first interaction term,  $\mathcal{L}_8^{(1)}$ , violates the Okubo–Zweig–Iizuka (OZI) rule [134]. The OZI rule has a phenomenological origin, created to justify the decay rates of some vector mesons by stating that QCD flavour changing processes are  $N_c$  suppressed [134–136]. One clear violation of this rule is the pion and eta meson masses which are very different in the real world, but would have equal values if such flavour changing processes were completely suppressed [134].

It is possible to include other types of symmetry preserving quark interactions in the NJL model besides scalar and pseudoscalar ones. For instance, when using the NJL Lagrangian to build the neutron star EoS, incorporating vector interactions in the model has been found to be essential to model the behaviour of the EoS at medium-high densities and predict  $2M_\odot$  neutron stars [61]. In [61], the following set of symmetry preserving four-quark vector and pseudovector interaction (vector-isoscalar) and the vector-isovector and pseudovector-isovector interaction (vector-isovector) were considered (for  $N_f = 3$ ):

$$\mathcal{L}_\omega \propto \left\{ (\bar{\psi} \gamma^\mu \lambda_0 \psi)^2 + (\bar{\psi} \gamma^\mu \gamma_5 \lambda_0 \psi)^2 \right\}, \quad (4.19)$$

$$\mathcal{L}_\rho \propto \left\{ \sum_{a=1}^8 \left[ (\bar{\psi} \gamma^\mu \lambda_a \psi)^2 + (\bar{\psi} \gamma^\mu \gamma_5 \lambda_a \psi)^2 \right] \right\}. \quad (4.20)$$

As for the scalar-pseudoscalar interactions, one can also include vector interactions amongst eight quarks. An example of chiral symmetry preserving eight-quark vector interactions, is to generalize the four-quark vector interactions introduced earlier. Consider (for  $N_f = 3$ ):

$$\mathcal{L}_{\omega\omega} \propto \left\{ (\bar{\psi} \gamma^\mu \lambda_0 \psi)^2 + (\bar{\psi} \gamma^\mu \gamma_5 \lambda_0 \psi)^2 \right\}^2, \quad (4.21)$$

$$\mathcal{L}_{\rho\rho} \propto \left\{ \sum_{a=1}^8 \left[ (\bar{\psi} \gamma^\mu \lambda_a \psi)^2 + (\bar{\psi} \gamma^\mu \gamma_5 \lambda_a \psi)^2 \right] \right\}^2, \quad (4.22)$$

$$\mathcal{L}_{\omega\rho} \propto \left\{ \sum_{a=1}^8 \left[ (\bar{\psi} \gamma^\mu \lambda_0 \psi)^2 + (\bar{\psi} \gamma^\mu \gamma_5 \lambda_0 \psi)^2 \right] \left[ (\bar{\psi} \gamma^\mu \lambda_a \psi)^2 + (\bar{\psi} \gamma^\mu \gamma_5 \lambda_a \psi)^2 \right] \right\}. \quad (4.23)$$

Of course, these are just some examples of eight-quark vector interactions. The inclusion of all possible chiral-symmetric sets of eight-quark vector interactions was performed in [137] in order to study the masses of the lowest spin-0 and spin-1 meson states.

Since we are treating this model as an effective theory of QCD without knowledge of how it emerges from QCD, the parameters of the NJL model need to be fixed in such a way that they

reproduce some physical observables like meson masses and leptonic decays in the vacuum [112, 130], lattice QCD results or, when dealing with the neutron star EoS, NS properties.

In Chapter 5, we will parametrize an extended version of the NJL model by reproducing some physical observables in the vacuum and analyse different parameter sets. While, in Chapter 6, the NJL model will be used to describe quark matter inside neutron stars. Some parameters of the model will be fixed by reproducing some meson masses while others, will left be free and their effect on the stability of NSs will be discussed.

### 4.1.1 Coupling to the Polyakov loop

A well-known shortcoming of using NJL-type Lagrangians as effective models of QCD, is the absence of dynamic gluons and the inability to describe the confinement-deconfinement transition. However, the model can be coupled to a static gluonic background field to describe not only the chiral but also the (statistical) deconfinement transition. These models are called Polyakov–NJL (PNJL) models [39, 40, 127, 128, 138–141]. To define such model, one simply substitutes the usual derivative by a covariant one to minimally couple the gluon background field to the fermion field:

$$\partial_\mu \rightarrow D_\mu = \partial_\mu - A_4 \delta_\mu^0. \quad (4.24)$$

Here,  $A_4 = iA_0$ , where  $A_0$  is the zeroth component of the gluon field. This covariant derivative is the zero component of the covariant derivative in QCD, defined in Eq. (2.3). One must also include an effective potential, written in terms of the Polyakov loop (see Eq. (3.1)) to the Lagrangian density,  $\mathcal{U}(\Phi[A_4], \bar{\Phi}[A_4]; T)$ . The Polyakov loop field  $\Phi$ , acts as an order parameter<sup>5</sup> for confinement/deconfinement. In the confined phase  $\Phi \rightarrow 0$  while in the deconfined phase,  $\Phi \rightarrow 1$ .

Usually, in these type of models, the Polyakov loop effective field,  $\Phi[A_4]$  and its conjugate  $\bar{\Phi}[A_4]$ , are not considered a dynamical degree of freedom: the Lagrangian does not contain any dynamical terms related to  $A_4$  and, when defining the generating functional of the model, no path integral over  $A_4$  is considered. The Polyakov loop is then calculated by the requirement of thermodynamical consistency: the grand canonical potential must be an extremum with respect to the Polyakov loop. This procedure is equivalent to considering a mean field approximation for the  $A_4$  field.

The effective potential,  $\mathcal{U}(\Phi, \bar{\Phi}; T)$ , can be written using Ginzburg–Landau theory of phase transitions. Within this approach, the effective potential has to respect the symmetries of the system in particular the  $Z(N_c)$  symmetry and to reproduce its spontaneous breaking at some

---

<sup>5</sup>For pure glue theory, the Polyakov loop is an exact order parameter. In the confined phase, the boundary conditions of QCD are respected by the  $Z(N_c)$  symmetry while in the deconfined phase it is broken.

high temperature. One widely used example is<sup>6</sup> [40, 142, 143]:

$$\frac{\mathcal{U}(\Phi, \bar{\Phi}; T)}{T^4} = -\frac{1}{2}a(T)\bar{\Phi}\Phi + b(T) \ln \left[ 1 - 6\bar{\Phi}\Phi + 4(\bar{\Phi}^3 + \Phi^3) - 3(\bar{\Phi}\Phi)^2 \right], \quad (4.25)$$

with the temperature dependent parameters [142, 143]:

$$a(T) = a_0 + a_1 \left( \frac{T_0}{T} \right) + a_2 \left( \frac{T_0}{T} \right)^2, \quad (4.26)$$

$$b(T) = b_3 \left( \frac{T_0}{T} \right)^3. \quad (4.27)$$

The parameters  $T_0$ ,  $a_0$ ,  $a_1$ ,  $a_2$  and  $a_3$  are fixed by reproducing lattice QCD results at  $\mu = 0$  [144–146]. It is important to mention that the NJL parameters and the Polyakov potential parameters are not on the same footing. In fact, while the NJL parameters can be directly related with physical quantities, the role of the Polyakov loop potential is to ensure the recovering of pure gauge lattice expectations.

The pure gauge critical temperature,  $T_0$ , is the only true parameter and fixes the temperature scale of the system. According to lattice findings, it is usually fixed to 270 MeV [147, 148]. However, in the Ginzburg–Landau framework, the characteristic temperature for a phase transition is not expected to be a prediction and different criteria for fixing  $T_0$  can be found in the literature. Indeed, in [149] an explicit  $N_f$  (number of flavours) dependence of  $T_0$  is considered, coming from renormalization group arguments. In Chapter 5, when studying the PNJL model, we will fix this parameter in order to reproduce the crossover temperature of the deconfinement transition coming from lattice QCD results.

#### 4.1.2 Regularization Procedure

An important aspect of both, NJL and PNJL models, is the lack of renormalizability which comes from the point-like nature of the quark-quark interaction allied to the mass dimension of the interactions couplings<sup>7</sup>. Indeed, in the mean field expansion, the NJL model is renormalizable in less than four spacetime dimensions while, for exactly four spacetime dimensions, it becomes a trivial theory of non-interacting bosons after renormalization [150].

As a consequence, a procedure to regularize divergent integrals in both models is required. The regularization process is part of the physical model and must be carried out in such a way that physically expected properties of the model and symmetry considerations are maintained [130]. Several regularization procedures are available: three dimensional cutoff [130], four dimensional cutoff [129, 130, 151], Pauli–Villars regularization [152–154], regularization in proper time

<sup>6</sup>In Chapter 5, we will study a version of the PNJL model considering the polynomial Polyakov loop potential (see Eq. (5.5)).

<sup>7</sup>The mass dimension of a coupling,  $m_D$ , can be used to measure the superficial degree of divergence of a particular field theory: for  $m_D > 0$  the theory is super-renormalizable, for  $m_D = 0$  it is renormalizable and for  $m_D < 0$  it is non-renormalizable [29]. The mass dimension of the scalar-pseudoscalar coupling is  $[2 - D]$  (where  $D$  is the spacetime dimension), rendering the NJL model non-renormalizable in perturbation theory in  $D = 4$ . In  $(1 + 1)$ -dimensions this model is renormalizable in perturbation theory and it is called the Gross–Neveu model.

[153, 155]. For a detailed analysis of the regularization procedures and more references to the corresponding literature see [130, 156].

A regularization that includes high momentum quark states ( $\Lambda \rightarrow \infty$  in the thermal convergent integrals), is necessary to get the required increase of extensive thermodynamic quantities, allowing the convergence to the Stefan–Boltzmann (SB) limit of QCD. However, this leads to unphysical behaviour of the quark condensates at very high temperatures (the quark condensates change sign and the constituent quark masses go below the respective current value) [157, 158]. In Chapter 5 of the present work, we will deal with these high momentum quark states when studying the phase diagram of the model. Following Ref. [159], one can include an extra temperature and chemical potential dependent term which leads to the correct asymptotic behaviour for all observables considered. Formally, such term arises as a constant of integration when one obtains the thermodynamic potential by integrating the gap equations (more details will be given in Chapter 5). For another regularization procedure, that prevents the unphysical behaviour of the quark condensates while ensuring that the pressure reaches the SB limit at high temperatures, see [160].

## 4.2 The Functional Renormalization Group

The Renormalization Group is an important tool in theoretical physics since it allows the study of physical phenomena on different scales of distance and/or energy. In contemporary physics, the Renormalization Group has a status of meta-theory, a theory about theories [161]. There are several applications of the Renormalization Group: study of the strong interaction, the electroweak phase transition, effective models of nuclear physics, condensed matter physics systems and even quantum gravity [162–164]. Some of its most important applications in the history of physics are the elimination of ultraviolet divergences in renormalizable quantum field theories and its application to explain the universality properties of continuous phase transitions.

The cancellation of ultraviolet divergences is essential in a theory which aims to make physical predictions. To remove this type of divergences Wilson proposed the application of a Renormalization Group transformation [29]. First, in the path integral approach of quantum field theory, consider the generating functional defined at a certain energy scale, a cutoff with physical meaning. In the case of a fundamental particle physics theory, this cutoff can be associated to a minimum length scale like the Planck distance. In condensed matter the inverse of the lattice spacing can be associated to this cutoff. Second, separate the slow and fast momentum modes of the field and integrate only the modes with high momenta, near the cutoff of the theory. Finally, rescale the Lagrangian to obtain a new effective Lagrangian with different couplings and new terms. Making the elimination of the fast modes in a arbitrarily thin momentum shell (a process called decimation in Renormalization Group language), rescaling and repeating the process, defines a continuous transformation of the Lagrangian [29]. These transformations create a trajectory in the space of all possible Lagrangians. The properties of this trajectory contains relevant information about the theory like renormalizability, asymptotic freedom, asymptotic

safety and, in the case of the FRG, grants access to the quantum effective action of the theory by incorporating quantum fluctuations in the calculation.

The construction of the renormalization group transformation (Decimation  $\oplus$  Rescaling) is not the same for all physical systems and finding such transformation is not trivial. The Functional Renormalization Group is a formal way of applying the Renormalization Group transformation to continuous field theories allowing to describe the macroscopic physics of a system from the microscopic description.

In the formalism of the FRG, the central object is the average effective action,  $\Gamma_k$ . This object depends explicitly on a momentum scale  $k$  and has well defined limits: in the momentum scale, where  $k = \Lambda$  the so-called ultraviolet (UV) scale, we have the classical action to be quantized called  $\mathcal{S}$ ; in the momentum scale  $k = 0$  the so-called infrared (IR) scale, all quantum fluctuations have been included and we obtain the full quantum effective action,  $\Gamma$ . The average effective action,  $\Gamma_k$ , acts as an interpolating functional between these two regimes in the space of all possible theories [165, 166].

To implement this idea, one has to modify the generating functional  $\mathcal{Z}$  (and, consequently, the effective action) to make it scale dependent. The modification has to be made in such a way that the two interpolating limits of the average effective action have to be respected i.e. [165, 166],

$$\Gamma_{k \rightarrow \Lambda} = \mathcal{S}, \quad (4.28)$$

$$\Gamma_{k \rightarrow 0} = \Gamma. \quad (4.29)$$

The simplest way of doing so, is to add the following regulator term,  $\Delta\mathcal{S}_k$ , to the generating functional, with the functional form (in a  $D$ -dimensional Euclidean spacetime):

$$\Delta\mathcal{S}_k[\phi] = \frac{1}{2} \int \frac{d^D q}{(2\pi)^D} \phi(-q) R_k(q) \phi(q), \quad (4.30)$$

where  $R_k(q)$  is the so-called regulator function. This regulator term can be interpreted as a scale dependent mass term since it is proportional to a term that is quadratic in the field. In principle the regulator function  $R_k$ , can have any functional form, as long as it respects the limits indicated above. These limits translate into three constraints for the regulator function. The first,

$$\lim_{q^2/k^2 \rightarrow 0} R_k(q) > 0, \quad (4.31)$$

ensures an infrared regularization with the regulator function representing a positive mass term (if  $q^2 \ll k^2$ ). The second constraint,

$$\lim_{k^2/q^2 \rightarrow 0} R_k(q) = 0, \quad (4.32)$$

implies a vanishing regulator function when  $k = 0$ , safeguarding the existence of the full quantum effective action when all quantum fluctuations have been included. The last condition is

$$\lim_{k^2 \rightarrow \infty} R_k(q) \rightarrow \infty. \quad (4.33)$$

In the ultraviolet limit, this last condition forces the regulator to go to infinity. Since it acts like a mass term, in this limit, the theory becomes classical because all the fluctuations are suppressed and the most important field configuration is the classical one. Formally, in such case, the functional integration is dominated by the stationary point (classical configuration). If,

$$\mathcal{Z} = \int \mathcal{D}\phi e^{-\mathcal{S}[\phi]}, \text{ with } \mathcal{S}[\phi] \rightarrow \infty, \quad (4.34)$$

one can use the saddle point approximation and expand  $\mathcal{S}[\phi]$  around its minimum  $\phi_0$ ,

$$\mathcal{S}[\phi] = \mathcal{S}[\phi_0] + \frac{1}{2} \left. \frac{\delta^2 \mathcal{S}[\phi]}{\delta \phi^2} \right|_{\phi=\phi_0} (\phi - \phi_0)^2 + O(\phi^3). \quad (4.35)$$

One can then write:

$$\mathcal{Z} \propto \exp \{-\mathcal{S}[\phi_0]\} \implies \Gamma_{k=\Lambda} = \mathcal{S} + \text{cte}. \quad (4.36)$$

Hence, in the UV, the effective average action,  $\Gamma_{k=\Lambda}$ , is given by the classical action,  $\mathcal{S}$ , without quantum fluctuations.

We are now ready to define the effective average action for a scalar field,  $\Gamma_k[\varphi]$ , as [165, 166]:

$$\Gamma_k[\varphi] = -\mathcal{W}_k[J_\varphi] + \int d^D x J_\varphi(x) \varphi(x) - \Delta \mathcal{S}_k[\varphi]. \quad (4.37)$$

Here,  $\mathcal{W}_k$  is the scale dependent energy functional,  $\varphi$ , is the so-called classical field and  $J_\varphi$  is the external source written as a functional of  $\varphi$ . This definition for the effective average action is very similar to the one of the effective action, defined in Eq. (4.4). The scale dependent energy functional,  $\mathcal{W}_k$ , also receives a modification from the regulator term  $\Delta \mathcal{S}_k$ , and can be defined as [165, 166]:

$$e^{\mathcal{W}_k[J]} = \int \mathcal{D}\phi \exp \left\{ -\mathcal{S}_E[\phi] - \Delta \mathcal{S}_k[\phi] + \int d^D x J(x) \phi(x) \right\}. \quad (4.38)$$

Where  $\mathcal{S}_E[\phi]$  is the Euclidean action of a scalar field  $\phi$  and  $J(x)$  is an external source. The classical field,  $\varphi$ , is defined as in the beginning of Chapter 4, but now one uses the scale dependent energy functional:

$$\langle \phi \rangle_J = \frac{\delta \mathcal{W}_k[J]}{\delta J(x)} = \varphi(x). \quad (4.39)$$

We highlight that the classical field, defined as a functional of the external source is scale dependent,  $\varphi = \varphi_k[J]$  as well as the external source, written as a functional of the classical field,  $J_\varphi = J_k[\phi]$  [165].

One is then interested in the behaviour of the effective average action as the scale  $k$  is changed from the ultraviolet scale, at  $k = \Lambda$  to the infrared scale at  $k = 0$ . To study this trajectory, it is necessary to compute the derivative of the effective average action,  $\Gamma_k$  (see Eq. (4.37)), with respect to the momentum scale  $k$ . After some functional calculus one can arrive at the Wetterich equation for bosonic fields [33, 165, 166],

$$\partial_k \Gamma_k[\varphi] = \frac{1}{2} \text{tr} \left\{ \partial_k R_k \left( \Gamma_k^{(2)}[\varphi] + R_k \right)^{-1} \right\}, \quad (4.40)$$

and, in the case of fermionic fields,  $\psi$  and  $\bar{\psi}$ , (using Grassmann variables) one arrives at:

$$\partial_k \Gamma_k[\bar{\psi}, \psi] = - \text{tr} \left\{ \partial_k R_k \left( \Gamma_k^{(1,1)}[\bar{\psi}, \psi] + R_k \right)^{-1} \right\}. \quad (4.41)$$

Here,  $\Gamma_k^{(2)}$  and  $\Gamma_k^{(1,1)}$  are the usual notations for boson and fermion fields derivatives, respectively given by:

$$\Gamma_k^{(a)}[\varphi] = \frac{\delta^a}{\delta \varphi^a} \Gamma_k[\varphi], \quad (4.42)$$

$$\Gamma_k^{(a,b)}[\psi, \bar{\psi}] = \frac{\overrightarrow{\delta^a}}{\delta \psi^a} \Gamma_k[\psi, \bar{\psi}] \frac{\overleftarrow{\delta^b}}{\delta \bar{\psi}^b}. \quad (4.43)$$

The Wetterich equation is an exact functional differential equation for the effective average action which, in principle, can be solved given a set of initial conditions. In the literature, this equation is said to have one-loop structure due to its similarity to the effective action in the one-loop approximation, see Eq. (4.12).

The Wetterich equation provides the flow of the effective action in the space of all possible theories. Solving the Wetterich equation is equivalent to completely solving a theory. However, such a task is mathematically impossible due to the highly coupled behaviour of the equation and some approximation scheme is needed. Fundamentally, when using the FRG approach to quantum field theory, one is exchanging the functional integration on the Feynman path integral approach, which may not be very well defined mathematically, by a functional differential equation with an one-loop structure.

Regarding the regulator, its purpose is both to ensure an infrared (IR) regularization and an ultraviolet (UV) regularization, as already explained. The IR regularization is achieved by the additional mass term in the denominator of Eqs. (4.40) and (4.41). The UV regularization is included by the derivative of the regulator present on the numerator of Wetterich's equations: the largest contribution to this term is given near  $p^2 \sim k^2$ , implementing the Wilsonian idea of gradual momentum integration. Even though the regulator function by itself is arbitrary, by fulfilling the requirements (4.31), (4.32) and (4.33), the endpoint of the flow trajectory will ideally be the same for every regulator. However, as in practice one has to make some truncation in a form of an *ansatz*, the flow may depend on the choice of the regulator function and truncation. To study the convergence of the solution one usually studies various regulators and truncations

schemes. For detailed reviews of the Functional Renormalization Group and its applications, see [161, 165–169].

As already stated, to solve Eqs. (4.40) and (4.41), some approximation scheme is required. In the literature, two schemes stand out: the vertex expansion (see Eq. (4.8)) and the operator expansion. In the first, the effective average action is expanded in a Taylor series:

$$\Gamma_k[\varphi] = \sum_{n=0}^{\infty} \frac{1}{n!} \int d^D x_1 \dots d^D x_n \Gamma_k^{(n)}(x_1, \dots, x_n) \varphi(x_1) \dots \varphi(x_n). \quad (4.44)$$

Where  $\Gamma_k^{(n)}(x_1, \dots, x_n) = \delta^n \Gamma_k / \delta \varphi(x_1) \dots \delta \varphi(x_n)$ . Inserting this *ansatz* in Eq. (4.12) leads to a tower of flow equations for the  $n$ -point vertex,  $\Gamma_k^{(n)}$  which interpolates between the *bare* vertex and the *dressed* one. This approach is very similar to the Dyson–Schwinger approach to quantum field theory, already addressed in Eq. (4.8). Although this type of calculation seems very close to Dyson–Schwinger approach, and they can even be used to calculate the Green’s functions of the theory, the approaches are slightly different. The first major difference is that by using the FRG, no renormalization is required, all the divergences are incorporated in the boundary conditions and in the flow [170]. Another difference is that it is simpler to improve the results systematically when using the FRG: one only needs to enlarge the theory space.

In the second approach, the operator expansion (also called derivative expansion), one builds an *ansatz* for the effective average action in powers of momentum. As an example, consider a field theory with a single scalar field:

$$\Gamma_k[\varphi] = \int d^D x \left[ V_k(\varphi) + \frac{1}{2} Z_k(\varphi) (\partial \varphi)^2 + \mathcal{O}(\partial^4) \right]. \quad (4.45)$$

The local potential approximation (LPA) consists of keeping the scale dependence only on the first term, the effective potential  $V_k(\varphi)$ . In this approximation, the scale dependent wave function renormalisation,  $Z_k$ , is neglected. In theory, improving this approximation is straightforward (although extremely challenging in practice): one can include scale dependence on the wave function renormalization (LPA’) and Yukawa coupling (LPA’+Y) [171].

### 4.2.1 Applying the FRG to NJL-type models

The FRG has been applied to the NJL model under different physical scenarios besides the vacuum: at finite temperature and chemical potential and even with finite magnetic field, for some examples see [116, 172–177]. In some of these works, the renormalization group flow of the scalar and pseudoscalar coupling  $G$  was studied which, as already mentioned, is fundamentally connected to the mechanism of chiral symmetry breaking in the NJL model.

In order to explain the advantages and disadvantages of applying the FRG method to the NJL we will follow very closely Refs. [178, 179]. In these works, the Wetterich equation for fermions (Eq. (4.41)) was applied to a simplified *ansatz* of the two flavour NJL effective action in the

vacuum:

$$\Gamma_k[\bar{\psi}, \psi] = \int d^4x \left\{ \bar{\psi} i \not{\partial} \psi + \frac{G}{2} [(\bar{\psi}\psi)^2 + (\bar{\psi} i \gamma_5 \boldsymbol{\tau} \psi)^2] \right\}. \quad (4.46)$$

Here, the only interaction included amongst massless quarks was the previously mentioned scalar and pseudoscalar, see Eq. (4.14). The coupling of this interaction depends on the renormalization group scale, i.e.,  $G = G_k$ . A possible contribution coming from the fermion wave-function renormalization is ignored.

Such procedure leads to the flow equation for the coupling  $G$ , also called the  $\beta$ -function for the scalar and pseudoscalar coupling. Deriving explicitly this flow equation is not a trivial task, leaving the scope of the present work. For further details on the derivation, see [178].

For the considered *ansatz*, the  $\beta$ -function has two zeros, representing two different fixed points, a trivial one,  $G^0 = 0$  (Gaussian fixed point), and a non trivial one,  $G^*$ . In order to solve the flow equation, an initial value for the coupling has to be chosen, i.e., one has to fix the coupling in the UV,  $G^{(\text{UV})}$ . Solving the  $\beta$ -function with  $G^{(\text{UV})} < G^*$  drives the system towards weak coupling in the IR, i.e., after all quantum fluctuations are taken into account, it will take the system to one of non-interacting fermions (the coupling constant is zero) leaving the chiral symmetry intact. Starting the flow with a different value for the coupling in the UV,  $G^{(\text{UV})} > G^*$ , leads the system to a diverging coupling in the IR, i.e.,  $G \rightarrow \infty$ . This diverging behaviour is natural and it is signalling chiral symmetry breaking. This can be understood by considering the partially bosonized version of the NJL model.

The partially bosonized version of this model can be obtained by introducing the scalar and pseudoscalar auxiliary fields,  $\sigma$  and  $\boldsymbol{\pi}$ , with the same quantum numbers as the interaction terms in the NJL model, see Eq. (4.46). Following Refs. [178, 179], consider the following Hubbard–Stratonovich transformations which introduce the two previously mentioned auxiliary fields<sup>8</sup>,  $\phi^T = (\sigma, \boldsymbol{\pi})$ :

$$e^{i \int d^4x \frac{\hbar^2}{2m^2} [(\bar{\psi}\psi)^2 + (\bar{\psi} i \gamma_5 \boldsymbol{\tau} \psi)^2]} \propto \int \mathcal{D}\sigma \mathcal{D}\boldsymbol{\pi} \exp \left\{ i \int d^4x \left[ -\frac{m^2}{2} \phi^2 - \hbar \bar{\psi} (\sigma + i \gamma_5 \boldsymbol{\tau} \cdot \boldsymbol{\pi}) \psi \right] \right\}, \quad (4.47)$$

where  $\phi^2 = \sigma^2 + \boldsymbol{\pi}^2$ . Defining the generating functional of the theory and applying the above transformations, alongside the identification,

$$G = \frac{\hbar^2}{m^2}, \quad (4.48)$$

one can define the partially bozonized NJL Lagrangian:

$$\mathcal{L} = \bar{\psi} i \not{\partial} \psi - \hbar \bar{\psi} (\sigma + i \gamma_5 \boldsymbol{\tau} \cdot \boldsymbol{\pi}) \psi - \frac{m^2}{2} \phi^2. \quad (4.49)$$

---

<sup>8</sup>This particular transformation can be obtained by considering the integral,  $\int \mathcal{D}\phi \exp \left\{ -i \int d^4x \frac{m^2}{2} \phi^2 \right\} \propto 1$ , and considering a shift in the field variables as:  $\sigma \rightarrow \sigma + \frac{\hbar}{m^2} \bar{\psi} \psi$  and  $\boldsymbol{\pi} \rightarrow \boldsymbol{\pi} + \frac{\hbar}{m^2} \bar{\psi} i \gamma_5 \boldsymbol{\tau} \psi$ .

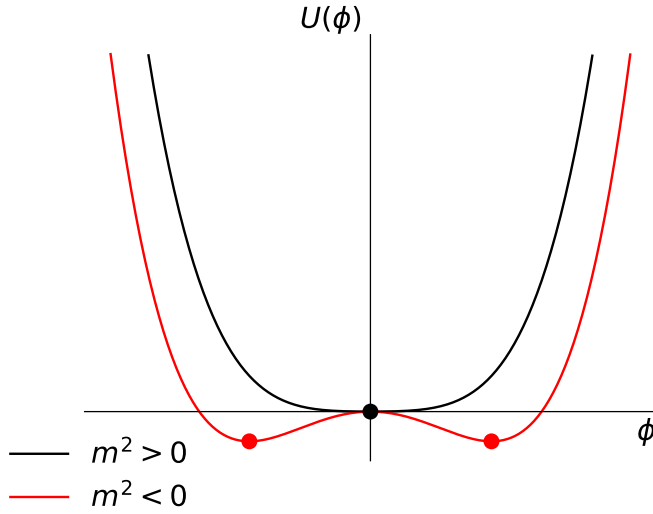


FIGURE 4.1: Sketch of the potential of the Quark-Meson given in Eq. (4.51) as a function of the field  $\phi$ , for two particular values of  $m^2$ :  $m^2 > 0$  (black line) and  $m^2 < 0$  (red line). For positive values of  $m^2$ , the potential only has one minimum, located at  $\phi = 0$ . For  $m^2 < 0$  the potential develops infinite non-vanishing expectation values for the field  $\phi$ , located at  $\phi^2 = -m^2/\lambda_\phi$  [180].

Here,  $\sigma$  and  $\boldsymbol{\pi}$  fields are the auxiliary fields which arise during the bosonization procedure and  $h$  is a Yukawa coupling which measures the strength of the interaction between the quarks and the auxiliary fields. The role of the parameter  $m$  will be discussed later. The generating functional of this theory is now quadratic in the quark fields. However, there is still a path integral over the auxiliary fields to be calculated.

One can maintain the need of the regularization scheme present in the original NJL Lagrangian or, one can introduce kinetic terms for the new fields, send the cutoff to infinity and define a new renormalizable model, the Quark-Meson model (or, equivalently, the linear  $\sigma$ -model coupled to quarks). In this model the previously auxiliary fields introduced to bosonize the NJL Lagrangian are promoted to dynamical fields that will correspond to the lowest mass mesons. One can also add wave function renormalization to the quark,  $Z_\psi$  and meson fields,  $Z_\phi$ . The Quark-Meson model Lagrangian density is then:

$$\mathcal{L} = Z_\psi \bar{\psi} i \not{\partial} \psi - h \bar{\psi} (\sigma + i \gamma_5 \boldsymbol{\tau} \cdot \boldsymbol{\pi}) \psi + \frac{Z_\phi}{2} (\partial_\mu \phi)^2 - U(\phi). \quad (4.50)$$

The potential,  $U(\phi)$ , contains the quadratic contribution,  $m^2 \phi^2/2$ , but can also be generalized to include higher order terms, as long as all the symmetries of the system are respected. An usual choice is,

$$U(\phi) = \frac{m^2}{2} \phi^2 + \frac{\lambda_\phi}{4} \phi^4, \quad (4.51)$$

where  $\lambda_\phi > 0$ . The second order term, proportional to  $m^2$ , dictates the curvature of the potential at the origin. Indeed, if  $m^2 > 0$ , the potential has one minimum at  $\langle \phi \rangle = 0$ . If  $m^2 < 0$  however, the potential has the famous *mexican hat* shape and infinite degenerate minima exist, implying a

non vanishing expectation value for the  $\phi$  field [180]. This behaviour is illustrated in Fig. 4.1 where the potential  $U(\phi)$  is sketched as a function of the field  $\phi$  (see Eq. (4.51)), for two particular values of  $m^2$ :  $m^2 > 0$  (black line) and  $m^2 < 0$  (red line). One can choose a particular vacuum state that preserves isospin symmetry, by fixing  $\langle \boldsymbol{\pi} \rangle = 0$  and getting  $\langle \phi \rangle = \langle \sigma \rangle = \sqrt{-m^2/\lambda_\phi}$ . From the classical Euler–Lagrange equation of motion, one can obtain a linear relation between the quark condensate,  $\langle \bar{\psi}\psi \rangle$ , and the vacuum expectation value of the  $\sigma$  field,  $\langle \sigma \rangle$ . Since the quark condensate acts as an order parameter for chiral symmetry, a non vanishing expectation value for the  $\sigma$  field, implies a non vanishing expectation value for the chiral condensate and chiral symmetry breaking. In the case of  $m^2 < 0$ , the system falls in one of the minima with non vanishing expectation value for the  $\sigma$  field. Thus, the limit  $m^2 \rightarrow 0$  can be understood as a signal of chiral symmetry breaking.

Coming back to the NJL model, and the behaviour of the  $\beta$ –function of the effective action given in Eq. (4.46), one can interpret the divergent scalar-pseudoscalar coupling  $G \rightarrow \infty$ , in the partially bosonized version of the model, as implying  $m^2 \rightarrow 0$  (see Eq. (4.48)), a change of sign, and chiral symmetry breaking [178, 181].

We have reached the conclusion that applying the FRG method directly to the NJL model leads to a naturally diverging coupling in the Renormalization Group flow, that signals spontaneous breaking of chiral symmetry. However, in order to study the behaviour of physical quantities like masses, spectral functions and thermodynamic quantities like pressure, energy density and entropy, after chiral symmetry is already broken, another scheme must be used to apply the FRG to a theory with four-Fermi interactions. This is a recent theoretical challenge and some ways to deal with this problem have been proposed:

- Study the fixed point structure of the four-Fermi coupling (or its inverse) will yield knowledge on the onset of chiral symmetry because one only has information on the curvature of the potential [116, 175, 178, 182]. Still, it will not grant access to the order of the phase transition and physical observables due to its diverging nature.
- A very recent approach proposed by some authors lies in the so-called Weak field method [183–186]. In this method a different approach to the Functional Renormalization Group in the form of the Wegner–Houghton equation is used [187]. The solution of the Renormalization Group equation with singularities that arises from this method is called the “weak” solution. The authors claim that this method is able not only to resolve the order of the transition as well to evaluate the dynamical mass and chiral condensate [184].
- From the partially bosonized Lagrangian density in Eq. (4.49) one can define the Quark-Meson model. The FRG can be applied to this model where the scale dependence is imposed in the effective potential (LPA). This method has been successfully used to study the QCD phase diagram in both two and three flavours, as well as used to compute spectral functions through an analytical continuation to imaginary time [188–190]. This strategy is widely used in the literature because it leads to relatively simple flow equation. However, more recently, it was also found that the application of the FRG to the two flavour QM model leads to an unphysical behaviour at low temperatures and high chemical potentials:

the existence of a region of negative entropy density near the first-order phase transition of the model which is not well understood [191].

# PART II

Studies in the mean field approximation



## Chapter 5

# The strange CEP and isentropic trajectories in the PNJL model

### 5.1 Introduction

In this chapter, we explore different vacuum parameter sets for an extended PNJL model with 't Hooft determinant and eight-quark interactions in the up, down and strange sectors. Besides, we also study the possible existence of several CEPs in the phase diagram of strongly interacting matter and the isentropic trajectories crossing both (light and strange) chiral phase transitions and around the CEP in both the crossover and first-order transition regions.

Along the lines of previous works where isentropic trajectories were studied (see [73, 76, 192, 193]) here we analyse the effect upon these of the inclusion of eight-quark interactions. Furthermore, contrarily to previous works, where a heat kernel expansion was used to derive the meson spectra (see [62–64, 194]), here we use a standard approach of expanding the Lagrangian to second order in the fields.

In HIC, the evolution of the fireball is accepted to be a hydrodynamic expansion of an ideal fluid thus being an isentropic process. This means that it will follow trajectories of constant entropy per baryon,  $s/\rho_B$  (the so-called isentropes), in the phase diagram. For AGS<sup>1</sup>, SPS, and RHIC, the values of  $s/\rho_B$  that can be explored in these experiments are 30, 45, and 300, respectively [195, 196]. Lattice QCD simulations for the isentropic (2+1)-flavour equation of state (EoS) at these values of  $s/\rho_B$  were presented in [197, 198].

The chapter is organized as follows. In Section 5.2 the extended PNJL model with eight-quark interactions is formally introduced. The Lagrangian is expanded to first order in quark bilinear operators to give access to the thermodynamical potential in the mean field approximation. The Lagrangian is also expanded to second order to yield the so-called meson projectors, used to calculate the meson masses. In Section 5.3 we present different parameter sets including eight-quark interactions which are used to build different scenarios for the phase diagram. The isentropic trajectories are also presented and analysed with and without an extra term in the

---

<sup>1</sup>Alternating Gradient Synchrotron.

grand canonical potential which accounts for high momentum modes. Finally, in Section 5.4 conclusions are drawn.

## 5.2 Model and formalism

The Lagrangian density of the  $SU(3)_f$  PNJL model including four, six and eight-quark interactions can be written as [124, 125]:

$$\begin{aligned}
\mathcal{L} = & \bar{\psi}(i\not{D} - \hat{m})\psi + \frac{G}{2} \left[ (\bar{\psi}\lambda_a\psi)^2 + (\bar{\psi}i\gamma^5\lambda_a\psi)^2 \right] \\
& + 8\kappa \left[ \det(\bar{\psi}P_R\psi) + \det(\bar{\psi}P_L\psi) \right] \\
& + 16g_1 \left[ (\bar{\psi}_i P_R \psi_j) (\bar{\psi}_j P_L \psi_i) \right]^2 \\
& + 16g_2 \left[ (\bar{\psi}_i P_R \psi_j) (\bar{\psi}_j P_L \psi_k) (\bar{\psi}_k P_R \psi_l) (\bar{\psi}_l P_L \psi_i) \right] \\
& - \mathcal{U}(\Phi, \bar{\Phi}; T).
\end{aligned} \tag{5.1}$$

Here,  $\psi$  is a 3-component vector in flavour space and  $\hat{m} = \text{diag}(m_u, m_d, m_s)$  is the quark current mass matrix and  $P_{R/L}$ , are the chiral projection operators, defined as:  $P_{R/L} = (1 \pm \gamma_5)/2$ . In this model the quark field is minimally coupled to a background gluonic field in the time direction,  $A^0 = g\mathcal{A}_a^0 \frac{\lambda_a}{2}$  through the covariant derivative,  $D^\mu = \partial^\mu - i\delta_0^\mu A^0$ ,  $A_0 = -iA_4$  and  $\mathcal{U}(\Phi, \bar{\Phi}; T)$  is the effective glue potential parametrized by the Polyakov loop (see Eq. (3.1)), as already mentioned in Chapter 4.1.1.

In the interaction terms,  $\lambda^a$  ( $a = 1, 2, \dots, 8$ ) are the Gell-Mann matrices of the  $SU(3)$  group and  $\lambda^0 = \sqrt{2/3}\mathbb{1}$ . The implicit sum and the determinant are to be carried out over flavour space. Finite density effects can be considered by including, in the Lagrangian density, the term  $\bar{\psi}\gamma^0\hat{\mu}\psi$ , with  $\hat{\mu} = \text{diag}(\mu_u, \mu_d, \mu_s)$  the chemical potential matrix.

The model defined in Eq. (5.1) includes the usual four-quark scalar and pseudoscalar interaction ( $G$ ), the 't Hooft determinant interaction (introduced to break the  $U_A(1)$  symmetry) and the most general spin-zero and chirally symmetry preserving interactions scalar and pseudoscalar eight-quark [124, 125]. We highlight that the first eight-quark interaction term, with the  $g_1$  coupling constant, exhibits OZI violating effects. The details about multi-quark interactions, were given in Chapter 4.1.

The inclusion of eight-quark interactions stabilizes the mean field vacuum of the model. This is only true, if the couplings  $G$ ,  $\kappa$ ,  $g_1$  and  $g_2$  respect certain stability conditions. These stability conditions were determined in [124] at mean field level by analysing the gap equation of the model and, for the Lagrangian density defined in Eq.(5.1), are given by:

$$g_1 > 0, \tag{5.2}$$

$$2g_1 + 3g_2 > 0, \tag{5.3}$$

$$Gg_1 - \frac{\kappa^2}{8} > 0. \tag{5.4}$$

In this chapter we will use the following polynomial potential [127]:

$$\frac{\mathcal{U}(\Phi, \bar{\Phi}; T)}{T^4} = -\frac{b_2(T)}{2}\bar{\Phi}\Phi - \frac{b_3}{6}(\Phi^3 + \bar{\Phi}^3) + \frac{b_4}{4}(\bar{\Phi}\Phi)^2, \quad (5.5)$$

$$b_2(T) = a_0 + a_1\left(\frac{T_0}{T}\right) + a_2\left(\frac{T_0}{T}\right)^2 + a_3\left(\frac{T_0}{T}\right)^3. \quad (5.6)$$

Here,  $a_0 = 6.75$ ,  $a_1 = -1.95$ ,  $a_2 = 2.625$ ,  $a_3 = -7.44$ ,  $b_3 = 0.75$  and  $b_4 = 7.5$  obtained with  $T_0 = 270$  MeV to reproduce lattice QCD data in the pure gauge sector [127]. We opted to use this simple form of the Polyakov potential so as to better isolate the effect of eight-quark interactions. Furthermore, it should be noticed that in our implementation of the thermodynamical potential, with the additional term to account for the high momentum modes (see below for discussion) the problem of the incorrect asymptotic value for the Polyakov loop does not occur [159].

We introduce the auxiliary scalar,  $s_a$ , and pseudoscalar field variables,  $p_a$ , written in terms of quark bilinear operators,  $s_a = \bar{\psi}\lambda_a\psi$  and  $p_a = \bar{\psi}i\gamma^5\lambda_a\psi$ , with indices  $a = 0, 1, 2, \dots, 8$ . One can now write the original Lagrangian density given in Eq. (5.1) using these new variables. In the following, we will use several results obtained in detail in Appendices B.1 and B.2.

The four-quark scalar-pseudoscalar interaction,  $\mathcal{L}_4$ , written in terms of  $s_a$  and  $p_a$  can be obtained by substitution:

$$\begin{aligned} \mathcal{L}_4 &= \frac{G}{2} \left[ (\bar{\psi}\lambda_a\psi)^2 + (\bar{\psi}i\gamma^5\lambda_a\psi)^2 \right] \\ &= \frac{G}{2} (s_a^2 + p_a^2). \end{aligned} \quad (5.7)$$

The remaining interaction terms are written in terms of the matrix elements of  $\bar{\psi}P_{R/L}\psi$ . Defining  $s = s_a\lambda_a$ ,  $p = p_a\lambda_a$  and using the relation (B.19), these matrix elements can be written as:

$$(s)_{kl} = s_a(\lambda_a)_{kl} = \bar{\psi}_i\psi_j(\lambda_a)_{ij}(\lambda_a)_{kl} = \bar{\psi}_i\psi_j 2\delta_{il}\delta_{kj} = 2\bar{\psi}_l\psi_k, \quad (5.8)$$

$$(p)_{kl} = p_a(\lambda_a)_{kl} = \bar{\psi}_i i\gamma^5\psi_j(\lambda_a)_{ij}(\lambda_a)_{kl} = \bar{\psi}_i i\gamma^5\psi_j 2\delta_{il}\delta_{kj} = 2\bar{\psi}_l i\gamma^5\psi_k. \quad (5.9)$$

The 't Hooft determinant interaction,  $\mathcal{L}_6$ , is the third term in Eq. (5.1), and it is defined as:

$$\mathcal{L}_6 = 8\kappa \left[ \det(\bar{\psi}P_R\psi) + \det(\bar{\psi}P_L\psi) \right]. \quad (5.10)$$

Applying Eqs. (5.8), (5.9) and relation (B.23), we can write:

$$\begin{aligned} \det(\bar{\psi}P_{R/L}\psi) &= \det\left(\frac{\bar{\psi}_i\psi_j}{2} \pm \frac{\bar{\psi}_i\gamma^5\psi_j}{2}\right) \\ &= \det\left(\frac{s}{4} \mp i\frac{p}{4}\right) \\ &= \frac{1}{4^3} A_{abc} (s_a \mp ip_a)(s_b \mp ip_b)(s_c \mp ip_c) \\ &= \frac{1}{4^3} A_{abc} (s_a s_b s_c \pm ip_a p_b p_c \mp 3ip_a s_b s_c - 3s_a p_b p_c). \end{aligned} \quad (5.11)$$

Where the quantity  $A_{abc}$  was derived in detail in Appendix B.2, and it is explicitly given by:

$$A_{abc} = \frac{2}{3}d_{abc} + \sqrt{\frac{2}{3}}(\delta_{a0}\delta_{b0}\delta_{c0} - \delta_{a0}\delta_{bc} - \delta_{b0}\delta_{ca} - \delta_{c0}\delta_{ab}). \quad (5.12)$$

Here,  $d_{abc}$  are the symmetric structure constants of the special unitary group  $SU(3)$ . Using this result, we can finally write:

$$\begin{aligned} \mathcal{L}_6 &= \frac{16\kappa}{4^3}A_{abc}s_a(s_b s_c - 3p_b p_c) \\ &= \frac{\kappa}{4}A_{abc}s_a(s_b s_c - 3p_b p_c). \end{aligned} \quad (5.13)$$

Using Eqs. (5.8), (5.9), the OZI violating eight-quark interaction,  $\mathcal{L}_8^{(1)}$  (proportional to  $g_1$ ), can be written as:

$$\begin{aligned} \mathcal{L}_8^{(1)} &= 16g_1 \left[ (\bar{\psi}_i P_R \psi_j) (\bar{\psi}_j P_L \psi_i) \right]^2 \\ &= \frac{16g_1}{4^4} [\text{tr}(s - ip)(s + ip)]^2 \\ &= \frac{16g_1}{4^4} [\text{tr}(s^2 + p^2)]^2 \\ &= \frac{16g_1}{4^4} [(s_a s_b + p_a p_b) \text{tr}(\lambda_a \lambda_b)]^2 \\ &= \frac{g_1}{4} [(s_a^2 + p_a^2)]^2. \end{aligned} \quad (5.14)$$

Where we applied Eq. (B.2), to calculate the trace between two Gell-Mann matrices. Likewise, the non-OZI violating eight-quark interaction,  $\mathcal{L}_8^{(2)}$  (proportional to  $g_2$ ), is given by:

$$\begin{aligned} \mathcal{L}_8^{(2)} &= 16g_2 \left[ (\bar{\psi}_i P_R \psi_j) (\bar{\psi}_j P_L \psi_k) (\bar{\psi}_k P_R \psi_l) (\bar{\psi}_l P_L \psi_i) \right] \\ &= \frac{16g_2}{4^4} [\text{tr}(s - ip)(s + ip)(s - ip)(s + ip)]^2 \\ &= \frac{16g_2}{4^4} [\text{tr}(s^4 + p^4 + 4s^2 p^2 - 2s p s p)]^2 \\ &= \frac{16g_2}{4^4} [(s_a s_b s_c s_d + p_a p_b p_c p_d + 4s_a s_b p_c p_d - 2s_a p_b s_c p_d) \text{tr}(\lambda_a \lambda_b \lambda_c \lambda_d)]^2 \\ &= \frac{g_2}{8} [d_{abe} d_{cde} (s_a s_b s_c s_d + 2s_a s_b p_c p_d + p_a p_b p_c p_d) + 4f_{abe} f_{cde} s_a p_b s_c p_d]. \end{aligned} \quad (5.15)$$

Here, we have used Eq. (B.20) to calculate the trace of four Gell-Mann matrices and several properties of the symmetric ( $d_{abc}$ ) and antisymmetric constants ( $f_{abc}$ ) of the  $U(3)$  algebra, including the Jacobi identity that is given in Eq. (B.11).

Using these results, we can write the extended  $SU(3)$  NJL Lagrangian in terms of quark bilinear operators,  $s_a = \bar{\psi}\lambda_a\psi$  and  $p_a = \bar{\psi}i\gamma^5\lambda_a\psi$  as:

$$\begin{aligned} \mathcal{L} = & \bar{\psi}(i\not{D} - \hat{m})\psi + \frac{G}{2}(s_a^2 + p_a^2) \\ & + \frac{\kappa}{4}A_{abc}s_a(s_b s_c - 3p_b p_c) \\ & + \frac{g_1}{4}(s_a^2 + p_a^2)^2 \\ & + \frac{g_2}{8}[d_{abc}d_{cde}(s_a s_b s_c s_d + 2s_a s_b p_c p_d + p_a p_b p_c p_d) + 4f_{abc}f_{cde}s_a p_b s_c p_d] \\ & - \mathcal{U}(\Phi, \bar{\Phi}; T). \end{aligned} \quad (5.16)$$

Once again,  $f_{abc}$  and  $d_{abc}$  are the totally antisymmetric and symmetric structure constants of the special unitary group  $SU(3)$ , respectively and the constants  $A_{abc}$  are defined in Eq. (5.12) (see the Appendices B.1 and B.2 for more details).

### 5.2.1 Thermodynamics

Using the Lagrangian density given in Eq. (5.1), one can calculate the generating functional of the theory and relate it to the grand canonical potential, in order to study thermodynamical properties of the model. The presence of more than two quark interactions at the Lagrangian level renders an exact integration of the quark fields, impossible. In order to derive the thermodynamical potential of the model we consider the MF approximation. In this approximation, all quark interactions are transformed into quadratic interactions by introducing auxiliary fields whose quantum fluctuations are neglected and only the classical configuration contributes to the path integral i.e., the functional integration is dominated by the stationary point. A quark bilinear operator,  $\hat{\mathcal{O}}$ , can be written as its mean field value plus a small perturbation,  $\hat{\mathcal{O}} = \langle \hat{\mathcal{O}} \rangle + \delta\hat{\mathcal{O}}$ . To linearise the product of  $N$ -operators, terms superior to  $(\delta\hat{\mathcal{O}})^2$  must be neglected. Conveniently, the linear product between  $N = n + 1$  operators can be written using the following formula<sup>2</sup>:

$$\prod_{i=1}^{n+1} \hat{\mathcal{O}}_i = \left[ \sum_{i=1}^{n+1} \frac{\hat{\mathcal{O}}_i}{\langle \hat{\mathcal{O}}_i \rangle} - n \right] \prod_{j=1}^{n+1} \langle \hat{\mathcal{O}}_j \rangle. \quad (5.17)$$

After the linear expansion of the quark bilinear operators, the now quadratic Lagrangian in the quark fields can be written as the one of fermions in a mean field potential with effective masses and chemical potentials. Using the results provided in the Appendix D, one can use the Matsubara formalism [199], to calculate the mean field grand canonical potential,  $\Omega$ , for the  $SU(3)$  PNJL model within the 3-momentum regularization scheme, at finite temperature and chemical potential, for the  $N_c = 3$  case. It is given by:

$$\Omega(T, \mu) = \Omega_0 + U + \mathcal{U}(\Phi, \bar{\Phi}; T) + C(T, \mu) - 6 \sum_i \int_0^\Lambda \frac{d^3p}{(2\pi)^3} [E_i + \mathcal{F}(T, \mu_i) + \mathcal{F}^*(T, \mu_i)]. \quad (5.18)$$

<sup>2</sup>This formula can be proved by induction. See Appendix C.1 for the proof.

with the sum made over  $i = \{u, d, s\}$ . The potential  $U$  and the thermal functions  $\mathcal{F}(T, \mu_i)$  and  $\mathcal{F}^*(T, \mu_i)$ , defined as:

$$U = G \sum_i \sigma_i^2 + 4\kappa \prod_i \sigma_i + 3g_1 \left( \sum_i \sigma_i^2 \right)^2 + 3g_2 \sum_i \sigma_i^4, \quad (5.19)$$

$$\mathcal{F}(T, \mu_i) = T \ln \left[ 1 + 3\bar{\Phi} e^{-\frac{1}{T}(E_i - \mu_i)} + 3\Phi e^{-\frac{2}{T}(E_i - \mu_i)} + e^{-\frac{3}{T}(E_i - \mu_i)} \right], \quad (5.20)$$

$$\mathcal{F}^*(T, \mu_i) = T \ln \left[ 1 + 3\Phi e^{-\frac{1}{T}(E_i + \mu_i)} + 3\bar{\Phi} e^{-\frac{2}{T}(E_i + \mu_i)} + e^{-\frac{3}{T}(E_i + \mu_i)} \right]. \quad (5.21)$$

with  $E_i = \sqrt{p^2 + M_i^2}$  and  $\langle \bar{\psi}_i \psi_i \rangle = \sigma_i$  the quark condensate. The constant  $\Omega_0$  is the thermodynamical potential in the vacuum,  $\Omega_0 = \Omega(T = 0, \mu = 0)$ , ensuring that the vacuum pressure is zero. The nature, relevance and mathematical definition of the  $C(T, \mu)$  term will be discussed later.

For  $i \neq j \neq k \in \{u, d, s\}$ , the  $i$ -quark effective mass,  $M_i$ , is given by the gap equation:

$$M_i = m_i - 2G\sigma_i - 2\kappa\sigma_j\sigma_k - 4g_1\sigma_i \sum_j \sigma_j^2 - 4g_2\sigma_i^3. \quad (5.22)$$

Minimizing the thermodynamic potential with respect to  $\sigma_i$ ,  $\Phi$ ,  $\bar{\Phi}$ ,

$$\frac{\partial \Omega}{\partial \sigma_i} = \frac{\partial \Omega}{\partial \Phi} = \frac{\partial \Omega}{\partial \bar{\Phi}} = 0, \quad (5.23)$$

we can determine the value of these quantities for a given temperature and chemical potential.

Consider the stationary condition applied to the quark condensate,  $\sigma_i$ . It can be written as:

$$\frac{\partial \Omega}{\partial \sigma_i} = \frac{\partial \Omega(\sigma_i)}{\partial \sigma_i} + \sum_i \frac{\partial \Omega(M_i)}{\partial M_i} \frac{\partial M_i(\sigma_i)}{\partial \sigma_i} = 0. \quad (5.24)$$

The simplest way to apply the stationary condition above and derive an equation for  $\sigma_i$ , is to consider the simpler PNJL model with  $\kappa = g_1 = g_2 = 0$ . For such model there is no flavour mixing, and the effective mass of a particular quark only depends on itself:  $M_i = m_i - 2G\sigma_i$ . In such simple scenario, we can write:

$$\frac{\partial \Omega(\sigma_i)}{\partial \sigma_i} = \frac{\partial U(\sigma_i)}{\partial \sigma_i} = 2G \sum_i \sigma_i, \quad (5.25)$$

$$\frac{\partial M_i(\sigma_i)}{\partial \sigma_i} = -2G, \quad (5.26)$$

$$\frac{\partial \Omega(M_i)}{\partial M_i} = -2N_c \int \frac{d^3p}{(2\pi)^3} \frac{M_i}{E_i} (1 - \nu_i - \bar{\nu}_i) = I_i. \quad (5.27)$$

Here,  $\nu_i$  and  $\bar{\nu}_i$  are the particle and antiparticle occupation numbers in the PNJL model:

$$\nu_i = \frac{e^{-3(E_i - \mu_i)/T} + \bar{\Phi}e^{-(E_i - \mu_i)/T} + 2\Phi e^{-2(E_i - \mu_i)/T}}{1 + e^{-3(E_i - \mu_i)/T} + 3\bar{\Phi}e^{-(E_i - \mu_i)/T} + 3\Phi e^{-2(E_i - \mu_i)/T}}, \quad (5.28)$$

$$\bar{\nu}_i = \frac{e^{-3(E_i + \mu_i)/T} + \Phi e^{-(E_i + \mu_i)/T} + 2\bar{\Phi}e^{-2(E_i + \mu_i)/T}}{1 + e^{-3(E_i + \mu_i)/T} + 3\Phi e^{-(E_i + \mu_i)/T} + 3\bar{\Phi}e^{-2(E_i + \mu_i)/T}}. \quad (5.29)$$

Using these results, we can write the stationary relation for the model with  $\kappa = g_1 = g_2 = 0$  as:

$$\frac{\partial \Omega}{\partial \sigma_i} = 2G \sum_i [\sigma_i - I_i] = 0. \quad (5.30)$$

For non-zero  $G$  the above equation only holds, if and only if,  $\sigma_i = I_i$ . Hence the  $i$ -flavour quark condensate,  $\langle \bar{\psi}_i \psi_i \rangle = \sigma_i$ , is then given by ( $N_c = 3$ ):

$$\sigma_i = \langle \bar{\psi}_i \psi_i \rangle = -2N_c \int \frac{d^3p}{(2\pi)^3} \frac{M_i}{E_i} (1 - \nu_i - \bar{\nu}_i). \quad (5.31)$$

For non-zero  $\kappa$ ,  $g_1$  and  $g_2$  the process is identical, but more algebra is involved due to the flavour mixing. However, it yields exactly the same result for  $\sigma_i$ .

The gap equations for the Polyakov loop fields,  $\Phi$  and  $\bar{\Phi}$ , can be directly applied to yield:

$$T^3 \left[ -\frac{b_2(T)}{2} \bar{\Phi} - \frac{b_3(T)}{2} \Phi^2 + \frac{b_4(T)}{2} \Phi \bar{\Phi}^2 \right] = 6 \sum_i \int \frac{d^3p}{(2\pi)^3} \left[ \frac{e^{-(E_i + \mu_i)/T}}{e^{\mathcal{F}^*(\mathbf{p}, T, \mu_i)/T}} + \frac{e^{-2(E_i - \mu_i)/T}}{e^{\mathcal{F}(\mathbf{p}, T, \mu_i)/T}} \right], \quad (5.32)$$

$$T^3 \left[ -\frac{b_2(T)}{2} \Phi - \frac{b_3(T)}{2} \bar{\Phi}^2 + \frac{b_4(T)}{2} \Phi^2 \bar{\Phi} \right] = 6 \sum_i \int \frac{d^3p}{(2\pi)^3} \left[ \frac{e^{-(E_i - \mu_i)/T}}{e^{\mathcal{F}(\mathbf{p}, T, \mu_i)/T}} + \frac{e^{-2(E_i + \mu_i)/T}}{e^{\mathcal{F}^*(\mathbf{p}, T, \mu_i)/T}} \right]. \quad (5.33)$$

In the  $T = 0$  limit, the PNJL grand canonical potential reduces to the usual NJL model. Indeed, in this limit, the Polyakov loop potential and the thermal function  $\mathcal{F}^*$  vanish while the function  $\mathcal{F}$  becomes a step-function<sup>3</sup>. We draw attention to the fact that this feature is a consequence of the definition of the Polyakov loop potential in Eq. (5.5). Actually, one can try to build a different Polyakov loop potential that does not vanish in the  $T \rightarrow 0$  limit by including, for example, an explicit dependence in the chemical potential. Of course, such a modified potential would have to respect the  $Z(N_c)$  of QCD, as well as, reproduce lattice observables.

Finally, we will analyse the temperature and chemical potential dependent term,  $C(T, \mu)$ , in the grand canonical potential (Eq. (5.18)) that is defined as (for the  $N_c = 3$  case):

$$C(T, \mu) = -6 \sum_i \int_{\Lambda}^{\infty} \frac{d^3p}{(2\pi)^3} T \ln \left[ 1 + e^{-(|p| + \mu_i)/T} \right] - 6 \sum_i \int_{\Lambda}^{\infty} \frac{d^3p}{(2\pi)^3} T \ln \left[ 1 + e^{-(|p| - \mu_i)/T} \right]. \quad (5.34)$$

Here,  $\mu$  is the quark chemical potential. This contribution represents an additional pressure of massless quarks coming from the thermodynamics of the high momentum modes, with

<sup>3</sup>The limits of the thermal functions (5.20) and (5.21) are:  $\lim_{T \rightarrow 0} \mathcal{F}(T, \mu_i) = 3(\mu_i - E_i)H(\mu_i - E_i)$  and  $\lim_{T \rightarrow 0} \mathcal{F}^*(T, \mu_i) = 0$ . Here  $H(\mu_i - E_i)$  is the Heaviside step function defined in Eq. (A.1). Using these results yields the thermodynamical potential for the  $N_c = 3$  NJL model at zero temperature.

$|\mathbf{p}| > \Lambda$ . These higher momentum modes are missing from the regularized PNJL grand canonical potential, where all integrations are limited to the cutoff,  $\Lambda$ . Adding such a contribution to the thermodynamics is essential to get the correct high-temperature behaviour of the thermodynamics in effective models [200, 201].

Indeed, by deriving the grand canonical potential of the model by integration of the gap equations, such contribution appears naturally [159]. In such case, when integrating the gap equations over the squared mass from 0 to  $M_i^2$  (with  $M_i$  the dynamical mass of the quark of flavour  $i$ ) a subtraction of the thermal functions evaluated at zero mass appears. This procedure can be viewed as the model dependent determination of how much we are deviated from the massless case (as such both the thermal functions at  $M_i$  and the zero mass subtraction should be regularized). In order to reproduce the correct thermodynamic behaviour we should add the baseline of the pressure of a gas of massless non interacting fermions. As this baseline is model independent it should not be regularized. In the particular case of the 3-momentum cutoff this results in the cancellation of the massless parts only up to the cutoff thus originating the additional term.

The thermodynamical quantities are determined via the thermodynamical potential (see [143]). The pressure is given by  $P(T, \mu) - P_0 = -\Omega(T, \mu)$  (with  $P_0$  the pressure in the vacuum) while the density of the  $i$ -quark,  $\rho_i(T, \mu)$ , and the entropy density,  $s(T, \mu)$ , are derived from the pressure using Eqs. (A.15) and (A.16), explicitly given by:

$$\begin{aligned}\rho_i(T, \mu) &= - \left( \frac{\partial \Omega(T, \mu)}{\partial \mu_i} \right)_T, \\ s(T, \mu) &= - \left( \frac{\partial \Omega(T, \mu)}{\partial T} \right)_\mu.\end{aligned}$$

The baryonic density,  $\rho_B$ , is given by  $\rho_B = (\rho_u + \rho_d + \rho_s)/3$ , with  $\rho_u$ ,  $\rho_d$  and  $\rho_s$  the densities of the up, down and strange quarks, respectively.

### 5.2.2 Meson masses

In the NJL model we assume that mesons can be described as pairs of quark-antiquark states. The meson masses can be calculated by writing an effective Lagrangian, built by expanding the Lagrangian in Eq. (5.16), up to second order in auxiliary meson fields introduced in the so-called bosonization procedure [202]. Following the linear expansion of the Lagrangian, to build the quadratic expansion, terms superior to  $(\delta\hat{\mathcal{O}})^3$  are neglected. More easily, the quadratic product between  $N = n + 2$  operators, with  $n \geq 1$ , can be written using the following formula<sup>4</sup>:

$$\prod_{i=1}^{n+2} \hat{\mathcal{O}}_i = \left[ \frac{1}{2} \sum_{i=1}^{n+2} \sum_{j=1}^{n+2} \frac{\hat{\mathcal{O}}_i}{\langle \hat{\mathcal{O}}_i \rangle} \frac{\hat{\mathcal{O}}_j}{\langle \hat{\mathcal{O}}_j \rangle} (1 - \delta_{ij}) - n \sum_{i=1}^{n+2} \frac{\hat{\mathcal{O}}_i}{\langle \hat{\mathcal{O}}_i \rangle} + \frac{n}{2}(n+1) \right] \prod_{k=1}^{n+2} \langle \hat{\mathcal{O}}_k \rangle. \quad (5.35)$$

<sup>4</sup>This formula can be proved by induction. See Appendix C.2 for the proof.

Following this approach, one can write an effective action,  $\mathcal{S}_{\text{eff}}$ , where all the interactions are written in terms of quadratic quark bilinear operators (fourth order terms in the quark fields):

$$\mathcal{S}_{\text{eff}}[\bar{\psi}, \psi] = \int d^4x \left[ \bar{\psi}(i\mathcal{D} - \hat{m})\psi + \frac{1}{2}s_a S_{ab}s_b + \frac{1}{2}p_a P_{ab}p_b - \mathcal{U}(\Phi, \bar{\Phi}; T) \right] + O(s^0, p^0, s, p, sp). \quad (5.36)$$

Here, the contribution  $O(s^0, p^0, s, p, sp)$ , includes terms that are proportional to zero order and first order in the auxiliary variables  $s_a^{0,1}$  and  $p_a^{0,1}$  and also mixed quadratic terms, proportional to  $s_a p_b$ . For our purposes this contribution will be neglected. The so-called pseudoscalar and scalar meson projectors,  $P_{ab}$  and  $S_{ab}$ , including four, six and eight-quark interactions, are given by:

$$\begin{aligned} P_{ab} = & G\delta_{ab} - \frac{3\kappa}{2}A_{abc} \langle s_c \rangle + g_1[\delta_{ab} \langle p_c \rangle \langle p_c \rangle + 2 \langle p_a \rangle \langle p_b \rangle + \delta_{ab} \langle s_c \rangle \langle s_c \rangle] \\ & + \frac{g_2}{2}[(d_{abe}d_{cde} + d_{ace}d_{bde} + d_{ade}d_{cbe}) \langle p_c \rangle \langle p_d \rangle + (d_{abe}d_{cde} + 2f_{dbe}f_{cae}) \langle s_c \rangle \langle s_d \rangle], \end{aligned} \quad (5.37)$$

$$\begin{aligned} S_{ab} = & G\delta_{ab} + \frac{3\kappa}{2}A_{abc} \langle s_c \rangle + g_1[\delta_{ab} \langle s_c \rangle \langle s_c \rangle + 2 \langle s_a \rangle \langle s_b \rangle + \delta_{ab} \langle p_c \rangle \langle p_c \rangle] \\ & + \frac{g_2}{2}[(d_{abe}d_{cde} + d_{ace}d_{bde} + d_{ade}d_{cbe}) \langle s_c \rangle \langle s_d \rangle + (d_{abe}d_{cde} + 2f_{dbe}f_{cae}) \langle p_c \rangle \langle p_d \rangle]. \end{aligned} \quad (5.38)$$

Here,  $\langle s_a \rangle = \langle \bar{\psi}\lambda_a\psi \rangle$  and  $\langle p_a \rangle = \langle \bar{\psi}i\gamma^5\lambda_a\psi \rangle$  i.e., the mean field values of the scalar and pseudoscalar quark bilinear operators.

The generating functional for the system, can be written as<sup>5</sup>:

$$\mathcal{Z}_{\text{eff}}[\eta, \bar{\eta}] \propto \int \mathcal{D}\bar{\psi}\mathcal{D}\psi \exp \left\{ i\mathcal{S}_{\text{eff}}[\bar{\psi}, \psi] + i \int d^4x (\bar{\psi}\eta + \bar{\eta}\psi) \right\}. \quad (5.39)$$

In order to integrate out the quark fields, one can bosonize the theory. This can be accomplished by introducing the auxiliary meson fields,  $\sigma_a$  and  $\pi_a$ , using the Hubbard–Stratonovich transformation:

$$\exp \left\{ i \int d^4x \frac{1}{2}s_a S_{ab}s_b \right\} \propto \int \mathcal{D}\sigma_a \mathcal{D}\sigma_b \exp \left\{ i \int d^4x \left[ -\frac{1}{2}\sigma_a S_{ab}^{-1}\sigma_b - s_a\sigma_a \right] \right\}, \quad (5.40)$$

$$\exp \left\{ i \int d^4x \frac{1}{2}p_a P_{ab}p_b \right\} \propto \int \mathcal{D}\pi_a \mathcal{D}\pi_b \exp \left\{ i \int d^4x \left[ -\frac{1}{2}\pi_a P_{ab}^{-1}\pi_b - p_a\pi_a \right] \right\}. \quad (5.41)$$

We recall that  $s_a = \bar{\psi}\lambda_a\psi$  and  $p_a = \bar{\psi}i\gamma^5\lambda_a\psi$ . Neglecting the contributions from  $O(s^0, p^0, s, p, sp)$ , we can use this exact transformation to write the generating functional as (omitting source

---

<sup>5</sup>In general, there should also be a path integral over the gluonic degrees of freedom that are included in the Polyakov loop. In our case however, we consider that those degrees of freedom were already integrated out to yield an effective Lagrangian written in terms of the Polyakov loop and its adjoint. For instance, in Ref. [203], the diagonal matrices of the  $SU(3)_c$  algebra were used to represent the Polyakov loop and its adjoint in the path integral. The non-diagonal matrices are integrated out to yield the Haar measure and, after applying a mean field approximation to the diagonal matrices, one can recover a model very similar to the PNJL.

terms):

$$\mathcal{Z}_{\text{eff}} \propto \int \mathcal{D}\bar{\psi}\mathcal{D}\psi\mathcal{D}\sigma_a\mathcal{D}\sigma_b\mathcal{D}\pi_a\mathcal{D}\pi_b \exp \left\{ i \int d^4x \left[ \bar{\psi}(i\mathcal{D} - \hat{m} - \lambda_a\sigma_a - i\gamma_5\lambda_a\pi_a)\psi - \frac{1}{2}\sigma_a S_{ab}^{-1}\sigma_b - \frac{1}{2}\pi_a P_{ab}^{-1}\pi_b - \mathcal{U}(\Phi, \bar{\Phi}; T) \right] \right\}. \quad (5.42)$$

Since the action is quadratic in the fermion fields, one can integrate out the quark fields to get:

$$\mathcal{Z}_{\text{eff}} \propto \int \mathcal{D}\sigma_a\mathcal{D}\sigma_b\mathcal{D}\pi_a\mathcal{D}\pi_b \exp \left\{ \text{tr} \ln (i\mathcal{D} - \hat{m} - \lambda_a\sigma_a - i\gamma_5\lambda_a\pi_a) + i \int d^4x \left[ -\frac{1}{2}\sigma_a S_{ab}^{-1}\sigma_b - \frac{1}{2}\pi_a P_{ab}^{-1}\pi_b - \mathcal{U}(\Phi, \bar{\Phi}; T) \right] \right\}. \quad (5.43)$$

We are now able to expand the action to second order in the auxiliary meson fields  $\sigma_a$  and  $\pi_a$ , in order to obtain the propagators of the auxiliary meson fields. In Eq. (5.43), the terms proportional to  $S_{ab}^{-1}$  and  $P_{ab}^{-1}$  are already second order in the auxiliary meson fields. Expanding the fermion determinant to second order in  $\sigma_a$  and  $\pi_a$  and using the series expansion of the logarithm, one can identify the following quadratic contribution to the effective action (in momentum space):

$$\mathcal{S}_{\text{eff}} = \int \frac{d^4q}{(2\pi)^4} \left[ -\frac{1}{2}\sigma_a(q) \left[ S_{ab}^{-1} - \Pi_{ab}^S(q) \right] \sigma_b(q) - \frac{1}{2}\pi_a(q) \left[ P_{ab}^{-1} - \Pi_{ab}^P(q) \right] \pi_b(q) \right] + \dots \quad (5.44)$$

Here  $\Pi_{ab}^S$  is the scalar polarization operator and  $\Pi_{ab}^P$  is the pseudoscalar polarization operator. They are defined by:

$$\Pi_{ab}^S(q) = iN_c \int \frac{d^4p}{(2\pi)^4} \text{tr} \left[ \frac{1}{\not{p} - \hat{M}} \lambda_a \frac{1}{\not{p} + \not{q} - \hat{M}} \lambda_b \right], \quad (5.45)$$

$$\Pi_{ab}^P(q) = iN_c \int \frac{d^4p}{(2\pi)^4} \text{tr} \left[ \frac{1}{\not{p} - \hat{M}} \lambda_a i\gamma_5 \frac{1}{\not{p} + \not{q} - \hat{M}} \lambda_b i\gamma_5 \right]. \quad (5.46)$$

The trace has to be made over flavour and Dirac indices and  $\hat{M}$  is the effective quark mass matrix.

As already stated, the inverse propagator of the auxiliary meson fields are defined as the second functional derivative of the effective action with respect to the specific auxiliary field. The pseudoscalar,  $G_{ab}^P$ , and scalar,  $G_{ab}^S$ , auxiliary meson propagators are given by:

$$G_{ab}^P(q) = \left[ P_{ab}^{-1} - \Pi_{ab}^P(q) \right]^{-1}, \quad (5.47)$$

$$G_{ab}^S(q) = \left[ S_{ab}^{-1} - \Pi_{ab}^S(q) \right]^{-1}. \quad (5.48)$$

Here, the indices  $a, b = 0, 1, 2, \dots, 8$ .

The correspondence between the auxiliary pseudoscalar fields,  $\pi_a$ , and the physical pseudoscalar mesons can be performed using:

$$\frac{\lambda_a \pi_a}{\sqrt{2}} = \begin{bmatrix} \frac{\pi_0}{\sqrt{3}} + \frac{\pi_3}{\sqrt{2}} + \frac{\pi_8}{\sqrt{6}} & \frac{\pi_1 - i\pi_2}{\sqrt{2}} & \frac{\pi_4 - i\pi_5}{\sqrt{2}} \\ \frac{\pi_1 + i\pi_2}{\sqrt{2}} & \frac{\pi_0}{\sqrt{3}} - \frac{\pi_3}{\sqrt{2}} + \frac{\pi_8}{\sqrt{6}} & \frac{\pi_6 - i\pi_7}{\sqrt{2}} \\ \frac{\pi_4 + i\pi_5}{\sqrt{2}} & \frac{\pi_6 + i\pi_7}{\sqrt{2}} & \frac{\pi_0 - \sqrt{2}\pi_8}{\sqrt{3}} \end{bmatrix} = \begin{bmatrix} \pi_u/\sqrt{2} & \pi^+ & K^+ \\ \pi^- & \pi_d/\sqrt{2} & K^0 \\ K^- & \bar{K}^0 & \pi_s/\sqrt{2} \end{bmatrix}. \quad (5.49)$$

Where the pseudoscalar nonet was represented in the usual way. For the auxiliary scalar fields,  $s_a$ , and the physical scalar fields, we use:

$$\frac{\lambda_a \sigma_a}{\sqrt{2}} = \begin{bmatrix} \frac{\sigma_0}{\sqrt{3}} + \frac{\sigma_3}{\sqrt{2}} + \frac{\sigma_8}{\sqrt{6}} & \frac{\sigma_1 - i\sigma_2}{\sqrt{2}} & \frac{\sigma_4 - i\sigma_5}{\sqrt{2}} \\ \frac{\sigma_1 + i\sigma_2}{\sqrt{2}} & \frac{\sigma_0}{\sqrt{3}} - \frac{\sigma_3}{\sqrt{2}} + \frac{\sigma_8}{\sqrt{6}} & \frac{\sigma_6 - i\sigma_7}{\sqrt{2}} \\ \frac{\sigma_4 + i\sigma_5}{\sqrt{2}} & \frac{\sigma_6 + i\sigma_7}{\sqrt{2}} & \frac{\sigma_0 - \sqrt{2}\sigma_8}{\sqrt{3}} \end{bmatrix} = \begin{bmatrix} \sigma_u/\sqrt{2} & a_0^+ & \kappa^+ \\ a_0^- & \sigma_d/\sqrt{2} & \kappa^0 \\ \kappa^- & \bar{\kappa}^0 & \sigma_s/\sqrt{2} \end{bmatrix}. \quad (5.50)$$

Using these correspondences one can now write an effective action for the physical meson fields and derive the respective meson propagators. For the neutral mesons,  $\pi^0$ ,  $\eta$  and  $\eta'$ , one must perform, as usual, a diagonalization of the quadratic contributions coming from the  $0 - 3 - 8$  channels. In the isotopic limit, one therefore obtains the straightforward extension of the results from [202] to include the eight-quark contributions. For more details see [202, 204]. The physical meson propagators can be written in terms of the pseudoscalar and scalar polarization functions for two quarks with flavours  $i$  and  $j$ , which are given by [202]:

$$\Pi_{ij}^P(q) = 4 \left[ I_i^{(1)} + I_j^{(1)} - (q^2 - (M_i - M_j)^2) I_{ij}^{(2)} \right], \quad (5.51)$$

$$\Pi_{ij}^S(q) = 4 \left[ I_i^{(1)} + I_j^{(1)} - (q^2 - (M_i + M_j)^2) I_{ij}^{(2)} \right]. \quad (5.52)$$

In the vacuum, where we will calculate the meson masses to fix the parameters, the integrals  $I_i^{(1)}$  and  $I_{ij}^{(2)}$  are:

$$I_i^{(1)} = \frac{N_c}{4\pi^2} \int_0^\Lambda dp \frac{p^2}{E_i}, \quad (5.53)$$

$$I_{ij}^{(2)} = \frac{N_c}{4\pi^2} \int_0^\Lambda dp \frac{p^2}{E_i E_j} \frac{(E_i + E_j)}{q^2 - (E_i + E_j)^2}. \quad (5.54)$$

The last integral,  $I_{ij}^{(2)}$ , must be calculated using the Sokhotski–Plemelj formula (see Eq. (A.7)) displaying, in some cases, an imaginary contribution. At finite temperature and chemical potential this integrals would contain terms proportional to the modified Fermi distribution function of Eqs. (5.28) and (5.29). Such extension would allow the study of the properties of the mesons at finite temperature and chemical potential. A very detailed study can be found in [193].

Using the diagonal matrices of  $SU(3)_f$  and the identity, we can write the mean field values of the bilinear operators in the  $0 - 3 - 8$  basis. One can switch to the quark flavour basis,  $u - d - s$ ,

doing a rotation as follows:

$$\langle s_a \rangle = T_{ai} \sigma_i. \quad (5.55)$$

Here, the elements of the matrix  $T_{ai}$  are given by:

$$(T_{ai}) = \begin{bmatrix} \sqrt{2/3} & \sqrt{2/3} & \sqrt{2/3} \\ 1 & -1 & 0 \\ 1/\sqrt{3} & 1/\sqrt{3} & -2/\sqrt{3} \end{bmatrix}. \quad (5.56)$$

The polarization functions can be rotated between basis using,

$$\Pi_{ab} = T_{ai} T_{bj} \Pi_{ij}. \quad (5.57)$$

The mass of a given meson,  $M_M$ , and its decay width,  $\Gamma_M$ , can then be calculated by searching for the complex pole of its inverse propagator,  $G_M$ , in the rest frame, i.e.,

$$\left[ G_M \left( M_M - i \frac{\Gamma_M}{2}, \mathbf{q} = \mathbf{0} \right) \right]^{-1} = 0. \quad (5.58)$$

These two quantities are extracted from the zeroes of the complete real and imaginary components of Eq. (5.58) that can be written in the form of a system of two coupled equations. Usually, different approaches can also be used to compute  $M_M$  and  $\Gamma_M$ . In [205], the meson masses were calculated by supposing that the pole is near the real axis and the imaginary part is neglected. In [206–208] only the  $\Gamma_M^2$  contribution coming from  $(M_M - i\Gamma_M/2)$  was neglected.

## 5.3 Results

### 5.3.1 Parameter fitting

The NJL and PNJL models are identical in the vacuum since the Polyakov loop potential vanishes at  $T = 0$  and the thermal part of the model becomes identical (see footnote 3). Since, in the vacuum, both models have exactly the same phenomenology, for the parameter fitting we will consider the NJL model.

The NJL model, as defined in Eq. (5.1), has seven free parameters in the isotopic limit: the light current quark mass,  $m_u = m_d = m_l$ , the strange quark current mass,  $m_s$ , the scalar couplings,  $G$ ,  $\kappa$ ,  $g_1$ ,  $g_2$  and the regularization cutoff,  $\Lambda$ . These parameters can be fixed by reproducing vacuum observables such as the experimental values of meson masses and weak decays.

Previous works have performed the parametrization of this model using the so-called heat kernel expansion [209–211], alongside a Pauli–Villars regularization [152] with two subtractions in the integrand [212]. In this work, to perform the parametrization, we calculate the vacuum meson masses using the more common quadratic expansion of the effective action using the 3-momentum regularization [130].

As a first approach to parametrize the model, the coupling  $g_1$  was considered a fixed positive parameter and the remaining six free parameters were found by requiring the model to reproduce the masses of the pion ( $M_{\pi^\pm} = 0.140$  GeV), the kaon ( $M_{K^\pm} = 0.494$  GeV), the eta prime ( $M_{\eta'} = 0.958$  GeV) and  $a_0^\pm$  ( $M_{a_0^\pm} = 0.960$  GeV) mesons, the leptonic decays of the pion ( $f_{\pi^+} = 0.0924$  GeV) and kaon,  $f_{K^+}$ . The empirical value of the ratio between the pion and kaon decays is  $f_{K^+}/f_{\pi^+} = 1.1928(26)$  [30], however we were not able to correctly reproduce this value while also, correctly reproducing the remaining observables.

The reason to fix the  $g_1$  coupling *a priori*, is connected to the aforementioned works that used the heat kernel expansion to calculate the meson masses. In these works it was observed that increasing the value of the  $g_1$  coupling had the effect of decreasing the predicted value for the  $\sigma$  and  $f_0$  mesons (the latter only slightly), while keeping the rest of the low-lying scalar and pseudoscalar meson spectra unchanged. The same conclusion is observed in our approach, as can be seen in Fig. 5.1. Of course, considering the stability condition in Eq. (5.2),  $g_1$  is considered as positive. We only present the case  $g_1 = 0$  because, within a quark model with eight-quark interactions, such a case is the one closer to the usual model with four and six-quark interactions.

We point out that the identification of the scalars with physical states is debatable (apart from the quantum numbers matching). For instance, it could be argued that, due to the dubious identification of the  $\sigma$  meson with a simple antiquark-quark state, the lowest lying scalar states should in fact be identified with the  $f_0(980)$  and the  $f_0(1370)$  physical states. It should be noted, however, that the only scalar meson used in the fitting procedure was  $M_{a_0^\pm} = (980 \pm 20)$  MeV. The remaining scalars are outputs of the model.

In order to define families of parameter sets, we used different values of the decay of the kaon meson:  $f_{K^+} = \{93.00, 93.25, 93.50, 93.75, 94.00, 94.25, 94.50, 94.75\}$  MeV, thus a given family of parameter sets is defined by its  $f_{K^+}$  value. We limited the values of this observable to this set because, for higher values of  $f_{K^+}$ , the CEP of the NJL disappears in the  $\mu_B = 0$  axis of the phase diagram, while still leaving a first-order phase transition for all the diagram, as we will see later. From lattice QCD, we know that the transition at finite temperature and zero chemical potential is a smooth crossover. Hence, such unphysical scenarios are not studied. This will be further explored in the following sections.

As already discussed within the heat kernel expansion, a particular family of parameter sets is only differentiated by the usual four-quark coupling constant,  $G$  and the OZI violating eight-quark interaction,  $g_1$  [134]. Indeed, the other parameters,  $m_l$ ,  $m_s$ ,  $\kappa$ ,  $g_2$  and  $\Lambda$ , are constant as a function of  $g_1$ . In Table 5.1 these parameters are displayed for each value of  $f_{K^+}$  (each corresponding to a family of parameter sets). The coupling  $G$  however, decreases with increasing  $g_1$ , as one can see in Fig. 5.2. In this figure, the usual four Fermi coupling,  $G$ , as a function of the OZI-violating eight-quark interaction,  $g_1$  is displayed for all the families of parameter sets. In Table 5.1 the quark current masses, the 't Hooft determinant, the  $g_2$  coupling and the cutoff are shown for each family of parameter sets, i.e., for a particular choice of  $f_{K^+}$ . In Table 5.2, some vacuum observables are shown for each value of  $f_{K^+}$ , including: the effective quark masses

$f_{K^+}$ [MeV]	$m_l$ [MeV]	$m_s$ [MeV]	$\kappa\Lambda^5$	$g_2\Lambda^8$	$\Lambda$ [GeV]	$\kappa$ [GeV $^{-5}$ ]	$g_2$ [GeV $^{-8}$ ]
93.00	6.00209	136.669	-10.714	14.186	0.576331	-168.493	1165.436
93.25	6.01204	137.436	-10.982	1.154	0.578633	-169.310	91.842
93.50	6.01593	138.052	-11.245	-9.309	0.581187	-169.583	-715.121
93.75	6.01401	138.526	-11.502	-17.671	0.583972	-169.354	-1306.542
94.00	6.00659	138.868	-11.752	-24.334	0.586968	-168.671	-1727.006
94.25	5.99408	139.090	-11.997	-29.628	0.590159	-167.582	-2013.505
94.50	5.97686	139.201	-12.237	-33.819	0.593532	-166.133	-2195.840
94.75	5.95530	139.211	-12.473	-37.113	0.597078	-164.367	-2297.614

TABLE 5.1: Parameter sets: each line corresponds to a particular family of parameters, differentiated by  $f_{K^+}$ . For a particular family, the following parameters are  $g_1$  independent: current masses of the light ( $m_l = m_u = m_d$ ) and strange quarks ( $m_s$ ), 't Hooft determinant ( $\kappa$ ), non OZI violating eight-quark ( $g_2$ ) interactions and 3-momentum cutoff used in the regularization ( $\Lambda$ ). The parameter  $G$  changes with  $g_1$  (see Fig. 5.2). These were obtained fitting the masses of the pion ( $M_{\pi^\pm} = 0.140$  GeV), the kaon ( $M_{K^\pm} = 0.494$  GeV), the eta prime ( $M_{\eta'} = 0.958$  GeV) and  $a_0^\pm$  ( $M_{a_0^\pm} = 0.960$  GeV) mesons and the weak decay of the pion ( $f_{\pi^+} = 0.0924$  GeV).

( $M_l$  and  $M_s$ ), the light and strange quark condensates ( $\langle\bar{\psi}_l\psi_l\rangle^{1/3}$  and  $\langle\bar{\psi}_s\psi_s\rangle^{1/3}$ ) and masses of the  $\eta$  ( $M_\eta$ ) and  $\kappa$  ( $M_\kappa$ ) mesons.

Since there is an almost perfect linear relation between the dimensionless couplings  $G\Lambda^2$  and  $g_1\Lambda^8$  (see Fig. 5.2), we fitted the coupling  $G\Lambda^2$  as a function of  $g_1\Lambda^8$ , using a linear function  $y = A + Bx$ , with  $y = G\Lambda^2$  and  $x = g_1\Lambda^8$ . The results of the fitting procedure, for every family of parameters, are displayed in Table 5.3. In this table we present the fitting parameters  $A$  and  $B$ , the standard error of these parameters,  $\delta A$  and  $\delta B$ , the residual sum of squares (RSS - the sum of the squares of the difference between the value predicted by the fit and the ‘‘empirical’’ value), and the coefficient of determination  $R^2$ . There is a linear relation between these parameters as we can see by the value of RSS and  $R^2$ . One is now able to reproduce, to very good approximation, every parameter set obtained. Choosing a particular family of parameters ( $f_{K^+}$ ), one can use the coefficients of the linear fits alongside Table 5.1, to reproduce every parameter set obtained for a particular choice of  $g_1\Lambda^8$  (to a very good approximation, taking into account the goodness-of-fit).

In both Figs. 5.1 and 5.2, each panel corresponds to a particular family of parameters, i.e. to a fixed  $f_{K^+}$ . The dashed vertical and dotted lines in the graphs are the minimum  $g_1$  values which fulfil the inequalities (5.3) and (5.4), respectively. Obviously, the first condition ( $g_1 > 0$ ) is not fulfilled in any family of parameter sets in the case with  $g_1 = 0$ . Hence, the grey region corresponds to parameter sets that obey all the stability conditions. Since the mass of the sigma meson,  $M_\sigma$ , decreases with increasing  $g_1$ , we decide to terminate the regions of stability when  $M_\sigma = 400$  MeV. We also highlight that, these conditions translate into vertical lines in Figs. 5.1 and 5.2 because the parameters  $\kappa$  and  $g_2$  do not change for increasing  $g_1$ , for a particular family of parameters (particular choice of  $f_{K^+}$ ).

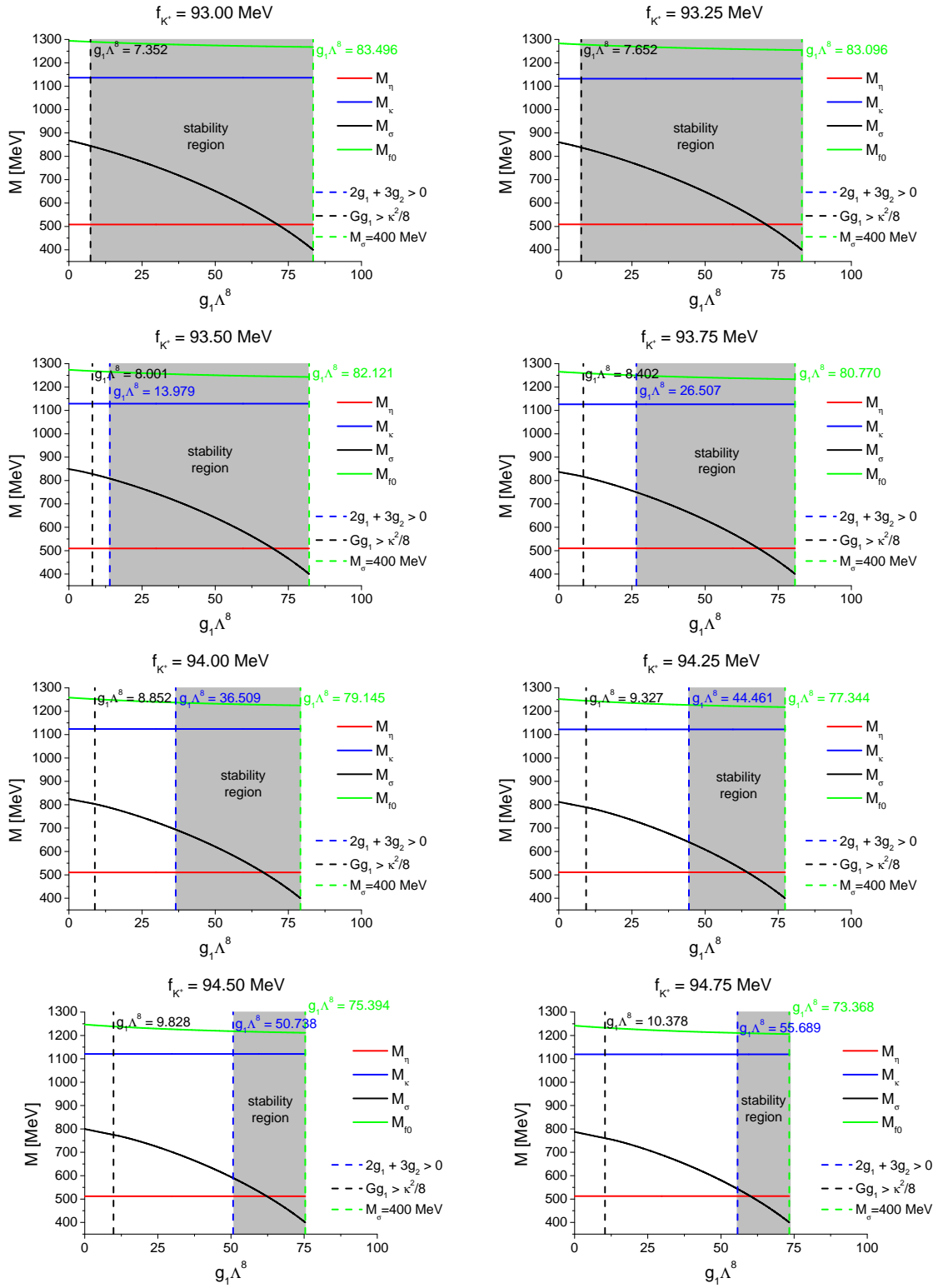


FIGURE 5.1: Non-fitted mesons masses: each panel corresponds to a particular family of parameters, differentiated by  $f_{K^+}$ . Predicted values of  $M_\eta$ ,  $M_\kappa$ ,  $M_\sigma$  and  $M_{f_0}$ , as a function of the dimensionless OZI violating eight-quark interaction parameter,  $g_1\Lambda^8$ . The grey region corresponds to the region of parameters where all stability conditions are satisfied (see Eqs. (5.2), (5.3) and (5.4)). The critical values of  $g_1\Lambda^8$  that bound the regions and the stability regions are terminated when  $M_\sigma = 400$  MeV.

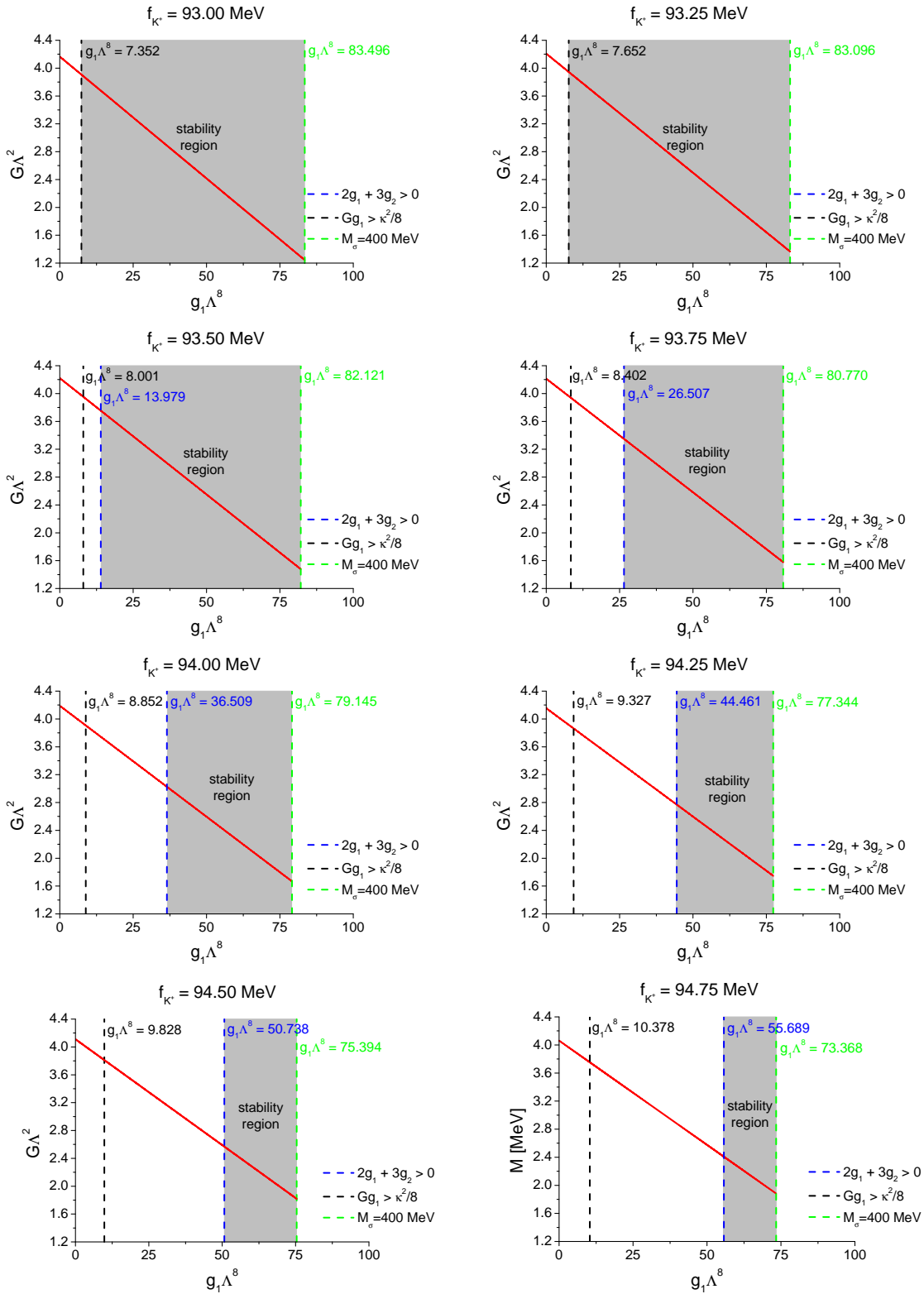


FIGURE 5.2: Four-quark interaction coupling,  $G\Lambda^2$ , as a function of the dimensionless OZI violating eight-quark interaction parameter,  $g_1\Lambda^8$ . Each panel corresponds to a particular family of parameters, differentiated by  $f_{K^+}$ . The grey region corresponds to the region of parameters where all stability conditions are satisfied (see Eqs. (5.2), (5.3) and (5.4)). The critical values of  $g_1\Lambda^8$  that bound the regions are pointed out and the stability regions are terminated when  $M_\sigma = 400$  MeV.

$f_{K^+}$	$M_l$	$M_s$	$\langle\bar{\psi}_l\psi_l\rangle^{1/3}$	$\langle\bar{\psi}_s\psi_s\rangle^{1/3}$	$M_\eta$	$M_\kappa$
[MeV]	[MeV]	[MeV]	[MeV]	[MeV]	[GeV]	[GeV]
93.00	443.3	619.1	-240.8	-251.3	0.5084	1.1362
93.25	432.3	604.9	-240.6	-251.6	0.5090	1.1322
93.50	421.9	591.9	-240.6	-252.0	0.5095	1.1289
93.75	412.0	580.0	-240.6	-252.5	0.5101	1.1263
94.00	402.7	569.1	-240.7	-253.0	0.5107	1.1241
94.25	394.0	559.0	-240.9	-253.7	0.5112	1.1223
94.50	385.7	549.6	-241.1	-254.4	0.5118	1.1207
94.75	378.0	540.9	-241.5	-255.2	0.5124	1.1192

TABLE 5.2: Vacuum observables: each line corresponds to a particular family of parameters, differentiated by  $f_{K^+}$ . For a particular family of parameters (see Table 5.1), the following observables are  $g_1$  independent: effective quark masses ( $M_l$  and  $M_s$ ) light and strange quark condensates ( $\langle\bar{\psi}_l\psi_l\rangle^{1/3}$  and  $\langle\bar{\psi}_s\psi_s\rangle^{1/3}$ ) and masses of the  $\eta$  ( $M_\eta$ ) and  $\kappa$  ( $M_\kappa$ ) mesons. The meson masses,  $M_\sigma$  and  $M_{f_0}$ , change with  $g_1$  (see Fig. 5.1).

$f_{K^+}$ [MeV]	$A$	$\delta A$	$B$	$\delta B$	RSS	$R^2$
93.00	4.166	$6.94 \times 10^{-12}$	-0.0350	$1.44 \times 10^{-13}$	$1.34 \times 10^{-16}$	1.000
93.25	4.208	$1.14 \times 10^{-11}$	-0.0342	$2.37 \times 10^{-13}$	$3.59 \times 10^{-16}$	1.000
93.50	4.221	$1.06 \times 10^{-11}$	-0.0334	$2.25 \times 10^{-13}$	$3.06 \times 10^{-16}$	1.000
93.75	4.213	$1.00 \times 10^{-11}$	-0.0326	$2.15 \times 10^{-13}$	$2.63 \times 10^{-16}$	1.000
94.00	4.189	$6.20 \times 10^{-12}$	-0.0319	$1.36 \times 10^{-13}$	$9.64 \times 10^{-17}$	1.000
94.25	4.154	$1.05 \times 10^{-11}$	-0.0311	$2.34 \times 10^{-13}$	$2.62 \times 10^{-16}$	1.000
94.50	4.110	$1.46 \times 10^{-11}$	-0.0304	$3.35 \times 10^{-13}$	$4.83 \times 10^{-16}$	1.000
94.75	4.061	$1.74 \times 10^{-11}$	-0.0297	$4.10 \times 10^{-13}$	$6.51 \times 10^{-16}$	1.000

TABLE 5.3: Results of the fit of the coupling  $G\Lambda^2$  as a function of  $g_1\Lambda^8$ , using a linear function  $y = A + Bx$ , with  $y = G\Lambda^2$  and  $x = g_1\Lambda^8$ : the fitting parameters  $A$  and  $B$ , the standard error of these parameters,  $\delta A$  and  $\delta B$ , the residual sum of squares, RSS and the coefficient of determination  $R^2$ . Each line corresponds to a particular family of parameters, differentiated by  $f_{K^+}$ .

For increasing  $f_{K^+}$ , the region with stable parameter sets is pushed towards higher values of  $g_1$ . The movement of this region is dictated by the behaviour of the model's parameters with increasing  $g_1$  and specially constrained by the relation between the two eight-quark couplings,  $g_1$  and  $g_2$ . This is understandable by analysing both Fig. 5.2 and Table 5.1. For the parameters sets with  $f_{K^+} = \{93.00, 93.25\}$  MeV the  $g_2$  coupling is positive, meaning that the constraint imposed by the condition (5.3) is automatically fulfilled for any positive value of  $g_1$  and the grey regions are dictated only by the stability condition in Eq. (5.4). For the remaining parameter sets  $g_2$  is negative and the constraint of Eq. (5.3) starts playing a very important role in defining the stable region of parameters. As soon as  $g_2$  becomes negative this constraint is the main force driving the onset of the stability region to the right. In fact, the stability condition of Eq. (5.4)

moves very slightly across every scenario. This is due to the fact that this condition depends on  $G$ ,  $\kappa$  and  $g_1$ : while  $\kappa$  remains constant for a given parameter family, for increasing  $g_1$ ,  $G$  decreases (see Fig. 5.2). Since these couplings are inversely proportional, the  $g_1$  onset of this inequality almost does not move. The stability condition of Eq. (5.3) however, depends only on the eight-quark couplings  $g_1$  and  $g_2$ . Since, for a given parameter family,  $g_2$  is the same for every  $g_1$ , and it becomes more negative for increasing  $f_{K^+}$ , the onset of stability is mainly driven by this constraint.

As already pointed out, for a particular family of parameters, only the masses of the  $\sigma$  and  $f_0$  mesons are changed with increasing  $g_1$ . In Fig. 5.1, the meson masses of the non-fitted mesons,  $M_\eta$ ,  $M_\kappa$ ,  $M_\sigma$ ,  $M_{f_0}$ , are displayed as a function of the coupling constant  $g_1$  (coloured lines). The  $\sigma$  meson mass in particular is very sensitive to the choice of the OZI violating eight-quark coupling. From Fig. 5.1 and Table 5.2, the pattern of the meson masses for different values of  $f_{K^+}$  is also evident: increasing  $f_{K^+}$  lowers the mass of the non-fitted scalar mesons while,  $M_\eta$ , slightly increases. Since increasing  $f_{K^+}$  is equivalent to lowering  $g_2$  (see Table 5.1), one can also relate the overall magnitude of  $|g_2|$  with the small decrease of  $M_\kappa$ ,  $M_\sigma$ ,  $M_{f_0}$  and small increase of  $M_\eta$ .

### 5.3.2 The NJL phase diagram

Our endgame is to study the phase diagram of the PNJL model and isentropic trajectories around the critical region, specially near the CEP. So, after building the parametrizations further restrictions on the parameters can be imposed by analysing the phase diagram of the model. In Fig. 5.3 we start to show the phase diagram of the NJL model for some specific sets (highlighted in the figures) for each family of parameter sets. In this figure, the full lines represent a first-order phase transition and the dots are the CEPs, associated to the partial<sup>6</sup> restoration of chiral symmetry. In each panel, the first set of parameters is the one which corresponds to the first stable model in that family, i.e., it corresponds to the value of  $g_1$  in which the stable region of parameters start (grey region in Figs. 5.1 and 5.2). The remaining sets of parameters in each panel corresponds to decreasing values of the  $\sigma$  meson mass,  $M_\sigma$ .

Every panel presents a critical scenario where there is a first-order chiral phase transition (associated with light quarks) at zero temperature but, the CEP is no longer found in the diagram. In these cases there is a first-order phase transition crossing the entire phase diagram up to  $\mu_B = 0$ . Such results do not agree with knowledge coming from lattice QCD calculations which predict a crossover in the  $\mu_B = 0$  axis of the phase diagram. Hence, we do not show the phase diagram for larger values of  $g_1$  in those cases. We highlight that, the last parameter set, which always corresponds to smallest  $\sigma$  meson mass in given family, is not the one in which the CEP is exactly in the  $\mu_B = 0$ . Such a critical value of  $g_1$  lies between the last two parameter sets in each panel. For the family of parameters with  $f_{K^+} = 94.75$  MeV, the first stable parametrization, corresponds already to an unphysical scenario. This is the reason why we only considered the maximum value of  $f_{K^+} = 94.75$  MeV.

<sup>6</sup>We use the partial restoration of chiral symmetry terminology because, after the transition, the values of the effective masses of the quarks are still different from the respective current quark masses, and the quark condensates are still non-zero.

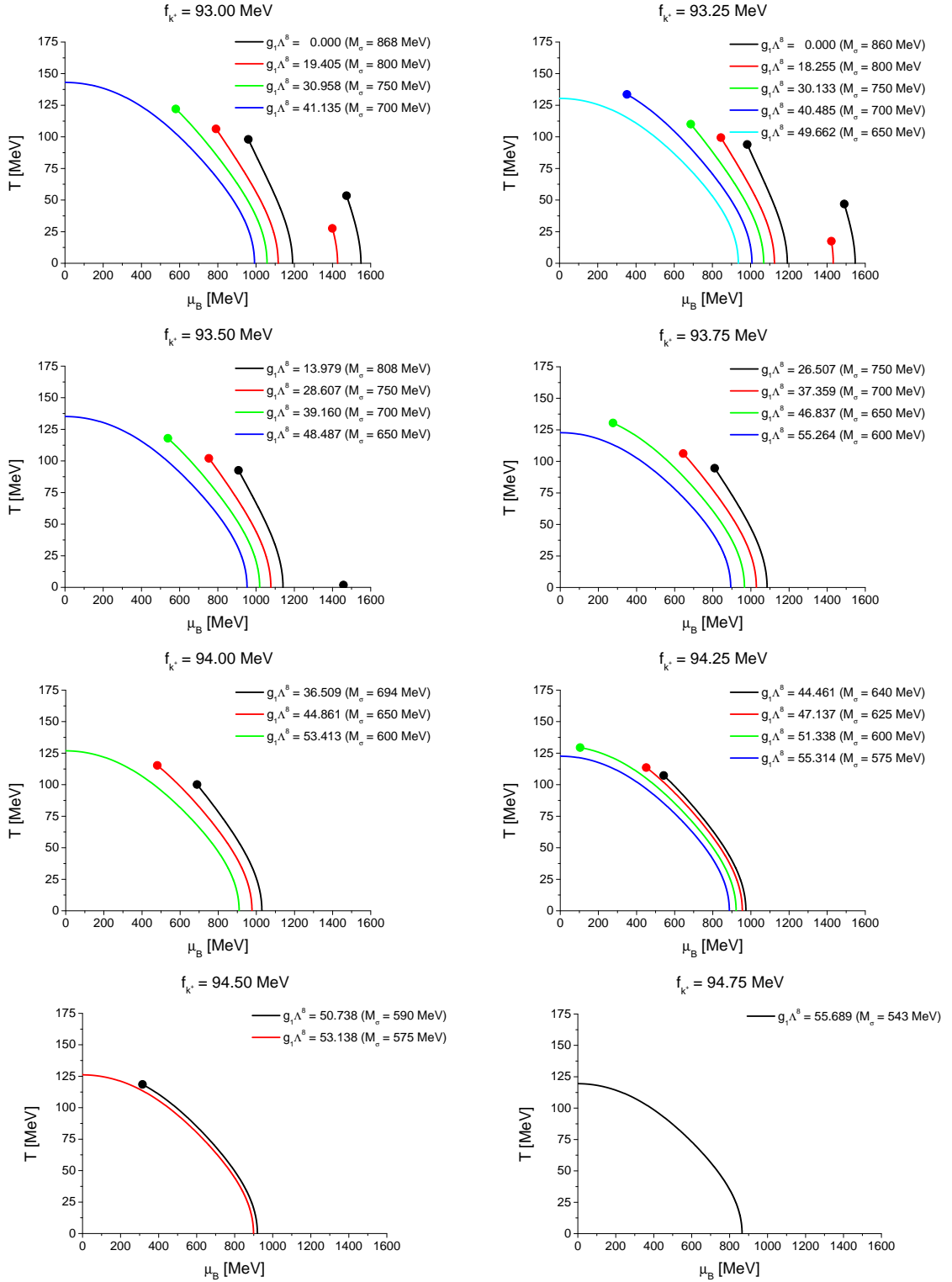


FIGURE 5.3: Phase diagram of the NJL model for specific parameter sets (highlighted in the panels). Each panel corresponds to a particular family of parameters, differentiated by  $f_{K^+}$ . The full lines are first-order phase transitions and the dots are the CEPs. The first value of  $g_1\Lambda^8$  corresponds to the start of the stable region (grey region in Figs. 5.1 and 5.2). The other scenarios correspond to parameter sets with decreasing  $M_\sigma$ .

One very interesting property of our approach is the existence of a second CEP in the phase diagram of some parameter sets, as one can see in Fig. 5.3. In particular the families of parameters with  $f_{K^+} = \{93.00, 93.25, 93.50\}$  MeV present some stable parameter sets where a second CEP can be found. Such CEP is associated with the restoration of chiral symmetry in the strange sector. This will be discussed with more detail in a later section.

Other studies [213], have demonstrated that the very low temperature region of the phase diagrams is identical in both the NJL and PNJL models and that differences arise at high temperatures: the CEP is usually pushed to higher temperatures and smaller chemical potentials. Indeed, if there is no first-order phase transition at  $T = 0$  in the NJL model, for certain there will be no first-order phase transition in the Polyakov version of the model, be it related to the light sector or the strange sector. This conclusion follows from the fact that both models are identical at  $T = 0$ . Hence, if there are two CEPs for the NJL model, there will be two CEPs in the PNJL model, unless one of them or both are pushed onto the  $\mu_B = 0$  axis, in which case it will be considered unphysical as it is not what is predicted by lattice QCD calculations.

In the next section we will use a couple of different parameter sets of one particular family (a particular choice of  $f_{K^+}$ ) and study the phase diagram of the PNJL models, and the isentropic trajectories for each parameter set.

### 5.3.3 The PNJL phase diagram: the strange critical endpoint and isentropic trajectories

In this section, as previously stated, we will study the phase diagram of the PNJL model and isentropic trajectories for a couple of different parameter sets found in the previous section. In particular we are interested in parameter sets which predict, in the NJL model, an extra CEP associated with the restoration of chiral symmetry in the light sector. By inspecting Fig. 5.3, we realized that the strange CEP is positioned at higher temperatures in the family of parameter sets with  $f_{K^+} = 93.00$  MeV. Since the inclusion of the Polyakov loop, within the same vacuum parameter set, is known to push the CEP to even higher temperatures [213], for this section, we will consider only parameter sets with  $f_{K^+} = 93.00$  MeV. Within this family of parameter sets, we considered four particular values for the OZI violating coupling  $g_1$ ,  $g_1 = \{0, 800, 1600, 2400\}$  GeV<sup>-8</sup> which are displayed in Table 5.4. For the considered parameter sets, only the  $g_1 = 0$  GeV<sup>-8</sup> does not fulfil all the stability conditions. We analyse this case nonetheless because it is the one which is closer to not considering eight-quark interactions in the model.

Introducing the Polyakov loop in the NJL model leads to the inclusion of additional parameters in the calculation (see Eq. (5.5)). At finite temperature and chemical potential, the Polyakov loop potential parameter  $T_0$  is responsible for controlling the temperature scale of the deconfinement transition. Its original value of  $T_0 = 0.270$  GeV, is chosen in order to reproduce the pure glue deconfinement transition [145]. In fact, some works suggest that this parameter should be  $N_f$  and chemical potential dependent [149]. In this work this parameter was fixed by requiring that

set	$G\Lambda^2$	$g_1\Lambda^8$	$G$ [GeV $^{-2}$ ]	$g_1$ [GeV $^{-8}$ ]	$T_0$ [GeV]
a)	4.166	0.000	12.542	0.000*	0.18257
b)	3.825	9.738	11.515	800.000*	0.18271
c)	3.484	19.476	10.489	1600.000*	0.18280
d)	3.143	29.214	9.463	2400.000*	0.18264

TABLE 5.4: Parameter sets: couplings for the NJL ( $G$ ), OZI violating eight-quark ( $g_1$ ) and  $T_0$  parameter used in the polynomial Polyakov potential. The remaining parameters do not change with different values of  $g_1$  and are given in the first row of Table 5.1 ( $f_{K^+} = 93.00$  MeV). For each set the  $T_0$  parameter is fixed by requiring a crossover deconfinement temperature (defined using the inflection point in the Polyakov loop) of  $T_c^\phi = 0.172$  GeV when using the polynomial Polyakov potential (see Eq. 5.5). The OZI violating coupling  $g_1$  is fixed at the listed values (and marked with \*).

set	$M_\sigma$ [GeV]	$M_{f_0}$ [GeV]
a)	0.868	1.294
b)	0.836	1.289
c)	0.800	1.284
d)	0.758	1.281

TABLE 5.5: Vacuum observables for each parameter set defined in Table 5.4: masses of the  $\sigma$  ( $M_\sigma$ ) and  $f_0$  ( $M_{f_0}$ ) mesons. The remaining observables do not change with different values of  $g_1$  and are given in the first row of Table 5.2 ( $f_{K^+} = 93.00$  MeV).

the crossover deconfinement<sup>7</sup> temperature of the model is  $T_c^\phi = 0.172$  GeV. This value was chosen in order to be bounded by the lattice QCD results from [214].

Of course, increasing  $g_1$  implies that we are changing the model, as such, a change in the deconfinement transition temperature at  $\mu_B = 0$  GeV for a fixed  $T_0$  is expected, which means that the  $T_0$  parameter should be different for each parameter set to ensure that  $T_c^\phi = 0.172$  GeV for every parameter set. The values for  $T_0$  span, however, a surprisingly narrow range, see Table 5.4, resulting in an effective independence of  $T_0$  on the  $g_1$  coupling choice.

One important aspect about the model, that deserves to be studied is the impact, in the phase diagram and isentropic trajectories, of the inclusion of  $C(T, \mu)$  in the thermodynamical potential of the model, using the a) parameter set in Table 5.4, with  $g_1 = 0$  GeV $^{-8}$ . Considering this parametrization, in Fig. 5.4, we present the first-order phase transition line, the spinodal lines, the CEP and several isentropic lines for symmetric matter i.e.,  $\mu = \mu_u = \mu_d = \mu_s = \mu_B/3$ . In the left panel, Fig. 5.4(a), the model does not include the  $C(T, \mu)$  term while, in the right panel, Fig. 5.4(b), it is included in the thermodynamical potential.

The chiral first-order phase transition line is calculated using the Maxwell construction, using the Gibbs conditions of thermal, chemical and mechanical equilibrium. The critical temperatures

<sup>7</sup>Defined using the inflection point in the Polyakov loop.

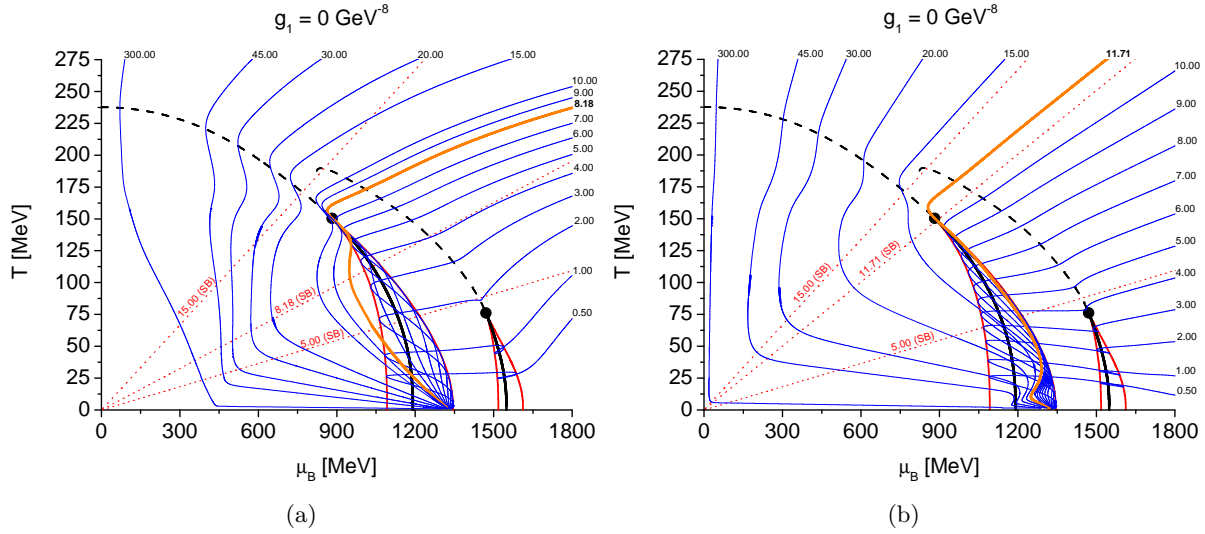


FIGURE 5.4: The impact of the inclusion of  $C(T, \mu)$  in the thermodynamical potential upon the determination of the isentropic lines (constant entropy per baryon number) is illustrated above in panels 5.4(a) and 5.4(b) (without/with  $C(T, \mu)$  respectively). The chosen parametrization for this case study is parameter set a) from Table 5.4. Full black lines correspond to the first-order transitions (ending in the CEPs marked with black circles) whereas dashed black lines correspond to crossover lines. The critical temperatures for the crossover lines are determined by using the inflexion point in  $\sigma_i$  ( $i = l$  for the leftmost line and  $i = s$  for the rightmost) at fixed chemical potential. The spinodals are marked by full red lines. The isentropic lines are displayed in full blue lines (the chosen value of entropy per baryon number is displayed in the end of the curve). The thicker orange line corresponds to the isentropic line that goes through the CEP. Red dashed straight lines irradiating from the origin correspond to the Stefan–Boltzmann limit of the  $s/\rho_B = 5$ , 8.18 or 11.71 (lines that cross the CEP in each scenario), and 15 cases.

for the crossover lines are determined using the inflexion point in  $\sigma_i$  ( $i = l$  for the light quarks and  $i = s$  for the strange quark) at fixed chemical potential.

As already expected from the NJL calculation performed in the previous section, there are two different first-order lines and CEPs: the leftmost one is due to the partial restoration of chiral symmetry in the light quark sector while the rightmost one is related with the partial restoration of chiral symmetry in the strange quark sector. The identification of these transitions with the restoration of chiral symmetry in the light and strange quarks sectors can be confirmed by observing Fig. 5.5. In this figure we plot the light quark condensate and the strange quark condensate as function of the baryonic chemical potential,  $\mu_B$  for a fixed temperature of  $T = 50$  MeV. The existence of two separate first-order phase transitions and two CEPs will be discussed in more detail later.

Focusing in the effect of the inclusion of the  $C(T, \mu)$  term, the chiral critical region, i.e., the first-order phase transition line, spinodal lines and CEPs are not affected by this extra term. As a matter of fact, both critical regions are identical. The reason for this behaviour is that the extra  $C(T, \mu)$  term does not depend on neither the condensate nor the Polyakov loop. Also, using the Gibbs conditions to define the first-order transition line, the chirally broken phase and the restored phase must be in thermal, chemical and mechanical equilibrium. In the latter requirement the pressure, for a given temperature and chemical potential, must be equal in both

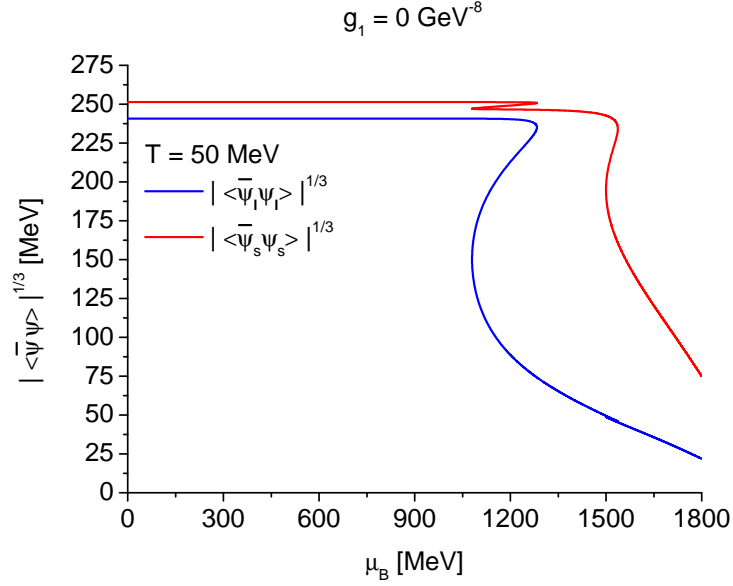


FIGURE 5.5: Absolute value of the light and strange quark condensates ( $|\langle\bar{\psi}_l\psi_l\rangle|^{1/3}$  and  $|\langle\bar{\psi}_s\psi_s\rangle|^{1/3}$ ) as a function of the baryon chemical potential,  $\mu_B$ , for  $T = 50$  MeV considering  $g_1 = 0$  GeV $^{-8}$ .

phases. Since the mass-independent  $C(T, \mu)$  term contribution to the pressure is the same in both phases, it does not change the phase transition point.

On the other hand, the effect of the  $C(T, \mu)$  term in the isentropic trajectories, is completely different in each scenario. The general behaviour for the isentropic lines inside the critical region (for both, the light and strange first-order regions) can be informally described as bouncing back and forth between spinodals [75]. In the previous section we claimed that the motivation to include such a term was to correctly reproduce the thermodynamic observables at finite temperature and chemical potential, such as the isentropic lines by including, in the model, the lacking higher momentum modes. For comparison purposes we also included the trajectories of constant entropy density of the quark-gluon gas, for three different scenarios: when the isentropic line crosses the first-order phase transition ( $s/\rho_B = 5$ ), the CEP ( $s/\rho_B = 8.18$  without  $C(T, \mu)$  and  $s/\rho_B = 11.71$  with  $C(T, \mu)$ ) and the crossover transition ( $s/\rho_B = 15$ ). In the Stefan Boltzmann limit, the isentropic trajectories for a gas of massless quarks and gluons in the  $N_c = 3$  and  $N_f = 3$  case are given by<sup>8</sup> (see for instance [215]):

$$\frac{s(T, \mu)}{\rho_B(T, \mu)} = \frac{\frac{(4N_c^2 + 7N_cN_f - 4)\pi^4}{5N_cN_f}T^3 + 3\pi^2T\mu^2}{\pi^2\mu T^2 + \mu^3}. \quad (5.59)$$

In the case without  $C(T, \mu)$ , Fig. 5.4(a), the isentropic trajectories for high values of temperature and chemical potential, where chiral symmetry is already restored, are completely different from

<sup>8</sup>The pressure for a gas of massless fermions and gluons with  $N_f$  and  $N_c$  internal degrees of freedom is given by:  $P(T, \mu) = (4N_c^2 + 7N_cN_f - 4)\pi^2T^4/180 + N_cN_fT^2\mu^2/6 + N_cN_f\mu^4/12\pi^2$ . The entropy density is computed to yield:  $s(T, \mu) = (\partial P(T, \mu)/\partial T)_\mu = (4N_c^2 + 7N_cN_f - 4)\pi^2T^3/45 + N_cN_fT\mu^2/3$ . Likewise, the baryon density is given by:  $\rho_B(T, \mu) = (\partial\mu/\partial\mu_B)_T(\partial P/\partial\mu)_T = (N_cN_f\pi^2T^2\mu + N_cN_f\mu^3)/9\pi^2$ . The lines of constant constant entropy per baryon number gas of massless quarks and gluons is then given by Eq. (5.59).

the one expected in a free gas of massless quarks and gluons. In the case with  $C(T, \mu)$ , Fig. 5.4(b), the isentropic trajectories have a very similar behaviour to what is expected from the Stefan Boltzmann limit case. Indeed, the same isentropic lines are parallel at high energies. It should be noted that a deviation from the ideal massless free quark-gluon gas is always expected due to the inclusion of a finite quark current mass (particularly in the case of the strange quark).

Besides, the asymptotic differences between the isentropic trajectories with and without  $C(T, \mu)$ , there are other important differences between both calculations. The isentropic lines that cross the light quark CEP ( $s/\rho_B = 8.18$  in the first case and  $s/\rho_B = 11.71$  in the second case) enter the critical region from the top, in the case without  $C(T, \mu)$ , the isentropic line gets out from the critical region while, in the case with  $C(T, \mu)$ , the isentropic line that cross the CEP remains bounded by the spinodal region of the chiral phase transition. Another difference is related with the larger isentropic trajectories with  $s/\rho_B = 15 - 300$ : in the case with  $C(T, \mu)$  these lines are more spread in the phase diagram and maintain a certain distance from one another while, in the other case they are closer together only getting more separated at high temperatures. In particular, the  $s/\rho_B = 300$  line in the case with  $C(T, \mu)$  is very close to the zero chemical potential axis for finite temperature.

We now turn our attention to the phase diagram and isentropic trajectories of models with different OZI violating coupling  $g_1$ , i.e., corresponding to each parametrization given in Table 5.4. Such results can be observed in Fig. 5.6 where the  $C(T, \mu)$  term was included.

As already mentioned the most striking feature of these calculations is the presence of two CEPs: one related to the partial restoration of the chiral symmetry on the light quark sector and, the other, associated with the partial restoration of chiral symmetry of the strange quark. Multiple first-order phase transitions and CEPs were observed when including the effect of a finite magnetic field [73]. In our calculation however, the strange CEP is present for all considered parameters sets (considering  $f_{K^+} = 93.00$  MeV, see Fig. 5.3).

The  $(\mu_B, T)$  coordinates of the light quark CEP for increasing values of  $g_1 = \{0, 800, 1600, 2400\}$  GeV are  $\text{CEP}_l = \{(882.1, 150.4), (777.3, 158.0), (631.3, 167.1), (407.6, 176.8)\}$  MeV while, for the strange CEP they are  $\text{CEP}_s = \{(1470.8, 76.1), (1434.7, 61.5), (1396.0, 44.0), (1347.2, 16.2)\}$  MeV. The light quark CEP moves to larger temperatures and smaller chemical potentials. This was already observed in other calculations where eight-quark interactions were incorporated [194, 216]. The behaviour of the strange CEP with increasing  $g_1$ , on the other hand, is very interesting: it moves to smaller baryon chemical and temperatures, contrary to the light CEP in the last case.

Focusing on the light quark phase transition, the first-order line and the leftmost spinodal line, at small temperatures, also moves towards smaller baryon chemical potentials. However, the rightmost spinodal line almost does not move with increasing  $g_1$ . This means that the critical region, at smaller temperatures, gets larger with increasing  $g_1$ . The crossover temperatures at  $\mu_B = 0$  also moves towards smaller temperatures with the increase of the OZI violating coupling,  $T_c = \{237.7, 221.8, 206.5, 192.1\}$  MeV.

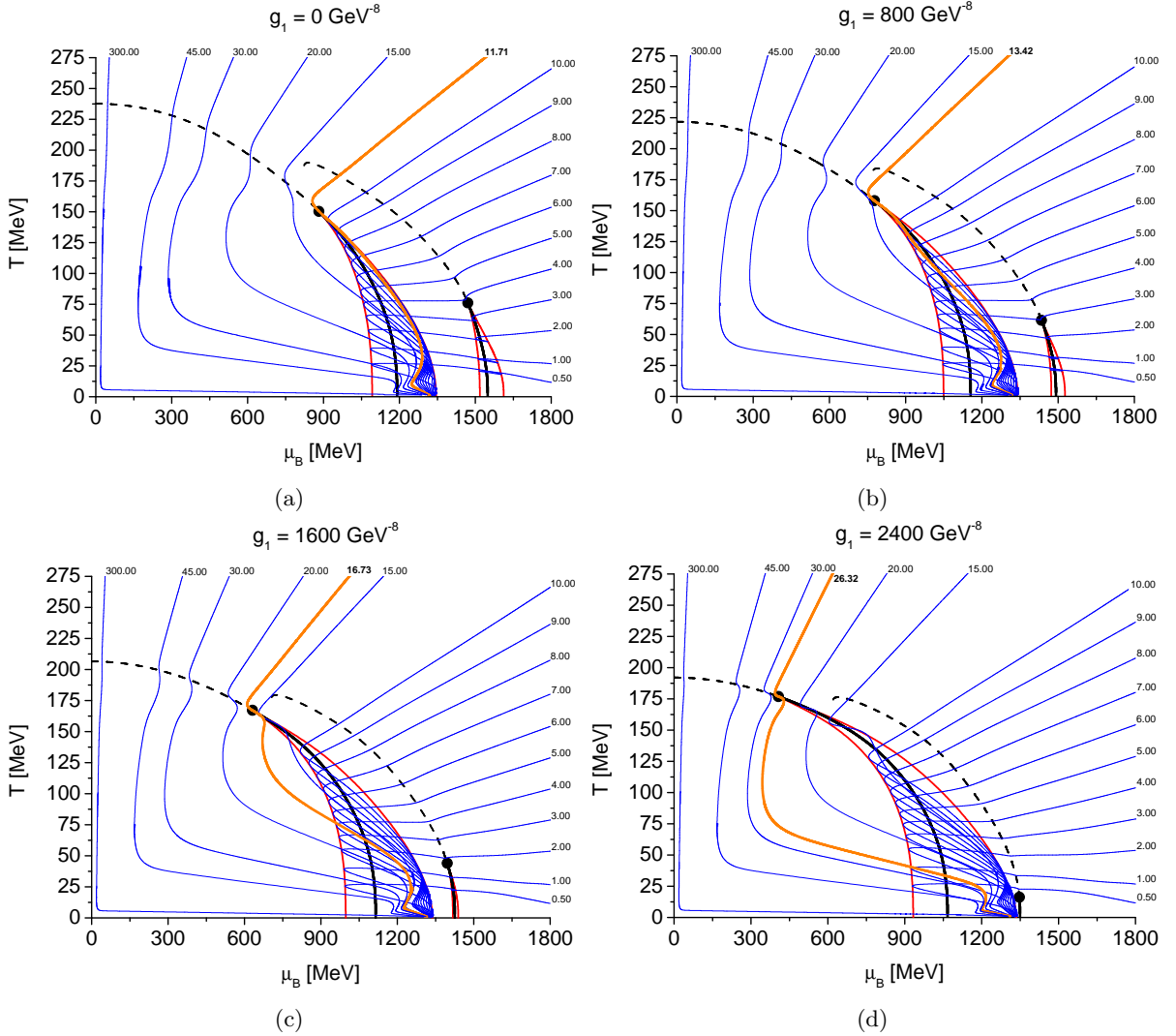


FIGURE 5.6: The impact of the OZI violating eight-quark interactions in the phase diagram and the isentropic lines determined by the model using parameter sets from Table 5.4 can be seen in the above panels. The line notation used is the same as in Fig. 5.4.

The hierarchy we found for the chiral and deconfinement transitions at  $\mu_B = 0$  is not consistent with lattice QCD calculations. From lattice QCD one expects the chiral transition temperature,  $T_c^\chi \approx 156$  MeV, to be at lower temperature than the deconfinement temperature,  $T_c^\phi \approx 172$  MeV [50]. In this work we observe the opposite behaviour. The inability to correctly reproduce the hierarchy of the transitions of the PNJL model is a known limitation of the model. It should be noted that one can obtain the correct ordering but only at the cost of missing the scale at which they occur, see [217]. Increasing  $T_0$  will drag both transitions to very high temperatures, although the order is correct. Also, using the Entangled PNJL (a Polyakov loop dependence on the four-quark coupling, see Ref. [218]), one can make the two transitions occur simultaneously.

Regarding the strange crossover, it does not extend all the way to the  $\mu_B = 0$  axis, in fact, there is a critical chemical potential for the appearance of this line.

The absence of the strange crossover line for small chemical potentials is simply due to the

disappearance of that particular inflection point. It does not mean that there is no smooth transition, but only that the surviving inflection point is the one close to the crossover transition for light quarks (we choose not to add such line).

The  $(\mu_B, T)$  position for the beginning of this line for the considered sets is, in increasing  $g_1$  order:  $\{(823.5, 187.5), (772.9, 182.7), (707.1, 177.7), (621.0, 174.3)\}$  MeV. Both the temperature and the chemical potential of the starting point of the strange crossover line are pushed towards lower values with increasing  $g_1$  with the effect being more pronounced in the reduction of the latter.

When analysing the difference in the isentropic lines obtained with the chosen parametrizations, one of the most interesting aspects is the small impact that the choice of  $g_1$  has outside the critical region bounded by the spinodal lines. The delimitation of this region is however, as already mentioned, strongly influenced by the model choice.

For the critical region around the light quark chiral restoration transition we observe the following behaviour: starting from the point where it crosses the rightmost spinodal (coming in from the higher temperature/chemical potential region) it will continue more or less in the same path until it approaches the leftmost spinodal, there it turns around and continues until it approaches the rightmost spinodal, here it performs another reversal and then, without reaching the leftmost spinodal, turns around one last time and follows the path dictated by the fact that all lines end at the critical chemical potential corresponding to the rightmost spinodal at vanishing temperature.

It is worthwhile pointing out that not all lines follow this behaviour. Consider for instance the lines that go through the CEP: in the two cases with weaker OZI-violating eight-quark interactions (see Figs. 5.6(c) and 5.6(d),  $g_1 = 0$  and  $800 \text{ GeV}^{-8}$ , with  $s/\rho_B = 11.71$  and  $s/\rho_B = 13.42$ , respectively) the lines stay inside the critical region, however, for the two cases with stronger OZI-violating eight-quark interactions ( $g_1 = 1600$  and  $2400 \text{ GeV}^{-8}$ ), lines corresponding to an entropy per baryon number close (or equal) to  $(s/\rho_B)_{\text{CEP}}$  ( $s/\rho_B = 16.73$  and  $s/\rho_B = 26.32$ , respectively) in fact leave the critical region before reentering it at a lower temperature (ending as all others at the critical chemical potential of the rightmost spinodal at vanishing temperature). The smallness of the portion of the path spent inside the critical region by these  $s_{\text{CEP}}$  isentropic lines for the strong  $g_1$  cases results, in fact, in a strong similarity to the path of the lines that go through the crossover (with a  $s/\rho_B$  slightly above that of the CEP). The isentropic lines that are currently under study ( $s/\rho_B = 30, 45, 300$ ), also display a bigger curvature when there is a CEP nearby.

Also note that as the leftmost spinodals are shifted towards lower chemical potential (broadening the critical region) with increasing  $g_1$ , this means that lower chemical potentials can be reached inside this critical region.

For isentropic lines which also cross the critical region delimited by the spinodals resulting from the strange quark partial chiral restoration an additional loop appears with the line turning around at both spinodals. As this critical region becomes increasingly smaller with increasing  $g_1$  this effect becomes almost imperceptible.

The presence of a first-order phase transition in the phase diagram causes the absorption, by the spinodal region, of certain low temperature isentropic lines. For a fixed low baryonic chemical potential, the existence of a given isentropic line at high temperatures and its disappearance at low temperatures indicates the existence of a first-order line in between the two temperature regimes. Hence, the experimental examination of heavy-ion collisions which follow isentropic lines with smaller values of  $s/\rho_B$  than the ones that are currently being studied ( $s/\rho_B = 30, 45, 300$ ), could lead to an indication of a first-order phase transition and indirectly the existence of the CEP.

## 5.4 Conclusions and outlook

In this chapter, we parametrized the NJL model including four, six and eight-quark interactions, in order to reproduce meson masses and leptonic decays using the 3-momentum regularization scheme. The meson masses were calculated using the usual quadratic expansion of the Lagrangian, different from other approaches where the heat kernel expansion was used. Some important conclusions related to the parametrization are:

- Considering a  $g_1 > 0$  and a family of parameter sets with  $g_2 > 0$ , only the constraint given in Eq. (5.4) plays a role. When  $g_2$  is negative the most important constraint comes from the relation between  $g_1$  and  $g_2$ , given by the stability condition in Eq. (5.3);
- In our approach it was not possible to reproduce correctly the ratio between the pion and kaon leptonic decays. This indicates the inability of the model to describe both the meson masses and leptonic decays, simultaneously. Other works, which include explicit chiral symmetry breaking interactions at the Lagrangian level, improve in this direction [219].

In the PNJL version of the model, the same parameters can be used, as both models are equal in the vacuum, and extra parameters, related to the Polyakov loop potential are calibrated in order to reproduce lattice QCD results at  $\mu_B = 0$ .

As observed in other works, [200, 201], the inclusion of high momentum modes in the model is essential to calculate thermodynamic observables at high temperatures and chemical potentials. Here, such modes were added by including in the thermodynamic potential the temperature and chemical potential dependent  $C(T, \mu)$  term, defined in Eq. (5.34).

The inclusion of eight-quark interactions, as already reported in other works [194, 216], pushes the CEP towards lower baryon chemical potentials and higher temperatures. Such behaviour is controlled by the overall magnitude of the coupling related to the OZI violating interaction,  $g_1$ . Phenomenologically, different values of this coupling change only the masses of the  $\sigma$  and, to a small extent,  $f_0$  scalar mesons. Within our parametrizations the presence of a new first-order phase transition and CEP was obtained, related to the partial restoration of chiral symmetry of the strange quark. Contrary to the light quark CEP, the strange CEP moves to smaller temperatures with increasing  $g_1$ . The isentropic trajectories inside both the light and strange critical regions, have the same general behaviour (a bouncing back and forth between spinodals)

while outside they are not very much affected by increasing values of this OZI violating coupling,  $g_1$ .

As future work one can further study the parametrization of the model: can the ratio of the leptonic decays of the kaon and pion mesons be reproduced to better accuracy? Another interesting study, involving the parametrization of the model, would be to construct a goodness-of-fit parameter, also called an objective function,  $\chi^2$ , instead of fitting the model to exactly reproduce some vacuum observables (as performed in the present work). The objective function, for a set of parameters  $\mathbf{p} = \{p_1, p_2, \dots\}$ , can be defined as,

$$\chi^2(\mathbf{p}) = \sum_{n=1}^N \frac{[\mathcal{O}_n^{(\text{mod})}(\mathbf{p}) - \mathcal{O}_n^{(\text{exp})}]^2}{\Delta\mathcal{O}_n^2}. \quad (5.60)$$

Here, we consider  $n$  possible observables and  $\mathcal{O}_n^{(\text{mod})}(\mathbf{p})$  is the value of the observable  $n$ , predicted by the model and  $\mathcal{O}_n^{(\text{exp})}$  is the respective experimental value. The associated error of a given observable,  $\Delta\mathcal{O}_n$ , contains the experimental error and can also contain some error due to the systematic uncertainties, that can be associated to the fact that the model does not incorporate all the expected dynamics. After minimizing this function, one can study the sensibility of the model to certain parameters, measure their importance to reproduce a given observable and associate errors to theoretical predictions. For an example of this procedure, applied to relativistic mean field models in the context of finite nuclei and neutron stars, see Ref. [220].

The study the speed of sound and fluctuations of conserved charges and their higher order cumulants along isentropic lines in this model is also a future line of research. Heavy ion collisions experiments can measure the probability distribution of conserved charges, using event-by-event analysis. Calculating the fluctuations of conserved charges at finite temperature and density from an effective model, as the one used in this chapter, can help interpret results coming from these experiments and look for observational signatures of the CEP or the first-order line.

Finally, the meson behaviour at finite temperature and density was already studied in the context of the NJL/PNJL model with four and six-quark interactions. It would also be interesting to study this including eight-quark interactions and also vector interaction.

## Chapter 6

# Quark matter in light neutron stars

### 6.1 Introduction

This chapter is devoted to describe neutron star (NS) matter using hybrid equations of state, where a first-order phase transition from hadronic to quark matter is realized. We explore the connection between the speed of sound at the central density of the star, the size of the quark core, the NS mass and the tidal deformability.

It is known that, after a quite rapid cooling, the temperature in NSs is negligible when compared to the chemical potentials and masses of the particles inside the NS [93]. Thus, matter inside the star is degenerate and the  $T = 0$  limit of the EoS can be considered.

Also, after the cooling process, the star is in  $\beta$ -equilibrium and the neutron decay and electron capture occur at the same rate:

$$n \rightleftharpoons p + e^- + \bar{\nu}_e \Leftrightarrow d \rightleftharpoons u + e^- + \bar{\nu}_e. \quad (6.1)$$

Considering strangeness, the following equilibrium condition must be verified:

$$d \rightleftharpoons s. \quad (6.2)$$

In the formalism we are going to use, these equilibrium relations act as constraints on the chemical potentials of the particles:

$$\mu_d = \mu_u + \mu_{e^-} + \mu_{\bar{\nu}_e} = \mu_s. \quad (6.3)$$

Here,  $\mu_u$ ,  $\mu_d$  and  $\mu_s$  are the chemical potentials of the up, down and strange quarks while,  $\mu_{e^-}$  and  $\mu_{\bar{\nu}_e}$  are the chemical potential of the electron and the antineutrino, respectively. Considering that the neutrinos escape the interior of the star due to their weak interaction with matter, their chemical potential can be ignored, yielding:

$$\mu_d = \mu_u + \mu_{e^-} = \mu_s. \quad (6.4)$$

We will further consider matter with local<sup>1</sup> charge neutrality [93], i.e.,

$$\rho_Q = 0. \quad (6.5)$$

Here,  $\rho_Q$  is the electric charge density. Considering quark matter with, up, down and strange quarks, this relation imposes the following constraint:

$$\frac{2}{3}\rho_u - \frac{1}{3}(\rho_d + \rho_s + 3\rho_e) = 0, \quad (6.6)$$

here  $\rho_u$ ,  $\rho_d$  and  $\rho_s$  are the densities of the up, down and strange quarks, respectively and  $\rho_e$  is the electron density.

In the hybrid EoS approach, two models are used to describe NS matter: one that describes the hadronic (confined) phase and a second describing the quark (deconfined) phase. The matching of the two EoS may be carried out within different methods. In the present work we will consider a Maxwell construction to describe a first-order phase transition from hadron to quark matter. This method is considered to be quite realistic if the surface tension between the hadron and quark phase, a still unknown quantity, is large. This methodology has been widely used, where an hadronic model and an independent quark model were considered, see [61, 221–225].

The description of the hadron phase is well known around the saturation density ( $\rho_0$ ) but, at higher densities, our knowledge about the EoS is very limited. Several techniques have been applied throughout the last decades to describe this type of matter such as: Skyrme interactions, relativistic mean field models and Taylor expansions around the saturation density [226–234]. One feature that these approaches have in common is that free parameters are usually fixed to reproduce nuclear properties at the saturation density. In this work, the hadronic sector of the EoS is described by a relativistic mean field nuclear model, the DDME2 model (density-dependent meson-exchange effective interaction in relativistic Hartree-Bogoliubov and quasiparticle random-phase approximation) [235].

The DDME2 model is based on the formalism of quantum hadrodynamics, the name given to effective relativistic nuclear field models, whose degrees of freedom are hadrons and the nuclear force is described by the exchange of mesons. In this framework, in order to model attractive long-range and repulsive short range nuclear forces, the scalar meson ( $\sigma$ ) and the vector meson ( $\omega_\mu$ ) were originally introduced in the effective Lagrangian [236–238]. To describe asymmetric nuclear matter correctly, another field is included, an isovector meson field ( $\rho_\mu$ ), an isospin triplet which couples to the isospin current of the nucleon and acts as an isospin restoring interaction. Further improvements on these types of models can be accomplished by incorporating mesonic non-linear self-interaction terms or, as an alternative, considering effective density dependent nucleon-meson couplings fitted to medium-dependent nucleon self-energies. The DDME2 model belongs to the latter category and was calibrated to reproduce properties of nuclear matter, ground state and excited state of spherical nuclei (nuclear binding energies, charge radii, and multipole giant resonances). It has the following nuclear properties at the

---

<sup>1</sup>One can also consider global charge neutrality, allowing for non-uniform phases inside the NS.

saturation density ( $\rho_0 = 0.152 \text{ fm}^{-3}$ ): binding energy  $E/A = -16.14 \text{ MeV}$ , incompressibility  $K = 251 \text{ MeV}$ , symmetry energy  $J = 32.3 \text{ MeV}$  and slope  $L = 51 \text{ MeV}$ . Beyond these properties, this model is also capable of reproducing a neutron matter EoS, at sub-saturation densities, in good agreement with calculations performed with chiral effective field theory [239], see [240].

For the quark phase, the MIT bag model or the Nambu–Jona-Lasinio (NJL) type models have been extensively used to study hybrid neutron stars [221, 241–245]. In the case of the NJL model, previous works have successfully predicted neutron stars with at least  $2M_\odot$  [61, 245]. In the context of this model, in Ref. [246] it was argued that the hadron-quark phase transition is controlled by the light quarks effective mass in the vacuum: smaller values shifts the zero pressure towards lower chemical potentials, favouring the appearance of stable quark matter for massive stars. One can also define an effective bag parameter in the NJL model which has a similar effect. The presence of the vector-isoscalar interaction was shown to be very important in stiffening the EoS to sustain  $2M_\odot$ . The inclusion of eight-quark interactions in the scalar and in the vector-isoscalar channels within the two-flavour NJL model was explored in [222, 223] in the context of hybrid stars. In [247], local and nonlocal NJL models with vector interactions were seen to typically give no hybrid stars (or just small quark branches). The eight-quark vector-isoscalar interaction should be interpreted as an effective interaction that includes non-linear terms to take into account medium effects, in a spirit similar to the one taken by G. Brown and M. Rho, to propose their scaling effective Lagrangians in a dense medium in [248]. The vector-isoscalar eight-quark interaction in the NJL model is equivalent to the non-linear  $(\omega^\mu \omega_\mu)^2$  term introduced in the Lagrangian density of the relativistic nuclear model TM1 [249, 250] to weaken effects of the repulsive  $\omega$ -meson contribution at high densities and reproduce Dirac–Brueckner–Hartree–Fock results. The inclusion of eight-quark interactions may be understood as an effective way of considering density dependent couplings at large densities. An alternative approach is to include the density dependence in quark models through the introduction of a chemical potential dependence [251–254].

It has been shown by several authors that the onset of the  $\Delta$  baryons may compete with the onset of hyperons, and due to its large isospin and lack of information to fix the couplings these particles may set in at densities below the onset of hyperons, just above the saturation density [255–258]. In particular, the onset of  $\Delta$ s may occur in low mass stars making compatible relativistic mean field models with the constraint set by GW170817 on the tidal deformability. In this chapter, we will show an alternative scenario: the onset of quarks at densities below twice the saturation density also have a similar effect of pushing down the tidal deformability of stars with masses  $\sim 1.4M_\odot$  or below.

Using a constant-sound-speed parametrization for the high-density EoS region in [259, 260], the authors concluded that for a strong first-order phase transition to quark matter to be compatible with  $M_{\text{max}} > 2M_\odot$ , large speed of sound is required in the quark phase,  $v_s^2 \gtrsim 0.5$ , for soft hadronic EoS and,  $v_s^2 \gtrsim 0.4$ , for stiff hadronic EoS. Using the same formalism, the work [261] points in the same direction: strong repulsive interactions in quark matter are required to support the NS masses  $M \gtrsim 2.0M_\odot$ .

In [262], the authors studied the possibility of occurrence of stars with quark cores, imposing well known constraints, both observational and theoretical ab-initio calculations, to a large set of EoS built using metamodels parametrized by the speed of sound. They proposed that  $1.4M_\odot$  stars are compatible with hadronic stars. Besides, they infer that massive stars with a mass  $\approx 2M_\odot$  and a speed of sound not far from the conformal limit will have large quark cores. It is important to understand whether it is possible to arrive at similar conclusions starting from a set of quark matter EoS that satisfy a given number of constraints established by properties of mesons in the vacuum which, also have been derived from a model with intrinsic chiral symmetry.

To attain this aim, the three-flavour NJL model will be used, and we will analyse the effect of four-quark and eight-quark vector-isoscalar interactions in hadron-quark hybrid EoS. Having the NJL functional with a eight-quark vector-isoscalar interaction as framework, it allows for the generation of hybrid EoS that satisfy nuclear matter constraints and observational constraints. Using this strategy we avoid meta-modelling the EoS using polytropes or the speed of sound approaches [262, 263] and a functional based on a relativistic and chiral symmetric framework is used instead. NJL models typically give rather low values for the speed of sound in the quark matter phase ( $v_s^2 \sim 0.2 - 0.3$ ) and have a small dependence on the density. We will explore the impact of the vector interactions on the speed of sound and on the quark phase and thus on the stability of hybrid stars sequences. Moreover, exploring these additional interactions, we will analyse the possibility of having quark cores in light NS and, at the same time, fulfil all observational constraints.

This chapter is organized as follows: in Section 6.2 the quark model is detailed. The results are presented in Section 6.3 followed by our conclusions and future perspectives, in Section 6.4.

## 6.2 Model and Formalism

The  $SU(3)_f$  NJL Lagrangian density, including four and six scalar-pseudoscalar interactions and four and eight vector-isoscalar interactions, can be written as [264]:

$$\begin{aligned} \mathcal{L} = & \bar{\psi}(i\not{\partial} - \hat{m} + \hat{\mu}\gamma^0)\psi + \frac{G}{2} \left[ (\bar{\psi}\lambda_a\psi)^2 + (\bar{\psi}i\gamma^5\lambda_a\psi)^2 \right] \\ & + 8\kappa \left[ \det(\bar{\psi}P_R\psi) + \det(\bar{\psi}P_L\psi) \right] \\ & - G_\omega \left[ (\bar{\psi}\gamma^\mu\lambda_0\psi)^2 + (\bar{\psi}\gamma^\mu\gamma_5\lambda_0\psi)^2 \right] \\ & - G_{\omega\omega} \left[ (\bar{\psi}\gamma^\mu\lambda_0\psi)^2 + (\bar{\psi}\gamma^\mu\gamma_5\lambda_0\psi)^2 \right]^2. \end{aligned} \quad (6.7)$$

Here,  $\hat{m} = \text{diag}(m_u, m_d, m_s)$  and  $\hat{\mu} = \text{diag}(\mu_u, \mu_d, \mu_s)$  are the quark current masses and chemical potential matrices, respectively. Once again,  $P_{R/L} = (1 \pm \gamma_5)/2$ , are the chiral projection operators and the matrices  $\lambda_a$ , with components  $a = 1, 2, \dots, 8$ , are the Gell-Mann matrices of the  $SU(3)$  group while, the zero component, is proportional to the identity matrix,  $\lambda^0 = \sqrt{2/3}\mathbb{1}$  (see the Appendices B.1 and B.2).

The multi-quark interactions considered in the above Lagrangian, are chiral symmetry preserving. For more details about each type of quark interaction considered here, see Chapter 4.1. The four

scalar and pseudoscalar quark interaction is essential to incorporate in the model spontaneous chiral symmetry breaking while, the 't Hooft determinant incorporates the explicit  $U(1)_A$  symmetry breaking in the model, as already seen. Introducing vector interaction in the model has been found to be essential to model the medium to high density behaviour of the EoS and predict  $2M_\odot$  NS. The inclusion of all possible chiral-symmetric set of eight-quark vector interactions was performed in [137] in order to study the masses of the lowest spin-0 and spin-1 meson states. Following previous works, the vector-isoscalar quark interactions have been showed to be essential to build  $2M_\odot$  neutron stars.

Here, we will restrict our analysis to four and eight vector-isoscalar quark interactions and study their influence on the EoS of hybrid neutron stars. These vector interactions have couplings,  $G_\omega$  and  $G_{\omega\omega}$  respectively. In general, both of these couplings can be fixed in the vacuum by fitting the omega meson mass. Indeed, while the masses and decay constants of the scalar and pseudoscalar mesons do not depend explicitly on the  $G_\omega$  and  $G_{\omega\omega}$  couplings, parametrizing the model using the omega-meson mass would affect the values of the interaction couplings, the quark current masses and cutoff, see [45]. However, in this chapter, we are not interested in studying the behaviour of vector mesons. The vector interactions are used as a way to parametrize unknown degrees of freedom that can make the EoS softer or stiffer at medium to large densities. Indeed, as discussed in the literature [45, 74], the vector-isoscalar terms are proportional to density degrees of freedom and their couplings might be density dependent. Hence, to take into account the possible in-medium dependence of the vector couplings  $G_\omega$  and  $G_{\omega\omega}$ , we will not fix their magnitudes in the vacuum and leave them as free parameters. As in previous works [61], we will study different models defined by different values for the ratios:

$$\xi_\omega = \frac{2G_\omega}{G}, \quad (6.8)$$

$$\xi_{\omega\omega} = \frac{16G_{\omega\omega}}{G^4}. \quad (6.9)$$

Exactly as done in the previous chapter, along with the Matsubara formalism to derive the thermodynamical potential, we are going to regularize the integrations using the 3-momentum cutoff regularization (the details about the NJL model and the regularization were given in Chapter 4.1).

The thermodynamical potential of the NJL model is calculated in the mean field approximation (MF), where the products between quark bilinear operators are linearised around their mean field values using again Eq. (5.17). After linearising the Lagrangian density, the quark fields can then be integrated out (for more details about the linear product between  $N$  operators see the Appendix C.1). Using the Matsubara formalism and the linear Lagrangian density, the MF thermodynamical potential of the NJL model,  $\Omega$ , can be derived (for the detailed derivation of the grand canonical potential for fermions in a mean field potential, see the Appendix D). At

finite temperature and chemical potential, the thermodynamical potential can be written as:

$$\begin{aligned}\Omega(T, \mu) = & \Omega_0 + G(\sigma_u^2 + \sigma_d^2 + \sigma_s^2) + 4\kappa\sigma_u\sigma_d\sigma_s \\ & - \frac{2}{3}G_\omega(\rho_u + \rho_d + \rho_s)^2 - \frac{4}{3}G_{\omega\omega}(\rho_u + \rho_d + \rho_s)^4 \\ & - 2TN_c \sum_{i=u,d,s} \int_0^\Lambda \frac{d^3p}{(2\pi)^3} \left[ \beta E_i + \ln \left( 1 + e^{-(E_i + \tilde{\mu}_i)/T} \right) + \ln \left( 1 + e^{-(E_i - \tilde{\mu}_i)/T} \right) \right].\end{aligned}\quad (6.10)$$

The constant  $\Omega_0$  is fixed in such a way that the potential vanishes in the vacuum. Also,  $E_i = \sqrt{p^2 + M_i^2}$  and  $\sigma_i$  and  $\rho_i$  are the condensate and density of the quarks with flavour  $i$ , respectively. For  $i \neq j \neq k \in \{u, d, s\}$ , the effective mass,  $M_i$ , and effective chemical potentials,  $\tilde{\mu}_i$ , are found to be:

$$M_i = m_i - 2G\sigma_i - 2\kappa\sigma_j\sigma_k, \quad (6.11)$$

$$\tilde{\mu}_i = \mu_i - \frac{4}{3}G_\omega(\rho_i + \rho_j + \rho_k) - \frac{16}{9}G_{\omega\omega}(\rho_i + \rho_j + \rho_k)^3. \quad (6.12)$$

In the MF approximation the thermodynamical potential must be stationary with respect to the effective mass,  $M_i$ , and effective chemical potentials [45],  $\tilde{\mu}_i$ , i.e., the following relation must hold<sup>2</sup>:

$$\frac{\partial\Omega}{\partial M} = \frac{\partial\Omega}{\partial\tilde{\mu}} = 0. \quad (6.13)$$

Applying these stationary conditions to the thermodynamical potential yields a closed expression for the quark condensate<sup>3</sup>,  $\sigma_i$ , and density,  $\rho_i$ :

$$\sigma_i = \langle \bar{\psi}_i \psi_i \rangle = -2N_c \int \frac{d^3p}{(2\pi)^3} \frac{M_i}{E_i} \left[ 1 - \frac{1}{e^{(E_i - \tilde{\mu}_i)/T} + 1} - \frac{1}{e^{(E_i + \tilde{\mu}_i)/T} + 1} \right], \quad (6.14)$$

$$\rho_i = 2N_c \int \frac{d^3p}{(2\pi)^3} \left[ \frac{1}{e^{(E_i - \tilde{\mu}_i)/T} + 1} - \frac{1}{e^{(E_i + \tilde{\mu}_i)/T} + 1} \right]. \quad (6.15)$$

The pressure ( $P$ ), particle densities ( $\rho_i$ ), entropy density ( $s$ ) and energy density ( $\epsilon$ ), can be derived from the thermodynamical potential given in Eq. (6.10), using Eqs. (A.14), (A.15),

<sup>2</sup>Or, equivalently, the thermodynamical potential must be stationary with respect to  $\sigma_i$  and  $\rho_i$ , with  $i \in \{u, d, s\}$ .

<sup>3</sup>This was already discussed in Chapter 5.2.1, for the stationary relation with respect to  $\sigma_i$ . For  $\rho_i$  it is analogous.

(A.16) and (A.17), which are explicitly given by:

$$\begin{aligned}
P(T, \mu) - P_0 &= -\Omega(T, \mu), \\
\rho_i(T, \mu) &= -\left(\frac{\partial\Omega(T, \mu)}{\partial\mu_i}\right)_T, \\
s(T, \mu) &= -\left(\frac{\partial\Omega(T, \mu)}{\partial T}\right)_\mu, \\
\epsilon(T, \mu) &= -P(T, \mu) + \sum_i \mu_i \rho_i(T, \mu).
\end{aligned}$$

The constant  $P_0$  is the vacuum pressure i.e.,  $P_0 = P(0, 0)$ .

Since we are interested in describing cold degenerate neutron star matter, we must use the  $T = 0$  limit of the above equations. In such limit, the  $i$  quark condensate and density, are given by:

$$\sigma_i = \langle \bar{\psi}_i \psi_i \rangle = -\frac{N_c}{\pi^2} \int_{\lambda_{F_i}}^{\Lambda} dp p^2 \frac{M_i}{\sqrt{p^2 + M_i^2}}, \quad (6.16)$$

$$\rho_i = \frac{N_c}{3\pi^2} \lambda_{F_i}^3, \quad (6.17)$$

where we defined the Fermi momentum,  $\lambda_{F_i} = \sqrt{\tilde{\mu}_i^2 - M_i^2}$ .

The NJL pressure, in this limit is,

$$\begin{aligned}
P(\mu) &= -\Omega_0 - G(\sigma_u^2 + \sigma_d^2 + \sigma_s^2) - 4\kappa\sigma_u\sigma_d\sigma_s \\
&\quad + \frac{2}{3}G_\omega(\rho_u + \rho_d + \rho_s)^2 + \frac{4}{3}G_{\omega\omega}(\rho_u + \rho_d + \rho_s)^4 \\
&\quad + \frac{N_c}{\pi^2} \sum_{i=u,d,s} \int_{\lambda_{F_i}}^{\Lambda} dp p^2 E_i + \frac{N_c}{\pi^2} \sum_{i=u,d,s} \tilde{\mu}_i \frac{\lambda_{F_i}^3}{3},
\end{aligned} \quad (6.18)$$

while the energy density is,

$$\begin{aligned}
\epsilon(\mu) &= \Omega_0 + G(\sigma_u^2 + \sigma_d^2 + \sigma_s^2) + 4\kappa\sigma_u\sigma_d\sigma_s \\
&\quad - \frac{2}{3}G_\omega(\rho_u + \rho_d + \rho_s)^2 - \frac{4}{3}G_{\omega\omega}(\rho_u + \rho_d + \rho_s)^4 \\
&\quad - \frac{N_c}{\pi^2} \sum_{i=u,d,s} \int_{\lambda_{F_i}}^{\Lambda} dp p^2 E_i + \frac{N_c}{\pi^2} \sum_{i=u,d,s} (\mu_i - \tilde{\mu}_i) \frac{\lambda_{F_i}^3}{3}.
\end{aligned} \quad (6.19)$$

Aside from the free vector couplings,  $G_\omega$  and  $G_{\omega\omega}$ , the remaining parameters of the model are fixed in order to reproduce the values of some meson masses and decay constants. The used parameter set can be found in Table 6.1. In Table 6.2 we present the values of some meson masses and leptonic decay constants within the parameter set in Table 6.1 and the respective experimental values.

The NJL model pressure and energy density are defined up to a constant  $B$ , analogous to the MIT bag constant [221]. It is essential in building hybrid EoS that sustain two-solar mass

$\Lambda$ [MeV]	$m_{u,d}$ [MeV]	$m_s$ [MeV]	$G\Lambda^2$	$\kappa\Lambda^5$	$M_{u,d}$ [MeV]	$M_s$ [MeV]
623.58	5.70	136.60	3.34	-13.67	332.2	510.7

TABLE 6.1: Parameters of the NJL model used in the present work:  $\Lambda$  is the model cutoff,  $m_{u,d}$  and  $m_s$  are the quark current masses,  $G$  and  $\kappa$  are coupling constants.  $M_{u,d}$  and  $M_s$  are the resulting constituent quark masses in the vacuum. This parameter set yields, in the vacuum, a light quark condensate of  $\langle\bar{\psi}_l\psi_l\rangle^{1/3} = -243.9$  MeV and strange quark condensate of  $\langle\bar{\psi}_s\psi_s\rangle^{1/3} = -262.9$  MeV.

	NJL $SU(3)$	Experimental [20]
$m_{\pi^\pm}$ [MeV]	139.6	139.6
$f_{\pi^\pm}$ [MeV]	92.0	92.2
$m_{K^\pm}$ [MeV]	493.7	493.7
$f_{K^\pm}$ [MeV]	96.4	110.4
$m_\eta$ [MeV]	515.6	547.9
$m_{\eta'}$ [MeV]	957.8	957.8

TABLE 6.2: The masses and decay constants of several mesons within the model and the respective experimental values.

neutrons stars. In [61, 221],  $B$  was fixed by requiring that the deconfinement occurs at the same baryonic chemical potential as the chiral phase transition. More recently in [261], an effective bag parameter was also used to control the density at which the phase transition from hadron to quark matter happened. In the presence of a finite bag parameter, the quark EoS is modified by  $P \rightarrow P + B$  and  $\epsilon \rightarrow \epsilon - B$ . Here, we will take the latter recipe and add a phenomenological bag pressure to the quark EoS. Thus, the NJL quark model will be defined by three parameters: the model vector coupling ratios,  $\xi_\omega = 2G_\omega/G$  and  $\xi_{\omega\omega} = 16G_{\omega\omega}/G^4$  and the bag parameter  $B$ .

As previously stated, for the hadronic part of the hybrid stars we use the DDME2 model [235]. This is a relativistic mean field model with density dependent couplings that describes two solar mass stars and satisfies a well established set of nuclear matter and finite nuclei constraints [230, 240], including the constraints set by the ab-initio calculations for neutron matter using a chiral effective field theoretical approach [239]. This has been the low density constraint set in [262].

### 6.3 Results

Herein, we analyse the effect of the vector-isoscalar couplings  $\xi_\omega = 2G_\omega/G$  and  $\xi_{\omega\omega} = 16G_{\omega\omega}/G^4$  on the hybrid EoS and respective NS properties. The effect of the bag parameter  $B$  was already studied in [61, 111, 221, 245, 264–271], where it was found that the onset of quark matter in the hybrid EoS happens at lower densities as  $B$  increases. Although we have explored several values for  $B$ , we have decided to keep it fixed in the following analysis to  $B = 15$  MeV/fm<sup>3</sup>. Increasing  $B$  shifts the hadron-quark transition to lower densities as discussed in [264]. The value of  $B$  should be constrained from below, by imposing that no quark matter exists for symmetric nuclear matter at the saturation density. We have chosen a value that does not predict unrealistic

physical scenarios such as quark matter at too low density and still allows for the presence of a quite large quark cores in low mass stars, as will be shown in the following. As free parameters, we consider  $\{\xi_\omega, \xi_{\omega\omega}\}$  which give a considerable flexibility to span a wide range of EoS with the required properties.

In the following, charge-neutral neutron star matter in  $\beta$ -equilibrium, with a first-order phase transition (via a Maxwell construction) from hadronic matter to quark matter, is studied. The transition between the quark and hadron phases is built using the Gibbs criteria. In such scenario, a phase transition occurs when both phases are in chemical, thermal and mechanical equilibrium and the following relations apply:

$$\mu_B^{(H)} = \mu_B^{(Q)}, \quad (6.20)$$

$$P^{(H)} = P^{(Q)}, \quad (6.21)$$

$$T^{(H)} = T^{(Q)}. \quad (6.22)$$

Here,  $\mu_B$  is the baryon chemical potential,  $P$  is the pressure and  $T$  is the temperature. The indices,  $H$  and  $Q$ , represent the hadronic and quark phases, respectively.

As already pointed out, to consider matter in  $\beta$ -equilibrium, one must add a contribution coming from electrons to the thermodynamical potential. Such contribution is given by:

$$\Omega_e = 2T \int \frac{d^3p}{(2\pi)^3} \left[ \beta E_e + \ln \left( 1 + e^{-(E_e + \mu_e)/T} \right) + \ln \left( 1 + e^{-(E_e - \mu_e)/T} \right) \right], \quad (6.23)$$

where  $E_e = \sqrt{p^2 + m_e^2}$ ,  $m_e = 0.510$  MeV, is the electron mass and  $\mu_e$  is the electron chemical potential. In the zero temperature limit we can define the Fermi momentum for electrons as:

$$\lambda_{F_j} = \sqrt{\mu_e^2 - m_e^2}. \quad (6.24)$$

Finally, the electron pressure ( $P_e$ ), electron density ( $\rho_e$ ) and energy density ( $\epsilon_e$ ) are:

$$P_e = \frac{1}{\pi^2} \int_{\lambda_{F_e}}^{+\infty} dp p^2 E_e + \mu_e \frac{\lambda_{F_e}^3}{3\pi^2} - \Omega_{0e}, \quad (6.25)$$

$$\rho_e = \frac{\lambda_{F_e}^3}{3\pi^2}, \quad (6.26)$$

$$\epsilon_e = \Omega_{0e} - \frac{1}{\pi^2} \int_{\lambda_{F_e}}^{+\infty} dp p^2 E_e. \quad (6.27)$$

It is important to include both vector interaction terms because they play different roles: the  $G_\omega$  term makes the EoS harder, a necessary condition to get two solar mass stars. However, if the EoS is too stiff no transition to quark matter is predicted. This can still be partially regulated with the inclusion of the bag pressure  $B$  but only allows for small quark cores. The effect of the  $G_{\omega\omega}$  term becomes more important at large densities. As a consequence, the stellar matter enters the quark phase as a quite soft EoS, but, as the density increases, the effect of the  $G_{\omega\omega}$  term becomes stronger and stronger, allowing for massive and stable stars with a large quark core.

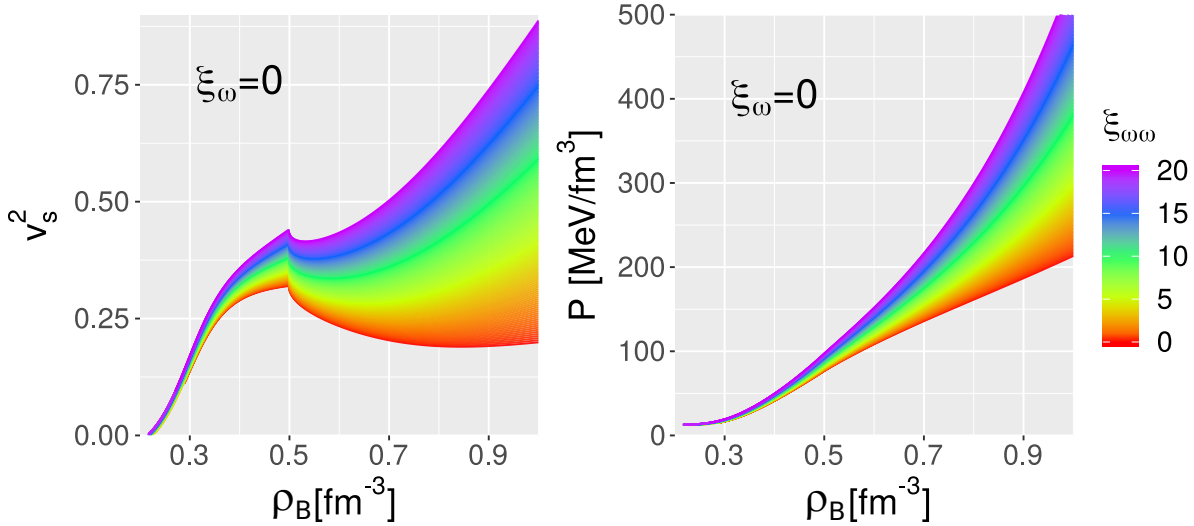


FIGURE 6.1: The speed of sound (left) and pressure (right) as a function of density for quark matter,  $\rho_B = (\rho_u + \rho_d + \rho_s)/3$ , with  $\xi_\omega = 0.0$ . The colour scale indicates the  $\xi_{\omega\omega}$  value.

The main effect of the four-quark vector term is to stiffen the quark EoS and shift the onset of quark matter to larger densities as discussed in [61, 270]. Moreover, the larger the coupling constant,  $\xi_\omega$  the smaller the quark core. This behaviour has been described considering a constant speed of sound model for the quark phase [272].

Let us now analyse how  $\xi_{\omega\omega}$  affects the quark matter EoS. Figure 6.1 shows the pressure (right) and the speed of sound squared (left) as a function of baryonic density,

$$\rho_B = \frac{1}{3}(\rho_u + \rho_d + \rho_s), \quad (6.28)$$

for  $\xi_\omega = 0$ . The speed of sound,

$$v_s^2 = \left. \frac{\partial p}{\partial \epsilon} \right|_s, \quad (6.29)$$

characterizes how stiff the EoS is. It is clear from both panels that the eight-quark term, characterized by the coupling  $\xi_{\omega\omega}$ , allows the quark EoS to become stiffer so that a larger quark core will be sustained in the hybrid NS: this term gives rise to a density dependent speed of sound that increases non-linearly with density. The main role of  $\xi_{\omega\omega}$  is played at large densities: it affects in a much smaller extension the onset of quark matter than the  $\xi_\omega$  coupling. This is clearly seen in Fig. 6.2, where the onset density of quark matter, for each hybrid EoS, is shown by a colour gradient in terms of the parameters  $\xi_{\omega\omega}$  and  $\xi_\omega$ . The change of colour is only slightly dependent on  $\xi_{\omega\omega}$ .

The sudden decrease of the speed of sound  $v_s^2$  at  $\rho_B \approx 0.5 \text{ fm}^{-3}$  is due to the onset of strangeness. Note, however, that the appearance of the strange quark occurs via a crossover and thus in a continuous way. Since the vector terms introduced are flavour invariant [45], the onset of strangeness does not depend of the vector terms and is completely defined by the properties of the model shown in Table 6.1. The amount of strangeness inside the star, will, therefore, be

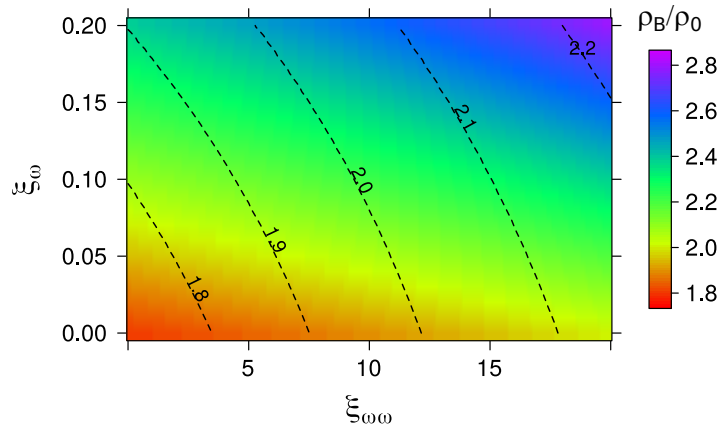


FIGURE 6.2: Onset density of quark matter,  $\rho_B/\rho_0$  (baryonic density in units of saturation density,  $\rho_0 = 0.155 \text{ fm}^{-3}$ ), as a function of both  $\xi_\omega$  and  $\xi_{\omega\omega}$ . The dashed lines represent the value of the maximum NS mass (in solar masses,  $M_\odot$ ) reached by each hybrid EoS, defined by  $(\xi_\omega, \xi_{\omega\omega})$ .

determined by the central density that depends on both vector terms.

In order to study the NS properties, one must solve Einstein's field equations of General Relativity. The energy–momentum tensor of the distribution of matter, in this case of the neutron star, must be calculated in order to solve these equations. Up to this point, we have only worked in flat spacetime, including the formalism to derive the EoS for the interior of the NS. Using the principle of general covariance<sup>4</sup>, one could obtain the energy–momentum tensor in curved spacetime by replacing the Minkowski metric  $\eta_{\mu\nu}$  with a general metric  $g_{\mu\nu}$  and promoting normal derivatives to covariant ones. This process however, would completely couple the field theory used to describe the EoS of the star with Einstein's field equations. In the limit of stellar collapse, the variation of the metric element in the radial direction, over the space occupied by a nucleon is of the order of  $10^{-19}$ . This small variation means that the change of the metric elements along the radial direction is negligible [93]. This, allied to the fact that the EoS is a valid description of the interior of a star, as proved by J. Wheeler and collaborators [273], allows the description of each small volume in the star by the laws of special relativity. Hence, we will partially decouple matter from gravity by computing the EoS in Minkowski spacetime and solving Einstein's field equations with a energy–momentum tensor of a perfect fluid. Such approximation amounts to solving the Tolmann–Oppenheimer–Volkoff (TOV) equations.

Treating NSs as being static, spherically symmetric and assuming the energy–momentum tensor of a perfect fluid, one can use General Relativity in order to calculate the metric tensor inside and

<sup>4</sup>The principle of general covariance states that, if some covariant law of physics holds in the absence of gravity, it also holds in a general gravitational field [93].

outside the static and spherically symmetric star. One can then arrive at the Tolmann–Oppenheimer–Volkoff (TOV) equations [274, 275]:

$$\frac{dP(r)}{dr} = -\frac{G_N}{r^2}[\epsilon(r) + P(r)][M(r) + 4\pi r^3 P(r)] \left[1 - \frac{2G_N M(r)}{r}\right]^{-1}, \quad (6.30)$$

$$M(r) = 4\pi \int_0^r dr' r'^2 \epsilon(r'). \quad (6.31)$$

In the above,  $G_N$  is the gravitational constant,  $P$  and  $\epsilon$  are the pressure and energy density of the matter distribution, i.e., the EoS. The initial conditions for the TOV equations are:  $P(r = R) = 0$ ,  $M(r = 0) = 0$ , where  $M$  is the total gravitational mass of the star and  $R$  is the total radius of the star, defined as the distance from the center at which the pressure vanishes.

We are also interested in calculating the dimensionless tidal deformability of a NS,  $\Lambda$  [93, 276–278]. This quantity is EoS dependent and can be measured by gravitational wave astronomy, in the latter stages of the merging of binary systems, both for NS-NS systems as for NS-black hole systems. This quantity can be related to the  $k_2$  Love number using:

$$\Lambda = \frac{2k_2 R^5}{3M^5}. \quad (6.32)$$

Considering a binary system, one component of the binary will create a tidal tensor  $\epsilon_{ij}$ , which will induce, in the other component of the binary, a quadrupole moment  $Q_{ij}$ . As a first approximation, one can write:  $Q_{ij} = -\lambda(\text{EoS}; m)\epsilon_{ij}$ , where  $m$  is the mass of the star that is experiencing the tidal deformation and  $\lambda(\text{EoS}; m)$  is the EoS dependent tidal deformability. The differential equations for the  $k_2$  Love number can be derived from General Relativity by considering a static, spherically symmetric star placed in a static external quadrupolar tidal field. For details on the derivation, see [276–278]. Explicitly, the differential equation for the  $k_2$  Love number is given by:

$$k_2^{(A)} = \frac{8}{5}C^5(1 - 2C)^2(2 + 2C(y_R - 1) - y_R), \quad (6.33)$$

$$k_2^{(B)} = 2C(6 - 3y_R + 3C(5y_R - 8)), \quad (6.34)$$

$$k_2^{(C)} = 4C^3[13 - 11y_R + C(3y_R - 2) + 2C^2(1 + y_R)], \quad (6.35)$$

$$k_2^{(D)} = 3(1 - 2C)^2[2 - y_R + 2C(y_R - 1)]\ln(1 - 2C), \quad (6.36)$$

$$k_2 = \frac{k_2^{(A)}}{k_2^{(B)} + k_2^{(C)} + k_2^{(D)}}. \quad (6.37)$$

Here,  $C = M/R$  is the compactness of the star and  $y_R = R \frac{dH(R)}{dr} / H(R)$ . The function  $H(r)$  and its derivative with respect to  $r$ ,  $\frac{dH(R)}{dr}$ , can be obtained by solving the following differential

equation for  $H(r)$ :

$$\begin{aligned} \frac{d^2 H(r)}{dr^2} + \left\{ \frac{2}{r} + \left[ \frac{2M(r)}{4\pi r^2} + r(P(r) - \epsilon(r)) \right] \frac{4\pi}{1 - \frac{2M(r)}{r}} \right\} \frac{dH(r)}{dr} \\ + \left\{ \left[ 5\epsilon(r) + 9P(r) + (P(r) + \epsilon(r)) \frac{d\epsilon}{dP} - \frac{3}{2\pi r^2} \right] \frac{4\pi}{1 - \frac{2M(r)}{r}} \right\} H(r) \\ - 4 \left\{ \frac{\frac{dP(r)}{dr}}{P(r) + \epsilon(r)} \right\}^2 H(r) = 0. \end{aligned} \quad (6.38)$$

This second order differential equation can be separated in two first-order differential equations which have to be solved alongside the TOV equations. Starting at the center of the star, one can use the expansion of  $H(r)$  near the origin,  $r \rightarrow 0$  to write,  $H(r) = a_0 r^2$  and  $H'(r) = 2a_0 r$ , with some constant  $a_0$ . Since we are interested in the ratio  $y_R = R \frac{dH(R)}{dr} / H(R)$ , the constant  $a_0$  can be fixed arbitrarily. In order to numerically solve the above equations we use as initial conditions  $H(r_0) = r_0^2$  and  $H'(r_0) = 2r_0$ , for very small  $r_0 \sim 0$ . For more details see [279, 280].

We plot in Fig. 6.3 our set of EoS on a pressure vs energy density graph for  $\xi_\omega = 0$ , and include in the background the acceptable region of EoS defined in [262]. We conclude that our set of EoS covers a quite large fraction of the proposed region. The red colour indicates a region with a speed of sound  $v_s^2 \lesssim 0.3$  as shown in Fig. 6.1. Our most massive stars (purple colour) lie close to the boarder of the region and are associated with central speed of sound well above the conformal limit, which can be as large as  $0.9c$ . Some interesting conclusions are:

- (a) our set of EoS also defines a change of slope. This could be due to the fact that we work with a model with chiral symmetry incorporated. This kind of “knee” is also present in other studies [263];
- (b) we get low mass stars with a quark core below the “knee”;
- (c) our heaviest stars with a large quark core have a speed of sound far from the conformal limit;
- (d) the red dots identify EoS with a speed of sound close to the conformal limit and lie in the center of the region as obtained in [262];
- (e) the vector interactions considered in this work do not span the whole region of the Fig. 6.3. Including extra four and eight-quark vector interactions, for instance in the scalar and vector-isovector channels, may increase this region. This is left as future work.

Figure 6.4 shows the  $M(R)$  diagram for each hybrid EoS, parametrized by  $(\xi_\omega, \xi_{\omega\omega})$ . For the sake of clarity, we have fixed  $\xi_\omega$  in each panel:  $\xi_\omega = 0.0$  (left),  $\xi_\omega = 0.1$  (center), and  $\xi_\omega = 0.2$  (right). The colour scale encodes the value of  $\xi_{\omega\omega}$ . The effect of  $\xi_\omega$  is clear: as its value increases, quarks appear at larger masses, shorter quark star branches are obtained, which reach higher  $M_{\max}$ . As expected, given that both represent repulsive interactions,  $\xi_{\omega\omega}$  shows the same trend as  $\xi_\omega$ . Higher values of  $\xi_{\omega\omega}$  originate longer quark branches capable of reproducing more massive NS. The most interesting cases occur for smaller values of  $\xi_\omega$  and for considerable high values of

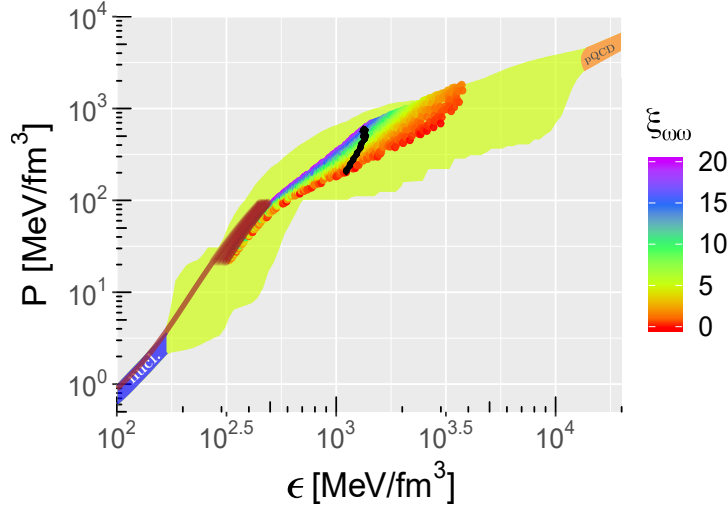


FIGURE 6.3: The EoS used in the present study in pressure vs energy density. The colour scale refers to the parameter  $\xi_{\omega\omega}$ . At low densities the DDME2 EoS is represented followed by the hadron-quark phase transition at constant pressure (Maxwell construction). All EoS shown are causal. On the background the contours of the region defined in [262] for the acceptable EoS that interpolate between the neutron matter EoS determined for a chiral effective field theory approach in [239] and the perturbative QCD EoS calculated in [281]. The black dots identify the maximum mass stars.

$\xi_{\omega\omega}$ , see left and center panels. Under these conditions, quarks are already present inside light NS,  $M > 1.1M_{\odot}$ , and it is still possible to attain quite massive and compact NS,  $M \approx 2.2M_{\odot}$  and  $R \approx 11$  km. For  $\xi_{\omega\omega} > 10$ , hybrid NS with  $M > 1.9M_{\odot}$  that predict already some quark content for  $M \approx 1.0M_{\odot}$  NS are possible.

We have represented two shaded regions in Fig. 6.4 that indicate the  $(M, R)$  constraints obtained by two independent analysis using the NICER x-ray data from the millisecond pulsar PSR J0030+0451 [97, 282]. The set of hybrid EoS in the present work are in agreement with both constraints.

The  $\Lambda(R)$  diagrams are shown in Fig. 6.5. Like in Fig. 6.4, we show three panels:  $\xi_{\omega} = 0.0$  (left),  $\xi_{\omega} = 0.1$  (center), and  $\xi_{\omega} = 0.2$  (right). The red dashed line represents the constraint  $70 < \Lambda_{1.4M_{\odot}} < 580$  (90% level) obtained from the GW170817 event [96]. We see that, with the combination of low  $\xi_{\omega}$  and high  $\xi_{\omega\omega}$ , it is possible to generate an hybrid EoS that softens the hadronic EoS (solid black line) at low baryonic densities, and satisfies the GW170817  $\Lambda_{1.4M_{\odot}}$  constraint. Another interesting result is that the radius of the heaviest stable NS,  $R_{\max}$ , is quite sensitive to the  $\xi_{\omega\omega}$  value, and it is possible to predict sequences in the  $\Lambda(R)$  diagram that clearly deviate from the purely hadronic EoS one. Small values of  $\Lambda$  for a low/intermediate mass star could be an important signature indicating the presence of quark matter in NS, which would be accessible through observational results on  $(M_i, R_i, \Lambda_i)$ .

In Fig. 6.6, we show how the central density,  $\rho_{\max}$  at the maximum NS,  $M_{\max}$ , depends on  $(\xi_{\omega}, \xi_{\omega\omega})$ . The overall effect of  $\xi_{\omega}$  is to decrease the central density of  $M_{\max}$ , while  $\xi_{\omega\omega}$  shows a clear non-monotonic impact on  $\rho_{\max}$ . The maximum value of  $\rho_{\max}$  is reached for  $\xi_{\omega} = 0$  and  $\xi_{\omega\omega} \approx 11$ . This is already seen in Fig. 6.4 (left panel), where the  $R_{\max}$  shows a non-monotonic

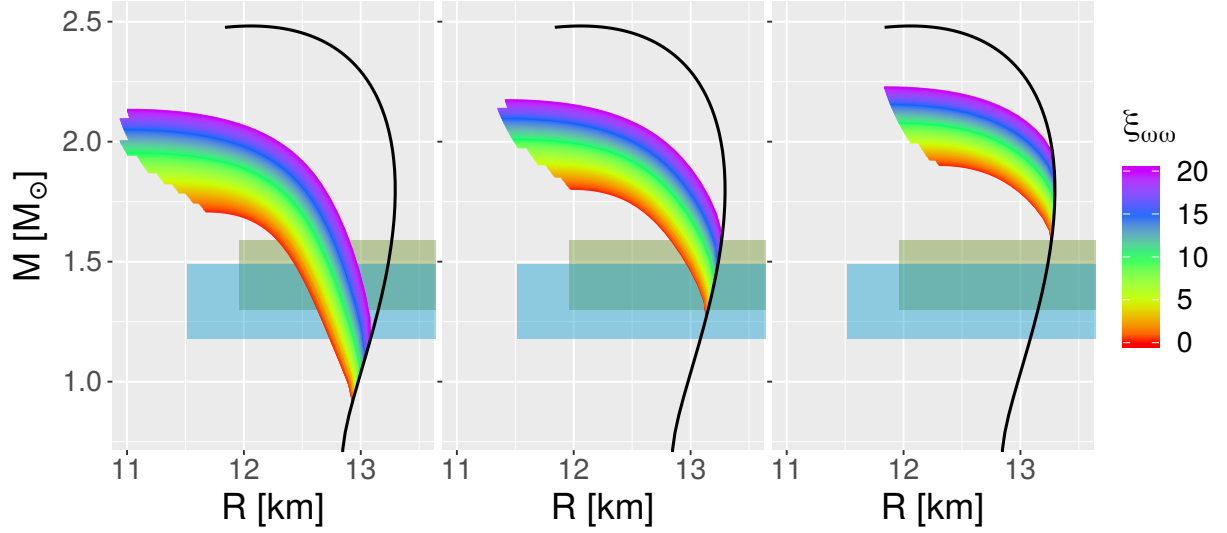


FIGURE 6.4:  $M(R)$  diagrams for  $\xi_\omega = 0$  (left),  $\xi_\omega = 0.1$  (center), and  $\xi_\omega = 0.2$  (right). The colour scale indicates the  $\xi_{\omega\omega}$  value and the black line represents the purely hadronic sequence. The bag parameter is fixed at  $B = 15 \text{ MeV}/\text{fm}^3$ . The coloured regions indicate the  $(M, R)$  constraints obtained by two independent analysis using the NICER x-ray data from the millisecond pulsar PSR J0030+0451 [97, 282].

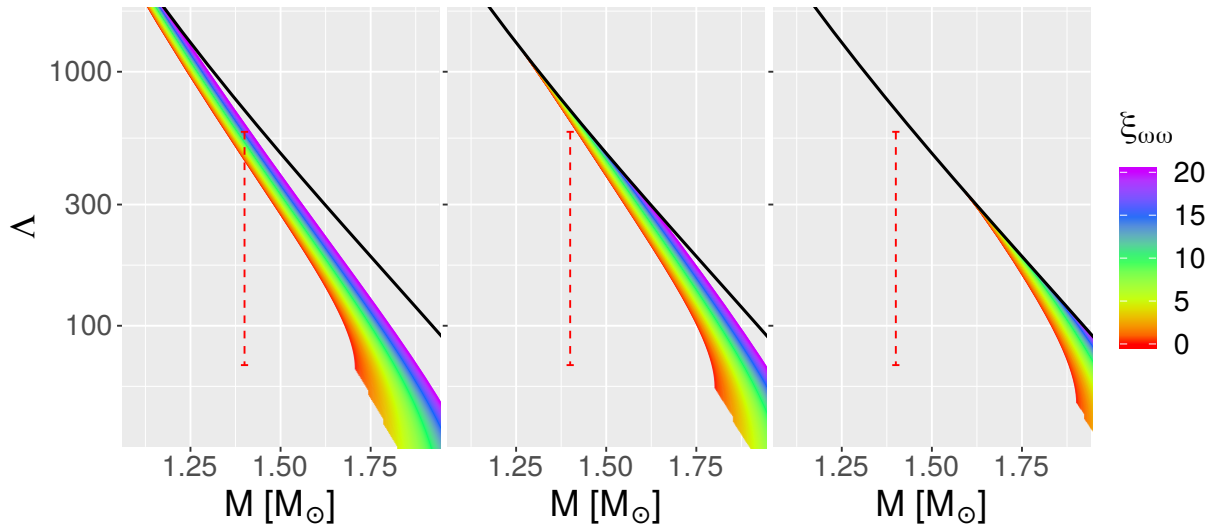


FIGURE 6.5:  $\Lambda(M)$  diagrams for  $\xi_\omega = 0$  (left),  $\xi_\omega = 0.1$  (center), and  $\xi_\omega = 0.2$  (right). The colour scale indicates the  $\xi_{\omega\omega}$  value and the black line represents the purely hadronic sequence. The bag parameter is fixed at  $B = 15 \text{ MeV}/\text{fm}^3$ . The dashed red line indicates the constraint  $70 < \Lambda_{1.4M_\odot} < 580$  (90% level) from the GW170817 event [96]

behaviour: it increases up to  $\xi_{\omega\omega} = 10$  and then starts to decrease for higher  $\xi_{\omega\omega}$  values. Since the onset of the strange quark occurs at  $\rho_B \approx 0.5 \text{ fm}^{-3}$  independently of the vector interaction, as we have seen before, we conclude that all stars have some fraction of strange quarks. However, if  $\xi_\omega > 0.1$  the amount of strangeness is quite small. This behaviour has also been found in hadronic matter with hyperons: if the coupling to the vector mesons is strong the strangeness content of the star is small [283, 284]. It is interesting, however, to realize that the eight-quark term stiffens the EoS but still allows very large central baryonic densities, and, as a consequence, a large strangeness content.

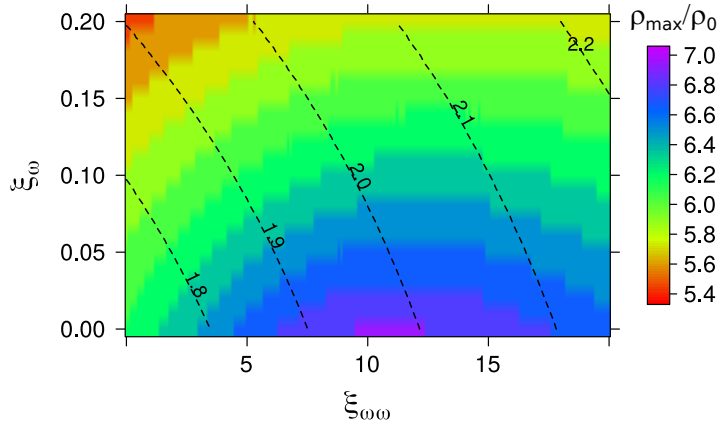


FIGURE 6.6: Central density at the maximum NS mass,  $\rho_{\max}$  [in units of saturation density,  $\rho_0 = 0.155 \text{ fm}^{-3}$ ], as a function of both  $\xi_\omega$  and  $\xi_{\omega\omega}$ . The dashed lines represent the value of the maximum NS mass [in  $M_\odot$ ] reached by each hybrid EoS, defined by  $(\xi_\omega, \xi_{\omega\omega})$ .

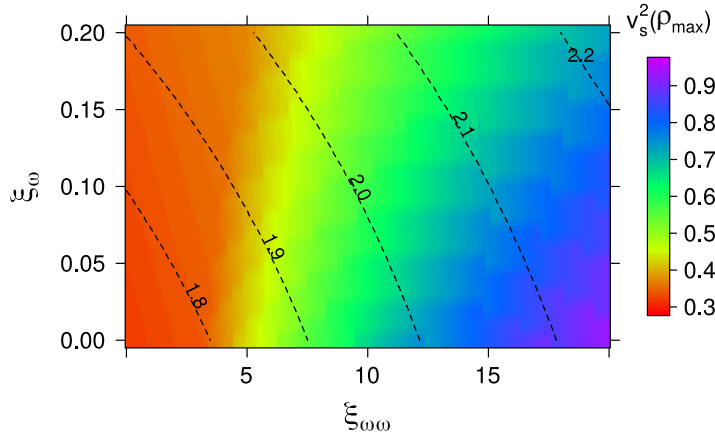


FIGURE 6.7: Speed of sound at the central density of the most massive stable NS,  $v_s^2(\rho_{\max})$ , as a function of both  $\xi_\omega$  and  $\xi_{\omega\omega}$ . The dashed lines represent the value of the maximum NS mass [in  $M_\odot$ ] reached by each hybrid EoS, defined by  $(\xi_\omega, \xi_{\omega\omega})$ .

In Fig. 6.7, we display the speed of sound squared,  $v_s^2$ , attained at the central density of the heavier NS ( $M_{\max}$ ) for each hybrid EoS, i.e.,  $v_s^2(\rho_{\max})$ , which is a function of  $(\xi_\omega, \xi_{\omega\omega})$ . Such quantity,  $v_s^2$ , is very sensitive to  $\xi_{\omega\omega}$  and is only slightly affected by  $\xi_\omega$ . To reach massive NS cores, it is crucial to have large  $v_s^2$  values. The quark core of  $M \approx 1.8M_\odot$  in Fig. 6.8, is possible only because the star has a very stiff quark matter phase, with  $v_s^2 \approx 0.93$ .

Finally, let us now analyse how the quark core size depends on  $(\xi_\omega, \xi_{\omega\omega})$ . Figure 6.8 displays both the mass of the quark core,  $M_{\text{QC}}$  (right panel), and the radii,  $R_{\text{QC}}$  (left panel), as a function of  $(\xi_\omega, \xi_{\omega\omega})$ . We further indicate the maximum mass reached by each hybrid stars through contour lines as before (black dashed lines). For a fixed  $\xi_\omega$  value,  $M_{\text{QC}}$  increases with  $\xi_{\omega\omega}$ , reaching a heavier quark core for low  $\xi_\omega$  and high  $\xi_{\omega\omega}$ . This is precisely when the central density is the largest. On the other hand, for a fixed  $\xi_{\omega\omega}$  value,  $M_{\text{QC}}$  decreases as the value of  $\xi_\omega$  gets bigger. Therefore, the extremes of  $M_{\text{QC}}(\xi_\omega, \xi_{\omega\omega})$  lie in opposite regions: the lighter quark core,

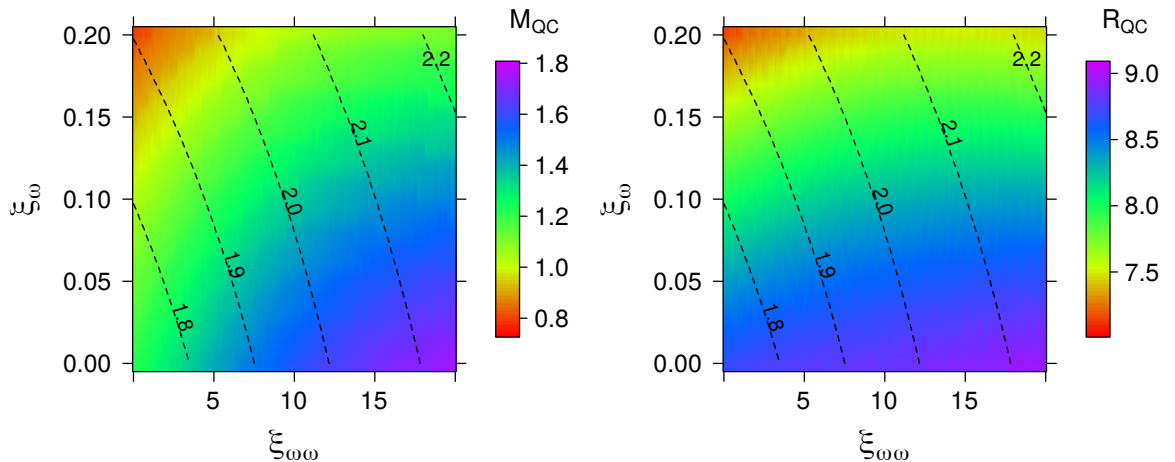


FIGURE 6.8: The quark core mass  $M_{\text{QC}}$  [in  $M_{\odot}$ ] (left) and radii  $R_{\text{QC}}$  [in km] (right) as a function of both  $\xi_{\omega}$  and  $\xi_{\omega\omega}$ . The dashed lines represent the value of the maximum NS mass [in  $M_{\odot}$ ] reached by each hybrid EoS, defined by  $(\xi_{\omega}, \xi_{\omega\omega})$ .

$M \approx 0.8M_{\odot}$ , is found for  $(\xi_{\omega} = 0.2, \xi_{\omega\omega} = 0)$  while the heavier,  $M \approx 1.8M_{\odot}$ , is generated for  $(\xi_{\omega} = 0, \xi_{\omega\omega} = 20)$ . Actually, a quark core of  $M \approx 1.8M_{\odot}$  is generated in a region where  $M_{\text{max}} \approx 2.1M_{\odot}$ , showing that 85% of the star has quark degrees of freedom. Even though  $R_{\text{QC}}$  displays a similar trend as  $M_{\text{QC}}$ , there is a greater sensitivity to  $\xi_{\omega}$  than  $\xi_{\omega\omega}$ . Even for low  $\xi_{\omega\omega}$  values, the quark core radii can reach values as high as 9 km, although two solar mass stars are not attained for these values. The contour lines representing  $M_{\text{max}}$  reflect a much stronger dependence on  $\xi_{\omega\omega}$  than on  $\xi_{\omega}$ .

## 6.4 Conclusions and outlook

In this chapter we have analysed the effect of four-quark and eight-quark vector-isoscalar interactions in hadron-quark hybrid EoS within the three flavour NJL model. Each hybrid EoS consists of charge-neutral matter in  $\beta$ -equilibrium, in which a first-order phase transition from hadronic to quark matter is realized. We have analysed how the stability of hybrid stars sequences and their properties depend on the four and eight vector-isoscalar couplings,  $\xi_{\omega} = 2G_{\omega}/G$  and  $\xi_{\omega\omega} = 16G_{\omega\omega}/G^4$ .

From the density dependence of the speed of sound of quark matter, one clearly recognizes the stiffening effect of both interactions. This behaviour imprints interesting features in the sequences of stable stars in the  $M(R)$  diagram. We show that the size of the quark star branch is quite sensitive to both couplings, particularly to the  $\xi_{\omega\omega}$  coupling. With a small value for  $\xi_{\omega}$ , there is a range of  $\xi_{\omega\omega}$  values that predict quark matter in light NS,  $\sim 1M_{\odot}$ , and, at the same time, are able to sustain a quark core in quite massive NS, i.e.,  $\sim 2.1M_{\odot}$ . Furthermore, the radius of the heaviest stable NS,  $R_{\text{max}}$ , is highly dependent on the strength of  $\xi_{\omega\omega}$ , leading to a considerable decrease of  $R_{\text{max}}$  as the coupling increases. As a consequence, for a hybrid EoS a considerable deviation from the purely hadronic matter EoS prediction for the tidal deformability

$\Lambda(M)$  is obtained. This occurs even for moderate NS masses,  $\sim 1.4 M_\odot$ , in accordance with the astrophysical constraints from NICER and LIGO/Virgo observations.

We have also discussed how the size of the quark core depends on  $\xi_\omega$  and  $\xi_{\omega\omega}$ . The main conclusion is that, for a fixed  $\xi_\omega$  value,  $M_{\text{QC}}$  increases with  $\xi_{\omega\omega}$ . While lighter quark cores,  $\sim 0.8M_\odot$ , are predicted for  $(\xi_\omega = 0.2, \xi_{\omega\omega} = 0)$ , the heaviest cores,  $\sim 1.8M_\odot$ , are generated in the opposite regime, i.e.,  $(\xi_\omega = 0, \xi_{\omega\omega} = 20)$ . Quite massive quark cores,  $\sim 1.8M_\odot$ , are predicted for hybrid EoS in which  $M_{\text{max}} \approx 2.1M_\odot$ , showing that there are quark degrees of freedom in 85% of the star.

Concerning the conclusions drawn in [262], we obtain some similar results, in particular, we are able to describe two solar mass stars with a central speed of sound squared below 0.4, but more massive stars require larger central values for the speed of sound. However, some other aspects in our study differ from the ones discussed in [262]. We have obtained low mass stars with a quark core, and we can describe very massive stars with large quark cores and a speed of sound far from the conformal limit. This is also in divergence with the conclusions drawn in [106] because we were able to get large quark cores even with a high central speed of sound. The reason for this behaviour is that the model used to perform our study, allows for a density dependent speed of sound, with a non-linear density dependence.

A low mass NS with a quark core would be confirmed if together with the binary neutron star tidal deformability and mass, also the dominant post-merger GW frequency<sup>5</sup>  $f_{\text{peak}}$  would be measured. In [286] it was shown that this frequency would identify a first-order phase transition. In the presence of a first-order phase transition the  $f_{\text{peak}}$  comes at a much larger frequency: the larger the baryonic density gap at the phase transition the larger the frequency.

A possible future research project is to add to the quark model other types of vector interactions like the vector-isovector channel both for four and eight-quark interactions. Such extension of the model could allow the model to span the whole region of the Fig. 6.3. One can also extend the model even further, to also include colour superconducting quark condensates or scalar and pseudoscalar eight-quark interactions, as performed in Chapter 5.

Another future project is to change the hadronic part of the hybrid EoS while also extending the quark model. In Ref. [264], the hadronic EoS was built using the Taylor expansion around saturation density. Using such approach, the space of possible parameters of the hadron phase are sampled and several meta-models can be considered, as long as they meet a given number of well established conditions. The reason to use such a procedure is simple: there is still an uncertainty in the hadronic phase and using a meta-model approach which does not rely on any specific physical model allows the study of a possible phase of quark matter inside a NS in a hadron-model independent way.

---

<sup>5</sup> $f_{\text{peak}}$  is the peak frequency, of the gravitational wave emission of the post-merger remnant, measured with the full width at half maximum [285].

# PART III

Studies beyond the mean field approximation



## Chapter 7

# One-meson-loop NJL model: collective and non-collective excitations

### 7.1 Introduction

In most applications, the NJL was studied in the standard mean field (MF) approximation, equivalent to the so-called Hartree plus random phase approximation (RPA) on the quark polarization function [287]. Within these schemes, only the quark loop is considered at the effective action level and quantum fluctuations caused by meson modes are neglected, see Chapter 4. Including fluctuations in the NJL model, however, is not an easy task [287]. For some works, including beyond MF corrections to the NJL model and linear sigma model see [180, 288–299].

Studying the model beyond the MF approximation, is very important to correctly inspect the physical behaviour near the critical region where the system displays long range correlations. At low temperatures and densities, before the restoration of chiral symmetry, it is expected that a major role is played by the thermal excitations of the pion modes [300]. These low mass degrees of freedom are the pseudo-Goldstone modes of the NJL model (the details on the importance of including quantum fluctuations to study the QCD phase diagram, were given in Chapters 3.1.3 and 4).

In a so-called symmetry conserving calculation, at any level of approximation, the symmetries of the model must be preserved. In the case of chiral symmetry and its breaking in the vacuum, the model must have a Goldstone mode in the chiral limit. The MF or Hartree plus RPA calculations are symmetry preserving [287, 301].

Different symmetry conserving schemes, to take the NJL model beyond the MF approximation, have been developed over the years like the  $1/N_c$  expansions, “ $\Phi$ -derivable” methods and functional methods [113, 287, 302–306]. The MF approximation represents the leading order in the  $N_c$  expansion and corrections to the MF approximation could be of order  $1/N_c$ . As already seen previously, the NJL is a non-renormalizable field theory in four spacetime dimensions and a regularization procedure must be applied, which will be directly related to the absolute size of

the corrections. This means that the magnitude of the corrections is not only dictated by the expansion parameter but also by the model parametrization and phenomenology [45].

A symmetry conserving method was developed by E. Nikolov et al. in [113], based on the effective action formalism. Such formalism was coined as the one-meson-loop approximation [113, 303] and represents the next to leading order correction in the  $N_c$  expansion of the NJL effective action. It was later extended to include low temperature effects in the gap equation [300] using an approximation: at low temperatures, only the lowest lying pion pole would contribute.

In this chapter, we do not deal with the system at finite density. Hence, vector-type interactions will not be considered even though these interactions can be present and are important in the NJL model, specially at finite density as seen in previous chapters.

In this chapter, we will take a step in the direction of calculating the NJL phase diagram beyond the MF approximation by extending the symmetry conserving scheme presented by E. Nikolov et al. to finite temperature [113, 300]. To accomplish this, we will solve the NJL gap equation including all contributions coming from the one-meson-loop correction terms. This will allow to study the impact of meson fluctuations on the quark condensate and in the restoration of chiral symmetry at finite temperature. Previous works have only considered the effect of the one-meson-loop terms in the vacuum quark condensate and did not develop the formalism of the integration technique and phenomenology to extend the calculation to finite temperature [113, 300, 301, 303]. In order to consider all contributions coming from the one-meson-loop correction terms, we will separate the contour integrations that arise in the calculation in two distinct contributions: the collective and non-collective modes [306, 307]. This calculation does not involve meson fields with kinetic boson terms at the Lagrangian level. In this formalism, mesons are composite collective and non-collective excitations of the underlying quark fields. A final remark is that we will use the NJL model in its two flavour version since the underlying physics of the calculation becomes less complicated.

This chapter is organized as follows. In Section 7.2 the NJL model and formalism, to derive the one-meson-loop gap equation, are presented. The separation of the collective and non-collective modes is laid out. In Section 7.3 the results from increasing the meson fluctuations in the vacuum and at finite temperature are studied. The separated effect of the collective modes and non-collective modes, on the quark condensate, is also considered. Finally, in Section 7.4 conclusions are discussed and further work is planned.

## 7.2 Model and Formalism

To derive the NJL gap equation including one-meson-loop corrections, we will use the effective action formalism. As E. Nikolov et al. in [113], we consider the two flavour NJL model, whose Lagrangian density in Minkowski spacetime is given by:

$$\mathcal{L}(\bar{\psi}, \psi) = \bar{\psi}(i\cancel{\partial} - \hat{m})\psi + \frac{G}{2} \left[ (\bar{\psi}\psi)^2 + (\bar{\psi}i\gamma^5\boldsymbol{\tau}\psi)^2 \right]. \quad (7.1)$$

Here,  $\psi$  is the quark field,  $\hat{m}$  is the current quark mass diagonal matrix,  $\hat{m} = \text{diag}(m_u, m_d)$ , which explicitly breaks chiral symmetry and  $G$  is the coupling constant of the scalar and pseudoscalar four-fermions interaction. We will work in the isotopic limit with  $m_u = m_d = m$  and the mass matrix  $\hat{m}$  can be written as  $m$  times the identity matrix in flavour space. As usual,  $\boldsymbol{\tau}$ , are the three Pauli matrices of the  $SU(2)$  group. If we define the operator  $\hat{\Gamma}_a$ :

$$\hat{\Gamma}_0 = \mathbb{1}, \quad \hat{\Gamma} = i\gamma^5 \boldsymbol{\tau} \rightarrow \hat{\Gamma}_a = \begin{cases} \mathbb{1} & , \quad a = 0, \\ i\gamma^5 \tau^a & , \quad a = 1, 2, 3, \end{cases} \quad (7.2)$$

we can rewrite the Lagrangian as:

$$\mathcal{L}(\bar{\psi}, \psi) = \bar{\psi}(i\not{\partial} - m)\psi + \frac{G}{2}(\bar{\psi}\hat{\Gamma}_a\psi)^2. \quad (7.3)$$

To include temperature we will use the Euclidean spacetime by performing a Wick rotation from real times to imaginary times,  $x_0 \rightarrow -i\tau$ , changing the metric,  $\eta_{ab} = -\delta_{ab}$  (see Table A.1 in the Appendix A). The Euclidean action now can be written as  $\mathcal{S}_E[\bar{\psi}, \psi] = -\int_0^{1/T} d\tau \int d^3x \mathcal{L}_E(\bar{\psi}, \psi)$ . The generating functional of the fully connected Green's functions, for a given temperature ( $T$ ), ignoring a normalization factor, can be written as:

$$\mathcal{W}[T; \eta, \bar{\eta}] = \ln \int \mathcal{D}\bar{\psi} \mathcal{D}\psi e^{-\mathcal{S}_E[\bar{\psi}, \psi] + \int_0^{1/T} d\tau \int d^3x (\bar{\psi}\eta + \bar{\eta}\psi)}. \quad (7.4)$$

Following the Wick rotation, the partial differential operator is defined as  $\partial_a = (-i\partial_0, \nabla) = (\partial_\tau, \partial_x)$  and the Euclidean Dirac matrices are  $\gamma_a = (i\gamma^0, \boldsymbol{\gamma}) = (\gamma_\tau, \boldsymbol{\gamma})$ , which respect the anti-commutation relation  $\{\gamma^a, \gamma^b\} = -2\delta^{ab}$ . For more details, see Appendix A.

As already pointed out in other chapters, when dealing with multi-quark interactions one can use the Hubbard–Stratonovich transformation to absorb these non-quadratic interactions with the use of auxiliary fields with the same quantum numbers as the quark bilinears operators. In the case of the NJL model considered in this chapter, it can be written as [308]:

$$\exp \left\{ \int_0^{1/T} d\tau \int d^3x \frac{G}{2} (\bar{\psi}\hat{\Gamma}_a\psi)^2 \right\} \propto \int \mathcal{D}\phi_a \exp \left\{ -\int_0^{1/T} d\tau \int d^3x \left[ \frac{\phi_a^2}{2G} + (\bar{\psi}\hat{\Gamma}_a\psi)\phi_a \right] \right\}. \quad (7.5)$$

This exact transformation leads to a partially bosonized version of the model with Yukawa-type of interactions between the fermions and the auxiliary fields without kinetic terms. The quadratic fermionic term can then be integrated out exactly. In this model the zeroth component of the field,  $\phi_0$ , corresponds to a scalar meson field and the other three  $\phi$ , to a pseudoscalar meson field i.e.,  $\phi_a = \{\phi_0, \boldsymbol{\phi}\}$ .

After using this transformation and shifting variables as  $\phi_a \rightarrow \phi_a - m\delta_{a0}$ , the generating functional in Euclidean spacetime, is:

$$\mathcal{Z}[\eta, \bar{\eta}, J] \propto \int \mathcal{D}\bar{\psi} \mathcal{D}\psi \mathcal{D}\phi_a e^{-\mathcal{S}_E[\bar{\psi}, \psi, \phi_a] + \int d\tau d^3x (\bar{\psi}\eta + \bar{\eta}\psi + J_a\phi_a)}, \quad (7.6)$$

where the Euclidean action,  $\mathcal{S}_E$ , is defined as:

$$\begin{aligned}\mathcal{S}_E[\bar{\psi}, \psi, \phi] &= - \int d\tau d^3x \mathcal{L}_E(\bar{\psi}, \psi, \phi_a) \\ &= \int d\tau d^3x \left[ \bar{\psi} \left( -i\gamma_a \partial_a + \hat{\Gamma}_a \phi_a \right) \psi + \frac{\phi_a^2}{2G} - \frac{m\phi_0}{G} + \frac{m^2}{2G} \right] \\ &= \int d\tau d^3x \left[ \bar{\psi} D \psi + \frac{\phi_a^2}{2G} - \frac{m\phi_0}{G} + \frac{m^2}{2G} \right].\end{aligned}\quad (7.7)$$

To write the above action, we used:  $\gamma_0 \partial_0 = \gamma_\tau \partial_\tau$  and  $\gamma_a \partial_a = \gamma_\tau \partial_\tau + \boldsymbol{\gamma} \cdot \boldsymbol{\nabla}$ , see Table A.1 in the Appendix A. The operator  $D$  is defined as:

$$D = -i\gamma_a \partial_a + \hat{\Gamma}_a \phi_a. \quad (7.8)$$

Since the generating functional is quadratic in the fermion fields we can integrate it exactly using the result for a Gaussian integral of  $N$  Grassman variables  $\xi_1, \xi_2 \dots \xi_N$ :

$$\int d\xi_1^\dagger d\xi_1 \dots d\xi_N^\dagger d\xi_N e^{\xi^\dagger D \xi} = \det D. \quad (7.9)$$

Using this result we obtain the following bosonized generating functional:

$$\mathcal{Z}[J] \propto \int \mathcal{D}\phi_a \det D \exp \left\{ - \int d\tau d^3x \left[ \frac{\phi_a^2}{2G} - \frac{m\phi_0}{G} + \frac{m^2}{2G} \right] + \int d\tau d^3x J_a \phi_a \right\}, \quad (7.10)$$

where the functional determinant is made over all fermionic internal indices i.e. Dirac, colour, flavour and continuous indices. Since  $D$  has no internal structure in colour space, the determinant over colour is simply  $D^{N_c}$ , with  $N_c$  the number of colours. We can rewrite the above as follows,

$$\begin{aligned}\mathcal{Z}[J] &\propto \int \mathcal{D}\phi_a e^{N_c \ln \det D} \exp \left\{ - \int d\tau d^3x \left[ \frac{\phi_a^2}{2G} - \frac{m\phi_0}{G} + \frac{m^2}{2G} \right] + \int d\tau d^3x J_a \phi_a \right\} \\ &\propto \int \mathcal{D}\phi_a e^{-\mathcal{S}_E[\phi_a] + \int d\tau d^3x J_a \phi_a},\end{aligned}\quad (7.11)$$

where  $\mathcal{S}_E[\phi_a]$  is the bosonized action defined as (using the identity  $\ln \det A = \text{tr} \ln A$ ):

$$\mathcal{S}_E[\phi] = -N_c \text{tr} \ln D + \int d\tau d^3x \left[ \frac{\phi_a^2}{2G} - \frac{m\phi_0}{G} + \frac{m^2}{2G} \right]. \quad (7.12)$$

As pointed out in [112, 113], for two quark flavours the complex part of the fermionic determinant vanishes. Indeed, a possible imaginary contribution to the Euclidean effective action is related to the non-invariance of the fermionic measure and to the measure of the vacuum persistence amplitude, effects that are not considered here [129, 134]. The fermionic determinant can be

written as:

$$\begin{aligned}\mathrm{tr} \ln D &= \frac{1}{2}(\mathrm{tr} \ln D + \mathrm{tr} \ln D) - \frac{1}{2}(\mathrm{tr} \ln D^\dagger - \mathrm{tr} \ln D^\dagger) \\ &= \frac{1}{2} \mathrm{tr} \ln (D^\dagger D) - \frac{1}{2} \mathrm{tr} \ln \left( \frac{D^\dagger}{D} \right).\end{aligned}\quad (7.13)$$

Neglecting the complex part, i.e.,  $D^\dagger = D$ , the second term is zero and we are allowed to write  $\mathrm{tr} \ln D = 1/2 \mathrm{tr} \ln D^\dagger D$ .

The operator  $D^\dagger D$  can be written in a covariant way. Consider the operator  $D$  defined in Eq. (7.8), its conjugate is<sup>1</sup>:

$$D^\dagger = (-i\gamma_a \partial_a + \hat{\Gamma}_a \phi_a)^\dagger = i\partial_a^\dagger \gamma_a^\dagger + \phi_a \hat{\Gamma}_a^\dagger = i\gamma_a \partial_a + \phi_a \hat{\Gamma}_a^\dagger. \quad (7.14)$$

Where we have used the fact that  $\gamma_a^\dagger = -\gamma_a$  and  $\partial_a^\dagger = -\partial_a$ . The product  $D^\dagger D$  can be written as:

$$D^\dagger D = \gamma_a \gamma_b \partial_a \partial_b + i\gamma_a \hat{\Gamma}_b (\partial_a \phi_b) + i\gamma_a \hat{\Gamma}_b \phi_b \partial_a - i\phi_a \hat{\Gamma}_a^\dagger \gamma_b \partial_b + \phi_a \hat{\Gamma}_a^\dagger \hat{\Gamma}_b \phi_b. \quad (7.15)$$

One can use the following results:

$$\phi_a \hat{\Gamma}_a^\dagger \gamma_b = (\phi_0 + i\gamma^5 \boldsymbol{\tau} \cdot \boldsymbol{\phi})^\dagger \gamma_b = (\phi_0 - i\gamma^5 \boldsymbol{\tau} \cdot \boldsymbol{\phi}) \gamma_b = \gamma_b (\phi_0 + i\gamma^5 \boldsymbol{\tau} \cdot \boldsymbol{\phi}) = \gamma_b \hat{\Gamma}_a \phi_a, \quad (7.16)$$

$$\gamma_a \gamma_b \partial_a \partial_b = \frac{1}{2}(\gamma_a \gamma_b + \gamma_b \gamma_a) \partial_a \partial_b = \frac{1}{2} \{\gamma_a, \gamma_b\} \partial_a \partial_b = -\delta_{ab} \partial_a \partial_b = -\partial_a \partial_a, \quad (7.17)$$

$$\phi_a \hat{\Gamma}_a^\dagger \hat{\Gamma}_b \phi_b = (\phi_0 - i\gamma^5 \boldsymbol{\tau} \cdot \boldsymbol{\phi})(\phi_0 + i\gamma^5 \boldsymbol{\tau} \cdot \boldsymbol{\phi}) = \phi_0^2 + (\gamma^5)^2 (\boldsymbol{\tau} \cdot \boldsymbol{\phi})^2 = \phi_0^2 + \boldsymbol{\phi}^2 = \phi_a \phi_a, \quad (7.18)$$

in order to write the operator  $D^\dagger D$  in a covariant way as:

$$D^\dagger D = -\partial_a \partial_a + i\gamma_a \hat{\Gamma}_b (\partial_a \phi_b) + \phi_a \phi_a. \quad (7.19)$$

Using this result, the bosonized Euclidean action in Eq. (7.12), can be written as:

$$\mathcal{S}_E[\phi] = -\frac{N_c}{2} \mathrm{tr} \ln D^\dagger D + \int_0^{1/T} d\tau \int d^3x \left[ \frac{\phi_a^2}{2G} - \frac{m\phi_0}{G} + \frac{m^2}{2G} \right]. \quad (7.20)$$

We can finally write the completely bosonic energy functional as:

$$\mathcal{W}[T; J] = \ln \int \mathcal{D}\phi_a e^{-\mathcal{S}_E[\phi_a] + \int_0^{1/T} d\tau \int d^3x J_a \phi_a}. \quad (7.21)$$

<sup>1</sup>The expectation value of the operator  $\partial$  and its hermitian conjugate are defined to be,  $\langle \partial \rangle = \int dx \Psi^* \partial \Psi$  and  $\langle \partial \rangle^* = \int dx \Psi^* \partial^\dagger \Psi$ . Integrating the first equation by parts and assuming that  $\Psi(x \rightarrow \infty) = 0$ , we write:

$$\langle \partial \rangle = \int dx \Psi^* \partial \Psi = - \int dx (\partial \Psi^*) \Psi = - \int dx \Psi^* \partial^\dagger \Psi.$$

Comparing the different definitions, one can conclude that  $\partial^\dagger = -\partial$ .

As already discussed in Chapter 4, we can use the energy functional defined above to get the effective action. The effective action can be expanded in the background field approximation to yield the one-loop effective action. Such quantity, in the context of the model presented here, is called the one-meson-loop effective action, from which the one-meson-loop gap equation was derived in Ref. [113].

The effective action of the model can be obtained through a Legendre transformation,

$$\Gamma[T; \varphi] = \int d\tau \int d^3x J_a \varphi_a - \mathcal{W}[T; J], \quad (7.22)$$

where  $\varphi_a$  is the vacuum expectation value of the fields in the presence of an external source,

$$\varphi = \langle \phi \rangle_J = \frac{\delta \mathcal{W}[J]}{\delta J}. \quad (7.23)$$

Considering small fluctuations around the background field, one can expand the effective action in terms of the action given by Eq. (7.20) and its functional derivatives [112]. Using such expansion, the one-meson-loop effective action is:

$$\Gamma[T; \varphi] = \mathcal{S}_E[\varphi] + \frac{1}{2} \text{tr} \ln \frac{\delta^2 \mathcal{S}_E[\varphi]}{\delta \varphi^2}. \quad (7.24)$$

The NJL one-meson-loop gap equation can be derived by requiring that, for a given constant field configuration, the effective action in Eq. (7.24) is stationary. To respect the symmetries of the vacuum, only the scalar field can have a non-vanishing expectation value,  $\bar{\varphi} = (S, \mathbf{0})$ . One writes:

$$\left. \frac{\delta \Gamma[\varphi]}{\delta \varphi_c} \right|_{\bar{\varphi}} = \left. \frac{\delta \mathcal{S}_E[\varphi]}{\delta \varphi_c} \right|_{\bar{\varphi}} + \frac{1}{2} \text{tr} \Delta_{ab}[\varphi] \left. \frac{\delta^3 \mathcal{S}_E[\varphi]}{\delta \varphi_a \delta \varphi_b \delta \varphi_c} \right|_{\bar{\varphi}} = 0. \quad (7.25)$$

Where, we have defined:

$$\Delta_{ab}[\varphi] = \left( \frac{\delta^2 \mathcal{S}_E[\varphi]}{\delta \varphi_a \delta \varphi_b} \right)^{-1}. \quad (7.26)$$

The first term in the gap equation is the MF contribution while the remaining terms correspond to the contribution coming from the meson fluctuations.

In the MF approximation, the pole of the quark propagator is given by  $\varphi_0 = S$ , meaning that the constituent MF-quark mass  $m_\psi$ , is given by  $m_\psi = S$ . As already pointed out by other authors [113, 303], the same does not occur on the one-meson-loop calculation and  $S$  is no longer identifiable with the quark mass. However, we will continue to call  $S$  the Hartree mass, since it can still be interpreted as a mass scale and it is essential for the definition of the masses of collective and non-collective modes that will contribute to the quark condensate, which can be

calculated using<sup>2</sup> [113, 303]:

$$\langle \bar{\psi}\psi \rangle = -\frac{(S-m)}{G}. \quad (7.27)$$

Using the interpretation of  $S$  as the MF or Hartree quark mass, will be important to understand the behaviour of the meson modes with increasing temperature.

The function  $\Delta_{ab}^{-1}(S, q)$ , needed to solve Eq. (7.25), is the second variation of the bosonic action  $\mathcal{S}_E[\varphi]$ , with respect to the fields at the stationary point. It can be calculated to yield:

$$\Delta_{ab}^{-1}(S, q) = \delta_{ab} \left[ 2N_c N_f f_1(S, q) (q^2 + 4S^2 \delta_{0\sigma}) - 4N_c N_f f_0(S) + G^{-1} \right]. \quad (7.28)$$

This is the meson propagator in the MF approximation which also agrees with the RPA meson propagator. The functions  $f_0(S)$  and  $f_1(S, q)$  are the so-called quark-loop functions and are given by (see Appendices E and F for more details):

$$f_0(S) = \int \frac{d^4k}{(2\pi)^4} \frac{1}{k^2 + S^2}, \quad (7.29)$$

$$f_1(S, q) = \int \frac{d^4k}{(2\pi)^4} \frac{1}{((k-q)^2 + S^2)(k^2 + S^2)}. \quad (7.30)$$

As suggested first by E. Nikolov [113] and after by M. Oertel [303], in order to have a symmetry conserving calculation, ensuring the pion as the Goldstone mode in the chiral limit, the quantity in Eq. (7.28), in every expression, has to be substituted by:

$$\tilde{\Delta}_M^{-1}(S, q) = 2N_c N_f f_1(S, q) (q^2 + 4S^2 \delta_{M\sigma}) + \frac{m}{GS}, \quad (7.31)$$

the meson-loop propagator, yielding the so-called meson-loop-approximation (with  $M = \{\sigma, \pi\}$ ). This substitution is exact in the MF approximation, where the MF-gap equation ensures its validity. In the first derivation of the one-meson-loop gap equation by E. Nikolov et al. [113], this substitution is justified in the basis of an  $N_c$  counting scheme. The first term in the gap equation (the quark loop term) is of order  $N_c$ . The second term will be of order  $1/N_c^0$ . Using the definition given in Eq. (7.28) would lead to contributions in the gap equation of order  $1/N_c$ , introducing higher order corrections in the calculation and ruining the  $N_c$  counting scheme. Substituting by Eq. (7.31) makes the calculation consistent and leads to massless pion in the chiral limit, as shown by the authors. For more details on their argument, see [113]. This substitution was also employed by M. Oertel et al. [303], where it is argued to be necessary in order to make the argument of the logarithm in Eq. (7.24) positive definite, yielding a real and positive solution to the one-meson-loop gap equation (for more details see Ref. [303]). In the present work we use this approximation since it is necessary to have a symmetry conserving approximation when adding meson loops in the effective action formalism. The functions  $\tilde{\Delta}_\sigma(S, q)$  and  $\tilde{\Delta}_\pi(S, q)$  do not correspond to the meson propagators with one-meson-loop corrections. To effectively calculate

<sup>2</sup>This relation follows from the Hellmann–Feynman theorem using the quark current mass,  $m$ , as a parameter:  $\langle \bar{\psi}\psi \rangle = \delta\Gamma[\varphi]/\delta m$ .

the meson propagators with one-meson-loop corrections, one would have to calculate the second functional derivative of the effective action including the one-meson-loop term, generating third and fourth order functional derivatives of the bosonic action given in Eq. (7.20). This is beyond the scope of the present work.

As already stated, the NJL model is non-renormalizable and some regularization scheme is needed in order to mathematically define the model (for more details, see Chapter 4.1.2). Here we will apply a 3-momentum regularization in all momentum integrations, effectively truncating the Hilbert space of the fields [156]. The quark loop momentum can be regularized with a hard 3D-momentum cutoff,  $\Lambda_f$ , the fermion cutoff. When including quantum fluctuations in the calculation, due to the non-renormalizable nature of the model, a new parameter has to be introduced in order to regularize the meson loops,  $\Lambda_b$ , the boson cutoff. When  $\Lambda_b = 0$ , one recovers the MF approximation. Upon studying the effect of quantum fluctuations beyond the mean field, in the NJL model, several authors have studied the ratio  $\alpha = \Lambda_b/\Lambda_f$ , or even fixed this ratio to an arbitrary value when building NJL models which dealt with meson loop corrections [113, 300, 303, 306, 309, 310]. In this study, we independently choose the values of  $\Lambda_f$  and  $\Lambda_b$  because the mathematical relation between them are not well determined in the NJL model at present.

We fix the ratio  $\alpha = \Lambda_b/\Lambda_f$  by fixing the energy scale of the model. The one-meson-loop contribution has a clear connection with the quark loop term: the mesons in this formalism are composite collective and non-collective excitations of the underlying quark fields and are not meson fields with kinetic boson terms at the Lagrangian level. This can be seen from the explicit dependence on the  $f_1(S, q)$  loop function in the one-meson-loop terms. In fact, the largest energy in the system will now be fixed by the  $f_1(S, q)$  loop function. In this function there will be a dispersion relation with total momentum  $P = q + k$ , with  $k$  the quark momentum (integrated up to  $\Lambda_f$ ) and  $q$  the external meson momentum (integrated up to  $\Lambda_b$ ). It is clear that the maximum momentum in the system will be the sum  $P_{\max} = \Lambda_f + \Lambda_b = (1 + \alpha)\Lambda_f$ . If one considers that the NJL model is valid up to a momentum scale of  $P_{\max} = 1$  GeV, then  $\alpha$  is limited by this energy scale for a given  $\Lambda_f$ . Hence, we will consider parametrizations where the ratio  $\alpha$ , yields a maximum momentum scale of the order of 1 GeV. More details will be given in Section 7.3.

### 7.2.1 The one-meson-loop gap equation at finite temperature

Calculating explicitly the functional derivatives in Eq. (7.25), one can arrive at the one-meson-loop gap equation, first derived in [113]:

$$\Sigma_q(S) + \Sigma_\sigma(S) + \Sigma_\pi(S) = 0. \quad (7.32)$$

The first term is the usual one-quark loop contribution while the remaining correspond to the  $\sigma$  and  $\pi$  one-meson-loop contributions to the gap equation. Each contribution is explicitly given

by:

$$\Sigma_q(S) = \frac{1}{G}(S - m) - 4N_c N_f S f_0(S), \quad (7.33)$$

$$\Sigma_\sigma(S) = 2N_c N_f S \{4I_{1\sigma}(S) + 2f_1(S, 0)I_\sigma(S) + I_{2\sigma}(S)\}, \quad (7.34)$$

$$\Sigma_\pi(S) = 6N_c N_f S \{2f_1(S, 0)I_\pi(S) + I_{2\pi}(S)\}. \quad (7.35)$$

Where  $I_M(S)$ ,  $I_{1M}(S)$  and  $I_{2M}(S)$ , with  $M = \{\sigma, \pi\}$ , are defined as:

$$I_M(S) = \int \frac{d^4q}{(2\pi)^4} \tilde{\Delta}_M(S, q), \quad (7.36)$$

$$I_{1M}(S) = \int \frac{d^4q}{(2\pi)^4} f_1(S, q) \tilde{\Delta}_M(S, q), \quad (7.37)$$

$$I_{2M}(S) = -2 \int \frac{d^4q}{(2\pi)^4} (q^2 + 4S^2 \delta_{M\sigma}) f_2(S, q) \tilde{\Delta}_M(S, q). \quad (7.38)$$

As will be discussed later, the function  $f_2(S, q)$  can be written as

$$f_2(S, q) = \int \frac{d^4k}{(2\pi)^4} \frac{1}{((k - q)^2 + S^2)(k^2 + S^2)^2}, \quad (7.39)$$

can be written as a derivative of the  $f_1(S, q)$  loop function with respect to  $S^2$ . In the chiral limit, the one-loop corrections,  $\Sigma_\sigma$  and  $\Sigma_\pi$ , are explicitly suppressed by an overall  $N_c$  factor, due to the extra  $N_c$  factor in the meson-loop propagator,  $\tilde{\Delta}_M(S, q)$ , meaning that these terms are of  $\mathcal{O}(N_c^0)$  [113, 300].

In the meson loop corrections terms present in the gap equation (Eqs. (7.34) and (7.35)), one is integrating over the meson four momentum  $q$  i.e., summing over all kinematic meson fluctuations that can contribute to the system.

At finite temperature, the meson-loop contributions can be calculated following the usual Matsubara sum technique and the vacuum can be calculated by taking the  $T \rightarrow 0$  limit. These infinite sums over residues, of a previous singular integrand, can be transformed into a contour integration in the complex plane which avoid poles located at the Matsubara frequencies. However, the available contours in the complex plane are constrained by the analytical structure of the integrand. In this calculation, the meson propagator, more specifically the loop function  $f_1(S, q)$ , imposes restrictions on the possible contours in the complex plane. Hence, due to the analytic properties of such a function, the Matsubara sum will be transformed into a contour integration as suggested in Fig. 7.1 (see Ref. [301]).

Each one-meson-loop term in the gap equation can be brought to a form of a contour integration of the function  $h(w)$  of a complex variable,  $w$ . The integral over the closed contour  $\mathcal{C}$  in the complex plane (see Fig. 7.1), of the complex function  $h(w)$  can be written as:

$$I = \oint_{\mathcal{C}} \frac{dw}{2\pi i} h(w). \quad (7.40)$$

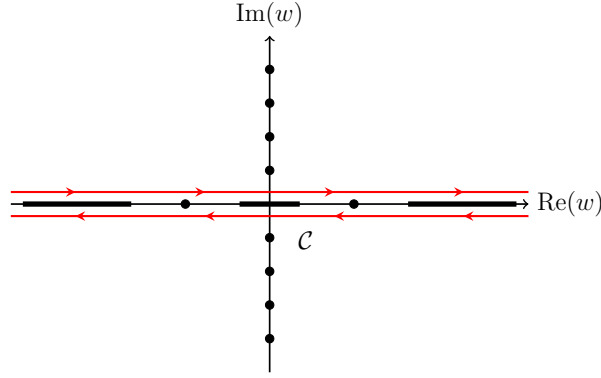


FIGURE 7.1: Contour used to calculate the meson-loop contributions to the gap equation. The dots in the vertical axis are poles that represent the bosonic Matsubara frequencies (see Fig. A.1(a) in the Appendix A.5). The poles and branch cuts on the horizontal axis are due to the analytical structure of the  $f_1(S, q)$  loop function. For more details on the Matsubara summation, see the Appendix A.5.

This integration, can then be written as an integration around the real axis as:

$$I = \int_{-\infty}^{+\infty} \frac{d\omega}{2\pi i} h(\omega + i\epsilon) + \int_{+\infty}^{-\infty} \frac{d\omega}{2\pi i} h(\omega - i\epsilon). \quad (7.41)$$

Following Refs. [306, 307, 311], we write the real part of  $w$  as  $\omega$ , and assume that the function  $h(w)$ , near the real axis (small  $\epsilon > 0$ ), can be decomposed in its real and imaginary parts as follows:

$$h(\omega \pm i\epsilon) = \text{Re}[h(\omega)] \pm i \text{Im}[h(\omega)]. \quad (7.42)$$

Using this decomposition we can write the integration in Eq. (7.40) as:

$$I = \frac{1}{\pi} \int_{-\infty}^{+\infty} d\omega \text{Im}[h(\omega)] \quad (7.43)$$

Only the imaginary part of the function under the original contour integration,  $\text{Im}[h(\omega)]$ , will contribute to the result. For our purposes the complex function  $h(w)$  will contain functions whose real and imaginary parts can be obtained using the Sokhotski–Plemelj formula,

$$\frac{1}{x - x_0 \pm i\epsilon} = \text{p.v.} \frac{1}{x - x_0} \mp i\pi\delta(x - x_0),$$

which indeed decomposes a function in a real and an imaginary part. For more details on this formula, see Appendix A.3.

In our framework, to calculate the meson contributions for a given meson channel  $M$ , two distinct contributions will be considered, the collective and non-collective modes (see Refs. [306, 307]). This separation is depicted in Fig. 7.2, where the first comes from the isolated poles in the complex plane while the latter, from the branch cuts.

In the chiral limit, Eq. (7.31) can be viewed as the propagator of a meson with effective mass  $4S^2\delta_{M\sigma}$  and a wave function renormalization proportional to  $f_1(S, q)$ . The function  $f_1(S, q)$

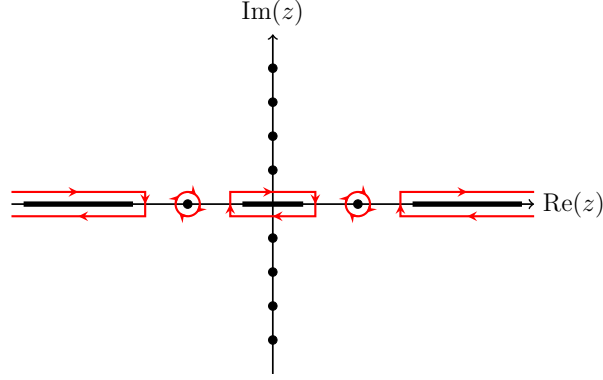


FIGURE 7.2: Definition of the collective meson mode (pole) and the non-collective meson mode (branch cut) terms in the meson-loop corrections.

amounts for the internal interacting quark substructure of the collective meson excitation. For convenience, we define the *collective* meson propagator in Eq. (7.31) as:

$$k_M(S, \mathbf{q}, q_0) = \frac{1}{(q^2 + 4S^2\delta_{M\sigma})} = \frac{1}{q_0^2 + E_M^2(S, \mathbf{q})}, \quad (7.44)$$

where the dispersion relation  $E_M^2 = \mathbf{q}^2 + 4S^2\delta_{M\sigma}$ , is a real quantity.

The collective mode contributions will be calculated by considering that only the *collective* meson propagator,  $k_M(S, \mathbf{q}, -iw)$ , has a non-vanishing imaginary part and  $f_1(S, \mathbf{q}, -iw)$  is a real quantity. These pole terms will appear as delta functions and will correspond to excitations of the underlying quark system with a precise dispersion relation. The non-collective modes come from the branch cuts, corresponding to the kinematic region where the imaginary part of  $f_1(S, \mathbf{q}, -iw)$  is non-zero and the *collective* meson propagator,  $k_M(S, \mathbf{q}, -iw)$  is a real quantity. The analytic continuation of the functions  $f_1(S, \mathbf{q}, q_0)$  to  $f_1(S, \mathbf{q}, -iq_0)$  and  $k_M(S, \mathbf{q}, q_0)$  to  $k_M(S, \mathbf{q}, -iq_0)$  have been defined as  $F(S, \mathbf{q}, \omega)$  and  $K_M(S, \mathbf{q}, \omega)$ , respectively, for real  $\omega$  (see Appendices F and I.1).

As pointed out by K. Yamazaki et al. in Refs. [306, 307], when chiral symmetry is not explicitly broken at the Lagrangian level i.e. when  $m = 0$ , these contributions are easily separated. When including the quark current mass however, these contributions get mixed and the separation must be done with care.

As the temperature increases, one expects chiral symmetry to get restored. This means that the absolute value of the quark condensate decreases, as well as the value for the expectation value of the scalar field,  $S$ . This implies that, both the position of the meson propagator pole in the complex plane, as well as the on-set of the branch cuts, can change with the temperature and  $S$ .

In the MF calculation of meson masses and decays, one can define the Mott temperature as the temperature at which the mass of a given meson channel, is equal to the sum of the constituent mass of its composing quarks (for a detailed discussion in the two flavour NJL model, see [128]). At this point the decay width of such a meson channel is non-zero and the previous quarks bound state, becomes a resonance. In the present chapter, this corresponds to the meson pole reaching the branch cut. At this point, both the *collective* meson propagator,  $k_M(S, \mathbf{q}, -iw)$

and the loop function  $f_1(S, \mathbf{q}, -iw)$  have non-vanishing imaginary parts. To calculate exactly such contributions, one should use a key-hole contour, avoiding both the pole as well as the branch cut singularity. However, that would introduce in the calculation a mixture between the imaginary contribution coming from the pole with the one coming from the cut, making very difficult to clearly separate both contributions. To avoid this, in the present framework, for a given kinematic contribution where the pole lies on top of the branch cut, only the non-collective mode will be calculated.

A collective meson mode exists, if there is an  $\omega_+$  value, in-between the branch cuts, where Eq. (7.31) is zero. This condition can be written as:

$$-\omega_+^2 + E_M^2(S, q) + \frac{\tilde{m}}{\text{Re}[F(S, \mathbf{q}, \omega_+)]} = 0, \quad (7.45)$$

where,

$$\tilde{m} = \frac{m}{2GN_c N_f S}. \quad (7.46)$$

Analysing  $\text{Im}[F(S, \mathbf{q}, \omega)]$ , one can recognize that the region in-between cuts is given by  $[\sqrt{(\Lambda_f + q)^2 + S^2} - \sqrt{\Lambda_f^2 + S^2}, E_\sigma]$ . One can also observe that the real part of  $F(S, \mathbf{q}, \omega)$  is always greater than zero in the  $\omega$ -region in-between the branch cuts. Thus, considering a finite current quark mass, Eq. (7.45) only has a zero for the pion meson mode. This means that excitations with the same quantum numbers as the  $\sigma$  field will not have collective mode contributions, only non-collective ones. For a deeper analysis about the non-existence of collective modes for the  $\sigma$ , see Appendix H.

In the following, the integrations defined in Eqs. (7.36), (7.37) and (7.38), will be separated in the collective and non-collective contributions. For the detailed calculation of all these contributions, see Appendix I.

Consider the contribution  $I_M(S)$ , for a given meson channel  $M = \{\sigma, \pi\}$ , given in Eq. (7.36) (for more details on this calculation, see Appendix I.1). As discussed earlier, it can be divided in the collective and non-collective contributions i.e., the pole  $\mathcal{P}_M(S)$  and a branch cut,  $\mathcal{B}_M(S)$  terms. This separation can be written as:

$$I_M(S) = \mathcal{P}_M(S) + \mathcal{B}_M(S). \quad (7.47)$$

The first term is the contribution coming from the collective modes. It can be calculated, as already stated, by considering that near the real axis, the loop function  $f_1(S, \mathbf{q}, -iw)$  is purely real and  $k_M^{-1}(S, \mathbf{q}, -iw)$  has both a real and an imaginary part. It can be calculated to yield:

$$\mathcal{P}_M(S) = \frac{1}{4N_c N_f} \int_{\mathbf{q}} \frac{\coth(\beta\omega_+/2)}{\text{Re}[F(S, \mathbf{q}, \omega_+)]} \frac{|\partial_\omega \chi_+(S, \mathbf{q}, \omega)|_{\omega_+}^{-1}}{\tilde{E}_M(S, \mathbf{q}, \omega_+)}. \quad (7.48)$$

Here, the collective mode dispersion relation  $\tilde{E}_M^2(S, \mathbf{q}, \omega)$  and the function  $\chi_+(S, \mathbf{q}, \omega)$ , are defined as:

$$\tilde{E}_M^2(S, \mathbf{q}, \omega) = E_M^2(S, \mathbf{q}) + \frac{\tilde{m}}{\text{Re}[F(S, \mathbf{q}, \omega)]}, \quad (7.49)$$

$$\chi_+(S, \mathbf{q}, \omega) = \omega - \tilde{E}_M(S, \mathbf{q}, \omega), \quad (7.50)$$

while  $\omega_+ = \omega_+(S, \mathbf{q})$  is the location of the pole on the real line of the  $\omega$ -complex plane. It can be calculated as a solution of

$$\chi_+(S, \mathbf{q}, \omega_+) = 0. \quad (7.51)$$

Now, one of the difficulties of including composite meson fluctuations in the calculation becomes clear. The pole location  $\omega_+$ , from which one calculates the collective mode dispersion relation  $\tilde{E}_M^2(S, \mathbf{q}, \omega_+)$ , depends on the Hartree mass ( $S$ ), on the meson 3-momentum ( $\mathbf{q}$ ) and implicitly on the temperature ( $T$ ), through  $\text{Re}[F(S, \mathbf{q}, \omega)]$ , which is related to the quark substructure of the collective mode.

From this, one can see that the pole contribution, does not simply correspond to an integration over the meson fluctuation momentum with a fixed collective meson mass. When integrating over the meson momentum, a certain value of Hartree mass and temperature are fixed and the pole location, for a single value of  $\mathbf{q}$ , is calculated self-consistently. We highlight that, in our calculation, the pole contributions are only non-zero if  $\omega_+$  exists in-between the cuts.

The second term,  $\mathcal{B}_M(S)$ , can be calculated by considering that, near the real axis,  $k_M^{-1}(S, \mathbf{q}, -i\omega)$  is real while  $f_1(S, \mathbf{q}, -i\omega)$  is complex. One can write:

$$\mathcal{B}_M(S) = \frac{1}{2\pi N_c N_f} \int_{\mathbf{q}} \int_0^{+\infty} d\omega \frac{\coth(\beta\omega/2)}{-\omega^2 + E_M^2(S, \mathbf{q})} \frac{-\text{Im}[F(S, \mathbf{q}, \omega)]}{\text{Re}[G(S, \mathbf{q}, \omega)]^2 + \text{Im}[F(S, \mathbf{q}, \omega)]^2}. \quad (7.52)$$

The function  $\text{Im}[F(S, \mathbf{q}, \omega)]$  have an Heaviside step function, which restricts the integration to the branch cuts in Fig. 7.2. The function  $\text{Re}[G(S, \mathbf{q}, \omega)]$ , is defined as:

$$\text{Re}[G(S, \mathbf{q}, \omega)] = \text{Re}[F(S, \mathbf{q}, \omega)] + \tilde{m}K_M(S, \mathbf{q}, \omega). \quad (7.53)$$

The integral in Eq. (7.37), only appears in the  $\sigma$  gap equation. Considering a finite quark current mass  $m$ , only the branch cut contribution will be non-zero,  $I_{1\sigma}(S) = \mathcal{B}_{1\sigma}(S)$  since, as previously stated, the  $\sigma$  mode does not have a pole. One can write this term as (see Appendix I.2 for more details on this derivation):

$$\mathcal{B}_{1\sigma}(S) = \frac{\tilde{m}}{2\pi N_c N_f} \int_{\mathbf{q}} \int_0^{+\infty} d\omega \frac{\coth(\beta\omega/2)}{-\omega^2 + E_\sigma^2(S, \mathbf{q})} \frac{K_\sigma(S, \mathbf{q}, \omega) \text{Im}[F(S, \mathbf{q}, \omega)]}{\text{Re}[G(S, \mathbf{q}, \omega)]^2 + \text{Im}[F(S, \mathbf{q}, \omega)]^2}. \quad (7.54)$$

It is clear that this contribution vanishes in the chiral limit, due to the overall factor  $\tilde{m}$ .

The last integration that needs attention, is given by Eq. (7.38) (for more details see Appendix I.3). It will have contributions coming both from the collective and non-collective modes:

$$I_{2M}(S) = \mathcal{P}_{2M}(S) + \mathcal{B}_{2M}(S). \quad (7.55)$$

To simplify the calculations one can write the integrand in terms of the  $f_1(S, q)$  loop function using the identity (see Appendix G):

$$f_2(S, q) = -\frac{1}{2} \frac{\partial}{\partial \xi^2} f_1(\xi, q)_{\xi=S}. \quad (7.56)$$

This will remove double poles that would otherwise appear when using the Matsubara sum technique.

Repeating the same process i.e., consider that  $f_1(S, \mathbf{q}, -i\omega)$  is purely real and  $k_M^{-1}(S, \mathbf{q}, -i\omega)$  is complex, near the real axis, after some calculations, one can arrive at:

$$\mathcal{P}_{2M}(S) = -\frac{\tilde{m}}{4N_c N_f} \int_{\mathbf{q}} \frac{\coth(\beta\omega_+/2)}{\tilde{E}_M(S, \mathbf{q}, \omega_+)} \frac{\partial_{S^2} \text{Re}[F(S, \mathbf{q}, \omega_+)]}{\text{Re}[F(S, \mathbf{q}, \omega_+)]^2} |\partial_\omega \chi_+(S, \mathbf{q}, \omega)|_{\omega_+}^{-1}. \quad (7.57)$$

The non-collective contribution to  $I_{2M}(S)$  can be calculated as before, near the real axis, the branch cut term is:

$$\mathcal{B}_{2M}(S) = \frac{1}{2\pi N_c N_f} \int_{\mathbf{q}} \int_0^{+\infty} d\omega \frac{\coth(\beta\omega/2)}{1 + A(S, \mathbf{q}, \omega)^2} \partial_{\xi^2} A(\xi, \mathbf{q}, \omega)_{\xi=S}. \quad (7.58)$$

Here, the function  $A(S, \mathbf{q}, \omega)$  is defined as

$$A(\xi, \mathbf{q}, \omega) = \frac{\text{Im}[F(\xi, \mathbf{q}, \omega)]}{\text{Re}[F(\xi, \mathbf{q}, \omega)] + \tilde{m}K_M(S, \mathbf{q}, \omega)}. \quad (7.59)$$

## 7.3 Results

In this section we present our results and discuss the influence of the one-meson-loop terms, separated in collective and non-collective contributions, on the quark condensate in the vacuum and at finite temperature. We also study the effect of including only the collective and non-collective contributions in the restoration of chiral symmetry with increasing temperature.

Here, we point out that, concerning the numerical calculations, the inclusion of the one-meson-loop terms is completely self-consistent: upon solving the gap equation for a given parametrization, for each value of Hartree mass,  $S$ , and temperature,  $T$ , one has to numerically check the existence of the collective modes and their influence on the non-collective modes.

### 7.3.1 Vacuum

To start our study, we find a parameter set which, at the MF level, reproduces the value of the light quark condensate obtained by two-flavour lattice QCD [312],  $\langle \bar{\ell}\ell \rangle^{1/3} = -256$  MeV, the pion

mass,  $m_\pi = 135$  MeV and the pion decay constant,  $f_\pi = 93$  MeV. This parameter set is displayed in Table 7.1.

$\Lambda_f$ [MeV]	$m$ [MeV]	$G\Lambda_f^2/2$	$S$ [MeV]
690.3	4.72	2.014	288.4

TABLE 7.1: Mean field parameter set and MF quark mass,  $S$ , in the vacuum.

To analyse the effect of the inclusion of meson-loop corrections in the vacuum condensate, we use the aforementioned MF parameter set and increase the value of  $\alpha$ , the ratio between the boson and fermion cutoff,  $\alpha = \Lambda_b/\Lambda_f$ , from zero (MF calculation) to a finite value. The results of such calculation can be seen in Fig. 7.3. Three different scenarios were considered:

- Quark loop and the collective modes,  $\Sigma_q(S) + \Sigma_P(S) = 0$ ;
- Quark loop and the non-collective modes,  $\Sigma_q(S) + \Sigma_B(S) = 0$ ;
- Quark loop and collective and non-collective modes,  $\Sigma_q(S) + \Sigma_P(S) + \Sigma_B(S) = 0$ .

Setting the boson cutoff to a non-zero value is equivalent to include the one-meson-loop correction terms. As one can see in the left panel of Fig. 7.3, by solving the gap equation with increasing  $\alpha$ , the value of the quark condensate decreases. For reference, the gray dashed line in the left panel of Fig. 7.3, corresponds to an  $1/N_c$ -reduction of the MF vacuum quark condensate. This decreasing behaviour is expected since the inclusion of bosonic degrees of freedom is known to restore chiral symmetry. The decreasing of the quark condensate with increasing  $\alpha$  happens until a point where, to further decrease the quark condensate, the boson cutoff has also to decrease. This behaviour of decreasing quark condensate with decreasing  $\alpha$ , continues up to the point at around where the pion collective mode with zero momentum reaches the branch cut i.e.,  $\tilde{E}_\pi(0) = E_\sigma(0)$ . This can be seen more clearly in the right panel of Fig. 7.3. After this point (red-dashed line in the right panel of Fig. 7.3) a smaller number of momentum modes will contribute to the collective modes. When the highest momentum mode, with  $q = \Lambda_b$ , reaches the branch cut i.e.,  $\tilde{E}_\pi(\Lambda_b) = E_\sigma(\Lambda_b)$ , the collective modes do not contribute any more to the calculation (full red line in the right panel of Fig. 7.3). At this point, no more solutions can be found for the gap equations. These points are represented in the right panel of Fig. 7.3 by the respective coloured dots.

### 7.3.2 Finite temperature

In this section we solve the gap equation at finite temperature for different sets of parameters that include one-meson-loop corrections and compare the results with the usual MF calculation.

To solve the gap equation at finite temperature it is necessary to evaluate the  $q \rightarrow 0$  limit of the  $f_1(S, q)$  loop function i.e.,  $f_1(S, 0)$  (see Eqs. (7.34) and (7.35)). This operation implies two distinct limits,  $q_0 \rightarrow 0$  and  $\mathbf{q} \rightarrow 0$ . After the extension of the discrete Matsubara frequencies to continuum values  $q_0$ , the function  $f_1(S, q)$  is no longer analytic in the origin [313]. This can be

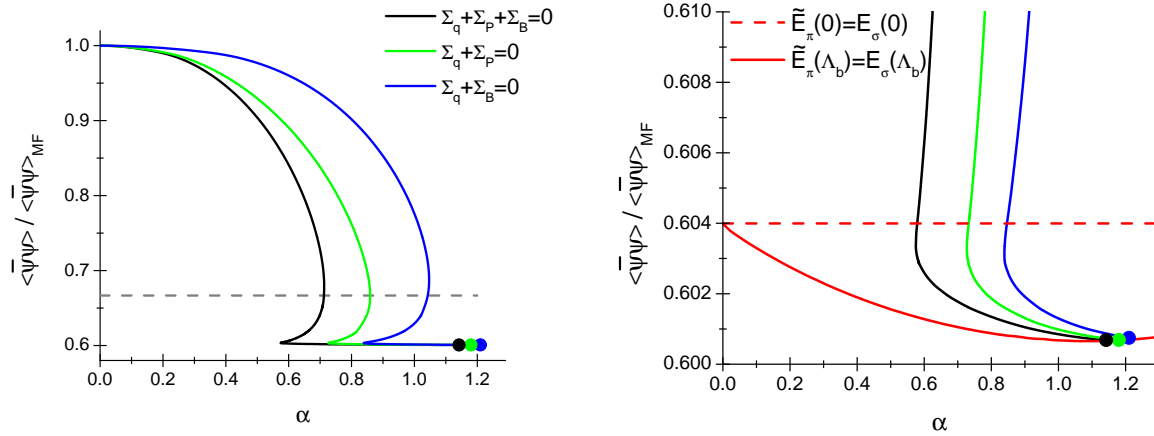


FIGURE 7.3: Ratio between the MF vacuum quark condensate and the one-meson-loop vacuum quark condensate, as a function of the ratio  $\alpha = \Lambda_b/\Lambda_f$ . The green line is the result of solving the gap equation with the collective contributions, the blue line with the non-collective contributions and the black line is the complete calculation. The gray dashed line in the left panel, corresponds to an  $1/N_c$ -reduction of the MF vacuum quark condensate. The red-dashed and red-full lines in the right panel, correspond to the Hartree mass points where the  $\pi$  collective mode reaches the branch cut, with  $q = 0$  and  $q = \Lambda_b$ , respectively.

demonstrated by noticing that the limiting operations,  $\mathbf{q} \rightarrow 0$  and  $q_0 \rightarrow 0$ , do not commute i.e.,

$$\lim_{\mathbf{q} \rightarrow 0} \lim_{q_0 \rightarrow 0} f_1(S, \mathbf{q}, q_0) \neq \lim_{q_0 \rightarrow 0} \lim_{\mathbf{q} \rightarrow 0} f_1(S, \mathbf{q}, q_0). \quad (7.60)$$

For the *plasmon* limit, one can write:

$$\lim_{q_0 \rightarrow 0} \lim_{\mathbf{q} \rightarrow 0} f_1(S, \mathbf{q}, q_0) = \int \frac{d^3k}{(2\pi)^3} \frac{1 - 2n_F(E_k)}{4E_k^3}. \quad (7.61)$$

For the *static* limit, one can write:

$$\lim_{\mathbf{q} \rightarrow 0} \lim_{q_0 \rightarrow 0} f_1(S, \mathbf{q}, q_0) = \int \frac{d^3k}{(2\pi)^3} \frac{1}{4E_k^3} \left\{ 1 - 2n_F(E_k) + \frac{2E_k}{T} n_F(E_k) [n_F(E_k) - 1] \right\}. \quad (7.62)$$

This is a consequence of the breaking of Lorentz symmetry by the heat bath. In fact, this feature is a well know property of finite temperature field theory and the limiting operations in Eq. (7.60) are related to two distinct approximations. The left hand side order of limiting operations is known as the *static* limit while, the one in the right hand side, is known as the *plasmon* limit. The analytical result for both limits is presented in Appendix F.7. For more details see [313]. We consider both the *static* and *plasmon* limits and compare both results in the calculation of the quark condensate as a function of temperature including collective and non-collective modes.

To study the finite temperature behaviour of the quark condensate and restoration of chiral symmetry with the one-meson-loops contribution, a set of parameters has to be provided which includes the boson cutoff. In order to do so, we fix the ratio between the boson and fermion cutoffs,  $\alpha$ , to different values and search for parametrizations which reproduce the same vacuum observables as in the MF case: the two flavour quark condensate, the pion mass and the pion

decay constant given previously. We also search for parametrizations in the three scenarios presented earlier, considering the complete one-meson-loop gap equation, and considering the quark loop with the collective excitations or with the non-collective excitations. The obtained parameter sets are displayed in Table 7.2.

To obtain the model parametrization, the pion mass and pion decay constant are calculated using the meson-loop pion propagator given in Eq. (7.31) (see also Ref. [130]). We highlight that this is an approximation since the vacuum quantities are not calculated using the one-meson-loop pion propagator i.e., the second functional derivative of the one-loop effective action. This approximation only changes the parametrization of the model and does not modify the qualitative effects of including collective and non-collective modes on the quark condensate and on the restoration of chiral symmetry.

$\alpha$	$\Sigma_P$	$\Sigma_B$	$\Lambda_f$ [MeV]	$m$ [MeV]	$G\Lambda_f^2/2$	$S$ [MeV]
0.1	✓	✓	690.9	4.72	2.015	288.1
	✓	✗	690.8	4.72	2.015	288.2
	✗	✓	690.4	4.72	2.015	288.4
0.2	✓	✓	694.4	4.72	2.022	286.2
	✓	✗	693.7	4.72	2.021	286.5
	✗	✓	691.0	4.72	2.016	288.1
0.3	✓	✓	702.2	4.72	2.038	282.1
	✓	✗	693.7	4.72	2.021	286.5
	✗	✓	692.6	4.72	2.019	287.2
0.4	✓	✓	714.7	4.72	2.065	276.0
	✓	✗	709.2	4.72	2.053	278.6
	✗	✓	695.7	4.72	2.025	285.5

TABLE 7.2: Parameter sets for different values of  $\alpha$ , considering three different scenarios: the complete calculation, considering only the quark sector and collective fluctuations and quark sector and non-collective fluctuations.

When calculating the collective modes contributions to the gap equation at finite temperature, for a given pair of values  $(T, S)$ , one is integrating over the meson momentum, from 0 to  $\Lambda_b$ . However, as temperature increases, the value of  $S$  decreases and chiral symmetry tends to get restored. As a consequence, the poles that originate the collective contributions and the branch cuts, move in the complex plane. Indeed, at a specific value of  $(T_0, S_0)$  the pole with momentum  $q = 0$ , enters the branch cut (see Fig. 7.2) and the mode with that dispersion relation no longer contributes as a collective excitation. As temperature continues to increase, more and more momentum modes generate pole contributions that overlap with the branch cuts and are not included as collective excitations. So, collective excitations are considered until the highest boson momentum mode, with momentum  $q = \Lambda_b$ , enters the branch cut.

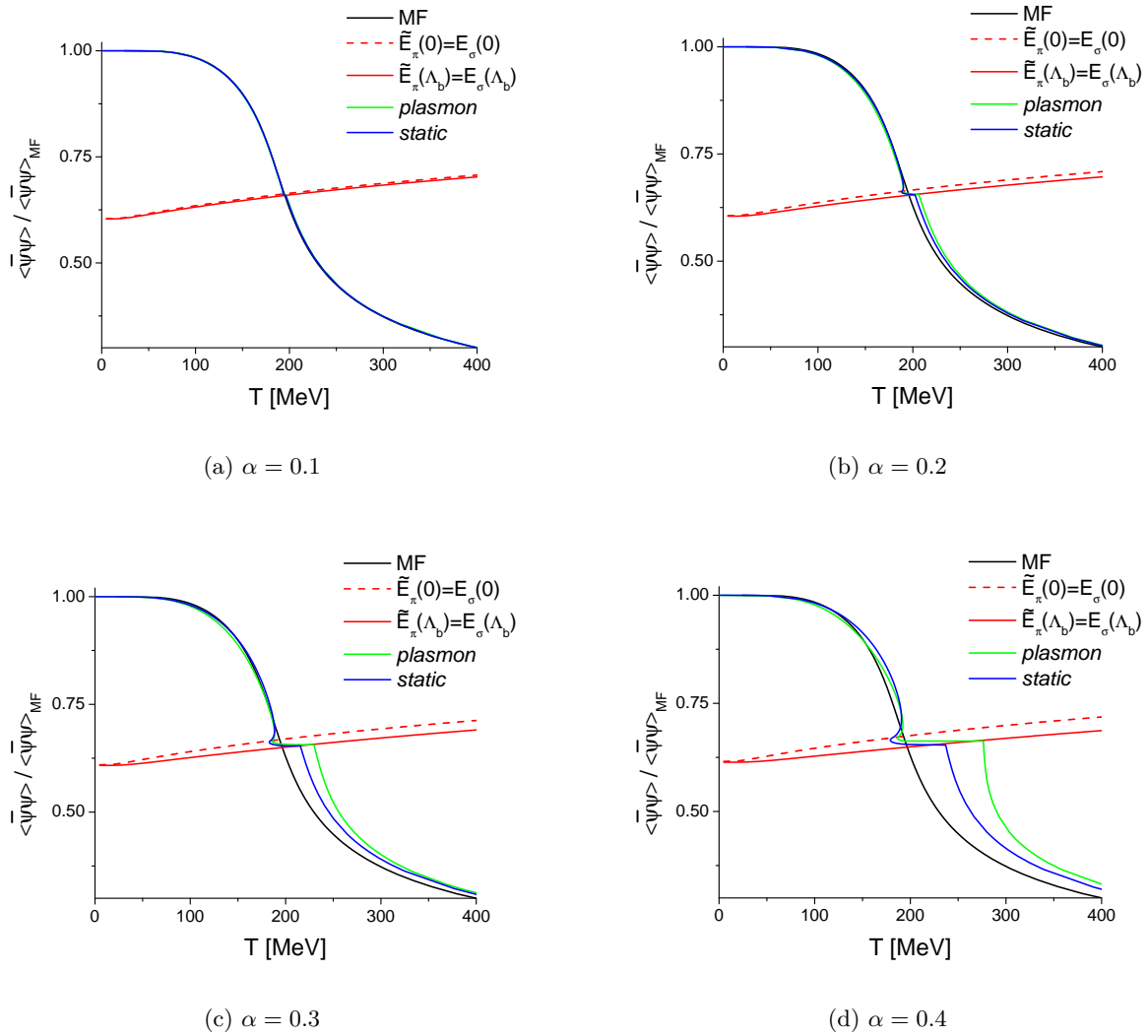


FIGURE 7.4: Solution of the gap equation at finite temperature including collective and non-collective fluctuations. Each panel represents the solution for a given ratio between the boson and fermion cutoff,  $\alpha = \Lambda_b/\Lambda_f$ . Both the *plasmon* and *static* limits are presented as well as the collective excitation melting lines for  $q = 0$  and  $q = \Lambda_b$ .

In Fig. 7.4, we present the results of solving the one meson loop gap equation, at finite temperature, increasing the boson cutoff. In all the panels we present the result of the MF model, using the parameters of Table 7.1, for reference. We also present the so-called pion melting lines for pion collective modes with momentum  $q = 0$  and  $q = \Lambda_b$  (dashed and full red lines of Fig. 7.4). For a given Hartree mass, these lines provide the respective melting temperature of the pion collective mode i.e., the temperature at which the poles with momentum modes  $q = 0$  and  $q = \Lambda_b$ , enter the branch cut. As already pointed out, for  $q = 0$ , this is known as the pion Mott temperature. The  $q = 0$  melting line, contrary to the  $q = \Lambda_b$  one, depends only on the fermionic parameters i.e., it does not depend on the boson cutoff. This means that these lines are almost the same in all scenarios presented in Fig. 7.4. Upon solving these complete gap equation, once the quark condensate reaches this temperature, a smaller number of momentum modes will contribute to the collective modes.

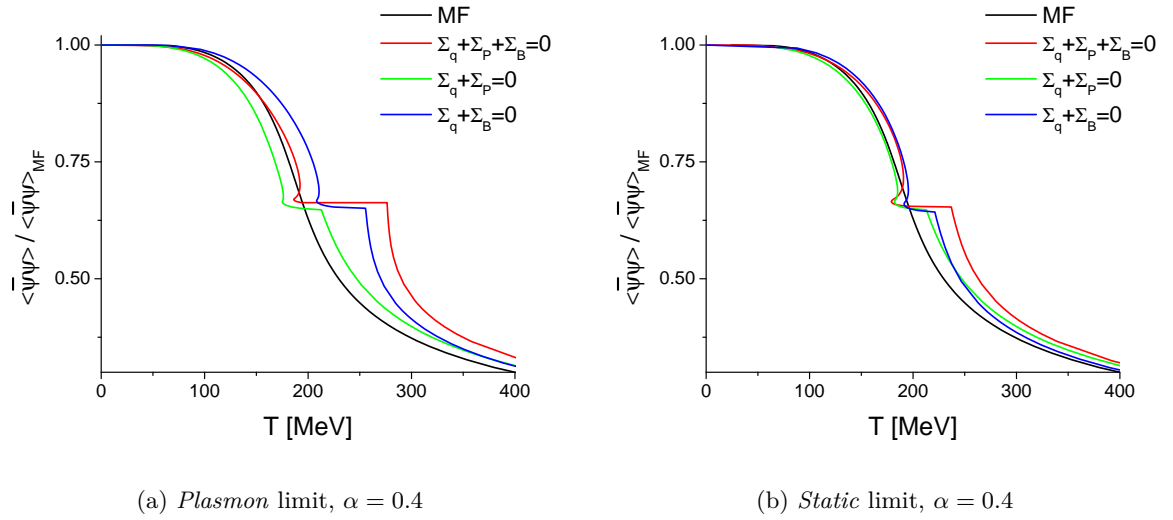


FIGURE 7.5: Solution of the gap equation at finite temperature with  $\alpha = \Lambda_b/\Lambda_f = 0.4$ . The left panel is the result in the *plasmon* limit while the right panel is the *static* limit. The green line is the result of solving the gap equation with the collective contributions, the blue line with the non-collective contributions and the red line is the complete calculation. The black line is the MF result using the parameters of Table 7.1.

In both the *plasmon* and *static* limits, the quark condensate at finite temperature, has a different behaviour with meson loop corrections, when compared to MF, see Fig. 7.5. There is a bending behaviour not seen at MF level: because of the inclusion of collective and non collective modes in the system and the crossing of cuts in the complex plane the quark condensate is not an analytical function of temperature.

Figure 7.5 also shows that this behaviour is present when solving the gap equation with both collective and non collective excitations (red line) or when considering these contributions separately (green and blue lines). Such observation leads us to conclude that this behaviour is a consequence of considering beyond MF corrections within this formalism, independently if they are collective or non collective excitations.

Due to the presence of this bend, the critical temperature of the crossover transition cannot be defined as the zero of the second derivative of the quark condensate with respect to temperature, as usual. Still, one can clearly distinguish two phases, one with a large quark condensate and the other with a small quark condensate. These phases are also separated by the Mott temperature line of the  $q = 0$  pion collective mode (see Fig. 7.4). Hence, in this calculation, it would be natural to associate this temperature with the partial restoration of chiral symmetry.

A non-standard quark condensate as a function of temperature was also obtained in [314] for a nonlocal version of the Polyakov–Nambu–Jona-Lasinio model beyond mean field. In that work, the authors found a “wobble” and attributed such a behaviour to the beyond MF corrections to the quark self-energy.

In conclusion, we expect to show that the inclusion of quantum fluctuations in the NJL model needs to be done with care, especially if one is trying to reproduce lattice QCD results. If one

wants to have a consistent model beyond the mean field, including collective and non-collective excitations, one should also include in the gap equation contributions coming from these modes, as performed in this work. We found, however, that such a calculation leads to an unexpected behaviour near the critical temperature of the model. This might indicate that the one-meson-loop NJL model, should be used with care as an effective model of QCD: taking our results into account, we conclude that to use the NJL with one-meson-loop corrections, the overall contribution from meson loops should be very small i.e.,  $\alpha$ , should be of the order of  $\alpha = 0.1 - 0.2$ , to get a chiral condensate which is bounded by the error bars coming from two flavour lattice QCD calculations [147].

## 7.4 Conclusions and outlook

Along this chapter, we have studied the effect of the inclusion of collective and non-collective modes in the quark condensate of the NJL model using a symmetry conserving approximation. This approximation is based on the effective action formalism and guarantees that the pion is the Goldstone mode in the chiral limit.

Adding quantum fluctuations, in a symmetric conserving way, by considering the influence of collective and non-collective modes in the NJL model is not a simple task [287]. The composite nature of the meson modes leads to a dynamical scenario where, depending on the temperature and Hartree mass, collective modes may, or may not exist. From the practical point of view, even evaluating some integrations analytically, one ends up effectively solving four dimensional integrals, numerically.

In the vacuum, using a mean field parametrization and adding the meson sector by increasing the boson cutoff, it was found a decreasing value for the quark condensate. This result is expected: the inclusion of boson degrees of freedom is known to drag the system into a state of restored chiral symmetry. It was also found that this decrease is limited by the existence of the collective modes. Decreasing the value of the quark condensate too much leads to the absence of pole contributions to the vacuum gap equation, which are essential to balance the gap equation, providing the existence of a solution, beyond the MF approximation.

This calculation shows that adding meson-loop correction terms to the NJL model, in a consistent way, is a very delicate process. There is a back reaction in the quark condensate and restoration of chiral symmetry, due to the existence of composite collective and non-collective modes. As temperature increases and chiral symmetry gets restored, the collective modes melt and its contribution to the gap equation vanishes.

As future work, testing the robustness of the results with different regularization procedures for the quark and meson loops, like the Pauli–Villars scheme, could be insightful. The calculation can be extended to finite density by including a finite chemical potential. With such an extension one could study the finite temperature and density behaviour of the collective and non-collective modes and their influence on the restoration of chiral symmetry at finite density. This would

also allow to obtain the phase diagram of the NJL model at one-meson-loop level and check the existence of a CEP and its robustness against an increasing  $\alpha = \Lambda_b/\Lambda_f$ .

Another interesting extension would be to apply the developed formalism to the calculation of transport coefficients at finite temperature.

Finally, extending the model to include the strange quark, further quark interactions, like eight scalar quark interactions or vector interactions (see Chapter 4.1) and the Polyakov loop, could bring additional insight to the importance of going beyond the mean field approximation.

Including the strange quark in the model would mean working with  $SU(3)$  flavour symmetry. While the current masses of the up and down quarks,  $m_u$  and  $m_d$ , are very small (in comparison with the pion mass for example see Table 2.1) and their ratio is not far from unity,  $m_u/m_d \approx 0.5$ , the mass of the strange quark,  $m_s$ , is much larger, and its ratio with the “average light current quark mass” is much larger than unity,  $m_s/(m_u/2 + m_d/2) \approx 27$  [30]. Indeed, while for  $SU(2)$  the isotopic limit is considered a valid approximation, for the strange sector that is not the case and usually one uses two different quark masses in these models, a light quark mass  $m_u = m_d = m_l$  and the strange quark mass,  $m_s$ , implying a diagonal, non-degenerate quark current mass matrix,  $\hat{m}$ . Such extension in the model seems trivial at first glance and, for the mean field approximation, that is indeed the case. However, in the one-meson-loop approximation, having a non-degenerate mass matrix,  $\hat{m}$  complicates the calculation. The problem stems from the expansion of the action in powers of the fields: the operator  $D^\dagger D$  will contain several contributions, one being the non-degenerate mass matrix  $\hat{m}$ , which now does not commute with other contributions present in the operator [134]. The same issue appears in the heat kernel expansion approach to the NJL model where the effective action of the model is written using the Schwinger proper time method, see [134]. This difficulty was overcome using resummation techniques, for more details see [209–211]. So, although including the strange quark is possible in the one-meson-loop NJL model, it is quite an intricate calculation.

The inclusion of further quark interactions can be interesting, but also intricate. Including other four-quark interactions, which can be “reduced” to quadratic quark interactions through the Hubbard–Stratonovich transformations is a straightforward process. One such example would be to include four-quark vector interactions, which would modify the quark chemical potential into an effective one. Considering six, eight and higher quark interactions however, would lead to further difficulties. Before writing the one-meson-loop effective action one has to bosonize the theory and the question on how to bosonize these higher than four-quark interactions arises. One idea would be to write the Lagrangian density, with all desired multi-quark interactions and then building an effective Lagrangian where all multi-quark interactions were written as four-quark interactions. Such effective Lagrangian can then be bosonized and the effective action formalism can be applied to yield the one-meson-loop NJL with multi-quark interactions. In order to write the multi-quark interactions as four-quark interactions, one can consider these interactions as products of quark bilinear operators and use the quadratic expansion of the product between N-operators we present in the Appendix C.2.

### 7.4.1 The one-meson-loop Polyakov–Nambu–Jona-Lasinio

In this section we comment on how one can extend the formalism developed previously to incorporate the Polyakov loop. Such extension of the model would allow to study the influence of the collective and non-collective modes on the breaking of  $Z(N_c)$  symmetry and statistical deconfinement. The Polyakov loop can be included in the model by coupling a background gluon field in the time direction,  $A_0 = -iA_4$ , to the Lagrangian density via the covariant derivative<sup>3</sup>

$$\mathcal{L}(\bar{\psi}, \psi, A_4) = \bar{\psi}(i\not{D} - m)\psi + \frac{G}{2}(\bar{\psi}\hat{\Gamma}_a\psi)^2 - \mathcal{U}(\Phi[A_4], \bar{\Phi}[A_4]). \quad (7.63)$$

Here the covariant derivative is defined as  $D^\mu = \partial^\mu - i\delta_0^\mu A^0$ ,  $A_0 = -iA_4$  and we added an effective potential for the Polyakov loop degrees of freedom,  $\mathcal{U}(\Phi[A_4], \bar{\Phi}[A_4])$ . The details on extending the NJL model to include the Polyakov loop were presented in Chapter 4.1.1.

In the mean field treatment of this model the quark fields  $\psi$  and the gluonic background field  $A_4$ , are considered static and only the classical trajectory of these fields is taken into account. Using the so-called Polyakov gauge,  $A_4$  is a diagonal traceless matrix [315] and everything can be written in terms of the normalized Polyakov loop,  $\Phi$  and its adjoint  $\bar{\Phi}$ . The main effect of the gluonic background field is to change the quarks chemical potential to effective ones which have structure in colour space. Hence, upon calculating traces over the colour space the thermodynamical potential will be different from the NJL model and the Fermi distribution functions will be replaced by modified Fermi distribution functions:  $n_{\pm\eta}^F(E) \rightarrow \nu_{\pm\eta}^F(E)$ . These modified distribution functions can be defined as:

$$\nu_{\pm\eta}^F(E) = \frac{e^{-3\beta(E\mp\eta\mu)} + \Phi_{\mp\eta}e^{-\beta(E\mp\eta\mu)} + 2\Phi_{\pm\eta}e^{-2\beta(E\mp\eta\mu)}}{1 + e^{-3\beta(E\mp\eta\mu)} + 3\Phi_{\mp\eta}e^{-\beta(E\mp\eta\mu)} + 3\Phi_{\pm\eta}e^{-2\beta(E\mp\eta\mu)}}. \quad (7.64)$$

With  $\eta = \pm 1$  and, by definition,  $\Phi_- = \bar{\Phi}$  and  $\Phi_+ = \Phi$ . In Chapter 5, we studied an extend version of the PNJL in the mean field approximation.

In order to obtain the one-meson-loop PNJL model, we write the Euclidean action of the Lagrangian defined in Eq. (7.63) as  $\mathcal{S}_E[\bar{\psi}, \psi] = -\int_0^{1/T} d\tau \int d^3x \mathcal{L}(\bar{\psi}, \psi, A_4)$ , and define the energy functional as:

$$\mathcal{W}[T; \eta, \bar{\eta}, j_4] = \ln \int \mathcal{D}\bar{\psi} \mathcal{D}\psi \mathcal{D}A_4 e^{-\mathcal{S}_E[\bar{\psi}, \psi, A_4] + \int_0^{1/T} d\tau \int d^3x (\bar{\psi}\eta + \bar{\eta}\psi + A_4 j_4)}. \quad (7.65)$$

The path integral over the temporal gluon field  $A_4$  is to be made over all of its eight generator components and  $j_4$  is a source for the temporal gluon field  $A_4$ . As laid out in Section 7.2, one can bosonize the model in order to obtain a quadratic Lagrangian in the quark fields. The energy

<sup>3</sup>In Chapter 5, we studied an extended version of the PNJL model with eight-quark interactions and their connection to the existence of two CEPs, related to restoration of chiral symmetry in the light and strange quark sectors.

functional becomes:

$$\begin{aligned}\mathcal{W}[T; J, j_4] &= \ln \int \mathcal{D}\phi_a \mathcal{D}A_4 e^{-\mathcal{S}_E[\phi_a, A_4] + \int_0^{1/T} d\tau \int d^3x (J_a \phi_a + A_4 j_4)} \\ &= \ln \int \mathcal{D}\phi_a e^{-\mathcal{S}'_E[\phi_a, j_4] + \int_0^{1/T} d\tau \int d^3x J_a \phi_a}.\end{aligned}\quad (7.66)$$

Where we have defined the action  $\mathcal{S}'_E[\phi_a, j_4]$  as:

$$\mathcal{S}'_E[\phi_a, j_4] = -\ln \int \mathcal{D}A_4 e^{-\mathcal{S}_E[\phi_a, A_4] + \int_0^{1/T} d\tau \int d^3x A_4 j_4}.\quad (7.67)$$

Omitting the source  $j_4$  in Eq. (7.66), one can realize that this expression is identical to the one presented in Eq. (7.21) but written for the action  $\mathcal{S}'_E[\phi_a]$ . Hence, the effective action in the one-meson-loop approximation for this model,  $\Gamma'$ , is given by Eq. (7.24) and can be written explicitly as:

$$\Gamma'[T; \varphi] = \mathcal{S}'_E[\varphi] + \frac{1}{2} \text{tr} \ln \frac{\delta^2 \mathcal{S}'_E[\varphi]}{\delta \varphi^2}.\quad (7.68)$$

The only thing left to do is to solve the path integral over the temporal gluon field in the definition of  $\mathcal{S}'_E[\varphi]$ . One could also include quantum fluctuations in the gluonic sector by using the background field expansion to solve the path integral. However, we consider that the Polyakov loop potential,  $\mathcal{U}(\Phi[A_4], \bar{\Phi}[A_4])$ , is an effective potential which contains free parameters that are fitted to reproduce lattice QCD results. Hence, in a way, the Polyakov loop effective potential already incorporates quantum fluctuations from the exact results coming from lattice QCD. So we will consider the mean field approximation in the  $A_4$  field. Considering the traceless property of  $A_4$ , for  $N_c = 3$ , only two degrees of freedom are needed to parametrize this field. We intended to parametrize  $A_4$  in terms of the Polyakov loop and its complex conjugate,  $\Phi$  and  $\bar{\Phi}$ . Indeed, without loss of generality, one can only consider the diagonal and traceless generators with  $a = 3$  and  $a = 8$  and integrate over the remaining non-diagonal components to obtain the Haar measure [203, 316]. Since we are not interested in a derivation of the Polyakov loop effective potential using the Haar measure, we absorb the Haar volume, coming from the integration over the non-diagonal components of the field, in the definition of Polyakov effective potential. We can finally write:

$$\mathcal{S}'_E[\phi_a] = -\ln \int \mathcal{D}A_4^3 \mathcal{D}A_4^8 e^{-\mathcal{S}_E[\phi_a, A_4^3, A_4^8]}.\quad (7.69)$$

In the mean field approximation, only the classical trajectory is considered and one can use the stationary phase approximation to write:

$$\mathcal{S}'_E[\phi_a] \approx \mathcal{S}_E[\phi_a, \tilde{A}_4^3, \tilde{A}_4^8].\quad (7.70)$$

Where the fields  $\tilde{A}_4^3$  and  $\tilde{A}_4^8$  in the right hand side are calculated from demanding the action,  $\mathcal{S}_E$ , to be an extremum with respect to the fields  $A_4^3$  and  $A_4^8$ , i.e.:

$$\frac{\partial \mathcal{S}_E[\phi_a, A_4^3, A_4^8]}{\partial A_4^3} = \frac{\partial \mathcal{S}_E[\phi_a, A_4^3, A_4^8]}{\partial A_4^8} = 0. \quad (7.71)$$

There is an infinitesimal connection between the fields  $A_4^3$  and  $A_4^8$  with the Polyakov loop [317], and one can demand instead for the action to be an extremum with respect to the Polyakov loop:

$$\frac{\partial \mathcal{S}_E[\phi_a, \Phi, \bar{\Phi}]}{\partial \Phi} = \frac{\partial \mathcal{S}_E[\phi_a, \Phi, \bar{\Phi}]}{\partial \bar{\Phi}} = 0. \quad (7.72)$$

We can now use these results to write the one-meson-loop effective for the PNJL model:

$$\Gamma'[T; \varphi, \Phi, \bar{\Phi}] = \mathcal{S}_E[\varphi, \Phi, \bar{\Phi}] + \frac{1}{2} \text{tr} \ln \frac{\delta^2 \mathcal{S}_E[\varphi, \Phi, \bar{\Phi}]}{\delta \varphi^2}. \quad (7.73)$$

Since we used the mean field approximation on the gluon sector, the stationary relation for the Polyakov loop is only applied to the action  $\mathcal{S}_E[\varphi, \Phi, \bar{\Phi}]$ . The gap equation for the model would imply the action  $\Gamma'[T; \varphi, \Phi, \bar{\Phi}]$  to be stationary with respect to the field  $\varphi$  as laid out in Eq. (7.25). Hence, to incorporate the Polyakov loop in the one-meson-loop gap equation defined in Eq. (7.32), one simply has to substitute the Fermi–Dirac distribution functions by the modified ones,  $n_{\pm\eta}^F(E) \rightarrow \nu_{\pm\eta}^F(E)$ , defined in Eq. (7.64). The Fermi–Dirac distribution only appears in the functions  $f_0(S)$ ,  $f_1(S, q)$  and  $f_2(S, q)$ . Hence modifying these functions to include the Polyakov loop yields the one-meson-loop PNJL model, where the gluon field is considered a mean field.

## Chapter 8

# FRG study of the critical region of the QM model with vector interactions

### 8.1 Introduction

In this chapter, the critical region of the two flavour Quark-Meson model with vector interactions is explored using the Functional Renormalization Group technique. For more details on this method see Chapter 4.2. The FRG has been extensively used to study the QCD phase diagram using chiral effective models beyond the MF, like the NJL model [116, 178, 182, 183] and the QM model [88, 110, 188, 318–321].

The application of the FRG method to the two flavour QM model leads to the presence of an unphysical negative entropy density region in the low temperature and high density region of the phase diagram, near the critical region where a first-order chiral phase transition and CEP are predicted by the model. This behaviour was first discussed in detail by R. Tripolt et al. in [191], although previous FRG studies have reported decreasing pressures with increasing temperatures [319, 320]. The authors have put forward some explanations for this unphysical region: the truncation used to derive the QM flow equation was not enough to define a thermodynamically consistent model beyond the mean field approximation or the specific choice of regulator, used to account for fluctuations in the model, was not appropriate. They also discuss the possibility that the source for such behaviour is physical like a pairing transition to a colour superconducting phase or to the existence of inhomogeneous phases. For more details see [191].

We will explore the connection between vector degrees of freedom, the critical region predicted by the model and the unphysical negative entropy density region. Vector interactions are very important to describe in-medium properties and are widely used to describe neutron stars (as we have seen in Chapter 6) [61, 322, 323], to study the curvature of the critical line [160] and vector meson masses. The general effect of these interactions on the phase diagram, in MF calculations, is to drive the first-order phase transition and CEP towards lower temperatures and higher

chemical potentials. For high enough vector couplings, the critical region disappears leaving a smooth crossover for the chiral transition for all values of temperature and chemical potential.

The isoscalar  $\omega_0$  and isovector  $\rho_0^3$  vector mesons will be considered. The  $\omega_0$  vector is known to stiffen the EoS of quark matter while the  $\rho_0^3$  can be very important in isospin asymmetric systems, acting as an isospin restoring interaction. Hence the inclusion of these degrees of freedom can be essential to describe certain physical systems at high densities like NSs.

This chapter is organized as follows. In Section 8.2 the two flavour QM model, including vector interactions and the FRG formalism are presented. The vector degrees of freedom are frozen and the flow equations for the effective potential and entropy density are laid out. In Section 8.3 the results are presented and the effect of the vector interactions on the critical region and on the unphysical negative entropy density are discussed. Finally, in Section 8.4 conclusions are drawn and further work is proposed.

## 8.2 Model and Formalism

The two flavour Quark-Meson model is invariant under chiral symmetry i.e.,  $SU(2)_L \times SU(2)_R$ . It can be built by considering a quark field  $\psi$ , interacting with dynamical meson fields via symmetry conserving terms at the Lagrangian level. Considering the scalar and pseudoscalar fields,  $\sigma$ ,  $\boldsymbol{\pi}$  and the isoscalar-vector and isovector-vector fields,  $\omega_\mu$  and  $\boldsymbol{\rho}_\mu$ , the following symmetry conserving Lagrangian density, in Minkowski spacetime, can be written<sup>1</sup>:

$$\begin{aligned} \mathcal{L} = & \bar{\psi} [i\cancel{\partial} - h(\sigma + i\boldsymbol{\tau} \cdot \boldsymbol{\pi}\gamma_5) - g_\omega\psi - g_\rho\boldsymbol{\tau} \cdot \boldsymbol{\rho} + \hat{\mu}\gamma_0] \psi \\ & + \frac{1}{2}(\partial_\mu\sigma)^2 + \frac{1}{2}(\partial_\mu\boldsymbol{\pi})^2 - \frac{1}{4}F_{\mu\nu}F^{\mu\nu} - \frac{1}{4}\mathbf{R}_{\mu\nu}\mathbf{R}^{\mu\nu} - U(\sigma, \boldsymbol{\pi}, \omega_\mu, \boldsymbol{\rho}_\mu). \end{aligned} \quad (8.1)$$

Here, the quark field  $\psi$  is an  $N_f$ -component vector in flavour space, where each component is a Dirac spinor and  $\boldsymbol{\tau}$  are the three Pauli matrices. In the above Lagrangian,  $h$  is the Yukawa coupling of the quarks with the  $\sigma$  and  $\boldsymbol{\pi}$  fields,  $g_\omega$  and  $g_\rho$ , are the Yukawa couplings of the quarks with the  $\omega_\mu$  and  $\boldsymbol{\rho}_\mu$  vector fields. To study the system at finite density, a diagonal quark chemical potential matrix,  $\hat{\mu} = \text{diag}(\mu_u, \mu_d)$ , was also included. The field strength tensors  $F_{\mu\nu}$  and  $\mathbf{R}_{\mu\nu}$  are used to define the kinetic terms for the  $\omega_\mu$  and  $\boldsymbol{\rho}_\mu$  fields, respectively, and are given by:

$$F_{\mu\nu} = \partial_\mu\omega_\nu - \partial_\nu\omega_\mu, \quad (8.2)$$

$$\mathbf{R}_{\mu\nu} = \partial_\mu\boldsymbol{\rho}_\nu - \partial_\nu\boldsymbol{\rho}_\mu - g_\rho\boldsymbol{\rho}_\mu \times \boldsymbol{\rho}_\nu. \quad (8.3)$$

The potential  $U(\sigma, \boldsymbol{\pi}, \omega_\mu, \boldsymbol{\rho}_\mu)$ , must be invariant under chiral symmetry except for an explicit chiral symmetry breaking term, that tilts the potential to give a finite mass to the Goldstone mode, the pion. This can be accomplished, in the QM model, by adding to the potential a

<sup>1</sup>A version of this model, without vector interactions, was introduced in Chapter 4.2.1, as a bosonized version of the two flavour NJL model.

non-vanishing expectation value for the  $\sigma$  field,

$$U(\sigma, \boldsymbol{\pi}, \omega_\mu, \boldsymbol{\rho}_\mu) \rightarrow U(\sigma, \boldsymbol{\pi}, \omega_\mu, \boldsymbol{\rho}_\mu) - c\sigma. \quad (8.4)$$

This field will behave as an order parameter for the chiral transition. In the above, the coupling of the explicit chiral symmetry breaking term,  $c$ , is chosen in such a way to reproduce pion vacuum observables, like  $f_\pi$  and  $m_\pi$ .

At the mean field level, for the  $\sigma$  and  $\boldsymbol{\pi}$  fields, this potential can include arbitrary powers of the chiral invariant combination<sup>2</sup>,  $\phi^2 = \sigma^2 + \boldsymbol{\pi}^2$ . Regarding the vector field contributions to the potential, several types of terms can be included, as long as the symmetries are respected. Due to the nature of the FRG calculation, one has only to specify the potential at the ultraviolet scale.

Finite temperature can be included, once again, using the Matsubara formalism in which a Wick rotation to Euclidean spacetime is applied to the action. To simplify the notation, we introduce the fields,  $\phi^i = \{\sigma, \boldsymbol{\pi}\}$  and  $V_\mu^i = \{\omega_\mu, \boldsymbol{\rho}_\mu\}$ . The Euclidean action can be written as:

$$\mathcal{S}_E = - \int_0^{1/T} d\tau \int d^3x \mathcal{L}_E, \quad (8.5)$$

where the Euclidean Lagrangian,  $\mathcal{L}_E$ , can be obtained by Wick rotating the Lagrangian given in Eq. (8.1),  $\mathcal{L}_E = \mathcal{L}(t \rightarrow -i\tau)$ . The generating functional of the fully connected Green's functions, for a given temperature ( $T$ ) and chemical potential ( $\mu$ ), is defined as:

$$\mathcal{W}[T, \mu; J^i, j_\mu^i] = \ln \int \mathcal{D}\psi \mathcal{D}\bar{\psi} \mathcal{D}\phi^i \mathcal{D}V_\mu^i e^{-\mathcal{S}_E[T, \mu; \psi, \bar{\psi}, \phi^i, V_\mu^i] + \int_0^{1/T} d\tau \int d^3x (J^i \phi^i + j_\mu^i V_\mu^i)}, \quad (8.6)$$

where we have included sources for the scalar fields ( $J^i$ ) and for the vector fields ( $j_\mu^i$ ), omitting the sources for the fermion fields which can be integrated out. First we are only interested in dealing with the path integral over the vector fields hence, we write:

$$\mathcal{W}[T, \mu; J^i, j_\mu^i] = \ln \int \mathcal{D}V_\mu^i e^{-\mathcal{S}_V[T, \mu; J^i, V_\mu^i] + \int_0^{1/T} d\tau \int d^3x j_\mu^i V_\mu^i}. \quad (8.7)$$

We have defined the effective action for vector degrees of freedom as:

$$\mathcal{S}_V[T, \mu; J^i, V_\mu^i] = - \ln \int \mathcal{D}\psi \mathcal{D}\bar{\psi} \mathcal{D}\phi^i e^{-\mathcal{S}_E[T, \mu; \psi, \bar{\psi}, \phi^i, V_\mu^i] + \int_0^{1/T} d\tau \int d^3x J^i \phi^i} \quad (8.8)$$

Writing explicitly only the functional dependence on  $j_\mu^i$ , the effective action can be computed by Legendre transforming  $\mathcal{W}[j_\mu^i]$  as follows:

$$\Gamma_V[\tilde{V}_\mu^i] = -\mathcal{W}[j_\mu^i] + \int_0^{1/T} d\tau \int d^3x j_\mu^i \tilde{V}_\mu^i, \quad (8.9)$$

<sup>2</sup>As already discussed in other chapters, the  $\sigma$  and  $\boldsymbol{\pi}$  fields have the same quantum numbers as the quark bilinear operators  $\bar{\psi}\psi$  and  $\bar{\psi}i\gamma_5\boldsymbol{\tau}\psi$ , respectively. The combination  $\phi^2 = \sigma^2 + \boldsymbol{\pi}^2$  can be checked to be invariant under vector and axial-vector transformations (see Table 2.2, for the transformation properties).

where  $\tilde{V}_\mu^i$  is the expectation value of the vector fields  $V_\mu^i$ , in the presence of an external source  $j_\mu^i$  (also called the classical field [56]) and it is defined as:

$$\frac{\delta \mathcal{W}[j_\mu^i]}{\delta j_\mu^i(x)} = \tilde{V}_\mu^i(x). \quad (8.10)$$

The effective action can be written as [56]:

$$e^{-\Gamma_V[\tilde{V}_\mu^i]} = \int \mathcal{D}V_\mu^i \exp \left\{ -\mathcal{S}_V[V_\mu^i + \tilde{V}_\mu^i] + \int_0^{1/T} d\tau \int d^3x \frac{\delta \Gamma_V[\tilde{V}_\mu^i]}{\delta \tilde{V}_\mu^i} V_\mu^i \right\}. \quad (8.11)$$

In a chiral effective model, the most important dynamics comes from chiral symmetry breaking. This means that the dynamics of the more massive fields, will play a secondary role. Hence, following previous approaches [324], the vector fields will be used to model unknown degrees of freedom at short distances. This allows the use of the saddle point approximation to solve the path integral in Eq. (8.11): the classical trajectories will be the most important for such fields, effectively freezing these heavier modes.

Using the saddle point approximation, the main contribution to the integral will come from the minimum of the action  $\mathcal{S}_V[V_\mu^i]$ . Taylor expanding the action  $\mathcal{S}_V[V_\mu^i + \tilde{V}_\mu^i]$  around  $\tilde{V}_\mu^i$  one can get the effective action in the mean field approximation (see Chapter 4 for a similar calculation),

$$e^{-\Gamma_V[\tilde{V}_\mu^i]} \approx e^{-\mathcal{S}_V[\tilde{V}_\mu^i]}. \quad (8.12)$$

Where the mean field configuration is calculated from:

$$\left. \frac{\partial \mathcal{S}_V(V_\mu^i)}{\partial V_\mu^i} \right|_{V_\mu^i = \tilde{V}_\mu^i} = \left. \frac{\partial \Gamma_V(V_\mu^i)}{\partial V_\mu^i} \right|_{V_\mu^i = \tilde{V}_\mu^i} = 0 \quad (8.13)$$

Due to rotational invariance, the spatial components of the mean fields  $\tilde{V}_j^i$ , vanish [324]. Since we are not interested in studying the condensation of mean fields that change the isospin properties of the vacuum, the non-diagonal elements  $\tilde{\rho}^1 = \tilde{\rho}^2 = 0$  will also be zero. Therefore, only the fields  $\tilde{\omega}_0$  and  $\tilde{\rho}_0^3$  can have non-zero values. These fields can be absorbed in the definition of the effective quark chemical potential matrix,  $\tilde{\mu}$ , as:

$$\tilde{\mu} = \hat{\mu} - g_\omega \tilde{\omega}_0 - g_\rho \tilde{\rho}_0^3 \tau^3. \quad (8.14)$$

As expected, the mean field  $\tilde{\rho}_0^3$ , introduces an isospin asymmetry [324].

Using Eqs. (8.8) and (8.12), we can write the effective action as:

$$\Gamma_V[T, \mu; \tilde{V}_\mu^i, J^i] = -\ln \int \mathcal{D}\psi \mathcal{D}\bar{\psi} \mathcal{D}\phi^i e^{-S_E[T, \tilde{\mu}; \psi, \bar{\psi}, \phi^i, \tilde{V}_\mu^i] + \int_0^{1/T} d\tau \int d^3x J^i \phi^i}, \quad (8.15)$$

where the mean field vector field configurations,  $\tilde{V}_\mu^i$ , are calculated by imposing Eq. (8.13):

$$\left. \frac{\partial \Gamma_V(V_\mu^i)}{\partial V_\mu^i} \right|_{V_\mu^i = \tilde{V}_\mu^i} = \left. \frac{\partial \mathcal{S}_E[T, \tilde{\mu}; V_\mu^i]}{\partial V_\mu^i} \right|_{V_\mu^i = \tilde{V}_\mu^i} = 0. \quad (8.16)$$

The same approximation could be performed in the remaining meson path integrals and the quarks can be integrated out exactly, yielding the Quark-Meson model, including vector interactions, in the mean field approximation. However, in the present work, we will go beyond the mean field by taking into account quantum fluctuations of the  $\sigma$  and  $\pi$  fields using the FRG method.

### 8.2.1 The FRG method

The FRG method was discussed in Chapter 4.2. In this section, we briefly summarize the FRG formalism.

The scale dependent effective average action,  $\Gamma_k$ , is the essential object in the FRG. This quantity interpolates between the bare action in the UV,  $k = \Lambda$ , and the effective action,  $\Gamma$ , in the IR,  $k = 0$ , containing all the quantum fluctuations:

$$\begin{aligned} \Gamma_{k \rightarrow \Lambda} &= \mathcal{S}, \\ \Gamma_{k \rightarrow 0} &= \Gamma. \end{aligned}$$

The behaviour of the effective average action, during the renormalization group flow, is governed by the so-called Wetterich equation [325] which, for bosonic and fermionic fields, can be written respectively as:

$$\begin{aligned} \partial_t \Gamma_k[\varphi] &= \frac{1}{2} \text{tr} \left\{ \partial_t R_k^{\text{B}} \left( \Gamma_k^{(2)}[\varphi] + R_k^{\text{B}} \right)^{-1} \right\}, \\ \partial_t \Gamma_k[\bar{\psi}, \psi] &= - \text{tr} \left\{ \partial_t R_k^{\text{F}} \left( \Gamma_k^{(1,1)}[\bar{\psi}, \psi] + R_k^{\text{F}} \right)^{-1} \right\}. \end{aligned}$$

Here, instead of writing the differential equations with respect to the momentum scale  $k$ , we introduced  $t$ ,

$$t = \ln \frac{k}{\Lambda}, \quad (8.17)$$

the adimensional renormalization “time” with respect to some UV cutoff momentum  $\Lambda$ . In the Wetterich equations,  $\Gamma_k^{(2)}$  and  $\Gamma_k^{(1,1)}$  are the usual notations for boson and fermion fields derivatives given by in Eqs. (4.42) and (4.43).

The regulator function  $R_k$  is introduced to regularize the flow both in the UV and in the IR. The regulators also guarantee that the flow reaches the full quantum effective action in the IR. To achieve those ends, the regulator functions must respect certain conditions (which were discussed in detail in Chapter 4.2):  $\lim_{q^2/k^2 \rightarrow 0} R_k(q) > 0$ ,  $\lim_{k^2/q^2 \rightarrow 0} R_k(q) = 0$  and  $\lim_{k^2 \rightarrow \infty} R_k(q) \rightarrow \infty$ .

Hence, to use Wetterich's equation, a regulator function  $R_k$ , which respects the interpolating limits of the effective average action, has to be chosen. As long as the interpolation between the UV and the IR is correct, the regulator can take any functional form since it will only interfere in the arbitrary path taken, between these points in the theory space. Of course, since from the numerical point of view it is impossible to reach  $k = 0$  [166], a finite infrared cutoff,  $k_{\text{IR}}$ , has to be applied in practical calculations. This means that different regulators might lead to different infrared effective actions.

In this work, we consider the three-dimensional Litim regulator functions [326, 327], for bosons and fermions, respectively given by<sup>3</sup>:

$$R_k^{\text{B}}(\mathbf{q}^2) = (k^2 - \mathbf{q}^2)H(k^2 - \mathbf{q}^2), \quad (8.18)$$

$$R_k^{\text{F}}(\mathbf{q}^2) = \mathbf{q} \cdot \boldsymbol{\gamma} \left( \sqrt{\frac{k^2}{\mathbf{q}^2}} - 1 \right) H(k^2 - \mathbf{q}^2). \quad (8.19)$$

Here,  $H(x)$  is the Heaviside step function (see Appendix A.2). These regulators were derived in Minkowski spacetime in Refs. [326, 327] considering an optimization criterion. These specific regulator functions allow the analytic separation between quantum fluctuations and thermal fluctuations and, given their analytical structure, usually allow for the Matsubara summation to be performed analytically, yielding a simpler flow equation [327]. At finite temperature, the Matsubara summations already acts as a regulator and only the three-dimensional version of the regulators can be considered [327, 328].

After solving the flow equation one can relate the effective action in the minimum, with the grand canonical potential,  $\Gamma_{k=k_{\text{IR}}}(T, \mu)_{\text{min}} = V\Omega(T, \mu)/T$ , to calculate several thermodynamic quantities of interest such as the pressure ( $P$ ), particle ( $\rho_i$ ), entropy ( $s$ ) and energy densities ( $\epsilon$ ), using the thermodynamic relations in Appendix A.5.1, which are explicitly given by:

$$\begin{aligned} P(T, \mu) - P_0 &= -\Omega(T, \mu), \\ \rho_i(T, \mu) &= - \left( \frac{\partial \Omega(T, \mu)}{\partial \mu_i} \right)_T, \\ s(T, \mu) &= - \left( \frac{\partial \Omega(T, \mu)}{\partial T} \right)_\mu, \\ \epsilon(T, \mu) &= -P(T, \mu) + Ts(T, \mu) + \sum_i \mu_i \rho_i(T, \mu). \end{aligned}$$

The constant  $P_0$  is the vacuum pressure i.e.,  $P_0 = P(0, 0)$ .

<sup>3</sup>We would like to draw attention to the conventions for the Dirac matrices that were used in this work,  $\gamma_0^M = -i\gamma_0^E = -i\gamma_\tau$  and  $\gamma_j^M = \gamma_j^E$ , with superscript  $M$  and  $E$  meaning Minkowski and Euclidean spacetime (see Appendix A). Using these conventions, the fermionic regulator is given by Eq. (8.19). However, in other works, a different convention was used:  $\gamma_0^M = \gamma_0^E$  and  $\gamma_j^M = i\gamma_j^E$ , see for example [33, 328, 329]. Using this different convention, the fermionic regulator is given by:  $R_k^{\text{F}}(\mathbf{q}^2) = i\boldsymbol{\gamma}(\sqrt{k^2/\mathbf{q}^2} - 1)H(k^2 - \mathbf{q}^2)$ .

### 8.2.2 The flow equations

As already stated, solving exactly the Wetterich equation is an impossible task due to the infinitely high coupled behaviour of the equation and some approximation scheme is needed. In this work, to build the *ansatz* for the effective average action of the Quark-Meson model with vector interactions, we will consider the operator expansion. In this approximation the effective action is expanded in powers of momentum. Keeping only the first term in the expansion corresponds to the local potential approximation (LPA). Hence, in this approximation, only the potential is scale dependent and contributions coming from the wave renormalizations for the fields are neglected.

We will write an *ansatz* for the effective average action based on the Euclidean action defined in Eq. (8.5), alongside the stationary condition of Eq. (8.16). The *ansatz* for the imaginary-time effective average action,  $\Gamma_k$ , that we will use in this chapter, can be written as<sup>4</sup>:

$$\Gamma_k[T, \mu] = \int_0^{1/T} d\tau \int d^3x \left\{ \bar{\psi} [ -i\gamma_a \partial_a + h(\sigma + i\boldsymbol{\tau} \cdot \boldsymbol{\pi} \gamma_5) - \tilde{\mu} \gamma_0 ] \psi + \frac{1}{2} (\partial_a \sigma)^2 + \frac{1}{2} (\partial_a \boldsymbol{\pi})^2 + U_k(\sigma, \boldsymbol{\pi}, \omega_0, \rho_0^3) \right\}. \quad (8.20)$$

Here, the partial differential operator is  $\partial_a = (-i\partial_0, \boldsymbol{\nabla}) = (\partial_\tau, \partial_x)$  and the Euclidean Dirac matrices are  $\gamma_a = (i\gamma^0, \boldsymbol{\gamma}) = (\gamma_\tau, \boldsymbol{\gamma})$  (see Appendix A). The scale dependent effective potential,  $U_k$ , is written in terms the chiral invariant combination,  $\phi^2 = \sigma^2 + \boldsymbol{\pi}^2$ , and of the vector fields:

$$U_k(\sigma, \boldsymbol{\pi}, \omega_0, \rho_0^3) = U_k^X(\sigma, \boldsymbol{\pi}, \omega_0, \rho_0^3) + U_k^V(\sigma, \boldsymbol{\pi}, \omega_0, \rho_0^3). \quad (8.21)$$

The contribution  $U_k^X$  is a function of the chiral invariant only and the term  $U_k^V$  represents the contribution from the vector degrees of freedom. While the functional dependence of the chiral part of the potential is calculated during the flow, a mean field approximation is performed in the vector channels, and a functional dependence for  $U_k^V$  must be chosen. In this work we use:

$$U_k^V(\sigma, \boldsymbol{\pi}, \omega_0, \rho_0^3) = -\frac{m_\omega^2}{2} \omega_0^2 - \frac{m_\rho^2}{2} (\rho_0^3)^2. \quad (8.22)$$

#### The effective potential flow equation

Considering the *ansatz* for the effective average action in Eq. (8.20), and the fact that the effective potential,  $U_k$ , is considered to be spacetime independent, calculating the scale derivative of the effective action is equivalent to calculating the scale derivative of the effective potential

<sup>4</sup>We would like to draw attention to the conventions for the Dirac matrices that were used in this work,  $\gamma_0^M = -i\gamma_0^E = -i\gamma_\tau$  and  $\gamma_j^M = \gamma_j^E$ , with superscript  $M$  and  $E$  meaning Minkowski and Euclidean spacetime (see Appendix A). Using these conventions, the Wick rotated Euclidean action yields the result presented in Eq. (8.20). However, in other works, a different convention was used:  $\gamma_0^M = \gamma_0^E$  and  $\gamma_j^M = i\gamma_j^E$ , see for example [33, 328, 329]. Using this different convention, the fermionic kinetic term is  $\not{\partial}$  instead of  $-i\gamma_a \partial_a$ .

[328], i.e.,

$$\partial_t \Gamma_k = \frac{V}{T} \partial_t U_k(\sigma, \boldsymbol{\pi}, \omega_0, \rho_0^3). \quad (8.23)$$

Where, the volume factor comes from the spacetime independence of the effective potential  $U_k$ , and,  $\int_0^{1/T} d\tau \int d^3x = V/T$ . Thus, solving the flow for the effective action is equivalent to solving the flow for the effective potential,  $U_k$ .

In our approach, when considering vector degrees of freedom, the effective action must be stationary with respect to the vector fields, following the mean field approximation applied to the vector sector (see Eq. (8.16)). Since we are interested in solving Wetterich's equation for the *ansatz* in Eq. (8.20), we will apply the stationary condition to the effective average action,  $\Gamma_k$ . Since the flow of the effective action and the flow of the effective potential are equivalent (see Eq. (8.23)), the condition that the effective average action must be stationary with respect to the vector fields is equivalent to requiring the same for the effective potential<sup>5</sup>,  $U_k(\sigma, \boldsymbol{\pi}, V_0^i)$  [324, 330], i.e.:

$$\left. \frac{\partial U_k(\sigma, \boldsymbol{\pi}, V_0^i)}{\partial V_0^i} \right|_{V_0^i = \tilde{V}_{0,k}^i} = 0 \implies \left. \frac{\partial U_k(\sigma, \boldsymbol{\pi}, \omega_0, \rho_0^3)}{\partial \omega_0} \right|_{\omega_0 = \tilde{\omega}_{0,k}} = \left. \frac{\partial U_k(\sigma, \boldsymbol{\pi}, \omega_0, \rho_0^3)}{\partial \rho_0^3} \right|_{\rho_0^3 = \tilde{\rho}_{0,k}^3} = 0. \quad (8.24)$$

Hence, the vector fields acquire an implicit dependence on the renormalization group scale  $k$  through the stationarity requirement. Such condition ensures that the flow equation follows a path, in theory space, where the effective potential is always in the minimum with respect to the vector fields.

Having the *ansatz* for the effective average action, one can use Wetterich's equation to derive a flow equation for the effective potential. Consider the scale derivative of the effective potential, with the previous stationary condition already applied. One can write it as follows:

$$\partial_t U_k(\sigma, \boldsymbol{\pi}, \tilde{V}_{0,k}^i) = \left. \partial_t U_k(\sigma, \boldsymbol{\pi}, V_0^i) \right|_{V_0^i = \tilde{V}_{0,k}^i} + \sum_i \frac{\partial \tilde{V}_{0,k}^i}{\partial t} \left. \frac{\partial U_k(\sigma, \boldsymbol{\pi}, V_0^i)}{\partial V_0^i} \right|_{V_0^i = \tilde{V}_{0,k}^i}. \quad (8.25)$$

In the first term we consider the explicit  $k$  dependence of the effective potential while, in the second term, the implicit scale dependence coming from the vector fields, is considered. The requirement for the effective action to be stationary with respect to the vector fields implies that the last term vanishes. Using Eq. (8.21), we can write the above equations as:

$$\partial_t U_k(\sigma, \boldsymbol{\pi}, \tilde{V}_{0,k}^i) = \left. \partial_t \left( U_k^X(\sigma, \boldsymbol{\pi}, V_0^i) + U_k^V(\sigma, \boldsymbol{\pi}, V_0^i) \right) \right|_{V_0^i = \tilde{V}_{0,k}^i}. \quad (8.26)$$

---

<sup>5</sup>We recall that  $V_0^i = \{\omega_0, \rho_0^3\}$ .

Since the vector contribution to the potential,  $U_k^V$ , does not depend explicitly on the renormalization group time (see Eq. (8.22)), the above equation simplifies and we can write:

$$\partial_t U_k(\sigma, \boldsymbol{\pi}, \tilde{V}_{0,k}^i) = \partial_t U_k^X(\sigma, \boldsymbol{\pi}, \tilde{V}_{0,k}^i) \quad (8.27)$$

Thus, ensuring, at each momentum shell, that the vector fields stationary conditions hold, one can simply solve the flow equation for  $U_k^X$  with effective quark chemical potentials modified by the mean field vector fields. The flow equation for the Quark-Meson model, using the *ansatz* of Eq. (8.20) without quark effective chemical potentials, has been derived in several works, for some derivations see [33, 328].

Deriving the flow equation for Eq. (8.20) and considering no pion condensation<sup>6</sup>, one can get the dimensionful LPA flow equation for the effective potential  $U_k^X(T, \mu; \sigma, \tilde{\omega}_{0,k}, \tilde{\rho}_{0,k}^3)$ :

$$\partial_t U_k^X(T, \mu; \sigma, \tilde{\omega}_{0,k}, \tilde{\rho}_{0,k}^3) = \frac{k^5}{12\pi^2} \left\{ \frac{1}{E_\sigma} [1 + 2n_B(E_\sigma)] + \frac{3}{E_\pi} [1 + 2n_B(E_\pi)] - \frac{4N_c}{E_\psi} \sum_{l=0,1} \left( 1 - \sum_{\eta=\pm 1} n_F(E_\psi - \eta \tilde{\mu}_{k,l}) \right) \right\}. \quad (8.28)$$

Here, the effective chemical potential,  $\tilde{\mu}_{k,l}$ , is defined as,

$$\tilde{\mu}_{k,l} = \mu_l - v_{k,l}, \quad (8.29)$$

with,  $l = 0$  for up quarks and  $l = 1$  for down quarks. The vector contribution,  $v_{k,l}$ , is defined as:

$$v_{k,l} = g_\omega \tilde{\omega}_{0,k} + (-1)^l g_\rho \tilde{\rho}_{0,k}^3. \quad (8.30)$$

The  $k$  dependence on the effective quark chemical potential and on the vector fields, is only manifest when the condition that the effective potential is stationary with respect to the vector fields is applied. The functions,  $n_B(E)$  and  $n_F(E)$  are the Bose–Einstein and Fermi–Dirac distribution functions respectively given by:

$$n_B(E) = \frac{1}{e^{E/T} - 1}, \quad (8.31)$$

$$n_F(E) = \frac{1}{e^{E/T} + 1}. \quad (8.32)$$

The energies  $E_\sigma$ ,  $E_\pi$  and  $E_\psi$  are:

$$E_\sigma^2 = k^2 + \partial_\sigma^2 U_k^X, \quad (8.33)$$

$$E_\pi^2 = k^2 + \frac{1}{\sigma} \partial_\sigma U_k^X, \quad (8.34)$$

$$E_\psi^2 = k^2 + h^2 \sigma^2. \quad (8.35)$$

The second term in Eqs. (8.33) and (8.34) will be labelled as the curvature mesons masses, or

<sup>6</sup>Only the radial direction of the field,  $\phi = \{\sigma, \mathbf{0}\}$ , will contribute and we can switch variables to  $\sigma$ .

simply meson masses  $m_M^2$ , i.e.,  $m_\sigma^2 = \partial_\sigma^2 U_k^\chi$  and  $m_\pi^2 = \frac{1}{\sigma} \partial_\sigma U_k^\chi$ . The second term in Eq. (8.35) is the quark mass,  $m_q^2 = h^2 \sigma^2$ .

After solving the above flow equation, one has access to  $U_{k=k_{\text{IR}}}^\chi$ . The full potential in the infrared,  $U_{k=k_{\text{IR}}}$ , containing the contribution coming from vector fields, can be calculated with  $k = k_{\text{IR}}$ :

$$U_{k=k_{\text{IR}}}(T, \mu; \sigma, \tilde{\omega}_0, \tilde{\rho}_0^3) = U_{k=k_{\text{IR}}}^\chi(T, \mu; \sigma, \tilde{\omega}_0, \tilde{\rho}_0^3) + U_{k=k_{\text{IR}}}^V(T, \mu; \sigma, \tilde{\omega}_0, \tilde{\rho}_0^3). \quad (8.36)$$

The contribution coming from the vector fields can be calculated using Eq. (8.22) in the infrared.

### Flow equations for the MF vector fields

Now, we will derive the self consistent equations for the vector fields that must be satisfied at each momentum shell,  $k$ . We will follow a very similar calculation performed in Ref. [328].

Consider the stationarity condition provided in Eq. (8.24). The effective potential,  $U_k$ , is a function of the vector fields,  $V_0^i$ , explicitly and implicitly through the effective chemical potential,  $\tilde{\mu}_{k,l}$ , and meson masses<sup>7</sup>,  $m_M^2$ , see Eqs. (8.29), (8.33) and (8.34), respectively. The stationary condition can be written as:

$$\left. \frac{\partial U_k(T, \mu; \sigma, V_0^i)}{\partial V_0^i} \right|_{V_0^i = \tilde{V}_{0,k}^i} = \left[ \sum_M \frac{\partial U_k}{\partial V_0^i} \frac{\partial m_M^2}{\partial U_k} \frac{\partial U_k}{\partial m_M^2} + \sum_{l=0,1} \frac{\partial \tilde{\mu}_l}{\partial V_0^i} \frac{\partial U_k}{\partial \tilde{\mu}_l} + \frac{\partial U_k}{\partial V_0^i} \right]_{V_0^i = \tilde{V}_{0,k}^i} = 0. \quad (8.37)$$

Applying the stationary condition itself, the first term is zero. Using the decomposition defined in Eq. (8.21), we can write:

$$\left. \frac{\partial U_k(T, \mu; \sigma, V_0^i)}{\partial V_0^i} \right|_{V_0^i = \tilde{V}_{0,k}^i} = \sum_{l=0,1} \frac{\partial \tilde{\mu}_l}{\partial V_0^i} \frac{\partial U_k^\chi}{\partial \tilde{\mu}_l} \Big|_{V_0^i = \tilde{V}_{0,k}^i} + \left. \frac{\partial U_k^V}{\partial V_0^i} \right|_{V_0^i = \tilde{V}_{0,k}^i} = 0. \quad (8.38)$$

The first term in the right-hand side of the above equation, can be written as:

$$\begin{aligned} \sum_{l=0,1} \frac{\partial \tilde{\mu}_l}{\partial V_0^i} \frac{\partial U_k^\chi}{\partial \tilde{\mu}_l} \Big|_{V_0^i = \tilde{V}_{0,k}^i} &= \sum_{l=0,1} \frac{\partial \tilde{\mu}_l}{\partial V_0^i} \frac{\partial}{\partial \tilde{\mu}_l} \left[ \int_\Lambda^k dp \frac{\partial}{\partial p} U_p^\chi + C^\chi \right] \Big|_{V_0^i = \tilde{V}_{0,k}^i} \\ &= \sum_{l=0,1} \frac{\partial \tilde{\mu}_l}{\partial V_0^i} \frac{\partial}{\partial \tilde{\mu}_l} \int_\Lambda^k dp \frac{\partial}{\partial p} U_p^\chi \Big|_{V_0^i = \tilde{V}_{0,k}^i} + \sum_{l=0,1} \frac{\partial \tilde{\mu}_l}{\partial V_0^i} \frac{\partial C^\chi}{\partial \tilde{\mu}_l} \Big|_{V_0^i = \tilde{V}_{0,k}^i}. \end{aligned} \quad (8.39)$$

In the above we have used the fundamental theorem of calculus<sup>8</sup> applied to the effective potential and we have also defined  $U_p^\chi = U_p^\chi(T, \mu; \sigma, V_0^i)$  and  $C^\chi = C^\chi(T, \mu; \sigma, V_0^i)$ . The integration is made from  $\Lambda$  to  $k$  since the effective potential is defined from the UV scale at  $k = \Lambda$ , to the IR

<sup>7</sup>The masses depend on the effective potential,  $U_k^\chi$ , which depend on the vector fields, see Eqs. (8.33) and (8.34).

<sup>8</sup>The fundamental theorem of calculus can be summarized in the following equation:

$$\int_a^b dx f(x) = F(b) - F(a),$$

where  $f(x)$  is continuous in the closed interval  $[a, b]$  and  $F(x)$  is its indefinite integral in that same interval.

at  $k = k_{\text{IR}}$ . The  $k$  independent term,  $C^X$ , is introduced with the integration in order to eliminate the extra freedom coming from the contribution of the lower bound in the integration. This term is going to be calculated later, by setting  $k = \Lambda$ . For simplicity, we redefine the overall contribution coming from this term as,  $C^i$ , by defining:

$$\sum_{l=0,1} \frac{\partial \tilde{\mu}_l}{\partial V_0^i} \frac{\partial}{\partial \tilde{\mu}_l} C^X(T, \mu; \sigma, V_0^i) \Big|_{V_0^i = \tilde{V}_{0,k}^i} = C^i(T, \mu; \sigma, \tilde{V}_{0,k}^i). \quad (8.40)$$

Making this substitution and using the right hand side of the flow Eq. (8.28), one can write:

$$\begin{aligned} \sum_{l=0,1} \frac{\partial \tilde{\mu}_l}{\partial V_0^i} \frac{\partial U_k^X}{\partial \tilde{\mu}_l} \Big|_{V_0^i = \tilde{V}_{0,k}^i} &= \sum_{l=0,1} \frac{\partial \tilde{\mu}_l}{\partial V_0^i} \frac{\partial}{\partial \tilde{\mu}_l} \int_{\Lambda} dp \frac{p^4}{12\pi^2} \left\{ \frac{1}{E_{\sigma}} [1 + 2n_{\text{B}}(E_{\sigma})] + \frac{3}{E_{\pi}} [1 + 2n_{\text{B}}(E_{\pi})] \right. \\ &\quad \left. - \frac{4N_c}{E_{\psi}} \sum_{j=0,1} \left( 1 - \sum_{\eta=\pm 1} n_{\text{F}}(E_{\psi} - \eta \tilde{\mu}_j) \right) \right\} \Big|_{V_0^i = \tilde{V}_{0,k}^i} + C^i. \end{aligned} \quad (8.41)$$

Commuting the effective chemical potential derivative with the integral, only the fermion terms will contribute:

$$\sum_{l=0,1} \frac{\partial \tilde{\mu}_l}{\partial V_0^i} \frac{\partial U_k^X}{\partial \tilde{\mu}_l} \Big|_{V_0^i = \tilde{V}_{0,k}^i} = \frac{N_c}{3\pi^2} \sum_{l=0,1} \frac{\partial \tilde{\mu}_l}{\partial V_0^i} \sum_{j=0,1} \sum_{\eta=\pm 1} \int_{\Lambda} dp \frac{p^4}{E_{\psi}} \frac{\partial}{\partial \tilde{\mu}_l} n_{\text{F}}(E_{\psi} - \eta \tilde{\mu}_j) \Big|_{V_0^i = \tilde{V}_{0,k}^i} + C^i. \quad (8.42)$$

As performed in [328], we can use the following identity<sup>9</sup>:

$$\frac{\partial}{\partial \mu_l} n_{\text{F}}(E_{\psi} - \eta \mu_j) = -\delta_{lj} \frac{\eta}{E_{\psi}} \frac{\partial}{\partial p} n_{\text{F}}(E_{\psi} - \eta \mu_j), \quad (8.43)$$

in order to write:

$$\sum_{l=0,1} \frac{\partial \tilde{\mu}_l}{\partial V_0^i} \frac{\partial U_k^X}{\partial \tilde{\mu}_l} \Big|_{V_0^i = \tilde{V}_{0,k}^i} = -\frac{N_c}{3\pi^2} \sum_{l=0,1} \frac{\partial \tilde{\mu}_l}{\partial V_0^i} \sum_{j=0,1} \delta_{lj} \sum_{\eta=\pm 1} \int_{\Lambda} dp \eta p^3 \frac{\partial}{\partial p} n_{\text{F}}(E_{\psi} - \eta \tilde{\mu}_j) \Big|_{V_0^i = \tilde{V}_{0,k}^i} + C^i. \quad (8.44)$$

Performing the sum over  $j$  and setting  $V_0^i = \tilde{V}_{0,k}^i$ , defines the scale dependent effective chemical potential,  $\tilde{\mu}_{k,l}$ , as previously defined in Eq. (8.29). We can write:

$$\sum_{l=0,1} \frac{\partial \tilde{\mu}_l}{\partial V_0^i} \frac{\partial U_k^X}{\partial \tilde{\mu}_l} \Big|_{V_0^i = \tilde{V}_{0,k}^i} = -\frac{N_c}{3\pi^2} \sum_{l=0,1} \sum_{\eta=\pm 1} \left[ \int_{\Lambda} dp \eta p^3 \frac{\partial}{\partial p} n_{\text{F}}(E_{\psi} - \eta \tilde{\mu}_{k,l}) \right] \frac{\partial \tilde{\mu}_l}{\partial V_0^i} \Big|_{V_0^i = \tilde{V}_{0,k}^i} + C^i. \quad (8.45)$$

<sup>9</sup>This identity can be proved by expanding both sides of the equation.

Integrating by parts, yields:

$$\sum_{l=0,1} \frac{\partial \tilde{\mu}_l}{\partial V_0^i} \frac{\partial U_k^X}{\partial \tilde{\mu}_l} \Big|_{V_0^i = \tilde{V}_{0,k}^i} = -\frac{N_c}{3\pi^2} \sum_{l=0,1} \sum_{\eta=\pm 1} I_{k,\eta l} \frac{\partial \tilde{\mu}_l}{\partial V_0^i} \Big|_{V_0^i = \tilde{V}_{0,k}^i} + C^i. \quad (8.46)$$

Where  $I_{k,\eta l} = I_{k,\eta l}(T, \mu; \sigma, \tilde{V}_{0,k}^i)$ , is given by:

$$I_{k,\eta l}(T, \mu; \sigma, \tilde{V}_{0,k}^i) = 3 \int_k^\Lambda dp \eta p^2 n_F(E_\psi - \eta \tilde{\mu}_{k,l}) - \left[ \eta p^3 n_F(E_\psi - \eta \tilde{\mu}_{k,l}) \right]_k^\Lambda. \quad (8.47)$$

To complete the calculation we just have to calculate the vector derivative of the vector potential,  $\partial_{V_0^i} U_k^V$ , needed in Eq. (8.38). At this point in the calculation of the stationary conditions for the vector fields, enters the specific functional dependence chosen for the vector potential,  $U_k^V$ . In this work we opted for the usual quadratic dependence in the vector fields, see Eq. (8.22). One can calculate this term to be:

$$\frac{\partial U_k^V}{\partial V_0^i} \Big|_{V_0^i = \tilde{V}_{0,k}^i} = -m_{V_0^i}^2 \tilde{V}_{0,k}^i. \quad (8.48)$$

From Eq. (8.38), the stationary equation for the vector fields can finally be written as:

$$\tilde{V}_{0,k}^i(T, \mu; \sigma, \tilde{V}_{0,k}^i) = -\frac{N_c}{3\pi^2} \frac{1}{m_{V_0^i}^2} \sum_{l=0,1} \sum_{\eta=\pm 1} I_{k,\eta l}(T, \mu; \sigma, \tilde{V}_{0,k}^i) \frac{\partial \tilde{\mu}_l}{\partial V_0^i} \Big|_{V_0^i = \tilde{V}_{0,k}^i} + C^i(T, \mu; \sigma, \tilde{V}_{0,k}^i). \quad (8.49)$$

We can also calculate explicitly the term,  $C^i(T, \mu; \sigma, \tilde{V}_{0,k}^i)$ , by setting  $k = \Lambda$ . From Eq. (8.47) it can be seen that the integral contribution vanishes and this term is given by:

$$C^i(T, \mu; \sigma) = \tilde{V}_{0,\Lambda}^i(T, \mu; \sigma). \quad (8.50)$$

That is the values for the vector fields as a function of temperature, chemical potential and the  $\sigma$  field, in the ultraviolet scale,  $k = \Lambda$ .

Using the general expression in Eq. (8.49) and Eq. (8.29) for the effective chemical potential, we are able to derive the stationary field equations for both the  $\tilde{\omega}_{0,k}$  and  $\tilde{\rho}_{0,k}$  vector fields:

$$g_\omega \tilde{\omega}_{0,k}(T, \mu; \sigma, \tilde{\omega}_{0,k}, \tilde{\rho}_{0,k}^3) = g_\omega \tilde{\omega}_{0,\Lambda} + \frac{4N_c}{12\pi^2} \left( \frac{g_\omega}{m_\omega} \right)^2 \sum_{\substack{l=0,1 \\ \eta=\pm 1}} I_{k,\eta l}(T, \mu; \sigma, \tilde{\omega}_{0,k}, \tilde{\rho}_{0,k}^3), \quad (8.51)$$

$$g_\rho \tilde{\rho}_{0,k}^3(T, \mu; \sigma, \tilde{\omega}_{0,k}, \tilde{\rho}_{0,k}^3) = g_\rho \tilde{\rho}_{0,\Lambda}^3 + \frac{4N_c}{12\pi^2} \left( \frac{g_\rho}{m_\rho} \right)^2 \sum_{\substack{l=0,1 \\ \eta=\pm 1}} (-1)^l I_{k,\eta l}(T, \mu; \sigma, \tilde{\omega}_{0,k}, \tilde{\rho}_{0,k}^3). \quad (8.52)$$

Since the equations depend only on the product  $g_\omega \tilde{\omega}_{0,k} = \tilde{\omega}_k$  and  $g_\rho \tilde{\rho}_{0,k}^3 = \tilde{\rho}_k$ , we take this combined quantity as variables. Likewise, the equations depend only on the combination  $\frac{g_\omega}{m_\omega} = G_\omega$  and  $\frac{g_\rho}{m_\rho} = G_\rho$ , we take these ratios as parameters.

### The entropy flow equation

We are also interested in studying the entropy of the system including quantum fluctuations in order to understand what happens to the low temperature behaviour of this quantity. Hence, a flow equation for the entropy must be derived. The scale dependent entropy density, can be obtained using Eq. (8.23) and the definition of entropy density given in Eq. (A.16). It is written as:

$$\begin{aligned} s_k(T, \mu; \sigma, \tilde{V}_{0,k}^i) &= -\frac{\partial}{\partial T} U_k(T, \mu; \sigma, \tilde{V}_{0,k}^i) \\ &= s_k^X(T, \mu; \sigma, \tilde{V}_{0,k}^i) + s_k^V(T, \mu; \sigma, \tilde{V}_{0,k}^i). \end{aligned} \quad (8.53)$$

Where we have defined,

$$s_k^X(T, \mu; \sigma, \tilde{V}_{0,k}^i) = -\frac{\partial}{\partial T} U_k^X(T, \mu; \sigma, \tilde{V}_{0,k}^i), \quad (8.54)$$

$$s_k^V(T, \mu; \sigma, \tilde{V}_{0,k}^i) = -\frac{\partial}{\partial T} U_k^V(T, \mu; \sigma, \tilde{V}_{0,k}^i). \quad (8.55)$$

Calculating the scale derivative of both sides, and commuting the scale derivative with the temperature derivative, one can write the entropy flow equation as:

$$\partial_t s_k(T, \mu; \sigma, \tilde{V}_{0,k}^i) = -\frac{\partial}{\partial T} \partial_t U_k(T, \mu; \sigma, \tilde{V}_{0,k}^i). \quad (8.56)$$

Using Eq. (8.27), we can write:

$$\partial_t s_k(T, \mu; \sigma, \tilde{V}_{0,k}^i) = -\frac{\partial}{\partial T} \partial_t U_k^X(T, \mu; \sigma, \tilde{V}_{0,k}^i) = \partial_t s_k^X(T, \mu; \sigma, \tilde{V}_{0,k}^i). \quad (8.57)$$

Finally, using Eq. (8.28), the flow equation for the entropy density,  $s_k^X$ , can be written as follows:

$$\partial_t s_k^X(T, \mu; \sigma, \tilde{V}_{0,k}^i) = -\frac{\partial}{\partial T} f_k^U(T, \mu; \sigma, \tilde{V}_{0,k}^i). \quad (8.58)$$

Where  $f_k^U(T, \mu; \sigma, \tilde{V}_{0,k}^i)$  is given by the right-hand side of Eq. (8.28) and its temperature derivative can be calculated as:

$$\begin{aligned} \frac{\partial f_k^U}{\partial T} &= \frac{k^5}{12\pi^2} \left\{ \frac{\partial}{\partial T} \left( \frac{1}{E_\sigma} [1 + 2n_B(E_\sigma)] \right) + \frac{\partial}{\partial T} \left( \frac{3}{E_\pi} [1 + 2n_B(E_\pi)] \right) \right. \\ &\quad \left. + \frac{4N_c}{E_\psi} \sum_{l=0,1} \sum_{\eta=\pm 1} \frac{\partial}{\partial T} n_F(E_\psi - \eta \tilde{\mu}_{k,l}) \right\}. \end{aligned} \quad (8.59)$$

The contribution coming from the meson fields is (using some results from Appendix J):

$$\begin{aligned} \frac{\partial}{\partial T} \left( \frac{1}{E_M} [1 + 2n_B(E_M)] \right) &= \frac{\partial E_M}{\partial T} \frac{\partial}{\partial E_M} \left( \frac{1}{E_M} [1 + 2n_B(E_M)] \right) + \frac{1}{E_M} \frac{\partial}{\partial T} [1 + 2n_B(E_M)] \\ &= -[1 + 2n_B(E_M)] \frac{1}{2E_M^3} \frac{\partial m_M^2}{\partial T} \\ &\quad + 2n_B(E_M) [1 + n_B(E_M)] \left( \frac{1}{T^2} - \frac{1}{2TE_M^2} \frac{\partial m_M^2}{\partial T} \right). \end{aligned} \quad (8.60)$$

The remaining temperature derivatives depend differently on each field,  $M = \{\sigma, \pi\}$ . The squared meson mass derivatives are given by:

$$\frac{\partial m_\sigma^2}{\partial T} = \frac{\partial}{\partial T} \partial_\sigma^2 U_k^\chi = -\partial_\sigma^2 s_k^\chi, \quad (8.61)$$

$$\frac{\partial m_\pi^2}{\partial T} = \frac{\partial}{\partial T} \frac{\partial_\sigma U_k^\chi}{\sigma} = -\frac{1}{\sigma} \partial_\sigma s_k^\chi. \quad (8.62)$$

In the above we used the definition of the entropy density (see Eq. (A.16)).

For the contribution coming from the quark fields, we must take into account that the effective chemical potential depends on temperature because of the vector fields, see Eqs. (8.51) and (8.52). Such contribution can be written as (using some results from Appendix J):

$$\begin{aligned} \frac{\partial}{\partial T} n_F(E_\psi - \eta \tilde{\mu}_{k,l}) &= \frac{\partial}{\partial T} n_F(E) + \frac{\partial(E_\psi - \eta \tilde{\mu}_{k,l})}{\partial T} \frac{\partial}{\partial E} n_F(E) \Big|_{E=E_\psi - \eta \tilde{\mu}_{k,l}} \\ &= \frac{n_F(E_\psi - \eta \tilde{\mu}_{k,l})}{T^2} [1 - n_F(E_\psi - \eta \tilde{\mu}_{k,l})] [E_\psi - \eta \tilde{\mu}_{k,l} + \eta T \partial_T \tilde{\mu}_{k,l}(T)]. \end{aligned} \quad (8.63)$$

If considering non-zero vector interactions, there is an extra contribution coming from the temperature dependence of the vector fields, at each momentum shell,  $\partial v_{k,l}/\partial T$ . At first sight, this seems to implicate that we need to have another set of self-consistent equations, now for the temperature derivative of the vector fields,  $\partial \tilde{\omega}_k/\partial T$  and  $\partial \tilde{\rho}_k/\partial T$ . However, the derivative is a linear operator which means that, when we apply the derivative operator to Eqs. (8.51) and (8.52), it will generate a set of coupled linear equations for these derivatives. Such equations can be solved to yield the value of  $\partial \tilde{\omega}_k/\partial T$  and  $\partial \tilde{\rho}_k/\partial T$ , given the value of the vector fields,  $\tilde{\omega}_k$  and  $\tilde{\rho}_k$ . For the detailed calculation of  $\partial v_{k,l}/\partial T$  quantity, see Appendix L.1.

Putting everything together, the following dimensionful flow equation for the chiral contribution to the average entropy density,  $s_k^\chi$ , can be written:

$$\partial_t s_k^\chi(T, \mu; \sigma, \tilde{\omega}_{0,k}, \tilde{\rho}_{0,k}^3) = -\frac{k^5}{12\pi^2} \sum_{i=\sigma, \pi, \psi} S_k^{(i)}(T, \mu; \sigma, \tilde{\omega}_{0,k}, \tilde{\rho}_{0,k}^3). \quad (8.64)$$

The contributions to the sum are given by (for simplicity, we omit the arguments of the functions):

$$S_k^{(\sigma)} = 2n_B(E_\sigma)[1 + n_B(E_\sigma)] \left( \frac{1}{T^2} + \frac{\partial_\sigma^2 s_k^\chi}{2TE_\sigma^2} \right) + \partial_\sigma^2 s_k^\chi \frac{[1 + 2n_B(E_\sigma)]}{2E_\sigma^3}, \quad (8.65)$$

$$S_k^{(\pi)} = 6n_B(E_\pi)[1 + n_B(E_\pi)] \left( \frac{1}{T^2} + \frac{\partial_\sigma s_k^\chi}{2\sigma TE_\pi^2} \right) + 3\partial_\sigma s_k^\chi \frac{[1 + 2n_B(E_\pi)]}{2\sigma E_\pi^3}, \quad (8.66)$$

$$S_k^{(\psi)} = \frac{4N_c}{E_\psi} \sum_{l=0,1} \sum_{\eta=\pm 1} \frac{n_F(E_\psi - \eta\tilde{\mu}_{k,l})}{T^2} [1 - n_F(E_\psi - \eta\tilde{\mu}_{k,l})] \left[ E_\psi - \eta\tilde{\mu}_{k,l} - \eta T \frac{\partial v_{k,l}}{\partial T} \right]. \quad (8.67)$$

The entropy density in the infrared,  $s_{k=k_{\text{IR}}}$ , containing the contribution coming from vector fields, can be calculated after solving the system of flow equations through:

$$s_{k=k_{\text{IR}}} (T, \mu; \sigma, \tilde{\omega}_0, \tilde{\rho}_0^3) = s_{k=k_{\text{IR}}}^\chi (T, \mu; \sigma, \tilde{\omega}_0, \tilde{\rho}_0^3) - \frac{\partial}{\partial T} U_{k=k_{\text{IR}}}^V (T, \mu; \sigma, \tilde{\omega}_0, \tilde{\rho}_0^3). \quad (8.68)$$

The contribution coming from the vector fields can be calculated using the stationary conditions for the vector fields given by Eqs. (8.51) and (8.52).

### The quark density flow equation

The calculation of the flow equation for the  $j$ -quark density is completely analogous to the calculation of the entropy density performed in the previous section. The scale dependent  $j$ -quark density,  $n_k^j$ , can be defined using Eq. (A.15):

$$\begin{aligned} n_k^j(T, \mu; \sigma, \tilde{V}_{0,k}^i) &= -\frac{\partial}{\partial \mu_j} U_k(T, \mu; \sigma, \tilde{V}_{0,k}^i) \\ &= n_k^{j,\chi}(T, \mu; \sigma, \tilde{V}_{0,k}^i) + n_k^{j,V}(T, \mu; \sigma, \tilde{V}_{0,k}^i). \end{aligned} \quad (8.69)$$

Here:

$$n_k^{j,\chi}(T, \mu; \sigma, \tilde{V}_{0,k}^i) = -\frac{\partial}{\partial \mu_j} U_k^\chi(T, \mu; \sigma, \tilde{V}_{0,k}^i), \quad (8.70)$$

$$n_k^{j,V}(T, \mu; \sigma, \tilde{V}_{0,k}^i) = -\frac{\partial}{\partial \mu_j} U_k^V(T, \mu; \sigma, \tilde{V}_{0,k}^i). \quad (8.71)$$

Calculating the scale derivative of both sides, and commuting the scale derivative with the chemical potential derivative, we can get the flow equation for the  $j$ -quark density:

$$\partial_t n_k^j(T, \mu; \sigma, \tilde{V}_{0,k}^i) = -\frac{\partial}{\partial \mu_j} \partial_t U_k(T, \mu; \sigma, \tilde{V}_{0,k}^i). \quad (8.72)$$

Using Eq. (8.27) yields:

$$\partial_t n_k^j(T, \mu; \sigma, \tilde{V}_{0,k}^i) = -\frac{\partial}{\partial \mu_j} \partial_t U_k^\chi(T, \mu; \sigma, \tilde{V}_{0,k}^i) = \partial_t n_k^{j,\chi}(T, \mu; \sigma, \tilde{V}_{0,k}^i). \quad (8.73)$$

Using the flow equation given in Eq. (8.28) we can write:

$$\partial_t n_k^{j,\chi}(T, \mu; \sigma, \tilde{V}_{0,k}^i) = -\frac{\partial}{\partial \mu_j} f_k^U(T, \mu; \sigma, \tilde{V}_{0,k}^i). \quad (8.74)$$

Where  $f_k^U(T, \mu; \sigma, \tilde{V}_{0,k}^i)$  is given by the right-hand side of Equation (8.28). We just have to calculate:

$$\begin{aligned} \frac{\partial f_k^U}{\partial \mu_j} = \frac{k^5}{12\pi^2} \left\{ \frac{\partial}{\partial \mu_j} \left( \frac{1}{E_\sigma} [1 + 2n_B(E_\sigma)] \right) + \frac{\partial}{\partial \mu_j} \left( \frac{3}{E_\pi} [1 + 2n_B(E_\pi)] \right) \right. \\ \left. + \frac{4N_c}{E_\psi} \sum_{l=0,1} \sum_{\eta=\pm 1} \frac{\partial}{\partial \mu_j} n_F(E_\psi - \eta \tilde{\mu}_{k,l}) \right\}. \quad (8.75) \end{aligned}$$

Consider first the contribution coming from the meson sector. Since the meson dispersion relations  $E_\sigma$  and  $E_\pi$  have mass terms which depend on derivatives of the effective action, there is a chemical potential dependence coming from these contributions. To calculate such contribution one can make use of the following result (using some results from Appendix J):

$$\begin{aligned} \frac{\partial}{\partial \mu_j} \left( \frac{1}{E_M} [1 + 2n_B(E_M)] \right) &= \frac{\partial E_M}{\partial \mu_j} \frac{\partial}{\partial E_M} \left( \frac{1}{E_M} [1 + 2n_B(E_M)] \right) \\ &= -\frac{1}{2E_M^2} \left( \frac{1}{E_M} [1 + 2n_B(E_M)] + \frac{2n_B(E_M)}{T} [1 + n_B(E_M)] \right) \frac{\partial m_M^2}{\partial \mu_j}. \end{aligned} \quad (8.76)$$

The remaining chemical potential derivatives depend differently on each field,  $M = \{\sigma, \pi\}$ . The squared meson mass derivatives are given by:

$$\frac{\partial m_\sigma^2}{\partial \mu_j} = \frac{\partial}{\partial \mu_j} \partial_\sigma^2 U_k = -\partial_\sigma^2 n_k^j, \quad (8.77)$$

$$\frac{\partial m_\pi^2}{\partial \mu_j} = \frac{\partial}{\partial \mu_j} \frac{\partial_\sigma U_k}{\sigma} = -\frac{1}{\sigma} \partial_\sigma n_k^j. \quad (8.78)$$

In the above we used the definition of the  $j$ -quark density (see Eq. (A.15)).

The contribution coming from the quark sector is simpler and can be calculated to yield (using some results from Appendix J):

$$\frac{\partial}{\partial \mu_j} n_F(E_\psi - \eta \tilde{\mu}_{k,l}) = \frac{\eta}{T} n_F(E_\psi - \eta \tilde{\mu}_{k,l}) [1 - n_F(E_\psi - \eta \tilde{\mu}_{k,l})] \left( \delta_{lj} - \frac{\partial v_{k,l}(\mu)}{\partial \mu_j} \right). \quad (8.79)$$

Similar to the case of the entropy density, the existence of vector degrees of freedom generates an additional contribution to the quark density in the term,  $\partial v_{k,l}/\partial \mu_j$ . This term can be calculated in exactly the same way as  $\partial v_{k,l}/\partial T$ . The calculation can be found in Appendix L.2.

Putting everything together we can explicitly write the flow equation for the  $j$ -quark density,

$$\partial_t n_k^j(T, \mu; \sigma, \tilde{\omega}_{0,k}, \tilde{\rho}_{0,k}^3) = -\frac{k^5}{12\pi^2} \sum_{i=\sigma,\pi,\psi} N_k^{(i)}(T, \mu; \sigma, \tilde{\omega}_{0,k}, \tilde{\rho}_{0,k}^3), \quad (8.80)$$

where the contributions to the sum are given by (for simplicity, we omit the arguments of the functions):

$$N_k^{(\sigma)} = \frac{\partial_\sigma^2 n_k^j}{2E_\sigma^2} \left( \frac{1}{E_\sigma} [1 + 2n_B(E_\sigma)] + \frac{2n_B(E_\sigma)}{T} [1 + n_B(E_\sigma)] \right), \quad (8.81)$$

$$N_k^{(\pi)} = \frac{3\partial_\sigma n_k^j}{2\sigma E_\pi^2} \left( \frac{1}{E_\pi} [1 + 2n_B(E_\pi)] + \frac{2n_B(E_\pi)}{T} [1 + n_B(E_\pi)] \right), \quad (8.82)$$

$$N_k^{(\psi)} = \frac{4N_c}{E_\psi} \sum_{l=0,1} \sum_{\eta=\pm 1} \frac{\eta}{T} n_F(E_\psi - \eta \tilde{\mu}_{k,l}) [1 - n_F(E_\psi - \eta \tilde{\mu}_{k,l})] \left( \delta_{lj} - \frac{\partial v_{k,l}}{\partial \mu_j} \right). \quad (8.83)$$

The  $j$ -quark density in the infrared,  $n_{k=k_{\text{IR}}}^j$ , containing the contribution coming from vector fields, can be calculated after solving the system of flow equations through:

$$n_{k=k_{\text{IR}}}^j(T, \mu; \sigma, \tilde{\omega}_0, \tilde{\rho}_0^3) = n_{k=k_{\text{IR}}}^{j,\chi}(T, \mu; \sigma, \tilde{\omega}_0, \tilde{\rho}_0^3) - \frac{\partial}{\partial \mu_j} U_{k=k_{\text{IR}}}^V(T, \mu; \sigma, \tilde{\omega}_0, \tilde{\rho}_0^3). \quad (8.84)$$

The contribution coming from the vector fields can be calculated using the stationary conditions for the vector fields given by Eqs. (8.51) and (8.52).

### Solving the flow equations

The system of coupled, partial differential equations, for the effective average action and average entropy, given in Eqs. (8.28) and (8.64) alongside the self-consistent equations for the vector fields, (8.51) and (8.52), must be solved numerically. One way to do so, is to use a Taylor expansion around the scale-dependent minimum of the effective potential  $U_k$ . This method however, is not well suited to study the low temperature and high density regime of the phase diagram, where for certain parametrizations, a first-order chiral phase transition is expected and two minima co-exist. In the present work we use the grid method, a much more powerful technique that provides full access to the effective potential, in a given range of the  $\sigma$  field. This allows the study of the phase diagram around a first-order phase transition. In this numerical approach, the field variable  $\sigma$  is discretized in an one-dimensional grid, and the first and second derivatives of the effective potential with respect to  $\sigma$  are calculated using finite differences. The details about this numerical approach are given in Appendix (K).

The value of the vector fields,  $\tilde{\omega}_{0,k}$  and  $\tilde{\rho}_{0,k}^3$ , are calculated using Eqs. (8.51) and (8.52) at each momentum shell  $k$ . In practice, by following this approach, the flow of the effective potential and the entropy density are automatically in the minimum with respect to the vector fields.

In the MF calculation, the self-consistent equation for the  $\tilde{\omega}_0$  field is directly related to the sum of the quark densities while the one for the  $\tilde{\rho}_0^3$  field is related to the difference of the quark densities. This means that the  $\tilde{\rho}_{0,k}^3$  field is zero for symmetric matter ( $\tilde{\rho}_{0,k}^3 = 0$ ), i.e. if considering  $\mu_u = \mu_d$ .

The FRG calculation leads to a similar scenario. Indeed, in [324] it was shown that neglecting the boson quantum fluctuations, the MF results can be recovered. However, the choice of non-zero ultraviolet value of the  $\tilde{\rho}_0^3$  vector field,  $\tilde{\rho}_{0,\Lambda}^3$ , would lead to an explicit isospin breaking interaction and to a non-zero  $\tilde{\rho}_0^3$  field, even for symmetric matter. Indeed, in [330], non-zero values for  $\tilde{\omega}_{0,\Lambda}$  were considered and their effect on the phase diagram was studied. However there is no reason to consider an ultraviolet potential with explicit isospin breaking by the  $\tilde{\rho}_0^3$  field. Hence, in the present work, we will take  $\tilde{\rho}_{0,\Lambda}^3 = 0$ .

In order to study the effect of the  $\tilde{\rho}_0^3$  field on the phase diagram and the unphysical negative entropy density region, an asymmetry between the quark flavours has to be considered. Following [45], we allow for different chemical potentials for each quark flavour,

$$\mu_u = \mu + \delta\mu, \quad (8.85)$$

$$\mu_d = \mu - \delta\mu. \quad (8.86)$$

In principle, upon considering a finite  $\delta\mu$ , pion condensation could happen. This means that the effective potential would be dependent on two different quantities,  $\phi^2 = \sigma^2 + \pi_3^2$  and  $\xi^2 = \pi_1^2 + \pi_2^2$ , as suggested in Ref. [331]. In such a scenario, not only the flow equations would be much more complicated but a two dimensional grid would have to be considered since there are two distinct chiral invariants. Following previous works [323, 324], to simplify the calculations, we will neglect the possibility of pion condensation and work only with one chiral invariant. To make this approximation valid, a very small difference between quark chemical potentials of  $\delta\mu = -30$  MeV will be considered [45]. For such a value of  $\delta\mu$ , we will be describing matter with more down quarks than up quarks, a very important scenario to study neutron stars, for example.

### 8.3 Results

In this section we present the phase diagram of the two flavour Quark-Meson model, calculated by solving the flow Eq. (8.28), for different values of temperature and chemical potential. Different vector couplings are considered in order to study their effect on the phase diagram. We also present, for the same scenarios, the results of solving the flow equation for the entropy, given in Eq. (8.64). From this calculation we are able to study the behaviour of the entropy density near the critical region with and without vector interactions where an unphysical region, of negative entropy density, is expected from previous calculations [191]. We also test the thermodynamical consistency by checking if the numerical temperature derivative of the effective potential agrees with the result coming from solving the flow equation for the entropy density (Eq. (8.64)).

Regarding the numerical calculation, solving the system of coupled flow equations in a grid is very computationally demanding. In fact, the computational time is not only dictated by the grid size and the infrared cutoff,  $k_{\text{IR}}$  but, in the case of finite vector couplings, of consistently solving Eqs. (8.51) and (8.52) for each grid point at every momentum shell (see the Appendix K).

$\Lambda$ [MeV]	$m_\Lambda/\Lambda$	$\lambda_\Lambda$	$c/\Lambda^3$	$h$
1000	0.969	0.001	0.00175	4.2

TABLE 8.1: Used parameter set [191]. It yields in the vacuum, for  $k_{\text{IR}} = 80$  MeV, the following observables:  $f_\pi = 92.4$  MeV,  $m_\pi = 137.6$  MeV,  $m_\sigma = 606.7$  MeV and  $m_q = 388.2$  MeV. From the Goldberger–Treiman relation (see Eqs. (2.14) and (2.15)) and the definition of the quark mass in this model (see Eq. (8.35)), the vacuum expectation value of the  $\sigma$  field,  $\langle\sigma\rangle$ , and the pion decay constant,  $f_\pi$ , are related:  $\langle\sigma\rangle = f_\pi$  [33, 180].

In order to make the numerical computations more efficient within the scope of the present work, we decided to use a higher infrared cutoff of  $k_{\text{IR}} = 80$  MeV then the one used in [191] of  $k_{\text{IR}} = 40$  MeV. We verified, by solving the flow equations for different values of  $k_{\text{IR}}$ , that this change does not influence the results qualitatively, allowing the study of the qualitative effect of different vector interactions in the phase diagram and in the unphysical negative density entropy region, using less computing resources. Using a finite value for the infrared cutoff ( $k_{\text{IR}}$ ) physically means neglecting, in the numerical calculation, low momentum modes of the meson fields at the level of the path integral.

Different grid sizes were also studied and, after some analysis, we decided to use a 80-point grid size in  $\sigma \in [2, 122]$  MeV. As for the infrared cutoff, using a thinner grid does not change the qualitative behaviour of the results and since the same grid is used for every scenario, considering a given grid size represents a systematic uncertainty.

The system of flow equations can then be solved from the UV scale,  $k = \Lambda$ , down to the infrared scale,  $k = k_{\text{IR}}$ , to yield  $U_{k=k_{\text{IR}}}$  and  $s_{k=k_{\text{IR}}}$ , the effective potential and entropy density in the infrared. In order to solve this system of coupled partial differential equations, a set of initial conditions has to be provided. In the case of Eqs. (8.28) and (8.64), these correspond to the effective action and entropy density in the  $k = \Lambda$  momentum shell. The effective potential in the UV,  $U_{k=\Lambda}$ , is chosen in such a way that it respects the symmetries of the system and to yield, in the infrared limit, the experimental values for the pion mass and its decay constant. In this work we use the usual potential:

$$U_{k=\Lambda}(T, \mu; \sigma) = \frac{1}{2}m_\Lambda^2\sigma^2 + \frac{1}{4}\lambda_\Lambda\sigma^4, \quad (8.87)$$

with the parameters given in Table 8.1. An explicitly chiral symmetry breaking term  $-c\sigma$  (see E. (8.4)), is added to the effective potential after the flow is calculated i.e., it is added to the effective potential in the IR,  $U_{k=k_{\text{IR}}}$ :

$$U_{k=k_{\text{IR}}}(T, \mu; \sigma) \rightarrow U_{k=k_{\text{IR}}}(T, \mu; \sigma) - c\sigma. \quad (8.88)$$

If this symmetry breaking term is neglected, the pion would be massless in the IR. This term is not considered as an initial condition in the UV since we assume that, at high energies, the UV potential is symmetry preserving.

The vector fields in the UV,  $\tilde{\omega}_{0,\Lambda}$  and  $\tilde{\rho}_{0,\Lambda}^3$ , in this work, were chosen to be zero,

$$g_\omega \tilde{\omega}_{0,\Lambda}(T, \mu; \sigma) = 0, \quad (8.89)$$

$$g_\rho \tilde{\rho}_{0,\Lambda}^3(T, \mu; \sigma) = 0. \quad (8.90)$$

This choice of UV conditions for the vector fields implies that, in the UV, the MF values of the vector fields,  $\tilde{\omega}_{0,\Lambda}$  and  $\tilde{\rho}_{0,\Lambda}^3$ , are constant, independent from the  $\sigma$  field. More, they are considered to be zero. Since the UV potential is chemical potential independent (see Eq. 8.87), one can argue that, in the UV scale, particle density is zero (in the sense of particle density being the chemical potential derivative of the pressure, see Eq. (A.15)). These vector fields are known to couple to density degrees of freedom. Since particle density in the UV is zero, it is natural to set the vector fields to be zero in the UV and allow for the generation of non vanishing values of  $\tilde{\omega}_{0,\Lambda}$  and  $\tilde{\rho}_{0,\Lambda}^3$  during the flow. In Ref. [330], the effect of a  $\sigma$  dependence for the  $\tilde{\omega}_{0,\Lambda}$  vector field was studied, which ended up not changing the phase structure significantly. In such study however, the chiral limit was considered.

We will consider the vector coupling constants,  $G_\omega = g_\omega/m_\omega$  and  $G_\rho = g_\rho/m_\rho$  as free parameters and study the influence of different values on the structure of the phase diagram. In [324], these parameters were considered as bounded by  $G_\omega = G_\rho = 0.001 - 0.01 \text{ MeV}^{-1}$ . These bounds were obtained using vacuum properties, by considering the vector fields as massive,  $m_\omega, m_\rho \sim 1 \text{ GeV}$  and  $g_\omega = g_\rho = 1 - 10$  [324]. However these parameters might be density dependent and in-medium modifications could change their magnitudes.

Due to the fact that there is no temperature dependence in the UV potential, the UV entropy density,  $s_{k=\Lambda}$ , is simply given by:

$$s_{k=\Lambda}(T, \mu; \sigma) = 0. \quad (8.91)$$

Since the UV scale is fixed at a finite value, there is no reason why the effective potential in the UV, should be temperature and chemical potential independent [321]. Indeed, in [332], only the purely thermal flow equation was solved, effectively generating a temperature and chemical dependent UV potential.

In Fig. 8.1, we show the result of solving the flow equation for the effective potential (Eq. (8.28)) in the vacuum i.e., with  $T = \mu = 0$ . For this particular calculation we enlarged the grid size to  $\sigma \in [1, 131] \text{ MeV}$  with 130-points<sup>10</sup>. Each panel in this figure represents the normalized effective potential,  $u_k(\sigma)$ , at a particular point in the trajectory of the flow equation, as a function of the  $\sigma$  field. For simplicity, we normalized the field as  $\sigma/f_\pi$  (with  $f_\pi = 92.4 \text{ MeV}$ ) and, to fix the value of the effective potential at zero as  $u_k(\sigma = 0) = 0$  during the flow, we choose to normalize the potential as,

$$u_k(\sigma) = \frac{U_k(\sigma) - U_k(\sigma_{\min})}{U_k(\sigma_{\max}) - U_k(\sigma_{\min})}. \quad (8.92)$$

<sup>10</sup>This change in grid size did not affect the vacuum observables that were presented in the caption of Table 8.1.

The first panel of Fig. 8.1, is simply the effective potential in the UV, i.e., the initial condition given in Eq. (8.87). Solving Eq. (8.28) until the IR is reached ( $k_{\text{IR}} = 80$  MeV) provides the evolution displayed in Fig. 8.1. We highlight that the plotted effective potential does not include the explicit chiral symmetry breaking term  $-\sigma$ , that must be included in the potential to make the pion massive, see Eq. (8.4). For this reason, the minimum of the potential in the IR, which corresponds to the last panel of Fig. 8.1, with  $k_{\text{IR}} = 80$  MeV, is not located at  $\sigma/f_\pi = 1$ , but it is slightly shifted. We opted to present the potential without the explicit chiral symmetry breaking term only for simplicity, if included, the minimum of the IR potential, in the vacuum, is located exactly at  $\sigma/f_\pi = 1$ . We also would like to comment that the minimum starts to move at around  $k \sim 630$  MeV, and below  $k \sim 100$  MeV, its position almost does not change (see Fig. 8.1). There is an analogous flow evolution for the effective potential for different values of temperature and chemical potential. In fact, for certain values of temperature and chemical potential, a first-order phase transition is expected, implying the existence of two minima. The effective entropy density, the effective quark density and the vector fields also have similar trajectories, starting in some initial condition and ending in the IR. To build the thermodynamics and the phase diagram one has to solve the flow equations for different values of temperature and chemical potential, yielding several evolutions like the one displayed in Fig. 8.1.

As previously mentioned, in the presence of a first-order chiral phase transition, the effective potential has two minima. The phase transition in this case will be defined through the Maxwell construction: when the effective potential has several minima, the one with lowest energy represents the stable phase. In Fig. 8.2, we present such a construction at  $T = 20$  MeV for the QM model using the FRG method. The dot is the chiral transition chemical potential while the squares are the chemical potentials of spinodal points.

In this first stage, the QM model without vector interactions is considered. In Fig. 8.3 we present the first-order phase transition of the model, the  $s_{k=k_{\text{IR}}} = 0$  line and the CEP. One can see that the region in-between spinodal lines is very narrow, different when compared to MF calculations. Indeed, for  $T = 20$  MeV one can analyse Fig. 8.2 and observe that the overall size of the region in-between spinodal points is less than 1.5 MeV. We also present the line  $s_{k=k_{\text{IR}}} = 0$  which separates the region of positive and negative entropy densities. This result is very similar to the one presented in [191]. However, in [191], a region of negative entropy density is only discussed on the right side of the first-order phase transition. Here, we find such an unphysical region on both sides of the phase transition line. This apparent difference can be of numerical origin. While we solved the flow equation for the entropy density, it can also be calculated as the derivative  $-\partial U_{k=k_{\text{IR}}}/\partial T|_\mu$ , after solving the flow equation for the effective potential.

More, we see that the  $s_{k=k_{\text{IR}}} = 0$  line behaves like an isentropic line that crosses the first-order phase transition: in [73, 75] when an isentropic line crosses the first-order phase transition it enters the critical region, touches each spinodal line once and exits the critical region. The branches entering from outside the spinodal region until touching the phase-transition line correspond to the entropy in the stable minimum of the potential. The two parts of the line between the phase transition line and touching the spinodal lines correspond to the entropy in the respective local minimum,  $\sigma$ , of the effective potential  $U_k = k_{\text{IR}}(\sigma)$ . Finally, the branch between touching both

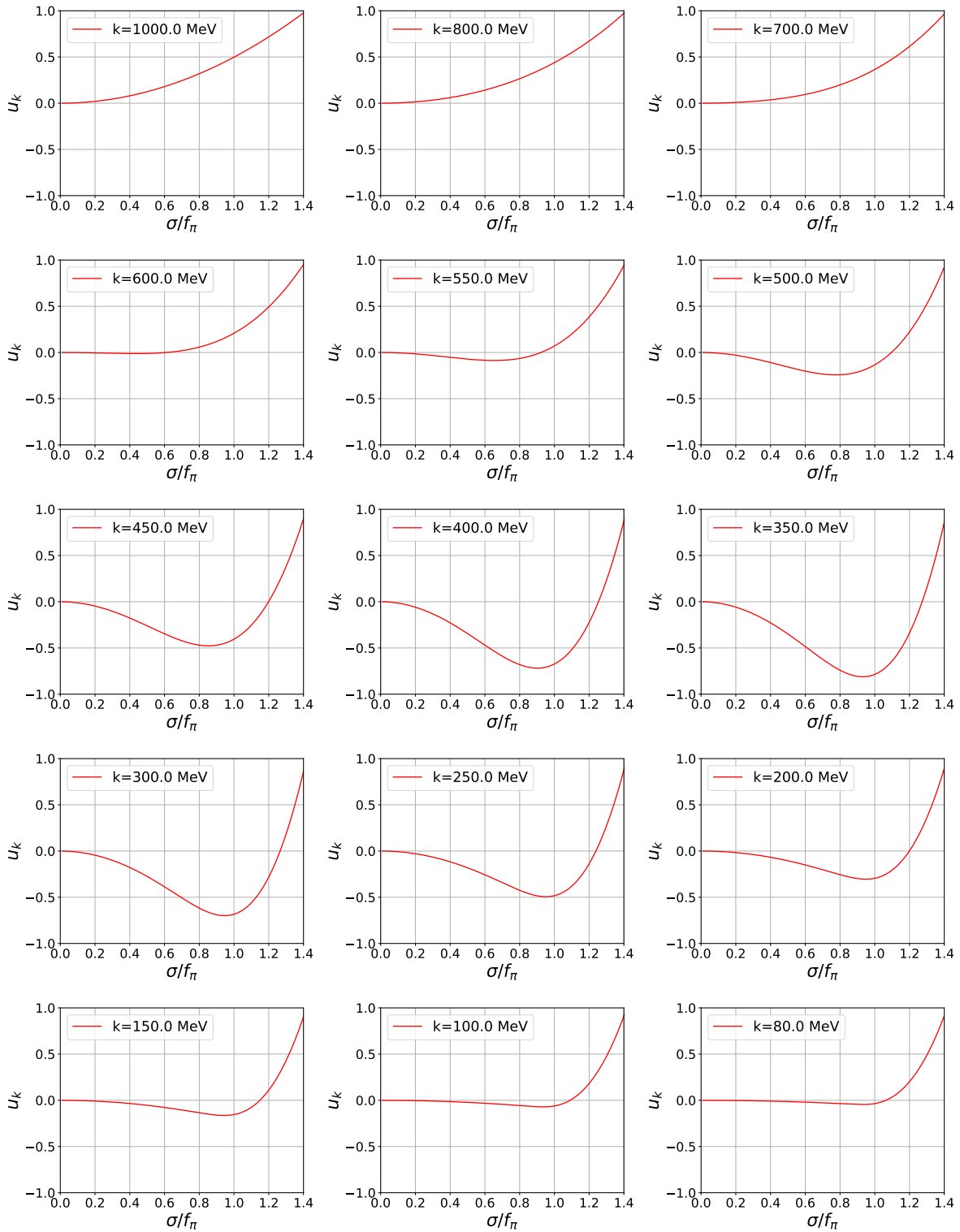


FIGURE 8.1: Evolution of the effective average potential,  $u_k$ , from the UV (with  $k = 1000$  MeV) down to the IR (with  $k_{\text{IR}} = 80$  MeV) as a function of the dimensionless  $\sigma/f_\pi$ . For this specific calculation we used a 130-point grid size in  $\sigma \in [1, 131]$  MeV. The effective potential is normalized as  $u_k(\sigma) = \frac{U_k(\sigma) - U_k(\sigma_{\text{min}})}{U_k(\sigma_{\text{max}}) - U_k(\sigma_{\text{min}})}$  and the  $f_\pi = 92.4$  MeV.

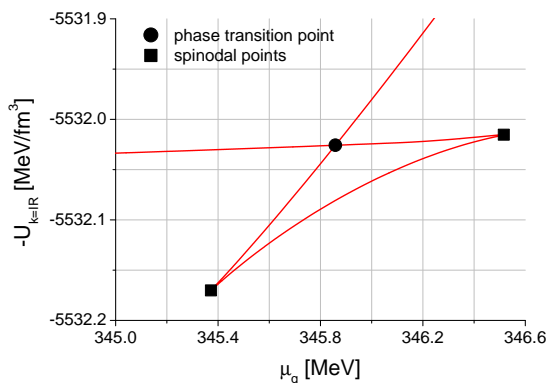


FIGURE 8.2: Extrema of the infrared effective potential as a function of the quark chemical potential for  $T = 20$  MeV. The phase transition point is represented by the dot while the squares are the spinodal points.

spinodal lines follows the solution in the maximum of the potential. Thermodynamically, the zero entropy density line must be located at the zero temperature axis. This leads us to observe that the  $s_{k=k_{\text{IR}}} = 0$  “isentropic line” is displaced from its  $T = 0$  location in this model within the FRG approach.

A possible origin for the displacement of this line and consequently the existence of the negative entropy density region is that finite chemical potential effects are not correctly accounted in the model beyond mean field. Upon considering an UV potential which is independent of the temperature and chemical potential, one is considering that the initial conditions to solve the differential equations are the same for every point in the phase diagram. Such case may not be true and considering temperature and chemical potential dependences in the UV potential are known to modify the thermodynamics and the phase structure [332]. Hence, building a temperature and/or chemical potential UV effective potential could provide more insights on the origin of the negative entropy density region. Such a study is beyond the scope of the present work and is left as future work.

The next step in our study is to consider the effect of finite vector interactions. First we just consider the effect of the  $\tilde{\omega}_0$  field, by setting  $G_\rho = 0$ , and increasing  $G_\omega$ . The critical region with increasing  $G_\omega$  can be seen in Fig. 8.4. For increasing vector coupling in the range  $G_\omega = [0.001, 0.004]$  MeV $^{-1}$  (see Fig. 8.4, panels (a), (b), (c), and (d)), there are two main effects regarding the critical region: the CEP is moved to much higher temperatures and smaller chemical potentials and the extension of the region in-between spinodal lines increases. The low temperature first-order phase transition line is slightly shifted to higher chemical potentials while for higher temperatures the first-order line is dragged along with the CEP to smaller chemical potentials. Further increasing the vector coupling,  $G_\omega = [0.006, 0.015]$  MeV $^{-1}$  (see Fig. 8.3, panels (e), (f), (g), (h), and (i)), a very different behaviour is observed: the CEP is moved towards smaller temperatures and higher chemical potentials while the region in-between spinodal lines gets imperceptibly smaller. The behaviour of the CEP for these values of  $G_\omega$  is very similar to the one found in [330] even though in that study, the chiral limit is used.

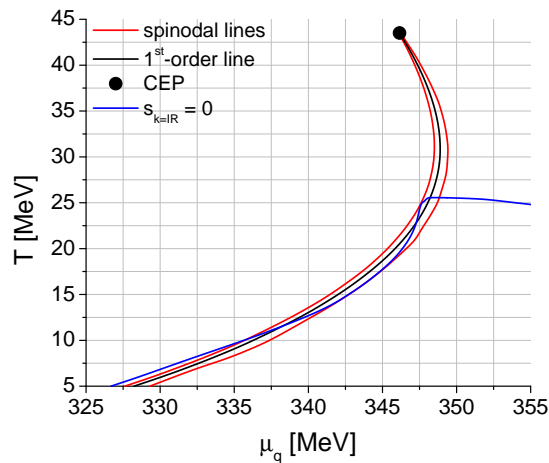


FIGURE 8.3: First-order phase transition of the QM model without vector interactions. The red lines are the spinodals, the black line is the first-order phase transition line and the CEP is the black dot. The blue line corresponds to the  $s_{k=k_{\text{IR}}} = 0$  line and below this line entropy density is negative.

The behaviour of the negative entropy density region and  $s_{k=k_{\text{IR}}} = 0$  line is very interesting: increasing the vector coupling  $G_\omega$  pushes this region to lower values of temperature. In fact, there is a critical value of  $G_\omega$  to which there is no more negative entropy density region on the phase diagram of the model.

As already discussed, we expect that the range of magnitudes that we considered for the vector couplings to be within acceptable and physical ranges. Specially since these couplings may be density dependent. Nonetheless, the vanishing of the negative entropy region for a given vector coupling is not a signal that such a coupling is physical. The critical vector coupling in which we do not observe a negative entropy density region is not unique, since it should be different for another parameter set (different values for  $\Lambda$ ,  $m_\Lambda$ ,  $\lambda_\Lambda$ ,  $c$  and  $h$ ). Also, for numerical reasons, we were only able to solve the flow equations down to a minimum temperature of 5 MeV. Hence, a given critical value of  $G_\omega$  and  $G_\rho$ , where no negative entropy density is found above  $T = 5$  MeV does not guarantee that, for lower temperatures, the negative entropy density region is not present.

From MF studies one expects that the inclusion of repulsive vector interactions would push the CEP towards lower values of temperature, making it disappear for a high enough vector coupling [75]. However, we observe a rather different and complex behaviour when including quantum fluctuations with the FRG. Indeed, the CEP and first-order phase transition do not disappear for the range of considered vector couplings and the previous unphysical negative entropy density region disappears for increasing  $G_\omega$ .

As already stated, in order to study the effect of the  $\vec{\rho}_0^3$  vector field on the first-order phase transition, the two flavour quark system must be on an asymmetric state. As already discussed, we will consider a finite isospin chemical potential of  $\delta\mu = -30$  MeV.

In Fig. 8.5, we show the results of comparing the critical region of the model with  $\delta\mu = 0$  and

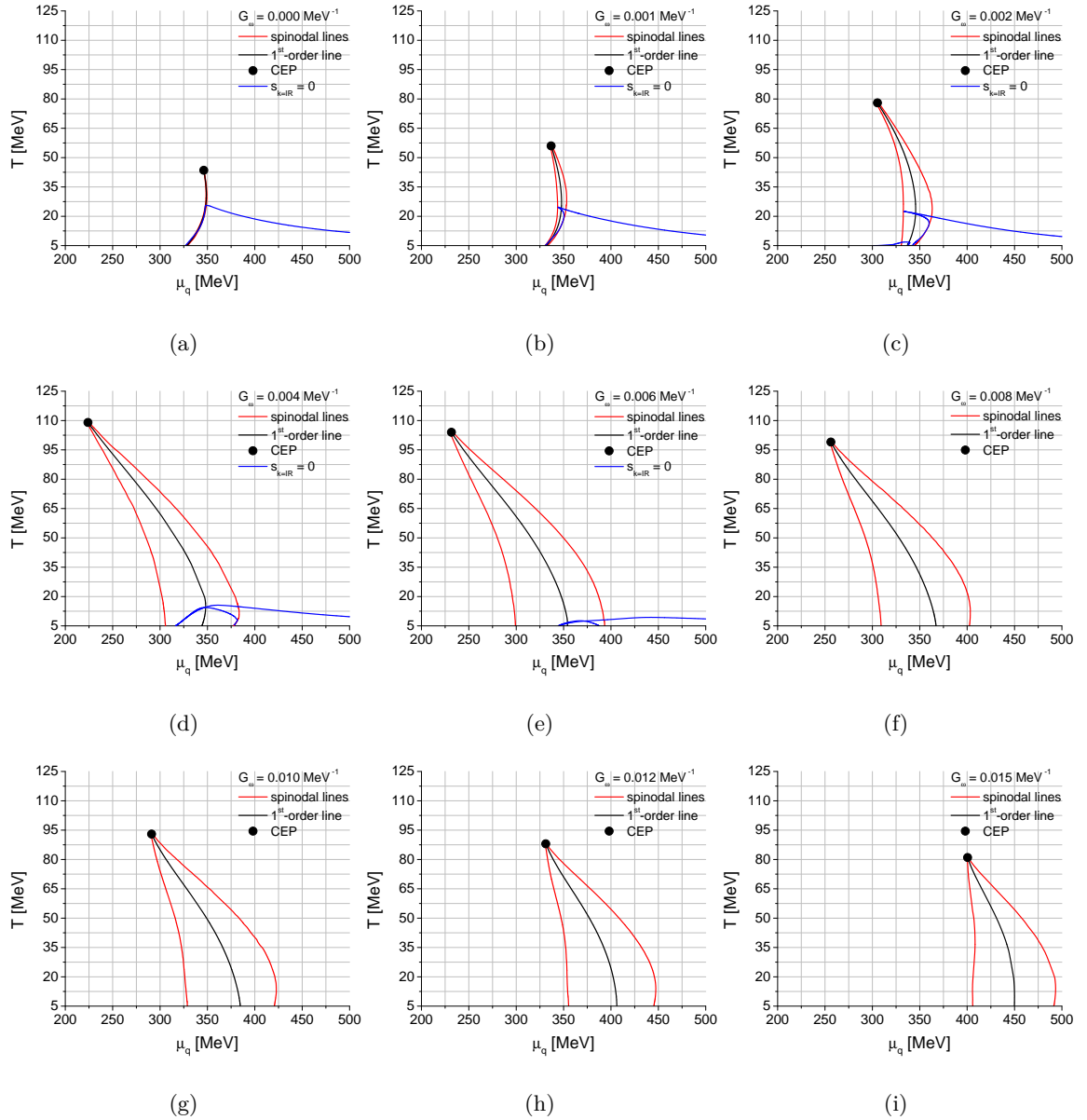


FIGURE 8.4: First-order phase transition of the QM model, for increasing values of  $G_\omega$  and fixed  $G_\rho = 0$ . The red, black and blue lines are the spinodals, first-order phase transition and the  $s_{k=k_{\text{IR}}} = 0$  lines, respectively, for each value of  $G_\omega$ . The CEPs are represented by the black dots. Entropy density is negative below the  $s_{k=k_{\text{IR}}} = 0$  line.

$\delta\mu = -30$  MeV, without vector interactions i.e.,  $G_\omega = G_\rho = 0$ . The effect of considering a finite isospin is the following: the first-order line is shifted to higher chemical potentials (at lower temperatures) and the CEP is marginally moved to lower quark chemical potentials but its temperature remains the same (within our level of numerical accuracy). Since the  $s_{k=k_{\text{IR}}} = 0$  “isentropic line” is connected to the spinodal region, moving the first-order line to higher chemical potentials also moves the unphysical negative entropy density region. The inclusion of a finite  $\delta\mu$  also enlarges the region in-between the spinodal lines.

In order to study the isolated effect of the  $\tilde{\rho}_0^3$  vector field with  $\delta\mu = -30$  MeV, we set  $G_\omega = 0$  and calculate the phase diagram for increasing values of  $G_\rho$ . The results can be seen in Fig.

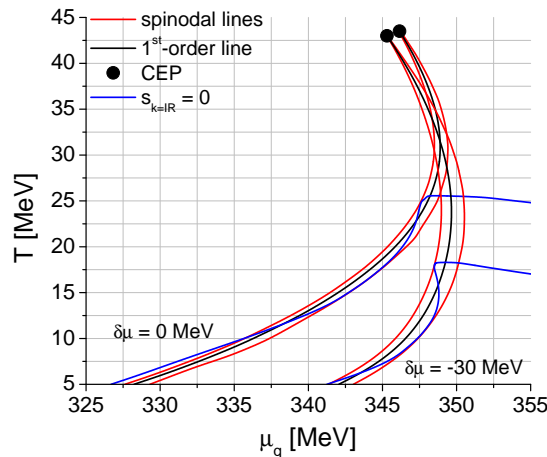


FIGURE 8.5: First-order phase transition of the QM model without vector interactions, for  $\delta\mu = 0$  and  $\delta\mu = -30$  MeV. The red, black and blue lines are the spinodals, first-order phase transitions and the  $s_{k=k_{\text{IR}}} = 0$  lines, respectively. The CEPs are represented by the black dots. Entropy density is negative below the  $s_{k=k_{\text{IR}}} = 0$  line.

8.6. Increasing the coupling  $G_\rho$ , has the opposite behaviour of considering a finite  $\delta\mu$ : it shifts the first-order line to smaller chemical potentials while the CEP is slightly moved to higher chemical potentials and low temperatures. The region in between spinodal lines is also larger with finite  $G_\rho$  when compared to the case without vector interactions, even though the effect is much less noticeable than when considering finite  $G_\omega$ . The first-order phase transition line at low temperatures is very close to its original location with  $\delta\mu = 0$  for  $G_\rho = 0.008 \text{ MeV}^{-1}$ . Thus, increasing this coupling is effectively restoring the isospin symmetry, broken by the finite  $\delta\mu$ . Indeed, in nuclear relativistic mean field models, the  $\tilde{\rho}_0^3$  vector field can be added to the theory as an isospin restoring interaction, mirroring the Bethe–Weizsäcker mass formula and the valley of beta stability in nuclear physics [93].

Finally, in Fig. 8.7 we consider  $G_\omega = G_\rho = 0.008 \text{ MeV}^{-1}$ , with  $\delta\mu = -30 \text{ MeV}$ . In this scenario we are taking into account the combined effects of the  $\tilde{\omega}_0$  and  $\tilde{\rho}_0^3$  vector fields. The obtained phase diagram is similar to the one obtained in the Fig. 8.4 panel (f), with  $G_\omega = 0.008 \text{ MeV}^{-1}$  and  $\delta\mu = 0$ . The only difference is on the location of the first-order line which is negligibly dislocated to smaller chemical potentials. Taking the previous results into account, this behaviour is expected: the  $\tilde{\rho}_0^3$  field is restoring the isospin symmetry while the influence of the  $\tilde{\omega}_0$  field is identical to the one observed in the isospin symmetric case.

## 8.4 Conclusions and outlook

We have calculated the critical region near the first-order phase transition of the two flavour QM model with vector interactions, within the FRG approach to include quantum fluctuations. Besides the first-order chiral transition and the CEP, the spinodal lines were presented. The unphysical region of negative entropy density reported by [191] was also found and its behaviour in the presence of vector interactions was studied.

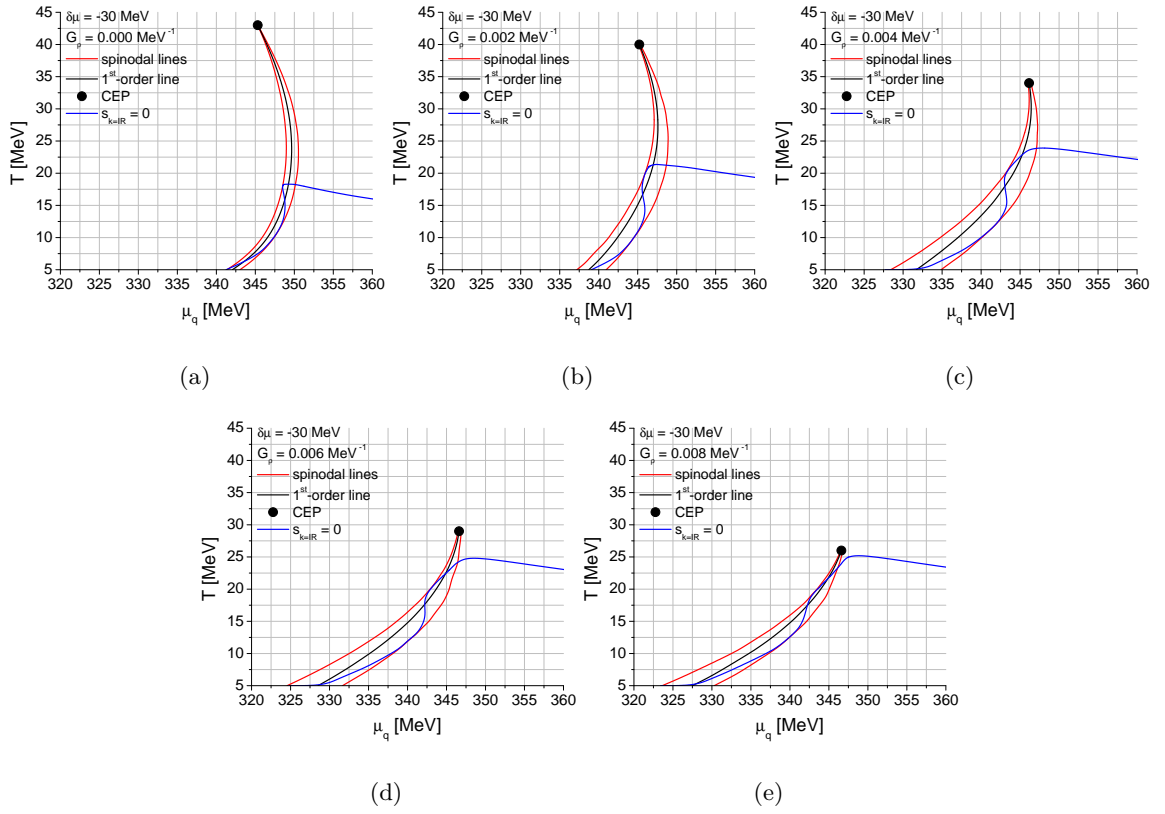


FIGURE 8.6: First-order phase transition of the QM model with  $\delta\mu = -30$  MeV, for increasing  $G_\rho$  with fixed  $G_\omega = 0$ . The red, black and blue lines are the spinodals, first-order phase transitions and the  $s_{k=k_{\text{IR}}} = 0$  lines, respectively. The CEPs are represented by the black dots. Entropy density is negative below the  $s_{k=k_{\text{IR}}} = 0$  line.

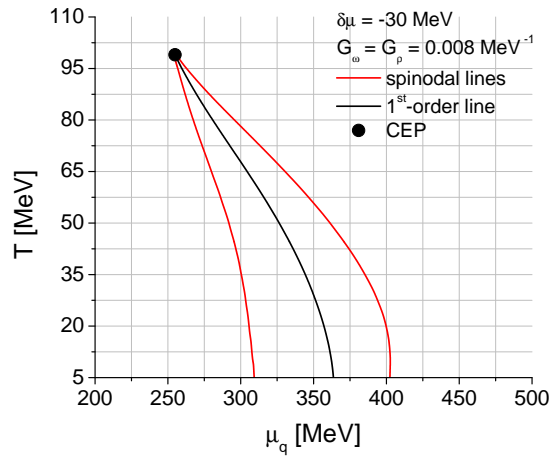


FIGURE 8.7: First-order phase transition of the QM model with  $\delta\mu = -30$  MeV, for  $G_\omega = G_\rho = 0.008$   $\text{MeV}^{-1}$ . The red lines are the spinodals, the black line is the first-order phase transition line and the black dot is the CEP.

The behaviour of the critical region under finite vector interactions is different from mean field calculations: increasing the repulsive vector interaction pushes the CEP towards higher values of temperature and lower values of chemical potential. Furthermore, increasing the vector

interaction drives the CEP to smaller temperatures and higher chemical potentials. Another important conclusion is that the region in-between spinodal lines increases in chemical potential with increasing vector couplings. Matter inside the spinodal region corresponds to unstable and metastable matter. Unstable matter can only be reached in a non-equilibrium evolution of the system in the form of clusterized matter. Very different from the case without vector interactions, the increase of this region in chemical potential, due to finite vector interactions, indicates that it is possible to have clusterized chiral symmetric matter in a wider region of chemical potentials [333].

We also found that the region of negative entropy density is present on both sides of the first-order phase transition line. The positive entropy density region and the negative entropy density region is separated by the  $s_{k=k_{\text{IR}}} = 0$  line. However, this line behaves like an “isentropic line”: it passes through the first-order line, touches one spinodal line, changes direction crossing the first-order line again, touches the other spinodal and changes direction again. This leads us to conclude that the appearance of the negative entropy density region is a consequence of the displacement of the  $s = 0$  “isentropic line” from its  $T = 0$  location. For a high enough vector interaction the negative entropy density regions disappears leaving a physical phase diagram with a first-order phase transition and CEP and without negative entropy.

Considering a difference of up and down quark chemical potentials  $\delta\mu$ , so a finite isospin chemical potential, has a big effect on the chemical potential of the first-order line but the location of the CEP is unchanged in temperature and marginally changed to smaller chemical potentials. Increasing at a finite  $\delta\mu$  the coupling of the  $\tilde{\rho}_0^3$  vector field,  $G_\rho$ , is equivalent to restoring isospin symmetry while pushing the CEP to lower values of temperature, leading to a phase structure similar to the one with  $\delta\mu = 0$  with a CEP at smaller temperatures.

To better understand the origin of the unphysical negative entropy density region, as previously found by [191], a flow equation beyond the LPA could be derived and the phase diagram and entropy density calculated. A different regulator function could also influence the results. Due to the mathematical nature of the QM flow equation, we were only able to calculate the phase diagram down to low temperatures ( $T = 5$  MeV) but not at zero temperature. Solving the  $T = 0$  flow equation exactly could also provide some new analytical and numerical insights. Some efforts in this direction have been done in [334], where the authors try to solve the flow equation at  $T = 0$  by executing a mathematical transformation to the differential equations in order to transform the rectangular initial condition on a circular one, due to the Fermi sphere.

Another possible source for the appearance of the negative entropy density region is the fact that the UV potential is temperature and chemical potential independent. As future work we plan to explore how different, temperature and chemical potential dependent UV potentials, affect the phase diagram and the negative density entropy region.

A different line of future research consists of studying the effect of conserved baryon and isospin charges beyond the MF using the model and techniques laid out in this chapter. Very recently such study has been performed in the context of the PNJL model in the MF approximation, see [333].

We would like to make a final comment on the introduction of vector degrees of freedom in the calculation. In our approach, the vector fields are regarded as mean fields. With this approximation we considered that the effective average action,  $\Gamma_k$ , and equivalently, the effective average potential,  $U_k$ , would be stationary with respect to these vector degrees of freedom along the flow. To make this demand, we derived self-consistent equations for the vector fields that should be verified at every momentum scale,  $k$ , implying that, at every momentum shell, the effective average potential is always stationary with respect to the vector fields. These equations imprinted scale ( $k$ ), temperature ( $T$ ), chemical potential ( $\mu$ ) and  $\sigma$  dependencies on the vector fields, i.e.,  $V_0 = V_{0,k}(T, \mu, \sigma)$ . Since the vector fields are scale dependent there is a direct effect of the vector fields in the flow at each scale.

Very recently in [335], a different approach to include mean field vector degrees of freedom, in the Quark-Meson model within the FRG, was used. In such work, the mesons are also considered in a mean field approximation but the stationary condition is only applied after the flow is solved: a specific constant value for the vector field is chosen, changing the chemical potential by a simple shift. The flow is then solved from the ultraviolet down to the infrared, with this constant vector field. This process is then repeated for several different values of constant vector field. In the end one has access to the effective potential as a function of  $\sigma$  and of the vector field. Applying the stationary condition of the effective action with respect to the vector field, implies that the desired value for the mean field vector field is the one which minimizes the effective potential in the infrared. In that approach, the flow is not directly affected at every momentum scale, but the chemical potential is shifted during the flow.

Indeed, both the approach presented in this chapter and the one in [335], are completely different. They lead to two distinct trajectories in theory space, which were drawn with different flow equations. Of course, solving two different flow equations leads to two different infrared physics. More studies are necessary in order to better understand which approach is best to model real physics.



# PART IV

## Conclusion



## Chapter 9

# Conclusion

In this work, we have explored different aspects of the phase diagram of strongly interacting matter using effective models of QCD in different approximations: the MF approximation, the one-loop approximation of the effective action and the FRG technique. In the first case, the generating functional of the model is computed by considering that only the classical configuration of the field contributes to the path integral. In the one-loop approximation of the effective action, correction terms to the MF approximation are included. The FRG technique consists on treating the quantum fluctuations successively, from scale to scale, making a gradual momentum integration.

Since different studies have been performed with different approximations and techniques, we have divided the work in two main studies: studies in the MF approximation and, studies beyond the MF approximation. The main tool to perform our researches is the NJL model in its two and three flavour versions, including different types of interactions in different studies. The QM model with vector interactions, which can be interpreted as a partially bosonized version of the NJL model, is also used.

Using an extended version of the NJL model, which includes the Polyakov loop to study the deconfinement transition, we have obtained, for some parametrizations of the model, a phase diagram containing two CEPs. One of the CEPs is associated with the light quarks while the other, is associated with the strange quark. We have concluded that, for a fixed baryon chemical potential, the existence of a particular isentropic trajectory at high temperatures and its vanishing at lower temperatures might be an indication of the existence of a first-order phase transition in-between these temperature regimes. Further research, including the study of fluctuations of conserved charges and their higher order cumulants along the isentropic lines should be performed. Such study could give more information about possible signatures for the presence of the first-order phase transitions and, consequently, the CEP, in the phase diagram.

Using the zero temperature, three flavour NJL model, in  $\beta$ -equilibrium, with four-quark and eight-quark vector-isoscalar interactions, we have explored the stability of neutron stars in accordance with the latest astrophysical constraints from NICER, LIGO/Virgo and the pulsars with approximately two solar masses, PSR J1614-2230 and PSR J0348+0432. The presence of a eight-quark vector-isoscalar interaction is crucial to generate large quark branches in the  $M(R)$

diagram. This is due to the stiffening effect on the quark matter EoS, which translates itself into a non-linear density dependence of the speed of sound. Indeed, we have found that the model predicts quark matter in the core of moderately low mass neutron stars,  $\sim 1M_\odot$ , while providing the necessary repulsion to preserve the star stability up to  $\sim 2.1M_\odot$ . The existence of quark matter inside low/intermediate mass neutron stars imprints the tidal deformability when compared to the expected results for purely hadronic neutron stars. It follows that, low values of tidal deformability for a low/intermediate mass stars ( $\sim 1.4M_\odot$ ), might be a possible observational signature for the existence of quark matter in the core of neutron stars.

Regarding the study of the NJL model beyond the mean field approximation, we have explored the effect of including quantum fluctuations in the two flavour NJL model at finite temperature. This is accomplished, in a symmetry preserving way, by including collective and non-collective modes in the one-meson-loop gap equation which originate from poles and branch cuts in the complex plane, respectively. The inclusion of a boson cutoff,  $\Lambda_b$ , is necessary to regularize the meson-loop momenta. This new parameter is used to study the influence of going beyond the usual mean field approximation in the quark condensate in the vacuum and at finite temperature. We have found that, with the increase of temperature, chiral symmetry tends to get restored, the collective modes melt and only non-collective modes contribute to the quark condensate. With the inclusion of such modes, the quark condensate at finite temperature has a different behaviour from the one found in MF calculations. However, it is still possible to distinguish two phases, one with a large quark condensate and another with a small quark condensate. These phases are separated by the melting temperature of the collective modes, the so-called Mott temperature.

We have applied the FRG formalism to the two flavour QM model with vector interactions. Special attention has been given to the low temperature and high density region of the phase diagram, where the applied formalism is known to lead to an unphysical region of negative entropy density near the first-order phase transition of the model. As in previous studies, without repulsive vector interactions, a region of negative entropy density has been found near the first-order chiral phase transition. We have explored the connection between this unphysical region and the chiral critical region, especially the first-order line and spinodal lines, using also different values for vector interactions. We have found that the unphysical negative entropy density region appears because the  $s = 0$  “isentropic line”, near the critical region, is displaced from its  $T = 0$  location. For certain values of vector interactions this region is pushed to lower temperatures and high chemical potentials in such way that the negative entropy density region present in the phase diagram of the model can even disappear. In the case of finite vector interactions, the location of the CEP has a non-trivial behaviour in the  $T - \mu_B$  plane, different from the one found in MF calculations.

We conclude with a comment on MF and beyond MF calculations. Although it is essential to study effective models beyond the MF approximation, such models should be used with care as effective models of QCD. Both in the one-meson-loop and FRG calculations performed in this work, it is evident that new dynamics are incorporated beyond the MF level. These extra dynamics seem to reflect properties of the models or of the technique used to incorporate quantum fluctuations. A question then arises: are these extra dynamics essential to model QCD, or are

---

they artefacts of using effective models? Hence, MF calculations are still an invaluable tool to study the QCD phase diagram as a first approximation due to its simplicity, not only of practical applicability but also on interpreting physical results. Nonetheless, calculations beyond the MF are of ultimate importance to better understand the models we use to study QCD, but they still require further investigations in the future.



# PART V

## Appendix



## Appendix A

# Units, conventions and the Matsubara summation

### A.1 Conventions

Throughout this work we use Planck units:

$$c = \hbar = k_B = 1,$$

where  $c$  is the speed of light,  $\hbar$  is the reduced Planck constant and  $k_B$  is the Boltzmann constant. In this system:

$$[\text{lenght}] = [\text{time}] = [\text{energy}]^{-1} = [\text{mass}]^{-1} = [\text{temperature}]^{-1}.$$

We use the following conversion factor:

$$\hbar c = 197.326 \text{ MeV fm}.$$

The Einstein convention for sum over repeated indices is assumed, unless stated otherwise.

We often work with Euclidean spacetime, which can be obtained from Minkowski spacetime, after the so-called Wick rotation,  $t \rightarrow -i\tau$ . After this transformation, the norm between four-vectors is given by the Euclidean norm. The conventions used in this thesis are summarized in Table A.1.

The following notation is used along the work for an  $n$ -dimensional integration in momentum space:

$$\int_{q_n} = \int \frac{d^n q}{(2\pi)^n}.$$

Minkowski spacetime	Euclidean spacetime
$(g_{\mu\nu}) = \text{diag}(1, -1, -1, -1)$	$(g_{ab}) = -\text{diag}(1, 1, 1, 1) = -(\delta_{ab})$
$(x^\mu) = (x^0, \mathbf{x})$	$(x_a) = (ix^0, \mathbf{x}) = (x_\tau, \mathbf{x})$
$(\partial_\mu) = (\partial_0, \nabla)$	$(\partial_a) = (-i\partial_0, \nabla) = (\partial_\tau, \nabla)$
$x^\mu x_\mu = x_0^2 - \mathbf{x} \cdot \mathbf{x}$	$x^a x_a = -x_\tau^2 - \mathbf{x} \cdot \mathbf{x}$
$(\gamma^\mu) = (\gamma^0, \boldsymbol{\gamma})$	$(\gamma_a) = (i\gamma^0, \boldsymbol{\gamma}) = (\gamma_\tau, \boldsymbol{\gamma})$
$(\gamma^\mu)^\dagger = (\gamma^0, -\boldsymbol{\gamma})$	$(\gamma_a)^\dagger = (-\gamma_\tau, -\boldsymbol{\gamma}) = -(\gamma_a)$
$\gamma^\mu, \gamma^\nu = 2g^{\mu\nu}$	$\gamma^a, \gamma^b = -2\delta^{ab}$
$\gamma^5 = i\gamma^0\gamma^1\gamma^2\gamma^3$	$\gamma^5 = \gamma_\tau\gamma^1\gamma^2\gamma^3$

TABLE A.1: Convention table.

## A.2 The Heaviside step function and the Dirac delta function

The Heaviside step function<sup>1</sup> centered at  $x_0$ ,  $H(x - x_0)$ , is defined as:

$$H(x - x_0) = \begin{cases} 0 & \text{if } x < x_0, \\ 1 & \text{if } x > x_0. \end{cases} \quad (\text{A.1})$$

This function is discontinuous at  $x_0$  and the value of the function at the discontinuity,  $H(0)$ , is usually chosen based on the problem to be solved. Indeed, in different applications one can find,  $H(0) = 0$ ,  $H(0) = 1/2$  or  $H(0) = 1$ .

The Dirac delta function<sup>1</sup> centered at  $x_0$ ,  $\delta(x - x_0)$ , is defined as the function which is zero everywhere in the real line, except at  $x_0$ , where it diverges. For an arbitrary continuous function  $f(x)$ , it satisfies:

$$\int_A^B dx f(x)\delta(x - x_0) = \begin{cases} f(x_0) & \text{if } A < x_0 < B, \\ 0 & \text{otherwise.} \end{cases} \quad (\text{A.2})$$

The Dirac delta function can be composed with another continuous function,  $g(x)$ , to yield,  $\delta(g(x))$ . This composition is non-zero only if  $g$  has real roots,  $x_i$ . In such case one can write:

$$\delta(g(x)) = \sum_i \frac{\delta(x - x_i)}{|g'(x_i)|}. \quad (\text{A.3})$$

This is only valid in the domain where  $g'$  is non-zero.

<sup>1</sup>Although called a function, it can be formally defined as a distribution or as a measure.

One can relate the Heaviside step function and Dirac delta function using:

$$H(x - x_0) = \int_{-\infty}^{x_0} dy \delta(y - x_0), \quad (\text{A.4})$$

$$\frac{dH(x)}{dx} = \delta(x). \quad (\text{A.5})$$

For our purposes we will often write Eq. (A.2), using the difference between Heaviside functions<sup>2</sup> as:

$$\int_A^B dx f(x) \delta(x - x_0) = f(x_0)[H(x_0 - A) - H(x_0 - B)]. \quad (\text{A.6})$$

### A.3 Sokhotski–Plemelj formula

The Sokhotski–Plemelj formula is given by:

$$\frac{1}{x - x_0 \pm i\epsilon} = \text{p.v.} \frac{1}{x - x_0} \mp i\pi \delta(x - x_0). \quad (\text{A.7})$$

Where  $\epsilon \geq 0$ , p.v. stands for the Cauchy Principal value and  $\delta$  is the Dirac delta function.

### A.4 Dirac matrices

The Dirac matrices are defined as  $\gamma^\mu = (\gamma^0, \boldsymbol{\gamma})$  and they obey the following anticommutation relations:

$$\{\gamma^\mu, \gamma^\nu\} = \gamma^\mu \gamma^\nu + \gamma^\nu \gamma^\mu = 2g_{\mu\nu}. \quad (\text{A.8})$$

They have the following properties:  $(\gamma^0)^\dagger = \gamma^0$ ,  $(\gamma^i)^\dagger = -\gamma^i$ ,  $(\gamma^0)^2 = \mathbb{1}_{4 \times 4}$ ,  $(\gamma^i)^2 = -\mathbb{1}_{4 \times 4}$ , where  $\mathbb{1}_{4 \times 4}$  is the identity matrix. The  $\gamma_5$  matrix, is defined as the product of the four gamma matrices as follows:

$$\gamma_5 \equiv i\gamma^0 \gamma^1 \gamma^2 \gamma^3. \quad (\text{A.9})$$

It anticommutes with the other Dirac matrices,  $\{\gamma_5, \gamma^\mu\} = 0$ , and its properties are:  $(\gamma_5)^\dagger = \gamma_5$  and  $(\gamma_5)^2 = \mathbb{1}_{4 \times 4}$ .

In the Dirac basis these matrices are given by:

$$\gamma^0 = \begin{pmatrix} \mathbb{1}_{2 \times 2} & 0 \\ 0 & -\mathbb{1}_{2 \times 2} \end{pmatrix}, \quad \gamma^i = \begin{pmatrix} 0 & \tau_i \\ -\tau_i & 0 \end{pmatrix}, \quad \gamma_5 = \begin{pmatrix} 0 & \mathbb{1}_{2 \times 2} \\ \mathbb{1}_{2 \times 2} & 0 \end{pmatrix}. \quad (\text{A.10})$$

Here,  $\tau_i$  are the three Pauli matrices of the  $SU(2)$  group (see Appendix B.1).

---

<sup>2</sup>Such a function is usually called a boxcar function.

## A.5 Matsubara summation

In quantum field theory at finite temperature, one can study the properties of the 2-point thermal Green functions for fermionic and bosonic fields. One can conclude that the 2-point thermal Green function is a periodic function for bosons and an antiperiodic function for fermions. Due to the (anti)periodicity of the thermal propagators, the fields are only allowed to take discrete frequencies. Such frequencies are known as Matsubara frequencies and are the allowed frequencies for bosonic and fermionic fields at finite temperature. Such frequencies are given by:

$$\omega_n = \begin{cases} 2n\pi T, & \text{for bosons,} \\ (2n+1)\pi T, & \text{for fermions,} \end{cases} \quad \text{with, } |n| = 0, 1, 2, \dots \quad (\text{A.11})$$

For more details, see [313].

The integration over the Euclidean frequency direction,  $k_0$ , can be performed using the Matsubara frequencies. The original integration of the function  $f(k_0)$  over  $k_0$ , can be written as a sum over the allowed Matsubara frequencies for the fermionic or bosonic field,  $\omega_n$ :

$$\int \frac{dk_0}{2\pi} f(k_0) \rightarrow \frac{1}{\beta} \sum_{n=-\infty}^{\infty} f(\omega_n). \quad (\text{A.12})$$

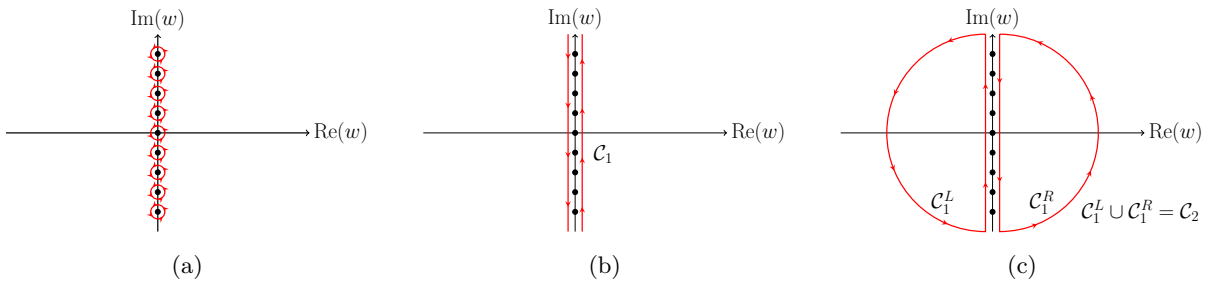


FIGURE A.1: Contours used to transform the Matsubara summation into a contour integration.

This infinite sum over the Matsubara frequencies can be converted into a contour integration on the complex plane. Considering that  $f(z)$  does not have poles on the imaginary axis, we can write the original Matsubara sum as the sum of residues of the function  $f(z)u_\beta(z)$ , with  $u_\beta(z)$  a function with simple poles located exactly at  $\omega_n$  (the Matsubara frequencies), and with residue 1. This sum of residues can be written as a sum of contour integrations where each contour surrounds a simple pole located at a particular allowed Matsubara frequency, see Fig. A.1(a). Using the residue theorem, one can recover the original summation.

The set of infinite contours around the Matsubara frequencies, can be deformed to give origin to a new contour,  $C_1$ , which goes around the entire imaginary axis, containing all the Matsubara frequencies, see Fig. A.1(b). As long as the function  $f(z)u_\beta(z)$ , goes to zero fast enough at infinity, the contour integration over  $C_1$  can be written as the contour integration over  $C_2$ , where the contour  $C_2$  contains the entire complex plane except the imaginary axes, see Fig. A.1(c).

We highlight that, in order to have the conventional orientation in the contour  $\mathcal{C}_2$ , we had to multiply the integration by  $-1$ .

This procedure can be summarized in the following substitution:

$$\int \frac{dk_0}{2\pi} f(k_0) \rightarrow \frac{1}{\beta} \sum_{n=-\infty}^{\infty} f(\omega_n) \rightarrow \frac{-1}{\beta} \oint_{\mathcal{C}_2} \frac{dw}{2\pi i} f(-iw) \times \begin{cases} \frac{\beta}{2} \coth\left(\frac{\beta w}{2}\right) & \text{for bosons,} \\ \frac{\beta}{2} \tanh\left(\frac{\beta w}{2}\right) & \text{for fermions.} \end{cases} \quad (\text{A.13})$$

The hyperbolic tangent functions chosen above, play the role of the function  $u_\beta(z)$ , which generate simple poles located at the Matsubara frequencies, for bosons or fermions. A much more detailed explanation about evaluating sums over the Matsubara frequencies can be found in [336].

### A.5.1 Thermodynamic relations

After calculating the thermodynamical potential,  $\Omega(T, \mu)$ , one can calculate several thermodynamic quantities of interest such as the pressure ( $P$ ), particle ( $\rho_i$ ), entropy ( $s$ ) and energy densities ( $\epsilon$ ), using the following relations [337]:

$$P(T, \mu) - P_0 = -\Omega(T, \mu), \quad (\text{A.14})$$

$$\rho_i(T, \mu) = - \left( \frac{\partial \Omega(T, \mu)}{\partial \mu_i} \right)_T, \quad (\text{A.15})$$

$$s(T, \mu) = - \left( \frac{\partial \Omega(T, \mu)}{\partial T} \right)_\mu, \quad (\text{A.16})$$

$$\epsilon(T, \mu) = -P(T, \mu) + T s(T, \mu) + \sum_i \mu_i \rho_i(T, \mu). \quad (\text{A.17})$$

The constant  $P_0$  is the vacuum pressure i.e.,  $P_0 = P(0, 0)$ .



## Appendix B

# $SU(N)$ and $U(N)$ matrices

### B.1 $SU(N)$ matrices

We designate the set of  $N^2 - 1$  traceless hermitian  $N \times N$  matrices, that form the algebra of the  $SU(N)$  group, by  $\lambda_a$  (we also use  $\lambda_a$  for the particular case with  $N = 3$ ). Unless stated otherwise, a sum over repeated indices is assumed. The matrices  $\frac{1}{2}\lambda_a$  are the generators of the  $SU(N)$  group and satisfy the following commutation relation:

$$[\lambda_a, \lambda_b] = 2if_{abc}\lambda_c, \quad (\text{B.1})$$

with  $(a, b, c) = 1, 2, \dots, N^2 - 1$  and  $f_{abc}$  a third rank tensor. By definition,  $\text{tr} \lambda_a = 0$ . We normalize the generators using:

$$\text{tr} \lambda_a \lambda_b = 2\delta_{ab}. \quad (\text{B.2})$$

With this conventions,  $f_{abc}$  is totally antisymmetric.

One can define a third rank totally symmetric tensor,  $d_{abc}$  by writing:

$$\lambda_a \lambda_b = \frac{2}{N} \delta_{ab} + (d_{abc} + if_{abc})\lambda_c. \quad (\text{B.3})$$

and using the commutation relation in Eq. (B.1), one can derive the following relations:

$$\{\lambda_a, \lambda_b\} = \frac{4}{N} \delta_{ab} + 2d_{abc}\lambda_c, \quad (\text{B.4})$$

$$\text{tr}([\lambda_a, \lambda_b]\lambda_c) = 4if_{abc}, \quad (\text{B.5})$$

$$\text{tr}(\{\lambda_a, \lambda_b\}\lambda_c) = 4d_{abc}. \quad (\text{B.6})$$

The totally symmetric,  $d_{abc}$ , and totally antisymmetric,  $f_{abc}$ , tensors are called the structure constants of the algebra.

Any  $N \times N$  matrix can be written as linear combination of the identity matrix,  $\mathbb{1}$ , and the generators,  $\lambda_a$ . Consider the  $N \times N$  matrix  $M$ , which can be linearly expanded as follows:

$$M = M_0 \mathbb{1} + M_a \lambda_a. \quad (\text{B.7})$$

This can be interpreted as a completeness relation. Calculating the trace of the above, multiplying it by  $\lambda_b$  and calculating the trace yields the components:

$$M_0 = \frac{1}{N} \text{tr } M, \quad (\text{B.8})$$

$$M_a = \frac{1}{2} \text{tr } (M \lambda_a). \quad (\text{B.9})$$

Plugging the components back in the completeness relation allows us to derive the following identity (also called the completeness relation):

$$\delta_{il} \delta_{kj} = \frac{1}{2} \left( \frac{2}{N} \delta_{ij} \delta_{kl} + (\lambda_a)_{ij} (\lambda_a)_{kl} \right). \quad (\text{B.10})$$

One important result concerning the totally antisymmetric structure constants that we will use, is the Jacobi identity, given by:

$$f_{abe} f_{ecd} + f_{cbe} f_{aed} + f_{dbe} f_{ace} = 0. \quad (\text{B.11})$$

For  $N = 2$ , the generators are the three Pauli matrices of  $SU(2)$ ,  $\tau_a$ , and can be written explicitly as:

$$\tau_1 = \begin{pmatrix} 0 & 1 \\ 1 & 0 \end{pmatrix}, \quad \tau_2 = \begin{pmatrix} 0 & -i \\ i & 0 \end{pmatrix}, \quad \tau_3 = \begin{pmatrix} 1 & 0 \\ 0 & -1 \end{pmatrix}. \quad (\text{B.12})$$

In this case the structure constants are:  $f_{abc} = \varepsilon_{abc}$  and  $d_{abc} = 0$ , with  $\varepsilon_{abc}$  the three dimensional Levi-Civita symbol.

For  $N = 3$ , the generators are the eight Gell-Mann matrices,  $\lambda_a$ , which can be written as:

$$\begin{aligned} \lambda_1 &= \begin{pmatrix} 0 & 1 & 0 \\ 1 & 0 & 0 \\ 0 & 0 & 0 \end{pmatrix}, & \lambda_2 &= \begin{pmatrix} 0 & -i & 0 \\ i & 0 & 0 \\ 0 & 0 & 0 \end{pmatrix}, & \lambda_3 &= \begin{pmatrix} 1 & 0 & 0 \\ 0 & -1 & 0 \\ 0 & 0 & 0 \end{pmatrix}, & \lambda_4 &= \begin{pmatrix} 0 & 0 & 1 \\ 0 & 0 & 0 \\ 1 & 0 & 0 \end{pmatrix}, \\ \lambda_5 &= \begin{pmatrix} 0 & 0 & -i \\ 0 & 0 & 0 \\ i & 0 & 0 \end{pmatrix}, & \lambda_6 &= \begin{pmatrix} 0 & 0 & 0 \\ 0 & 0 & 1 \\ 0 & 1 & 0 \end{pmatrix}, & \lambda_7 &= \begin{pmatrix} 0 & 0 & 0 \\ 0 & 0 & -i \\ 0 & i & 0 \end{pmatrix}, & \lambda_8 &= \begin{pmatrix} \frac{1}{\sqrt{3}} & 0 & 0 \\ 0 & \frac{1}{\sqrt{3}} & 0 \\ 0 & 0 & \frac{-2}{\sqrt{3}} \end{pmatrix}. \end{aligned} \quad (\text{B.13})$$

The non-vanishing structure constants for the  $N = 3$  case are presented in Table B.1.

## B.2 $U(N)$ matrices

In this section we consider the  $N^2$  matrices of the  $U(N)$  algebra. Basically, we upgrade the algebra of  $SU(N)$  by including also the a generator,  $\lambda_0$ , proportional to the identity matrix,  $\mathbb{1}$ .

$abc$	$f_{abc}$	$abc$	$d_{abc}$
123	1	118, 228, 338	$\frac{1}{\sqrt{3}}$
147, 246, 257, 345	$\frac{1}{2}$	146, 157, 256, 344, 355	$\frac{1}{2}$
156, 367	$-\frac{1}{2}$	247, 366, 377	$-\frac{1}{2}$
458, 678	$\frac{\sqrt{3}}{2}$	448, 558, 668, 778	$-\frac{1}{2\sqrt{3}}$
		888	$-\frac{1}{\sqrt{3}}$

TABLE B.1: Non-vanishing antisymmetric and symmetric structure constants,  $f_{abc}$  (left) and  $d_{abc}$  (right), respectively, for the  $SU(3)$  group.

It can be defined in the following way:

$$\lambda_0 = \sqrt{\frac{2}{N}} \mathbb{1}, \quad (\text{B.14})$$

which follows by requiring the same normalization as in the  $SU(N)$  algebra:

$$\text{tr } \lambda_a \lambda_b = 2\delta_{ab}, \quad (\text{B.15})$$

From this convention, it follows:

$$\text{tr } (\lambda_a) = N \sqrt{\frac{2}{N}} \delta_{0a}. \quad (\text{B.16})$$

The commutation relation of the  $U(N)$  algebra has the same structure as the commutation relation of  $SU(N)$  and it is given by Eq. (B.1). In this case however, the totally antisymmetric constants must also be enlarged to include the zero component, and one can write  $f_{0ab} = 0$ .

As for the  $SU(N)$  algebra, one can also define a totally symmetric rank three tensor,  $d_{abc}$ , for this algebra by writing:

$$\lambda_a \lambda_b = (d_{abc} + i f_{abc}) \lambda_c. \quad (\text{B.17})$$

The totally symmetric structure constants are the same as for the  $SU(N)$  algebra while also including,  $d_{0ab} = \frac{2}{N} \delta_{ab}$ . The anticommutation relation for this algebra can be written as:

$$\{\lambda_a, \lambda_b\} = 2d_{abc} \lambda_c. \quad (\text{B.18})$$

The relations given in Eq. (B.5) and (B.6) for the  $SU(N)$ , are still valid for the  $U(N)$  algebra but with the new structure constants.

As before, one can write any  $N \times N$  matrix as linear combination of the  $U(N)$  generators,  $\lambda_a$  i.e., any matrix  $M$  can be written as  $M = M_a \lambda_a$ . Proceeding like for the  $SU(N)$  algebra, one

can derive the following completeness relation:

$$\delta_{il}\delta_{kj} = \frac{1}{2}(\lambda_a)_{ij}(\lambda_a)_{kl}. \quad (\text{B.19})$$

One important result that will be used in this work is the trace of the product between four  $U(N)$  generators:

$$\text{tr}(\lambda_a\lambda_b\lambda_c\lambda_d) = 2(d_{abe}d_{cde} + id_{abe}f_{cde} + if_{abe}d_{cde} - f_{abe}f_{cde}). \quad (\text{B.20})$$

For  $N = 2$  and  $N = 3$ , the additional matrices,  $\tau_0$  and  $\lambda_0$  respectively, are explicitly given by:

$$\tau_0 = \begin{pmatrix} 1 & 0 \\ 0 & 1 \end{pmatrix}, \quad \lambda_0 = \begin{pmatrix} \sqrt{\frac{2}{3}} & 0 & 0 \\ 0 & \sqrt{\frac{2}{3}} & 0 \\ 0 & 0 & \sqrt{\frac{2}{3}} \end{pmatrix}. \quad (\text{B.21})$$

Another important result for the calculations in this thesis is calculating the determinant of an  $n \times n$  matrix,  $B = [b_{ij}]$ . Formally, it can be defined as:

$$\det(B) = \frac{1}{n!}\varepsilon_{i_1\dots i_n}\varepsilon_{j_1\dots j_n}b_{i_1j_1}\dots b_{i_nj_n}. \quad (\text{B.22})$$

Where the  $\varepsilon_{i_1,\dots,i_n}$  is the  $n$ -dimensional Levi-Civita symbol. Consider the case with  $n = 3$ . Expanding the matrix on the basis of the Gell-Mann matrices and the identity,  $\lambda_0$ ,  $B = B_a\lambda_a$ , we can write:

$$\det(B) = \det(B_a\lambda_a) = \frac{1}{3!}\varepsilon_{ijk}\varepsilon_{lmn}(B_a\lambda_a)_{il}(B_b\lambda_b)_{jm}(B_c\lambda_c)_{kn} = A_{abc}B_aB_bB_c, \quad (\text{B.23})$$

where,

$$A_{abc} = \frac{1}{3!}\varepsilon_{ijk}\varepsilon_{lmn}(\lambda_a)_{il}(\lambda_b)_{jm}(\lambda_c)_{kn}. \quad (\text{B.24})$$

Decomposing the product of two Levi-Civita symbols in Kronecker deltas<sup>1</sup> and using results from the algebra (Eqs. (B.16) and (B.6)), one can get:

$$A_{abc} = \frac{2}{3}d_{abc} + \sqrt{\frac{2}{3}}(\delta_{a0}\delta_{b0}\delta_{c0} - \delta_{a0}\delta_{bc} - \delta_{b0}\delta_{ca} - \delta_{c0}\delta_{ab}). \quad (\text{B.25})$$

<sup>1</sup>With:  $\varepsilon_{ijk}\varepsilon_{lmn} = \delta_{il}(\delta_{jm}\delta_{kn} - \delta_{jn}\delta_{km}) - \delta_{im}(\delta_{jl}\delta_{kn} - \delta_{jn}\delta_{kl}) + \delta_{in}(\delta_{jl}\delta_{km} - \delta_{jm}\delta_{kl})$ .

## Appendix C

# Expansion of the product between $N$ operators

### C.1 Linear expansion of the product between $N$ operators

First we write an operator  $\hat{O}_i$  as its own expectation value, plus a small perturbation  $\delta\hat{O}_i$  around it:

$$\hat{O}_i = \langle \hat{O}_i \rangle + (\hat{O}_i - \langle \hat{O}_i \rangle) = \langle \hat{O}_i \rangle + \delta\hat{O}_i, \quad (\text{C.1})$$

here, the perturbation is defined as:

$$\delta\hat{O}_i = \hat{O}_i - \langle \hat{O}_i \rangle. \quad (\text{C.2})$$

The linear product between  $N$  operators can be obtained by writing each operator as in Eq. (C.1) and neglecting higher order perturbations, i.e., for  $n \geq 2$ ,  $(\delta\hat{O})^n = 0$ .

The linear product between two operators,  $\hat{O}_1\hat{O}_2$ , can then be calculated to yield:

$$\hat{O}_1\hat{O}_2 = (\langle \hat{O}_1 \rangle + \delta\hat{O}_1)(\langle \hat{O}_2 \rangle + \delta\hat{O}_2) = \langle \hat{O}_1 \rangle \langle \hat{O}_2 \rangle + \langle \hat{O}_1 \rangle \delta\hat{O}_2 + \delta\hat{O}_1 \langle \hat{O}_2 \rangle + \delta\hat{O}_1\delta\hat{O}_2, \quad (\text{C.3})$$

using  $\delta\hat{O}_1\delta\hat{O}_2 = 0$  and writing the perturbation as in Eq. (C.2), yields the final result:

$$\hat{O}_1\hat{O}_2 = \hat{O}_1 \langle \hat{O}_2 \rangle + \hat{O}_2 \langle \hat{O}_1 \rangle - \langle \hat{O}_1 \rangle \langle \hat{O}_2 \rangle. \quad (\text{C.4})$$

#### C.1.1 The general formula

The linear product between  $N = n + 1$  operators, with  $n \geq 1$ , can be written using the following formula:

$$\prod_{i=1}^{n+1} \hat{O}_i = \left[ \sum_{i=1}^{n+1} \frac{\hat{O}_i}{\langle \hat{O}_i \rangle} - n \right] \prod_{j=1}^{n+1} \langle \hat{O}_j \rangle. \quad (\text{C.5})$$

This formula can be proved by induction.

First, we start with the base case and show that the proposition is valid for  $n = 1$ . Substituting  $n = 1$ , in Eq. (C.5), it yields the linear 2-operator product:

$$\begin{aligned}\hat{\mathcal{O}}_1\hat{\mathcal{O}}_2 &= \left[ \sum_{i=1}^2 \frac{\hat{\mathcal{O}}_i}{\langle \hat{\mathcal{O}}_i \rangle} - 1 \right] \prod_{j=1}^2 \langle \hat{\mathcal{O}}_j \rangle \\ &= \hat{\mathcal{O}}_1 \langle \hat{\mathcal{O}}_2 \rangle + \hat{\mathcal{O}}_2 \langle \hat{\mathcal{O}}_1 \rangle - \langle \hat{\mathcal{O}}_1 \rangle \langle \hat{\mathcal{O}}_2 \rangle.\end{aligned}\quad (\text{C.6})$$

Which is exactly the result given by the definition of the linear product between two operators, see in Eq. (C.4). This establishes the validity of the formula for the  $n = 1$  case.

The next step is the inductive step. The goal is to show that, if one assumes that the formula is valid for any given  $n = m$ , then it also holds for  $n = m + 1$ . Hence, assuming that the formula is valid for  $n = m$ :

$$\prod_{i=1}^{m+1} \hat{\mathcal{O}}_i = \left[ \sum_{i=1}^{m+1} \frac{\hat{\mathcal{O}}_i}{\langle \hat{\mathcal{O}}_i \rangle} - m \right] \prod_{j=1}^{m+1} \langle \hat{\mathcal{O}}_j \rangle, \quad (\text{C.7})$$

we must show that the  $n = m + 1$  case is also true, i.e., show that the following equality holds:

$$\prod_{i=1}^{m+2} \hat{\mathcal{O}}_i = \left[ \sum_{i=1}^{m+2} \frac{\hat{\mathcal{O}}_i}{\langle \hat{\mathcal{O}}_i \rangle} - (m + 1) \right] \prod_{j=1}^{m+2} \langle \hat{\mathcal{O}}_j \rangle. \quad (\text{C.8})$$

Consider the right-hand side of this equation:

$$\text{RHS} = \left[ \sum_{i=1}^{m+2} \frac{\hat{\mathcal{O}}_i}{\langle \hat{\mathcal{O}}_i \rangle} - (m + 1) \right] \prod_{j=1}^{m+2} \langle \hat{\mathcal{O}}_j \rangle. \quad (\text{C.9})$$

Write the  $m + 2$  contribution in the sum explicitly:

$$\text{RHS} = \left[ \sum_{i=1}^{m+1} \frac{\hat{\mathcal{O}}_i}{\langle \hat{\mathcal{O}}_i \rangle} + \frac{\hat{\mathcal{O}}_{m+2}}{\langle \hat{\mathcal{O}}_{m+2} \rangle} - (m + 1) \right] \prod_{j=1}^{m+2} \langle \hat{\mathcal{O}}_j \rangle. \quad (\text{C.10})$$

Now, let us deal with the left-hand side of Eq. (C.8). We write:

$$\begin{aligned}\text{LHS} &= \prod_{i=1}^{m+2} \hat{\mathcal{O}}_i \\ &= \prod_{i=1}^{m+1} \hat{\mathcal{O}}_i \hat{\mathcal{O}}_{m+2} \\ &= \left[ \sum_{i=1}^{m+1} \frac{\hat{\mathcal{O}}_i}{\langle \hat{\mathcal{O}}_i \rangle} - m \right] \prod_{j=1}^{m+1} \langle \hat{\mathcal{O}}_j \rangle \hat{\mathcal{O}}_{m+2} \\ &= \left[ \sum_{i=1}^{m+1} \frac{1}{\langle \hat{\mathcal{O}}_i \rangle} \hat{\mathcal{O}}_i \hat{\mathcal{O}}_{m+2} - m \hat{\mathcal{O}}_{m+2} \right] \prod_{j=1}^{m+1} \langle \hat{\mathcal{O}}_j \rangle.\end{aligned}\quad (\text{C.11})$$

Here we wrote the  $m + 2$  contribution in the product explicitly and have used the assumption in Eq. (C.7). The first term can be expanded using the result for the linear product of two operators, using the base case given in Eq. (C.6). We write:

$$\begin{aligned}
\text{LHS} &= \left[ \sum_{i=1}^{m+1} \frac{1}{\langle \hat{\mathcal{O}}_i \rangle} \left( \frac{\hat{\mathcal{O}}_i}{\langle \hat{\mathcal{O}}_i \rangle} + \frac{\hat{\mathcal{O}}_{m+2}}{\langle \hat{\mathcal{O}}_{m+2} \rangle} - 1 \right) \langle \hat{\mathcal{O}}_i \rangle \langle \hat{\mathcal{O}}_{m+2} \rangle - m \hat{\mathcal{O}}_{m+2} \right] \prod_{j=1}^{m+1} \langle \hat{\mathcal{O}}_j \rangle \\
&= \left[ \sum_{i=1}^{m+1} \frac{\hat{\mathcal{O}}_i}{\langle \hat{\mathcal{O}}_i \rangle} + \sum_{i=1}^{m+1} \frac{\hat{\mathcal{O}}_{m+2}}{\langle \hat{\mathcal{O}}_{m+2} \rangle} - \sum_{i=1}^{m+1} 1 - m \frac{\hat{\mathcal{O}}_{m+2}}{\langle \hat{\mathcal{O}}_{m+2} \rangle} \right] \prod_{j=1}^{m+1} \langle \hat{\mathcal{O}}_j \rangle \langle \hat{\mathcal{O}}_{m+2} \rangle \\
&= \left[ \sum_{i=1}^{m+1} \frac{\hat{\mathcal{O}}_i}{\langle \hat{\mathcal{O}}_i \rangle} + (m+1) \frac{\hat{\mathcal{O}}_{m+2}}{\langle \hat{\mathcal{O}}_{m+2} \rangle} - (m+1) - m \frac{\hat{\mathcal{O}}_{m+2}}{\langle \hat{\mathcal{O}}_{m+2} \rangle} \right] \prod_{j=1}^{m+2} \langle \hat{\mathcal{O}}_j \rangle \\
&= \left[ \sum_{i=1}^{m+1} \frac{\hat{\mathcal{O}}_i}{\langle \hat{\mathcal{O}}_i \rangle} + \frac{\hat{\mathcal{O}}_{m+2}}{\langle \hat{\mathcal{O}}_{m+2} \rangle} - (m+1) \right] \prod_{j=1}^{m+2} \langle \hat{\mathcal{O}}_j \rangle \\
&= \text{RHS}.
\end{aligned} \tag{C.12}$$

Since both sides of Eq. (C.8) are equal, the formula also holds for  $n = m + 1$ , completing the inductive step. Hence, by mathematical induction, Eq. (C.5) is valid for  $n \geq 1$ .

## C.2 Quadratic expansion of the product between $N$ operators

Similarly to the linear product between  $N$  operators, the quadratic product between  $N$  operators can be obtained by writing each operator as in Eq. (C.1) and neglecting cubic perturbations, i.e., for  $n \geq 3$ ,  $(\delta \hat{\mathcal{O}})^n = 0$ .

The quadratic expansion of the product between three operators,  $\hat{\mathcal{O}}_1 \hat{\mathcal{O}}_2 \hat{\mathcal{O}}_3$ , can then be calculated to yield:

$$\begin{aligned}
\hat{\mathcal{O}}_1 \hat{\mathcal{O}}_2 \hat{\mathcal{O}}_3 &= \left( \langle \hat{\mathcal{O}}_1 \rangle + \delta \hat{\mathcal{O}}_1 \right) \left( \langle \hat{\mathcal{O}}_2 \rangle + \delta \hat{\mathcal{O}}_2 \right) \left( \langle \hat{\mathcal{O}}_3 \rangle + \delta \hat{\mathcal{O}}_3 \right) \\
&= \delta \hat{\mathcal{O}}_1 \delta \hat{\mathcal{O}}_2 \langle \hat{\mathcal{O}}_3 \rangle + \delta \hat{\mathcal{O}}_3 \delta \hat{\mathcal{O}}_1 \langle \hat{\mathcal{O}}_2 \rangle + \delta \hat{\mathcal{O}}_2 \delta \hat{\mathcal{O}}_3 \langle \hat{\mathcal{O}}_1 \rangle \\
&\quad + \delta \hat{\mathcal{O}}_1 \langle \hat{\mathcal{O}}_2 \rangle \langle \hat{\mathcal{O}}_3 \rangle + \delta \hat{\mathcal{O}}_3 \langle \hat{\mathcal{O}}_1 \rangle \langle \hat{\mathcal{O}}_2 \rangle + \delta \hat{\mathcal{O}}_2 \langle \hat{\mathcal{O}}_3 \rangle \langle \hat{\mathcal{O}}_1 \rangle + \delta \hat{\mathcal{O}}_1 \delta \hat{\mathcal{O}}_2 \delta \hat{\mathcal{O}}_3,
\end{aligned} \tag{C.13}$$

using  $\delta \hat{\mathcal{O}}_1 \delta \hat{\mathcal{O}}_2 \delta \hat{\mathcal{O}}_3 = 0$  and writing the perturbation as in Eq. (C.2), yields the final result:

$$\begin{aligned}
\hat{\mathcal{O}}_1 \hat{\mathcal{O}}_2 \hat{\mathcal{O}}_3 &= \hat{\mathcal{O}}_1 \hat{\mathcal{O}}_2 \langle \hat{\mathcal{O}}_3 \rangle + \hat{\mathcal{O}}_3 \hat{\mathcal{O}}_1 \langle \hat{\mathcal{O}}_2 \rangle + \hat{\mathcal{O}}_2 \hat{\mathcal{O}}_3 \langle \hat{\mathcal{O}}_1 \rangle \\
&\quad - \hat{\mathcal{O}}_1 \langle \hat{\mathcal{O}}_2 \rangle \langle \hat{\mathcal{O}}_3 \rangle - \hat{\mathcal{O}}_3 \langle \hat{\mathcal{O}}_1 \rangle \langle \hat{\mathcal{O}}_2 \rangle - \hat{\mathcal{O}}_2 \langle \hat{\mathcal{O}}_3 \rangle \langle \hat{\mathcal{O}}_1 \rangle + \langle \hat{\mathcal{O}}_1 \rangle \langle \hat{\mathcal{O}}_2 \rangle \langle \hat{\mathcal{O}}_3 \rangle.
\end{aligned} \tag{C.14}$$

### C.2.1 The general formula

The quadratic product between  $N = n + 2$  operators, with  $n \geq 1$ , can be written using the following formula:

$$\prod_{i=1}^{n+2} \hat{\mathcal{O}}_i = \left[ \frac{1}{2} \sum_{i=1}^{n+2} \sum_{j=1}^{n+2} \frac{\hat{\mathcal{O}}_i}{\langle \hat{\mathcal{O}}_i \rangle} \frac{\hat{\mathcal{O}}_j}{\langle \hat{\mathcal{O}}_j \rangle} (1 - \delta_{ij}) - n \sum_{i=1}^{n+2} \frac{\hat{\mathcal{O}}_i}{\langle \hat{\mathcal{O}}_i \rangle} + \frac{n}{2} (n+1) \right] \prod_{k=1}^{n+2} \langle \hat{\mathcal{O}}_k \rangle. \tag{C.15}$$

As for the linear product expansion, this formula can be proved very easily by induction.

First we consider the base case and show that the expression is valid for  $n = 1$ , i.e., for the quadratic expansion of the product between three operators. We write:

$$\begin{aligned}\hat{\mathcal{O}}_1\hat{\mathcal{O}}_2\hat{\mathcal{O}}_3 &= \left[ \frac{1}{2} \sum_{i=1}^3 \sum_{j=1}^3 \frac{\hat{\mathcal{O}}_i}{\langle \hat{\mathcal{O}}_i \rangle} \frac{\hat{\mathcal{O}}_j}{\langle \hat{\mathcal{O}}_j \rangle} (1 - \delta_{ij}) - \sum_{i=1}^3 \frac{\hat{\mathcal{O}}_i}{\langle \hat{\mathcal{O}}_i \rangle} + 1 \right] \prod_{k=1}^3 \langle \hat{\mathcal{O}}_k \rangle \\ &= \hat{\mathcal{O}}_1\hat{\mathcal{O}}_2 \langle \hat{\mathcal{O}}_3 \rangle + \hat{\mathcal{O}}_1\hat{\mathcal{O}}_3 \langle \hat{\mathcal{O}}_2 \rangle + \hat{\mathcal{O}}_2\hat{\mathcal{O}}_3 \langle \hat{\mathcal{O}}_1 \rangle \\ &\quad - \hat{\mathcal{O}}_1 \langle \hat{\mathcal{O}}_2 \rangle \langle \hat{\mathcal{O}}_3 \rangle - \hat{\mathcal{O}}_2 \langle \hat{\mathcal{O}}_1 \rangle \langle \hat{\mathcal{O}}_3 \rangle - \hat{\mathcal{O}}_3 \langle \hat{\mathcal{O}}_1 \rangle \langle \hat{\mathcal{O}}_2 \rangle + \langle \hat{\mathcal{O}}_1 \rangle \langle \hat{\mathcal{O}}_2 \rangle \langle \hat{\mathcal{O}}_3 \rangle. \quad (\text{C.16})\end{aligned}$$

This result agrees with Eq. (C.14) validating the formula for the base case with  $n = m$ . Next, we assume the formula holds for  $n = m$ , i.e.,

$$\prod_{i=1}^{m+2} \hat{\mathcal{O}}_i = \left[ \frac{1}{2} \sum_{i=1}^{m+2} \sum_{j=1}^{m+2} \frac{\hat{\mathcal{O}}_i}{\langle \hat{\mathcal{O}}_i \rangle} \frac{\hat{\mathcal{O}}_j}{\langle \hat{\mathcal{O}}_j \rangle} (1 - \delta_{ij}) - m \sum_{i=1}^{m+2} \frac{\hat{\mathcal{O}}_i}{\langle \hat{\mathcal{O}}_i \rangle} + \frac{m}{2}(m+1) \right] \prod_{k=1}^{m+2} \langle \hat{\mathcal{O}}_k \rangle. \quad (\text{C.17})$$

Now we must demonstrate that it is also valid for  $n = m + 1$ . Hence, we have to show that the following relations holds ( $n = m + 1$  case):

$$\prod_{i=1}^{m+3} \hat{\mathcal{O}}_i = \left[ \frac{1}{2} \sum_{i=1}^{m+3} \sum_{j=1}^{m+3} \frac{\hat{\mathcal{O}}_i}{\langle \hat{\mathcal{O}}_i \rangle} \frac{\hat{\mathcal{O}}_j}{\langle \hat{\mathcal{O}}_j \rangle} (1 - \delta_{ij}) - (m+1) \sum_{i=1}^{m+3} \frac{\hat{\mathcal{O}}_i}{\langle \hat{\mathcal{O}}_i \rangle} + \frac{(m+1)}{2}(m+2) \right] \prod_{k=1}^{m+3} \langle \hat{\mathcal{O}}_k \rangle. \quad (\text{C.18})$$

Let us focus on the right-hand side of Eq. (C.18). Separating the  $m + 3$  contribution in the sums we can write:

$$\begin{aligned}\text{RHS} &= \left[ \frac{1}{2} \sum_{i=1}^{m+2} \sum_{j=1}^{m+2} \frac{\hat{\mathcal{O}}_i}{\langle \hat{\mathcal{O}}_i \rangle} \frac{\hat{\mathcal{O}}_j}{\langle \hat{\mathcal{O}}_j \rangle} (1 - \delta_{ij}) + \frac{\hat{\mathcal{O}}_{m+3}}{\langle \hat{\mathcal{O}}_{m+3} \rangle} \sum_{i=1}^{m+2} \frac{\hat{\mathcal{O}}_i}{\langle \hat{\mathcal{O}}_i \rangle} \right. \\ &\quad \left. - (m+1) \sum_{i=1}^{m+2} \frac{\hat{\mathcal{O}}_i}{\langle \hat{\mathcal{O}}_i \rangle} - (m+1) \frac{\hat{\mathcal{O}}_{m+3}}{\langle \hat{\mathcal{O}}_{m+3} \rangle} + \frac{(m+1)}{2}(m+2) \right] \prod_{k=1}^{m+3} \langle \hat{\mathcal{O}}_k \rangle. \quad (\text{C.19})\end{aligned}$$

The left-hand side of Eq. (C.18) can be written:

$$\begin{aligned}\text{LHS} &= \prod_{i=1}^{m+3} \hat{\mathcal{O}}_i \\ &= \prod_{i=1}^{m+2} \hat{\mathcal{O}}_i \hat{\mathcal{O}}_{m+3} \\ &= \left[ \frac{1}{2} \sum_{i=1}^{m+2} \sum_{j=1}^{m+2} \frac{\hat{\mathcal{O}}_i}{\langle \hat{\mathcal{O}}_i \rangle} \frac{\hat{\mathcal{O}}_j}{\langle \hat{\mathcal{O}}_j \rangle} (1 - \delta_{ij}) - m \sum_{i=1}^{m+2} \frac{\hat{\mathcal{O}}_i}{\langle \hat{\mathcal{O}}_i \rangle} + \frac{m}{2}(m+1) \right] \prod_{k=1}^{m+2} \langle \hat{\mathcal{O}}_k \rangle \hat{\mathcal{O}}_{m+3}, \quad (\text{C.20})\end{aligned}$$

$$\begin{aligned} \text{LHS} = & \left[ \frac{1}{2} \sum_{i=1}^{m+2} \sum_{j=1}^{m+2} \frac{\hat{\mathcal{O}}_i}{\langle \hat{\mathcal{O}}_i \rangle} \frac{\hat{\mathcal{O}}_j}{\langle \hat{\mathcal{O}}_j \rangle} \frac{\hat{\mathcal{O}}_{m+3}}{\langle \hat{\mathcal{O}}_{m+3} \rangle} (1 - \delta_{ij}) \right. \\ & \left. - m \sum_{i=1}^{m+2} \frac{\hat{\mathcal{O}}_i}{\langle \hat{\mathcal{O}}_i \rangle} \frac{\hat{\mathcal{O}}_{m+3}}{\langle \hat{\mathcal{O}}_{m+3} \rangle} + \frac{m}{2} (m+1) \frac{\hat{\mathcal{O}}_{m+3}}{\langle \hat{\mathcal{O}}_{m+3} \rangle} \right] \prod_{k=1}^{m+3} \langle \hat{\mathcal{O}}_k \rangle. \end{aligned} \quad (\text{C.21})$$

Here, we separated the  $i = m + 3$  contribution of the product and used Eq. (C.17). Consider the first term inside the brackets,  $t$ :

$$t = \frac{1}{2} \sum_{i=1}^{m+2} \sum_{j=1}^{m+2} \frac{\hat{\mathcal{O}}_i}{\langle \hat{\mathcal{O}}_i \rangle} \frac{\hat{\mathcal{O}}_j}{\langle \hat{\mathcal{O}}_j \rangle} \frac{\hat{\mathcal{O}}_{m+3}}{\langle \hat{\mathcal{O}}_{m+3} \rangle} (1 - \delta_{ij}). \quad (\text{C.22})$$

Using Eq. (C.16), we can write  $t$  as:

$$\begin{aligned} t = & \frac{1}{2} \sum_{i=1}^{m+2} \sum_{j=1}^{m+2} \frac{1}{\langle \hat{\mathcal{O}}_i \rangle} \frac{1}{\langle \hat{\mathcal{O}}_j \rangle} \frac{1}{\langle \hat{\mathcal{O}}_{m+3} \rangle} (1 - \delta_{ij}) \left\{ \hat{\mathcal{O}}_i \hat{\mathcal{O}}_j \langle \hat{\mathcal{O}}_{m+3} \rangle + \hat{\mathcal{O}}_{m+3} \hat{\mathcal{O}}_i \langle \hat{\mathcal{O}}_j \rangle + \hat{\mathcal{O}}_j \hat{\mathcal{O}}_{m+3} \langle \hat{\mathcal{O}}_i \rangle \right. \\ & - \hat{\mathcal{O}}_i \langle \hat{\mathcal{O}}_j \rangle \langle \hat{\mathcal{O}}_{m+3} \rangle - \hat{\mathcal{O}}_{m+3} \langle \hat{\mathcal{O}}_i \rangle \langle \hat{\mathcal{O}}_j \rangle \\ & \left. - \hat{\mathcal{O}}_j \langle \hat{\mathcal{O}}_{m+3} \rangle \langle \hat{\mathcal{O}}_i \rangle + \langle \hat{\mathcal{O}}_i \rangle \langle \hat{\mathcal{O}}_j \rangle \langle \hat{\mathcal{O}}_{m+3} \rangle \right\}. \end{aligned} \quad (\text{C.23})$$

After some straightforward algebra, we can write:

$$\begin{aligned} t = & \frac{1}{2} \sum_{i=1}^{m+2} \sum_{j=1}^{m+2} \frac{\hat{\mathcal{O}}_i}{\langle \hat{\mathcal{O}}_i \rangle} \frac{\hat{\mathcal{O}}_j}{\langle \hat{\mathcal{O}}_j \rangle} (1 - \delta_{ij}) + \frac{\hat{\mathcal{O}}_{m+3}}{\langle \hat{\mathcal{O}}_{m+3} \rangle} \sum_{i=1}^{m+2} \sum_{j=1}^{m+2} \frac{\hat{\mathcal{O}}_i}{\langle \hat{\mathcal{O}}_i \rangle} (1 - \delta_{ij}) \\ & - \sum_{i=1}^{m+2} \sum_{j=1}^{m+2} \frac{\hat{\mathcal{O}}_i}{\langle \hat{\mathcal{O}}_i \rangle} (1 - \delta_{ij}) - \frac{1}{2} \frac{\hat{\mathcal{O}}_{m+3}}{\langle \hat{\mathcal{O}}_{m+3} \rangle} \sum_{i=1}^{m+2} \sum_{j=1}^{m+2} (1 - \delta_{ij}) + \frac{1}{2} \sum_{i=1}^{m+2} \sum_{j=1}^{m+2} (1 - \delta_{ij}). \end{aligned} \quad (\text{C.24})$$

Using:

$$\sum_{i=1}^{m+2} \sum_{j=1}^{m+2} \frac{\hat{\mathcal{O}}_i}{\langle \hat{\mathcal{O}}_i \rangle} (1 - \delta_{ij}) = (m+1) \sum_{i=1}^{m+2} \frac{\hat{\mathcal{O}}_i}{\langle \hat{\mathcal{O}}_i \rangle}, \quad (\text{C.25})$$

$$\sum_{i=1}^{m+2} \sum_{j=1}^{m+2} (1 - \delta_{ij}) = (m+2)(m+1), \quad (\text{C.26})$$

we can finally write:

$$\begin{aligned} t = & \frac{1}{2} \sum_{i=1}^{m+2} \sum_{j=1}^{m+2} \frac{\hat{\mathcal{O}}_i}{\langle \hat{\mathcal{O}}_i \rangle} \frac{\hat{\mathcal{O}}_j}{\langle \hat{\mathcal{O}}_j \rangle} (1 - \delta_{ij}) + \frac{\hat{\mathcal{O}}_{m+3}}{\langle \hat{\mathcal{O}}_{m+3} \rangle} (m+1) \sum_{i=1}^{m+2} \frac{\hat{\mathcal{O}}_i}{\langle \hat{\mathcal{O}}_i \rangle} \\ & - (m+1) \sum_{i=1}^{m+2} \frac{\hat{\mathcal{O}}_i}{\langle \hat{\mathcal{O}}_i \rangle} - \frac{1}{2} (m+2)(m+1) \frac{\hat{\mathcal{O}}_{m+3}}{\langle \hat{\mathcal{O}}_{m+3} \rangle} + \frac{1}{2} (m+2)(m+1). \end{aligned} \quad (\text{C.27})$$

The left-hand side of Eq. (C.18) can finally be written as:

$$\begin{aligned} \text{LHS} &= \left[ \frac{1}{2} \sum_{i=1}^{m+2} \sum_{j=1}^{m+2} \frac{\hat{\mathcal{O}}_i}{\langle \hat{\mathcal{O}}_i \rangle} \frac{\hat{\mathcal{O}}_j}{\langle \hat{\mathcal{O}}_j \rangle} (1 - \delta_{ij}) + \frac{\hat{\mathcal{O}}_{m+3}}{\langle \hat{\mathcal{O}}_{m+3} \rangle} \sum_{i=1}^{m+2} \frac{\hat{\mathcal{O}}_i}{\langle \hat{\mathcal{O}}_i \rangle} \right. \\ &\quad \left. - (m+1) \sum_{i=1}^{m+2} \frac{\hat{\mathcal{O}}_i}{\langle \hat{\mathcal{O}}_i \rangle} - (m+1) \frac{\hat{\mathcal{O}}_{m+3}}{\langle \hat{\mathcal{O}}_{m+3} \rangle} + \frac{(m+1)}{2} (m+2) \right] \prod_{k=1}^{m+3} \langle \hat{\mathcal{O}}_k \rangle \\ &= \text{RHS}. \end{aligned} \tag{C.28}$$

Hence, the left-hand side is equivalent to the right-hand side given in Eq. (C.19), the formula also holds for  $n = m + 1$ , completing the inductive step. Hence, by mathematical induction, Eq. (C.15) is valid for  $n \geq 1$ .

## Appendix D

# Grand canonical potential for fermions in the mean field approximation

In this work we study fermionic systems in the mean field approximation. In such scheme, the Lagrangian density of the system can be written as the one of quasiparticles with an effective mass, effective chemical potential and effective potential, that accounts for the interaction at mean field level. One can always write the Lagrangian density of such a system in the following way<sup>1</sup>:

$$\begin{aligned}\mathcal{L} &= \bar{\psi} \left[ i\gamma^\mu \left( \partial_\mu + iV_0\delta_\mu^0 \right) - (\hat{m} + S) \right] \psi + U(V_0, S) \\ &= \bar{\psi} (i\mathcal{D} - \hat{M}) \psi + U.\end{aligned}\tag{D.1}$$

Here,  $\mathcal{D}_\mu = \partial_\mu + iV_0\delta_\mu^0$ , can be interpreted as a covariant derivative and  $\hat{M} = \hat{m} + S$  as an effective mass. The field variables  $V_0$  and  $S$ , are the ground state of some homogeneous fields  $V_\mu(x)$  and  $S(x)$ , i.e.,  $\langle V_0 \rangle = V_0$  and  $\langle S \rangle = S$ . In the mean field approximation, the system is in equilibrium and dynamic currents are not considered, i.e.,  $\langle V_i \rangle = 0$ . The mean field potential  $U(V_0, S)$  is independent from the fermion field and from spacetime, but may depend on the ground state of the auxiliary fields. The fermion field  $\psi(x)$ , as well as the auxiliary fields and effective mass, may have several indices like flavour ( $f$ ) or colour ( $c$ ), which will be denoted by  $I = \{f, c, \dots\}$ .

Following Noether's theorem, an invariance of the Lagrangian under a global symmetry leads to a conserved current. In this case the conserved current is  $j^\mu = \bar{\psi}\gamma^\mu\psi$ , with a corresponding conserved charge given by  $Q = \int_V dV \bar{\psi}\gamma^0\psi$ . The presence of a conserved charge allows the addition of a chemical potential  $\hat{\mu}$ , to the system. Here, we consider the chemical potential as a diagonal matrix in the space of the internal indices,  $I$ . The partition function in the imaginary

---

<sup>1</sup>This derivation is a generalization of the derivation performed in [338].

time formalism is:

$$\begin{aligned}
\mathcal{Z} &= \mathcal{N} \int \mathcal{D}\bar{\psi}(\tau, \mathbf{x}) \mathcal{D}\psi(\tau, \mathbf{x}) e^{\mathcal{S}_E[\bar{\psi}, \psi]} \\
&= \mathcal{N} \int \mathcal{D}\bar{\psi} \mathcal{D}\psi \exp \left[ \int_0^\beta d\tau \int_V d^3x \left( \mathcal{L} + \hat{\mu} \bar{\psi} \gamma^0 \psi \right) \right] \\
&= \mathcal{N} \int \mathcal{D}\bar{\psi} \mathcal{D}\psi \exp \left[ \int_0^\beta d\tau \int_V d^3x \left( \bar{\psi} D \psi + U \right) \right], \tag{D.2}
\end{aligned}$$

the functional integration is to be made over  $\bar{\psi}$  and  $\psi$  (considered as independent fields) and  $\mathcal{S}_E$ , is the Euclidean action. Here, was defined the operator  $D$  and the effective chemical potential  $\tilde{\mu}$ :

$$D = i\gamma^\mu \partial_\mu - \hat{M} + \tilde{\mu} \gamma^0, \tag{D.3}$$

$$\tilde{\mu} = \hat{\mu} - V_0. \tag{D.4}$$

The fermion field can be expressed as:

$$\psi(\tau, \mathbf{x}) = \langle \tau, \mathbf{x} | \psi \rangle = \sum_{n, \mathbf{p}=-\infty}^{+\infty} \langle \tau, \mathbf{x} | \omega_n, \mathbf{p} \rangle \langle \omega_n, \mathbf{p} | \psi \rangle = \frac{1}{\sqrt{\beta V}} \sum_{n, \mathbf{p}=-\infty}^{+\infty} e^{i(\mathbf{p} \cdot \mathbf{x} + \omega_n \tau)} \hat{\psi}_n(\mathbf{p}), \tag{D.5}$$

where  $\omega_n = (2n + 1) \pi / \beta$  are the allowed Matsubara frequencies for fermions. Fourier transforming the fields using (D.5), gives a discrete version of the action in the  $(\omega_n, \mathbf{p})$ -space (the sum's bounds are omitted for simplicity):

$$\mathcal{S}_E[\bar{\psi}, \psi] = \int_0^\beta d\tau \int_V d^3x \left[ U + \frac{1}{\beta V} \sum_{m, \mathbf{q}} e^{-i(\mathbf{q} \cdot \mathbf{x} + \omega_m \tau)} \hat{\bar{\psi}}_m(\mathbf{q}) D \sum_{n, \mathbf{p}} e^{i(\mathbf{p} \cdot \mathbf{x} + \omega_n \tau)} \hat{\psi}_n(\mathbf{p}) \right]. \tag{D.6}$$

The action of the operator  $D$  in the discrete fermion field  $\hat{\psi}_n(\mathbf{p})$  is:

$$\begin{aligned}
D \sum_{n, \mathbf{p}} e^{i(\mathbf{p} \cdot \mathbf{x} + \omega_n \tau)} \hat{\psi}_n(\mathbf{p}) &= \sum_{n, \mathbf{p}} e^{i(\mathbf{p} \cdot \mathbf{x} + \omega_n \tau)} \left[ - \left( \gamma^0 i \frac{\partial}{\partial \tau} \omega_n \tau + \gamma^i p^j \frac{\partial}{\partial x^i} x_j \right) - \hat{M} + \tilde{\mu} \gamma^0 \right] \hat{\psi}_n(\mathbf{p}) \\
&= \sum_{n, \mathbf{p}} e^{i(\mathbf{p} \cdot \mathbf{x} + \omega_n \tau)} \hat{D} \hat{\psi}_n(\mathbf{p}). \tag{D.7}
\end{aligned}$$

The operator  $\hat{D}$  is defined as:

$$\hat{D} = -i\omega_n \gamma^0 - \gamma^j p_j - \hat{M} + \tilde{\mu} \gamma^0. \tag{D.8}$$

Inserting this results in the discrete action in Eq. (D.6), making the integral over the mean field potential (independent from spacetime) and applying the relations:

$$\int_0^\beta d\tau e^{i\tau(\omega_n - \omega_m)} = \beta \delta(\omega_n - \omega_m), \tag{D.9}$$

$$\int_V d^3x e^{i\mathbf{x} \cdot (\mathbf{p} - \mathbf{q})} = V \delta^{(3)}(\mathbf{p} - \mathbf{q}), \tag{D.10}$$

yields:

$$\mathcal{S}_E[\bar{\psi}, \psi] = \beta V U + \sum_{n, \mathbf{p}} \hat{\bar{\psi}}_n(\mathbf{p}) \hat{D} \hat{\psi}_n(\mathbf{p}). \quad (\text{D.11})$$

Assuming that any changes caused by the Fourier transformation on the integral measure  $\mathcal{D}\bar{\psi}\mathcal{D}\psi$ , can be absorbed in a new normalization constant,  $\mathcal{N}'$ , we write:

$$\begin{aligned} \mathcal{Z} &= \mathcal{N}' e^{\beta V U} \int \mathcal{D}\hat{\bar{\psi}}(\omega_n, \mathbf{p}) \mathcal{D}\hat{\psi}(\omega_n, \mathbf{p}) \exp \left[ \sum_{n, \mathbf{p}} \hat{\bar{\psi}}_n(\mathbf{p}) \hat{D} \hat{\psi}_n(\mathbf{p}) \right] \\ &= \mathcal{N}' e^{\beta V U} \prod_{n, \mathbf{p}} \int d\hat{\bar{\psi}}_n d\hat{\psi}_n e^{\hat{\bar{\psi}}_n(\mathbf{p}) \hat{D} \hat{\psi}_n(\mathbf{p})}. \end{aligned} \quad (\text{D.12})$$

Using the known result for  $N$  Grassmann variables,  $\int d\xi_1^\dagger d\xi_1 \dots d\xi_N^\dagger d\xi_N e^{\xi^\dagger D \xi} = \det D$ , we are able to do the integral in Eq. (D.12) to yield:

$$\mathcal{Z} = \mathcal{N}' e^{\beta V U} \det_{n, \mathbf{p}, d, I} \hat{D}. \quad (\text{D.13})$$

This determinant is usually called the fermionic determinant and it must be computed over all indices (Dirac, momentum, frequency and, the set of internal indices,  $I$ ).

Ignoring a constant term, the grand canonical potential can finally be written as<sup>2</sup>:

$$\Omega = -\frac{T}{V} \ln [\mathcal{Z}] = -U - \frac{T}{V} \ln \det_{n, \mathbf{p}, d, I} \hat{D} = -U - \frac{T}{V} \text{tr}_{n, \mathbf{p}, I} \left( \ln \det_d \hat{D} \right). \quad (\text{D.14})$$

The determinant over the Dirac space can be easily calculated by choosing a specific representation for the gamma matrices. Using the Dirac basis for the Dirac matrices (see the Appendix A.4), the operator  $\hat{D}$  is:

$$\hat{D} = -i\omega_n \gamma^0 - \gamma^j p_j - \hat{M} + \tilde{\mu} \gamma^0 = \begin{pmatrix} -i\omega_n - \hat{M} + \tilde{\mu} & -\boldsymbol{\sigma} \cdot \mathbf{p} \\ \boldsymbol{\sigma} \cdot \mathbf{p} & i\omega_n - \hat{M} - \tilde{\mu} \end{pmatrix}. \quad (\text{D.15})$$

Evaluating the determinant and substituting it in Eq. (D.14) yields:

$$\Omega = -U - \frac{T}{V} \text{tr}_{n, \mathbf{p}, I} \left[ \ln \left( E^2 + (\omega_n + i\tilde{\mu})^2 \right)^2 \right]. \quad (\text{D.16})$$

Where  $E = \sqrt{p^2 + \hat{M}^2}$ . Making the allowed substitution,  $\omega_n \rightarrow -\omega_n$ , and carrying out some simple calculations, one can get:

$$\Omega = -U - \frac{T}{V} \text{tr}_I \sum_{\mathbf{p}=-\infty}^{+\infty} \sum_{n=-\infty}^{+\infty} \left[ \ln \left( \omega_n^2 + (E + \tilde{\mu})^2 \right) + \ln \left( \omega_n^2 + (E - \tilde{\mu})^2 \right) \right]. \quad (\text{D.17})$$

<sup>2</sup>Applying the identity:  $\ln \det A = \text{tr} \ln A$ .

Remembering that  $\omega_n = (2n + 1)\pi T$ , the Matsubara summation can be calculated using several methods to yield the following result (ignoring a possible constant [339, 340]):

$$\sum_{n=-\infty}^{+\infty} \ln \left( \omega_n^2 + (E \pm \tilde{\mu})^2 \right) = \beta(E \pm \tilde{\mu}) + 2 \ln \left( 1 + e^{-\beta(E \pm \tilde{\mu})} \right). \quad (\text{D.18})$$

Substituting this result and taking the continuum limit<sup>3</sup>, the grand canonical potential (D.17) yields:

$$\Omega(T, \mu) = \Omega_0 - U(V_0, S) - 2T \operatorname{tr}_I \int \frac{d^3 p}{(2\pi)^3} \left[ \beta E + \ln \left( 1 + e^{-\beta(E + \tilde{\mu})} \right) + \ln \left( 1 + e^{-\beta(E - \tilde{\mu})} \right) \right]. \quad (\text{D.19})$$

Here  $\Omega_0$  is a constant, which can be chosen in order to make the pressure vanish in the vacuum. The trace operation over the indices  $I$  must be done if the field has any additional index otherwise, it simply yields 1. The factor of 2 represents the spin degeneracy of the  $1/2$  spin particles (fermions). There is a contribution from the vacuum energy  $\beta E$ , and a term for particles (positive chemical potential) and another for antiparticles (negative chemical potential).

We can relate the grand canonical potential of a field theory (D.14), with the theory's effective action in the imaginary time formalism. Their definitions suggest that one can write the grand canonical potential of a theory with a set of fields  $\phi$  as  $\Omega[\phi] \propto \Gamma[\phi]$ . The effective action must be stationary in relation to the fields,  $\phi$ . The ground state value of the fields,  $\phi_c$ , can be derived from this requirement. Hence, the thermodynamical potential must also be stationary to any fields present and we can write:

$$\left. \frac{\delta \Omega[\phi]}{\delta \phi} \right|_{\phi=\phi_c} = 0. \quad (\text{D.20})$$

Applying this condition to the fields  $S$  and  $V_0$  of Eq. (D.19) yields a self-consistent equation, which allow to calculate their values for a given temperature and chemical potential. The relation (D.20) is also called thermodynamic consistency relation.

---

<sup>3</sup>The sum over momentum can be replaced by an integral:  $\frac{1}{V} \sum_{\mathbf{p}=-\infty}^{+\infty} \rightarrow \int \frac{d^3 p}{(2\pi)^3}$ .

## Appendix E

### $f_0(S)$ loop function

The thermal loop function  $f_0(S)$  is defined as:

$$f_0(S) = \int \frac{d^4k}{(2\pi)^4} \frac{1}{k^2 + S^2}. \quad (\text{E.1})$$

We can separate the time dependence by defining,  $E_{\mathbf{k}}^2 = \mathbf{k}^2 + S^2$ . We write:

$$f_0(S) = \int \frac{d^3k}{(2\pi)^3} \int \frac{dk_0}{2\pi} \frac{1}{k_0^2 + E_{\mathbf{k}}^2} = \int \frac{d^3k}{(2\pi)^3} g_0(S, \mathbf{k}). \quad (\text{E.2})$$

To perform the integration over  $k_0$ , we write the integral as a sum over the allowed Matsubara frequencies,  $\omega_n = (2n+1)\pi/\beta$ ,  $n \in \mathbb{Z}$ , for fermionic fields. We write:

$$g_0(S, \mathbf{k}) = \int \frac{dk_0}{2\pi} \frac{1}{k_0^2 + E_{\mathbf{k}}^2} = \frac{1}{\beta} \sum_{n=-\infty}^{\infty} \frac{1}{\omega_n^2 + E_{\mathbf{k}}^2}. \quad (\text{E.3})$$

It can be shown that, for a system at finite density, the chemical potential can easily be introduced in this step of the calculation. If the chemical potential matrix in flavour space  $\hat{\mu}$ , at the Lagrangian level, is diagonal and degenerate i.e.,  $\hat{\mu} = \text{diag}(\mu_1, \dots, \mu_{N_f}) = \text{diag}(\mu, \dots, \mu)$ , the simple substitution [341]:

$$\omega_n \rightarrow \omega_n + i\mu, \quad (\text{E.4})$$

includes density effects in the calculation. The present work deals with meson loops, in which bosonic Matsubara sums have also to be considered. Hence, we remark that only fermionic frequencies must be altered by this recipe, since the simple bosonic field does not have any conserved charged associated to it. This yields:

$$g_0(S, \mathbf{k}) = \frac{1}{\beta} \sum_{n=-\infty}^{\infty} \frac{1}{(\omega_n + i\mu)^2 + E_{\mathbf{k}}^2}. \quad (\text{E.5})$$

To evaluate the sum we use the usual contour technique ( $\omega_n \rightarrow -iw$ , for more details see Appendix A.5):

$$g_0(S, \mathbf{k}) = -\frac{1}{\beta} \oint_{C_2} \frac{dw}{2\pi i} \frac{1}{(-iw + i\mu)^2 + E_{\mathbf{k}}^2} \frac{\beta}{2} \tanh\left(\frac{\beta w}{2}\right). \quad (\text{E.6})$$

Defining the integrand as a function of the integration variable,  $w$ , we can write it as:

$$h_0(w) = \frac{1}{2} \frac{1}{(w - \mu)^2 - E_{\mathbf{k}}^2} \tanh\left(\frac{\beta w}{2}\right) \quad (\text{E.7})$$

The off-imaginary axis poles of the integrand are given by the zeroes of denominator. We note that all poles are of order one. The poles are:  $w = \pm E_{\mathbf{k}} + \mu$ . The denominator in  $h_0(w)$ , can be written as:

$$(w - \mu)^2 - E_{\mathbf{k}}^2 = (w - \mu - E_{\mathbf{k}})(w - \mu + E_{\mathbf{k}}). \quad (\text{E.8})$$

The residues at the poles  $w = \pm E_{\mathbf{k}} + \mu$ , are:

$$\text{Res}(h_0, +E_{\mathbf{k}} + \mu) = \frac{1}{2} \frac{1}{2E_{\mathbf{k}}} \tanh\left(\frac{\beta(E_{\mathbf{k}} + \mu)}{2}\right) = \frac{1}{4E_{\mathbf{k}}} (1 - 2n_{\text{F}}(E_{\mathbf{k}} + \mu)). \quad (\text{E.9})$$

$$\text{Res}(h_0, -E_{\mathbf{k}} + \mu) = \frac{1}{2} \frac{1}{-2E_{\mathbf{k}}} \tanh\left(\frac{-\beta(E_{\mathbf{k}} - \mu)}{2}\right) = \frac{1}{4E_{\mathbf{k}}} (1 - 2n_{\text{F}}(E_{\mathbf{k}} - \mu)). \quad (\text{E.10})$$

The loop function  $f_0(S)$  is finally given by:

$$f_0(S) = \int \frac{d^3k}{(2\pi)^3} \frac{1}{2E_{\mathbf{k}}} [1 - n_{\text{F}}(E_{\mathbf{k}} + \mu) - n_{\text{F}}(E_{\mathbf{k}} - \mu)]. \quad (\text{E.11})$$

## Appendix F

### $f_1(S, q)$ loop function

The thermal loop function  $f_1(S, q)$  is defined as:

$$f_1(S, q) = \int \frac{d^4k}{(2\pi)^4} \frac{1}{((k-q)^2 + S^2)(k^2 + S^2)}. \quad (\text{F.1})$$

We can separate the time dependence by defining,  $E_{\mathbf{k}}^2 = \mathbf{k}^2 + S^2$  and  $E_{\mathbf{k}-\mathbf{q}}^2 = (\mathbf{k} - \mathbf{q})^2 + S^2$ . We write:

$$f_1(S, \mathbf{q}, q_0) = \int \frac{d^3k}{(2\pi)^3} \int \frac{dk_0}{2\pi} \frac{1}{((k_0 - q_0)^2 + E_{\mathbf{k}-\mathbf{q}}^2)(k_0^2 + E_{\mathbf{k}}^2)} = \int \frac{d^3k}{(2\pi)^3} g_1(S, \mathbf{q}, q_0, \mathbf{k}). \quad (\text{F.2})$$

To perform the integration over  $k_0$ , we write the integral as a sum over the allowed Matsubara frequencies,  $\omega_n = (2n+1)\pi/\beta$ ,  $n \in \mathbb{Z}$ , for fermionic fields. We write:

$$g_1(S, \mathbf{q}, q_0, \mathbf{k}) = \int \frac{dk_0}{2\pi} \frac{1}{((k_0 - q_0)^2 + E_{\mathbf{k}-\mathbf{q}}^2)(k_0^2 + E_{\mathbf{k}}^2)} = \frac{1}{\beta} \sum_{n=-\infty}^{\infty} \frac{1}{((\omega_n - q_0)^2 + E_{\mathbf{k}-\mathbf{q}}^2)(\omega_n^2 + E_{\mathbf{k}}^2)}. \quad (\text{F.3})$$

To include the chemical potential in this calculation, we follow the previous section and use Eq. (E.4). Making the proper substitutions, it yields:

$$g_1(S, \mathbf{q}, q_0, \mathbf{k}) = \frac{1}{\beta} \sum_{n=-\infty}^{\infty} \frac{1}{((\omega_n + i\mu - q_0)^2 + E_{\mathbf{k}-\mathbf{q}}^2)((\omega_n + i\mu)^2 + E_{\mathbf{k}}^2)}. \quad (\text{F.4})$$

To calculate the sum we use the usual contour technique ( $\omega_n \rightarrow -iw$ , for more details see A.5):

$$g_1(S, \mathbf{q}, q_0, \mathbf{k}) = -\frac{1}{\beta} \oint_{C_2} \frac{dw}{2\pi i} \frac{1}{((-iw + i\mu - q_0)^2 + E_{\mathbf{k}-\mathbf{q}}^2)((-iw + i\mu)^2 + E_{\mathbf{k}}^2)} \frac{\beta}{2} \tanh\left(\frac{\beta w}{2}\right). \quad (\text{F.5})$$

To evaluate the integral we proceed to apply Cauchy's residue theorem, calculating the sum of residues at each pole. For simplicity, we define the integrand<sup>1</sup> only as a function of the integration

<sup>1</sup>We ignore the factor  $2\pi i$  in the integrand since it cancels with the same factor in Cauchy's residue theorem.

variable,  $w$ :

$$h_1(w) = -\frac{1}{2} \frac{1}{((w - \mu - iq_0)^2 - E_{\mathbf{k}-q}^2)((w - \mu)^2 - E_{\mathbf{k}}^2)} \tanh\left(\frac{\beta w}{2}\right). \quad (\text{F.6})$$

The denominator in the above can be written as:

$$\begin{aligned} ((w - \mu - iq_0)^2 - E_{\mathbf{k}-q}^2)((w - \mu)^2 - E_{\mathbf{k}}^2) &= (w - \mu - iq_0 - E_{\mathbf{k}-q})(w - \mu - iq_0 + E_{\mathbf{k}-q}) \\ &\quad \times (w - \mu - E_{\mathbf{k}})(w - \mu + E_{\mathbf{k}}). \end{aligned} \quad (\text{F.7})$$

The off-imaginary axis poles of the integrand are then given by the zeroes of Eq. (F.7). We note that all poles are of order one. The poles are:  $w = iq_0 \pm E_{\mathbf{k}-q} + \mu$  and  $w = \pm E_{\mathbf{k}} + \mu$ . In the residue calculation, we will use the following definitions,

$$E_+ \equiv E_+(S, \mathbf{q}, \mathbf{k}) = E_{\mathbf{k}} + E_{\mathbf{k}-q}, \quad (\text{F.8})$$

$$E_- \equiv E_-(S, \mathbf{q}, \mathbf{k}) = E_{\mathbf{k}} - E_{\mathbf{k}-q} \quad (\text{F.9})$$

and properties:  $\tanh(-z) = -\tanh(z)$  and  $\tanh\left(\frac{\beta z}{2}\right) = 1 - 2n_{\text{F}}(z) = 1 - \frac{2}{e^{\beta z} + 1}$ , where  $n_{\text{F}}(z)$  is the Fermi–Dirac distribution.

The residues at the poles  $w = \pm E_{\mathbf{k}} + \mu$ , are:

$$\begin{aligned} \text{Res}(h_1, +E_{\mathbf{k}} + \mu) &= \frac{-1}{2} \frac{1}{2E_{\mathbf{k}}(E_{\mathbf{k}} - iq_0)^2 - E_{\mathbf{k}-q}^2} \tanh\left(\frac{\beta(E_{\mathbf{k}} + \mu)}{2}\right) \\ &= \frac{1}{8E_{\mathbf{k}}E_{\mathbf{k}-q}} \left[ \frac{1}{iq_0 - E_+} - \frac{1}{iq_0 - E_-} \right] (2n_{\text{F}}(E_{\mathbf{k}} + \mu) - 1), \end{aligned} \quad (\text{F.10})$$

$$\begin{aligned} \text{Res}(h_1, -E_{\mathbf{k}} + \mu) &= \frac{-1}{2} \frac{1}{-2E_{\mathbf{k}}(E_{\mathbf{k}} + iq_0)^2 - E_{\mathbf{k}-q}^2} \tanh\left(\frac{-\beta(E_{\mathbf{k}} - \mu)}{2}\right) \\ &= \frac{1}{8E_{\mathbf{k}}E_{\mathbf{k}-q}} \left[ \frac{1}{iq_0 + E_-} - \frac{1}{iq_0 + E_+} \right] (2n_{\text{F}}(E_{\mathbf{k}} - \mu) - 1), \end{aligned} \quad (\text{F.11})$$

When calculating the remaining residues, we will have contributions proportional to

$$\tanh\left(\frac{\beta iq_0 + \beta E_{\mathbf{k}-q}}{2}\right) = 1 - 2n_{\text{F}}(iq_0 + E_{\mathbf{k}-q}), \quad (\text{F.12})$$

where  $n_{\text{F}}(iq_0 + E_{\mathbf{k}-q}) = 1/(e^{\beta iq_0} e^{\beta E_{\mathbf{k}-q}} + 1)$ . The variable  $q_0$  corresponds to the Matsubara frequency of the external particle. In this case, the external particles are bosons (sigma and pions mesons). Hence  $q_0 = 2n\pi/\beta$ ,  $n \in \mathbb{Z}$ . We can then make use of Euler's identity and write:

$$n_{\text{F}}(iq_0 + E_{\mathbf{k}-q}) = \frac{1}{e^{\beta iq_0} e^{\beta E_{\mathbf{k}-q}} + 1} = \frac{1}{e^{\beta E_{\mathbf{k}-q}} + 1} = n_{\text{F}}(E_{\mathbf{k}-q}). \quad (\text{F.13})$$

In the case of fermionic external particle extra minus signs would appear. This can also be

seen from the fact that  $\tanh(z)$  is periodic in  $z$  with period  $i\pi$ . For the  $q_0$  mentioned above,  $\tanh\left(z + \frac{\beta iq_0}{2}\right) = \tanh(z + in\pi) = \tanh(z)$ .

The residues at the poles  $w = iq_0 \pm E_{\mathbf{k}-q} + \mu$ , are:

$$\begin{aligned} \text{Res}(h_1, iq_0 + E_{\mathbf{k}-q} + \mu) &= \frac{-1}{2} \frac{1}{2E_{\mathbf{k}-q}} \frac{1}{(iq_0 + E_{\mathbf{k}-q})^2 - E_{\mathbf{k}}^2} \tanh\left(\frac{\beta(iq_0 + E_{\mathbf{k}-q} + \mu)}{2}\right) \\ &= \frac{1}{8E_{\mathbf{k}}E_{\mathbf{k}-q}} \left[ \frac{1}{iq_0 - E_-} - \frac{1}{iq_0 + E_+} \right] (2n_{\text{F}}(E_{\mathbf{k}-q} + \mu) - 1), \end{aligned} \quad (\text{F.14})$$

$$\begin{aligned} \text{Res}(h_1, iq_0 - E_{\mathbf{k}-q} + \mu) &= \frac{-1}{2} \frac{1}{-2E_{\mathbf{k}-q}} \frac{1}{(iq_0 - E_{\mathbf{k}-q})^2 - E_{\mathbf{k}}^2} \tanh\left(\frac{\beta(iq_0 - E_{\mathbf{k}-q} + \mu)}{2}\right) \\ &= \frac{1}{8E_{\mathbf{k}}E_{\mathbf{k}-q}} \left[ \frac{1}{iq_0 - E_+} - \frac{1}{iq_0 + E_-} \right] (2n_{\text{F}}(E_{\mathbf{k}-q} - \mu) - 1). \end{aligned} \quad (\text{F.15})$$

Adding all contributions yields the final result:

$$\begin{aligned} g_1(S, \mathbf{q}, q_0, \mathbf{k}) &= \frac{1}{4E_{\mathbf{k}}E_{\mathbf{k}-q}} \left\{ \frac{[n_{\text{F}}(E_{\mathbf{k}} + \mu) + n_{\text{F}}(E_{\mathbf{k}-q} - \mu) - 1]}{iq_0 - E_+} - \frac{[n_{\text{F}}(E_{\mathbf{k}} + \mu) - n_{\text{F}}(E_{\mathbf{k}-q} + \mu)]}{iq_0 - E_-} \right. \\ &\quad \left. + \frac{[n_{\text{F}}(E_{\mathbf{k}} - \mu) - n_{\text{F}}(E_{\mathbf{k}-q} - \mu)]}{iq_0 + E_-} - \frac{[n_{\text{F}}(E_{\mathbf{k}} - \mu) + n_{\text{F}}(E_{\mathbf{k}-q} + \mu) - 1]}{iq_0 + E_+} \right\}. \end{aligned} \quad (\text{F.16})$$

In order to write the equations in a more compact way we define:

$$G_+(S, \mu) \equiv G_+(S, \mathbf{q}, \mathbf{k}, \mu) = 1 - n_{\text{F}}(E_{\mathbf{k}} - \mu) - n_{\text{F}}(E_{\mathbf{k}-q} + \mu), \quad (\text{F.17})$$

$$G_-(S, \mu) \equiv G_-(S, \mathbf{q}, \mathbf{k}, \mu) = n_{\text{F}}(E_{\mathbf{k}} + \mu) - n_{\text{F}}(E_{\mathbf{k}-q} + \mu). \quad (\text{F.18})$$

Finally,  $f_1(S, \mathbf{q}, q_0)$  is:

$$f_1(S, \mathbf{q}, q_0) = \int \frac{d^3k}{(2\pi)^3} \frac{1}{4E_{\mathbf{k}}E_{\mathbf{k}-q}} \left\{ \frac{G_+(S, \mu)}{iq_0 + E_+} - \frac{G_+(S, -\mu)}{iq_0 - E_+} + \frac{G_-(S, -\mu)}{iq_0 + E_-} - \frac{G_-(S, \mu)}{iq_0 - E_-} \right\}. \quad (\text{F.19})$$

Following [306, 307, 311], it is useful to decompose Eq. (F.19) in two different contributions as follows:

$$f_1(S, \mathbf{q}, q_0) = f_{1\text{p}}(S, \mathbf{q}, q_0) + f_{1\text{s}}(S, \mathbf{q}, q_0), \quad (\text{F.20})$$

where:

$$f_{1\text{p}}(S, \mathbf{q}, q_0) = \int \frac{d^3k}{(2\pi)^3} \frac{1}{4E_{\mathbf{k}}E_{\mathbf{k}-q}} \left\{ \frac{G_+(S, \mu)}{iq_0 + E_+} - \frac{G_+(S, -\mu)}{iq_0 - E_+} \right\}, \quad (\text{F.21})$$

$$f_{1\text{s}}(S, \mathbf{q}, q_0) = \int \frac{d^3k}{(2\pi)^3} \frac{1}{4E_{\mathbf{k}}E_{\mathbf{k}-q}} \left\{ \frac{G_-(S, -\mu)}{iq_0 + E_-} - \frac{G_-(S, \mu)}{iq_0 - E_-} \right\}. \quad (\text{F.22})$$

Each term is connected to different physical processes [306, 307, 311, 342]: the so-called pair-creation and annihilation process, related to  $f_{1p}(S, \mathbf{q}, q_0)$ , and the scattering process (also called absorption/emission mode), related to  $f_{1s}(S, \mathbf{q}, q_0)$ .

The variable  $q_0$  is complex. In the calculations, we will be interested in the case where  $q_0$  is a pure imaginary number hence, we consider Wick rotation,  $q_0 = -i\omega$ , for real  $\omega$ . We define:

$$F(S, \mathbf{q}, \omega) = f_1(S, \mathbf{q}, -i\omega) = F_p(S, \mathbf{q}, \omega) + F_s(S, \mathbf{q}, \omega). \quad (\text{F.23})$$

Where,

$$F_p(S, \mathbf{q}, \omega) = \int \frac{d^3k}{(2\pi)^3} \frac{1}{4E_k E_{k-q}} \left\{ \frac{G_+(S, \mu)}{\omega + E_+} - \frac{G_+(S, -\mu)}{\omega - E_+} \right\}, \quad (\text{F.24})$$

$$F_s(S, \mathbf{q}, \omega) = \int \frac{d^3k}{(2\pi)^3} \frac{1}{4E_k E_{k-q}} \left\{ \frac{G_-(S, -\mu)}{\omega + E_-} - \frac{G_-(S, \mu)}{\omega - E_-} \right\}. \quad (\text{F.25})$$

One important observation regarding the vacuum limit of  $F(S, \mathbf{q}, \omega)$ , is that, in this limit ( $T = \mu = 0$ ), the scattering contribution,  $F_s(S, \mathbf{q}, \omega)$ , is zero while the pair creation/annihilation term,  $F_p(S, \mathbf{q}, \omega)$ , is non-zero. Such behaviour is expected since, only in the medium, at finite temperature and/or density (chemical potential), there will be matter available for scattering processes. In the vacuum, only the creation/annihilation of pairs occur.

## F.1 The Real and Imaginary parts of $F(S, \mathbf{q}, \omega)$

The real and imaginary parts of  $F(S, \mathbf{q}, \omega)$  can be defined with an analytical continuation near the real axis:

$$F(S, \mathbf{q}, \omega) \rightarrow F(S, \mathbf{q}, \omega \pm i\epsilon) = \text{Re}[F(S, \mathbf{q}, \omega)] \pm i \text{Im}[F(S, \mathbf{q}, \omega)]. \quad (\text{F.26})$$

Here, we comment on the fact that, from the definition of  $F(S, \mathbf{q}, \omega)$  in Eq. (F.23), this function is an even function of  $\omega$  (if accompanied by changing  $\mu \rightarrow -\mu$ ). By defining the real and imaginary parts as in Eq. (F.26), this property implies that, the real part will be an even function of  $\omega$  while, the imaginary part, will be an odd function [29]. Indeed one can write:

$$F(S, \mathbf{q}, \omega \pm i\epsilon) = F(S, \mathbf{q}, -(\omega \pm i\epsilon)) = \text{Re}[F(S, \mathbf{q}, -\omega)] \mp i \text{Im}[F(S, \mathbf{q}, -\omega)] \quad (\text{F.27})$$

Hence, by definition, the following must hold,

$$\text{Re}[F(S, \mathbf{q}, \omega)] \pm i \text{Im}[F(S, \mathbf{q}, \omega)] = \text{Re}[F(S, \mathbf{q}, -\omega)] \mp i \text{Im}[F(S, \mathbf{q}, -\omega)], \quad (\text{F.28})$$

which implies:

$$\text{Re}[F(S, \mathbf{q}, \omega)] = \text{Re}[F(S, \mathbf{q}, -\omega)], \quad (\text{F.29})$$

$$\text{Im}[F(S, \mathbf{q}, \omega)] = -\text{Im}[F(S, \mathbf{q}, -\omega)]. \quad (\text{F.30})$$

Thus, the imaginary part of  $F(S, \mathbf{q}, \omega)$  must be an odd function of  $\omega$ .

Each contribution defined in (F.26) can be explicitly calculated by applying the Sokhotski–Plemelj formula for distributions defined in Eq. (A.7).

## F.2 Change of variables

To proceed with the calculations in a more cleaner and simpler form, it is easier to consider a change of variables. We follow the substitution proposed in [306]. We define:  $E = \frac{1}{2}(E_{\mathbf{k}} + E_{\mathbf{k}-\mathbf{q}}) = E_+/2$  and  $\varepsilon = E_{\mathbf{k}-\mathbf{q}} - E_{\mathbf{k}} = -E_-$ . From these, we can write:

$$E_{\mathbf{k}} = E - \varepsilon/2, \quad (\text{F.31})$$

$$E_{\mathbf{k}-\mathbf{q}} = E + \varepsilon/2. \quad (\text{F.32})$$

One can see from the definition of  $\varepsilon$  can be positive or negative while  $E$  is always a positive quantity. We also point out that the expressions in Eqs. (F.31) and (F.32) are always positive after all,  $E_{\mathbf{k}}$  and  $E_{\mathbf{k}-\mathbf{q}}$  are positive quantities (energies). This is important when considering the zero temperature limit of the Fermi functions with these dispersion relations.

The Jacobian of this transformation<sup>2</sup> is:

$$\frac{\partial(E, \varepsilon)}{\partial(k, \cos \theta)} = \left( \frac{\partial E}{\partial k} \right) \left( \frac{\partial \varepsilon}{\partial \cos \theta} \right) - \left( \frac{\partial E}{\partial \cos \theta} \right) \left( \frac{\partial \varepsilon}{\partial k} \right) = -\frac{k^2 q}{E_{\mathbf{k}} E_{\mathbf{k}-\mathbf{q}}}. \quad (\text{F.33})$$

Here,  $k = |\mathbf{k}|$  and  $q = |\mathbf{q}|$ . The change of variables yields:

$$dE d\varepsilon = \left| \frac{\partial(E, \varepsilon)}{\partial(k, \cos \theta)} \right| dk d(\cos \theta) = q \frac{dk k^2 d(\cos \theta)}{E_{\mathbf{k}} E_{\mathbf{k}-\mathbf{q}}}. \quad (\text{F.34})$$

The phase space integration is:

$$\frac{d^3 k}{E_{\mathbf{k}} E_{\mathbf{k}-\mathbf{q}}} = \frac{dk k^2 d \cos \theta d\phi}{E_{\mathbf{k}} E_{\mathbf{k}-\mathbf{q}}} = \frac{dE d\varepsilon d\phi}{q}. \quad (\text{F.35})$$

To complete the process one has to change the limits of integration accordingly. As noted in [311], by construction, the following equality holds:  $E_{\mathbf{k}-\mathbf{q}}^2 - E_{\mathbf{k}}^2 = 2E\varepsilon = q^2 - 2kq \cos \theta$ . This

<sup>2</sup>Considering a two-dimensional integral, the Jacobian of the transformation  $x = x(u, v)$  and  $y = y(u, v)$  is:

$$\frac{\partial(x, y)}{\partial(u, v)} = \begin{vmatrix} \partial_u x & \partial_v x \\ \partial_u y & \partial_v y \end{vmatrix}.$$

The integration measure is changed as:

$$dA = \left| \frac{\partial(x, y)}{\partial(u, v)} \right| du dv.$$

implies:

$$\cos \theta = -\frac{E\varepsilon - q^2/2}{kq} \implies \cos^2 \theta = \left( \frac{E\varepsilon - q^2/2}{kq} \right)^2. \quad (\text{F.36})$$

The function  $\cos \theta$  is limited to the interval  $[0, 1]$ . So, the following inequality holds:

$$\left( \frac{E\varepsilon - q^2/2}{kq} \right)^2 \leq 1. \quad (\text{F.37})$$

Writing  $k$  using the definition of  $E_{\mathbf{k}} = \sqrt{k^2 + S^2}$ , one can write:

$$k = \sqrt{E_{\mathbf{k}}^2 - S^2} = \sqrt{(E - \varepsilon/2)^2 - S^2}. \quad (\text{F.38})$$

Plugging this into inequality (F.37), one gets:

$$E^2 \varepsilon^2 \leq q^2 \left[ E^2 - S^2 + \varepsilon^2/4 - q^2/4 \right]. \quad (\text{F.39})$$

The region of integration is further restricted by the regularization of the theory itself. As previously mentioned, being a non-renormalizable field theory, the NJL model is only mathematically defined once a proper regularization scheme is chosen. In the present work we consider the 3-momentum cutoff, meaning that the 3-momentum of a single quark is restricted to a maximum value  $\Lambda_f$ , i.e.,  $k \leq \Lambda_f$ . Applying this restriction to Eq. (F.38),  $\sqrt{(E - \varepsilon/2)^2 - S^2} \leq \Lambda_f$ , and solving for  $E$  and  $\varepsilon$  yields the final constraint in the region of integration<sup>3</sup>:

$$E \leq \frac{|\varepsilon|}{2} + \sqrt{\Lambda_f^2 + S^2}, \quad (\text{F.40})$$

$$|\varepsilon| \geq 2E - 2\sqrt{\Lambda_f^2 + S^2}. \quad (\text{F.41})$$

Choosing a different regularization scheme would imply a different restriction on the region of integration, effectively changing the function  $F(S, \mathbf{q}, \omega)$  and functions derived from it. As we will later see, the one-meson-loop contributions require the calculation of the  $S^2$  and  $\omega$  derivatives of  $F(S, \mathbf{q}, \omega)$ . The chosen regularization, by affecting the region of integration will, directly, affect the mathematical structure of such derivatives. Hence, the regularization of the fermion sector will directly affect the one-meson-loop contributions.

The region of integration  $\mathcal{R}$ , spans the two-dimensional surface, in the  $(\varepsilon/q, E/q)$  space, displayed in red in Fig. F.1. Depending on the integrand, it will be more convenient to use the two possible ordered integrations i.e.,  $\int_{\mathcal{R}} d\varepsilon dE$  or  $\int_{\mathcal{R}} dE d\varepsilon$ . Of course, the integration region is the same for both order of integration, however the functions that bound the integration region are different.

<sup>3</sup>Here we make an approximation by imposing the absolute value of  $\varepsilon$  in the integration region. We do this in order to simplify the calculation: the integration region becomes symmetric, allowing for several simplifications. This approximation amounts to considering that some contributions to the loop function go above the fermion cutoff,  $\Lambda_f$ . This approximation is not expected to change the qualitative behaviour of the calculation.

So, we decided to show the integration region for both integration orders,  $\int_{\mathcal{R}} d\varepsilon dE$  (panel F.1(a)) and  $\int_{\mathcal{R}} dE d\varepsilon$  (panel F.1(b)).

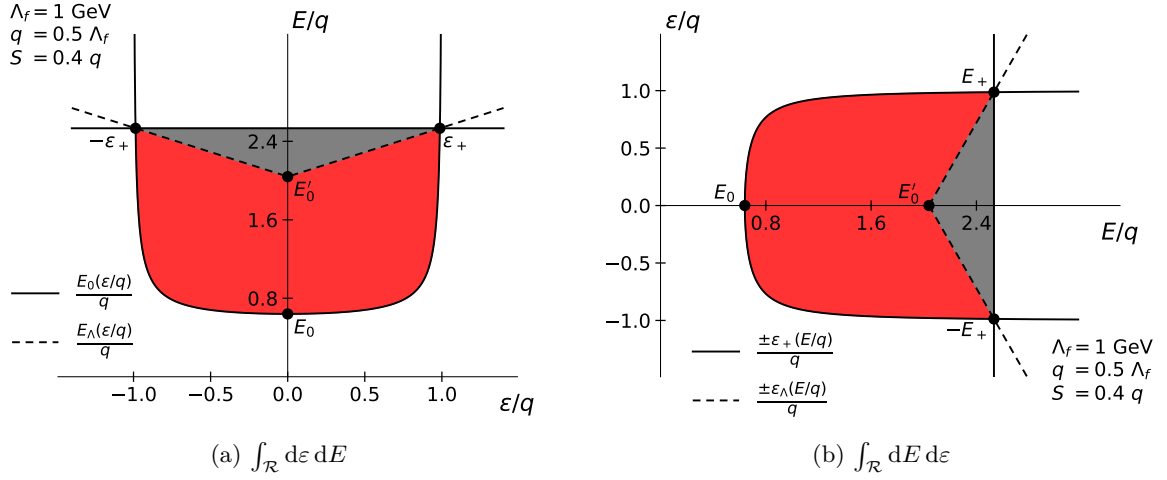


FIGURE F.1: The region of integration  $\mathcal{R}$  is displayed by red and curves that limit this region are the full and dashed lines. The gray region is needed to calculate the integrations when using the  $dE d\varepsilon$  integration order, being subtracted from the total region, bounded by full lines.

Consider first the integration order,  $d\varepsilon dE$  (see Fig. F.1(a)). The integration over the region  $\mathcal{R}$ , can be formally defined as:

$$\int_{\mathcal{R}} d\varepsilon dE = \int_a^b d\varepsilon \int_{c(\varepsilon)}^{d(\varepsilon)} dE. \quad (\text{F.42})$$

The curve which bounds the region from below,  $E_0(\varepsilon) = c(\varepsilon)$ , may be found by solving Eq. (F.39) with respect to  $E$ :

$$E_0(\varepsilon) = \frac{q}{2} \sqrt{1 + \frac{4S^2}{q^2 - \varepsilon^2}} = c(\varepsilon). \quad (\text{F.43})$$

The upper curve,  $d(\varepsilon) = E_\Lambda(\varepsilon)$ , is given by the equality in Eq. (F.40):

$$E_\Lambda(\varepsilon) = \frac{|\varepsilon|}{2} + \sqrt{\Lambda_f^2 + S^2} = d(\varepsilon). \quad (\text{F.44})$$

The left and right bound of the integration region,  $-\varepsilon_+ = a$  and  $\varepsilon_+ = b$  can be found by calculating the  $\varepsilon$  coordinate at which  $E_0(\varepsilon) = E_\Lambda(\varepsilon)$ . This yields:

$$\varepsilon_+ = \sqrt{(\Lambda_f + q)^2 + S^2} - \sqrt{\Lambda_f^2 + S^2} = -a = b, \quad (\text{F.45})$$

The remaining intersection points are given by:

$$E_0 = c(0) = \frac{1}{2} \sqrt{q^2 + 4S^2} = \frac{1}{2} E_\sigma, \quad (\text{F.46})$$

$$E'_0 = d(0) = \sqrt{\Lambda_f^2 + S^2}. \quad (\text{F.47})$$

We can then write the integration over the region  $\mathcal{R}$ , as defined in Eq. (F.42), as:

$$\int_{\mathcal{R}} d\varepsilon dE = \int_a^b d\varepsilon \int_{c(\varepsilon)}^{d(\varepsilon)} dE = \int_{-\varepsilon_+}^{\varepsilon_+} d\varepsilon \int_{E_0(\varepsilon)}^{E_{\Lambda}(\varepsilon)} dE. \quad (\text{F.48})$$

Consider now the opposite order of integration,  $dE d\varepsilon$ . For this case the region  $\mathcal{R}$  must be decomposed in two different regions,  $\mathcal{R}_1$  (red plus gray regions in Fig. F.1(b)) and  $\mathcal{R}_2$  (gray in Fig. F.1(b)). The integration over  $\mathcal{R}$  can be written as:

$$\begin{aligned} \int_{\mathcal{R}} dE d\varepsilon &= \int_{\mathcal{R}_1} dE d\varepsilon - \int_{\mathcal{R}_2} dE d\varepsilon \\ &= \int_{A_1}^{B_1} dE \int_{C_1(E)}^{D_1(E)} d\varepsilon - \int_{A_2}^{B_2} dE \int_{C_2(E)}^{D_2(E)} d\varepsilon \\ &= \sum_{k=1}^2 (-1)^{k+1} \int_{A_k}^{B_k} dE \int_{C_k(E)}^{D_k(E)} d\varepsilon. \end{aligned} \quad (\text{F.49})$$

To simplify the notation we will define the sum over  $k$  as:

$$\sum_{k=1}^2 (-1)^{k+1} \equiv \sum_k. \quad (\text{F.50})$$

The upper and lower curves of  $\mathcal{R}_1$ ,  $\varepsilon_+(E) = D_1(E)$  and  $-\varepsilon_+(E) = C_1(E)$ , are given by the positive and negative branches, respectively, of the solution of Eq. (F.39), with respect to  $\varepsilon$ , i.e.,

$$\varepsilon_+(E) = \pm q \sqrt{1 - \frac{4S^2}{4E^2 - q^2}} = \pm q \frac{\sqrt{4E^2 - E_\sigma^2}}{\sqrt{4E^2 - q^2}} = D_1(E) = -C_1(E). \quad (\text{F.51})$$

The upper and lower curves of  $\mathcal{R}_2$ ,  $\varepsilon_{\Lambda_+}(E) = D_2(E)$  and  $-\varepsilon_{\Lambda_+}(E) = C_2(E)$ , are given by the positive and negative branches, respectively, of the solution of Eq. (F.41):

$$\varepsilon_{\Lambda_+}(E) = \pm \left( 2E - 2\sqrt{\Lambda_f^2 + S^2} \right) = D_2(E) = -C_2(E). \quad (\text{F.52})$$

The left bound for the integration over the regions  $\mathcal{R}_1$  and  $\mathcal{R}_2$ ,  $E_0 = A_1$  and  $E'_0 = A_2$ , are given in Eqs. (F.46) and (F.47), respectively. The right bound,  $E_+ = B_k$ , can be found by the intersections amongst these curves, by searching the  $E$  coordinate at which  $\varepsilon_+(E) = \varepsilon_{\Lambda_+}(E)$ , yielding:

$$E_+ = \frac{1}{2} \left( \sqrt{(\Lambda_f + q)^2 + S^2} + \sqrt{\Lambda_f^2 + S^2} \right) = B_k. \quad (\text{F.53})$$

Following the subdivision proposed above, the integration region can be written as:

$$\begin{aligned} \int_{\mathcal{R}} dE d\varepsilon &= \sum_k \int_{A_k}^{B_k} dE \int_{C_k(E)}^{D_k(E)} d\varepsilon \\ &= \int_{E_0}^{E_+} dE \int_{-\varepsilon_+(E)}^{\varepsilon_+(E)} d\varepsilon - \int_{E'_0}^{E_+} dE \int_{-\varepsilon_{\Lambda_+}(E)}^{\varepsilon_{\Lambda_+}(E)} d\varepsilon. \end{aligned} \quad (\text{F.54})$$

Original Definition	Equation
Eq. (F.8)	$E_+(S, \mathbf{q}, \mathbf{k}) = E_{\mathbf{k}} + E_{\mathbf{k}-\mathbf{q}}$
Eq. (F.9)	$E_-(S, \mathbf{q}, \mathbf{k}) = E_{\mathbf{k}} - E_{\mathbf{k}-\mathbf{q}}$
Eq. (F.17)	$G_+(S, \mathbf{q}, \mathbf{k}, \mu) = 1 - n_F(E_{\mathbf{k}} - \mu) - n_F(E_{\mathbf{k}-\mathbf{q}} + \mu)$
Eq. (F.18)	$G_-(S, \mathbf{q}, \mathbf{k}, \mu) = n_F(E_{\mathbf{k}} + \mu) - n_F(E_{\mathbf{k}-\mathbf{q}} + \mu)$
Eq. (F.24)	$F_p(S, \mathbf{q}, \omega) = \int \frac{d^3k}{(2\pi)^3} \frac{1}{4E_{\mathbf{k}}E_{\mathbf{k}-\mathbf{q}}} \left\{ \frac{G_+(S, \mu)}{\omega + E_+} - \frac{G_+(S, -\mu)}{\omega - E_+} \right\}$
Eq. (F.25)	$F_s(S, \mathbf{q}, \omega) = \int \frac{d^3k}{(2\pi)^3} \frac{1}{4E_{\mathbf{k}}E_{\mathbf{k}-\mathbf{q}}} \left\{ \frac{G_-(S, -\mu)}{\omega + E_-} - \frac{G_-(S, \mu)}{\omega - E_-} \right\}$
Eq. (F.45)	$\varepsilon_+ = \sqrt{(\Lambda_f + q)^2 + S^2} - \sqrt{\Lambda_f^2 + S^2} = -a = b$
Eq. (F.46)	$E_0 = c(0) = \frac{1}{2}\sqrt{q^2 + 4S^2} = \frac{1}{2}E_\sigma$
Eq. (F.47)	$E'_0 = d(0) = \sqrt{\Lambda_f^2 + S^2}$
Eq. (F.52)	$\varepsilon_{\Lambda_+}(E) = \pm \left( 2E - 2\sqrt{\Lambda_f^2 + S^2} \right) = D_2(E) = -C_2(E)$
Eq. (F.53)	$E_+ = \frac{1}{2} \left( \sqrt{(\Lambda_f + q)^2 + S^2} + \sqrt{\Lambda_f^2 + S^2} \right) = B_k$
Eq. (F.50)	$\sum_{k=1}^2 (-1)^{k+1} \equiv \sum_k$

TABLE F.1: Important equations that will be used throughout the calculations.

The intersection points  $E_0$  and  $E'_0$ , by definition, respect,  $\pm\varepsilon_+(E_0) = 0$  and  $\pm\varepsilon_{\Lambda_+}(E'_0) = 0$ , (see Fig. F.1(b)). This allows us to write the following identity:

$$C_k(A_k) = D_k(A_k) = 0, \quad (\text{F.55})$$

which will be important in the calculation of the one-meson-loop contributions.

For simplicity, we gather some important equations in Table F.1, that will be used several times during the remaining calculations.

### F.3 The pair creation/annihilation contribution, $F_p(S, \mathbf{q}, \omega)$

Using the change of variables suggested in the previous section and performing the integration over the azimuthal angle  $\phi$  (which yields a simple  $2\pi$  factor), the pair creation/annihilation contribution of  $F(S, \mathbf{q}, \omega)$ , as defined in Eq. (F.24), can be written as:

$$\begin{aligned} 16\pi^2 q F_p(S, \mathbf{q}, \omega) &= \int_{\mathcal{R}} dE d\varepsilon \left\{ \frac{G_+(S, \mu)}{\omega + 2E} - \frac{G_+(S, -\mu)}{\omega - 2E} \right\} \\ &= \frac{1}{2} \int_{\mathcal{R}} dE d\varepsilon \sum_{\eta=\pm 1} \frac{G_+(S, \eta\mu)}{E + \eta\omega/2}. \end{aligned} \quad (\text{F.56})$$

Where,

$$G_+(S, \eta\mu, E, \varepsilon) = 1 - n_F(E - \varepsilon/2 - \eta\mu) - n_F(E + \varepsilon/2 + \eta\mu). \quad (\text{F.57})$$

Using the order of integration  $dE d\varepsilon$ ,

$$16\pi^2 q F_p(S, \mathbf{q}, \omega) = \frac{1}{2} \sum_{\eta=\pm 1} \sum_k \int_{A_k}^{B_k} \frac{dE}{E + \eta\omega/2} \int_{C_k(E)}^{D_k(E)} d\varepsilon G_+(S, \eta\mu) \quad (\text{F.58})$$

and to simplify the calculations, we define:

$$g_+^k(S, E, \eta\mu) = \int_{C_k(E)}^{D_k(E)} d\varepsilon G_+(S, \eta\mu), \quad (\text{F.59})$$

to finally obtain

$$16\pi^2 q F_p(S, \mathbf{q}, \omega) = \frac{1}{2} \sum_{\eta=\pm 1} \sum_k \int_{A_k}^{B_k} dE \frac{1}{E + \eta\omega/2} g_+^k(S, E, \eta\mu). \quad (\text{F.60})$$

The integration in Eq. (F.59) can be performed analytically by separating each term, making the proper change of variables and using identity (J.11). This is very useful since it allows to reduce the dimension of the numerical integration by one, saving computation time. One can write:

$$\begin{aligned} g_+^k(S, E, \eta\mu) &= \int_{C_k(E)}^{D_k(E)} d\varepsilon \{1 - n_F(E - \varepsilon/2 - \eta\mu) - n_F(E + \varepsilon/2 + \eta\mu)\} \\ &= 2D_k(E) - \int_{C_k(E)}^{D_k(E)} d\varepsilon n_{-\eta}^F(E - \varepsilon/2) - \int_{C_k(E)}^{D_k(E)} d\varepsilon n_{+\eta}^F(E + \varepsilon/2). \end{aligned} \quad (\text{F.61})$$

Where we have used the following definition:

$$n_{\pm\eta}^F(E) = \frac{1}{e^{\beta(E \pm \eta\mu)} + 1}. \quad (\text{F.62})$$

To calculate the remaining integrals, we just have to calculate the following quantity:

$$I_{\pm\eta}(S, E, \eta\mu) = \int_{C_k}^{D_k} d\varepsilon n_{\pm\eta}^F(E \pm \varepsilon/2) = \int_{C_k}^{D_k} \frac{d\varepsilon}{e^{\beta(E \pm \varepsilon/2 \pm \eta\mu)} + 1} = \pm \frac{2}{\beta} \int_{x(C_k)}^{x(D_k)} \frac{dx}{e^x + 1}. \quad (\text{F.63})$$

In the last step we changed variables,  $x(\varepsilon) = \beta(E \pm \varepsilon/2 \pm \eta\mu)$ ,  $d\varepsilon = \pm \frac{2}{\beta} dx$  and

$$x(D_k) = \beta(E \pm D_k/2 \pm \eta\mu), \quad (\text{F.64})$$

$$x(C_k) = \beta(E \pm C_k/2 \pm \eta\mu) = \beta(E \mp D_k/2 \pm \eta\mu). \quad (\text{F.65})$$

Using the identity given in Eq. (J.11), one can get:

$$\begin{aligned} I_{\pm\eta}(S, E, \eta\mu) &= \pm \frac{2}{\beta} \left\{ x(D_k) - \ln [e^{x(D_k)} + 1] - x(C_k) + \ln [e^{x(C_k)} + 1] \right\} \\ &= \pm \frac{2}{\beta} \left\{ \pm \beta D_k - \ln \left[ \frac{e^{\beta(E \pm D_k/2 \pm \eta\mu)} + 1}{e^{\beta(E \mp D_k/2 \pm \eta\mu)} + 1} \right] \right\} \\ &= \mp \frac{2}{\beta} \ln \left[ \frac{e^{\beta(E \pm \eta\mu)} + e^{\mp \beta D_k/2}}{e^{\beta(E \pm \eta\mu)} + e^{\pm \beta D_k/2}} \right]. \end{aligned} \quad (\text{F.66})$$

In the last step we wrote the logarithm as:

$$\ln \left[ \frac{e^{\beta(E \pm D_k/2 \pm \eta\mu)} + 1}{e^{\beta(E \mp D_k/2 \pm \eta\mu)} + 1} \right] = \pm \beta D_k + \ln \left[ \frac{e^{\beta(E \pm \eta\mu)} + e^{\mp \beta D_k/2}}{e^{\beta(E \pm \eta\mu)} + e^{\pm \beta D_k/2}} \right]. \quad (\text{F.67})$$

Substituting  $I_{\pm\eta}(S, E, \eta\mu)$ , one can finally write  $g_{\pm}^k(S, E, \eta\mu)$  as:

$$g_{\pm}^k(S, E, \eta\mu) = 2D_k + 2T \ln \left[ \frac{e^{\beta(E - \eta\mu)} + e^{-\beta D_k/2}}{e^{\beta(E - \eta\mu)} + e^{\beta D_k/2}} \right] + 2T \ln \left[ \frac{e^{\beta(E + \eta\mu)} + e^{-\beta D_k/2}}{e^{\beta(E + \eta\mu)} + e^{\beta D_k/2}} \right]. \quad (\text{F.68})$$

In the vacuum limit, the Fermi–Dirac distribution functions vanish and only the first term in the original integration will contribute, yielding simply  $g_{\pm}^k(S, E) = 2D_k$ . Here we point out that  $g_{\pm}^k(S, E, \eta\mu)$  is an odd function with respect to  $E$  (while also changing  $\mu \rightarrow -\mu$ ) i.e.,  $g_{\pm}^k(S, -E, \mu) = -g_{\pm}^k(S, E, -\mu)$ .

In order to obtain the real and imaginary parts of  $F_p(S, \mathbf{q}, \omega)$ , we apply the Sokhotski–Plemelj formula by shifting the poles as  $\omega/2 \rightarrow \omega/2 - i\epsilon$ . We write:

$$16\pi^2 q F_p(S, \mathbf{q}, \omega) = \frac{1}{2} \sum_{\eta=\pm 1} \sum_k \int_{A_k}^{B_k} dE \frac{1}{E + \eta(\omega/2 - i\epsilon)} g_{\pm}^k(S, E, \eta\mu). \quad (\text{F.69})$$

To explicitly write the real and imaginary contributions we apply Eq. (A.7). The real part is:

$$16\pi^2 q \text{Re} [F_p(S, \mathbf{q}, \omega)] = \frac{1}{2} \sum_{\eta=\pm 1} \sum_k \text{p.v.} \int_{A_k}^{B_k} dE \frac{g_{\pm}^k(S, E, \eta\mu)}{E + \eta\omega/2}, \quad (\text{F.70})$$

where p.v. stands for the Cauchy Principal value of the integral. The imaginary part is given by

$$16\pi^2 q \text{Im} [F_p(S, \mathbf{q}, \omega)] = \frac{\pi}{2} \sum_{\eta=\pm 1} \sum_k \eta \int_{A_k}^{B_k} dE \delta\left(E + \eta\frac{\omega}{2}\right) g_{\pm}^k(S, E, \eta\mu). \quad (\text{F.71})$$

The integration over  $E$  can be made using the Dirac delta function to yield:

$$\begin{aligned} 16\pi^2 q \text{Im} [F_p(S, \mathbf{q}, \omega)] = & + \frac{\pi}{2} \sum_k g_{\pm}^k\left(S, -\frac{\omega}{2}, \mu\right) \left[ H\left(-\frac{\omega}{2} - A_k\right) - H\left(-\frac{\omega}{2} - B_k\right) \right] \\ & - \frac{\pi}{2} \sum_k g_{\pm}^k\left(S, \frac{\omega}{2}, -\mu\right) \left[ H\left(\frac{\omega}{2} - A_k\right) - H\left(\frac{\omega}{2} - B_k\right) \right]. \end{aligned} \quad (\text{F.72})$$

Here,  $H(x)$  is the Heaviside step function defined in the Appendix A.2. Since both  $A_k$  and  $B_k$  are always positive quantities, the first term is only non-zero for negative  $\omega$  while the second term only for positive  $\omega$ . So, using the fact that  $g_{\pm}^k(S, -E, \mu) = -g_{\pm}^k(S, E, -\mu)$ , we can extend the result for all values of  $\omega$ ,

$$16\pi^2 q \text{Im} [F_p(S, \mathbf{q}, \omega)] = -\frac{\pi}{2} \sum_k g_{\pm}^k\left(S, \frac{\omega}{2}, -\mu\right) \left[ H\left(\frac{\omega}{2} - A_k\right) - H\left(\frac{\omega}{2} - B_k\right) \right]. \quad (\text{F.73})$$

#### F.4 The scattering contribution, $F_s(S, \mathbf{q}, \omega)$

The same process used previously can be applied to Eq. (F.25), the scattering contribution. We have:

$$16\pi^2 q F_s(S, \mathbf{q}, \omega) = \int_{\mathcal{R}} dE d\varepsilon \left\{ \frac{G_-(S, -\mu)}{\omega - \varepsilon} - \frac{G_-(S, \mu)}{\omega + \varepsilon} \right\} = - \int_{\mathcal{R}} dE d\varepsilon \sum_{\eta=\pm 1} \frac{G_-(S, \eta\mu)}{\varepsilon + \eta\omega}. \quad (\text{F.74})$$

Where,

$$G_-(S, \eta\mu, E, \varepsilon) = n_F(E - \varepsilon/2 + \eta\mu) - n_F(E + \varepsilon/2 + \eta\mu). \quad (\text{F.75})$$

Using the order of integration  $d\varepsilon dE$ , we can write:

$$16\pi^2 q F_s(S, \mathbf{q}, \omega) = - \sum_{\eta=\pm 1} \int_a^b \frac{d\varepsilon}{\varepsilon + \eta\omega} \int_{c(\varepsilon)}^{d(\varepsilon)} dE G_-(S, \eta\mu). \quad (\text{F.76})$$

Again, by defining,

$$g_-(S, \varepsilon, \eta\mu) = \int_{c(\varepsilon)}^{d(\varepsilon)} dE G_-(S, \eta\mu), \quad (\text{F.77})$$

one gets:

$$16\pi^2 q F_s(S, \mathbf{q}, \omega) = - \sum_{\eta=\pm 1} \int_a^b d\varepsilon \frac{g_-(S, \varepsilon, \eta\mu)}{\varepsilon + \eta\omega}. \quad (\text{F.78})$$

The integration in Eq. (F.77), like the pair creation/annihilation term, can also be performed analytically. Using Eq. (F.62), we write:

$$\begin{aligned} g_-(S, \varepsilon, \eta\mu) &= \int_{c(\varepsilon)}^{d(\varepsilon)} dE \{ n_F(E - \varepsilon/2 + \eta\mu) - n_F(E + \varepsilon/2 + \eta\mu) \} \\ &= \int_{c(\varepsilon)}^{d(\varepsilon)} dE \{ n_{+\eta}^F(E - \varepsilon/2) - n_{+\eta}^F(E + \varepsilon/2) \}. \end{aligned} \quad (\text{F.79})$$

Like before, we just have to calculate:

$$I_{\pm}(S, \varepsilon, \eta\mu) = \int_c^d dE n_{+\eta}^F(E \pm \varepsilon/2) = \int_c^d \frac{dE}{e^{\beta(E \pm \varepsilon/2 + \eta\mu)} + 1} = \frac{1}{\beta} \int_{x(c)}^{x(d)} \frac{dx}{e^x + 1}. \quad (\text{F.80})$$

Where the following change of variables was considered:  $x(E) = \beta(E \pm \varepsilon/2 + \eta\mu)$ ,  $dE = \frac{1}{\beta} dx$  and

$$x(d) = \beta(d \pm \varepsilon/2 + \eta\mu), \quad (\text{F.81})$$

$$x(c) = \beta(c \pm \varepsilon/2 + \eta\mu). \quad (\text{F.82})$$

Using the result in Eq. (J.11), we can write:

$$\begin{aligned} I_{\pm}(S, \varepsilon, \eta\mu) &= \frac{1}{\beta} \left\{ x(d) - \ln \left[ e^{x(d)} + 1 \right] - x(c) + \ln \left[ e^{x(c)} + 1 \right] \right\} \\ &= (d - c) - \frac{1}{\beta} \ln \left[ e^{\beta(d \pm \varepsilon/2 + \eta\mu)} + 1 \right] + \frac{1}{\beta} \ln \left[ e^{\beta(c \pm \varepsilon/2 + \eta\mu)} + 1 \right]. \end{aligned} \quad (\text{F.83})$$

Using this result and the fact that  $c = E_0$  and  $d = E_{\Lambda}$  (see also Table F.1), we can finally write:

$$\begin{aligned} g_-(S, \varepsilon, \eta\mu) &= T \ln \left[ \frac{e^{\beta(E_{\Lambda} + \varepsilon/2 + \eta\mu)} + 1}{e^{\beta(E_{\Lambda} - \varepsilon/2 + \eta\mu)} + 1} \right] - T \ln \left[ \frac{e^{\beta(E_0 + \varepsilon/2 + \eta\mu)} + 1}{e^{\beta(E_0 - \varepsilon/2 + \eta\mu)} + 1} \right] \\ &= T \ln \left[ \frac{e^{\beta(E_{\Lambda} + \eta\mu)} + e^{-\beta\varepsilon/2}}{e^{\beta(E_{\Lambda} + \eta\mu)} + e^{\beta\varepsilon/2}} \right] - T \ln \left[ \frac{e^{\beta(E_0 + \eta\mu)} + e^{-\beta\varepsilon/2}}{e^{\beta(E_0 + \eta\mu)} + e^{\beta\varepsilon/2}} \right]. \end{aligned} \quad (\text{F.84})$$

In the vacuum limit ( $T, \mu \rightarrow 0$ ), the Fermi–Dirac distributions vanish and this contribution is zero. Indeed, it is this fact that makes all the scattering contributions vanish in the vacuum limit.

As before, to calculate the real and imaginary contributions of  $F_s(S, \mathbf{q}, \omega)$ , we shift the pole,  $\omega/2 \rightarrow \omega/2 - i\epsilon$ , and apply the Sokhotski–Plemelj formula. Consider:

$$16\pi^2 q \operatorname{Re} [F_s(S, \mathbf{q}, \omega)] = - \sum_{\eta=\pm 1} \int_a^b d\varepsilon \frac{g_-(S, \varepsilon, \eta\mu)}{\varepsilon + \eta(\omega - i\epsilon)}. \quad (\text{F.85})$$

The real contribution is:

$$16\pi^2 q \operatorname{Re} [F_s(S, \mathbf{q}, \omega)] = - \sum_{\eta=\pm 1} \text{p.v.} \int_a^b d\varepsilon \frac{g_-(S, \varepsilon, \eta\mu)}{\varepsilon + \eta\omega}. \quad (\text{F.86})$$

The imaginary part is:

$$16\pi^2 q \operatorname{Im} [F_s(S, \mathbf{q}, \omega)] = -\pi \sum_{\eta=\pm 1} \eta \int_a^b d\varepsilon \delta(\varepsilon + \eta\omega) g_-(S, \varepsilon, \eta\mu). \quad (\text{F.87})$$

Making the integration over  $\varepsilon$  yields:

$$\begin{aligned} 16\pi^2 q \operatorname{Im} [F_s(S, \mathbf{q}, \omega)] &= -\pi g_-(S, -\omega, \mu) [H(-\omega - a) - H(-\omega - b)] \\ &\quad + \pi g_-(S, \omega, -\mu) [H(\omega - a) - H(\omega - b)]. \end{aligned} \quad (\text{F.88})$$

Since  $a = -b$  and  $g_-(S, -\omega, \mu) = -g_-(S, \omega, -\mu)$ , both terms are equal. One gets:

$$16\pi^2 q \operatorname{Im} [F_s(S, \mathbf{q}, \omega)] = 2\pi g_-(S, \omega, -\mu) [H(\omega - a) - H(\omega - b)]. \quad (\text{F.89})$$

## F.5 Calculation of $\partial_{S^2} F(S, \mathbf{q}, \omega)$

To calculate some contributions of the  $SU(2)_f$  NJL gap equation, it will be necessary to calculate  $\partial_{S^2} F(S, \mathbf{q}, \omega)$ . In this section we will calculate these contributions explicitly by calculating,

separately, the real and imaginary components of  $\partial_{S^2} F(S, \mathbf{q}, \omega)$  for the pair creation/annihilation,  $F_p(S, \mathbf{q}, \omega)$ , and scattering contributions,  $F_s(S, \mathbf{q}, \omega)$ .

### F.5.1 Calculation of $\partial_{S^2} 16\pi^2 q \operatorname{Re} [F_p(S, \mathbf{q}, \omega)]$

The derivative of the real part, with respect to  $S^2$ , is defined as:

$$\partial_{S^2} 16\pi^2 q \operatorname{Re} [F_p(S, \mathbf{q}, \omega)] = \frac{1}{2} \frac{\partial}{\partial S^2} \sum_{\eta=\pm 1} \sum_k \text{p.v.} \int_{A_k(S)}^{B_k(S)} dE \frac{g_+^k(S, E, \eta\mu)}{E + \eta\omega/2} \quad (\text{F.90})$$

To calculate the derivative w.r.t.  $S^2$ , we will apply the Leibniz integral rule defined in the Appendix J.2. Assuming that the derivative and the Cauchy Principal value operations commute, we can change the order of these operations and write:

$$\begin{aligned} \partial_{S^2} 16\pi^2 q \operatorname{Re} [F_p(S, \mathbf{q}, \omega)] &= \frac{1}{2} \sum_{\eta=\pm 1} \sum_k \text{p.v.} \int_{A_k(S)}^{B_k(S)} dE \frac{\partial_{S^2} g_+^k(S, E, \eta\mu)}{E + \eta\omega/2} \\ &\quad + \frac{1}{2} \sum_{\eta=\pm 1} \sum_k \frac{g_+^k(S, B_k, \eta\mu)}{B_k + \eta\omega/2} \partial_{S^2} B_k(S) \\ &\quad - \frac{1}{2} \sum_{\eta=\pm 1} \sum_k \frac{g_+^k(S, A_k, \eta\mu)}{A_k + \eta\omega/2} \partial_{S^2} A_k(S). \end{aligned} \quad (\text{F.91})$$

The last term is zero because, for every  $k$ , the following holds:

$$g_+^k(S, A_k, \eta\mu) = 0. \quad (\text{F.92})$$

This identity comes from the definition of  $g_+^k(S, E, \eta\mu)$  in Eq. (F.59). Since,  $C_k(A_k) = D_k(A_k) = 0$  for every  $k$  (see Eq. (F.55)), this implies that the integration bounds in Eq. (F.59) are equal and null, implying Eq. (F.92). The second term also vanishes owing to  $B_k$  being the same<sup>4</sup> for every  $k$ . This fact implies that the sum over  $k$ , defined in (F.50), sum up to zero. Thus, the following holds for any function  $h(E)$ :

$$\sum_k h(B_k) = \sum_{k=1}^2 (-1)^{k+1} h(B_k) = 0. \quad (\text{F.93})$$

Hence, the derivative can be written as:

$$\partial_{S^2} 16\pi^2 q \operatorname{Re} [F_p(S, \mathbf{q}, \omega)] = \frac{1}{2} \sum_{\eta=\pm 1} \sum_k \text{p.v.} \int_{A_k(S)}^{B_k(S)} dE \frac{\partial_{S^2} g_+^k(S, E, \eta\mu)}{E + \eta\omega/2}. \quad (\text{F.94})$$

We proceed to calculate the explicit expression. We first point out that to calculate the derivatives one has to use the Leibniz integral rule. However, the derivatives,

$$\partial_{S^2} g_+^k(S, E, \eta\mu) = \frac{\partial}{\partial S^2} \int_{C_k(S, E)}^{D_k(S, E)} d\varepsilon G_+(E, \varepsilon, \eta\mu), \quad (\text{F.95})$$

<sup>4</sup>Indeed, explicitly,  $B_1 = B_2 = E_+$  (see Eq. (F.53)).

are simple to calculate since the integrand does not depend on  $S$  (here we only omitted the  $q$  dependency). This means that, by application of the Leibniz integral rule, only the boundary derivatives will contribute. Using the fact that for any  $k$ ,  $D_k = -C_k$ , one gets:

$$\partial_{S^2} g_+^k(S, E, \eta\mu) = 2G_+(S, E, D_k(S, E), \eta\mu) \frac{\partial}{\partial S^2} D_k(S, E). \quad (\text{F.96})$$

Using this result in Eq. (F.94) and simplifying the expressions, one can write:

$$\partial_{S^2} 16\pi^2 q \operatorname{Re} [F_p(S, \mathbf{q}, \omega)] = \frac{1}{\omega^2 - E_\sigma^2} \sum_k J_k(S, \mathbf{q}, \omega). \quad (\text{F.97})$$

Where we have defined:

$$\frac{J_k(S, \mathbf{q}, \omega)}{\omega^2 - E_\sigma^2} = \sum_{\eta=\pm 1} \text{p.v.} \int_{A_k}^{B_k} dE \frac{G_+(S, E, D_k, \eta\mu)}{E + \eta\omega/2} \frac{\partial}{\partial S^2} D_k(S, E) \quad (\text{F.98})$$

Lets consider each contribution separately. For  $k = 1$ , we can write:

$$\frac{J_1(S, \mathbf{q}, \omega)}{\omega^2 - E_\sigma^2} = \sum_{\eta=\pm 1} \text{p.v.} \int_{A_1}^{B_1} dE \frac{G_+(S, E, D_1, \eta\mu)}{E + \eta\omega/2} \frac{\partial}{\partial S^2} D_1(S, E). \quad (\text{F.99})$$

The derivative is given by (see Table F.1):

$$\frac{\partial}{\partial S^2} D_1(S, E) = \frac{\partial}{\partial S^2} \varepsilon_+(S, E) = \frac{-2q}{\sqrt{4E^2 - q^2}} \frac{1}{\sqrt{4E^2 - E_\sigma^2}}. \quad (\text{F.100})$$

Which yields:

$$\frac{J_1(S, \mathbf{q}, \omega)}{\omega^2 - E_\sigma^2} = \sum_{\eta=\pm 1} \text{p.v.} \int_{A_1}^{B_1} dE \frac{-2q}{\sqrt{4E^2 - q^2}} \frac{1}{\sqrt{4E^2 - E_\sigma^2}} \frac{G_+(D_1, \eta\mu)}{E + \eta\omega/2}. \quad (\text{F.101})$$

It is useful to use the identity (see Appendix (J.3) for more details about the derivation):

$$\sum_{\eta=\pm 1} \frac{1}{\sqrt{4E^2 - E_\sigma^2}} \frac{G_+(\eta\mu)}{E + \eta\omega/2} = \frac{(-1)}{\omega^2 - E_\sigma^2} \sum_{\eta=\pm 1} \left[ K_+(\eta\mu) \frac{\sqrt{2E - \eta E_\sigma}}{\sqrt{2E + \eta E_\sigma}} - G_+(\eta\mu) \frac{\sqrt{4E^2 - E_\sigma^2}}{E + \eta\omega/2} \right], \quad (\text{F.102})$$

where,

$$K_+(\eta\mu) = G_+(\eta\mu) + G_+(-\eta\mu) + \frac{\omega}{E_\sigma} [G_+(\eta\mu) - G_+(-\eta\mu)]. \quad (\text{F.103})$$

In the  $\mu = 0$  case, one gets  $K_+ = 2G_+$ . Finally, the function  $J_1(S, \mathbf{q}, \omega)$  is given by:

$$\begin{aligned} J_1(S, \mathbf{q}, \omega) &= \sum_{\eta=\pm 1} \text{p.v.} \int_{A_1}^{B_1} dE \frac{2q}{\sqrt{4E^2 - q^2}} \left[ K_+(D_1, \eta\mu) \frac{\sqrt{2E - \eta E_\sigma}}{\sqrt{2E + \eta E_\sigma}} - G_+(D_1, \eta\mu) \frac{\sqrt{4E^2 - E_\sigma^2}}{E + \eta\omega/2} \right] \\ &= j_\sigma(S, \mathbf{q}, \omega) - j_\omega(S, \mathbf{q}, \omega). \end{aligned} \quad (\text{F.104})$$

The function  $j_\sigma(S, \mathbf{q}, \omega)$  is:

$$j_\sigma(S, \mathbf{q}, \omega) = 2 \sum_{\eta=\pm 1} \text{p.v.} \int_{A_1}^{B_1} dE q \frac{K_+(D_1, \eta\mu) \sqrt{2E - \eta E_\sigma}}{\sqrt{4E^2 - q^2} \sqrt{2E + \eta E_\sigma}}. \quad (\text{F.105})$$

The function  $j_\omega(S, \mathbf{q}, \omega)$  is:

$$j_\omega(S, \mathbf{q}, \omega) = 2 \sum_{\eta=\pm 1} \text{p.v.} \int_{A_1}^{B_1} dE D_1(E) \frac{G_+(D_1, \eta\mu)}{E + \eta\omega/2}. \quad (\text{F.106})$$

When  $\omega = E_\sigma$ , the above contributions are equal and  $J_1(S, \mathbf{q}, E_\sigma) = 0$ .

For  $k = 2$ , the calculations are simpler. The derivative is

$$\frac{\partial}{\partial S^2} D_2(S, E) = \frac{\partial}{\partial S^2} \varepsilon_{\Lambda^+}(S, E) = -\frac{1}{\sqrt{\Lambda_f^2 + S^2}}. \quad (\text{F.107})$$

Yielding the following final result for  $J_2(S, \mathbf{q}, \omega)$ :

$$J_2(S, \mathbf{q}, \omega) = -(\omega^2 - E_\sigma^2) \sum_{\eta=\pm 1} \text{p.v.} \int_{A_2}^{B_2} dE \frac{G_+(E, D_2, \eta\mu)}{\sqrt{\Lambda_f^2 + S^2}} \frac{1}{E + \eta\omega/2}. \quad (\text{F.108})$$

### F.5.2 Calculation of $\partial_{S^2} 16\pi^2 q \text{Im} [F_p(S, \mathbf{q}, \omega)]$

The  $S^2$  derivative of the imaginary part is defined as:

$$\partial_{S^2} 16\pi^2 q \text{Im} [F_p(S, \mathbf{q}, \omega)] = -\frac{\pi}{2} \frac{\partial}{\partial S^2} \sum_k g_+^k \left( S, \frac{\omega}{2}, -\mu \right) \left[ H \left( \frac{\omega}{2} - A_k(S) \right) - H \left( \frac{\omega}{2} - B_k(S) \right) \right]. \quad (\text{F.109})$$

We write:

$$\begin{aligned} \partial_{S^2} 16\pi^2 q \text{Im} [F_p(S, \mathbf{q}, \omega)] &= \frac{\pi}{2} \sum_k g_+^k \left( S, \frac{\omega}{2}, -\mu \right) \left[ \delta \left( \frac{\omega}{2} - A_k \right) \partial_{S^2} A_k(S) - \delta \left( \frac{\omega}{2} - B_k \right) \partial_{S^2} B_k(S) \right] \\ &\quad - \frac{\pi}{2} \sum_k \left[ H \left( \frac{\omega}{2} - A_k \right) - H \left( \frac{\omega}{2} - B_k \right) \right] \partial_{S^2} g_+^k \left( S, \frac{\omega}{2}, -\mu \right). \end{aligned} \quad (\text{F.110})$$

When integrating over  $\omega$ , the last term will vanish by application of the identities presented in Eqs. (F.92) and (F.93). Hence, we have:

$$\partial_{S^2} 16\pi^2 q \text{Im} [F_p(S, \mathbf{q}, \omega)] = -\frac{\pi}{2} \sum_k \left[ H \left( \frac{\omega}{2} - A_k \right) - H \left( \frac{\omega}{2} - B_k \right) \right] \partial_{S^2} g_+^k \left( S, \frac{\omega}{2}, -\mu \right). \quad (\text{F.111})$$

This derivative can easily be calculated explicitly, for each  $k$ , by using Eqs. (F.96), (F.100) and (F.107).

**F.5.3 Calculation of  $\partial_{S^2} 16\pi^2 q \operatorname{Re} [F_s(S, \mathbf{q}, \omega)]$** 

The derivative of the real part, with respect to  $S^2$ , is defined as:

$$\partial_{S^2} 16\pi^2 q \operatorname{Re} [F_s(S, \mathbf{q}, \omega)] = - \sum_{\eta=\pm 1} \frac{\partial}{\partial S^2} \text{p.v.} \int_{a(S)}^{b(S)} d\varepsilon \frac{g_-(S, \varepsilon, \eta\mu)}{\varepsilon + \eta\omega}. \quad (\text{F.112})$$

Again, changing the derivative operation with the Cauchy Principal value integral and applying the Leibniz integral formula, we write:

$$\begin{aligned} \partial_{S^2} 16\pi^2 q \operatorname{Re} [F_s(S, \mathbf{q}, \omega)] = & - \sum_{\eta=\pm 1} \text{p.v.} \int_{a(S)}^{b(S)} d\varepsilon \frac{\partial_{S^2} g_-(S, \varepsilon, \eta\mu)}{\varepsilon + \eta\omega} \\ & - \sum_{\eta=\pm 1} \frac{g_-(S, b(S), \eta\mu)}{b(S) + \eta\omega} \partial_{S^2} b(S) \\ & + \sum_{\eta=\pm 1} \frac{g_-(S, a(S), \eta\mu)}{a(S) + \eta\omega} \partial_{S^2} a(S). \end{aligned} \quad (\text{F.113})$$

The second and third terms are zero due to

$$g_-(S, a(S), \eta\mu) = g_-(S, b(S), \eta\mu) = 0. \quad (\text{F.114})$$

Similarly to the pair creation/annihilation contribution, this is a consequence of the definition of  $g_-(S, \varepsilon, \eta\mu)$  in Eq. (F.77). Since  $a(S) = -b(S)$  and by definition,  $c(a(S)) = d(a(S))$  (see Eq. (F.45)), the integration in (F.77) yields zero (see Table F.1). We get:

$$\partial_{S^2} 16\pi^2 q \operatorname{Re} [F_s(S, \mathbf{q}, \omega)] = - \sum_{\eta=\pm 1} \text{p.v.} \int_{a(S)}^{b(S)} d\varepsilon \frac{\partial_{S^2} g_-(S, \varepsilon, \eta\mu)}{\varepsilon + \eta\omega}. \quad (\text{F.115})$$

The derivative,

$$\partial_{S^2} g_-(S, \varepsilon, \eta\mu) = \frac{\partial}{\partial S^2} \int_{c(S, \varepsilon)}^{d(S, \varepsilon)} dE G_-(S, \eta\mu) \quad (\text{F.116})$$

is calculated, as before, using the Leibniz integral rule. One gets:

$$\partial_{S^2} g_-(S, \varepsilon, \eta\mu) = G_-(d(S, \varepsilon), \varepsilon, S, \eta\mu) \frac{\partial}{\partial S^2} d(S, \varepsilon) - G_-(c(S, \varepsilon), \varepsilon, S, \eta\mu) \frac{\partial}{\partial S^2} c(S, \varepsilon). \quad (\text{F.117})$$

The derivatives are (see Table F.1):

$$\frac{\partial}{\partial S^2} d(S, \varepsilon) = \frac{\partial}{\partial S^2} E_\Lambda(S, \varepsilon) = \frac{1}{2\sqrt{\Lambda_f^2 + S^2}}, \quad (\text{F.118})$$

$$\frac{\partial}{\partial S^2} c(S, \varepsilon) = \frac{\partial}{\partial S^2} E_0(S, \varepsilon) = \frac{-q}{\sqrt{(\varepsilon^2 - q^2)(\varepsilon^2 - E_\sigma^2)}}. \quad (\text{F.119})$$

So, one can write:

$$\partial_{S^2} g_-(S, \varepsilon, \eta\mu) = \frac{G_-(d(S, \varepsilon), \varepsilon, S, \eta\mu)}{2\sqrt{\Lambda_f^2 + S^2}} + q \frac{G_-(c(S, \varepsilon), \varepsilon, S, \eta\mu)}{\sqrt{(\varepsilon^2 - q^2)(\varepsilon^2 - E_\sigma^2)}}. \quad (\text{F.120})$$

#### F.5.4 Calculation of $\partial_{S^2} 16\pi^2 q \text{Im} [F_s(S, \mathbf{q}, \omega)]$

The derivative of the real part, with respect to  $S^2$ , is defined as:

$$\partial_{S^2} 16\pi^2 q \text{Im} [F_s(S, \mathbf{q}, \omega)] = 2\pi \partial_{S^2} \{g_-(S, \omega, -\mu)[H(\omega - a(S)) - H(\omega - b(S))]\}. \quad (\text{F.121})$$

We can write:

$$\begin{aligned} \partial_{S^2} 16\pi^2 q \text{Im} [F_s(S, \mathbf{q}, \omega)] &= 2\pi [H(\omega - a(S)) - H(\omega - b(S))] \partial_{S^2} g_-(S, \omega, -\mu) \\ &\quad - 2\pi g_-(S, \omega, -\mu) [\delta(\omega - a(S)) \partial_{S^2} a(S) - \delta(\omega - b(S)) \partial_{S^2} b(S)]. \end{aligned} \quad (\text{F.122})$$

Like before, upon integrating over  $\omega$ , the last term will vanish due to Eq. (F.114). Hence, we finally get:

$$\partial_{S^2} 16\pi^2 q \text{Im} [F_s(S, \mathbf{q}, \omega)] = 2\pi [H(\omega - a(S)) - H(\omega - b(S))] \partial_{S^2} g_-(S, \omega, -\mu). \quad (\text{F.123})$$

Here, the explicit expression for the derivative is given by Eq. (F.120).

## F.6 Calculation of $\partial_\omega \text{Re} [F(S, \mathbf{q}, \omega)]$

The pole contributions, due to the Dirac delta function, introduce a multiplicative factor dependent on  $\partial_\omega \text{Re} [F(S, \mathbf{q}, \omega)]$ . Indeed, this contribution seems to be essential to protect the calculation from a divergence when the pion pole reaches exactly the sigma branch cut, effectively dissolving all collective mode contributions to the dynamics. As performed in previous sections, this contribution will be calculated explicitly by separating the pair creation/annihilation and scattering contributions.

### F.6.1 Calculation of $\partial_\omega 16\pi^2 q \text{Re} [F_p(S, \mathbf{q}, \omega)]$

This  $\omega$ -derivative of the real part of the pair creation/annihilation contribution is defined as:

$$\partial_\omega 16\pi^2 q \text{Re} [F_p(S, \mathbf{q}, \omega)] = \frac{1}{2} \frac{\partial}{\partial \omega} \sum_{\eta=\pm 1} \sum_k \text{p.v.} \int_{A_k}^{B_k} dE \frac{g_+^k(S, E)}{E + \eta\omega/2}. \quad (\text{F.124})$$

Since the right-hand side only depends on  $\omega$  in the denominator, calculating the derivative directly (by commuting the integration with the derivative) would lead to a quadratic divergence when  $E = -\eta\omega/2$ . This would mean that the Cauchy principal value would not be well defined. A partial integration would have to be carried in order to reach an expression where a meaningful value can be assigned to integration through the Cauchy principal value. To avoid this we make

a change of variables in the integral and then apply the Leibniz integral rule. Of course, both methods have to yield the same results. Considering the new variable  $x = E + \eta\omega/2$ , we can write:

$$\partial_\omega 16\pi^2 q \text{Re} [F_p(S, \mathbf{q}, \omega)] = \frac{1}{2} \frac{\partial}{\partial \omega} \sum_{\eta=\pm 1} \sum_k \text{p.v.} \int_{A_k + \eta\omega/2}^{B_k + \eta\omega/2} \frac{dx}{x} g_+^k(x - \eta\omega/2). \quad (\text{F.125})$$

Applying the Leibniz integral rule, we can write:

$$\begin{aligned} \partial_\omega 16\pi^2 q \text{Re} [F_p(S, \mathbf{q}, \omega)] &= \frac{1}{2} \sum_{\eta=\pm 1} \sum_k \text{p.v.} \int_{A_k + \eta\omega/2}^{B_k + \eta\omega/2} \frac{dx}{x} \partial_\omega g_+^k(x - \eta\omega/2) \\ &\quad + \frac{1}{4} \sum_{\eta=\pm 1} \sum_k \eta \frac{g_+^k(S, B_k)}{B_k + \eta\omega/2} \\ &\quad - \frac{1}{4} \sum_{\eta=\pm 1} \sum_k \eta \frac{g_+^k(S, A_k)}{A_k + \eta\omega/2}. \end{aligned} \quad (\text{F.126})$$

Like in the previous section, the second and third terms are zero owing to Eqs. (F.93) and (F.92), respectively.

The derivative in the integrand can be written as:

$$\partial_\omega g_+^k(x - \eta\omega/2) = -\frac{\eta}{2} \partial_a g_+^k(a)_{a=x-\eta\omega/2}. \quad (\text{F.127})$$

Switching back to the original integration variables, we can write:

$$\partial_\omega 16\pi^2 q \text{Re} [F_p(S, \mathbf{q}, \omega)] = -\frac{1}{4} \sum_{\eta=\pm 1} \sum_k \text{p.v.} \int_{A_k}^{B_k} dE \frac{\eta}{E + \eta\omega/2} \partial_E g_+^k(E). \quad (\text{F.128})$$

The derivative in the integrand, using the definition in Eq. (F.59) and the fact that  $D_k(E) = -C_k(E)$ , can be written as:

$$\begin{aligned} \partial_E g_+^k(E) &= \frac{\partial}{\partial E} \int_{C_k(E)}^{D_k(E)} d\varepsilon G_+(E, \varepsilon) \\ &= 2G_+(E, D_k) \partial_E D_k(E) + 2 \int_0^{D_k(E)} d\varepsilon \partial_E G_+(E, \varepsilon). \end{aligned} \quad (\text{F.129})$$

Bringing everything together we can write the derivative in a more compact way:

$$\partial_\omega 16\pi^2 q \text{Re} [F_p(S, \mathbf{q}, \omega)] = \frac{1}{\omega^2 - E_\sigma^2} \sum_k [X_p^k(S, \mathbf{q}, \omega) + Y_p^k(S, \mathbf{q}, \omega)]. \quad (\text{F.130})$$

Where we have defined:

$$\frac{X_p^k(S, \mathbf{q}, \omega)}{\omega^2 - E_\sigma^2} = -\frac{1}{2} \sum_{\eta=\pm 1} \text{p.v.} \int_{A_k}^{B_k} dE G_+(E, D_k) \frac{\eta}{E + \eta\omega/2} \partial_E D_k(E), \quad (\text{F.131})$$

$$\frac{Y_p^k(S, \mathbf{q}, \omega)}{\omega^2 - E_\sigma^2} = -\frac{1}{2} \sum_{\eta=\pm 1} \text{p.v.} \int_{A_k}^{B_k} dE \frac{\eta}{E + \eta\omega/2} \int_0^{D_k(E)} d\varepsilon \partial_E G_+(E, \varepsilon). \quad (\text{F.132})$$

Lets calculate each contribution, individually. Consider Eq. (F.131) for  $k = 1$ , we can write:

$$\frac{X_p^1(S, \mathbf{q}, \omega)}{\omega^2 - E_\sigma^2} = -\frac{1}{2} \sum_{\eta=\pm 1} \text{p.v.} \int_{A_1}^{B_1} dE G_+(E, D_1) \frac{\eta}{E + \eta\omega/2} \partial_E D_1(E) \quad (\text{F.133})$$

The derivative is given by (see Table F.1):

$$\partial_E D_1(E) = \partial_E \varepsilon_+(E) = \frac{16EqS^2}{(4E^2 - q^2)^{3/2}} \frac{1}{\sqrt{4E^2 - E_\sigma^2}}. \quad (\text{F.134})$$

Meaning we get:

$$\frac{X_p^1(S, \mathbf{q}, \omega)}{\omega^2 - E_\sigma^2} = -8 \sum_{\eta=\pm 1} \text{p.v.} \int_{A_1}^{B_1} dE G_+(E, D_1) \frac{EqS^2}{(4E^2 - q^2)^{3/2}} \frac{1}{\sqrt{4E^2 - E_\sigma^2}} \frac{\eta}{E + \eta\omega/2}. \quad (\text{F.135})$$

For practical calculations, it is easier to use the identity,

$$\frac{1}{\sqrt{4E^2 - E_\sigma^2}} \sum_{\eta=\pm 1} \frac{\eta}{E + \eta\omega/2} = \frac{(-1)}{\omega^2 - E_\sigma^2} \sum_{\eta=\pm 1} \left[ \frac{2\omega}{E_\sigma} \eta \frac{\sqrt{2E - \eta E_\sigma}}{\sqrt{2E + \eta E_\sigma}} - \eta \frac{\sqrt{4E^2 - E_\sigma}}{E + \eta\omega/2} \right], \quad (\text{F.136})$$

to simplify the expression. The proof of this equality is presented in the Appendix (J.3). This means we can write the function  $X_p^1(S, \mathbf{q}, \omega)$  as:

$$\begin{aligned} X_p^1(S, \mathbf{q}, \omega) &= 8 \sum_{\eta=\pm 1} \text{p.v.} \int_{A_1}^{B_1} dE G_+(E, D_1) \frac{EqS^2}{(4E^2 - q^2)^{3/2}} \left[ \frac{2\omega}{E_\sigma} \eta \frac{\sqrt{2E - \eta E_\sigma}}{\sqrt{2E + \eta E_\sigma}} - \eta \frac{\sqrt{4E^2 - E_\sigma}}{E + \eta\omega/2} \right] \\ &= x_\sigma(S, \mathbf{q}, \omega) - x_\omega(S, \mathbf{q}, \omega). \end{aligned} \quad (\text{F.137})$$

Here,

$$x_\sigma(S, \mathbf{q}, \omega) = 16 \sum_{\eta=\pm 1} \text{p.v.} \int_{A_1}^{B_1} dE G_+(E, D_1) \frac{EqS^2}{(4E^2 - q^2)^{3/2}} \frac{\omega}{E_\sigma} \eta \frac{\sqrt{2E - \eta E_\sigma}}{\sqrt{2E + \eta E_\sigma}}, \quad (\text{F.138})$$

$$x_\omega(S, \mathbf{q}, \omega) = 8 \sum_{\eta=\pm 1} \text{p.v.} \int_{A_1}^{B_1} dE G_+(E, D_1) \frac{EqS^2}{(4E^2 - q^2)^{3/2}} \eta \frac{\sqrt{4E^2 - E_\sigma}}{E + \eta\omega/2}. \quad (\text{F.139})$$

To finish, we just point out that for  $\omega = E_\sigma$ , both contributions are equal and  $X_p^1(S, \mathbf{q}, E_\sigma) = 0$ .

For  $k = 2$ , the derivative is much simpler,  $\partial_E D_2(E) = \partial_E \varepsilon_{\Lambda_+}(E) = 2$  (see Table F.1). Hence,  $X_p^2(S, \mathbf{q}, \omega)$  is given by:

$$X_p^2(S, \mathbf{q}, \omega) = -(\omega^2 - E_\sigma^2) \sum_{\eta=\pm 1} \text{p.v.} \int_{A_2}^{B_2} dE G_+(E, D_2) \frac{\eta}{E + \eta\omega/2}. \quad (\text{F.140})$$

To finish the calculation, we just have to calculate the term  $Y_p^k(S, \mathbf{q}, \omega)$ , defined in Eq. (F.132). The derivative in the integrand can be written as:

$$\partial_E G_+(E, \varepsilon) = \partial_E [1 - n_F(E - \varepsilon/2) - n_F(E + \varepsilon/2)] = - \sum_{\eta=\pm 1} \partial_E n_F(E + \eta\varepsilon/2). \quad (\text{F.141})$$

The inner most integration in Eq. (F.132) can be written as (considering a change of variables as  $z = E + \eta\varepsilon/2$ ):

$$\begin{aligned} \int_0^{D_k(E)} d\varepsilon \partial_E G_+(E, \varepsilon) &= - \sum_{\eta=\pm 1} \int_0^{D_k(E)} d\varepsilon \partial_E n_F(E + \eta\varepsilon/2) \\ &= - \sum_{\eta=\pm 1} \frac{2}{\eta} \int_E^{E+\eta D_k(E)/2} dz \partial_z n_F(z) \\ &= -2 \left[ n_F\left(E + \frac{D_k(E)}{2}\right) - n_F\left(E - \frac{D_k(E)}{2}\right) \right]. \end{aligned} \quad (\text{F.142})$$

So we can finally write:

$$\frac{Y_p^k(S, \mathbf{q}, \omega)}{\omega^2 - E_\sigma^2} = \sum_{\eta=\pm 1} \text{p.v.} \int_{A_k}^{B_k} dE \frac{\eta}{E + \eta\omega/2} \left[ n_F\left(E + \frac{D_k(E)}{2}\right) - n_F\left(E - \frac{D_k(E)}{2}\right) \right]. \quad (\text{F.143})$$

### F.6.2 Calculation of $\partial_\omega 16\pi^2 q \text{Re} [F_s(S, \mathbf{q}, \omega)]$

This  $\omega$ -derivative of the real part of the scattering contribution is defined as:

$$\partial_\omega 16\pi^2 q \text{Re} [F_s(S, \mathbf{q}, \omega)] = -\frac{\partial}{\partial \omega} \sum_{\eta=\pm 1} \text{p.v.} \int_a^b d\varepsilon \frac{g_-(\varepsilon)}{\varepsilon + \eta\omega}. \quad (\text{F.144})$$

Following the previous section, consider the new variable  $x = \varepsilon + \eta\omega$ , we can write:

$$\partial_\omega 16\pi^2 q \text{Re} [F_s(S, \mathbf{q}, \omega)] = -\frac{\partial}{\partial \omega} \sum_{\eta=\pm 1} \text{p.v.} \int_{a+\eta\omega}^{b+\eta\omega} \frac{dx}{x} g_-(x - \eta\omega). \quad (\text{F.145})$$

Applying the Leibniz integral rule, we can write:

$$\begin{aligned} \partial_\omega 16\pi^2 q \text{Re} [F_s(S, \mathbf{q}, \omega)] &= - \sum_{\eta=\pm 1} \text{p.v.} \int_{a+\eta\omega}^{b+\eta\omega} \frac{dx}{x} \partial_\omega g_-(x - \eta\omega) \\ &\quad - \sum_{\eta=\pm 1} \eta \frac{g_-(S, b)}{b + \eta\omega} + \sum_{\eta=\pm 1} \eta \frac{g_-(S, a)}{a + \eta\omega}. \end{aligned} \quad (\text{F.146})$$

The second and third terms are zero due to identity (F.114).

The derivative in the integrand can be written as:

$$\partial_\omega g_-(x - \eta\omega) = -\eta \partial_a g_-(a)_{a=x-\eta\omega}. \quad (\text{F.147})$$

Which means we can write:

$$\partial_\omega 16\pi^2 q \operatorname{Re} [F_s(S, \mathbf{q}, \omega)] = \sum_{\eta=\pm 1} \text{p.v.} \int_a^b d\varepsilon \frac{\eta}{\varepsilon + \eta\omega} \partial_\varepsilon g_-(\varepsilon). \quad (\text{F.148})$$

The derivative can be calculated, again by application of the Leibniz integral rule:

$$\partial_\varepsilon g_-(\varepsilon) = G_-(d, \varepsilon) \partial_\varepsilon d(\varepsilon) - G_-(c, \varepsilon) \partial_\varepsilon c(\varepsilon) + \int_c^d dE \partial_\varepsilon G_-(E, \varepsilon) \quad (\text{F.149})$$

We write:

$$\partial_\omega 16\pi^2 q \operatorname{Re} [F_s(S, \mathbf{q}, \omega)] = \frac{1}{\omega^2 - E_\sigma^2} [X_s(S, \mathbf{q}, \omega) + Y_s(S, \mathbf{q}, \omega) + Z_s(S, \mathbf{q}, \omega)], \quad (\text{F.150})$$

with

$$\frac{X_s(S, \mathbf{q}, \omega)}{\omega^2 - E_\sigma^2} = \sum_{\eta=\pm 1} \text{p.v.} \int_a^b d\varepsilon \eta \frac{G_-(d, \varepsilon)}{\varepsilon + \eta\omega} \partial_\varepsilon d(\varepsilon), \quad (\text{F.151})$$

$$\frac{Y_s(S, \mathbf{q}, \omega)}{\omega^2 - E_\sigma^2} = - \sum_{\eta=\pm 1} \text{p.v.} \int_a^b d\varepsilon \eta \frac{G_-(c, \varepsilon)}{\varepsilon + \eta\omega} \partial_\varepsilon c(\varepsilon), \quad (\text{F.152})$$

$$\frac{Z_s(S, \mathbf{q}, \omega)}{\omega^2 - E_\sigma^2} = \sum_{\eta=\pm 1} \text{p.v.} \int_a^b d\varepsilon \frac{\eta}{\varepsilon + \eta\omega} \int_c^d dE \partial_\varepsilon G_-(E, \varepsilon). \quad (\text{F.153})$$

Consider each contribution individually. The first and second derivatives are (see Table F.1):

$$\partial_\varepsilon d(\varepsilon) = \partial_\varepsilon E_\Lambda(\varepsilon) = \frac{\varepsilon}{2|\varepsilon|}, \quad (\text{F.154})$$

$$\partial_\varepsilon c(\varepsilon) = \partial_\varepsilon E_0(\varepsilon) = \frac{2\varepsilon q S^2}{(q^2 - \varepsilon^2)^{3/2}} \frac{1}{\sqrt{E_\sigma^2 - \varepsilon^2}}. \quad (\text{F.155})$$

The innermost integrand in  $Z_s(S, \mathbf{q}, \omega)$  is:

$$\begin{aligned}
\int_c^d dE \partial_\varepsilon G_-(E, \varepsilon) &= \int_c^d dE \partial_\varepsilon n_F(E - \varepsilon/2) - \int_c^d dE \partial_\varepsilon n_F(E + \varepsilon/2) \\
&= \sum_{\eta=\pm 1} \eta \int_c^d dE \partial_\varepsilon n_F(E - \eta\varepsilon/2) \\
&= -\frac{1}{2} \sum_{\eta=\pm 1} \int_{c-\eta\frac{\varepsilon}{2}}^{d-\eta\frac{\varepsilon}{2}} dz \partial_z n_F(z) \\
&= \frac{1}{2} \sum_{\eta'=\pm 1} \left[ n_F\left(c - \eta'\frac{\varepsilon}{2}\right) - n_F\left(d - \eta'\frac{\varepsilon}{2}\right) \right]. \tag{F.156}
\end{aligned}$$

Finally, we can write:

$$\frac{X_s(S, \mathbf{q}, \omega)}{\omega^2 - E_\sigma^2} = \frac{1}{2} \sum_{\eta=\pm 1} \text{p.v.} \int_a^b d\varepsilon \eta \frac{G_-(d, \varepsilon)}{\varepsilon + \eta\omega} \frac{\varepsilon}{|\varepsilon|}, \tag{F.157}$$

$$\frac{Y_s(S, \mathbf{q}, \omega)}{\omega^2 - E_\sigma^2} = -2 \sum_{\eta=\pm 1} \text{p.v.} \int_a^b d\varepsilon \eta \frac{G_-(c, \varepsilon)}{\varepsilon + \eta\omega} \frac{\varepsilon q S^2}{(q^2 - \varepsilon^2)^{3/2}} \frac{1}{\sqrt{E_\sigma^2 - \varepsilon^2}}, \tag{F.158}$$

$$\frac{Z_s(S, \mathbf{q}, \omega)}{\omega^2 - E_\sigma^2} = \frac{1}{2} \sum_{\eta=\pm 1} \text{p.v.} \int_a^b d\varepsilon \frac{\eta}{\varepsilon + \eta\omega} \sum_{\eta'=\pm 1} \left[ n_F\left(c - \eta'\frac{\varepsilon}{2}\right) - n_F\left(d - \eta'\frac{\varepsilon}{2}\right) \right]. \tag{F.159}$$

## F.7 Noncommutative limits of the $f_1(S, q \rightarrow 0)$ loop function

In the meson contributions to the  $SU(2)_f$  NJL gap equation, it is necessary to evaluate the  $q \rightarrow 0$  limit of the  $f_1(S, q)$  loop function i.e.,  $f_1(S, 0)$ . This operation implies two distinct limits,  $q_0 \rightarrow 0$  and  $\mathbf{q} \rightarrow 0$ .

After the extension of the discrete Matsubara frequencies to continuum values  $q_0$ , the function  $f_1(S, q)$  is no longer analytic in the origin [313]. This can easily be demonstrated by seeing that the limiting operations,  $\mathbf{q} \rightarrow 0$  and  $q_0 \rightarrow 0$ , do not commute, see Eq. (7.60). This fact is a consequence of the breaking of Lorentz symmetry by the heath bath: at zero temperature functions derived from Lorentz invariant field theories only depend on  $q^\mu$  while at finite temperature the dependence on  $q_0$  and  $\mathbf{q}$  can be different. In fact this feature is a well know property of finite temperature field theory and the limiting operations in Eq. (7.60) are related two two distinct approximations. The left hand side limit is known as the *static* limit while the one in the right hand side is known as the *plasmon* limit. For more details see [313]. To explicitly calculate both limits, consider the function  $f_1(S, \mathbf{q}, q_0)$  with zero chemical potential defined in Eq. (F.19).

For the *plasmon* limit, one gets:

$$\begin{aligned}
\lim_{q_0 \rightarrow 0} \lim_{\mathbf{q} \rightarrow 0} f_1(S, \mathbf{q}, q_0) &= \lim_{q_0 \rightarrow 0} f_1(S, \mathbf{q} = 0, q_0) \\
&= \lim_{q_0 \rightarrow 0} \int \frac{d^3k}{(2\pi)^3} \frac{1 - 2n_{\text{F}}(E_{\mathbf{k}})}{4E_{\mathbf{k}}^2} \left[ \frac{1}{iq_0 + 2E_{\mathbf{k}}} - \frac{1}{iq_0 - 2E_{\mathbf{k}}} \right] \\
&= \int \frac{d^3k}{(2\pi)^3} \frac{1 - 2n_{\text{F}}(E_{\mathbf{k}})}{4E_{\mathbf{k}}^3}. \tag{F.160}
\end{aligned}$$

For the *static* limit, we write:

$$\begin{aligned}
\lim_{q \rightarrow 0} \lim_{q_0 \rightarrow 0} f_1(S, \mathbf{q}, q_0) &= \lim_{q \rightarrow 0} f_1(S, \mathbf{q}, q_0 = 0) \\
&= \lim_{q \rightarrow 0} \int \frac{d^3k}{(2\pi)^3} \frac{1}{2E_{\mathbf{k}}E_{\mathbf{k}-q}} \left\{ \frac{1 - n_{\text{F}}(E_{\mathbf{k}}) - n_{\text{F}}(E_{\mathbf{k}-q})}{E_{\mathbf{k}} + E_{\mathbf{k}-q}} + \frac{n_{\text{F}}(E_{\mathbf{k}}) - n_{\text{F}}(E_{\mathbf{k}-q})}{E_{\mathbf{k}} - E_{\mathbf{k}-q}} \right\} \\
&= \int \frac{d^3k}{(2\pi)^3} \frac{1 - 2n_{\text{F}}(E_{\mathbf{k}})}{4E_{\mathbf{k}}^3} + \int \frac{d^3k}{(2\pi)^3} \frac{1}{2E_{\mathbf{k}}} \lim_{q \rightarrow 0} \frac{n_{\text{F}}(E_{\mathbf{k}}) - n_{\text{F}}(E_{\mathbf{k}-q})}{E_{\mathbf{k}-q}(E_{\mathbf{k}} - E_{\mathbf{k}-q})} \\
&= \int \frac{d^3k}{(2\pi)^3} \frac{1}{4E_{\mathbf{k}}^3} \left\{ 1 - 2n_{\text{F}}(E_{\mathbf{k}}) + \frac{2E_{\mathbf{k}}}{T} n_{\text{F}}(E_{\mathbf{k}}) [n_{\text{F}}(E_{\mathbf{k}}) - 1] \right\}. \tag{F.161}
\end{aligned}$$

Where second term can be calculated by application of L'Hôpital's rule as follows:

$$\begin{aligned}
\lim_{q \rightarrow 0} \frac{n_{\text{F}}(E_{\mathbf{k}}) - n_{\text{F}}(E_{\mathbf{k}-q})}{E_{\mathbf{k}-q}(E_{\mathbf{k}} - E_{\mathbf{k}-q})} &= \lim_{q \rightarrow 0} \frac{\frac{d}{dq}(n_{\text{F}}(E_{\mathbf{k}}) - n_{\text{F}}(E_{\mathbf{k}-q}))}{\frac{d}{dq}E_{\mathbf{k}-q}(E_{\mathbf{k}} - E_{\mathbf{k}-q})} = \lim_{q \rightarrow 0} \frac{-\frac{dn_{\text{F}}(E_{\mathbf{k}-q})}{dE_{\mathbf{k}-q}} \frac{dE_{\mathbf{k}-q}}{dq}}{-\frac{dE_{\mathbf{k}-q}}{dq}(2E_{\mathbf{k}-q} - E_{\mathbf{k}})} \\
&= \lim_{q \rightarrow 0} \frac{\beta n_{\text{F}}(E_{\mathbf{k}-q}) [n_{\text{F}}(E_{\mathbf{k}-q}) - 1]}{2E_{\mathbf{k}-q} - E_{\mathbf{k}}} = \frac{n_{\text{F}}(E_{\mathbf{k}})}{TE_{\mathbf{k}}} [n_{\text{F}}(E_{\mathbf{k}}) - 1]. \tag{F.162}
\end{aligned}$$

We highlight that in the zero temperature limit, both expressions agree.

## Appendix G

### $f_2(S, q)$ loop function

The thermal loop function  $f_2(S, q)$  is defined as:

$$f_2(S, q) = \int \frac{d^4k}{(2\pi)^4} \frac{1}{((k-q)^2 + S^2)(k^2 + S^2)^2}. \quad (\text{G.1})$$

If one wishes to proceed as before and integrate over  $k_0$  using the Matsubara trick, one would have to deal with poles of order two. This feature would make the residue calculation quite complicated leading to lengthy expressions. We have also to stress that this function will be integrated again over  $q$ . This means that  $q_0$  will be integrated over and by the use of the Matsubara formalism, another residue calculation will have to be made. Hence, to simplify the residue calculation, we will use a trick. One can show that the loop functions  $f_1(S, q)$  and  $f_2(S, q)$ , are connected through a derivative with respect to the parameter  $S$ :

$$f_2(S, q) = -\frac{1}{2} \frac{\partial}{\partial S^2} f_1(S, q). \quad (\text{G.2})$$

To prove Eq. (G.2), we write  $f_2(S, q)$  as:

$$f_2(S, q) = \frac{1}{2} \int \frac{d^4k}{(2\pi)^4} \left[ \frac{1}{((k-q)^2 + S^2)(k^2 + S^2)^2} + \frac{1}{((k-q)^2 + S^2)(k^2 + S^2)^2} \right]. \quad (\text{G.3})$$

Change variables in one of the terms using  $k - q = -p$  and  $d^4k = d^4p$ , to yield:

$$\begin{aligned} f_2(S, q) &= \frac{1}{2} \int \frac{d^4k}{(2\pi)^4} \frac{1}{((k-q)^2 + S^2)(k^2 + S^2)^2} + \frac{1}{2} \int \frac{d^4p}{(2\pi)^4} \frac{1}{(p^2 + S^2)((p-q)^2 + S^2)^2} \\ &= \frac{1}{2} \int \frac{d^4k}{(2\pi)^4} \left[ \frac{1}{((k-q)^2 + S^2)(k^2 + S^2)^2} + \frac{1}{(k^2 + S^2)((k-q)^2 + S^2)^2} \right]. \end{aligned} \quad (\text{G.4})$$

We can use the following identity

$$-\frac{\partial}{\partial S^2} \frac{1}{((k-q)^2 + S^2)(k^2 + S^2)} = \frac{1}{((k-q)^2 + S^2)(k^2 + S^2)^2} + \frac{1}{(k^2 + S^2)((k-q)^2 + S^2)^2}, \quad (\text{G.5})$$

to write Eq. (G.4) as:

$$f_2(S, q) = -\frac{1}{2} \int \frac{d^4 k}{(2\pi)^4} \frac{\partial}{\partial S^2} \frac{1}{((k-q)^2 + S^2)(k^2 + S^2)} = -\frac{1}{2} \frac{\partial}{\partial S^2} f_1(S, q). \quad (\text{G.6})$$

## Appendix H

# Non-existence of the $\sigma$ -meson collective excitation at finite temperature

In this section we argue that the  $\sigma$ -meson integrals will not have contributions originated from the collective excitations modes, i.e., contributions coming from the poles. A collective excitation for this meson exists, for given positive values of temperature ( $T$ ), Hartree mass ( $S$ ) and 3-momentum ( $\mathbf{q}$ ), if there is an  $\omega \in [\varepsilon_+, E_\sigma]$  (the  $\omega$ -region in-between the branch cuts<sup>1</sup>) which fulfils the following equality:

$$-\omega^2 + E_\sigma^2(S, q) + \frac{\tilde{m}}{\operatorname{Re}[F(S, \mathbf{q}, \omega)]} = 0. \quad (\text{H.1})$$

If  $\operatorname{Re}[F(S, \mathbf{q}, \omega)] > 0$  for  $\omega \in [\varepsilon_\Lambda, E_\sigma]$ , this equality will never hold for real  $E_\sigma^2(S, q)$ , which means that, in the range of  $\omega$  in-between cuts, there will not be any pole contributions coming from excitations with the same quantum numbers as the  $\sigma$  field. Hence, to show that there is no  $\sigma$ -meson collective excitation at finite temperature we will argue that, for any positive values of  $T$ ,  $S$  and  $\mathbf{q}$ , for  $\omega \in [\varepsilon_\Lambda, E_\sigma]$ , the following holds:  $\operatorname{Re}[F(S, \mathbf{q}, \omega)] > 0$ .

Although we checked numerically that Eq. (H.1) had no solutions for  $\omega \in [\varepsilon_+, E_\sigma]$  when we were solving the one-meson-loop gap equation, here we give an analytical argument to why such behaviour is expected.

Some equations used in this appendix are also presented in Table F.1.

### H.1 The zero temperature case, $T = 0$

For the zero temperature case, the scattering contribution,  $\operatorname{Re}[F_s(\omega)]$ , vanishes (see the definition in Eq. (F.25)), and the only contribution to  $\operatorname{Re}[F(\omega)]$  comes from the pair creation/annihilation

---

<sup>1</sup>This region corresponds to the region where the imaginary part of  $F(S, \mathbf{q}, \omega)$  is zero. The aforementioned range can be obtained by analysing Eqs. (F.73) and (F.89).

term,  $\text{Re}[F(\omega)] \equiv \text{Re}[F_p(\omega)]$ . It can be written as:

$$16\pi^2 q \text{Re}[F(\omega)] = \frac{1}{2} \sum_k \int_{A_k}^{B_k} dE \frac{2E}{E^2 - \omega^2/4} g_+^k(E). \quad (\text{H.2})$$

As discussed in the Appendix F.2, here,  $B_k = E_+$ ,  $A_1 = E_0 = E_\sigma/2$  and  $A_2 = E'_0$  (see Eqs. (F.53), (F.46) and (F.47)). One can verify that  $E_+ > E_\sigma$ , and  $E'_0 \geq E_0$ , as long as  $|q/\Lambda_f| \leq 2$ . Consider a particular contribution to the sum  $k$ , in  $\text{Re}[F_p(\omega)]$ :

$$f_k = \frac{1}{2} \int_{A_k}^{B_k} dE \frac{2E}{E^2 - \omega^2/4} g_+^k(E). \quad (\text{H.3})$$

In the range of  $\omega$  values we are interested in,  $\omega \in [\varepsilon_+, E_\sigma]$ , and considering the range of the integration variable,  $E \in [A_k, B_k]$ , the quotient in the integrand is always positive, i.e.,  $E^2 - \omega^2/4 \geq 0$ . This can be seen by considering the largest value of  $\omega$ ,  $\omega = E_\sigma$  and realizing that the quotient is always non-negative for  $E \in [E_\sigma/2, E_+]$  or  $E \in [E'_0, E_+]$ . The function  $g_+^k(E)$  in the integrand, is defined in Eq. (F.68). In the zero temperature and chemical potential limit, it is simply given by  $g_+^k(E) = 2D_k$ . For  $k = 1$ , this function is  $D_1 = \varepsilon_+(E)$  (see Eq. (F.51)) while, for  $k = 2$ , it is  $D_2 = \varepsilon_\Lambda(E)$  (see Eq. (F.52)). Again, in the range of the integration variable  $E$ , these functions are non-negative, i.e.,  $g_+^k(E) \geq 0$  for  $E \in [E_0, E_+]$  ( $k = 1$ ) and  $E \in [E'_0, E_+]$  ( $k=2$ ). Since the integration range is positive and the integrand is a non-negative function, the Riemann integral is positive i.e., for  $\omega \in [\varepsilon_+, E_\sigma]$ ,

$$f_k = \left( \frac{1}{2} \int_{A_k}^{B_k} dE \left| \frac{2E}{E^2 - \omega^2/4} g_+^k(E) \right| \right) > 0. \quad (\text{H.4})$$

Thus, in the original sum in Eq. (H.2), each term is positive. However the sum in  $k$  is actually a subtraction, with the  $k = 2$  term being negative, see Eq. (F.50). Writing the sum in  $k$  explicitly, we find:

$$16\pi^2 q \text{Re}[F_p(\omega)] = \frac{1}{2} \left( \int_{E_0}^{E_+} dE \left| \frac{2E}{E^2 - \omega^2/4} g_+^1(E) \right| - \int_{E'_0}^{E_+} dE \left| \frac{2E}{E^2 - \omega^2/4} g_+^2(E) \right| \right). \quad (\text{H.5})$$

Since each term is non-negative, the function  $16\pi^2 q \text{Re}[F_p(\omega)]$  is non-negative if the first term with  $k = 1$  is bigger than the second term with  $k = 2$ :

$$\int_{E_0}^{E_+} dE \left| \frac{2E}{E^2 - \omega^2/4} g_+^1(E) \right| > \int_{E'_0}^{E_+} dE \left| \frac{2E}{E^2 - \omega^2/4} g_+^2(E) \right|. \quad (\text{H.6})$$

As already stated,  $E'_0 \geq E_0$  and they are equal in the ‘‘extreme’’ case when one considers  $q/\Lambda_f = 2$ . For smaller values of  $q/\Lambda_f$ , the integration region with  $k = 2$  gets smaller, in fact, for  $q/\Lambda_f \rightarrow 0$ , the second term in Eq. (H.5) vanishes. Hence, the region of integration in the second term is

---

<sup>2</sup>As a matter of fact, the boson momentum,  $q$ , is limited by the boson cutoff,  $\Lambda_b$ . We will study different values of  $\Lambda_b/\Lambda_f \leq \alpha$ . In the extreme case with  $|q/\Lambda_f| = 2$ , it is trivial to check that  $E'_0 = E_0$ . This will be important to argue that  $\text{Re}[F_p(\omega)] \geq 0$ .

larger when  $q/\Lambda_f = 2$ . This can also be observed formally by performing the integration in Eq. (F.63) with the two different values of  $q/\Lambda_f$  and comparing the two resulting integrands. Taking these considerations into account, the following inequality must hold for the  $k = 2$  term:

$$\int_{E_0}^{E_+} dE \left| \frac{2E}{E^2 - \omega^2/4} g_+^2(E) \right| \geq \int_{E'_0}^{E_+} dE \left| \frac{2E}{E^2 - \omega^2/4} g_+^2(E) \right|. \quad (\text{H.7})$$

Thereby, if the following holds:

$$\int_{E_0}^{E_+} dE \left| \frac{2E}{E^2 - \omega^2/4} g_+^1(E) \right| > \int_{E_0}^{E_+} dE \left| \frac{2E}{E^2 - \omega^2/4} g_+^2(E) \right|, \quad (\text{H.8})$$

then, using Eq. (H.7), the original inequality in (H.6) holds, and  $16\pi^2 q \text{Re} [F_p(\omega)] > 0$ . To show this, we write the previous inequality, given in (H.8), as:

$$\int_{E_0}^{E_+} dE \left| \frac{2E}{E^2 - \omega^2/4} \left( |g_+^1(E)| - |g_+^2(E)| \right) \right| > 0 \implies |g_+^1(E)| > |g_+^2(E)|. \quad (\text{H.9})$$

In the positive range of the integration variable,  $E \in [E_0, E_+]$ , the condition above is true because,  $\varepsilon_+(E) \geq \varepsilon_\Lambda(E)$ . So, as already mentioned, the original inequality in (H.6) must also hold for any  $E'_0 \geq E_0$  because of relation (H.7). Hence, from (H.6) and (H.5), for  $T = 0$  and  $\omega \in [\varepsilon_+, E_\sigma]$ , the function  $16\pi^2 q \text{Re} [F(\omega)]$  is positive and there is no solution to Eq. (H.1) in the range  $\omega \in [\varepsilon_+, E_\sigma]$ . This means that there is no pole contribution coming from excitations with the same quantum numbers as the  $\sigma$ .

## H.2 The finite temperature case, $T > 0$

The finite temperature scenario is a little bit more complicated, but the reasoning is completely analogous to the zero temperature case. In this case, one can decompose  $\text{Re} [F(\omega)]$  in two distinct contributions, and write:

$$16\pi^2 q \text{Re} [F(\omega)] = 16\pi^2 q \text{Re} [F_p(\omega)] + 16\pi^2 q \text{Re} [F_s(\omega)]. \quad (\text{H.10})$$

Consider the scattering contribution,  $\text{Re} [F_s(\omega)]$ . It is defined in Eq.(F.86) and can be written as:

$$16\pi^2 q \text{Re} [F_s(\omega)] = \int_{-\varepsilon_+}^0 d\varepsilon \frac{2\varepsilon}{\omega^2 - \varepsilon^2} g_-(\varepsilon) + \int_0^{\varepsilon_+} d\varepsilon \frac{2\varepsilon}{\omega^2 - \varepsilon^2} g_-(\varepsilon). \quad (\text{H.11})$$

For zero chemical potential, the integrand,  $g_-(\varepsilon)$ , is (see Eq.(F.84)):

$$g_-(\varepsilon) = T \ln \left[ \left( \frac{e^{\beta E_\Lambda} + e^{-\beta \varepsilon/2}}{e^{\beta E_\Lambda} + e^{\beta \varepsilon/2}} \right) \left( \frac{e^{\beta E_0} + e^{\beta \varepsilon/2}}{e^{\beta E_0} + e^{-\beta \varepsilon/2}} \right) \right]. \quad (\text{H.12})$$

We wish to study the sign of this function for positive and negative values of  $\varepsilon$ . Since we are dealing with finite temperature,  $T > 0$ , we can consider instead how the sign of this function

behaves for different values of  $y = \beta\varepsilon/2$ . So, in an equivalent way:

$$\frac{g_-(y)}{T} = \ln \left[ \left( \frac{e^{\beta E_\Lambda} + e^{-y}}{e^{\beta E_\Lambda} + e^y} \right) \left( \frac{e^{\beta E_0} + e^y}{e^{\beta E_0} + e^{-y}} \right) \right]. \quad (\text{H.13})$$

As before, in the region of the integration variable, one has:  $E_\Lambda(\varepsilon) \geq E_0(\varepsilon) > 0$ . In order to parametrize this, we define:  $e^{\beta E_\Lambda} = a_\Lambda > 1$ ,  $e^{\beta E_0} = a_\Lambda/c$  with  $c \geq 1$ . Using this, the logarithm in the previous equations is:

$$\ln \left[ \left( \frac{a_\Lambda + e^{-y}}{a_\Lambda + e^y} \right) \left( \frac{a_\Lambda/c + e^y}{a_\Lambda/c + e^{-y}} \right) \right]. \quad (\text{H.14})$$

If the argument in the logarithm is larger or equal to one, then:  $g_-(y) \geq 0$ . In such case:

$$\left( \frac{a_\Lambda + e^{-y}}{a_\Lambda + e^y} \right) \left( \frac{a_\Lambda/c + e^y}{a_\Lambda/c + e^{-y}} \right) \geq 1 \implies (e^y - e^{-y}) \geq \frac{(e^y - e^{-y})}{c} \quad (\text{H.15})$$

By definition,  $c \geq 1$ , and the above inequality only holds for  $y \geq 0$ . Hence, for  $\varepsilon \geq 0$ , the argument of the logarithm is larger or equal to one, implying that  $g_-(y) \geq 0$ . In the other case, if the argument is smaller or equal to one,  $g_-(\varepsilon) \leq 0$ . In this case,

$$\left( \frac{a_\Lambda + e^{-y}}{a_\Lambda + e^y} \right) \left( \frac{a_\Lambda/c + e^y}{a_\Lambda/c + e^{-y}} \right) \leq 1 \implies (e^y - e^{-y}) \leq \frac{(e^y - e^{-y})}{c}. \quad (\text{H.16})$$

This inequality holds for  $c \geq 1$  and  $y \leq 0$ , which means that, for  $\varepsilon \leq 0$ ,  $g_-(\varepsilon) \leq 0$ . Summarizing, in the region of integration,  $\varepsilon \in [-\varepsilon_+, \varepsilon_+]$ ,  $g_-(\varepsilon) = |g_-(\varepsilon)|$  for  $\varepsilon \geq 0$  and  $g_-(\varepsilon) = -|g_-(\varepsilon)|$  for  $\varepsilon \leq 0$ .

Consider the second term in Eq. (H.11),  $I_+$ . It is given by:

$$I_+ = \int_0^{\varepsilon_+} d\varepsilon \frac{2\varepsilon}{\omega^2 - \varepsilon^2} g_-(\varepsilon). \quad (\text{H.17})$$

In this term, the integration variable is non-negative as well as the function  $g_-(\varepsilon)$ . In the interval of  $\omega$  that we are interested in,  $\omega \in [\varepsilon_+, E_\sigma]$ , the fraction is also a non-negative function. So, the integrand is a non-negative function in the region of integration and the Riemann integral is non-negative:

$$I_+ = \int_0^{\varepsilon_+} d\varepsilon \left| \frac{2\varepsilon}{\omega^2 - \varepsilon^2} g_-(\varepsilon) \right| \geq 0. \quad (\text{H.18})$$

For the first term in Eq. (H.11),  $I_-$ , the integration variable is non-positive,  $\varepsilon \leq 0$ . Using a change of variables as,  $\varepsilon = -|x|$ , yields:

$$I_- = \int_{-\varepsilon_+}^0 d\varepsilon \frac{2\varepsilon}{\omega^2 - \varepsilon^2} g_-(\varepsilon) = - \int_0^{\varepsilon_+} d|x| \frac{2|x|}{\omega^2 - |x|^2} g_-(|x|). \quad (\text{H.19})$$

As before, the fraction in the integrand is a non-negative function for  $\omega \in [\varepsilon_+, E_\sigma]$ . Recalling the previous discussion about  $g_-(y)$ , the integrand is a non-negative function in the range of

integration, the Riemann integral is non-negative and we can write:

$$I_- = \int_0^{\varepsilon_+} dx \left| \frac{2|x|}{\omega^2 - |x|^2} g_-(-|x|) \right| \geq 0. \quad (\text{H.20})$$

Finally, we can conclude that the scattering term, as defined in Eq. (H.11), is non-negative, i.e.  $16\pi^2 q \operatorname{Re}[F_s(\omega)] \geq 0$ .

To show that the pair creation/annihilation term, at finite temperature is positive, i.e.,  $16\pi^2 q \operatorname{Re}[F_p(\omega)] > 0$ , the reasoning is identical to the one presented for the zero temperature case. The previous arguments rest in two major pillars: (1) each contribution in the  $k$  sum is positive; (2) the term with  $k = 1$  is larger than the term with  $k = 2$  (in absolute value). The only change when considering finite temperature comes from the analytical structure of the functions  $g_+^k(E)$ . At finite temperature, for an arbitrary  $k$ , this function is defined as (see Eq. (F.68 with zero chemical potential)):

$$g_+^k(E) = 2D_k + 4T \ln \left[ \frac{e^{\beta E} + e^{-\beta D_k/2}}{e^{\beta E} + e^{\beta D_k/2}} \right] = 4T \ln \left[ e^{\beta D_k/2} \left( \frac{e^{\beta E} + e^{-\beta D_k/2}}{e^{\beta E} + e^{\beta D_k/2}} \right) \right]. \quad (\text{H.21})$$

Assuming that  $g_+^k(E) > 0$ , the argument in the logarithm must be bigger than one:

$$e^{\beta D_k/2} \left( \frac{e^{\beta E} + e^{-\beta D_k/2}}{e^{\beta E} + e^{\beta D_k/2}} \right) > 1 \implies (e^{\beta D_k/2} - 1) > \frac{(e^{\beta D_k/2} - 1)}{e^{\beta E}}. \quad (\text{H.22})$$

This inequality holds, since  $\beta E > 0$  in the integration range and  $D_k > 0$  for any  $k$ . This confirms that the argument of the logarithm is indeed bigger than one, and that  $g_+^k(E) > 0$  for any  $k$ , exactly like in the  $T = 0$  case.

Let us check now whether the condition that the contribution with  $k = 1$ , is indeed larger than the one for  $k = 2$ , like in the zero temperature case. As before we consider the extreme case with  $q/\Lambda_f = 2 \implies E'_0 = E_0$ . From Eq. (H.9), we can write, at finite temperature:

$$\left| g_+^1(E) \right| - \left| g_+^2(E) \right| > 0 \implies \ln \left[ e^{\beta D_1/2} \left( \frac{e^{\beta E} + e^{-\beta D_1/2}}{e^{\beta E} + e^{\beta D_1/2}} \right) e^{-\beta D_2/2} \left( \frac{e^{\beta E} + e^{\beta D_2/2}}{e^{\beta E} + e^{-\beta D_2/2}} \right) \right] > 0 \quad (\text{H.23})$$

Here, we have used the previous result that the logarithm is a positive function for any  $k$  and the integration variable is positive in the range of integration,  $E > 0$ . For simplicity, we define  $a = e^{\beta E} > 0$ ,  $y_1 = \beta D_1/2$  and  $y_2 = \beta D_2/2$ . Since  $D_1 \geq D_2$ , we can parametrize  $y_2 = y_1/c$  with  $c \geq 1$ . This inequality only holds if the argument is larger than one, assuming such to be the case, we write:

$$e^{y_1 - y_1/c} \left( \frac{a + e^{-y_1}}{a + e^{y_1}} \right) \left( \frac{a + e^{y_1/c}}{a + e^{-y_1/c}} \right) > 1 \implies \frac{(a^2 - 1)(e^{y_1} - e^{y_1/c})}{(a + e^{y_1})(ae^{y_1/c} + 1)} > 0 \quad (\text{H.24})$$

This indeed holds for  $a > 0$ ,  $c \geq 1$  and  $y_1 > 0$ . So, the inequality written in (H.23) is also true and the contribution coming from  $k = 1$  is larger than the one with  $k = 2$ . Thereby, for finite temperature, the pair creation/annihilation term is also larger than zero,  $16\pi^2 q \operatorname{Re}[F_p(\omega)] > 0$ .

Finally, since both contributions in the definition of  $\text{Re}[F(\omega)]$  are larger than zero in the range  $\omega \in [\varepsilon_+, E_\sigma]$ , then Eq. (H.1) has no solutions in such range and the  $\sigma$  will not have contributions coming from collective modes at finite temperature.

## Appendix I

# Integral contributions to the one-meson-loop gap equation

### I.1 The $I_M(S)$ contribution

Consider the term given in Eq. (7.36), for a given meson channel  $M = \{\sigma, \pi\}$ . We can write it as:

$$I_M(S) = \frac{1}{2N_c N_f} \int_{\mathbf{q}} \int \frac{dq_0}{2\pi} \left[ f_1(S, \mathbf{q}, q_0) k_M^{-1}(S, \mathbf{q}, q_0) + \tilde{m} \right]^{-1}. \quad (\text{I.1})$$

Here,  $\tilde{m}$  is defined in Eq. (7.46) as  $\tilde{m} = m/2GN_c N_f S$ . Changing the integration over  $q_0$  into a sum over Matsubara frequencies  $\omega_n$ , one gets,

$$I_M(S) = \frac{1}{2N_c N_f} \int_{\mathbf{q}} \frac{1}{\beta} \sum_{n=-\infty}^{\infty} \left[ f_1(S, \mathbf{q}, \omega_n) k_M^{-1}(S, \mathbf{q}, \omega_n) + \tilde{m} \right]^{-1}. \quad (\text{I.2})$$

As already stated,  $q$  corresponds to the momentum of a composite boson hence,  $\omega_n = \frac{2n\pi}{\beta}$ , the bosonic Matsubara frequencies. This sum can be converted into a contour integration, using contour  $\mathcal{C}$  of Fig. I.1. One gets,

$$I_M(S) = \frac{1}{2N_c N_f} \int_{\mathbf{q}} \frac{1}{2} \oint_{\mathcal{C}} \frac{dw}{2\pi i} \coth\left(\frac{\beta w}{2}\right) \left[ f_1(S, \mathbf{q}, -iw) k_M^{-1}(S, \mathbf{q}, -iw) + \tilde{m} \right]^{-1}. \quad (\text{I.3})$$

Applying the formalism discussed earlier after Eq. (7.43), the contour integral can be converted into an integration around the real axis, in which only the imaginary part of the integrand will contribute to the final result. The integral can then be divided in the collective and non-collective contributions as indicated in Eq. (7.47):

$$I_M(S) = \mathcal{P}_M(S) + \mathcal{B}_M(S). \quad (\text{I.4})$$

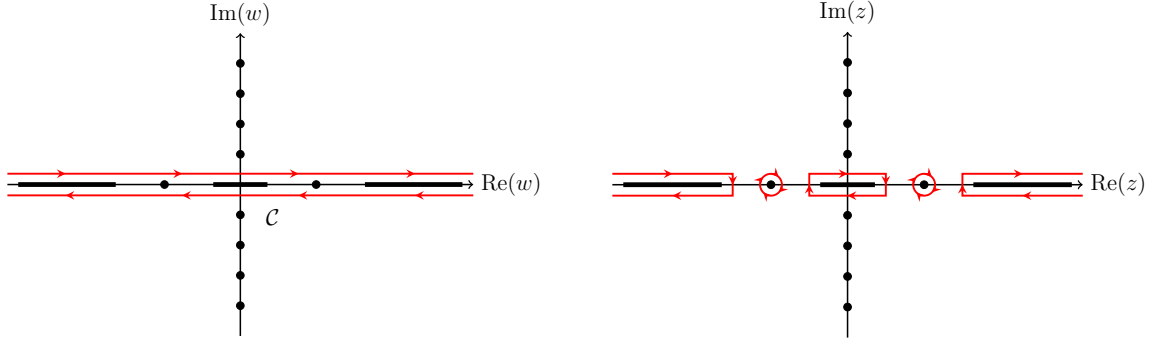


FIGURE I.1: Left panel: Contour used to calculate the meson-loop contributions to the gap equation. Right panel: Definition of the collective meson mode (pole) and the non-collective meson mode (branch cut) terms in the meson-loop corrections.

The first term,  $\mathcal{P}_M(S)$ , can be calculated by considering that, near the real axis, the loop function  $f_1(S, \mathbf{q}, -i\omega)$  is purely real and  $k_M^{-1}(S, \mathbf{q}, -i\omega)$  as an imaginary part. One can write,

$$\mathcal{P}_M(S) = \frac{1}{4\pi N_c N_f} \int_{\mathbf{q}} \int_{-\infty}^{+\infty} d\omega \frac{\coth(\beta\omega/2)}{\text{Re}[F(S, \mathbf{q}, \omega)]} \text{Im} \left[ \left( K_M(S, \mathbf{q}, \omega + i\epsilon)^{-1} + \frac{\tilde{m}}{\text{Re}[F(S, \mathbf{q}, \omega)]} \right)^{-1} \right]. \quad (\text{I.5})$$

The term in brackets can be written as:

$$\left( K_M(S, \mathbf{q}, \omega + i\epsilon)^{-1} + \frac{\tilde{m}}{\text{Re}[F(S, \mathbf{q}, \omega)]} \right)^{-1} = \frac{1}{2\tilde{E}_M(S, \mathbf{q}, \omega)} \sum_{\eta=\pm 1} \frac{\eta}{\omega + \eta\tilde{E}_M(S, \mathbf{q}, \omega) + i\epsilon}. \quad (\text{I.6})$$

Where  $\tilde{E}_M$  was defined in Eq. (7.49). Using the Sokhotski–Plemelj formula and the properties of the Dirac delta function, the imaginary part of the integrand is,

$$\text{Im} \left[ \left( K_M(S, \mathbf{q}, \omega + i\epsilon)^{-1} + \frac{\tilde{m}}{\text{Re}[F(S, \mathbf{q}, \omega)]} \right)^{-1} \right] = \frac{\pi}{2\tilde{E}_M(S, \mathbf{q}, \omega)} \sum_{\eta=\pm 1} \frac{\eta \delta(\omega - \omega_\eta)}{|\partial_\omega \chi_\eta(S, \mathbf{q}, \omega)|_{\omega_\eta}}, \quad (\text{I.7})$$

where the quantity  $\chi_\eta(S, \mathbf{q}, \omega)$  and its  $\omega$ -derivative are given by:

$$\chi_\eta(S, \mathbf{q}, \omega) = \omega - \eta\tilde{E}_M(S, \mathbf{q}, \omega), \quad (\text{I.8})$$

$$\partial_\omega \chi_\eta(S, \mathbf{q}, \omega) = 1 + \frac{\eta\tilde{m}}{2\tilde{E}_M(S, \mathbf{q}, \omega)} \frac{\partial_\omega \text{Re}[F(S, \mathbf{q}, \omega)]}{(\text{Re}[F(S, \mathbf{q}, \omega)])^2}. \quad (\text{I.9})$$

With  $\omega_\eta$  a solution to Eq. (7.51):  $\chi_+(S, \mathbf{q}, \omega) = \omega - \tilde{E}_M(S, \mathbf{q}, \omega) = 0$ . Plugging the imaginary part in the integral, and using the delta function to integrate over  $\omega$  yields the final result:

$$\begin{aligned} \mathcal{P}_M(S) &= \frac{1}{4\pi N_c N_f} \int_{\mathbf{q}} \int_{-\infty}^{+\infty} d\omega \frac{\coth(\beta\omega/2)}{\text{Re}[F(S, \mathbf{q}, \omega)]} \frac{\pi}{2\tilde{E}_M(S, \mathbf{q}, \omega)} \sum_{\eta=\pm 1} \eta \frac{\delta(\omega - \omega_\eta)}{|\partial_\omega \chi_\eta(S, \mathbf{q}, \omega)|_{\omega_\eta}} \\ &= \frac{1}{4N_c N_f} \int_{\mathbf{q}} \frac{\coth(\beta\omega_+/2)}{\text{Re}[F(S, \mathbf{q}, \omega_+)]} \frac{|\partial_\omega \chi_+(S, \mathbf{q}, \omega)|_{\omega_+}^{-1}}{\tilde{E}_M(S, \mathbf{q}, \omega_+)}. \end{aligned} \quad (\text{I.10})$$

It is more convenient to write this expression as:

$$\mathcal{P}_M(S) = \frac{2}{N_c N_f} \int_0^{\Lambda_b} dq \frac{\coth(\beta\omega_+/2)}{16\pi^2 q \operatorname{Re}[F(S, \mathbf{q}, \omega_+)]} \frac{q^3}{\tilde{E}_M(S, \mathbf{q}, \omega_+)} |\partial_\omega \chi_+(S, \mathbf{q}, \omega)|_{\omega_+}^{-1}. \quad (\text{I.11})$$

We highlight that this contribution is only non-zero if  $\omega_+$  exists in-between the cuts.

The second term,  $\mathcal{B}_M(S)$ , can be calculated by considering that, near the real axis,  $k_M^{-1}(S, \mathbf{q}, -i\omega)$  is real while  $f_1(S, \mathbf{q}, -i\omega)$  is complex. One can write:

$$\mathcal{B}_M(S) = \frac{1}{4\pi N_c N_f} \int_{\mathbf{q}} \int_{-\infty}^{+\infty} d\omega \frac{\coth(\beta\omega/2)}{-\omega^2 + E_M^2(S, \mathbf{q})} \operatorname{Im} \left[ (F(S, \mathbf{q}, \omega) + \tilde{m}K_M(S, \mathbf{q}, \omega))^{-1} \right]. \quad (\text{I.12})$$

We define the real quantity,  $M(S, \mathbf{q}, \omega) = \tilde{m}K_M(S, \mathbf{q}, \omega)$ , and write the imaginary factor as:

$$(F(S, \mathbf{q}, \omega) + M(S, \mathbf{q}, \omega))^{-1} = \frac{1}{\operatorname{Re}[F(S, \mathbf{q}, \omega)] + i \operatorname{Im}[F(S, \mathbf{q}, \omega)] + M(S, \mathbf{q}, \omega)}. \quad (\text{I.13})$$

Since  $M(S, \mathbf{q}, \omega)$  is real, we can absorb it in  $\operatorname{Re}[F(S, \mathbf{q}, \omega)]$  by defining  $\operatorname{Re}[G(S, \mathbf{q}, \omega)]$ , see Eq. (7.53). We can then write:

$$\begin{aligned} (F(S, \mathbf{q}, \omega) + M(S, \mathbf{q}, \omega))^{-1} &= \frac{1}{\operatorname{Re}[G(S, \mathbf{q}, \omega)] + i \operatorname{Im}[F(S, \mathbf{q}, \omega)]} \\ &= \frac{\operatorname{Re}[G(S, \mathbf{q}, \omega)] - i \operatorname{Im}[F(S, \mathbf{q}, \omega)]}{\operatorname{Re}[G(S, \mathbf{q}, \omega)]^2 + \operatorname{Im}[F(S, \mathbf{q}, \omega)]^2}. \end{aligned} \quad (\text{I.14})$$

One may drop the real part of this expression and, considering that the integrand is even in  $\omega$ , write:

$$\mathcal{B}_M(S) = \frac{1}{2\pi N_c N_f} \int_{\mathbf{q}} \int_0^{+\infty} d\omega \frac{\coth(\beta\omega/2)}{-\omega^2 + E_M^2(S, \mathbf{q})} \frac{-\operatorname{Im}[F(S, \mathbf{q}, \omega)]}{\operatorname{Re}[G(S, \mathbf{q}, \omega)]^2 + \operatorname{Im}[F(S, \mathbf{q}, \omega)]^2}. \quad (\text{I.15})$$

At this point we separate the imaginary part of the loop function present in the numerator,  $\operatorname{Im}[F(S, \mathbf{q}, \omega)]$ , in its pair creation/annihilation and scattering parts,  $\mathcal{B}_M(S) = \mathcal{B}_{M_p}(S) + \mathcal{B}_{M_s}(S)$ . For  $\mathcal{B}_{M_p}$ , we have

$$\mathcal{B}_{M_p}(S) = \frac{1}{2\pi N_c N_f} \int_{\mathbf{q}} \int_0^{+\infty} d\omega \frac{\coth(\beta\omega/2)}{-\omega^2 + E_M^2(S, \mathbf{q})} \frac{-\operatorname{Im}[F_p(S, \mathbf{q}, \omega)]}{\operatorname{Re}[G(S, \mathbf{q}, \omega)]^2 + \operatorname{Im}[F(S, \mathbf{q}, \omega)]^2}. \quad (\text{I.16})$$

Using Eq. (F.73) and the properties of the Heaviside step function (see Appendix A.2) yields:

$$\mathcal{B}_{M_p}(S) = \frac{2}{(16\pi^2)^2 N_c N_f} \sum_k \int_0^{\Lambda_b} \int_{2A_k}^{2B_k} \frac{dq d\omega}{-\omega^2 + E_M^2(S, \mathbf{q})} \frac{q \coth(\beta\omega/2) g_+^k(S, \frac{\omega}{2})}{\operatorname{Re}[G(S, \mathbf{q}, \omega)]^2 + \operatorname{Im}[F(S, \mathbf{q}, \omega)]^2}. \quad (\text{I.17})$$

The scattering contribution,  $\mathcal{B}_{Ms}$ , can be calculated in exactly the same way. Using Eq. (F.89), we write:

$$\mathcal{B}_{Ms}(S) = -\frac{8}{(16\pi^2)^2 N_c N_f} \int_0^{\Lambda_b} \int_0^b \frac{dq d\omega}{-\omega^2 + E_M^2(S, \mathbf{q})} \frac{q \coth(\beta\omega/2) g_-(S, \omega)}{\text{Re}[G(S, \mathbf{q}, \omega)]^2 + \text{Im}[F(S, \mathbf{q}, \omega)]^2}. \quad (\text{I.18})$$

## I.2 The $I_{1M}(S)$ contribution

As already stated, only the branch cut contribution of the  $I_{1\sigma}(S)$  integral needs to be calculated (for more details, see Appendix H). Consider,

$$I_{1\sigma}(S) = \frac{1}{2N_c N_f} \int_{\mathbf{q}} \int \frac{dq_0}{2\pi} f_1(S, \mathbf{q}, q_0) [f_1(S, \mathbf{q}, q_0) k_\sigma^{-1}(S, \mathbf{q}, q_0) + \tilde{m}]^{-1}. \quad (\text{I.19})$$

By changing the integral into a Matsubara sum and then to a contour integration using contour  $\mathcal{C}$ , we get:

$$I_{1\sigma}(S) = \frac{1}{2N_c N_f} \int_{\mathbf{q}} \frac{1}{2} \oint_{\mathcal{C}} \frac{dw}{2\pi i} \coth\left(\frac{\beta w}{2}\right) f_1(S, \mathbf{q}, -iw) [f_1(S, \mathbf{q}, -iw) k_\sigma^{-1}(S, \mathbf{q}, -iw) + \tilde{m}]^{-1}. \quad (\text{I.20})$$

Considering that, near the real axis,  $k_\sigma^{-1}(S, \mathbf{q}, -iw)$  is real while  $f_1(S, \mathbf{q}, -iw)$  is complex, one can write the branch-cut term as:

$$\mathcal{B}_{1\sigma}(S) = \frac{1}{4\pi N_c N_f} \int_{\mathbf{q}} \int_{-\infty}^{+\infty} d\omega \frac{\coth(\beta\omega/2)}{-\omega^2 + E_\sigma^2(S, \mathbf{q})} \text{Im} \left[ \frac{F(S, \mathbf{q}, \omega)}{F(S, \mathbf{q}, \omega) + M(S, \mathbf{q}, \omega)} \right]. \quad (\text{I.21})$$

Here,  $M(S, \mathbf{q}, \omega) = \tilde{m} K_\sigma(S, \mathbf{q}, \omega)$ . The imaginary factor can be found as follows:

$$\begin{aligned} \frac{F(S, \mathbf{q}, \omega + i\epsilon)}{F(S, \mathbf{q}, \omega + i\epsilon) + M(S, \mathbf{q}, \omega)} &= \frac{\text{Re}[F(S, \mathbf{q}, \omega)] + i \text{Im}[F(S, \mathbf{q}, \omega)] + \{M(S, \mathbf{q}, \omega) - M(S, \mathbf{q}, \omega)\}}{\text{Re}[F(S, \mathbf{q}, \omega)] + i \text{Im}[F(S, \mathbf{q}, \omega)] + M(S, \mathbf{q}, \omega)} \\ &= 1 - \frac{M(S, \mathbf{q}, \omega)}{\text{Re}[G(S, \mathbf{q}, \omega)] + i \text{Im}[F(S, \mathbf{q}, \omega)]} \\ &= 1 - M(S, \mathbf{q}, \omega) \frac{\text{Re}[G(S, \mathbf{q}, \omega)] - i \text{Im}[F(S, \mathbf{q}, \omega)]}{\text{Re}[G(S, \mathbf{q}, \omega)]^2 + \text{Im}[F(S, \mathbf{q}, \omega)]^2}. \end{aligned} \quad (\text{I.22})$$

Hence, the imaginary component of this equation is:

$$\text{Im} \left[ \frac{F(S, \mathbf{q}, \omega + i\epsilon)}{F(S, \mathbf{q}, \omega + i\epsilon) + M(S, \mathbf{q}, \omega)} \right] = \frac{M(S, \mathbf{q}, \omega) \text{Im}[F(S, \mathbf{q}, \omega)]}{\text{Re}[G(S, \mathbf{q}, \omega)]^2 + \text{Im}[F(S, \mathbf{q}, \omega)]^2}. \quad (\text{I.23})$$

Again, taking into consideration that the integrand is even in  $\omega$ , we write:

$$\mathcal{B}_{1\sigma}(S) = \frac{1}{2\pi N_c N_f} \int_{\mathbf{q}} \int_0^{+\infty} d\omega \frac{\coth(\beta\omega/2)}{-\omega^2 + E_\sigma^2(S, \mathbf{q})} \frac{M(S, \mathbf{q}, \omega) \text{Im}[F(S, \mathbf{q}, \omega)]}{\text{Re}[G(S, \mathbf{q}, \omega)]^2 + \text{Im}[F(S, \mathbf{q}, \omega)]^2} \quad (\text{I.24})$$

In this expression it is clear that this contribution vanishes in the chiral limit due to the overall factor of  $\tilde{m}$  in the numerator,  $M(S, \mathbf{q}, \omega) = \tilde{m} K_\sigma(S, \mathbf{q}, \omega)$  with  $\tilde{m} = m/2GN_c N_f S$ . One can

follow the same steps as in the calculation of  $\mathcal{B}_M(S)$ . Separating  $\text{Im}[F(S, \mathbf{q}, \omega)]$ , in its pair creation/annihilation and scattering parts, we have:  $\mathcal{B}_{1\sigma}(S) = \mathcal{B}_{1\sigma p}(S) + \mathcal{B}_{1\sigma s}(S)$ . For the first, we use Eq. (F.73), use the Heaviside step function and write:

$$\mathcal{B}_{1\sigma p}(S) = -\frac{2}{(16\pi^2)^2 N_c N_f} \sum_k \int_0^{\Lambda_b} \int_{2A_k}^{2B_k} \frac{dq d\omega}{-\omega^2 + E_\sigma^2(S, \mathbf{q})} \frac{q \coth(\beta\omega/2) M(S, \mathbf{q}, \omega) g_+^k(S, \frac{\omega}{2})}{\text{Re}[G(S, \mathbf{q}, \omega)]^2 + \text{Im}[F(S, \mathbf{q}, \omega)]^2}. \quad (\text{I.25})$$

The second term becomes:

$$\mathcal{B}_{1\sigma s}(S) = \frac{8}{(16\pi^2)^2 N_c N_f} \int_0^{\Lambda_b} \int_0^b \frac{dq d\omega}{-\omega^2 + E_\sigma^2(S, \mathbf{q})} \frac{q \coth(\beta\omega/2) M(S, \mathbf{q}, \omega) g_-(S, \omega)}{\text{Re}[G(S, \mathbf{q}, \omega)]^2 + \text{Im}[F(S, \mathbf{q}, \omega)]^2}. \quad (\text{I.26})$$

### I.3 The $I_{2M}(S)$ contribution

The final and more complicated contribution comes from integrals  $I_{2\sigma}(S)$  and  $I_{2\pi}(S)$ . We can define the quantity,  $I_{2M}(S)$ , which depends on the meson channel  $M = \{\sigma, \pi\}$  as:

$$I_{2M}(S) = -2 \int \frac{d^4 q}{(2\pi)^4} (q^2 + 4S^2 \delta_{M\sigma}) f_2(S, q) \tilde{\Delta}_M(S, q). \quad (\text{I.27})$$

To simplify the calculations, we make use of the identity presented in Eq. (7.56) (see its proof in Appendix G) and write  $-2f_2(S, q) = \partial f_1(\xi, q)/\partial \xi^2 |_{\xi=S}$ . Noticing that the numerator in the integrand, is the  $\xi^2$  derivative of the denominator, we can write this contribution as:

$$I_{2M}(S) = \frac{1}{2N_c N_f} \int_{\mathbf{q}} \frac{\partial}{\partial \xi^2} \int \frac{dq_0}{2\pi} \ln \left\{ f_1(\xi, \mathbf{q}, q_0) k_M^{-1}(S, \mathbf{q}, q_0) + \tilde{m} \right\}_{\xi=S}. \quad (\text{I.28})$$

Here,  $\tilde{m}$  is defined by Eq. (7.46),  $\tilde{m} = m/2GN_c N_f S$ , and the  $\xi^2$  derivative commutes with the integration since the integral bounds are  $\xi$ -independent. Following the usual recipe, the  $q_0$  integration can be transformed into a Matsubara sum. The sum is then converted into a contour integration, using contour  $\mathcal{C}$ , see Fig. I.1. We can now write,

$$I_{2M}(S) = \frac{1}{2N_c N_f} \int_{\mathbf{q}} \frac{\partial}{\partial \xi^2} \frac{1}{2} \oint_{\mathcal{C}} \frac{dw}{2\pi i} \coth\left(\frac{\beta w}{2}\right) \ln \left\{ f_1(\xi, \mathbf{q}, -iw) k_M^{-1}(S, \mathbf{q}, -iw) + \tilde{m} \right\}_{\xi=S}. \quad (\text{I.29})$$

The separation in the pole and branch cut contributions is performed using Eq. (7.55):

$$I_{2M}(S) = \mathcal{P}_{2M}(S) + \mathcal{B}_{2M}(S). \quad (\text{I.30})$$

For the pole contribution  $\mathcal{P}_{2M}(S)$ , one can write:

$$\mathcal{P}_{2M}(S) = \frac{1}{4\pi N_c N_f} \int_{\mathbf{q}} \frac{\partial}{\partial \xi^2} \int_{-\infty}^{+\infty} dw \coth\left(\frac{\beta w}{2}\right) \text{Im} \left[ \ln \left\{ \text{Re}[F(\xi, \mathbf{q}, \omega)] K_M^{-1}(S, \mathbf{q}, \omega) + \tilde{m} \right\} \right]_{\xi=S}. \quad (\text{I.31})$$

The logarithm in the integrand can be written as,

$$\ln \left\{ \operatorname{Re} [F(\xi, \mathbf{q}, \omega)] K_M^{-1}(S, \mathbf{q}, \omega) + \tilde{m} \right\} = \ln \operatorname{Re} [F(\xi, \mathbf{q}, \omega)] + \ln \left\{ K_M^{-1}(S, \mathbf{q}, \omega) + \frac{\tilde{m}}{\operatorname{Re} [F(\xi, \mathbf{q}, \omega)]} \right\}. \quad (\text{I.32})$$

The first term is real and can be dropped. Hence,

$$\mathcal{P}_{2M}(S) = \frac{1}{4\pi N_c N_f} \int_{\mathbf{q}} \frac{\partial}{\partial \xi^2} \int_{-\infty}^{+\infty} d\omega \coth \left( \frac{\beta\omega}{2} \right) \operatorname{Im} \left[ \ln \left\{ K_M^{-1}(S, \mathbf{q}, \omega) + \frac{\tilde{m}}{\operatorname{Re} [F(\xi, \mathbf{q}, \omega)]} \right\} \right]_{\xi=S}. \quad (\text{I.33})$$

Calculating the derivative yields:

$$\begin{aligned} \mathcal{P}_{2M}(S) &= \frac{1}{4\pi N_c N_f} \int_{\mathbf{q}} \int_{-\infty}^{+\infty} d\omega \coth \left( \frac{\beta\omega}{2} \right) \left[ \frac{\partial}{\partial \xi^2} \operatorname{Re} [F(\xi, \mathbf{q}, \omega)]_{\xi=S} \right] \\ &\quad \times \operatorname{Im} \left[ \left\{ K_M^{-1}(S, \mathbf{q}, \omega) + \frac{\tilde{m}}{\operatorname{Re} [F(S, \mathbf{q}, \omega)]} \right\}^{-1} \right]. \end{aligned} \quad (\text{I.34})$$

The derivative can be calculated to yield:

$$\frac{\partial}{\partial \xi^2} \operatorname{Re} [F(\xi, \mathbf{q}, \omega)]_{\xi=S} = -16\pi^2 q \tilde{m} \frac{\partial_{S^2} R_F(S, \mathbf{q}, \omega)}{R_F(S, \mathbf{q}, \omega)^2}, \quad (\text{I.35})$$

where we defined  $R_F(S, \mathbf{q}, \omega) = 16\pi^2 q \operatorname{Re} [F(S, \mathbf{q}, \omega)]$  and its derivative with respect to  $S^2$  is calculated in Appendix F.5. Using Eq. (I.7), the final result is given by:

$$\mathcal{P}_{2M}(S) = -\frac{2\tilde{m}}{N_c N_f} \int_0^{\Lambda_b} dq q^3 \frac{\coth(\beta\omega_+/2)}{\tilde{E}_M(S, \mathbf{q}, \omega_+)} \frac{\partial_{S^2} R_F(S, \mathbf{q}, \omega_+)}{R_F(S, \mathbf{q}, \omega_+)^2} \Big|_{\partial_\omega \chi_+(S, \mathbf{q}, \omega)|_{\omega_+}^{-1}}. \quad (\text{I.36})$$

Again, considering that  $k_M^{-1}(S, \mathbf{q}, -i\omega)$  is real and  $f_1(S, \mathbf{q}, -i\omega)$  complex near the real axis, the branch-cut is:

$$\mathcal{B}_{2M}(S) = \frac{1}{4\pi N_c N_f} \int_{\mathbf{q}} \frac{\partial}{\partial \xi^2} \int_{-\infty}^{+\infty} d\omega \coth \left( \frac{\beta\omega}{2} \right) \operatorname{Im} \left[ \ln \left\{ F(\xi, \mathbf{q}, \omega) K_M^{-1}(S, \mathbf{q}, \omega) + \tilde{m} \right\} \right]_{\xi=S}. \quad (\text{I.37})$$

The logarithm can be written as:

$$\ln \left\{ F(\xi, \mathbf{q}, \omega) K_M^{-1}(S, \mathbf{q}, \omega) + \tilde{m} \right\} = -\ln K_M(S, \mathbf{q}, \omega) + \ln \left\{ F(\xi, \mathbf{q}, \omega) + \tilde{m} K_M(S, \mathbf{q}, \omega) \right\}. \quad (\text{I.38})$$

The first term can be dropped since it is a real number and  $\mathcal{B}_{2M}(S)$  can be written as:

$$\mathcal{B}_{2M}(S) = \frac{1}{4\pi N_c N_f} \int_{\mathbf{q}} \frac{\partial}{\partial \xi^2} \int_{-\infty}^{+\infty} d\omega \coth \left( \frac{\beta\omega}{2} \right) \operatorname{Im} \left[ \ln \left\{ F(\xi, \mathbf{q}, \omega) + \tilde{m} K_M(S, \mathbf{q}, \omega) \right\} \right]_{\xi=S}. \quad (\text{I.39})$$

To calculate this term, the definition of  $\operatorname{Re} [G(\xi, \mathbf{q}, \omega)]$  is slightly different from the one in

Eq. (7.53). The term coming from  $\tilde{m}K_M(S, \mathbf{q}, \omega)$  does not depend on  $\xi$ :  $\text{Re}[G(\xi, \mathbf{q}, \omega)] = \text{Re}[F(\xi, \mathbf{q}, \omega)] + M(S, \mathbf{q}, \omega)$ . The argument of the logarithm, near the real axis, can be written as:

$$F(\xi, \mathbf{q}, \omega + i\epsilon) + \tilde{m}K_M(S, \mathbf{q}, \omega) = \text{Re}[G(\xi, \mathbf{q}, \omega)] + i \text{Im}[F(\xi, \mathbf{q}, \omega)]. \quad (\text{I.40})$$

The real part of the function  $F(S, \mathbf{q}, \omega)$  is even and its imaginary part is odd, with respect to  $\omega$ . Using these properties, the integration is broken at  $\omega = 0$  and a variable change in the integration for negative  $\omega$  as  $\omega = -\omega$ , provides:

$$\mathcal{B}_{2M}(S) = \frac{1}{4\pi N_c N_f} \int_{\mathbf{q}} \frac{\partial}{\partial \xi^2} \int_0^{+\infty} d\omega \coth\left(\frac{\beta\omega}{2}\right) \text{Im} \left[ \ln \left\{ \frac{\text{Re}[G(\xi, \mathbf{q}, \omega)] + i \text{Im}[F(\xi, \mathbf{q}, \omega)]}{\text{Re}[G(\xi, \mathbf{q}, \omega)] - i \text{Im}[F(\xi, \mathbf{q}, \omega)]} \right\} \right]_{\xi=S}. \quad (\text{I.41})$$

The complex numbers in the logarithm argument can be written in the polar representation by defining their absolute value  $L(\xi, \mathbf{q}, \omega)$  and argument  $A(\xi, \mathbf{q}, \omega)$  as,

$$L(\xi, \mathbf{q}, \omega) = \sqrt{\text{Re}[G(\xi, \mathbf{q}, \omega)]^2 + \text{Im}[F(\xi, \mathbf{q}, \omega)]^2}, \quad (\text{I.42})$$

$$A(\xi, \mathbf{q}, \omega) = \frac{\text{Im}[F(\xi, \mathbf{q}, \omega)]}{\text{Re}[G(\xi, \mathbf{q}, \omega)]}. \quad (\text{I.43})$$

which allows to write,

$$\text{Re}[G(\xi, \mathbf{q}, \omega)] \pm i \text{Im}[F(\xi, \mathbf{q}, \omega)] = L(\xi, \mathbf{q}, \omega) \exp \left[ \pm i \arctg A(\xi, \mathbf{q}, \omega) \right]. \quad (\text{I.44})$$

Using the polar representation and commuting the  $\xi^2$  derivative with the  $\omega$  integral, it gives:

$$\begin{aligned} \mathcal{B}_{2M}(S) &= \frac{1}{4\pi N_c N_f} \int_{\mathbf{q}} \frac{\partial}{\partial \xi^2} \int_0^{+\infty} d\omega \coth\left(\frac{\beta\omega}{2}\right) \text{Im} [2i \arctg A(\xi, \mathbf{q}, \omega)]_{\xi=S} \\ &= \frac{1}{2\pi N_c N_f} \int_{\mathbf{q}} \int_0^{+\infty} d\omega \frac{\coth(\beta\omega/2)}{1 + A(S, \mathbf{q}, \omega)^2} \partial_{\xi^2} A(\xi, \mathbf{q}, \omega)_{\xi=S}. \end{aligned} \quad (\text{I.45})$$

As expected, this contribution is non-zero only if the imaginary part of  $F(S, \mathbf{q}, \omega)$  is non-zero. The final task lies in calculating explicitly the derivative of the argument. Several terms will be generated due to the complexity of the involved functions. To simplify the calculation, it is easier to consider each contribution. Explicitly, we write:

$$\partial_{\xi^2} A(\xi, \mathbf{q}, \omega)_{\xi=S} = \frac{\partial}{\partial \xi^2} \frac{\text{Im}[F(\xi, \mathbf{q}, \omega)]}{\text{Re}[G(\xi, \mathbf{q}, \omega)]_{\xi=S}} = A_I(S, \mathbf{q}, \omega) + A(S, \mathbf{q}, \omega) A_R(S, \mathbf{q}, \omega). \quad (\text{I.46})$$

Here,

$$A_I(S, \mathbf{q}, \omega) = \frac{\partial_{S^2} \text{Im}[F(S, \mathbf{q}, \omega)]}{\text{Re}[G(S, \mathbf{q}, \omega)]}, \quad (\text{I.47})$$

$$A_R(S, \mathbf{q}, \omega) = -\frac{\partial_{S^2} \text{Re}[F(S, \mathbf{q}, \omega)]}{\text{Re}[G(S, \mathbf{q}, \omega)]}. \quad (\text{I.48})$$

Since  $F(S, \mathbf{q}, \omega)$  can be separated in the pair creation/annihilation and scattering terms, the functions  $A_I$  and  $A_R$  can also be further decomposed. For later convenience we write:

$$A_I(S, \mathbf{q}, \omega) = \frac{\partial_{S^2} \text{Im} [F_p(S, \mathbf{q}, \omega)]}{\text{Re} [G(S, \mathbf{q}, \omega)]} + \frac{\partial_{S^2} \text{Im} [F_s(S, \mathbf{q}, \omega)]}{\text{Re} [G(S, \mathbf{q}, \omega)]} = A_{Ip}(S, \mathbf{q}, \omega) + A_{Is}(S, \mathbf{q}, \omega), \quad (\text{I.49})$$

$$A_R(S, \mathbf{q}, \omega) = -\frac{\partial_{S^2} \text{Re} [F_p(S, \mathbf{q}, \omega)]}{\text{Re} [G(S, \mathbf{q}, \omega)]} - \frac{\partial_{S^2} \text{Re} [F_s(S, \mathbf{q}, \omega)]}{\text{Re} [G(S, \mathbf{q}, \omega)]} = A_{Rp}(S, \mathbf{q}, \omega) + A_{Rs}(S, \mathbf{q}, \omega). \quad (\text{I.50})$$

Hence, each contribution to the derivative of the argument, can be separated in two different parts (omitting the  $\omega$  and  $\mathbf{q}$  dependences):

$$\partial_{\xi^2} A(\xi)_{\xi=S} = A_{Ip}(S) + A_{Is}(S) + A_p(S)A_{Rp}(S) + A_p(S)A_{Rs}(S) + A_s(S)A_{Rp}(S) + A_s(S)A_{Rs}(S). \quad (\text{I.51})$$

To calculate each integration individually, we separate  $\mathcal{B}_{2M}(S)$  in a sum of different terms in the same way. Each term comes from the decomposition made in Eq. (I.51). We can write:

$$\mathcal{B}_{2M}(S) = \mathcal{B}_{2M}^{(Ip)}(S) + \mathcal{B}_{2M}^{(Is)}(S) + \mathcal{B}_{2M}^{(pRp)}(S) + \mathcal{B}_{2M}^{(pRs)}(S) + \mathcal{B}_{2M}^{(sRp)}(S) + \mathcal{B}_{2M}^{(sRs)}(S). \quad (\text{I.52})$$

When evaluating each contribution separately we will need the derivatives with respect to  $S^2$  of the real and imaginary parts of the pair creation/annihilation term, and the scattering term. These contribution were calculated in Appendix F.5 and are given in Eqs. (F.97), (F.111), (F.115) and (F.123). Below we present each contribution explicitly:

- $\mathcal{B}_{2M}^{(Ip)}(S)$

The first term,  $\mathcal{B}_{2M}^{(Ip)}(S)$ , can be written as:

$$\begin{aligned} \mathcal{B}_{2M}^{(Ip)}(S) &= \frac{1}{2\pi N_c N_f} \int_{\mathbf{q}} \int_0^{+\infty} d\omega \frac{\coth(\beta\omega/2)}{1 + A(S, \mathbf{q}, \omega)^2} A_{Ip}(S) \\ &= \frac{1}{2\pi N_c N_f} \int_{\mathbf{q}} \int_0^{+\infty} d\omega \frac{\coth(\beta\omega/2)}{1 + A(S, \mathbf{q}, \omega)^2} \frac{\partial_{S^2} 16\pi^2 q \text{Im} [F_p(S, \mathbf{q}, \omega)]}{R_G(S, \mathbf{q}, \omega)}. \end{aligned} \quad (\text{I.53})$$

Here,  $R_G(S, \mathbf{q}, \omega) = 16\pi^2 q \text{Re} [G(S, \mathbf{q}, \omega)]$ , and the derivative in the integrand is given by Eq. (F.111). Carrying out the calculation, one can get:

$$\mathcal{B}_{2M}^{(Ip)}(S) = \frac{-1}{4\pi^2 N_c N_f} \sum_k \int_0^{\Lambda_b} dq \int_{2A_k}^{2B_k} d\omega q^2 \frac{\coth(\beta\omega/2)}{1 + A(S, \mathbf{q}, \omega)^2} \frac{G_+(S, \omega/2, D_k)}{R_G(S, \mathbf{q}, \omega)} \frac{\partial}{\partial S^2} D_k \left( S, \frac{\omega}{2} \right), \quad (\text{I.54})$$

where we have used:

$$\partial_{S^2} g_+^k \left( S, \frac{\omega}{2} \right) = 2G_+(S, \omega/2, D_k) \frac{\partial}{\partial S^2} D_k \left( S, \frac{\omega}{2} \right). \quad (\text{I.55})$$

For  $k = 1$  and  $k = 2$  respectively, the derivatives are given by:

$$\frac{\partial}{\partial S^2} D_1\left(S, \frac{\omega}{2}\right) = \frac{\partial}{\partial S^2} \varepsilon_+\left(S, \frac{\omega}{2}\right) = \frac{-q}{E_\sigma \sqrt{\omega^2 - q^2}} \sum_{\eta=\pm 1} \eta \frac{\sqrt{\omega + \eta E_\sigma}}{\sqrt{\omega - \eta E_\sigma}}, \quad (\text{I.56})$$

$$\frac{\partial}{\partial S^2} D_2\left(S, \frac{\omega}{2}\right) = \frac{\partial}{\partial S^2} \varepsilon_{\Lambda^+}\left(S, \frac{\omega}{2}\right) = -\frac{1}{\sqrt{\Lambda_f^2 + S^2}}. \quad (\text{I.57})$$

- $\mathcal{B}_{2M}^{(\text{Is})}(S)$

The second term,  $\mathcal{B}_{2M}^{(\text{Is})}(S)$ , is defined as:

$$\begin{aligned} \mathcal{B}_{2M}^{(\text{Is})}(S) &= \frac{1}{2\pi N_c N_f} \int_{\mathbf{q}} \int_0^{+\infty} d\omega \frac{\coth(\beta\omega/2)}{1 + A(S, \mathbf{q}, \omega)^2} A_{\text{Is}}(S) \\ &= \frac{1}{2\pi N_c N_f} \int_{\mathbf{q}} \int_0^{+\infty} d\omega \frac{\coth(\beta\omega/2)}{1 + A(S, \mathbf{q}, \omega)^2} \frac{\partial_{S^2} 16\pi^2 q \text{Im}[F_s(S, \mathbf{q}, \omega)]}{R_G(S, \mathbf{q}, \omega)}. \end{aligned} \quad (\text{I.58})$$

Using Eq. (F.123) for the derivative in the integrand, we can write:

$$\mathcal{B}_{2M}^{(\text{Is})}(S) = \frac{1}{\pi^2 N_c N_f} \int_0^{\Lambda_b} dq \int_0^b d\omega q^2 \frac{\coth(\beta\omega/2)}{1 + A(S, \mathbf{q}, \omega)^2} \frac{\partial_{S^2} g_-(S, \omega)}{R_G(S, \mathbf{q}, \omega)}. \quad (\text{I.59})$$

In the last step we have used the fact that  $a = -b$  and that the integrand is even in  $\omega$ . The derivative is:

$$\partial_{S^2} g_-(S, \varepsilon) = \frac{G_-(d(\omega), \omega, S)}{2\sqrt{\Lambda_f^2 + S^2}} + q \frac{G_-(c(\omega), \omega, S)}{\sqrt{(\omega^2 - q^2)(\omega^2 - E_\sigma^2)}}. \quad (\text{I.60})$$

- $\mathcal{B}_{2M}^{(\text{pRp})}(S)$

The third term in the sum,  $\mathcal{B}_{2M}^{(\text{pRp})}(S)$ , is given by:

$$\begin{aligned} \mathcal{B}_{2M}^{(\text{pRp})}(S) &= \frac{1}{2\pi N_c N_f} \int_{\mathbf{q}} \int_0^{+\infty} d\omega \frac{\coth(\beta\omega/2)}{1 + A(S, \mathbf{q}, \omega)^2} A_{\text{p}}(S) A_{\text{Rp}}(S) \\ &= \frac{2}{N_c N_f} \sum_k \int_0^{\Lambda_b} dq \int_{2A_k}^{2B_k} d\omega \frac{q^3 \coth(\beta\omega/2)}{1 + A(S, \mathbf{q}, \omega)^2} \frac{g_+^k(S, \frac{\omega}{2})}{R_G(S, \mathbf{q}, \omega)^2} \partial_{S^2} \text{Re}[F_{\text{p}}(S, \mathbf{q}, \omega)]. \end{aligned} \quad (\text{I.61})$$

- $\mathcal{B}_{2M}^{(\text{pRs})}(S)$

The fourth term,  $\mathcal{B}_{2M}^{(\text{pRs})}(S)$ , is given by:

$$\begin{aligned} \mathcal{B}_{2M}^{(\text{pRs})}(S) &= \frac{1}{2\pi N_c N_f} \int_{\mathbf{q}} \int_0^{+\infty} d\omega \frac{\coth(\beta\omega/2)}{1 + A(S, \mathbf{q}, \omega)^2} A_{\text{p}}(S) A_{\text{Rs}}(S) \\ &= \frac{2}{N_c N_f} \sum_k \int_0^{\Lambda_b} dq \int_{2A_k}^{2B_k} d\omega \frac{q^3 \coth(\beta\omega/2)}{1 + A(S, \mathbf{q}, \omega)^2} \frac{g_+^k(S, \frac{\omega}{2})}{R_G(S, \mathbf{q}, \omega)^2} \partial_{S^2} \text{Re}[F_s(S, \mathbf{q}, \omega)]. \end{aligned} \quad (\text{I.62})$$

- $\mathcal{B}_{2M}^{(\text{sRp})}(S)$

The fifth term in the sum,  $\mathcal{B}_{2M}^{(\text{sRp})}(S)$ , is defined as:

$$\begin{aligned} \mathcal{B}_{2M}^{(\text{sRp})}(S) &= \frac{1}{2\pi N_c N_f} \int_{\mathbf{q}} \int_0^{+\infty} d\omega \frac{\coth(\beta\omega/2)}{1 + A(S, \mathbf{q}, \omega)^2} A_s(S) A_{\text{Rp}}(S) \\ &= \frac{-16}{N_c N_f} \int_0^{\Lambda_b} dq \int_0^b d\omega \frac{q^3 \coth(\beta\omega/2)}{1 + A(S, \mathbf{q}, \omega)^2} \frac{g_-(S, \omega)}{R_G(S, \mathbf{q}, \omega)^2} \partial_{S^2} \text{Re} [F_p(S, \mathbf{q}, \omega)]. \quad (\text{I.63}) \end{aligned}$$

- $\mathcal{B}_{2M}^{(\text{sRs})}(S)$

The sixth and final term in the sum,  $\mathcal{B}_{2M}^{(\text{sRs})}(S)$ , is defined as:

$$\begin{aligned} \mathcal{B}_{2M}^{(\text{sRp})}(S) &= \frac{1}{2\pi N_c N_f} \int_{\mathbf{q}} \int_0^{+\infty} d\omega \frac{\coth(\beta\omega/2)}{1 + A(S, \mathbf{q}, \omega)^2} A_s(S) A_{\text{Rs}}(S) \\ &= \frac{-16}{N_c N_f} \int_0^{\Lambda_b} dq \int_0^b d\omega \frac{q^3 \coth(\beta\omega/2)}{1 + A(S, \mathbf{q}, \omega)^2} \frac{g_-(S, \omega)}{R_G(S, \mathbf{q}, \omega)^2} \partial_{S^2} \text{Re} [F_s(S, \mathbf{q}, \omega)]. \quad (\text{I.64}) \end{aligned}$$

## Appendix J

# Useful identities and important results

### J.1 Useful identities

$$n_{\text{F}}(E) = \frac{1}{e^{E/T} + 1}, \quad (\text{J.1})$$

$$n_{\text{B}}(E) = \frac{1}{e^{E/T} - 1}, \quad (\text{J.2})$$

$$\frac{\partial n_{\text{F}}(E)}{\partial E} = -\frac{n_{\text{F}}(E)}{T} [1 - n_{\text{F}}(E)] \quad (\text{J.3})$$

$$\frac{\partial n_{\text{B}}(E)}{\partial E} = -\frac{n_{\text{B}}(E)}{T} [1 + n_{\text{B}}(E)] \quad (\text{J.4})$$

$$\frac{\partial n_{\text{F}}(E)}{\partial T} = \frac{E}{T^2} n_{\text{F}}(E) (1 - n_{\text{F}}(E)), \quad (\text{J.5})$$

$$\frac{\partial n_{\text{B}}(E)}{\partial T} = \frac{E}{T^2} n_{\text{B}}(E) (1 + n_{\text{B}}(E)), \quad (\text{J.6})$$

$$\tanh\left(\frac{E}{2T}\right) = 1 - 2n_{\text{F}}(E), \quad (\text{J.7})$$

$$\coth\left(\frac{E}{2T}\right) = 1 + 2n_{\text{B}}(E), \quad (\text{J.8})$$

$$\text{sech}^2\left(\frac{E}{2T}\right) = 4n_{\text{F}}(E)[1 - n_{\text{F}}(E)], \quad (\text{J.9})$$

$$\text{csch}^2\left(\frac{E}{2T}\right) = 4n_{\text{B}}(E)[1 + n_{\text{B}}(E)], \quad (\text{J.10})$$

$$\int \frac{dx}{e^x + 1} = x - \ln(e^x + 1) + \text{cte}. \quad (\text{J.11})$$

### J.2 Leibniz integral rule

The Leibniz integral rule can be stated as:

$$\frac{d}{dx} \int_{a(x)}^{b(x)} dt f(x, t) = f(x, b(x)) \frac{db(x)}{dx} - f(x, a(x)) \frac{da(x)}{dx} + \int_{a(x)}^{b(x)} dt \frac{\partial f(x, t)}{\partial x}. \quad (\text{J.12})$$

### J.3 $\eta$ -Sum Identity

$$\sum_{\eta=\pm 1} \frac{\eta^A}{\sqrt{4E^2 - E_\sigma^2}} \frac{G_+(\eta\mu)}{E + \eta\omega/2} = \begin{cases} \frac{(-1)}{\omega^2 - E_\sigma^2} \sum_{\eta=\pm 1} \left[ K_+(\eta\mu) \frac{\sqrt{2E - \eta E_\sigma}}{\sqrt{2E + \eta E_\sigma}} - G_+(\eta\mu) \frac{\sqrt{4E^2 - E_\sigma^2}}{E + \eta\omega/2} \right], & A = \text{even}, \\ \frac{(-1)}{\omega^2 - E_\sigma^2} \sum_{\eta=\pm 1} \eta \left[ L_+(\eta\mu) \frac{\sqrt{2E - \eta E_\sigma}}{\sqrt{2E + \eta E_\sigma}} - G_+(\eta\mu) \frac{\sqrt{4E^2 - E_\sigma^2}}{E + \eta\omega/2} \right], & A = \text{odd}. \end{cases} \quad (\text{J.13})$$

Here,

$$K_+(\eta\mu) = G_+(\eta\mu) + G_+(-\eta\mu) + \frac{\omega}{E_\sigma} [G_+(\eta\mu) - G_+(-\eta\mu)], \quad (\text{J.14})$$

$$L_+(\eta\mu) = G_+(\eta\mu) - G_+(-\eta\mu) + \frac{\omega}{E_\sigma} [G_+(\eta\mu) + G_+(-\eta\mu)]. \quad (\text{J.15})$$

These expressions are very useful to simplify the analytical and numerical calculations. More specifically, they are needed in the explicit calculation of  $\partial_{S^2} \text{Re} [F(S, \mathbf{q}, \omega)]$  and  $\partial_\omega \text{Re} [F(S, \mathbf{q}, \omega)]$ .

To derive this identity, we consider separately the cases when  $A$  is an even or an odd number. If  $A$  is even,  $A = 2n$  with  $n \in \mathbb{N}_0$ , we can write:

$$\frac{1}{\sqrt{4E^2 - E_\sigma^2}} \sum_{\eta=\pm 1} \eta^{2n} \frac{G_+(\eta\mu)}{E + \eta\omega/2} = \frac{1}{\sqrt{4E^2 - E_\sigma^2}} \sum_{\eta=\pm 1} \frac{G_+(\eta\mu)}{E + \eta\omega/2}. \quad (\text{J.16})$$

Next, to have only linear polynomials in  $E$  in the denominators, we write the sum in  $\eta$  explicitly and write the fractions in its the partial components (with respect to  $E$ ). We do this for numerical reasons: the integration in  $E$  can have singularities in the integration region and appropriate integration methods should be used for each term. Write:

$$\begin{aligned} \frac{1}{\sqrt{4E^2 - E_\sigma^2}} \sum_{\eta=\pm 1} \frac{G_+(\eta\mu)}{E + \eta\omega/2} &= \sqrt{4E^2 - E_\sigma^2} \sum_{\eta=\pm 1} \frac{1}{4E^2 - E_\sigma^2} \frac{G_+(\eta\mu)}{E + \eta\omega/2} \\ &= \frac{-\sqrt{4E^2 - E_\sigma^2}}{\omega^2 - E_\sigma^2} \sum_{\eta=\pm 1} \left[ \frac{G_+(\eta\mu) + G_+(-\eta\mu) + \frac{\omega}{E_\sigma} [G_+(\eta\mu) - G_+(-\eta\mu)]}{2E + \eta E_\sigma} - \frac{G_+(\eta\mu)}{E + \eta\omega/2} \right] \\ &= \frac{(-1)}{\omega^2 - E_\sigma^2} \sum_{\eta=\pm 1} \left[ K_+(\eta\mu) \frac{\sqrt{4E^2 - \eta^2 E_\sigma^2}}{2E + \eta E_\sigma} - G_+(\eta\mu) \frac{\sqrt{4E^2 - E_\sigma^2}}{E + \eta\omega/2} \right] \\ &= \frac{(-1)}{\omega^2 - E_\sigma^2} \sum_{\eta=\pm 1} \left[ K_+(\eta\mu) \frac{\sqrt{2E - \eta E_\sigma}}{\sqrt{2E + \eta E_\sigma}} - G_+(\eta\mu) \frac{\sqrt{4E^2 - E_\sigma^2}}{E + \eta\omega/2} \right]. \end{aligned} \quad (\text{J.17})$$

Which proves the identity for even  $A$ . For odd  $A$  i.e.,  $A = 2n + 1$  with  $n \in \mathbb{N}_0$ , the calculation is very similar:

$$\frac{1}{\sqrt{4E^2 - E_\sigma^2}} \sum_{\eta=\pm 1} \eta^{2n+1} \frac{G_+(\eta\mu)}{E + \eta\omega/2} = \frac{1}{\sqrt{4E^2 - E_\sigma^2}} \sum_{\eta=\pm 1} \eta \frac{G_+(\eta\mu)}{E + \eta\omega/2}. \quad (\text{J.18})$$

Trivially,  $\eta^{2n+1} = \eta$  for  $n \in \mathbb{N}_0$ . Following the same procedure as before, we write:

$$\begin{aligned}
\frac{1}{\sqrt{4E^2 - E_\sigma^2}} \sum_{\eta=\pm 1} \eta \frac{G_+(\eta\mu)}{E + \eta\omega/2} &= \sqrt{4E^2 - E_\sigma^2} \sum_{\eta=\pm 1} \frac{\eta}{4E^2 - E_\sigma^2} \frac{G_+(\eta\mu)}{E + \eta\omega/2} \\
&= \frac{-\sqrt{4E^2 - E_\sigma^2}}{\omega^2 - E_\sigma^2} \sum_{\eta=\pm 1} \eta \left[ \frac{G_+(\eta\mu) - G_+(-\eta\mu) + \frac{\omega}{E_\sigma} [G_+(\eta\mu) + G_+(-\eta\mu)]}{2E + \eta E_\sigma} - \frac{G_+(\eta\mu)}{E + \eta\omega/2} \right] \\
&= \frac{(-1)}{\omega^2 - E_\sigma^2} \sum_{\eta=\pm 1} \eta \left[ L_+(\eta\mu) \frac{\sqrt{2E - \eta E_\sigma}}{\sqrt{2E + \eta E_\sigma}} - G_+(\eta\mu) \frac{\sqrt{4E^2 - E_\sigma^2}}{E + \eta\omega/2} \right]. \tag{J.19}
\end{aligned}$$

Proving the equality for odd  $A$ .



## Appendix K

# FRG applied to the QM model: numerical details

In [329] it was demonstrated how to ensure numerical stability during the integration of a generalized version of Eq. (8.28), through an optimal step size. To derive such optimal step, for simplicity, it was considered that the function derivatives are calculated with low order finite difference methods: forward difference for the renormalization group time variable,  $t$ , and three-point rule for the  $\sigma$ -direction. It is supposed that the numerical stability condition derived within this simpler scheme, is also valid for the fourth order Runge–Kutta method, used in the  $t$  variable and higher order finite differences used for the  $\sigma$  derivatives. Following this approach the following conditions for the step size  $\Delta t$  was derived:

$$|\Delta t| \leq \frac{2|G|}{|F^2|}, \quad (\text{K.1})$$

$$|\Delta t| \leq \frac{\Delta\sigma^2}{2|G|}. \quad (\text{K.2})$$

Here,  $G$  and  $F$  are given by:

$$G = -\frac{k^5}{24\pi^2 E_\sigma^3} \left[ \coth\left(\frac{E_\sigma}{2T}\right) + \frac{E_\sigma}{2T} \operatorname{csch}^2\left(\frac{E_\sigma}{2T}\right) \right], \quad (\text{K.3})$$

$$F = -\frac{k^5}{8\pi^2 \sigma E_\pi^3} \left[ \coth\left(\frac{E_\pi}{2T}\right) + \frac{E_\pi}{2T} \operatorname{csch}^2\left(\frac{E_\pi}{2T}\right) \right]. \quad (\text{K.4})$$

As in [329], we do not consider these conditions for  $\sigma \sim 0$ . Since these conditions only depend on the bosonic sector of the flow equation, the fact that one is dealing with effective finite chemical potentials does not change the conditions directly. The effect of finite chemical potential and finite vector mesons only change these conditions indirectly, since the potential and its derivatives will be different during the flow.

To solve the set of coupled differential equations, in such a way to get full access to the full effective potential, we employed the grid method. In this method, the field variable  $\sigma$  is discretized in an one-dimensional grid, and the first and second derivatives of the effective potential with

respect to  $\sigma$  are calculated using finite differences. The five point midpoint rule was used except in the grid endpoints where the forward and backward rules were used.

Consider a set of  $N$  equally spaced discrete points  $x_i$ , with  $i = 0, 1, \dots, N - 1$  and a function evaluated at these points,  $f(x_i)$ . In our calculation the set of points corresponds to a grid in the  $\sigma$  field and the function corresponds to the effective potential,  $U_k^X(\sigma)$ , the entropy density  $s_k^X(\sigma)$  or the  $j$ -quark density,  $n_k^{j,X}(\sigma)$ . Since we consider the grid to be equally spaced, one can define  $\Delta = x_{i+1} - x_i$ , which is the same for all  $i$ .

For the first derivative, for  $i \in [2, N - 3]$  we used:

$$\frac{df(x_i)}{dx} = \frac{f(x_{i-2}) - 8f(x_{i-1}) + 8f(x_{i+1}) - f(x_{i+2})}{12\Delta} + O(\Delta^4), \quad (\text{K.5})$$

while, for the edges, we used the appropriate forward/backwards five point rules:

$$\frac{df(x_0)}{dx} = \frac{-25f(x_0) + 48f(x_1) - 36f(x_2) + 16f(x_3) - 3f(x_4)}{12\Delta} + O(\Delta^4), \quad (\text{K.6})$$

$$\frac{df(x_1)}{dx} = \frac{-3f(x_0) - 10f(x_1) + 18f(x_2) - 6f(x_3) + f(x_4)}{12\Delta} + O(\Delta^4), \quad (\text{K.7})$$

$$\frac{df(x_{N-2})}{dx} = \frac{3f(x_{N-1}) + 10f(x_{N-2}) - 18f(x_{N-3}) + 6f(x_{N-4}) - f(x_{N-5})}{12\Delta} + O(\Delta^4), \quad (\text{K.8})$$

$$\frac{df(x_{N-1})}{dx} = \frac{25f(x_{N-1}) - 48f(x_{N-2}) + 36f(x_{N-3}) - 16f(x_{N-4}) + 3f(x_{N-5})}{12\Delta} + O(\Delta^4). \quad (\text{K.9})$$

Likewise, for the second derivative, for  $i \in [2, N - 3]$  we used:

$$\frac{d^2f(x_i)}{dx^2} = \frac{-f(x_{i-2}) + 16f(x_{i-1}) - 30f(x_i) + 16f(x_{i+1}) - f(x_{i+2})}{12\Delta^2} + O(\Delta^4). \quad (\text{K.10})$$

As for the first derivatives, the edges are calculated with appropriate forward/backwards five point rules:

$$\frac{d^2f(x_0)}{dx^2} = \frac{35f(x_0) - 104f(x_1) + 114f(x_2) - 56f(x_3) + 11f(x_4)}{12\Delta^2} + O(\Delta^4), \quad (\text{K.11})$$

$$\frac{d^2f(x_1)}{dx^2} = \frac{11f(x_0) - 20f(x_1) + 6f(x_2) + 4f(x_3) - f(x_4)}{12\Delta^2} + O(\Delta^4), \quad (\text{K.12})$$

$$\frac{d^2f(x_{N-2})}{dx^2} = \frac{11f(x_{N-1}) - 20f(x_{N-2}) + 6f(x_{N-3}) + 4f(x_{N-4}) - f(x_{N-5})}{12\Delta^2} + O(\Delta^4), \quad (\text{K.13})$$

$$\frac{d^2f(x_{N-1})}{dx^2} = \frac{35f(x_{N-1}) - 104f(x_{N-2}) + 114f(x_{N-3}) - 56f(x_{N-4}) + 11f(x_{N-5})}{12\Delta^2} + O(\Delta^4). \quad (\text{K.14})$$

One starts the calculation in the UV scale i.e., at  $k = \Lambda$ . At this momentum scale the effective potential and entropy density are calculated using the initial conditions provided in Eqs. (8.87) and (8.91), respectively. The needed derivatives with respect to  $\sigma$  are calculated for every  $\sigma$ -grid point, using finite differences. Next, an optimal step size in the renormalization group time,  $\Delta t$ , is calculated using Eqs. (K.1) and (K.2): the smaller  $\Delta t$  is used. The flow equations are then solved using the fourth order Runge–Kutta method, to provide the  $\sigma$ -dependent effective potential

and entropy density in the next step  $t - \Delta t$ , i.e.,  $U_{k=\Lambda \exp(t-\Delta t)}(\sigma)$  and  $s_{k=\Lambda \exp(t-\Delta t)}(\sigma)$ . This process is repeated until the infrared scale is reached at  $k = k_{\text{IR}}$ . After reaching the infrared scale, one is in possession of the  $U_{k=k_{\text{IR}}}(\sigma)$  and  $s_{k=k_{\text{IR}}}(\sigma)$  and can then calculate the minimum of the effective potential, in which all observables are defined.

When considering finite vector interactions, the self-consistent Eqs. (8.51) and (8.52) have to be solved at every  $\sigma$ -grid point, at every momentum scale  $k$ . Hence, for a given  $k$ , for every  $\sigma$ -grid point, a 2-dimensional root finding algorithm is used to find the values of  $g_\omega \tilde{\omega}_{0,k}$  and  $g_\rho \tilde{\rho}_{0,k}^3$  that fulfil this system of equations. To speed up the root finding process, the solutions at the momentum scale  $k$  are provided as guesses for the next momentum shell. Since we are using the fourth order Runge–Kutta method this process has to be performed four times to be able to calculate the effective potential and entropy density in a given momentum scale.

The computing time is then related to the  $\sigma$  grid size, the infrared cutoff,  $k_{\text{IR}}$ , and the root finding precision, when considering vector interactions. The complexity of the flow equations also dictates the computing time since the step size  $\Delta t$  dictates how fast one goes from the UV down to the IR and different values of temperature and chemical potential influence the overall magnitude of the adaptive step size.

One very important observation is that the optimal step size calculated using Eqs. (K.3) and (K.4) does not depend on the chemical potential and can still be used in the calculation with finite vector interactions.

In order to calculate the phase diagram, the flow equation was solved multiple times for different values of temperature and chemical potential. In order to speed-up calculations, the OpenMP interface was used to run the computer code in parallel.



## Appendix L

# FRG applied to the QM model: derivatives of the vector field

### L.1 Derivative of the vector fields with respect to temperature

In order to calculate the entropy flow equation, it is necessary to calculate, at each momentum shell  $k$  the following quantity<sup>1</sup>:

$$\frac{\partial v_{k,l}}{\partial T} = \frac{\partial \tilde{\omega}_k}{\partial T} + (-1)^l \frac{\partial \tilde{\rho}_k}{\partial T}. \quad (\text{L.1})$$

Here,  $l = 0$  is for up quarks and  $l = 1$  is for down quarks. Considering that the vector stationary conditions hold, for a given momentum shell,  $k$ , we can use Eqs. (8.51), (8.52) and (8.47), to write the temperature derivatives of the vector fields as:

$$\frac{\partial \tilde{\omega}_k(T; \tilde{\omega}_k, \tilde{\rho}_k)}{\partial T} = a_\omega \sum_{\eta=\pm 1} \sum_{l=0,1} \frac{\partial}{\partial T} I_{k,\eta l}(T; \tilde{\omega}_k, \tilde{\rho}_k), \quad (\text{L.2})$$

$$\frac{\partial \tilde{\rho}_k(T; \tilde{\omega}_k, \tilde{\rho}_k)}{\partial T} = a_\rho \sum_{\eta=\pm 1} \sum_{l=0,1} (-1)^l \frac{\partial}{\partial T} I_{k,\eta l}(T; \tilde{\omega}_k, \tilde{\rho}_k). \quad (\text{L.3})$$

With  $a_\omega = N_c G_\omega^2 / 3\pi^2$  and  $a_\rho = N_c G_\rho^2 / 3\pi^2$ . We only need to calculate  $\frac{\partial}{\partial T} I_{k,\eta l}$ , which can be written as:

$$\frac{\partial}{\partial T} I_{k,\eta l}(T; \tilde{\omega}_k, \tilde{\rho}_k) = J_{k,\eta l}^{(1)}(T; \tilde{\omega}_k, \tilde{\rho}_k) - J_{k,\eta l}^{(2)}(T; \tilde{\omega}_k, \tilde{\rho}_k) \left[ \frac{\partial \tilde{\omega}_k(T; \tilde{\omega}_k, \tilde{\rho}_k)}{\partial T} + (-1)^l \frac{\partial \tilde{\rho}_k(T; \tilde{\omega}_k, \tilde{\rho}_k)}{\partial T} \right]. \quad (\text{L.4})$$

---

<sup>1</sup>In this section we use,  $\tilde{\omega}_k = g_\omega \tilde{\omega}_{0,k}$ ,  $\tilde{\rho}_k = g_\rho \tilde{\rho}_{0,k}^3$ ,  $G_\omega = \frac{g_\omega}{m_\omega}$  and  $G_\rho = \frac{g_\rho}{m_\rho}$ .

Here,

$$J_{k,\eta l}^{(1)}(T, \mu; \sigma, \tilde{\omega}_k, \tilde{\rho}_k) = 3 \int_k^\Lambda dp \eta p^2 \frac{n_F(E_\psi - \eta \tilde{\mu}_{k,l})}{T^2} (1 - n_F(E_\psi - \eta \tilde{\mu}_{k,l})) (E_\psi - \eta \tilde{\mu}_{k,l}) - \left[ \eta p^3 \frac{n_F(E_\psi - \eta \tilde{\mu}_{k,l})}{T^2} (1 - n_F(E_\psi - \eta \tilde{\mu}_{k,l})) (E_\psi - \eta \tilde{\mu}_{k,l}) \right]_k^\Lambda, \quad (\text{L.5})$$

$$J_{k,\eta l}^{(2)}(T, \mu; \sigma, \tilde{\omega}_k, \tilde{\rho}_k) = 3 \int_k^\Lambda dp p^2 \frac{n_F(E_\psi - \eta \tilde{\mu}_{k,l})}{T} (1 - n_F(E_\psi - \eta \tilde{\mu}_{k,l})) - \left[ p^3 \frac{n_F(E_\psi - \eta \tilde{\mu}_{k,l})}{T} (1 - n_F(E_\psi - \eta \tilde{\mu}_{k,l})) \right]_k^\Lambda. \quad (\text{L.6})$$

The derivatives of the vector fields with respect to temperature are given by:

$$\tilde{\omega}'_k(T; \tilde{\omega}_k, \tilde{\rho}_k) = a_\omega \sum_{\eta=\pm 1} \sum_{l=0,1} \left\{ J_{k,\eta l}^{(1)}(T; \tilde{\omega}_k, \tilde{\rho}_k) - J_{k,\eta l}^{(2)}(T; \tilde{\omega}_k, \tilde{\rho}_k) \left[ \tilde{\omega}'_k(T; \tilde{\omega}_k, \tilde{\rho}_k) + (-1)^l \tilde{\rho}'_k(T; \tilde{\omega}_k, \tilde{\rho}_k) \right] \right\}, \quad (\text{L.7})$$

$$\tilde{\rho}'_k(T; \tilde{\omega}_k, \tilde{\rho}_k) = a_\rho \sum_{\eta=\pm 1} \sum_{l=0,1} (-1)^l \left\{ J_{k,\eta l}^{(1)}(T; \tilde{\omega}_k, \tilde{\rho}_k) - J_{k,\eta l}^{(2)}(T; \tilde{\omega}_k, \tilde{\rho}_k) \left[ \tilde{\omega}'_k(T; \tilde{\omega}_k, \tilde{\rho}_k) + (-1)^l \tilde{\rho}'_k(T; \tilde{\omega}_k, \tilde{\rho}_k) \right] \right\}. \quad (\text{L.8})$$

This system of equations can be solved analytically for  $\tilde{\omega}'_k$  and  $\tilde{\rho}'_k$ . Omitting the functions dependencies, we can write:

$$\tilde{\omega}'_k = A_k - B_k \tilde{\omega}'_k - C_k \tilde{\rho}'_k, \quad (\text{L.9})$$

$$\tilde{\rho}'_k = D_k - E_k \tilde{\omega}'_k - F_k \tilde{\rho}'_k. \quad (\text{L.10})$$

Where we have defined,

$$A_k(T; \tilde{\omega}_k, \tilde{\rho}_k) = a_\omega \sum_{\eta=\pm 1} \sum_{l=0,1} J_{k,\eta l}^{(1)}(T; \tilde{\omega}_k, \tilde{\rho}_k), \quad (\text{L.11})$$

$$B_k(T; \tilde{\omega}_k, \tilde{\rho}_k) = a_\omega \sum_{\eta=\pm 1} \sum_{l=0,1} J_{k,\eta l}^{(2)}(T; \tilde{\omega}_k, \tilde{\rho}_k), \quad (\text{L.12})$$

$$C_k(T; \tilde{\omega}_k, \tilde{\rho}_k) = a_\omega \sum_{\eta=\pm 1} \sum_{l=0,1} (-1)^l J_{k,\eta l}^{(2)}(T; \tilde{\omega}_k, \tilde{\rho}_k), \quad (\text{L.13})$$

$$D_k(T; \tilde{\omega}_k, \tilde{\rho}_k) = a_\rho \sum_{\eta=\pm 1} \sum_{l=0,1} (-1)^l J_{k,\eta l}^{(1)}(T; \tilde{\omega}_k, \tilde{\rho}_k), \quad (\text{L.14})$$

$$E_k(T; \tilde{\omega}_k, \tilde{\rho}_k) = a_\rho \sum_{\eta=\pm 1} \sum_{l=0,1} (-1)^l J_{k,\eta l}^{(2)}(T; \tilde{\omega}_k, \tilde{\rho}_k) = \frac{a_\rho}{a_\omega} C_k(T; \tilde{\omega}_k, \tilde{\rho}_k), \quad (\text{L.15})$$

$$F_k(T; \tilde{\omega}_k, \tilde{\rho}_k) = a_\rho \sum_{\eta=\pm 1} \sum_{l=0,1} J_{k,\eta l}^{(2)}(T; \tilde{\omega}_k, \tilde{\rho}_k) = \frac{a_\rho}{a_\omega} B_k(T; \tilde{\omega}_k, \tilde{\rho}_k). \quad (\text{L.16})$$

Very easily one can solve the system of linear equations to get:

$$\frac{\partial \tilde{\omega}_k}{\partial T} = \frac{A_k - C_k D_k + A_k F_k}{1 + B_k - C_k E_k + F_k + B_k F_k}, \quad (\text{L.17})$$

$$\frac{\partial \tilde{\rho}_k}{\partial T} = \frac{D_k + B_k D_k - A_k E_k}{1 + B_k - C_k E_k + F_k + B_k F_k}. \quad (\text{L.18})$$

When considering only one vector field i.e., if  $G_\rho = 0$  or  $G_\omega = 0$ , the temperature derivatives are much simpler:

$$G_\rho = 0 \implies \frac{\partial \tilde{\omega}_k}{\partial T} = \frac{A_k}{1 + B_k}, \quad (\text{L.19})$$

$$G_\omega = 0 \implies \frac{\partial \tilde{\rho}_k}{\partial T} = \frac{D_k}{1 + F_k}. \quad (\text{L.20})$$

## L.2 Derivative of the vector fields with respect to chemical potential

The existence of finite vector interactions imply an extra contribution to the density flow equation coming from the chemical potential derivative of the vector fields. Considering Eq. (8.30), the chemical potential derivative in the density flow equation can be written as:

$$\frac{\partial v_{k,l}(\mu; \tilde{\omega}_k, \tilde{\rho}_k)}{\partial \mu_j} = \frac{\partial \tilde{\omega}_k(\mu; \tilde{\omega}_k, \tilde{\rho}_k)}{\partial \mu_j} + (-1)^l \frac{\partial \tilde{\rho}_k(\mu; \tilde{\omega}_k, \tilde{\rho}_k)}{\partial \mu_j}. \quad (\text{L.21})$$

Here,  $l = 0$  is for up quarks and  $l = 1$  is for down quarks. We need to calculate the vector fields chemical potential derivatives. Following the previous calculation related to the temperature derivative of the vector fields (see Appendix L.1), using the self-consistent equations for the vector fields given in Eqs. (8.51) and (8.52), we can write:

$$\frac{\partial \tilde{\omega}_k(\mu; \tilde{\omega}_k, \tilde{\rho}_k)}{\partial \mu_j} = a_\omega \sum_{\eta=\pm 1} \sum_{l=0,1} \frac{\partial}{\partial \mu_j} I_{k,\eta l}(\mu; \tilde{\omega}_k, \tilde{\rho}_k), \quad (\text{L.22})$$

$$\frac{\partial \tilde{\rho}_k(\mu; \tilde{\omega}_k, \tilde{\rho}_k)}{\partial \mu_j} = a_\rho \sum_{\eta=\pm 1} \sum_{l=0,1} (-1)^l \frac{\partial}{\partial \mu_j} I_{k,\eta l}(\mu; \tilde{\omega}_k, \tilde{\rho}_k). \quad (\text{L.23})$$

Using Eq. (8.47), we can write:

$$\begin{aligned} \frac{\partial}{\partial \mu_j} I_{k,\eta l}(\mu; \tilde{\omega}_k, \tilde{\rho}_k) &= \delta_{lj} J_{k,\eta l}^{(2)}(\mu; \tilde{\omega}_k, \tilde{\rho}_k) - J_{k,\eta l}^{(2)}(\mu; \tilde{\omega}_k, \tilde{\rho}_k) \left( \frac{\partial v_{k,l}(\mu; \tilde{\omega}_k, \tilde{\rho}_k)}{\partial \mu_j} \right) \\ &= \delta_{lj} J_{k,\eta l}^{(2)}(\mu; \tilde{\omega}_k, \tilde{\rho}_k) - J_{k,\eta l}^{(2)}(\mu; \tilde{\omega}_k, \tilde{\rho}_k) \left[ \frac{\partial \tilde{\omega}_k(\mu; \tilde{\omega}_k, \tilde{\rho}_k)}{\partial \mu_j} + (-1)^l \frac{\partial \tilde{\rho}_k(\mu; \tilde{\omega}_k, \tilde{\rho}_k)}{\partial \mu_j} \right]. \end{aligned} \quad (\text{L.24})$$

Here,  $J_{k,\eta l}^{(2)}(T, \mu; \sigma, \tilde{\omega}_k, \tilde{\rho}_k)$ , is given by Eq. (L.6).

The derivatives of the vector fields with respect to chemical potential can be written as:

$$\tilde{\omega}'_k(\mu; \tilde{\omega}_k, \tilde{\rho}_k) = a_\omega \sum_{\eta=\pm 1} \sum_{l=0,1} \left\{ \delta_{lj} J_{k,\eta l}^{(2)}(\mu; \tilde{\omega}_k, \tilde{\rho}_k) - J_{k,\eta l}^{(2)}(\mu; \tilde{\omega}_k, \tilde{\rho}_k) \left[ \tilde{\omega}'_k(\mu; \tilde{\omega}_k, \tilde{\rho}_k) + (-1)^l \tilde{\rho}'_k(\mu; \tilde{\omega}_k, \tilde{\rho}_k) \right] \right\}, \quad (\text{L.25})$$

$$\tilde{\rho}'_k(\mu; \tilde{\omega}_k, \tilde{\rho}_k) = a_\rho \sum_{\eta=\pm 1} \sum_{l=0,1} (-1)^l \left\{ \delta_{lj} J_{k,\eta l}^{(2)}(\mu; \tilde{\omega}_k, \tilde{\rho}_k) - J_{k,\eta l}^{(2)}(\mu; \tilde{\omega}_k, \tilde{\rho}_k) \left[ \tilde{\omega}'_k(\mu; \tilde{\omega}_k, \tilde{\rho}_k) + (-1)^l \tilde{\rho}'_k(\mu; \tilde{\omega}_k, \tilde{\rho}_k) \right] \right\}. \quad (\text{L.26})$$

As before, this system of equations can be solved analytically for  $\tilde{\omega}'_k$  and  $\tilde{\rho}'_k$ . Omitting the functions dependencies, we can write:

$$\tilde{\omega}'_k = L_{k,j} - M_k \tilde{\omega}'_k - N_k \tilde{\rho}'_k, \quad (\text{L.27})$$

$$\tilde{\rho}'_k = O_{k,j} - P_k \tilde{\omega}'_k - Q_k \tilde{\rho}'_k. \quad (\text{L.28})$$

Where:

$$L_{k,j}(\mu; \tilde{\omega}_k, \tilde{\rho}_k) = a_\omega \sum_{\eta=\pm 1} J_{k,\eta j}^{(2)}(\mu; \tilde{\omega}_k, \tilde{\rho}_k), \quad (\text{L.29})$$

$$M_k(\mu; \tilde{\omega}_k, \tilde{\rho}_k) = a_\omega \sum_{\eta=\pm 1} \sum_{l=0,1} J_{k,\eta l}^{(2)}(\mu; \tilde{\omega}_k, \tilde{\rho}_k), \quad (\text{L.30})$$

$$N_k(\mu; \tilde{\omega}_k, \tilde{\rho}_k) = a_\omega \sum_{\eta=\pm 1} \sum_{l=0,1} (-1)^l J_{k,\eta l}^{(2)}(\mu; \tilde{\omega}_k, \tilde{\rho}_k), \quad (\text{L.31})$$

$$O_{k,j}(\mu; \tilde{\omega}_k, \tilde{\rho}_k) = a_\rho \sum_{\eta=\pm 1} (-1)^j J_{k,\eta j}^{(2)}(\mu; \tilde{\omega}_k, \tilde{\rho}_k), \quad (\text{L.32})$$

$$P_k(\mu; \tilde{\omega}_k, \tilde{\rho}_k) = a_\rho \sum_{\eta=\pm 1} \sum_{l=0,1} (-1)^l J_{k,\eta l}^{(2)}(\mu; \tilde{\omega}_k, \tilde{\rho}_k) = \frac{a_\rho}{a_\omega} N_k(\mu; \tilde{\omega}_k, \tilde{\rho}_k), \quad (\text{L.33})$$

$$Q_k(\mu; \tilde{\omega}_k, \tilde{\rho}_k) = a_\rho \sum_{\eta=\pm 1} \sum_{l=0,1} J_{k,\eta l}^{(2)}(\mu; \tilde{\omega}_k, \tilde{\rho}_k) = \frac{a_\rho}{a_\omega} M_k(\mu; \tilde{\omega}_k, \tilde{\rho}_k). \quad (\text{L.34})$$

The linear system of equations for the chemical potential derivatives of the vector fields can be calculated to yield:

$$\frac{\partial \tilde{\omega}_k}{\partial \mu_j} = \frac{L_{k,j} - N_k O_{k,j} + L_{k,j} Q_k}{1 + M_k - N_k P_k + Q_k + M_k Q_k}, \quad (\text{L.35})$$

$$\frac{\partial \tilde{\rho}_k}{\partial \mu_j} = \frac{O_{k,j} + M_k O_{k,j} - L_{k,j} P_k}{1 + M_k - N_k P_k + Q_k + M_k Q_k}. \quad (\text{L.36})$$

When considering only one vector field i.e., if  $G_\rho = 0$  or  $G_\omega = 0$  the chemical potential derivatives of the vector fields are:

$$G_\rho = 0 \implies \frac{\partial \tilde{\omega}_k}{\partial \mu_j} = \frac{L_{k,j}}{1 + M_k}, \quad (\text{L.37})$$

$$G_\omega = 0 \implies \frac{\partial \tilde{\rho}_k}{\partial \mu_j} = \frac{O_{k,j}}{1 + Q_k}. \quad (\text{L.38})$$



# Bibliography

- [1] Adam Miklos Halasz et al. “On the phase diagram of QCD”. In: *Phys.Rev.* D58 (1998), p. 096007. DOI: 10.1103/PhysRevD.58.096007. arXiv: hep-ph/9804290 [hep-ph].
- [2] Sourendu Gupta et al. “Scale for the Phase Diagram of Quantum Chromodynamics”. In: *Science* 332 (2011), pp. 1525–1528. DOI: 10.1126/science.1204621. arXiv: 1105.3934 [hep-ph].
- [3] Miklos Gyulassy. “The QGP discovered at RHIC”. In: *Structure and dynamics of elementary matter. Proceedings, NATO Advanced Study Institute, Camyuwa-Kemer, Turkey, September 22-October 2, 2003.* 2004, pp. 159–182. arXiv: nucl-th/0403032 [nucl-th].
- [4] N. Brambilla et al. “QCD and Strongly Coupled Gauge Theories: Challenges and Perspectives”. In: *Eur. Phys. J. C* 74.10 (2014), p. 2981. DOI: 10.1140/epjc/s10052-014-2981-5. arXiv: 1404.3723 [hep-ph].
- [5] Robert C. Duncan and Christopher Thompson. “Formation of very strongly magnetized neutron stars - implications for gamma-ray bursts”. In: *Astrophys. J.* 392 (1992), p. L9. DOI: 10.1086/186413.
- [6] C. Kouveliotou et al. “An X-ray pulsar with a superstrong magnetic field in the soft gamma-ray repeater SGR 1806-20.” In: *Nature* 393 (1998), pp. 235–237. DOI: 10.1038/30410.
- [7] V. Skokov, A. Yu. Illarionov, and V. Toneev. “Estimate of the magnetic field strength in heavy-ion collisions”. In: *Int. J. Mod. Phys. A* 24 (2009), pp. 5925–5932. DOI: 10.1142/S0217751X09047570. arXiv: 0907.1396 [nucl-th].
- [8] Dmitri E. Kharzeev, Larry D. McLerran, and Harmen J. Warringa. “The Effects of topological charge change in heavy ion collisions: ‘Event by event P and CP violation’”. In: *Nucl. Phys.* A803 (2008), pp. 227–253. DOI: 10.1016/j.nuclphysa.2008.02.298. arXiv: 0711.0950 [hep-ph].
- [9] T. Vachaspati. “Magnetic fields from cosmological phase transitions”. In: *Phys. Lett.* B265 (1991), pp. 258–261. DOI: 10.1016/0370-2693(91)90051-Q.
- [10] K. Enqvist and P. Olesen. “On primordial magnetic fields of electroweak origin”. In: *Phys. Lett.* B319 (1993), pp. 178–185. DOI: 10.1016/0370-2693(93)90799-N. arXiv: hep-ph/9308270 [hep-ph].
- [11] H. Leutwyler. “On the history of the strong interaction”. In: (2014). Ed. by Antonino Zichichi, pp. 29–43. DOI: 10.1142/S0217732314300237. arXiv: 1211.6777 [physics.hist-ph].
- [12] Peter Skands. “Introduction to QCD”. In: *Proceedings, Theoretical Advanced Study Institute in Elementary Particle Physics: Searching for New Physics at Small and Large Scales (TASI 2012): Boulder, Colorado, June 4-29, 2012.* 2013, pp. 341–420. DOI: 10.

- 1142/9789814525220\_0008. arXiv: 1207.2389 [hep-ph]. URL: <http://inspirehep.net/record/1121892/files/arXiv:1207.2389.pdf>.
- [13] Harald Fritzsch. “The history of QCD”. In: (2012). URL: <https://cerncourier.com/a/the-history-of-qcd/>.
- [14] David J. Gross and Frank Wilczek. “Ultraviolet Behavior of Nonabelian Gauge Theories”. In: *Phys. Rev. Lett.* 30 (1973), pp. 1343–1346. DOI: 10.1103/PhysRevLett.30.1343.
- [15] H. David Politzer. “Reliable Perturbative Results for Strong Interactions?” In: *Phys. Rev. Lett.* 30 (1973), pp. 1346–1349. DOI: 10.1103/PhysRevLett.30.1346.
- [16] David J. Gross. “Twenty five years of asymptotic freedom”. In: *Nucl. Phys. Proc. Suppl.* 74 (1999), pp. 426–446. DOI: 10.1016/S0920-5632(99)00208-X. arXiv: hep-th/9809060 [hep-th].
- [17] E. D. Bloom et al. “High-Energy Inelastic  $e - p$  Scattering at  $6^\circ$  and  $10^\circ$ ”. In: *Phys. Rev. Lett.* 23 (16 Oct. 1969), pp. 930–934. DOI: 10.1103/PhysRevLett.23.930. URL: <https://link.aps.org/doi/10.1103/PhysRevLett.23.930>.
- [18] M. Breidenbach et al. “Observed Behavior of Highly Inelastic Electron-Proton Scattering”. In: *Phys. Rev. Lett.* 23 (16 Oct. 1969), pp. 935–939. DOI: 10.1103/PhysRevLett.23.935. URL: <https://link.aps.org/doi/10.1103/PhysRevLett.23.935>.
- [19] Siegfried Bethke. “Experimental tests of asymptotic freedom”. In: *Prog. Part. Nucl. Phys.* 58 (2007), pp. 351–386. DOI: 10.1016/j.pnpnp.2006.06.001. arXiv: hep-ex/0606035 [hep-ex].
- [20] K. A. Olive et al. “Review of Particle Physics”. In: *Chin. Phys.* C38 (2014), p. 090001. DOI: 10.1088/1674-1137/38/9/090001.
- [21] Giorgio Cortiana. “Top-quark mass measurements: review and perspectives”. In: *Rev. Phys.* 1 (2016), pp. 60–76. DOI: 10.1016/j.revip.2016.04.001. arXiv: 1510.04483 [hep-ex].
- [22] P. G. Harris et al. “New experimental limit on the electric dipole moment of the neutron”. In: *Phys. Rev. Lett.* 82 (1999), pp. 904–907. DOI: 10.1103/PhysRevLett.82.904.
- [23] Antonio Pich. “Effective Field Theory with Nambu-Goldstone Modes”. In: *Les Houches Lect. Notes* 108 (2020). Ed. by Sacha Davidson et al. DOI: 10.1093/oso/9780198855743.003.0003. arXiv: 1804.05664 [hep-ph].
- [24] E. Witten. Unpublished paper.
- [25] Steven Weinberg. “The U(1) Problem”. In: *Phys. Rev.* D11 (1975), pp. 3583–3593. DOI: 10.1103/PhysRevD.11.3583.
- [26] Gerard 't Hooft. “How Instantons Solve the U(1) Problem”. In: *Phys. Rept.* 142 (1986), pp. 357–387. DOI: 10.1016/0370-1573(86)90117-1.
- [27] Gerard 't Hooft. “Computation of the Quantum Effects Due to a Four-Dimensional Pseudoparticle”. In: *Phys. Rev.* D14 (1976). [Erratum: *Phys. Rev.* D18,2199(1978)], pp. 3432–3450. DOI: 10.1103/PhysRevD.18.2199.3, 10.1103/PhysRevD.14.3432.
- [28] Pedro Costa et al. “Effective restoration of the U(A)(1) symmetry with temperature and density”. In: *Phys. Rev.* D70 (2004), p. 116013. DOI: 10.1103/PhysRevD.70.116013. arXiv: hep-ph/0408177.

- [29] M.E. Peskin and D.V. Schroeder. *An Introduction To Quantum Field Theory*. Frontiers in physics. Westview Press, 1995. ISBN: 9780813345437. URL: <https://books.google.pt/books?id=EVeNNcslvX0C>.
- [30] M. Tanabashi et al. “Review of Particle Physics”. In: *Phys. Rev. D* 98.3 (2018), p. 030001. DOI: 10.1103/PhysRevD.98.030001.
- [31] Murray Gell-Mann, R. J. Oakes, and B. Renner. “Behavior of Current Divergences under  $SU_3 \times SU_3$ ”. In: *Phys. Rev.* 175 (5 Nov. 1968), pp. 2195–2199. DOI: 10.1103/PhysRev.175.2195. URL: <https://link.aps.org/doi/10.1103/PhysRev.175.2195>.
- [32] Stefano Carignano, Michael Buballa, and Bernd-Jochen Schaefer. “Inhomogeneous phases in the quark-meson model with vacuum fluctuations”. In: *Phys. Rev. D* 90.1 (2014), p. 014033. DOI: 10.1103/PhysRevD.90.014033. arXiv: 1404.0057 [hep-ph].
- [33] Ralf-Arno Tripolt. “Spectral Functions and Transport Coefficients from the Functional Renormalization Group”. PhD thesis. Technischen Universität Darmstadt, 2015.
- [34] N. Cabibbo and G. Parisi. “Exponential Hadronic Spectrum and Quark Liberation”. In: *Phys. Lett.* 59B (1975), pp. 67–69. DOI: 10.1016/0370-2693(75)90158-6.
- [35] Peter Braun-Munzinger et al. “Properties of hot and dense matter from relativistic heavy ion collisions”. In: *Phys. Rept.* 621 (2016), pp. 76–126. DOI: 10.1016/j.physrep.2015.12.003. arXiv: 1510.00442 [nucl-th].
- [36] Adam Bzdak et al. “Mapping the Phases of Quantum Chromodynamics with Beam Energy Scan”. In: *Phys. Rept.* 853 (2020), pp. 1–87. DOI: 10.1016/j.physrep.2020.01.005. arXiv: 1906.00936 [nucl-th].
- [37] J.M. Yeomans. *Statistical Mechanics of Phase Transitions*. Clarendon Press, 1992. ISBN: 9780191589706. URL: <https://books.google.pt/books?id=3IUVSvOUtTMC>.
- [38] Gregg Jaeger. “The Ehrenfest Classification of Phase Transitions: Introduction and Evolution”. In: *Archive for History of Exact Sciences* 53 (May 1998), pp. 51–81. DOI: 10.1007/s004070050021.
- [39] Robert D. Pisarski. “Notes on the deconfining phase transition”. In: *QCD perspectives on hot and dense matter. Proceedings, NATO Advanced Study Institute, Summer School, Cargese, France, August 6-18, 2001*. 2002, pp. 353–384. arXiv: hep-ph/0203271 [hep-ph]. URL: <http://alice.cern.ch/format/showfull?sysnb=2302511>.
- [40] Kenji Fukushima. “Chiral effective model with the Polyakov loop”. In: *Phys. Lett.* B591 (2004), pp. 277–284. DOI: 10.1016/j.physletb.2004.04.027. arXiv: hep-ph/0310121 [hep-ph].
- [41] Claudia Ratti. “Thermodynamics of the Quark-Gluon Plasma”. In: *International School on Quark-Gluon Plasma and Heavy Ion Collisions : past, present, future*.
- [42] B.O. Kerbikov. “Color superconducting state of quarks”. In: (Oct. 2001). arXiv: hep-ph/0110197.
- [43] Kenji Fukushima and Tetsuo Hatsuda. “The phase diagram of dense QCD”. In: *Rept. Prog. Phys.* 74 (2011), p. 014001. DOI: 10.1088/0034-4885/74/1/014001. arXiv: 1005.4814 [hep-ph].
- [44] Krishna Rajagopal. “Mapping the QCD phase diagram”. In: *Nucl. Phys.* A661 (1999), pp. 150–161. DOI: 10.1016/S0375-9474(99)85017-9. arXiv: hep-ph/9908360 [hep-ph].

- [45] Michael Buballa. “NJL model analysis of quark matter at large density”. In: *Phys. Rept.* 407 (2005), pp. 205–376. DOI: 10.1016/j.physrep.2004.11.004. arXiv: hep-ph/0402234 [hep-ph].
- [46] Andrei Kryjevski, David B. Kaplan, and Thomas Schäfer. “New phases in CFL quark matter”. In: *Phys. Rev. D* 71 (2005), p. 034004. DOI: 10.1103/PhysRevD.71.034004. arXiv: hep-ph/0404290.
- [47] M. A. Stephanov. “QCD phase diagram: An Overview”. In: *PoS LAT2006* (2006), p. 024. arXiv: hep-lat/0701002 [hep-lat].
- [48] Christian Schmidt and Sayantan Sharma. “The phase structure of QCD”. In: *J. Phys. G44.10* (2017), p. 104002. DOI: 10.1088/1361-6471/aa824a. arXiv: 1701.04707 [hep-lat].
- [49] Erhard Seiler. “Status of Complex Langevin”. In: *EPJ Web Conf.* 175 (2018), p. 01019. DOI: 10.1051/epjconf/201817501019. arXiv: 1708.08254 [hep-lat].
- [50] Szabolcs Borsanyi et al. “Is there still any  $T_c$  mystery in lattice QCD? Results with physical masses in the continuum limit III”. In: *JHEP* 09 (2010), p. 073. DOI: 10.1007/JHEP09(2010)073. arXiv: 1005.3508 [hep-lat].
- [51] A. Bazavov et al. “The chiral and deconfinement aspects of the QCD transition”. In: *Phys.Rev.* D85 (2012), p. 054503. DOI: 10.1103/PhysRevD.85.054503. arXiv: 1111.1710 [hep-lat].
- [52] R. Bellwied et al. “The QCD phase diagram from analytic continuation”. In: *Phys. Lett. B* 751 (2015), pp. 559–564. DOI: 10.1016/j.physletb.2015.11.011. arXiv: 1507.07510 [hep-lat].
- [53] A. Bazavov et al. “Chiral crossover in QCD at zero and non-zero chemical potentials”. In: *Phys. Lett. B* 795 (2019), pp. 15–21. DOI: 10.1016/j.physletb.2019.05.013. arXiv: 1812.08235 [hep-lat].
- [54] Y. Aoki et al. “The QCD transition temperature: Results with physical masses in the continuum limit”. In: *Phys. Lett. B* 643 (2006), pp. 46–54. DOI: 10.1016/j.physletb.2006.10.021. arXiv: hep-lat/0609068.
- [55] Kenji Fukushima and Chihiro Sasaki. “The phase diagram of nuclear and quark matter at high baryon density”. In: *Prog. Part. Nucl. Phys.* 72 (2013), pp. 99–154. DOI: 10.1016/j.pnpnp.2013.05.003. arXiv: 1301.6377 [hep-ph].
- [56] A. Das. *Field Theory: A Path Integral Approach*. World Scientific Lecture Notes in Physics. 1993. ISBN: 9789814504195. URL: <https://books.google.pt/books?id=UbzsCgAAQBAJ>.
- [57] Christian S. Fischer. “QCD at finite temperature and chemical potential from Dyson–Schwinger equations”. In: *Prog. Part. Nucl. Phys.* 105 (2019), pp. 1–60. DOI: 10.1016/j.pnpnp.2019.01.002. arXiv: 1810.12938 [hep-ph].
- [58] Christian S. Fischer et al. “Polyakov loop potential at finite density”. In: *Phys. Lett. B* 732 (2014), pp. 273–277. DOI: 10.1016/j.physletb.2014.03.057. arXiv: 1306.6022 [hep-ph].
- [59] Christian S. Fischer, Jan Luecker, and Christian A. Welzbacher. “Phase structure of three and four flavor QCD”. In: *Phys. Rev.* D90.3 (2014), p. 034022. DOI: 10.1103/PhysRevD.90.034022. arXiv: 1405.4762 [hep-ph].

- [60] Philipp Isserstedt et al. “Baryon number fluctuations in the QCD phase diagram from Dyson-Schwinger equations”. In: *Phys. Rev. D* 100.7 (2019), p. 074011. DOI: 10.1103/PhysRevD.100.074011. arXiv: 1906.11644 [hep-ph].
- [61] Renan Câmara Pereira, Pedro Costa, and Constança Providência. “Two-solar-mass hybrid stars: a two model description with the Nambu-Jona-Lasinio quark model”. In: *Phys. Rev. D* 94.9 (2016), p. 094001. DOI: 10.1103/PhysRevD.94.094001. arXiv: 1610.06435 [nucl-th].
- [62] A.A. Osipov, B. Hiller, and A.H. Blin. “Light Quark Masses in Multi-Quark Interactions”. In: *Eur.Phys.J. A* 49 (2013), p. 14. DOI: 10.1140/epja/i2013-13014-y. arXiv: 1206.1920 [hep-ph].
- [63] A.A. Osipov, B. Hiller, and A.H. Blin. “Effective multiquark interactions with explicit breaking of chiral symmetry”. In: *Phys.Rev.* D88.5 (2013), p. 054032. DOI: 10.1103/PhysRevD.88.054032. arXiv: 1309.2497 [hep-ph].
- [64] J. Moreira et al. “Strange quark matter in the presence of explicit symmetry breaking interactions”. In: *Phys. Rev.* D91 (2015), p. 116003. DOI: 10.1103/PhysRevD.91.116003. arXiv: 1409.0336 [hep-ph].
- [65] Jens O. Andersen, William R. Naylor, and Anders Tranberg. “Phase diagram of QCD in a magnetic field: A review”. In: *Rev. Mod. Phys.* 88 (2016), p. 025001. DOI: 10.1103/RevModPhys.88.025001. arXiv: 1411.7176 [hep-ph].
- [66] Szabolcs Borsanyi et al. “The QCD equation of state with dynamical quarks”. In: *JHEP* 11 (2010), p. 077. DOI: 10.1007/JHEP11(2010)077. arXiv: 1007.2580 [hep-lat].
- [67] G. S. Bali et al. “The QCD phase diagram for external magnetic fields”. In: *JHEP* 02 (2012), p. 044. DOI: 10.1007/JHEP02(2012)044. arXiv: 1111.4956 [hep-lat].
- [68] G. S. Bali et al. “QCD quark condensate in external magnetic fields”. In: *Phys. Rev.* D86 (2012), p. 071502. DOI: 10.1103/PhysRevD.86.071502. arXiv: 1206.4205 [hep-lat].
- [69] Falk Bruckmann, Gergely Endrodi, and Tamas G. Kovacs. “Inverse magnetic catalysis and the Polyakov loop”. In: *JHEP* 04 (2013), p. 112. DOI: 10.1007/JHEP04(2013)112. arXiv: 1303.3972 [hep-lat].
- [70] Gergely Endrodi. “Critical point in the QCD phase diagram for extremely strong background magnetic fields”. In: *JHEP* 07 (2015), p. 173. DOI: 10.1007/JHEP07(2015)173. arXiv: 1504.08280 [hep-lat].
- [71] M. Ferreira et al. “Inverse magnetic catalysis in the (2+1)-flavor Nambu-Jona-Lasinio and Polyakov-Nambu-Jona-Lasinio models”. In: *Phys. Rev.* D89.11 (2014), p. 116011. DOI: 10.1103/PhysRevD.89.116011. arXiv: 1404.5577 [hep-ph].
- [72] Pedro Costa et al. “Influence of the inverse magnetic catalysis and the vector interaction in the location of the critical end point”. In: *Phys. Rev. D* 92.3 (2015), p. 036012. DOI: 10.1103/PhysRevD.92.036012. arXiv: 1508.07870 [hep-ph].
- [73] Márcio Ferreira, Pedro Costa, and Constança Providência. “Multiple critical endpoints in magnetized three flavor quark matter”. In: *Phys. Rev.* D97.1 (2018), p. 014014. DOI: 10.1103/PhysRevD.97.014014. arXiv: 1712.08378 [hep-ph].
- [74] Kenji Fukushima. “Phase diagrams in the three-flavor Nambu-Jona-Lasinio model with the Polyakov loop”. In: *Phys. Rev.* D77 (2008). [Erratum: *Phys. Rev.* D78,039902(2008)],

- p. 114028. DOI: 10.1103/PhysRevD.77.114028, 10.1103/PhysRevD.78.039902. arXiv: 0803.3318 [hep-ph].
- [75] Pedro Costa. “Influence of the vector interaction and an external magnetic field on the isentropes near the chiral critical end point”. In: *Phys. Rev. D* 93.11 (2016), p. 114035. DOI: 10.1103/PhysRevD.93.114035. arXiv: 1610.06433 [nucl-th].
- [76] Márcio Ferreira, Pedro Costa, and Constança Providência. “Presence of a critical endpoint in the QCD phase diagram from the net-baryon number fluctuations”. In: *Phys. Rev. D* 98.3 (2018), p. 034006. DOI: 10.1103/PhysRevD.98.034006. arXiv: 1806.05757 [hep-ph].
- [77] Lisa M. Haas et al. “Improved Polyakov-loop potential for effective models from functional calculations”. In: *Phys. Rev. D* 87.7 (2013), p. 076004. DOI: 10.1103/PhysRevD.87.076004. arXiv: 1302.1993 [hep-ph].
- [78] Kenji Morita et al. “Role of mesonic fluctuations in the Polyakov loop extended quark-meson model at imaginary chemical potential”. In: *Phys. Rev. D* 84 (2011), p. 074020. DOI: 10.1103/PhysRevD.84.074020. arXiv: 1108.0735 [hep-ph].
- [79] E. Nakano et al. “Fluctuations and isentropes near the chiral critical endpoint”. In: *Phys. Lett. B* 682 (2010), pp. 401–407. DOI: 10.1016/j.physletb.2009.11.027. arXiv: 0907.1344 [hep-ph].
- [80] V. Skokov, B. Friman, and K. Redlich. “Quark number fluctuations in the Polyakov loop-extended quark-meson model at finite baryon density”. In: *Phys. Rev. C* 83 (2011), p. 054904. DOI: 10.1103/PhysRevC.83.054904. arXiv: 1008.4570 [hep-ph].
- [81] Matthias Drews and Wolfram Weise. “Functional renormalization group studies of nuclear and neutron matter”. In: *Prog. Part. Nucl. Phys.* 93 (2017), p. 69. DOI: 10.1016/j.pnpnp.2016.10.002. arXiv: 1610.07568 [nucl-th].
- [82] P.K. Srivastava, S.K. Tiwari, and C.P. Singh. “QCD Critical Point in a Quasiparticle Model”. In: *Phys. Rev. D* 82 (2010), p. 014023. DOI: 10.1103/PhysRevD.82.014023. arXiv: 1002.4780 [hep-ph].
- [83] Alexandre Biguet et al. “Sensitivity of predictions in an effective model – application to the chiral critical end point position in the Nambu–Jona-Lasinio model”. In: *Eur. Phys. J. A* 51.9 (2015), p. 121. DOI: 10.1140/epja/i2015-15121-1. arXiv: 1409.0990 [hep-ph].
- [84] Moritz Greif, Carsten Greiner, and Zhe Xu. “Magnetic field influence on the early time dynamics of heavy-ion collisions”. In: *Phys. Rev. C* 96.1 (2017), p. 014903. DOI: 10.1103/PhysRevC.96.014903. arXiv: 1704.06505 [hep-ph].
- [85] B. Friman et al. “The CBM Physics Book”. In: *Lect. Notes Phys.* 814 (2011), p. 681.
- [86] Masayuki Asakawa and Masakiyo Kitazawa. “Fluctuations of conserved charges in relativistic heavy ion collisions: An introduction”. In: *Prog. Part. Nucl. Phys.* 90 (2016), pp. 299–342. DOI: 10.1016/j.pnpnp.2016.04.002. arXiv: 1512.05038 [nucl-th].
- [87] Frithjof Karsch. “Determination of Freeze-out Conditions from Lattice QCD Calculations”. In: *Central Eur. J. Phys.* 10 (2012), pp. 1234–1237. DOI: 10.2478/s11534-012-0074-3. arXiv: 1202.4173 [hep-lat].

- [88] Christopher Jung et al. “In-Medium Spectral Functions of Vector- and Axial-Vector Mesons from the Functional Renormalization Group”. In: *Phys. Rev. D* 95.3 (2017), p. 036020. DOI: 10.1103/PhysRevD.95.036020. arXiv: 1610.08754 [hep-ph].
- [89] M. Oertel et al. “Equations of state for supernovae and compact stars”. In: *Rev. Mod. Phys.* 89.1 (2017), p. 015007. DOI: 10.1103/RevModPhys.89.015007. arXiv: 1610.03361 [astro-ph.HE].
- [90] Isaac Vidaña. “Short introduction to the physics of neutron stars”. In: *EPJ Web Conf.* 227 (2020). Ed. by C. Spitaleri et al., p. 01018. DOI: 10.1051/epjconf/202022701018.
- [91] A. Hewish et al. “Observation of a rapidly pulsating radio source”. In: *Nature* 217 (1968), pp. 709–713. DOI: 10.1038/217709a0.
- [92] Anthony Mezzacappa. “ASCERTAINING THE CORE COLLAPSE SUPERNOVA MECHANISM: The State of the Art and the Road Ahead”. In: *Annual Review of Nuclear and Particle Science* 55.1 (2005), pp. 467–515. DOI: 10.1146/annurev.nucl.55.090704.151608. eprint: <https://doi.org/10.1146/annurev.nucl.55.090704.151608>. URL: <https://doi.org/10.1146/annurev.nucl.55.090704.151608>.
- [93] N.K. Glendenning. *Compact Stars: Nuclear Physics, Particle Physics and General Relativity*. Astronomy and Astrophysics Library. Springer New York, 2012. ISBN: 9781468404913. URL: <https://books.google.pt/books?id=cCD1BwAAQBAJ>.
- [94] Norman K. Glendenning. “First order phase transitions with more than one conserved charge: Consequences for neutron stars”. In: *Phys. Rev. D* 46 (1992), pp. 1274–1287. DOI: 10.1103/PhysRevD.46.1274.
- [95] B. P. Abbott et al. “GW170817: Observation of Gravitational Waves from a Binary Neutron Star Inspiral”. In: *Phys. Rev. Lett.* 119.16 (2017), p. 161101. DOI: 10.1103/PhysRevLett.119.161101. arXiv: 1710.05832 [gr-qc].
- [96] B.P. Abbott et al. “GW170817: Measurements of neutron star radii and equation of state”. In: *Phys. Rev. Lett.* 121.16 (2018), p. 161101. DOI: 10.1103/PhysRevLett.121.161101. arXiv: 1805.11581 [gr-qc].
- [97] Thomas E. Riley et al. “A *NICER* View of PSR J0030+0451: Millisecond Pulsar Parameter Estimation”. In: *Astrophys. J. Lett.* 887.1 (2019), p. L21. DOI: 10.3847/2041-8213/ab481c. arXiv: 1912.05702 [astro-ph.HE].
- [98] John Antoniadis et al. “A Massive Pulsar in a Compact Relativistic Binary”. In: *Science* 340 (2013), p. 6131. DOI: 10.1126/science.1233232. arXiv: 1304.6875 [astro-ph.HE].
- [99] B. P. Abbott et al. “Gravitational Waves and Gamma-rays from a Binary Neutron Star Merger: GW170817 and GRB 170817A”. In: *Astrophys. J.* 848.2 (2017), p. L13. DOI: 10.3847/2041-8213/aa920c. arXiv: 1710.05834 [astro-ph.HE].
- [100] B. P. Abbott et al. “Multi-messenger Observations of a Binary Neutron Star Merger”. In: *Astrophys. J.* 848.2 (2017), p. L12. DOI: 10.3847/2041-8213/aa91c9. arXiv: 1710.05833 [astro-ph.HE].
- [101] David Radice et al. “Probing Extreme-Density Matter with Gravitational Wave Observations of Binary Neutron Star Merger Remnants”. In: *Astrophys. J.* 842.2 (2017), p. L10. DOI: 10.3847/2041-8213/aa775f. arXiv: 1612.06429 [astro-ph.HE].

- [102] David Radice et al. “GW170817: Joint Constraint on the Neutron Star Equation of State from Multimessenger Observations”. In: *Astrophys. J.* 852.2 (2018), p. L29. DOI: 10.3847/2041-8213/aaa402. arXiv: 1711.03647 [astro-ph.HE].
- [103] Andreas Bauswein et al. “Equation-of-state Constraints and the QCD Phase Transition in the Era of Gravitational-Wave Astronomy”. In: *AIP Conf. Proc.* 2127.1 (2019), p. 020013. DOI: 10.1063/1.5117803. arXiv: 1904.01306 [astro-ph.HE].
- [104] Michael W. Coughlin et al. “Constraints on the neutron star equation of state from AT2017gfo using radiative transfer simulations”. In: *Mon. Not. Roy. Astron. Soc.* 480.3 (2018), pp. 3871–3878. DOI: 10.1093/mnras/sty2174. arXiv: 1805.09371 [astro-ph.HE].
- [105] Yuan-Zhu Wang et al. “GW170817: The energy extraction process of the off-axis relativistic outflow and the constraint on the equation of state of neutron stars”. In: *Astrophys. J.* 877.1 (2019), p. 2. DOI: 10.3847/1538-4357/ab1914. arXiv: 1811.02558 [astro-ph.HE].
- [106] Mark G. Alford, Sophia Han, and Kai Schwenzer. “Signatures for quark matter from multi-messenger observations”. In: *J. Phys.* G46.11 (2019), p. 114001. DOI: 10.1088/1361-6471/ab337a. arXiv: 1904.05471 [nucl-th].
- [107] Elias R. Most et al. “Signatures of quark-hadron phase transitions in general-relativistic neutron-star mergers”. In: *Phys. Rev. Lett.* 122.6 (2019), p. 061101. DOI: 10.1103/PhysRevLett.122.061101. arXiv: 1807.03684 [astro-ph.HE].
- [108] Lukas R. Weih, Matthias Hanauske, and Luciano Rezzolla. “Postmerger Gravitational-Wave Signatures of Phase Transitions in Binary Mergers”. In: *Phys. Rev. Lett.* 124.17 (2020), p. 171103. DOI: 10.1103/PhysRevLett.124.171103. arXiv: 1912.09340 [gr-qc].
- [109] Ivo Sengo et al. “Neutron star inner crust: effects of rotation and magnetic fields”. In: *Phys. Rev. D* 102.6 (2020), p. 063013. DOI: 10.1103/PhysRevD.102.063013. arXiv: 2006.07248 [nucl-th].
- [110] Jens O. Andersen, William R. Naylor, and Anders Tranberg. “Chiral and deconfinement transitions in a magnetic background using the functional renormalization group with the Polyakov loop”. In: *JHEP* 04 (2014), p. 187. DOI: 10.1007/JHEP04(2014)187. arXiv: 1311.2093 [hep-ph].
- [111] Débora P. Menezes et al. “Repulsive Vector Interaction in Three Flavor Magnetized Quark and Stellar Matter”. In: *Phys. Rev.* C89.5 (2014), p. 055207. DOI: 10.1103/PhysRevC.89.055207. arXiv: 1403.2502 [nucl-th].
- [112] G. Ripka. *Quarks Bound by Chiral Fields: The Quark Structure of the Vacuum and of Light Mesons and Baryons*. Oxford science publications. Clarendon Press, 1997. ISBN: 9780198517849. URL: <https://books.google.pt/books?id=ntrPDA6zE1wC>.
- [113] Emil N. Nikolov et al. “Meson loops in the Nambu-Jona-Lasinio model”. In: *Nucl. Phys.* A608 (1996), pp. 411–436. DOI: 10.1016/0375-9474(96)00231-X. arXiv: hep-ph/9602274 [hep-ph].
- [114] Kazuhiko Kamikado and Takuya Kanazawa. “Chiral dynamics in a magnetic field from the functional renormalization group”. In: *JHEP* 03 (2014), p. 009. DOI: 10.1007/JHEP03(2014)009. arXiv: 1312.3124 [hep-ph].

- [115] Niklas Mueller and Jan M. Pawłowski. “Magnetic catalysis and inverse magnetic catalysis in QCD”. In: *Phys. Rev. D* 91.11 (2015), p. 116010. DOI: 10.1103/PhysRevD.91.116010. arXiv: 1502.08011 [hep-ph].
- [116] Kenji Fukushima and Jan M. Pawłowski. “Magnetic catalysis in hot and dense quark matter and quantum fluctuations”. In: *Phys. Rev. D* 86 (2012), p. 076013. DOI: 10.1103/PhysRevD.86.076013. arXiv: 1203.4330 [hep-ph].
- [117] Yoichiro Nambu and G. Jona-Lasinio. “Dynamical model of elementary particles based on an analogy with superconductivity. I”. In: *Phys. Rev.* 122 (1961), pp. 345–358. DOI: 10.1103/PhysRev.122.345.
- [118] Yoichiro Nambu and G. Jona-Lasinio. “Dynamical model of elementary particles based on an analogy with superconductivity. II”. In: *Phys. Rev.* 124 (1961), pp. 246–254. DOI: 10.1103/PhysRev.124.246.
- [119] Tohru Eguchi. “A New Approach to Collective Phenomena in Superconductivity Models”. In: *Phys. Rev. D* 14 (1976), p. 2755. DOI: 10.1103/PhysRevD.14.2755.
- [120] Keiji Kikkawa. “Quantum Corrections in Superconductor Models”. In: *Prog. Theor. Phys.* 56 (1976), p. 947. DOI: 10.1143/PTP.56.947.
- [121] M.k. Volkov and D. Ebert. “FOUR - QUARK INTERACTIONS AS A COMMON SOURCE OF THE VECTOR MESON DOMINANCE AND SIGMA MODEL. (IN RUSSIAN)”. In: *Yad. Fiz.* 36 (1982), pp. 1265–1277.
- [122] D. Ebert and M.K. Volkov. “Composite Meson Model with Vector Dominance Based on U(2) Invariant Four Quark Interactions”. In: *Z. Phys.* C16 (1983), p. 205. DOI: 10.1007/BF01571607.
- [123] M.K. Volkov. “Meson Lagrangians in a Superconductor Quark Model”. In: *Annals Phys.* 157 (1984), pp. 282–303. DOI: 10.1016/0003-4916(84)90055-1.
- [124] Alexander A. Osipov, Brigitte Hiller, and Joao da Providencia. “Multi-quark interactions with a globally stable vacuum”. In: *Phys. Lett.* B634 (2006), pp. 48–54. DOI: 10.1016/j.physletb.2006.01.008. arXiv: hep-ph/0508058.
- [125] Alexander A. Osipov et al. “Effects of eight-quark interactions on the hadronic vacuum and mass spectra of light mesons”. In: *Annals Phys.* 322 (2007), pp. 2021–2054. DOI: 10.1016/j.aop.2006.08.004. arXiv: hep-ph/0607066.
- [126] A. A. Osipov et al. “OZI violating eight-quark interactions as a thermometer for chiral transitions”. In: *Phys. Lett.* B659 (2008), pp. 270–274. DOI: 10.1016/j.physletb.2007.11.007. arXiv: hep-ph/0709.3507 [hep-ph].
- [127] Claudia Ratti, Michael A. Thaler, and Wolfram Weise. “Phases of QCD: Lattice thermodynamics and a field theoretical model”. In: *Phys. Rev. D* 73 (2006), p. 014019. DOI: 10.1103/PhysRevD.73.014019. arXiv: hep-ph/0506234.
- [128] H. Hansen et al. “Mesonic correlation functions at finite temperature and density in the Nambu-Jona-Lasinio model with a Polyakov loop”. In: *Phys. Rev. D* 75 (2007), p. 065004. DOI: 10.1103/PhysRevD.75.065004. arXiv: hep-ph/0609116.
- [129] U. Vogl and W. Weise. “The Nambu and Jona Lasinio model: Its implications for hadrons and nuclei”. In: *Prog. Part. Nucl. Phys.* 27 (1991), pp. 195–272. DOI: 10.1016/0146-6410(91)90005-9.

- [130] S. P. Klevansky. “The Nambu-Jona-Lasinio model of quantum chromodynamics”. In: *Rev. Mod. Phys.* 64 (1992), pp. 649–708. DOI: 10.1103/RevModPhys.64.649.
- [131] Tetsuo Hatsuda and Teiji Kunihiro. “QCD phenomenology based on a chiral effective Lagrangian”. In: *Phys. Rept.* 247 (1994), pp. 221–367. DOI: 10.1016/0370-1573(94)90022-1. arXiv: hep-ph/9401310.
- [132] M. Kobayashi and T. Maskawa. “CHIRAL SYMMETRY AND  $\eta$ - $X$  MIXING.” In: *Progr. Theor. Phys. (Kyoto)* 44: 1422-4(Nov 1970). (Jan. 1970). DOI: 10.1143/PTP.44.1422.
- [133] Alexander A. Osipov et al. “Aspects of  $U(A)(1)$  breaking in the Nambu and Jona-Lasinio model”. In: *Annals Phys.* 321 (2006), pp. 2504–2534. DOI: 10.1016/j.aop.2006.02.010. arXiv: hep-ph/0507226.
- [134] João Miguel Carvalho Alves Moreira. “Nambu–Jona-Lasinio Model with six and eight quark interactions”. PhD thesis. University of Coimbra, 2008.
- [135] S. Okubo. “Phi meson and unitary symmetry model”. In: *Phys. Lett.* 5 (1963), pp. 165–168. DOI: 10.1016/S0375-9601(63)92548-9.
- [136] Jugoro Iizuka. “Systematics and phenomenology of meson family”. In: *Prog. Theor. Phys. Suppl.* 37 (1966), pp. 21–34.
- [137] Jorge Morais, Brigitte Hiller, and Alexander A. Osipov. “Masses of the lowest spin-0 and spin-1 meson nonets: explicit symmetry breaking effects”. In: *Phys. Rev. D* 95.7 (2017), p. 074033. DOI: 10.1103/PhysRevD.95.074033. arXiv: 1702.06894 [hep-ph].
- [138] Peter N. Meisinger and Michael C. Ogilvie. “Chiral symmetry restoration and  $Z(N)$  symmetry”. In: *Phys. Lett. B* 379 (1996), pp. 163–168. DOI: 10.1016/0370-2693(96)00447-9. arXiv: hep-lat/9512011.
- [139] Robert D. Pisarski. “Quark-gluon plasma as a condensate of  $SU(3)$  Wilson lines”. In: *Phys. Rev. D* 62 (2000), p. 111501. DOI: 10.1103/PhysRevD.62.111501. arXiv: hep-ph/0006205.
- [140] Peter N. Meisinger, Travis R. Miller, and Michael C. Ogilvie. “Phenomenological equations of state for the quark gluon plasma”. In: *Phys. Rev. D* 65 (2002), p. 034009. DOI: 10.1103/PhysRevD.65.034009. arXiv: hep-ph/0108009.
- [141] Agnes Mocsy, Francesco Sannino, and Kimmo Tuominen. “Confinement versus chiral symmetry”. In: *Phys. Rev. Lett.* 92 (2004), p. 182302. DOI: 10.1103/PhysRevLett.92.182302. arXiv: hep-ph/0308135.
- [142] Simon Roessner, Claudia Ratti, and W. Weise. “Polyakov loop, diquarks and the two-flavour phase diagram”. In: *Phys. Rev. D* 75 (2007), p. 034007. DOI: 10.1103/PhysRevD.75.034007. arXiv: hep-ph/0609281 [hep-ph].
- [143] Pedro Costa et al. “Phase diagram and critical properties within an effective model of QCD: the Nambu-Jona-Lasinio model coupled to the Polyakov loop”. In: *Symmetry* 2 (2010), pp. 1338–1374. DOI: 10.3390/sym2031338. arXiv: 1007.1380 [hep-ph].
- [144] S. Ejiri, Y. Iwasaki, and K. Kanaya. “Nonperturbative determination of anisotropy coefficients in lattice gauge theories”. In: *Phys. Rev. D* 58 (1998), p. 094505. DOI: 10.1103/PhysRevD.58.094505. arXiv: hep-lat/9806007 [hep-lat].
- [145] G. Boyd et al. “Thermodynamics of  $SU(3)$  lattice gauge theory”. In: *Nucl. Phys.* B469 (1996), pp. 419–444. DOI: 10.1016/0550-3213(96)00170-8. arXiv: hep-lat/9602007 [hep-lat].

- [146] O. Kaczmarek et al. “Heavy quark anti-quark free energy and the renormalized Polyakov loop”. In: *Phys. Lett.* B543 (2002), pp. 41–47. DOI: 10.1016/S0370-2693(02)02415-2. arXiv: hep-lat/0207002 [hep-lat].
- [147] F. Karsch. “Lattice QCD at high temperature and density”. In: *Lect. Notes Phys.* 583 (2002), pp. 209–249. DOI: 10.1007/3-540-45792-5\_6. arXiv: hep-lat/0106019 [hep-lat].
- [148] Sz. Borsanyi et al. “Precision SU(3) lattice thermodynamics for a large temperature range”. In: *JHEP* 07 (2012), p. 056. DOI: 10.1007/JHEP07(2012)056. arXiv: 1204.6184 [hep-lat].
- [149] Bernd-Jochen Schaefer, Jan M. Pawłowski, and Jochen Wambach. “The Phase Structure of the Polyakov–Quark–Meson Model”. In: *Phys.Rev.* D76 (2007), p. 074023. DOI: 10.1103/PhysRevD.76.074023. arXiv: 0704.3234 [hep-ph].
- [150] Andre L. Mota et al. “Meson properties in a renormalizable version of the NJL model”. In: *Nucl.Phys.* A652 (1999), pp. 73–87. DOI: 10.1016/S0375-9474(99)00147-5. arXiv: hep-ph/9901455 [hep-ph].
- [151] Bruno Van den Bossche. “The Three flavor A scaled Nambu–Jona–Lasinio model”. In: *Ph.D. thesis, Université de Liège* (1996).
- [152] W. Pauli and F. Villars. “On the Invariant regularization in relativistic quantum theory”. In: *Rev.Mod.Phys.* 21 (1949), pp. 434–444. DOI: 10.1103/RevModPhys.21.434.
- [153] C. Schuren et al. “Vector mesons in the Nambu–Jona–Lasinio model”. In: *Nucl. Phys.* A565 (1993), pp. 687–739. DOI: 10.1016/0375-9474(93)90001-E.
- [154] Veljko Dmitrasinovic et al. “Chirally symmetric O (1/N(c corrections to the Nambu–Jona–Lasinio model”. In: *Annals Phys.* 238 (1995), pp. 332–369. DOI: 10.1006/aphy.1995.1024.
- [155] Julian S. Schwinger. “On gauge invariance and vacuum polarization”. In: *Phys. Rev.* 82 (1951), pp. 664–679. DOI: 10.1103/PhysRev.82.664.
- [156] G. Ripka. “Quarks bound by chiral fields: The quark-structure of the vacuum and of light mesons and baryons”. In: (). Oxford, UK: Clarendon Pr. (1997) 205 p.
- [157] Pedro Costa, M. C. Ruivo, and C. A. de Sousa. “Effects of the regularization on the restoration of chiral and axial symmetries”. In: *Phys. Rev.* D77 (2008), p. 096009. DOI: 10.1103/PhysRevD.77.096009. arXiv: 0710.5491 [hep-ph].
- [158] Pedro Costa et al. “How parameters and regularization affect the PNJL model phase diagram and thermodynamic quantities”. In: *Phys. Rev.* D81 (2010), p. 016007. DOI: 10.1103/PhysRevD.81.016007. arXiv: 0909.5124 [hep-ph].
- [159] J. Moreira et al. “Thermodynamic potential with correct asymptotics for PNJL model”. In: *Int.J.Mod.Phys.* A27 (2012), p. 1250060. DOI: 10.1142/S0217751X12500601. arXiv: 1008.0569 [hep-ph].
- [160] Nino M. Bratovic, Tetsuo Hatsuda, and Wolfram Weise. “Role of Vector Interaction and Axial Anomaly in the PNJL Modeling of the QCD Phase Diagram”. In: *Phys. Lett.* B719 (2013), pp. 131–135. DOI: 10.1016/j.physletb.2013.01.003. arXiv: 1204.3788 [hep-ph].

- [161] P. Kopietz, L. Bartosch, and F. Schütz. *Introduction to the Functional Renormalization Group*. Lecture Notes in Physics. Springer Berlin Heidelberg, 2010. ISBN: 9783642050947. URL: <https://books.google.pt/books?id=o05tCQAAQBAJ>.
- [162] Benjamín Jaramillo Ávila and Michael C. Birse. “Four-boson bound states from a functional renormalization group”. In: *Phys. Rev. A* 92.2 (2015), p. 023601. DOI: 10.1103/PhysRevA.92.023601. arXiv: 1506.04949 [cond-mat.quant-gas].
- [163] Frank Saueressig et al. “Black holes in Asymptotically Safe Gravity”. In: *PoS FFP14* (2016), p. 174. arXiv: 1503.06472 [hep-th].
- [164] Mahmoud Safari and Gian Paolo Vacca. “Multi-critical  $\square^k$  scalar theories: A perturbative RG approach with  $\epsilon$ -expansion”. In: (2017). arXiv: 1708.09795 [hep-th].
- [165] Christof Wetterich. “Effective average action in statistical physics and quantum field theory”. In: *Int. J. Mod. Phys. A* 16 (2001). Ed. by Z. Horvath and L. Palla, pp. 1951–1982. DOI: 10.1142/S0217751X01004591. arXiv: hep-ph/0101178.
- [166] Holger Gies. “Introduction to the functional RG and applications to gauge theories”. In: *Lect. Notes Phys.* 852 (2012), pp. 287–348. DOI: 10.1007/978-3-642-27320-9\_6. arXiv: hep-ph/0611146 [hep-ph].
- [167] Jan M. Pawłowski. “Aspects of the functional renormalisation group”. In: *Annals Phys.* 322 (2007), pp. 2831–2915. DOI: 10.1016/j.aop.2007.01.007. arXiv: hep-th/0512261 [hep-th].
- [168] Bertrand Delamotte. “An Introduction to the nonperturbative renormalization group”. In: *Lect. Notes Phys.* 852 (2012), pp. 49–132. DOI: 10.1007/978-3-642-27320-9\_2. arXiv: cond-mat/0702365 [cond-mat.stat-mech].
- [169] N. Dupuis et al. “The nonperturbative functional renormalization group and its applications”. In: (June 2020). arXiv: 2006.04853 [cond-mat.stat-mech].
- [170] Fei Gao and Jan M. Pawłowski. “Chiral phase structure and critical end point in QCD”. In: (Oct. 2020). arXiv: 2010.13705 [hep-ph].
- [171] Nils Strodthoff. “Self-consistent spectral functions in the  $O(N)$  model from the functional renormalization group”. In: *Phys. Rev. D* 95.7 (2017), p. 076002. DOI: 10.1103/PhysRevD.95.076002. arXiv: 1611.05036 [hep-th].
- [172] Jens Braun and Alexander Janot. “Dynamical Locking of the Chiral and the Deconfinement Phase Transition in QCD”. In: *Phys. Rev. D* 84 (2011), p. 114022. DOI: 10.1103/PhysRevD.84.114022. arXiv: 1102.4841 [hep-ph].
- [173] Jens Braun and Tina K. Herbst. “On the Relation of the Deconfinement and the Chiral Phase Transition in Gauge Theories with Fundamental and Adjoint Matter”. In: (May 2012). arXiv: 1205.0779 [hep-ph].
- [174] A. Jakovac and A. Patkos. “Local potential approximation for the renormalization group flow of fermionic field theories”. In: *Phys. Rev. D* 88 (2013), p. 065008. DOI: 10.1103/PhysRevD.88.065008. arXiv: 1306.2660 [hep-th].
- [175] Ken-Ichi Aoki, Hidenari Uoi, and Masatoshi Yamada. “Functional renormalization group study of the Nambu–Jona-Lasinio model at finite temperature and density in an external magnetic field”. In: *Phys. Lett. B* 753 (2016), pp. 580–585. DOI: 10.1016/j.physletb.2015.12.063. arXiv: 1507.02527 [hep-ph].

- [176] Jens Braun, Marc Leonhardt, and Martin Pospiech. “Fierz-complete NJL model study: Fixed points and phase structure at finite temperature and density”. In: *Phys. Rev. D* 96.7 (2017), p. 076003. DOI: 10.1103/PhysRevD.96.076003. arXiv: 1705.00074 [hep-ph].
- [177] Wei-jie Fu and Yu-xin Liu. “Four-fermion interactions and the chiral symmetry breaking in an external magnetic field”. In: *Phys. Rev. D* 96.7 (2017), p. 074019. DOI: 10.1103/PhysRevD.96.074019. arXiv: 1705.09841 [hep-ph].
- [178] Jens Braun. “Fermion Interactions and Universal Behavior in Strongly Interacting Theories”. In: *J. Phys.* G39 (2012), p. 033001. DOI: 10.1088/0954-3899/39/3/033001. arXiv: 1108.4449 [hep-ph].
- [179] Tina Katharina Herbst. “Polyakov-Loops and the QCD Phase Structure”. PhD thesis. Institut für Physik - FB Theoretische Physik der Karl-Franzens-Universität Graz, 2012.
- [180] Nicholas Petropoulos. “Linear sigma model at finite temperature”. Other thesis. Feb. 2004. arXiv: hep-ph/0402136.
- [181] Jan M. Pawłowski. “Equation of state and phase diagram of strongly interacting matter”. In: *Nucl. Phys.* A931 (2014), pp. 113–124. DOI: 10.1016/j.nuclphysa.2014.09.074.
- [182] Ken-Ichi Aoki and Masatoshi Yamada. “The RG flow of Nambu–Jona-Lasinio model at finite temperature and density”. In: *Int. J. Mod. Phys.* A30.27 (2015), p. 1550180. DOI: 10.1142/S0217751X15501808. arXiv: 1504.00749 [hep-ph].
- [183] Ken-Ichi Aoki, Shin-Ichiro Kumamoto, and Daisuke Sato. “Weak solution of the non-perturbative renormalization group equation to describe dynamical chiral symmetry breaking”. In: *PTEP* 2014.4 (2014), 043B05. DOI: 10.1093/ptep/ptu039. arXiv: 1403.0174 [hep-th].
- [184] Ken-Ichi Aoki, Shin-Ichiro Kumamoto, and Masatoshi Yamada. “Phase structure of NJL model with weak renormalization group”. In: (2017). arXiv: 1705.03273 [hep-th].
- [185] Ken-Ichi Aoki and Daisuke Sato. “Weak solution method of the non-perturbative renormalization group equation to describe dynamical chiral symmetry breaking and its application to beyond the ladder analysis in QCD”. In: *Proceedings, KMI-GCOE Workshop on Strong Coupling Gauge Theories in the LHC Perspective (SCGT 12): Nagoya, Japan, December 4-7, 2012*. 2014, pp. 448–451. DOI: 10.1142/9789814566254\_0055. arXiv: 1304.5276 [hep-th]. URL: <https://inspirehep.net/record/1229052/files/arXiv:1304.5276.pdf>.
- [186] Ken-Ichi Aoki, Shin-Ichiro Kumamoto, and Daisuke Sato. “Uniqueness and Significance of Weak Solution of Non-perturbative Renormalization Group Equation to Analyze Dynamical Chiral Symmetry Breaking”. In: *Proceedings, KMI-GCOE Workshop on Strong Coupling Gauge Theories in the LHC Perspective (SCGT 12): Nagoya, Japan, December 4-7, 2012*. 2014, pp. 423–426. DOI: 10.1142/9789814566254\_0049. arXiv: 1304.3289 [hep-th]. URL: <https://inspirehep.net/record/1227962/files/arXiv:1304.3289.pdf>.
- [187] Franz J. Wegner and Anthony Houghton. “Renormalization group equation for critical phenomena”. In: *Phys. Rev.* A8 (1973), pp. 401–412. DOI: 10.1103/PhysRevA.8.401.

- [188] Ralf-Arno Tripolt et al. “Spectral Functions for the Quark-Meson Model Phase Diagram from the Functional Renormalization Group”. In: *Phys. Rev. D* 89.3 (2014), p. 034010. DOI: 10.1103/PhysRevD.89.034010. arXiv: 1311.0630 [hep-ph].
- [189] Ralf-Arno Tripolt et al. “Finite-Temperature Spectral Functions from the Functional Renormalization Group”. In: *PoS LATTICE2013* (2014), p. 457. arXiv: 1311.4304 [hep-lat].
- [190] Jochen Wambach et al. “Spectral Functions from the Functional Renormalization Group”. In: *Nucl. Phys. A* 928 (2014), pp. 156–167. DOI: 10.1016/j.nuclphysa.2014.04.027. arXiv: 1404.7312 [hep-ph].
- [191] Ralf-Arno Tripolt et al. “Low-temperature behavior of the quark-meson model”. In: *Phys. Rev. D* 97.3 (2018), p. 034022. DOI: 10.1103/PhysRevD.97.034022. arXiv: 1709.05991 [hep-ph].
- [192] Pedro Costa. “Isentropic thermodynamics and scalar-mesons properties near the QCD critical end point”. In: *Eur. Phys. J. A* 52.8 (2016), p. 228. DOI: 10.1140/epja/i2016-16228-5. arXiv: 1610.05942 [hep-ph].
- [193] Pedro Costa and Renan Câmara Pereira. “Phase Diagram, Scalar-Pseudoscalar Meson Behavior and Restoration of Symmetries in  $(2 + 1)$  Polyakov-Nambu-Jona-Lasinio Model”. In: *Symmetry* 11.4 (2019), pp. 507–538. DOI: 10.3390/sym11040507. arXiv: 1904.05805 [hep-ph].
- [194] B. Hiller et al. “The phase diagram for the Nambu–Jona-Lasinio model with ’t Hooft and eight-quark interactions”. In: *Phys. Rev. D* 81 (2010), p. 116005. DOI: 10.1103/PhysRevD.81.116005. arXiv: 0812.1532 [hep-ph].
- [195] S. Ejiri et al. “The Isentropic equation of state of 2-flavor QCD”. In: *Phys. Rev. D* 73 (2006), p. 054506. DOI: 10.1103/PhysRevD.73.054506. arXiv: hep-lat/0512040.
- [196] M. Bluhm et al. “A family of equations of state based on lattice QCD: Impact on flow in ultrarelativistic heavy-ion collisions”. In: *Phys. Rev. C* 76 (2007), p. 034901. DOI: 10.1103/PhysRevC.76.034901. arXiv: 0705.0397 [hep-ph].
- [197] C. DeTar et al. “QCD thermodynamics with nonzero chemical potential at  $N_t = 6$  and effects from heavy quarks”. In: *Phys. Rev. D* 81 (2010), p. 114504. DOI: 10.1103/PhysRevD.81.114504. arXiv: 1003.5682 [hep-lat].
- [198] Sz. Borsanyi et al. “QCD equation of state at nonzero chemical potential: continuum results with physical quark masses at order  $mu^2$ ”. In: *JHEP* 08 (2012), p. 053. DOI: 10.1007/JHEP08(2012)053. arXiv: 1204.6710 [hep-lat].
- [199] Joseph I. Kapusta. *Finite-temperature field theory*. Cambridge University Press, 1989.
- [200] V. Skokov et al. “Meson fluctuations and thermodynamics of the Polyakov loop extended quark-meson model”. In: *Phys. Rev. C* 82 (2010), p. 015206. DOI: 10.1103/PhysRevC.82.015206. arXiv: 1004.2665 [hep-ph].
- [201] Tina Katharina Herbst, Jan M. Pawłowski, and Bernd-Jochen Schaefer. “The phase structure of the Polyakov–quark–meson model beyond mean field”. In: *Phys. Lett. B* 696 (2011), pp. 58–67. DOI: 10.1016/j.physletb.2010.12.003. arXiv: 1008.0081 [hep-ph].

- [202] P. Rehberg, S.P. Klevansky, and J. Hufner. “Hadronization in the SU(3) Nambu–Jona-Lasinio model”. In: *Phys.Rev.* C53 (1996), pp. 410–429. DOI: 10.1103/PhysRevC.53.410. arXiv: hep-ph/9506436 [hep-ph].
- [203] T. Hell et al. “Dynamics and thermodynamics of a non-local PNJL model with running coupling”. In: *Phys. Rev. D* 79 (2009), p. 014022. DOI: 10.1103/PhysRevD.79.014022. arXiv: 0810.1099 [hep-ph].
- [204] Pedro Costa et al. “Pseudoscalar mesons in hot, dense matter”. In: *Phys. Rev. C* 70 (2004), p. 025204. DOI: 10.1103/PhysRevC.70.025204. arXiv: hep-ph/0304025.
- [205] Juan M. Torres-Rincon and Joerg Aichelin. “Equation of state of a quark-meson mixture in the improved Polyakov–Nambu–Jona-Lasinio model at finite chemical potential”. In: *Phys. Rev. C* 96.4 (2017), p. 045205. DOI: 10.1103/PhysRevC.96.045205. arXiv: 1704.07858 [nucl-th].
- [206] M.C. Ruivo et al. “Effective restoration of chiral and axial symmetries at finite temperature and density”. In: *J. Phys. G* 31.6 (2005). Ed. by J. Cleymans, Z. Vilakazi, and P. Steinberg, S1183–S1186. DOI: 10.1088/0954-3899/31/6/083. arXiv: hep-ph/0411246.
- [207] Pedro Costa et al. “Analysis of the U(A)(1) symmetry-breaking and restoration effects on scalar-pseudoscalar spectrum”. In: *Phys. Rev. D* 71 (2005), p. 116002. DOI: 10.1103/PhysRevD.71.116002. arXiv: hep-ph/0503258.
- [208] Pedro Costa et al. “Scalar-pseudoscalar meson behavior and restoration of symmetries in SU(3) PNJL model”. In: *Phys. Rev. D* 79 (2009), p. 116003. DOI: 10.1103/PhysRevD.79.116003. arXiv: 0807.2134 [hep-ph].
- [209] A. A. Osipov and B. Hiller. “Inverse mass expansion of the one-loop effective action”. In: *Phys. Lett.* B515 (2001), pp. 458–462. DOI: 10.1016/S0370-2693(01)00889-9.
- [210] Alexander A. Osipov and Brigitte Hiller. “Large mass invariant asymptotics of the effective action”. In: *Phys.Rev.* D64 (2001), p. 087701. DOI: 10.1103/PhysRevD.64.087701. arXiv: hep-th/0106226 [hep-th].
- [211] Alexandre A. Osipov and Brigitte Hiller. “Generalized proper-time approach for the case of broken isospin symmetry”. In: *Phys. Rev. D* 63 (2001), p. 094009. DOI: 10.1103/PhysRevD.63.094009. arXiv: hep-ph/0012294.
- [212] M. K. Volkov and A. A. Osipov. “B,H,H’,Q1, and Q2 meson decays in the superconductor quark model”. In: *Sov. J. Nucl. Phys.* 41 (1985). [*Yad. Fiz.*41,785(1985)], pp. 500–503.
- [213] Pedro Costa et al. “The QCD critical end point in the PNJL model”. In: *EPL* 86.3 (2009), p. 31001. DOI: 10.1209/0295-5075/86/31001. arXiv: 0801.3616 [hep-ph].
- [214] Y. Aoki et al. “The QCD transition temperature: results with physical masses in the continuum limit II”. In: *JHEP* 06 (2009), p. 088. DOI: 10.1088/1126-6708/2009/06/088. arXiv: 0903.4155 [hep-lat].
- [215] C. R. Allton et al. “Thermodynamics of two flavor QCD to sixth order in quark chemical potential”. In: *Phys. Rev. D* 71 (2005), p. 054508. DOI: 10.1103/PhysRevD.71.054508. arXiv: hep-lat/0501030 [hep-lat].
- [216] Abhijit Bhattacharyya et al. “Investigation of Phase Diagram and Bulk Thermodynamic Properties using PNJL Model with Eight-Quark Interactions”. In: *Phys. Rev. D* 82 (2010), p. 014021. DOI: 10.1103/PhysRevD.82.014021. arXiv: 1003.3337 [hep-ph].

- [217] Hubert Hansen, Rainer Stiele, and Pedro Costa. “Quark and Polyakov-loop correlations in effective models at zero and nonvanishing density”. In: *Phys. Rev. D* 101.9 (2020), p. 094001. DOI: 10.1103/PhysRevD.101.094001. arXiv: 1904.08965 [hep-ph].
- [218] Yuji Sakai et al. “Entanglement between deconfinement transition and chiral symmetry restoration”. In: *Phys. Rev. D* 82 (2010), p. 076003. DOI: 10.1103/PhysRevD.82.076003. arXiv: 1006.3648 [hep-ph].
- [219] J. Moreira et al. “Thermodynamical properties of strongly interacting matter in a model with explicit chiral symmetry breaking interactions”. In: *Phys. Rev. D* 98.7 (2018), p. 074010. DOI: 10.1103/PhysRevD.98.074010. arXiv: 1806.00327 [hep-ph].
- [220] Wei-Chia Chen and J. Piekarewicz. “Building relativistic mean field models for finite nuclei and neutron stars”. In: *Phys. Rev. C* 90.4 (2014), p. 044305. DOI: 10.1103/PhysRevC.90.044305. arXiv: 1408.4159 [nucl-th].
- [221] G. Pagliara and J. Schaffner-Bielich. “Stability of CFL cores in Hybrid Stars”. In: *Phys. Rev. D* 77 (2008), p. 063004. DOI: 10.1103/PhysRevD.77.063004. arXiv: 0711.1119 [astro-ph].
- [222] Sanjin Benic. “Heavy hybrid stars from multi-quark interactions”. In: *Eur. Phys. J. A* 50 (2014), p. 111. DOI: 10.1140/epja/i2014-14111-1. arXiv: 1401.5380 [nucl-th].
- [223] Sanjin Benic et al. “A new quark-hadron hybrid equation of state for astrophysics - I. High-mass twin compact stars”. In: *Astron. Astrophys.* 577 (2015), A40. DOI: 10.1051/0004-6361/201425318. arXiv: 1411.2856 [astro-ph.HE].
- [224] Andreas Zacchi, Matthias Hanauske, and Jürgen Schaffner-Bielich. “Stable hybrid stars within a SU(3) Quark-Meson-Model”. In: *Phys. Rev. D* 93.6 (2016), p. 065011. DOI: 10.1103/PhysRevD.93.065011. arXiv: 1510.00180 [nucl-th].
- [225] Xuhao Wu, Akira Ohnishi, and Hong Shen. “Effects of quark-matter symmetry energy on hadron-quark coexistence in neutron-star matter”. In: *Phys. Rev. C* 98.6 (2018), p. 065801. DOI: 10.1103/PhysRevC.98.065801. arXiv: 1806.03760 [nucl-th].
- [226] D. Vautherin and D.M. Brink. “Hartree-Fock calculations with Skyrme’s interaction. 1. Spherical nuclei”. In: *Phys. Rev. C* 5 (1972), pp. 626–647. DOI: 10.1103/PhysRevC.5.626.
- [227] F. Douchin and P. Haensel. “A unified equation of state of dense matter and neutron star structure”. In: *Astron. Astrophys.* 380 (2001), p. 151. DOI: 10.1051/0004-6361:20011402. arXiv: astro-ph/0111092 [astro-ph].
- [228] Camille Ducoin et al. “Core-crust transition in neutron stars: predictivity of density developments”. In: *Phys. Rev. C* 83 (2011), p. 045810. DOI: 10.1103/PhysRevC.83.045810. arXiv: 1102.1283 [nucl-th].
- [229] M. Dutra et al. “Skyrme Interaction and Nuclear Matter Constraints”. In: *Phys. Rev. C* 85 (2012), p. 035201. DOI: 10.1103/PhysRevC.85.035201. arXiv: 1202.3902 [nucl-th].
- [230] M. Dutra et al. “Relativistic Mean-Field Hadronic Models under Nuclear Matter Constraints”. In: *Phys. Rev. C* 90.5 (2014), p. 055203. DOI: 10.1103/PhysRevC.90.055203. arXiv: 1405.3633 [nucl-th].
- [231] Jérôme Margueron, Rudiney Hoffmann Casali, and Francesca Gulminelli. “Equation of state for dense nucleonic matter from metamodeling. I. Foundational aspects”. In: *Phys.*

- Rev. C*97.2 (2018), p. 025805. DOI: 10.1103/PhysRevC.97.025805. arXiv: 1708.06894 [nucl-th].
- [232] Nai-Bo Zhang, Bao-An Li, and Jun Xu. “Combined Constraints on the Equation of State of Dense Neutron-rich Matter from Terrestrial Nuclear Experiments and Observations of Neutron Stars”. In: *Astrophys. J.* 859.2 (2018), p. 90. DOI: 10.3847/1538-4357/aac027. arXiv: 1801.06855 [nucl-th].
- [233] Tuhin Malik et al. “Tides in merging neutron stars: Consistency of the GW170817 event with experimental data on finite nuclei”. In: *Phys. Rev. C* 99.5 (2019), p. 052801. DOI: 10.1103/PhysRevC.99.052801. arXiv: 1901.04371 [nucl-th].
- [234] Jia Jie Li and Armen Sedrakian. “Constraining compact star properties with nuclear saturation parameters”. In: *Phys. Rev. C* 100.1 (2019), p. 015809. DOI: 10.1103/PhysRevC.100.015809. arXiv: 1903.06057 [astro-ph.HE].
- [235] G. A. Lalazissis et al. “New relativistic mean-field interaction with density-dependent meson-nucleon couplings”. In: *Phys. Rev. C* 71 (2 Feb. 2005), p. 024312. DOI: 10.1103/PhysRevC.71.024312. URL: <https://link.aps.org/doi/10.1103/PhysRevC.71.024312>.
- [236] M. H. Johnson and E. Teller. “Classical Field Theory of Nuclear Forces”. In: *Phys. Rev.* 98 (3 May 1955), pp. 783–787. DOI: 10.1103/PhysRev.98.783. URL: <https://link.aps.org/doi/10.1103/PhysRev.98.783>.
- [237] Hans-Peter Duerr. “Relativistic Effects in Nuclear Forces”. In: *Phys. Rev.* 103 (2 July 1956), pp. 469–480. DOI: 10.1103/PhysRev.103.469. URL: <https://link.aps.org/doi/10.1103/PhysRev.103.469>.
- [238] J.D Walecka. “A theory of highly condensed matter”. In: *Annals of Physics* 83.2 (1974), pp. 491–529. ISSN: 0003-4916. DOI: [https://doi.org/10.1016/0003-4916\(74\)90208-5](https://doi.org/10.1016/0003-4916(74)90208-5). URL: <http://www.sciencedirect.com/science/article/pii/0003491674902085>.
- [239] K. Hebeler et al. “Equation of state and neutron star properties constrained by nuclear physics and observation”. In: *Astrophys. J.* 773 (2013), p. 11. DOI: 10.1088/0004-637X/773/1/11.
- [240] M. Fortin et al. “Neutron star radii and crusts: uncertainties and unified equations of state”. In: *Phys. Rev. C* 94.3 (2016), p. 035804. DOI: 10.1103/PhysRevC.94.035804. arXiv: 1604.01944 [astro-ph.SR].
- [241] A. Chodos et al. “Baryon Structure in the Bag Theory”. In: *Phys. Rev. D*10 (1974), p. 2599. DOI: 10.1103/PhysRevD.10.2599.
- [242] Klaus Schertler, Stefan Leupold, and Jurgen Schaffner-Bielich. “Neutron stars and quark phases in the NJL model”. In: *Phys. Rev. C*60 (1999), p. 025801. DOI: 10.1103/PhysRevC.60.025801. arXiv: astro-ph/9901152 [astro-ph].
- [243] M. Baldo et al. “Neutron stars and the transition to color superconducting quark matter”. In: *Phys. Lett. B*562 (2003), pp. 153–160. DOI: 10.1016/S0370-2693(03)00556-2. arXiv: nucl-th/0212096 [nucl-th].
- [244] Igor Shovkovy, Matthias Hanauske, and Mei Huang. “Nonstrange hybrid compact stars with color superconducting matter”. In: *Phys. Rev. D*67 (2003), p. 103004. DOI: 10.1103/PhysRevD.67.103004. arXiv: hep-ph/0303027 [hep-ph].

- [245] Luca Bonanno and Armen Sedrakian. “Composition and stability of hybrid stars with hyperons and quark color-superconductivity”. In: *Astron. Astrophys.* 539 (2012), A16. DOI: 10.1051/0004-6361/201117832. arXiv: 1108.0559 [astro-ph.SR].
- [246] M. Buballa et al. “Quark mass effects on the stability of hybrid stars”. In: *Phys. Lett.* B595 (2004), pp. 36–43. DOI: 10.1016/j.physletb.2004.05.064. arXiv: nucl-th/0312078 [nucl-th].
- [247] Ignacio F. Ranea-Sandoval et al. “Constant-sound-speed parametrization for Nambu–Jona-Lasinio models of quark matter in hybrid stars”. In: *Phys. Rev. C* 93.4 (2016), p. 045812. DOI: 10.1103/PhysRevC.93.045812. arXiv: 1512.09183 [nucl-th].
- [248] G. E. Brown and Mannque Rho. “Scaling effective Lagrangians in a dense medium”. In: *Phys. Rev. Lett.* 66 (21 May 1991), pp. 2720–2723. DOI: 10.1103/PhysRevLett.66.2720. URL: <https://link.aps.org/doi/10.1103/PhysRevLett.66.2720>.
- [249] Y. Sugahara and H. Toki. “Relativistic mean field theory for unstable nuclei with nonlinear sigma and omega terms”. In: *Nucl. Phys. A* 579 (1994), pp. 557–572. DOI: 10.1016/0375-9474(94)90923-7.
- [250] K. Sumiyoshi, H. Kuwabara, and H. Toki. “Relativistic mean-field theory with non-linear  $\sigma$  and  $\omega$  terms for neutron stars and supernovae”. In: *Nucl. Phys. A* 581 (1995), pp. 725–746. DOI: 10.1016/0375-9474(94)00335-K.
- [251] R. Casalbuoni et al. “Aspects of the color flavor locking phase of QCD in the Nambu–Jona-Lasinio approximation”. In: *Phys. Rev. D* 68 (3 Aug. 2003), p. 034024. DOI: 10.1103/PhysRevD.68.034024. URL: <https://link.aps.org/doi/10.1103/PhysRevD.68.034024>.
- [252] Mark I. Gorenstein and Shin Nan Yang. “Gluon plasma with a medium-dependent dispersion relation”. In: *Phys. Rev. D* 52 (9 Nov. 1995), pp. 5206–5212. DOI: 10.1103/PhysRevD.52.5206. URL: <https://link.aps.org/doi/10.1103/PhysRevD.52.5206>.
- [253] K. Schertler, C. Greiner, and M.H. Thoma. “Medium effects in strange quark matter and strange stars”. In: *Nucl. Phys. A* 616 (1997). Ed. by S. Kubono, T. Kobayashi, and I. Tanihata, pp. 659–679. DOI: 10.1016/S0375-9474(97)00014-6. arXiv: hep-ph/9611305.
- [254] David Blaschke et al. “Was GW170817 a Canonical Neutron Star Merger? Bayesian Analysis with a Third Family of Compact Stars”. In: *Universe* 6.6 (2020), p. 81. DOI: 10.3390/universe6060081. arXiv: 2005.02759 [astro-ph.HE].
- [255] Alessandro Drago et al. “Early appearance of  $\Delta$  isobars in neutron stars”. In: *Phys. Rev. C* 90.6 (2014), p. 065809. DOI: 10.1103/PhysRevC.90.065809. arXiv: 1407.2843 [astro-ph.SR].
- [256] Patricia Ribes et al. “Interplay between  $\Delta$  Particles and Hyperons in Neutron Stars”. In: *Astrophys. J.* 883 (2019), p. 168. DOI: 10.3847/1538-4357/ab3a93. arXiv: 1907.08583 [astro-ph.HE].
- [257] Jia Jie Li and Armen Sedrakian. “Implications from GW170817 for  $\Delta$ -isobar Admixed Hypernuclear Compact Stars”. In: *Astrophys. J. Lett.* 874.2 (2019), p. L22. DOI: 10.3847/2041-8213/ab1090. arXiv: 1904.02006 [nucl-th].

- [258] Jia Jie Li, Armen Sedrakian, and Mark Alford. “Relativistic hybrid stars with sequential first-order phase transitions and heavy-baryon envelopes”. In: *Phys. Rev. D* 101.6 (2020), p. 063022. DOI: 10.1103/PhysRevD.101.063022. arXiv: 1911.00276 [astro-ph.HE].
- [259] Mark G. Alford, Sophia Han, and Madappa Prakash. “Generic conditions for stable hybrid stars”. In: *Phys. Rev. D* 88.8 (2013), p. 083013. DOI: 10.1103/PhysRevD.88.083013. arXiv: 1302.4732 [astro-ph.SR].
- [260] Mark G. Alford and Sophia Han. “Characteristics of hybrid compact stars with a sharp hadron-quark interface”. In: *Eur. Phys. J. A* 52.3 (2016), p. 62. DOI: 10.1140/epja/i2016-16062-9. arXiv: 1508.01261 [nucl-th].
- [261] Sophia Han et al. “Treating quarks within neutron stars”. In: *Phys. Rev. D* 100.10 (2019), p. 103022. DOI: 10.1103/PhysRevD.100.103022. arXiv: 1906.04095 [astro-ph.HE].
- [262] Eemeli Annala et al. “Evidence for quark-matter cores in massive neutron stars”. In: *Nature Phys.* (2020). DOI: 10.1038/s41567-020-0914-9. arXiv: 1903.09121 [astro-ph.HE].
- [263] I. Tews, J. Margueron, and S. Reddy. “Critical examination of constraints on the equation of state of dense matter obtained from GW170817”. In: *Phys. Rev. C* 98.4 (2018), p. 045804. DOI: 10.1103/PhysRevC.98.045804. arXiv: 1804.02783 [nucl-th].
- [264] Márcio Ferreira, Renan Câmara Pereira, and Constança Providência. “Neutron stars with large quark cores”. In: *Phys. Rev. D* 101.12 (2020), p. 123030. DOI: 10.1103/PhysRevD.101.123030. arXiv: 2005.10543 [nucl-th].
- [265] M. Hanauske et al. “Strange quark stars within the Nambu-Jona-Lasinio model”. In: *Phys. Rev. D* 64 (2001), p. 043005. DOI: 10.1103/PhysRevD.64.043005. arXiv: astro-ph/0101267.
- [266] T. Klähn et al. “Modern compact star observations and the quark matter equation of state”. In: *Phys. Lett. B* 654 (2007), pp. 170–176. DOI: 10.1016/j.physletb.2007.08.048. arXiv: nucl-th/0609067 [nucl-th].
- [267] C. H. Lenzi and G. Lugones. “Hybrid stars in the light of the massive pulsar PSR J1614-2230”. In: *Astrophys. J.* 759 (2012), p. 57. DOI: 10.1088/0004-637X/759/1/57. arXiv: 1206.4108 [astro-ph.SR].
- [268] Kota Masuda, Tetsuo Hatsuda, and Tatsuyuki Takatsuka. “Hadron–quark crossover and massive hybrid stars”. In: *PTEP* 2013.7 (2013), p. 073D01. DOI: 10.1093/ptep/ptt045. arXiv: 1212.6803 [nucl-th].
- [269] T. Klähn, R. Łastowiecki, and D. B. Blaschke. “Implications of the measurement of pulsars with two solar masses for quark matter in compact stars and heavy-ion collisions: A Nambu–Jona-Lasinio model case study”. In: *Phys. Rev. D* 88.8 (2013), p. 085001. DOI: 10.1103/PhysRevD.88.085001. arXiv: 1307.6996 [nucl-th].
- [270] Domenico Logoteta, Constança Providência, and Isaac Vidaña. “Formation of hybrid stars from metastable hadronic stars”. In: *Phys. Rev. C* 88.5 (2013), p. 055802. DOI: 10.1103/PhysRevC.88.055802. arXiv: 1311.0618 [nucl-th].
- [271] Thomas Klähn and Tobias Fischer. “Vector interaction enhanced bag model for astrophysical applications”. In: *Astrophys. J.* 810.2 (2015), p. 134. DOI: 10.1088/0004-637X/810/2/134. arXiv: 1503.07442 [nucl-th].

- [272] Mark G. Alford and Sophia Han. “Characteristics of hybrid compact stars with a sharp hadron-quark interface”. In: *Eur. Phys. J. A* 52.3 (2016), p. 62. DOI: 10.1140/epja/i2016-16062-9. arXiv: 1508.01261 [nucl-th].
- [273] B.K. HARRISON et al. *Gravitation Theory and Gravitational Collapse. [By] B. Kent Harrison ... Kip S. Thorne ... Masami Wakano ... John Archibald Wheeler*. Chicago & London, 1965. URL: <https://books.google.pt/books?id=8S0dMwEACAAJ>.
- [274] Richard C. Tolman. “Static solutions of Einstein’s field equations for spheres of fluid”. In: *Phys. Rev.* 55 (1939), pp. 364–373. DOI: 10.1103/PhysRev.55.364.
- [275] J. R. Oppenheimer and G. M. Volkoff. “On Massive neutron cores”. In: *Phys. Rev.* 55 (1939), pp. 374–381. DOI: 10.1103/PhysRev.55.374.
- [276] Tanja Hinderer. “Tidal Love numbers of neutron stars”. In: *Astrophys. J.* 677 (2008), pp. 1216–1220. DOI: 10.1086/533487. arXiv: 0711.2420 [astro-ph].
- [277] Tanja Hinderer. “Tidal Love numbers of neutron stars”. In: *Astrophys. J.* 677 (2008), pp. 1216–1220. DOI: 10.1086/533487. arXiv: 0711.2420 [astro-ph].
- [278] Sergey Postnikov, Madappa Prakash, and James M. Lattimer. “Tidal Love Numbers of Neutron and Self-Bound Quark Stars”. In: *Phys. Rev. D* 82 (2010), p. 024016. DOI: 10.1103/PhysRevD.82.024016. arXiv: 1004.5098 [astro-ph.SR].
- [279] Tanja Hinderer et al. “Tidal deformability of neutron stars with realistic equations of state and their gravitational wave signatures in binary inspiral”. In: *Phys. Rev. D* 81 (2010), p. 123016. DOI: 10.1103/PhysRevD.81.123016. arXiv: 0911.3535 [astro-ph.HE].
- [280] Andrea Sabatucci. “Tidal deformation of neutron stars”. PhD thesis. Sapienza – University of Rome, 2018.
- [281] Aleksi Kurkela, Paul Romatschke, and Aleksi Vuorinen. “Cold Quark Matter”. In: *Phys. Rev. D* 81 (2010), p. 105021. DOI: 10.1103/PhysRevD.81.105021. arXiv: 0912.1856 [hep-ph].
- [282] M.C. Miller et al. “PSR J0030+0451 Mass and Radius from *NICER* Data and Implications for the Properties of Neutron Star Matter”. In: *Astrophys. J. Lett.* 887.1 (2019), p. L24. DOI: 10.3847/2041-8213/ab50c5. arXiv: 1912.05705 [astro-ph.HE].
- [283] S. Weissenborn, D. Chatterjee, and J. Schaffner-Bielich. “Hyperons and massive neutron stars: Vector repulsion and strangeness”. In: *Nucl. Phys.* A914 (2013), pp. 421–426. DOI: 10.1016/j.nuclphysa.2013.04.003.
- [284] M. Oertel et al. “Hyperons in neutron star matter within relativistic mean-field models”. In: *J. Phys.* G42.7 (2015), p. 075202. DOI: 10.1088/0954-3899/42/7/075202.
- [285] A. Bauswein and H.-Th. Janka. “Measuring neutron-star properties via gravitational waves from binary mergers”. In: *Phys. Rev. Lett.* 108 (2012), p. 011101. DOI: 10.1103/PhysRevLett.108.011101. arXiv: 1106.1616 [astro-ph.SR].
- [286] Andreas Bauswein et al. “Identifying a first-order phase transition in neutron star mergers through gravitational waves”. In: *Phys. Rev. Lett.* 122.6 (2019), p. 061102. DOI: 10.1103/PhysRevLett.122.061102. arXiv: 1809.01116 [astro-ph.HE].
- [287] P. Zhuang, J. Hüfner, and S.P. Klevansky. “Thermodynamics of a quark-meson plasma in the Nambu-Jona-Lasinio model”. In: *Nuclear Physics A* 576.4 (1994), pp. 525–552.

- ISSN: 0375-9474. DOI: [https://doi.org/10.1016/0375-9474\(94\)90743-9](https://doi.org/10.1016/0375-9474(94)90743-9). URL: <http://www.sciencedirect.com/science/article/pii/0375947494907439>.
- [288] H. Guo et al. “Nambu–Jona–Lasinio Model Beyond the Mean-Field Approximation”. In: *Communications in Theoretical Physics* 27.1 (Jan. 1997), pp. 61–66. DOI: 10.1088/0253-6102/27/1/61. URL: <https://doi.org/10.1088/0253-6102/27/1/61>.
- [289] D. Blaschke et al. “Mott dissociation of pions and kaons in hot, dense quark matter”. In: *Phys. Rev. D* 96.9 (2017), p. 094008. DOI: 10.1103/PhysRevD.96.094008. arXiv: 1608.05383 [hep-ph].
- [290] David Fuseau, Thorsten Steinert, and Joerg Aichelin. “The phase diagram of the Polyakov Nambu Jona-Lasinio approach for finite chemical potentials”. In: (2019). arXiv: 1908.08122 [hep-ph].
- [291] D. Blaschke et al. “Generalized Beth–Uhlenbeck approach to mesons and diquarks in hot, dense quark matter”. In: *Annals Phys.* 348 (2014), pp. 228–255. DOI: 10.1016/j.aop.2014.06.002. arXiv: 1305.3907 [hep-ph].
- [292] Yin Jiang and Pengfei Zhuang. “Gluon Condensate in Pion Superfluid beyond Mean Field Approximation”. In: *Phys. Rev. C* 83 (2011), p. 038201. DOI: 10.1103/PhysRevC.83.038201. arXiv: 1012.2158 [nucl-th].
- [293] S. Rößner et al. “The chiral and deconfinement crossover transitions: PNJL model beyond mean field”. In: *Nuclear Physics A* 814.1 (2008), pp. 118–143. ISSN: 0375-9474. DOI: <https://doi.org/10.1016/j.nuclphysa.2008.10.006>. URL: <http://www.sciencedirect.com/science/article/pii/S0375947408007513>.
- [294] T. Hell et al. “Thermodynamics of a three-flavor nonlocal Polyakov–Nambu–Jona-Lasinio model”. In: *Phys. Rev. D* 81 (2010), p. 074034. DOI: 10.1103/PhysRevD.81.074034. arXiv: 0911.3510 [hep-ph].
- [295] D. Blaschke, A. Dubinin, and M. Buballa. “Polyakov-loop suppression of colored states in a quark-meson-diquark plasma”. In: *Phys. Rev. D* 91.12 (2015), p. 125040. DOI: 10.1103/PhysRevD.91.125040. arXiv: 1412.1040 [hep-ph].
- [296] Y. Nemoto, K. Naito, and M. Oka. “Effective potential of O(N) linear sigma model at finite temperature”. In: *Eur. Phys. J. A* 9 (2000), pp. 245–259. DOI: 10.1007/s100500070042. arXiv: hep-ph/9911431 [hep-ph].
- [297] Jurgen Baacke and Stefan Michalski. “The O(N) linear sigma model at finite temperature beyond the Hartree approximation”. In: *Phys. Rev. D* 67 (2003), p. 085006. DOI: 10.1103/PhysRevD.67.085006. arXiv: hep-ph/0210060 [hep-ph].
- [298] J. Baacke and Stefan Michalski. “O(N) linear sigma model beyond the Hartree approximation at finite temperature”. In: (Jan. 2004).
- [299] Jens O. Andersen and Tomas Brauner. “Linear sigma model at finite density in the 1/N expansion to next-to-leading order”. In: *Phys. Rev. D* 78 (2008), p. 014030. DOI: 10.1103/PhysRevD.78.014030. arXiv: 0804.4604 [hep-ph].
- [300] Wojciech Florkowski and Wojciech Broniowski. “Melting of the quark condensate in the NJL model with meson loops”. In: *Phys. Lett. B* 386 (1996), pp. 62–68. DOI: 10.1016/0370-2693(96)00935-5. arXiv: hep-ph/9605315 [hep-ph].

- [301] J. Hufner et al. “Thermodynamics of a Quark Plasma Beyond the Mean Field: A Generalized Beth-Uhlenbeck Approach”. In: *Annals of Physics* 234.2 (1994), pp. 225–244. ISSN: 0003-4916. DOI: <https://doi.org/10.1006/aphy.1994.1080>. URL: <http://www.sciencedirect.com/science/article/pii/S0003491684710803>.
- [302] Daniel Muller, Michael Buballa, and Jochen Wambach. “The Quark Propagator in the NJL Model in a self-consistent  $1/N_c$  Expansion”. In: *Phys. Rev. D* 81 (2010), p. 094022. DOI: 10.1103/PhysRevD.81.094022. arXiv: 1002.4252 [hep-ph].
- [303] M. Oertel, M. Buballa, and J. Wambach. “Meson loop effects in the NJL model at zero and nonzero temperature”. In: *Phys. Atom. Nucl.* 64 (2001). [*Yad. Fiz.*64,757(2001)], pp. 698–726. DOI: 10.1134/1.1368226. arXiv: hep-ph/0008131 [hep-ph].
- [304] Robert S. Plant and Michael C. Birse. “Mesonic fluctuations in a nonlocal NJL model”. In: *Nucl. Phys. A* 703 (2002), pp. 717–744. DOI: 10.1016/S0375-9474(01)01669-4. arXiv: hep-ph/0007340 [hep-ph].
- [305] D. Blaschke et al. “ $1/N(c)$  expansion of the quark condensate at finite temperature”. In: *Phys. Rev. C* 53 (1996), pp. 2394–2400. DOI: 10.1103/PhysRevC.53.2394. arXiv: nucl-th/9511003 [nucl-th].
- [306] Kanako Yamazaki and T. Matsui. “Quark–hadron phase transition in the PNJL model for interacting quarks”. In: *Nuclear Physics A* 913 (2013), pp. 19–50. ISSN: 0375-9474. DOI: <https://doi.org/10.1016/j.nuclphysa.2013.05.018>. URL: <http://www.sciencedirect.com/science/article/pii/S0375947413005939>.
- [307] Kanako Yamazaki and T. Matsui. “Quark–hadron phase transition in a three flavor PNJL model for interacting quarks”. In: *Nuclear Physics A* 922 (2014), pp. 237–261. ISSN: 0375-9474. DOI: <https://doi.org/10.1016/j.nuclphysa.2013.12.010>. URL: <http://www.sciencedirect.com/science/article/pii/S0375947413008099>.
- [308] D. Ebert. “Bosonization in particle physics”. In: *Lect. Notes Phys.* 508 (1998), pp. 103–114. DOI: 10.1007/BFb0106879. arXiv: hep-ph/9710511 [hep-ph].
- [309] Juan M. Torres-Rincon and Joerg Aichelin. “Equation of state of a quark-meson mixture in the improved Polyakov–Nambu–Jona-Lasinio model at finite chemical potential”. In: *Phys. Rev. C* 96 (4 Oct. 2017), p. 045205. DOI: 10.1103/PhysRevC.96.045205. URL: <https://link.aps.org/doi/10.1103/PhysRevC.96.045205>.
- [310] D. Blaschke et al. “Effects of composite pions on the chiral condensate within the PNJL model at finite temperature”. In: *Phys. Part. Nucl. Lett.* 15.3 (2018), pp. 230–235. DOI: 10.1134/S1547477118030056. arXiv: 1712.09322 [hep-ph].
- [311] Kanako Yamazaki. “Effective theory for the quark-hadron phase transition”. PhD thesis. Tokyo U., 2014.
- [312] Krzysztof Cichy, Elena Garcia-Ramos, and Karl Jansen. “Chiral condensate from the twisted mass Dirac operator spectrum”. In: *JHEP* 10 (2013), p. 175. DOI: 10.1007/JHEP10(2013)175. arXiv: 1303.1954 [hep-lat].
- [313] A. Das. *Finite Temperature Field Theory*. World scientific lecture notes in physics. World Scientific, 1997. ISBN: 9789810228569. URL: <https://books.google.pt/books?id=F7yhQgAACAAJ>.

- [314] A. E. Radzhabov et al. “Nonlocal PNJL model beyond mean field and the QCD phase transition”. In: *Phys. Rev. D* 83 (2011), p. 116004. DOI: 10.1103/PhysRevD.83.116004. arXiv: 1012.0664 [hep-ph].
- [315] E. Megias, E. Ruiz Arriola, and L.L. Salcedo. “Polyakov loop at finite temperature in chiral quark models”. In: (2004), pp. 1–6. arXiv: hep-ph/0410053 [hep-ph].
- [316] Chihiro Sasaki and Krzysztof Redlich. “An Effective gluon potential and hybrid approach to Yang-Mills thermodynamics”. In: *Phys. Rev. D* 86 (2012), p. 014007. DOI: 10.1103/PhysRevD.86.014007. arXiv: 1204.4330 [hep-ph].
- [317] Simon Rößner. “Field theoretical modelling of the QCD phase diagram”. PhD thesis. Technische Universität München, 2006.
- [318] Bernd-Jochen Schaefer and Jochen Wambach. “The Phase diagram of the quark meson model”. In: *Nucl. Phys. A* 757 (2005), pp. 479–492. DOI: 10.1016/j.nuclphysa.2005.04.012. arXiv: nucl-th/0403039 [nucl-th].
- [319] Tina K. Herbst, Jan M. Pawłowski, and Bernd-Jochen Schaefer. “Phase structure and thermodynamics of QCD”. In: *Phys. Rev. D* 88.1 (2013), p. 014007. DOI: 10.1103/PhysRevD.88.014007. arXiv: 1302.1426 [hep-ph].
- [320] Wei-jie Fu and Jan M. Pawłowski. “Relevance of matter and glue dynamics for baryon number fluctuations”. In: *Phys. Rev. D* 92.11 (2015), p. 116006. DOI: 10.1103/PhysRevD.92.116006. arXiv: 1508.06504 [hep-ph].
- [321] Tina Katharina Herbst et al. “Thermodynamics of QCD at vanishing density”. In: *Phys. Lett. B* 731 (2014), pp. 248–256. DOI: 10.1016/j.physletb.2014.02.045. arXiv: 1308.3621 [hep-ph].
- [322] Andreas Zacchi, Rainer Stiele, and Juergen Schaffner-Bielich. “Compact stars in a SU(3) Quark-Meson Model”. In: *Phys. Rev. D* 92.4 (2015), p. 045022. DOI: 10.1103/PhysRevD.92.045022. arXiv: 1506.01868 [astro-ph.HE].
- [323] Konstantin Otto, Micaela Oertel, and Bernd-Jochen Schaefer. “Hybrid and quark star matter based on a non-perturbative equation of state”. In: (2019). arXiv: 1910.11929 [hep-ph].
- [324] Matthias Drews and Wolfram Weise. “From asymmetric nuclear matter to neutron stars: a functional renormalization group study”. In: *Phys. Rev. C* 91.3 (2015), p. 035802. DOI: 10.1103/PhysRevC.91.035802. arXiv: 1412.7655 [nucl-th].
- [325] Christof Wetterich. “Exact evolution equation for the effective potential”. In: *Phys. Lett. B* 301 (1993), pp. 90–94. DOI: 10.1016/0370-2693(93)90726-X. arXiv: 1710.05815 [hep-th].
- [326] Daniel F. Litim. “Optimization of the exact renormalization group”. In: *Phys. Lett. B* 486 (2000), pp. 92–99. DOI: 10.1016/S0370-2693(00)00748-6. arXiv: hep-th/0005245.
- [327] Daniel F. Litim. “Optimized renormalization group flows”. In: *Phys. Rev. D* 64 (2001), p. 105007. DOI: 10.1103/PhysRevD.64.105007. arXiv: hep-th/0103195 [hep-th].
- [328] Matthias Drews. “Renormalization group approach to dense baryonic matter”. PhD thesis. Technical University Munich, 2014.

- [329] Takeru Yokota, Teiji Kunihiro, and Kenji Morita. “Functional renormalization group analysis of the soft mode at the QCD critical point”. In: *PTEP* 2016.7 (2016), p. 073D01. DOI: 10.1093/ptep/ptw062. arXiv: 1603.02147 [hep-ph].
- [330] Hui Zhang et al. “Functional renormalization group study of the quark-meson model with  $\omega$  meson”. In: *Phys. Rev. D* 96.11 (2017), p. 114029. DOI: 10.1103/PhysRevD.96.114029. arXiv: 1709.05654 [hep-ph].
- [331] Kazuhiko Kamikado et al. “Fluctuations in the quark-meson model for QCD with isospin chemical potential”. In: *Phys. Lett. B* 718 (2013), pp. 1044–1053. DOI: 10.1016/j.physletb.2012.11.055. arXiv: 1207.0400 [hep-ph].
- [332] Nils Strodthoff and Lorenz von Smekal. “Polyakov-Quark-Meson-Diquark Model for two-color QCD”. In: *Phys. Lett. B* 731 (2014), pp. 350–357. DOI: 10.1016/j.physletb.2014.03.008. arXiv: 1306.2897 [hep-ph].
- [333] Pedro Costa, Renan Câmara Pereira, and Constança Providência. “Role of the conserved charges in the chiral symmetry restoration phase transition”. In: *Phys. Rev. D* 102.5 (2020), p. 054010. DOI: 10.1103/PhysRevD.102.054010. arXiv: 2009.01781 [hep-ph].
- [334] G. G. Barnafoldi, A. Jakovac, and P. Posfay. “Harmonic expansion of the effective potential in a functional renormalization group at finite chemical potential”. In: *Phys. Rev. D* 95.2 (2017), p. 025004. DOI: 10.1103/PhysRevD.95.025004. arXiv: 1604.01717 [hep-th].
- [335] Konstantin Otto, Micaela Oertel, and Bernd-Jochen Schaefer. “Nonperturbative quark matter equations of state with vector interactions”. In: (July 2020). arXiv: 2007.07394 [hep-ph].
- [336] Agustin Nieto. “Evaluating sums over the Matsubara frequencies”. In: *Comput. Phys. Commun.* 92 (1995), pp. 54–64. DOI: 10.1016/0010-4655(95)00061-J. arXiv: hep-ph/9311210.
- [337] J. I. Kapusta and Charles Gale. *Finite-temperature field theory: Principles and applications*. Cambridge Monographs on Mathematical Physics. Cambridge University Press, 2011. ISBN: 9780521173223, 9780521820820, 9780511222801. DOI: 10.1017/CB09780511535130.
- [338] Topi Kähärä. “THERMODYNAMICS OF TWO-FLAVOR QCD FROM CHIRAL MODELS WITH POLYAKOV LOOP”. PhD thesis. University of Jyväskylä, 2010.
- [339] M.L. Bellac. *Thermal Field Theory*. Cambridge Monographs on Mathematical Physics. Cambridge University Press, 2000. ISBN: 9780521654777. URL: [https://books.google.pt/books?id=00\\_x6GR8GXoC](https://books.google.pt/books?id=00_x6GR8GXoC).
- [340] J.I. Kapusta and C. Gale. *Finite-Temperature Field Theory: Principles and Applications*. Cambridge Monographs on Mathematical Physics. Cambridge University Press, 2006. ISBN: 9781139457620. URL: <https://books.google.pt/books?id=r118dJ2iTpsC>.
- [341] Mikko Laine and Aleksi Vuorinen. *Basics of Thermal Field Theory*. Vol. 925. Springer, 2016. DOI: 10.1007/978-3-319-31933-9. arXiv: 1701.01554 [hep-ph].
- [342] H. Fujii and M. Ohtani. “Sigma and hydrodynamic modes along the critical line”. In: *Phys. Rev. D* 70 (1 July 2004), p. 014016. DOI: 10.1103/PhysRevD.70.014016. URL: <https://link.aps.org/doi/10.1103/PhysRevD.70.014016>.